Distribution Agreement

In presenting this thesis or dissertation as a partial fulfillment of the requirements for an advanced degree from Emory University, I hereby grant to Emory University and its agents the non-exclusive license to archive, make accessible, and display my thesis or dissertation in whole or in part in all forms of media, now or hereafter known, including display on the world wide web. I understand that I may select some access restrictions as part of the online submission of this thesis or dissertation. I retain all ownership rights to the copyright of the thesis or dissertation. I also retain the right to use in future works (such as articles or books) all or part of this thesis or dissertation.

Signature:

______________________________ ______________

Anna R. Kaplan Date

Leveraging Organic Synthesis to Disrupt and Understand Essential Bacterial Processes

By

Anna R. Kaplan

Doctor of Philosophy

Chemistry

William, M. Wuest, Ph.D.
Advisor

Huw M. L. Davies, Ph.D.
Committee Member

Frank E. McDonald, Ph.D.
Committee Member

Accepted:

Kimberly J. Arriola, Ph.D.
Dean of the James T. Laney School of Graduate Studies

Date

Leveraging Organic Synthesis to Disrupt and Understand Essential Bacterial Processes

By

Anna R. Kaplan

B.A., Bowdoin College, 2017

Advisor: William M. Wuest, Ph.D.

An abstract of
A dissertation submitted to the faculty of the
James T. Laney School of Graduate Studies of Emory University
in partial fulfillment of the requirements for the degree of
Doctor of Philosophy in Chemistry
2022

Abstract

Leveraging Organic Synthesis to Disrupt and Understand Essential Bacterial Processes

By Anna R. Kaplan

Since the serendipitous discovery of penicillin in 1928, antibiotics have revolutionized modern medicine and the way we treat bacterial infections, saving numerous lives in cases that were previously viewed as death sentences. However, this so-called "Golden-Age" of antibiotics has come to a screeching halt in recent years due to the discovery of increasing numbers of antibiotic-resistant bacteria and the lack of discovery of novel antibiotics to treat such infections. The threat of antibiotic resistance is now one of the biggest threats to the medical community, and thus finding new ways to combat these pathogens is now a major priority for both the Center for Disease Control and Prevention and the World Health Organization. With this in mind, my dissertation focuses on drawing inspiration primarily from natural sources to synthesize organic small molecules with the goal of perturbing or understanding essential bacterial processes. To this end, I have focused on two main pathogens that are key contributors to life-threatening and often times hospital-acquired infections particularly immunocompromised patients: *Pseudomonas aeruginosa* and *Staphylococcus aureus*. I will first give a more detailed introduction to antibiotics and antibiotic resistance, laying the foundation for the rest of my dissertation, which will first discuss two projects aimed at combatting and further understanding *P. aeruginosa* followed by two projects focused on targeting *S. aureus*.

Leveraging Organic Synthesis to Disrupt and Understand Essential Bacterial Processes

By

Anna R. Kaplan
B.A., Bowdoin College, 2017

Advisor: William M. Wuest, Ph.D.

A dissertation submitted to the faculty of the
James T. Laney School of Graduate Studies of Emory University
in partial fulfillment of the requirements for the degree of
Doctor of Philosophy in Chemistry
2022

Acknowledgements:

First and foremost, I want to thank my parents. From a young age, they have instilled in me the value of hard work and perseverance in whatever I was pursuing. In addition to having a strong work ethic, they also encouraged me to explore my interests and gave me the freedom to pursue my passions at the highest level possible, which is something I truly cannot repay. Although they didn't entirely understand the field of Chemistry or how to navigate a PhD, they were fully supportive of my endeavors and were always there for me. Whether it be letting me vent about a failed experiment or welcoming me home for random visits, they were always there to pick me up when I needed it. More importantly however, I want to thank them for always believing in me, even when I made a mistake in school or in life, because without your unwavering belief in me, I don't think I would have had the courage to pursue this journey.

In addition to my parents, I want to thank the rest of my family for their support in this process. I have been especially grateful to my grandparents Garney and Boppy, whom I visited more times than I can count throughout my PhD. Having the freedom to get in the car and see them, particularly during the pandemic when things were especially lonely was truly a blessing. I want to thank my brother Alex for his support; although he is my younger brother, he offered a lot of wise and sometimes unsolicited advice.

I also want to thank two people in my family who have served as a special inspiration to me throughout my entire life, but particularly during my PhD. First, my Uncle Guy who has Friedreich's Ataxia, a rare inherited disease that ultimately results in loss of motor function, ultimately resulting in living a life dependent on others. He invited me to go to a Friedreich's Ataxia conference with him and my grandfather in Atlanta in 2018 where I learned more about this currently incurable disease. This has spurred my motivation through the last four years and beyond in the hopes that one day my work can contribute to the treatment or cure of diseases like his. I am also tremendously indebted to my Grandpa Ben. He passed in 2019 at the age of 95 after living a life devoted to making others healthier as a cardiologist. I always looked up to him growing up and his encouragement definitely led me pursue the path that I am on today. One thing that I remember a lot of my family members talking about at his funeral was his devotion to his patients both in his medical advice and treatment as well as with his bedside manner. He truly believed in

helping people however he could, and I intend to carry that value with me in my career as well as in life. However, he was not only devoted to his patients; he also cared deeply about his family, particularly our education, and I cannot express enough my gratitude towards him for all of his support, financially and emotionally, of my academic and professional pursuits.

I want to extend a special thank you to two people who have unconditionally supported me through all of the challenges of grad school. I want to thank my best friend Ari who has always picked up the phone no matter what and listened to all of my complaints from experiments that didn't work to the most unreasonably stupid things that happened to bother me. She truly kept me sane through this entire process and always made sure I knew that she was just a phone call away. One of my favorite memories in grad school was the weekend that she surprised me in Atlanta because I had been having a stressful time; she just got on the plane and came to see me. However, I have to give credit to my boyfriend Leon who also played an instrumental role in making that weekend happen, as well as so many other memories in the final years of my PhD. Just like Ari, Leon has been unconditionally supportive of me no matter what, and always made sure that I knew that he always had my best interest at heart. He was always there for me to vent my frustrations about chemistry, struggles with job hunting, life problems, the list goes on. He always made sure I felt supported whether it was in getting me that extra cup of tea to get me through the day or helping me think through my science. I truly cannot express my gratitude enough for both of them.

I want to thank my boss Bill Wuest, as well as the entire Wuest lab for supporting and guiding me through my PhD acting as sounding boards for my ideas and offering feedback and advice as well. I always felt like I could talk to anybody in our lab about science and feel like I learned something, which was truly enriching. Additionally, I am incredibly grateful to be a member of a lab filled with good people who cared about my success as a scientist but also my wellness as a human being. I thank them all or that.

Finally, I want to extend my gratitude to the Emory Chemistry Department as a whole in supporting me both scientifically but also mentally and emotionally through this journey. I particularly want to thank my committee members, Dr. Huw Davies and Dr. Frank McDonald, whose advice and feedback throughout my PhD has been so truly valuable to me and I will carry it with me in my future career endeavors.

Table of Contents

1. INTRODUCTION 1

1.1. BACTERIA 1
1.2. THE EARLY DAYS OF ANTIBIOTICS 2
1.3. THE GOLDEN ERA OF ANTIBIOTICS 3
1.4. THE POST-GOLDEN ERA AND THE THREAT OF ANTIBIOTIC RESISTANCE 4
  1.4.1. Broad Spectrum vs. Narrow Spectrum Treatments 6
  1.4.2. The ESKAPEE Pathogens 6
1.5. A BRIEF INTERLUDE INTO NOVEL ANTIBIOTIC TREATMENTS 8
  1.5.1. Designing Species-Specific Antibiotics 9
  1.5.2. Trojan Horse Antibiotics 10
  1.5.3. Prevention of Bacterial Infections 10
  1.5.4. Anti-Persister Antibiotics 11
  1.5.5. Novel Scaffolds: Trans-Decalin-Containing Antimicrobials 11
1.6. MY APPROACH TO THIS DISSERTATION 15
1.7. REFERENCES 16

2. TARGET BASED DESIGN AND SYNTHESIS OF A NEW PROMYSALIN ANALOG 21

2.1. BACKGROUND 21
  2.1.1. Isolation of Promysalin[7] 22
  2.1.2. Total Synthesis of Promysalin[8] 23
  2.1.3. SAR Studies[9] 24
  2.1.4. Target Identification[10] 25
  2.1.5. Species Specificity of Promysalin 26
2.2. SIDE CHAIN ANALOGS 29
  3.2.1. Computational Analysis 31
  3.2.2. Terminal Aryl Analogs 31
3.3. COMPOUND 2.01 32
  3.3.1. Synthesis of 2.01 32
  3.3.2. Biological Evaluation of 2.01 37
3.4. NEW TERMINAL ARYL ANALOGS 38
3.5. REFERENCES 39

3. SYNTHESIS AND BIOLOGICAL EVALUATION OF IRON-BINDING BACTERIAL METABOLITES 41

3.1. THE ROLE OF IRON IN BACTERIA 41
3.2. BACTERIAL IRON ACQUISITION 41
  3.2.1. Methods for Iron Uptake 42
  3.2.2. Siderophores 42
3.3. *PSEUDOMONAS* METABOLITES 43
  3.3.1. Pyochelin and Pyoverdine 44
  3.3.2. Pyochelin Biosynthesis 45
  3.3.3. Pyochelin Biosynthetic Shunt Products 45
  3.3.4. IQS and Other Pseudomonad Metabolites 46
3.4. HYPOTHESIS FOR PYOCHELIN SHUNT METABOLITES 47
3.5. INVESTIGATION OF PYOCHELIN SHUNT METABOLITES 48
  3.5.1. Synthesis 48
  3.5.2. Iron-Binding Evaluation 50
  3.5.3. Biological Evaluation 55
3.6. CONCLUSIONS AND BROADER IMPACTS 57

3.7. Oxazoline and Oxazole Analogs ... 59
  3.7.1. *Synthesis* ... *59*
  3.7.2. *Fe^{III}-Binding Properties* ... *60*
  3.7.3. *Biological Evaluation* ... *62*
  3.7.4. *Conclusions* ... *63*
3.8. Acinetobacter Siderophores ... 63
  3.8.1. *Acinetobactin Biosynthesis* ... *64*
  3.8.2. *Synthesis of 3.22* ... *65*
  3.8.3. *Iron-Binding Properties* ... *65*
  3.8.4. *Biological Evaluation* ... *66*
  3.8.5. *Conclusions* ... *69*
3.9. References ... 70

4. INVESTIGATION OF QUATERNARY AMMONIUM COMPOUNDS (QACS) ... 76

4.1. (Methicillin-Resistant) *Staphylococcus aureus* and Prevention of Infections ... 76
4.2. QAC Background ... 76
  4.2.1. *Previous Work* ... *78*
  4.2.2. *Wuest and Minbiole* ... *79*
4.3. 3-Alkylpyridine Alkaloids (3-APAs) ... 82
  4.3.1. *Arctic 3-APAs* ... *82*
  4.3.2. *Previous Biological and Synthetic Investigations* ... *83*
4.4. Haliclocyclins as QACs ... 84
4.5. Synthesis of Haliclocyclins ... 84
4.6. Biological Evaluation of Haliclocyclins ... 85
4.7. Conclusions and Further SAR Efforts ... 87
4.8. References ... 90

5. EVALUATING THE EFFECT OF BROMINATION ON INDOLE-CONTAINING ANTIBIOTICS ... 95

5.1. Indole as a Bacterial Metabolite ... 95
5.2. The Potential of Indole-Containing Antibiotics ... 97
  5.2.1. *Indole-Containing Anti-Persister Compounds* ... *97*
  5.2.2. *Indole-Containing Anti-Biofilm Compounds* ... *98*
  5.2.3. *Halogenated Indole Antibiotics* ... *100*
5.3. Brominated Bis- and Tris- Indole Antimicrobial Compounds ... 101
  5.3.1. *Isolation and Biological Activity of Tulongicin and Dihydrospongotine C* ... *102*
  5.3.2. *Synthetic Library* ... *102*
  5.3.3. *Conclusions and Future Directions* ... *107*
5.4. References ... 108

6. SUPPORTING INFORMATION ... 113

List of Figures:

Chapter 1:

Figure 1.01. Image of bacterial leaf spot and bacterial sepsis rash.
Figure 1.02. Structures of active pyocyanase molecules, Prontosil and sulfanilamide, and Salvarsan**.**
Figure 1.03. Image of Alexander Fleming, structure of penicillin, and agar plate contaminated with *Penicillium* fungus.
Figure 1.04. Structures of tetracycline, erythromycin, methicillin, and gentamycin.
Figure 1.05. Timeline showing introduction of antibiotics into the clinic and discovery of resistance.
Figure 1.06. Schematic comparison of broad-spectrum and narrow-spectrum antibiotics.
Figure 1.07. High magnification image of *Pseudomonas aeruginosa*.
Figure 1.08. High magnification image of *Staphylococcus aureus*.
Figure 1.09. Workflow of developing natural-product-inspired antimicrobials.
Figure 1.10. Structure of promysalin.
Figure 1.11. Structure of Trojan Horse antibiotic Fetroja ® (cefiderocol).
Figure 1.12. Structure of quaternary ammonium compounds discussed in chapter 4.
Figure 1.13. Schematic representation of bacterial persistence.
Figure 1.14. General structures of QACs, haliclocyclins, and brominate indole antibiotics.
Figure 1.15. Structure of anthracimycin and chlorotonil A.

Chapter 2:

Figure 2.01. Schematic representation of broad-spectrum and species-specific antibiotics.
Figure 2.02. Structure of promysalin with undeduced stereochemistry.
Figure 2.03. Summary of modifications made to promysalin and analogs with retained activity.
Figure 2.04. Postulated hydrolysis of promysalin and structure of acid-catalyzed cyclization product.
Figure 2.05. Schematic representation of AfBPP approach to identifying the biological target of promysalin.
Figure 2.06. Feeding studies: promysalin with *P. aeruginosa* and *P. putida* in TSB and M9 minimal media.
Figure 2.07. Structure of siccanin, a known Sdh inhibitor.
Figure 2.08. Molecular docking of promysalin (green) and extended side chain analog (orange) in the SdhC binding pocket.
Figure 2.09. Molecular docking of terminal aryl promysalin analog in the SdhC binding pocket.
Figure 2.10. Structures and corresponding biological activity of promysalin, extended side-chain analog and terminal aryl analog.
Figure 2.11. Structures of proposed promysalin terminal aryl analogs.

Chapter 3:

Figure 3.01. Structures of siderophores containing the combination of a phenolate/catecholate motif and an oxazoline/thiazoline and the corresponding producing organisms.
Figure 3.02. Structures of selected *Pseudomonas* metabolites.
Figure 3.03. Structures of ulbactin F and promysalin.
Figure 3.04. Structures of mindapyrrole B and malleonitrone.
Figure 3.05. Structure of yersiniabactin and its biosynthetic shunt product escheriachelin and its inhibition of the growth of pyoverdine-deficient P. aeruginosa growth via an Fe^{III}-binding mechanism.
Figure 3.06. $FeCl_3$ assay shows Fe^{III} chelation by **3.01, 3.04, 3.08, 3.05, 3.07, 3.14,** and control EDTA.
Figure 3.07. Fluorescence titration curves of **3.01**, **3.04**, **3.08**, **3.05**, **3.07**, and **3.14** titrated with $FeCl_3$.

Figure 3.08. Fluorescence titration curves of **3.01** and **3.04** titrated with $FeCl_3$ $Fe(acac)_3$, $CoCl_2$, $CuCl_2$, $MgCl_2$, $MnCl_2$, and $NiCl_2$.
Figure 3.09. Ball-and-stick model of minimal energy structures of **3.01**-$FeCl_3$ complex.
Figure 3.10. Binding curves for **3.01**, **3.04**, **3.08**, **3.05**, **3.07**, and **3.14**.
Figure 3.11. Growth curves of PAO1 and ΔpvdDΔpchEF in Fe^{III}-depleted media with free ligands.
Figure 3.12. Growth curves of PAO1 and ΔpvdDΔpchEF Fe^{III}-depleted media with ligand:Fe^{III} complexes.
Figure 3.13. Structure of Fetroja® (cefiderocol) and hypothetical species-specific Trojan Horse antibiotic.
Figure 3.14. $FeCl_3$ assay shows Fe^{III} chelation by compounds **3.17, 3.18, 3.20,** and **3.21**.
Figure 3.15. Fluorescence titration curves for **3.16**, **3.17**, **3.19**, and **3.20** titrated with $FeCl_3$.
Figure 3.16. Binding curves for **3.16**, **3.17**, **3.19**, and **3.20**.
Figure 3.17. Growth curves of PAO1 and ΔpvdDΔpchEF with free ligand and ligand:Fe^{III} complex of each compound.
Figure 3.18. Structures of preacinetobactin, acinetobactin, fimsbactins A-F, and baumannoferrins A&B.
Figure 3.19. $FeCl_3$ assay shows Fe^{III} chelation by **3.22**.
Figure 3.20. Fluorescence titration curve for **3.22** titrated with $FeCl_3$.
Figure 3.21. Binding curves for **3.22**.
Figure 3.22. Growth curves of *A. baumannii* wild-type and ΔbasGΔbfnLΔfbsE grown in Fe^{III}-depleted media supplemented with 32 μM EDTA with free ligand **3.22**, **3.22**:Fe^{III} complex, and $FeCl_3$.
Figure 3.23. Growth curves of *A. baumannii* wild-type and ΔbasGΔbfnLΔfbsE grown in MH media in the with free ligand **3.22** and **3.22**:Fe^{III} complex.

Chapter 4:

Figure 4.01. Structure of generic QAC and commercial QACs.
Figure 4.02. Schematic representation of QAC mechanisms of action.
Figure 4.03. Structures of berberine and batzelladine K.
Figure 4.04. Structures of natural product-inspired QACs.
Figure 4.05. Summary of initial QAC series synthesized and evaluated by Wuest and Minbiole.
Figure 4.06. General structures of QACs synthesized in the rigidity-activity series.
Figure 4.07. General structures of pyridine alkyl and amide bisQACs with alkane, alkene, and alkyne linkers.
Figure 4.08. Structures of 3-APAs isolated from *Haliclona* sp.
Figure 4.09. Structures of the five classes of 3-APAs isolated from *Haliclona viscosa.*
Figure 4.10. CPC and its macrocyclic counterpart interacting with a cell membrane.
Figure 4.11. Structure of 2-APAs and comparison of 3-APA and 2-APA aliphatic portion lengths.

Chapter 5:

Figure 5.01. Schematic representation of bacterial persistence.
Figure 5.02. Structures of indole-containing anti-persister compounds.
Figure 5.03. Structures of indole-containing anti-biofilm compounds.
Figure 5.04. Structures of indole-containing compounds investigated by the Melander group.
Figure 5.05. Structures of bioactive bis-indole compounds.
Figure 5.06. Structures of tulongicin, dihydrospongotine C, spongotine C, and dibromodeoxytopsentin.
Figure 5.07. Structures of proposed bis- and tris-indole compounds for our synthetic library.

List of Schemes:

Chapter 1:

Scheme 1.01. Key synthetic steps to (-)-anthracimycin, (-)-terpentecin, (-)UCT4B, (-)-equisetin, (-)-tetrodecamycin.
Scheme 1.02. Retrosynthetic analysis of halichonadin C.

Chapter 2:

Scheme 2.01. Retrosynthesis of promysalin and confirmation of biological activity.
Scheme 2.02. Tricarboxylic acid cycle and glyoxylate shunt used by *Pseudomonads*.
Scheme 2.03. Synthesis of previously reported compounds **2.03** and **2.06**.
Scheme 2.04. Asymmetric Keck allylation used to synthesize stereoenriched homoallylic alcohols.
Scheme 2.05. Initial synthetic route to side chain **2.09**.
Scheme 2.06. Failed troubleshooting routes to side chain **2.09**.
Scheme 2.07. Full synthetic route to terminal aryl analog **2.01**.

Chapter 3:

Scheme 3.01. Abbreviated biosynthetic pathways to pyochelin and pyrrolnitrin, shunt pathway to Dha and redox breakdown to aeruginoic acid, IQS, and aeruginol, structure of aerugine, and postulated spontaneous nonenzymatic Pictet Spengler reaction between IQS and amino pyrrolnitrin to form pyonitrins A-D.
Scheme 3.02. Synthesis of Dha (**3.01**), aeruginoic (**3.04**), IQS (**3.08**), aeruginol (**3.05**), aerugine (**3.07**), pyonitrin C (**3.14**).
Scheme 3.03. Synthetic route to compounds **3.17**, **3.18**, **3.20**, **3.21**.
Scheme 3.04. Abbreviated biosynthetic pathway to preacinetobactin, its pH dependent isomerization to acinetobactin, and the hypothetical premature release of compound **3.22**.
Scheme 3.05. Synthesis of **3.24** achieved in three steps.

Chapter 4:

Scheme 4.01. Synthetic route previously employed to access common intermediate **A**.
Scheme 4.02. Hydroarylation reaction developed by the Jui group.
Scheme 4.03. Synthesis of haliclocyclins and analogs and corresponding yields.
Scheme 4.04. Unsuccessful reactions between functionalized 3-iodopyridines and **4.04**.
Scheme 4.05. Alternative photocatalytic conditions to access functionalized pyridine analogs.

Chapter 5:

Scheme 5.01. Biosynthesis of indole and derivatives in bacteria, plants, and animals.
Scheme 5.02. General synthetic outline to bis- and tris-indole compounds.
Scheme 5.03. Synthesis of 2-oxoacetaldehydes **5.03** and **5.04** and 1,2-diamines **5.11** and **5.12.**
Scheme 5.04. Synthesis of library of non-halogenated bis- and tris-indole compounds.
Scheme 5.05. Resonance form of topsentin D, reaction of dihydrospongotine with MeI and K_2CO_3, and alternative approaches to accessing the secondary alcohol in "dihydrotopsentin D" and dihydrospongotine.
Scheme 5.06. Proposed route to secondary alcohol and tris-indole analogs.

List of Tables:

Chapter 2:

Table 2.01. Structures of promysalin side chain analogs and their activity against *P. aeruginosa*.

Chapter 3:

Table 3.01. Binding stoichiometries and K_d values for **3.01**, **3.04**, **3.08**, **3.05**, **3.07**, **3.20** and pyochelin.
Table 3.02. Binding stoichiometries and K_d values for **3.16**, **3.17**, **3.19**, and **3.20**.

Chapter 4:

Table 4.01. Antimicrobial activity and red blood cell lysis activity of rigidity-activity bisQAC series.
Table 4.02. . Minimum inhibitory concentration and red blood cell hemolysis values for **4.14-4.22** and positive controls CPC and BAC.

1. Introduction

1.1. Bacteria

Bacteria are a class of prokaryotic single-celled organisms that have inhabited Earth long before most other domains of life, and continue to be a prominent life form today, with a population of approximately 2x10^{30} bacteria.[1,2] They occupy nearly all environments on the planet as mild as the soil in your back yard or the countertop in your kitchen and as extreme as acidic hot springs, hydrothermal vents, and even outer space.[3-6] Moreover, it's not surprising that bacteria play a crucial role in the vitality of nearly all ecosystems, particularly in various stages of nutrient cycling including nitrogen fixation, production of secondary metabolites, and decomposition and recycling of dead material.[5-7] In fact, human beings have exploited the versatility of bacteria in many man-made processes ranging from waste processing and treatment, to production of fermented foods like cheese, yogurt, and wine, and even the recovery of rare earth metals like ytterbium and lutetium.[8-10] It is not an exaggeration to say that the livelihood of humankind is heavily reliant on bacteria for these processes, as well as the homeostasis and well-being of our bodies, especially our gut and immune system.[6,11,12]

While the majority of bacteria are completely harmless, and often have a beneficial symbiotic relationship with the host, pathogenic bacterial infections can have devastating consequences. They can cause a range of infectious diseases affecting human health including pneumonia, meningitis, and sepsis. Pathogenic bacteria can be equally as devastating to agriculture causing leaf spot, fire blight, and wilts in plants or salmonella, mastitis, or anthrax in farm animals (Fig. 1.01).[13] For most of human history, bacterial infections have been quite catastrophic, and were often viewed as a death sentence when contracted. However, this all changed with the dawn of a new era of antibiotics.

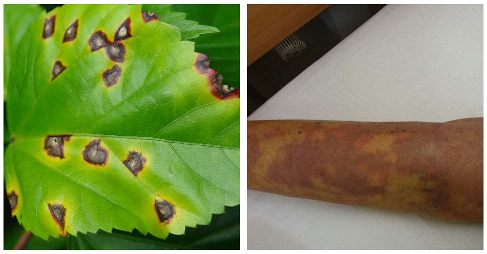

Figure 1.01. Image of bacterial leaf spot (left) and bacterial sepsis rash (right).[14,15]

1.2. The Early Days of Antibiotics

The use of antimicrobial treatments was first observed in ancient civilizations in China, Egypt, Greece, Rome, and Serbia.[16,17] Skeletons from ancient Sudanese Nubia and the Dakhleh Oasis in Egypt contain traces of tetracycline, which may be explained by consumption of tetracycline-containing materials.[16,18] Application of moldy bread to treat infections dates back to 1550 BCE, as referenced in Eber's papyrus.[16,17] Another ripe source of early antimicrobials were found in traditional Chinese medicines, wherein plants and herbs were often used to treat infections. For example, the anti-malarial drug artemisinin (qinghaosu), extracted from *Artemisia* plants in the 1970s, was used for thousands of years prior to treat a variety of illnesses.[16] It wasn't until the late 19th century that antibiotic research efforts evolved into the more modern and largely small-molecule-based approach.

Early efforts to treat bacterial infections were primarily focused on reducing the spread of gonorrhea and syphilis.[16] These infections were initially treated with heavy metals including arsenic, bismuth, and mercury. However there were several major drawbacks to these treatments including difficulty administering as well as harsh side effects often worse than the disease itself.[16] Pyocyanase, the first antibiotic treatment reported in a hospital setting, was produced by Emmerich and Löw in 1899.[16-18] This drug originated from a *Pseudomonas aeruginosa* supernatant containing two biologically active molecules, 2-heptyl-4-quinolone and 2-heptyl-3-hyroxy-4-quinolone, and was serendipitously found to be highly active against other bacterial pathogens (Fig. 1.02).[16-18] Gerhard Domagk, a bacteriologist at Bayer discovered Prontosil, the prodrug to sulfanilamide, which he used to treat an infection on his daughter's

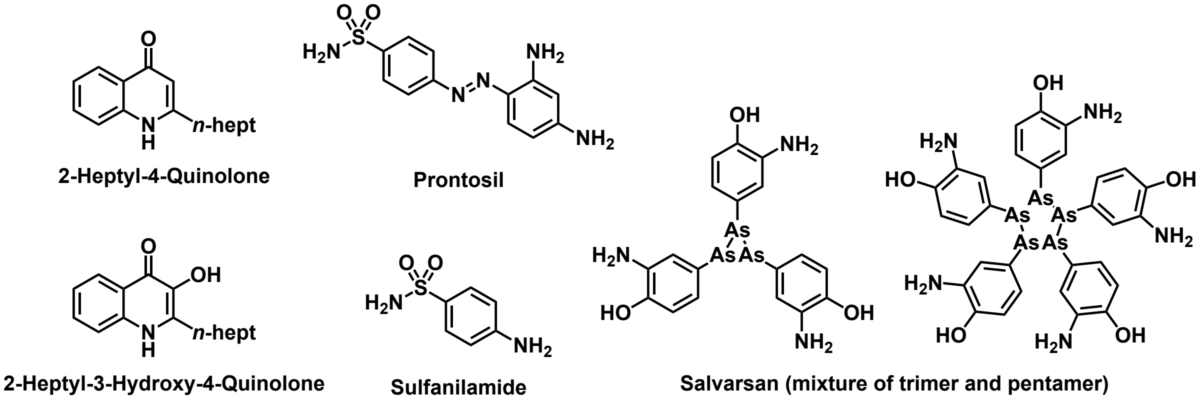
2-Heptyl-4-Quinolone
Prontosil
2-Heptyl-3-Hydroxy-4-Quinolone
Sulfanilamide
Salvarsan (mixture of trimer and pentamer)

Figure 1.02. Structures of active pyocyanase molecules, prodrug Prontosil and sulfanilamide, and Salvarsan.[14-18]

arm saving it from amputation (Fig. 1.02).[16-18] In 1911, Paul Ehrlich's "magic bullet" organoarsenic antibiotic Salvarsan first appeared in the medical literature (Fig. 1.02).[16-19] Used to treat otherwise incurable syphilis infections, Salvarsan was far more effective than the inorganic mercury salts that it replaced and it was also selectively active against bacterial cells exclusively over human cells, making it the most frequently prescribed drug until ultimately being replaced by penicillin in the 1940s.[18]

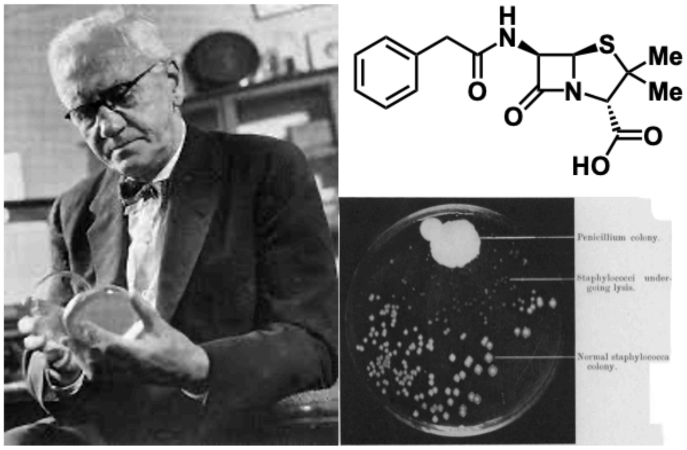
H
N
S
Me
Me
O
O
N
HO
O
Penicillium colony.
Staphylococci undergoing lysis.
Normal staphylococcus colony.

Figure 1.03. Image of Alexander Fleming, structure of penicillin, and agar plate contaminated with *Penicillium* fungus.[21,22]

In 1928, the Scottish bacteriologist Alexander Fleming returned from a vacation and noticed a zone of inhibition on an agar plate containing *Staphylococcus aureus* that had become contaminated with an invading fungus. Further isolation and extraction identified a fungus belonging to the *Penicillium* genus as the producer of the active agent now known as penicillin (Fig. 1.03).[22,23] Over the next decade, scientists worked tirelessly to isolate this promising new antibiotic compound and enable its mass production. After its isolation in 1941, penicillin was released into the clinic in 1943, revolutionizing modern medicine and opening up the door to what is now known as the "Golden Era" of Antibiotics.[23-25]

1.3. The Golden Era of Antibiotics

The years following the introduction of penicillin into the clinic were rich with antibiotic discovery; between 1940 and 1964, more than 20 new classes of antibiotics were reported and introduced into the clinic (Fig. 1.04).[16] Near the start of this era, the tetracyclines, were discovered as natural products from soil bacteria, actinomycetes, in 1948, and by the mid-1950s, three of them, chlortetracycline (Aureomycin), oxytetracycline (Terramycin), and tetracycline, had been used in the hospitals.[16,26] Shortly thereafter, erythromycin became the first macrolide antibiotic released into the clinic in 1952 working in a similar manner as the tetracyclines.[16] Methicillin was introduced in 1959 as a second generation β-lactam to treat penicillin-resistant *S. aureus* infections.[16,27,28] Finally, gentamicin was discovered by scientists at Schering Corporation in 1963 and has since been one of the leading agents to treat Gram-negative infections, particularly sepsis.[29,30] These are just a few examples of revolutionary antibiotics that have seen tremendous success in their medical applications. However, this booming era of antibiotics has since taken a dramatic turn in the years following the Golden Era leading us into what some refer to as the Post-Golden Era.

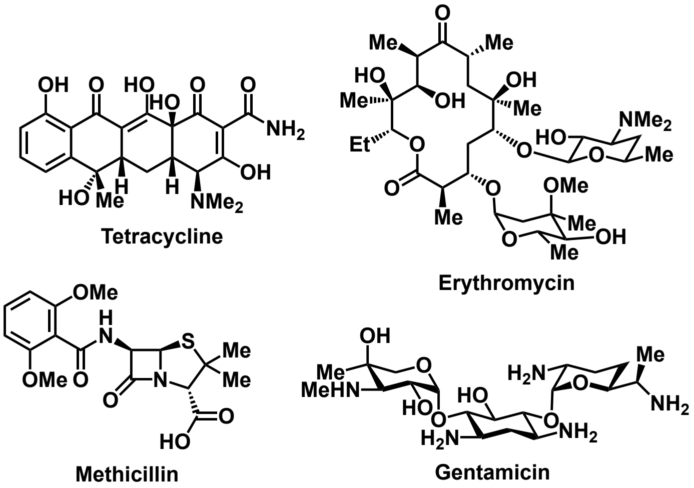
Tetracycline
Erythromycin
Methicillin
Gentamicin

Figure 1.04. Structures of tetracycline, erythromycin, methicillin, and gentamicin.

1.4. The Post-Golden Era and the Threat of Antibiotic Resistance

While it seemed that antibiotics had made a miraculous impact on the medical community and completely addressed the longstanding challenges associated bacterial infections, this sentiment was short lived, as strains of bacteria resistant to nearly all antibiotic classes were observed (Fig. 1.05).[31] Alarmingly, these strains were frequently discovered shortly after the release of these antibiotics into the clinic. In the case of penicillin, the discovery of penicillin-resistant *S. aureus* actually occurred three years prior to its commercial use. Resistant bacteria have continued to plague the healthcare industry, causing nearly 2.9 million infections resulting in almost 36,000 deaths with a cost of over 4.6 billion dollars in a single year in the United States alone.[32] In addition, antibiotic-resistant infections are responsible for over 1.7 million cases of sepsis per year and can often be implicated in complications associated with chronic conditions such as diabetes, surgeries, dialysis treatments for kidney disease, and cancer care.[32]

There are a number of factors contributing to the onset of antibiotic resistance, some of which are more difficult to avoid than others. Bacteria's ability to adapt quickly to survive antibiotic treatments by means of horizontal gene transfer, the movement of genetic material from one organism to another, is a major contributor to resistance.[16,33,34] Additionally, many bacteria have some inherent resistance to antibiotics, including β-lactamase enzymes which render antibiotics like penicillin useless or efflux pumps which recognize foreign molecules and eject them from the cell.[16,34] In contrast, clinical and agricultural overuse and inappropriate prescribing of antibiotics drive the evolution of resistance and have thus been main contributors to the crisis we are facing today. Additionally, the extensive use of antibiotics in agriculture may improve the overall health of animals, but these antibiotics along with the resistant bacteria get transferred to humans when they consume these animal products.[16,31,34] All of these factors are further compounded by the lack of discovery of novel antibiotic classes and targets since the end of the golden era.[30] Thus, it is clear that we need to rethink our outlook on treating bacterial infections and develop novel therapeutics with significantly diminished susceptibility to antimicrobial resistance.

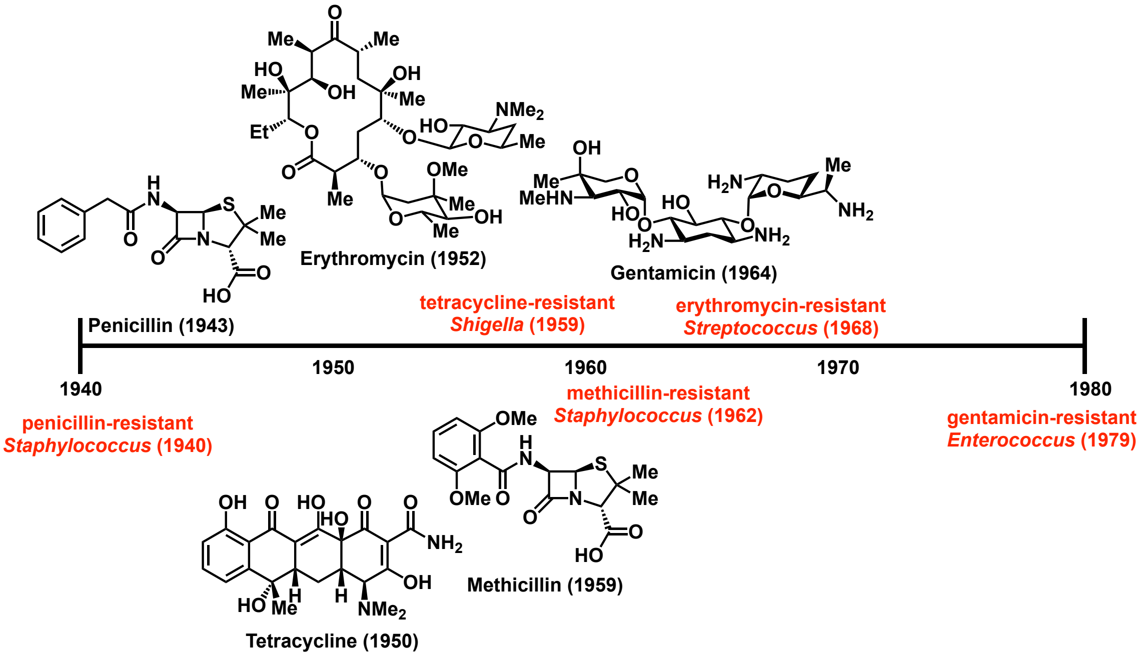
Penicillin (1943)
Erythromycin (1952)
Gentamicin (1964)
tetracycline-resistant *Shigella* (1959)
erythromycin-resistant *Streptococcus* (1968)
1940
1950
1960
1970
1980
penicillin-resistant *Staphylococcus* (1940)
methicillin-resistant *Staphylococcus* (1962)
gentamicin-resistant *Enterococcus* (1979)
Methicillin (1959)
Tetracycline (1950)

Figure 1.05. Timeline showing introduction of antibiotics into the clinic and discovery of resistance.[31]

1.4.1.Broad Spectrum vs. Narrow Spectrum Treatments

One key contributor to the prevalence of antibiotic resistance is the abundance of broad-spectrum antibiotics compared to those with narrow-spectrum activity. While broad-spectrum treatments are quite effective against a vast array of bacterial species, particularly when the identity of the infecting pathogen is unknown, their lack of selectivity creates a major drawback. As shown in figure 1.06, these types of antibiotics will effectively eradicate the infecting species, but in so doing, may also decimate a large portion of the commensal population. This damages the host microbiome, and enables any surviving resistant bacteria to monopolize the resources within the host and proliferate freely (Fig 1.06).[35-39] In contrast, a narrow-spectrum antibiotic will eradicate far fewer species therefore minimizing overall disruption to the host microbiome, thereby hampering the ability of resistant microbes to overtake and wreak havoc on the host (Fig. 1.06).[37] To this end, antibiotic resistance will likely be diminished if there are more effective narrow-spectrum therapeutics available.

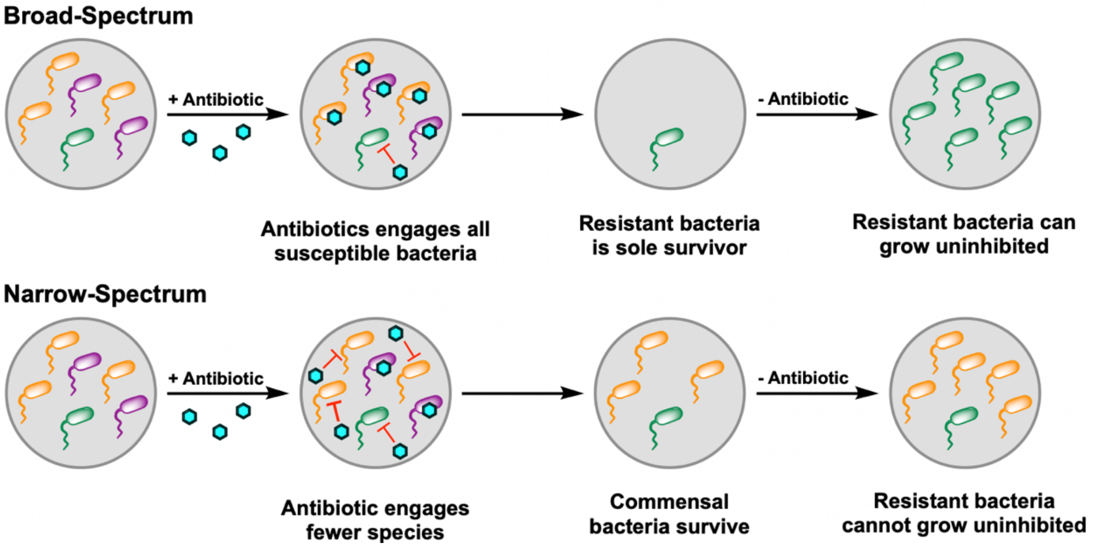
Broad-Spectrum
+ Antibiotic
Antibiotics engages all susceptible bacteria
Resistant bacteria is sole survivor
- Antibiotic
Resistant bacteria can grow uninhibited
Narrow-Spectrum
+ Antibiotic
Antibiotic engages fewer species
Commensal bacteria survive
- Antibiotic
Resistant bacteria cannot grow uninhibited

Figure 1.06. Schematic comparison of broad-spectrum and narrow-spectrum antibiotics.[34-38]

1.4.2.The ESKAPEE Pathogens

There are seven main bacterial species that deserve special attention when it comes to developing narrow-spectrum therapeutics, and these are the ESKAPEE pathogens. This group is comprised of *Enterococcus facium, Staphylococcus aureus, Klebsiella pneumoniae, Acinetobacter baumannii, Pseudomonas aeruginosa, Enterobacter* spp. and recently added *Escherichia coli*, all of which are key contributors to the antibiotic resistance statistics listed previously.[32,40] The World Health Organization recently listed all seven as antibiotic-resistant priority pathogens.[40] Additionally it has been shown that approximately 10% of Covid-19 patients became coinfected with ESKAPEE pathogens, most frequently *A. baumannii, K. pneumoniae,* and *E. faecium*, ultimately lengthening hospitalization time and increasing mortality rates.[42] With this in mind, most of my PhD work has been focused on combatting two ESKAPEE pathogens, *P. aeruginosa* and *S. aureus*.

1.4.2.1. Pseudomonas Aeruginosa

Multidrug-resistant *P. aeruginosa*, recently listed as a serious threat by the CDC, is a Gram-negative pathogen that can commonly cause many severe infections including pneumonia, bloodstream infections, urinary tract infections, and surgical site infections (Fig. 1.07).[43] In 2017, *P. aeruginosa* infections hospitalized over 32,000 people resulting in approximately 2,700 deaths.[43] *P. aeruginosa* infections are incredibly detrimental to those with compromised immune systems, greatly effecting cystic fibrosis (CF) patients. CF is caused by a variety of structural mutations in the cystic fibrosis transmembrane conductance regulator (CFTR), an ATP-gated ion channel responsible for the transport of chlorine ions within the lung and other cell types. These mutations cause rapid degradation of the ion channel, resulting in irregular ion and water transport with leads to buildup of thick layers of mucus in the lungs providing an ideal environment for pathogens like *P. aeruginosa* to colonize.[44] By the age of 18, an alarming 80% of CF patients are infected with *P. aeruginosa*, forcing them to continuously take high doses of antibiotics for the rest of their lives.[45,46] It is therefore imperative to develop new narrow-spectrum treatments for *P. aeruginosa* in order to minimize collateral damage to the CF patient microbiome.

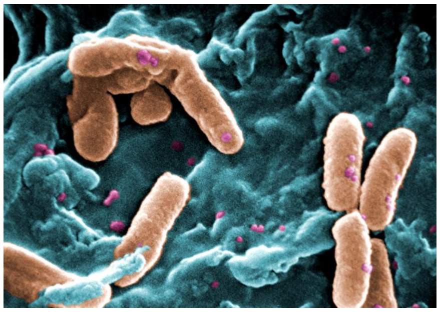

Figure 1.07. High magnification image of *Pseudomonas aeruginosa*.[43]

1.4.2.2. Staphylococcus Aureus

Methicillin-resistant *S. aureus* (MRSA), also listed as a serious threat by the CDC, is a Gram-positive pathogen accounting for 323,7000 cases of hospitalization in a single year (Fig. 1.08).[47] This pathogen accounts for nearly a third of all deaths and over one third of the overall healthcare cost associated with antibiotic resistant infections in one year.[47] Moreover, treatment of these infections has become increasingly difficult due to the fact that MRSA has become resistant to many first line antibiotics including B-lactams like penicillin and methicillin, linezolid, and vancomycin.[31,47] It is therefore clear that we are in dire need of new treatments for MRSA.

Figure 1.08. High magnification image of *Staphylococcus aureus*.[47]

1.5. A Brief Interlude into Novel Antibiotic Treatments

As previously mentioned, one of the major factors contributing to antibiotic resistance is the complete lack of novel antibiotic classes or targets. To this end, there are many treatment methods that are currently being explored to address this issue including combination therapies and phage treatments.[48] One major platform is the Waksman platform, wherein the inherent bioactivity in natural products, particularly bacterial metabolites, can be exploited in order to develop new lead therapeutics.[49-51] Our lab has adopted this approach as one core aspect of our research, wherein we will look to various natural sources, marine, terrestrial, microbial, etc. for inspiration. Once we identify a target antimicrobial natural product, we synthesize it then conduct a series of SAR studies with the ultimate goal of identifying the biological target and mechanism of action. This will then enable us to perform more informed target-guided SAR studies allowing us to optimize antibiotic potential (Fig. 1.09). Throughout my PhD, I have worked on projects at various stages in this pipeline which has served as a unifying aspect for all of my work.

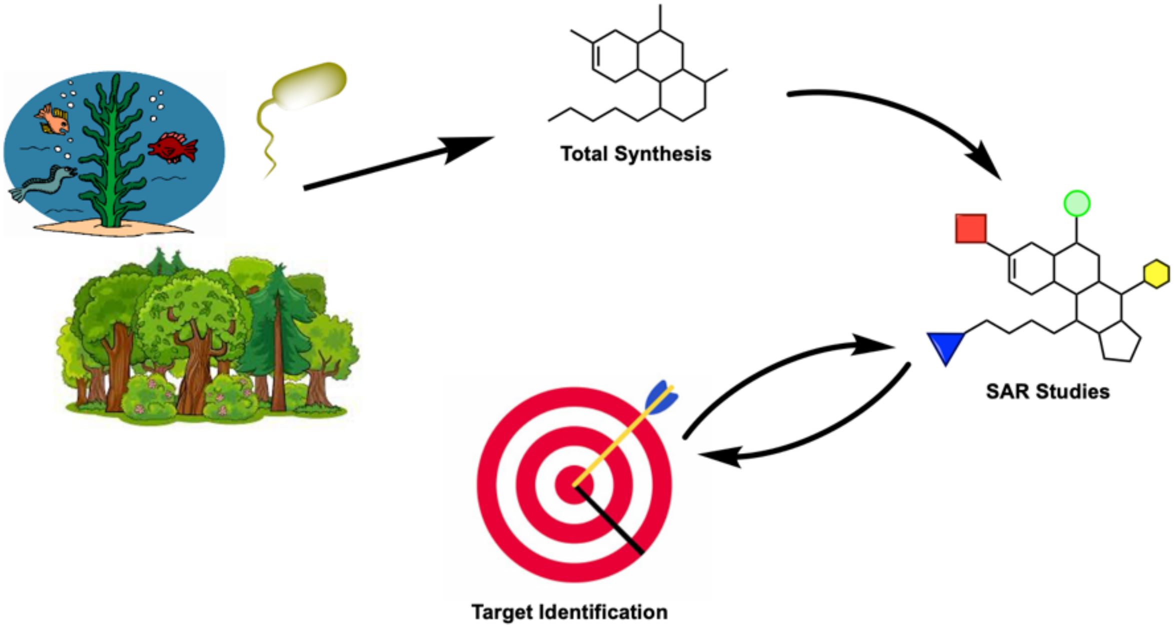
Total Synthesis
SAR Studies
Target Identification

Figure 1.09. Workflow of developing natural-product-inspired antimicrobials.

1.5.1. Designing Species-Specific Antibiotics

As previously mentioned, narrow-spectrum antibiotics represent a promising treatment strategy for combatting highly infective pathogens while significantly minimizing the risk of developing resistance. A species-specific antibiotic would offer even less risk of resistance. In so doing, this method of treatment would cause the least collateral damage to the host microbiome while still eradicating the infecting pathogen.[49] In chapter 2, I will discuss my work on promysalin, a natural product that has potent and species-specific activity against *P. aeruginosa* (Fig. 1.10).

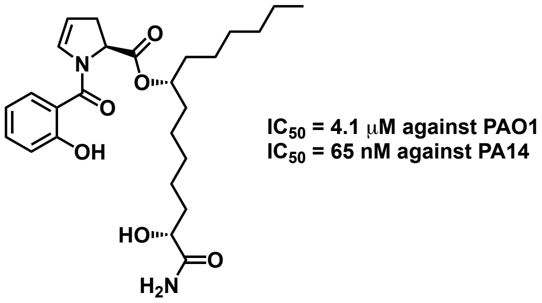
N
O
O
O
OH
HO
H2N
O
IC50 = 4.1 μM against PAO1
IC50 = 65 nM against PA14

Figure 1.10. Structure of promysalin.

1.5.2. Trojan Horse Antibiotics

Another platform of antibiotic research hinges on exploiting essential Fe^{III}-acquisition pathways in bacteria to develop siderophore-antibiotic conjugates known as "Trojan-Horse" antibiotics.[52] This strategy can either recapitulate activity of antibiotics prone to efflux resistance mechanisms, or more importantly enable antibiotics to bypass the difficult to penetrate cell membrane of Gram-negative bacteria by tricking the bacteria into taking in essential Fe^{III} by means of a siderophore (Fe^{III}-binding motif).[52] One recently approved Trojan Horse antibiotic, Fetroja ® (cefiderocol) contains a cephalosporin (purple) linked to an iron-binding catechol (orange) and is now approved to treat Gram-negative infections (Fig. 1.11).[53] In chapter 3, I will discuss my work with metabolites produced by *P. aeruginosa* pertaining to this platform.

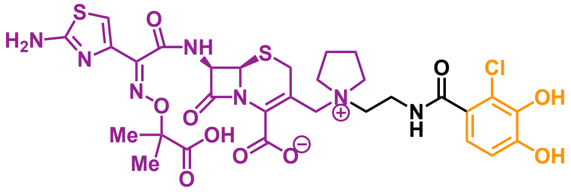

Fetroja ® (cefiderocol)

Figure 1.11. Structure of Trojan Horse antibiotic Fetroja ® (cefiderocol).[53]

1.5.3. Prevention of Bacterial Infections

Although it is important to have an arsenal of antibiotics effective at combatting bacterial infections as well as resistance, a complimentary strategy is to prevent these infections before they occur. According to the CDC, MRSA is capable of surviving on a variety of surfaces including towels, razors, and furniture for hours, days, or in some cases weeks. Without proper disinfection, contact with these surfaces, particularly with any type of open wound can lead to serious MRSA infections.[54] As previously mentioned, bacterial coinfection is directly correlated with higher levels of fatality in Covid-19 patients, making infection prevention an even greater priority in recent years.[42] In chapter 4, I will discuss my work on two different projects involving a class of potent antimicrobials known as quaternary ammonium compounds (Fig. 1.12).

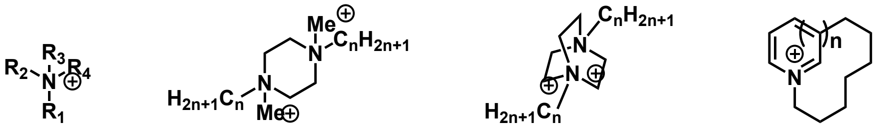

QACs **Piperazine bisQACs** **DABCO bisQACs** **Haliclocyclins**

Figure 1.12. Structure of quaternary ammonium compounds discussed in chapter 4.

1.5.4. Anti-Persister Antibiotics

One of the major obstacles in treating *S. aureus* infections is the increasing prevalence of bacterial persister cells, a subset of cells that are dormant, and therefore metabolically inactive.[54] Because they are not engaging in normal cellular activity, they are not susceptible to antibiotics with intracellular targets.[55] Upon completion of antibiotic treatment, these cells can revert back to a normal growing wild-type phenotype, exploit the host for readily available nutrients and repopulate (Fig. 1.13).[56]

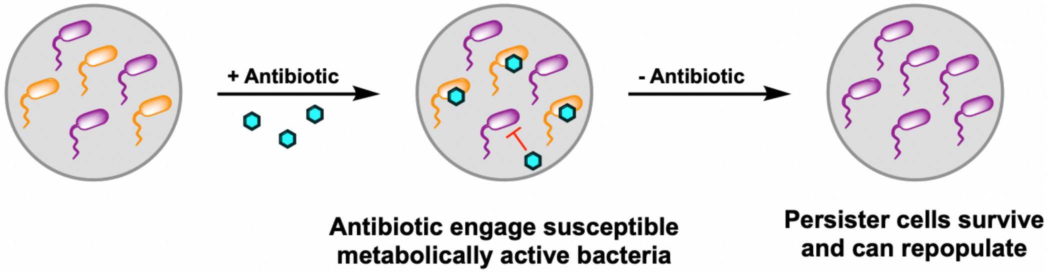
+ Antibiotic
- Antibiotic
Antibiotic engage susceptible metabolically active bacteria
Persister cells survive and can repopulate

Figure 1.13. Schematic representation of bacterial persistence.[54-56]

Persister cells present a unique challenge for development of novel antimicrobials, particularly due to their metabolically inactive state. In chapter 5, I will discuss my work on a class of indole-containing antibiotic compounds that are thought to specifically target persister cells (Fig. 1.14).

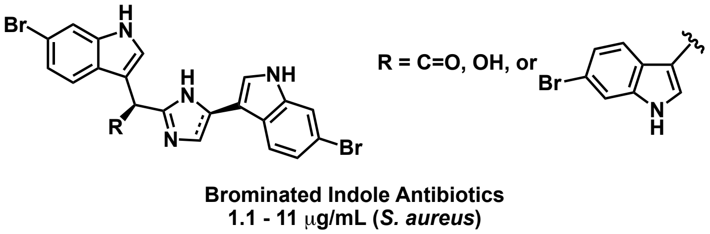
Br
H
N
R
H
N
N
NH
Br
R = C=O, OH, or
Br
N
H
Brominated Indole Antibiotics
1.1 - 11 μg/mL (*S. aureus*)

Figure 1.14. General structures of brominated indole antibiotics.

1.5.5.Novel Scaffolds: *Trans*-Decalin-Containing Antimicrobials

Another promising strategy for developing novel antimicrobials has been to search for new scaffolds yet to be observed in antibiotics. In theory, a new scaffold would lend itself to a new target or mechanism of action, rendering these types of compounds less susceptible to resistance. Of increasing interest to our group are natural products containing the trans-decalin modality. These frameworks are found in a variety of natural products, often displaying promising biological activity.[57] They are produced by a diverse array of organisms, and many are active against (methicillin-resistant) *Staphylococcus aureus* and various *Bacillus* species.[57-60] In fact, Quave and Melander recently showed that this scaffold may play a role in resensitizing MRSA to β-lactam antibiotics.[59] Notwithstanding, a portion my PhD work has involved synthesis and investigation of these scaffolds, which I will discuss briefly in this introductory chapter.

1.5.5.1. Anthracimycin

Anthracymicin is a *trans*-decalin-containing macrolide with potent antibiotic activity against both MRSA (63 ng/mL) and *Bacillus anthracis* (31 ng/mL), a highly lethal bioterrorism agent (Fig. 6.01).[57] Isolated in 2013 from *Streptomyces* sp. CNH365, this tricyclic polyketide contains a unique 14-member macrocycle fused with a *trans*-decalin motif, a scaffold that has never been seen before in antibiotics, with the exception of one other highly related scaffold, chlorotonil A (Fig. 6.01).[62-64] Interestingly, while most macrolide antibiotics inhibit protein synthesis, preliminary studies have shown that anthracimycin inhibits DNA and RNA synthesis, but does so in a manner not fully elucidated albeit distinct from the commonly observed DNA intercalation mechanism.[63] With its unique chemical scaffold as well as its broadly characterized mechanism of action, this natural product could belong to a new class of antibiotic compounds with potential for further study.

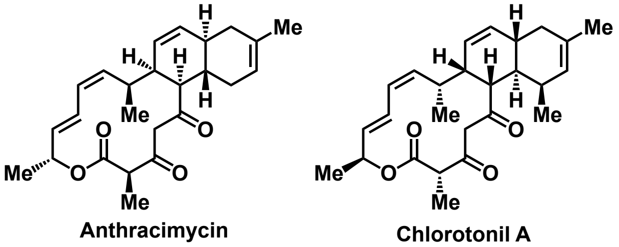

Figure 1.15. Structures of anthracimycin and chlorotonil A.[55-57]

I proposed the total synthesis of this natural product along with some preliminary SAR studies in my National Science Foundation Graduate Research Fellowships Program (NSF-GRFP) proposal in 2018 and was fortunate enough to receive funding for my proposal in 2019. Our group then joined forces with the Brimble group at the University of Auckland, who had just completed the partial synthesis of the natural product using an intramolecular Diels-Alder reaction to construct the *trans*-decalin system.[65] We aimed to optimize the stereoselectivity of this reaction while Brimble lab members constructed the macrocycle using chemistry similar to what I had proposed in the original route. Ultimately, the COVID-19 pandemic forced us out of the lab and ultimately the total synthesis was completed and published without any major changes to this Diels-Alder.[66] Work to construct analogs of anthracimycin was ultimately halted due to a lengthy route with moderate selectivity in several steps, thus requiring production of large amounts of material that could only be carried through in smaller batches early in the route. Additionally, the lack of reproducibility of the late stage Mukaiyama Aldol reaction added another degree of difficulty in making analogs.

1.5.5.2. Synthesis of Other *Trans*-Decalin-Containing Antibiotics

Zhang, W.†.; **Kaplan, A. R**.†.; Davison, E. K.; Freeman, J. L.; Brimble, M. A.; Wuest, W. M. Building *trans*-bicyclo[4.4.0]decanes/decenes in complex multifunctional frameworks: the case for antibiotic development. *Nat. Prod. Rep.* **2020**, *38*(5), 880-889. https://doi.org/10.10002/cbic.201800383

During the pandemic, myself and labmate, Wanli Zhang, as well as our collaborators Emma Davison and Jared Freeman wrote a highlight article discussing various strategies that have been employed to synthesize *trans*-decalin-containing antibiotics (Scheme 6.01). Several main approaches were discussed, including intramolecular Diels-Alder cyclizations, such as in the synthesis of (–)-anthracimycin, and exploiting the inherent stereoconfiguration of the Wieland-Miescher ketone to guide stereospecific formation of the *trans*-decalin rings as was the case in the synthesis of (–)-terpentecin and (+)-UCT4B.[65-67] We also discussed some less common strategies including sigmatropic rearrangements used to access the *trans*-decalin scaffold in the synthesis of equisetin and a SmI_2-mediated radical cyclization process utilized in the synthesis of (–)-tetrodecamycin.[68-70] Our hopes in writing this highlight article was that it would motivate synthetic chemists to draw inspiration from the established work in this field to continue to exploit and build upon these robust strategies to enable the construction of more *trans*-decalin-containing compounds, particularly those with potential use as antibiotics.

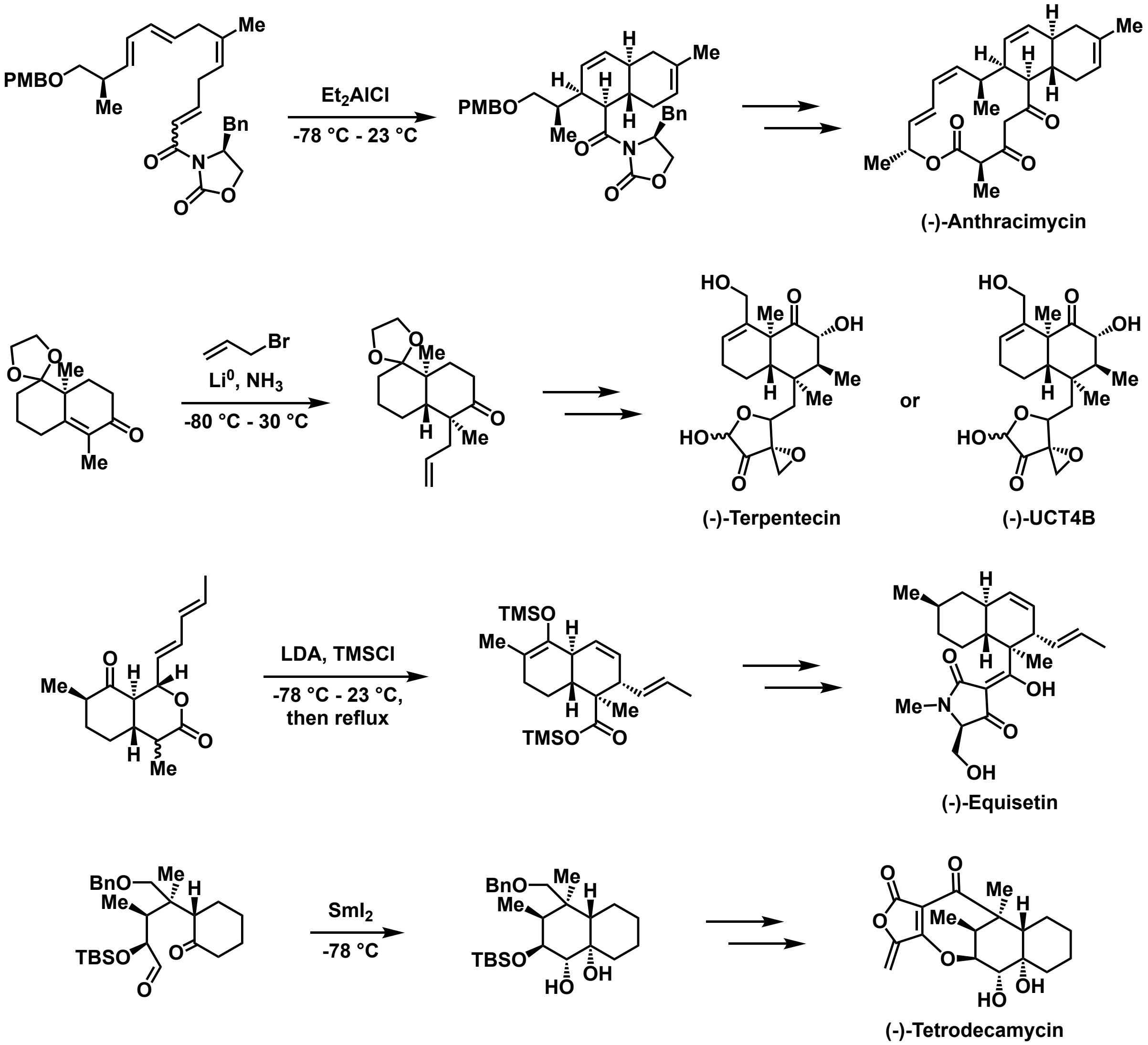

PMBO
Me
Bn
Et$_2$AlCl
-78 °C - 23 °C
Me
(-)-Anthracimycin
Br
Li^0, NH$_3$
-80 °C - 30 °C
HO
OH
(-)-Terpentecin
or
(-)-UCT4B
LDA, TMSCl
-78 °C - 23 °C, then reflux
TMSO
(-)-Equisetin
BnO
TBSO
SmI$_2$
-78 °C
(-)-Tetrodecamycin

Scheme 1.01. Key synthetic steps to (-)-anthracimycin, (-)-terpentecin, (-)UCT4B, (-)-equisetin, (-)-tetrodecamycin.[65-70]

1.5.5.3. Halichonadin C

After we wrote this highlight article, I became inspired to design and pursue the synthesis of another *trans*-decalin-containing antibiotic, halichonadin C (Scheme 1.02). This natural product was isolated from the marine sponge *Halichondria* sp. and its Cu(I) complex displayed antimicrobial activity against *Micrococcus luteus*, *Trichophyton mentagrophytes*, and *Cryptococcus neoformans* with MIC values of 4 μg/mL, 8 μg/mL, and 16 μg/mL, respectively.[71] In addition, bioactive Cu(I) complex led me to wonder if this natural product also acts as a bacterial Cu^I-binding metallophore, otherwise known as a chalkophore. To this end, Cassie Schrank and I devised a synthetic route to this natural product, which will then enable us to conduct a more extensive biological evaluation as well as Cu^I-binding studies. The route we have elected to pursue hinges on a Conia-ene cyclization to generate the *trans*-decalin framework (Scheme 6.02).[72] The precursor to this reaction can be accessed from the 3-alkylated cyclohexanone by first regioselectively alkylating the sp^3 a-carbon followed by a sequential conjugate addition then reaction of the aluminum enolate with an electrophilic ester precursor to generate the dicarbonyl species necessary for Conia-ene reaction.[73,74] The 3-alkylated cyclohexenone is synthesized in two steps by via Barbier alkylation between cyclohexenone and 1-chlro-5-trimethylsilyl-4-pentyne followed by oxidation.[75] This route is efficient in terms of step count and additionally, the sequential introduction of stereogenic centers is advantageous because it will enable the systematic evaluation of each alkyl stereocenter and the influence on biological activity. Additionally, the Conia-ene cyclization is powerful in that it automatically generates the exo-olefin without the need for any other olefin-generating chemistry.

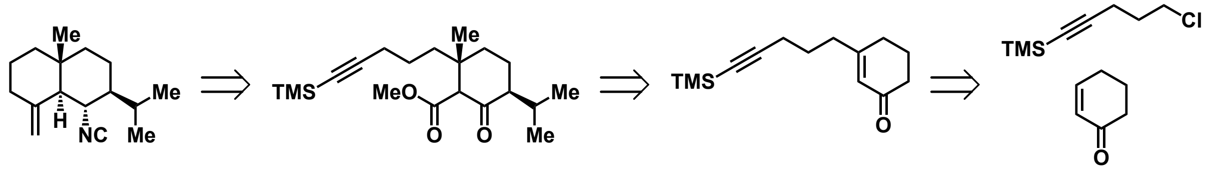

Halichonadin C

Scheme 1.02. Retrosynthetic analysis of halichonadin C.[71-74]

We are currently working towards the synthesis of halichonadin C and have thus far been successful in construction of the alkylated enone intermediate as well as stereoselective conjugate addition reactions in model systems. In the future, we look forward to completing the synthesis and further biological evaluation.

1.6. My Approach to This Dissertation

Throughout my PhD, I sought to find connections between my own work as well as the work done by others in order to find solutions to key questions I had within the realm of antimicrobial research. One of my main goals throughout my PhD was to expose myself to as many different avenues of antibiotic research as I could. However, I also wanted to find connections from one avenue of research to the next, thereby tying my thesis into a cohesive body of work. I have thus arranged this dissertation in a manner that will hopefully describe my work in an orderly fashion but also give perspective on my thought process in designing and pursuing the projects that I did.

1.7. References

1 Hall, B. (2008). Strickberger's Evolution: the integration of genes, organisms and populations. Sudbury, Mass: Jones and Bartlett.

2 Fleming, H. C.; Wuertz, S. Bacteria and archaea on Earth and their abundance in biofilms. *Nat. Rev. Microbiol.* **2019**, *17*(4), 247-260.

3 Baker-Austin, C.; Dopson, M. Life in acid: pH homeostasis in acidophiles. *Trends. Microbiol.* **2007**, *15*(4), 165-171.

4 Krasner, R. (2014). The Microbial Challenge: a public health perspective. Burlington, Mass: Jones & Bartlett Learning.

5 Pommerville, J. C. (2014). Fundamentals of Microbiology (10th ed.). Boston: Jones and Bartlett.

6 Wheelis, M. (2008). Principles of modern microbiology. Sudbury, Mass: Jones and Bartlett Publishers.

7 Barea, J. M.; Pozo, M. J.; Azcón, R.; Azcón-Aguilar, C. Microbial co-operation in the rhizosphere. *J. Exp. Bot.* **2005**, *56*(417), 1761-1778.

8 Johnson, M. E.; Lucey, J. A. Major technological advances and trends in cheese. *J. Dairy. Sci.* **2006**, *89*(4), 1174-1178.

9 Cohen, Y. Bioremediation of oil by marine microbial mats. *Int. Microbiol.* **2002**, *5*(4), 189-193.

10 Bonificio, W. D.; Clarke, D. R. Rare-Earth Separation Using Bacteria. *Environ. Sci. Technol. Lett.* **2016**, *3*, 180-184.

11 Sears, C. L. A dynamic partnership: celebrating our gut flora. *Anaerobe.* **2005**, *11*(5), 247-251.

12 Khan, R.; Petersen, F. C.; Shekhar, S. Commensal Bacteria: An Emerging Player in Defense Against Respiratory Pathogens. *Front. Immun.* **2019**, *10*(1203), 1-9.

13 Fish, D. N. Optimal antimicrobial therapy for sepsis. *Am. J. Health. Syst. Pharm.* **2002**, *59*, S13-S19.

14 Nelson, S. **2008**. Flickr description, Hibiscus: Bacterial leaf spot caused by *Pseudomonas cichorii*. Accessed 28 March, 2022. https://commons.wikimedia.org/wiki/File:Hibiscus_Bacterial_leaf_spot_caused_by_Pseudomonas_cichorii_(5684575818).jpg

15 Emergency doc. **2014**. Own work, Deutsch: Patientin mit schwerem septischen Schock und Ischämiezonene an der Haut bei Mikrothromben. Accessed 28 March, 2022. https://commons.wikimedia.org/wiki/File:Sepsis-Mikrothomben1.JPG

16 Gould, K. Antibiotics: from prehistory to the present day. *J. Antimicrob. Chemother.* **2016**, *71*, 572-575.

17 Hutchings, M. I.; Truman, A. W.; Wilkinson, B. Antibiotics: past, present and future. *Curr. Opin.*

Microbiol. **2019**, *51*, 72-80.

18 Aminov, R. I. A brief history of the antibiotic era: lessons learned and challenges for the future. *Front. Microbiol.* **2010**, *1*(134), 1-7.

19 Sepkowitz, K. A. One Hundred Years of Salvarsan. *N. Engl. J. Med.* **2011**, *365*(4), 291-293.

20 Dubern, J-F.; Diggle, S. P. Quorum sensing by 2-alkyl-4-quinolones in *Pseudomonas aeruginosa* and other bacterial species. *Mol. Biosyst.* **2008**, *4*, 882-888.

21 Welcome Collection gallery. **2018**. Welcome Images, Sir Alexander Fleming. Accessed 28 March, 2022. https://commons.wikimedia.org/wiki/File:Sir_Alexander_Fleming._Wellcome_L0000655.jpg

22 Fleming, A. On the Antibacterial Action of Cultures of a Penicillium with Special Reference to their Use in the Isolation of *B. influenzae*. *Br. J. Exp. Pathol.* **1929**, *10*(3), 226-236.

23 Gaynes, R. The Discovery of Penicillin – New Insights After More Than 75 Years of Clinical Use. *Emerg. Infect. Dis.* **2017**, *23*(5), 849-853.

24 Fleming, A. Penicillin. *BMJ.* **1941**, *2*(4210), 386.

25 Abraham, E. P.; Chain, E.; Fletcher, C. M.; Gardner, A. D.; Heatley, N. G.; Jennings, M. A.; Florey, H. W. Further observations on penicillin. *The Lancet.* **1941**, *238*(6155), 177-189.

26 Nelson, M. L.; Levy, S. B. The history of the tetracyclines. *Antimicrob. Ther. Rev.* **2011**, *1241*(1), 17-32.

27 Enright, M. C.; Robinson, . A.; Randle, G.; Feil, E. J.; Grundmann, H.; Spratt, B. G. The evolutionary history of methicillin-resistant *Staphylococcus aureus*. *PNAS.* **2002**, *99*(11),7687-7692.

28 LiverTox: Clinical and Research Information on Drug-Induced Liver Injury. Bethesa (MD): National Institute of Diabetes and Digestive and Kidney Diseases; 2012-. Penicillins (2nd Generation).

29 Weinstein, M. J.; Luedemann, G. M.; Oden, E. M.; Wagman, G. H.; Rosselet, J. P.; Marquez, J. A.; Coniglio, C. T.; Charney, W.; Herzog, H. L.; Black, J. Gentamicin,[1] a New Antibiotic Complex from Micromonospora. *J. Med. Chem.* **1963**, *6*(4), 463-464.

30 Germovsek, E.; Barker, C. I.; Sharland, M. What do I need to know about aminoglycoside antibiotics? *Arch. Dis. Child. Educ. Pract. Ed.* **2017**, *102*, 89-93.

31 Ventola, C. L. The Antibiotic Resistance Crisis: Causes and Threats. *P. T. J.* **2015**, *40*, 277-283.

32 Biggest Threats and Data. *CDC's Antibiotic Resistance Threats Report*. 2019.

33 Davies, J. Where have all the antibiotics gone? *Can. J. Infect. Dis. Med. Microbiol.* **2006**, *17*(5), 287-290.

34 Davies, J.; Davies, D. Origins and Evolution of Antibiotic Resistance? *Microbiol Mol. Biol. Rev.* **2010**, *74*, 417-433.

35 Ory, E. M.; Yow, E. M. Broad Spectrum Antibiotics. *JAMA*. **1963**, *185*, 273-279.

36 Leekha, S.; Terrell, C. L.; Edson, R. S. General Principles of Antimicrobial Therapy. *Mayo. Clin. Proc*. **2011**, *86*, 156-167.

37 Garland, M.; Loscher, M.; Bogyo, M. Chemical Strategies to Target Bacterial Virulence. *Chem. Rev*. **2017**, *117*, 4422-4461.

38 Canton, R.; Morosini, M. Emergence and spread of antibiotic resistance following exposure to antibiotics. *FEMS. Microbiol. Rev*. **2011**, *35*, 977-991.

39 Lobanovska, M.; Pilla, G. Penicillin's Discovery and Antibiotic Resistance: Lessons for the Future? *Yale. J. Biol. Med*. **2017**, *90*, 135-145.

40 Pendelton, J. N.; Gorman, S. P.; Gilmore, B. F. Clinical relevance of the ESKAPE pathogens. *Expert. Rev. Anti. Infect. Ther*. **2013**, *11*(3), 297-308.

41 Tacconelli, E.; Carrara, E.; Savoldi, A.; Harbarth, S.; Mendelson, M.; Monnet, . L.; Pulcini, C.; Kahlmeter, G.; Kluytmans, J.; Carmeli, Y.; Ouellett, M.; Outterson, K.; Patel, J.; Cavaleri, M.; Cox, E. M.; Houchens, C. R.; Grayson, M. L.; Hansen, P.; Singh, N.; Theuretzbacher, U.; Magrini, N.; WHO Pathogens Priority List Working Group. Discovery, research, and development of new antibiotics: the WHO priority list of antibiotic-resistant bacteria and tuberculosis. *Lancet. Infect. Dis*. **2018**, *18*, 318-327.

42 Protonotarious, E.; Mantzana, P.; Meletis, G.; Tychala, A.; Kassomenaki, A.; Vasilaki, O.; Kagkalou, G.; Gkeka, I.; Archonti, M.; Kati, S.; Metallidis, S.; Skoura, L. Microbiological characteristics of bacteremias among COVID-19 hospitalized patients in a tertiary referral hospital in Northern Greece during the second epidemic wave. *FEMS. Microbes*. **2021**, *2*, xtab021.

43 Multidrug-Resistant *Pseudomonas Aeruginosa*. *CDC's Antibiotic Resistance Threats Report.* 2019.

44 Heijerman, H. Infection and Inflammation in Cystic Fibrosis: A Short Review. *J. Cyst. Fibros.* **2005**, *4*, 3-5.

45 Crull, M. R.; Ramos, K. J.; Caldwell, E.; Mayer-Hamblett, N.; Aitken, M. L.; Goss, C. H. Change in *Pseudomonas Aeruginosa* Prevalence in Cystic Fibrosis Adults over Time. *BMC. Pulm. Med.* **2016**, *16*, 176.

46 Bhagirath, A. Y.; Li, Y.; Somoyajula, D.; Dadishi, M.; Badr, S.; Duan, K. Cystic Fibrosis Lung Environment and Pseudomonas Aeruginosa Infection. *BMC. Pulm. Med.* **2016**, *16*, 17.

47 Methicillin-Resistant *Staphylococcus aureus*. *CDC's Antibiotic Resistance Threats Report.* 2019.

48 Mulani, M. S.; Kamble, E. E.; Kumkar, S. N.; Tawre, M. S.; Pardesi, K. R. Emerging Strategies to Combat ESKAPE Pathogens in the Era of Antimicrobial Resistance: A Review. *Front. Microbiol.* **2019**, *10*(539), 1-24.

49 Lewis, K. Platforms for Antibiotic Discovery. *Nat. Rev. Drug. Discov.* **2013**, *12*, 371-378.

50 Rossiter, S. E.; Fletcher, M. H.; Wuest, W. M. Natural Products as Platforms to Overcome Antibiotic Resistance. *Chem. Rev.* **2017**, *117*, 12415-12474.

51 Abouelhassan, Y.; Garrison, A. T.; Yang, H.; Chávez-Riveros, A.; Burch, G. M.; Huigens, R. W. Recent Progress in Natural-Product-Inspired Programs Aimed to Address Antibiotic Resistance and Tolerance. *J. Med. Chem.* **2019**, *62*, 7618-7642.

52 Cheng, A. V.; Wuest, W. M. Signed, Sealed, Delivered: Conjugate and Prodrug Strategies as Targeted Delivery Vectors for Antibiotics. *ACS. Infect. Dis.* **2019**, *5*(6), 816-828.

53 Zhanel, G. G.; Golden, A. R.; Zelenitsky, S.; Wiebe, K.; Lawrence, C. K.; Adam, H. J.; Idow, T.; Domalaon, R.; Schweizer, F.; Zhanel, M. A.; Lagacé-Wiens, P. R. S.; Walkty, A. J.; Noreddin, A.; Lynch Iii, J. P.; Karlowsky, J. A. Cefiderocol: A Siderophore Cephalosporin with Activity Against Carbepenem-Resistant and Multidrug-Resistant Gram-Negative Bacilli. *Drugs.* **2019**, *79*(3), 271-289.

54 Fridman, O.; Goldberg, A.; Ronin, I.; Shoresh, N.; Balaban, N. Q. Optimization of lag time underlies antibiotic tolerance in evolved bacterial populations. *Nature.* **2014**, *513*(7518), 418-421.

55 Trastoy, R.; Manso, T.; Fernández-García, L.; Blasco, L.; Ambroa, A.; Pérez del Molino, M. L.; Bou, G.; García-Contreras, R.; Wood, T. K.; Tomás, M. Mechanisms of Bacterial Tolerance and Persistence in the Gastrointestinal and Respiratory Environments. *Clin. Microbiol. Rev.* **2018**, *31*(4), e00023-18.

56 Petchiappan, A.; Chatterji, D. Antibiotic Resistance: Current Perspectives. *ACS. Omega.* **2017**, *2*(10), 7400-7409.

57 Li, G.; Kusari, S.; Lamshöft, M.; Schüffler, A.; Laatsch, H.; Spiteller, M. Antibacterial Secondary Metabolites from an Endophytic Fungus, *Eupenicillium* sp. LG41 . *J. Nat. Prod.* **2014**, *77*(11), 2335-2341.

58 Burmeister, H. R.; Bennett, G. A.; Vesonder, R. F.; Hesseltine, C. W. Antibiotic Produced by *Fusarium equiseti* NRRL 5537. *Antimicrob. Agents. Chemother.* **1974**, *5*(6), 634-639.

59 Halecker, S.; Surup, F.; Kuhnert, E.; Mohr, K. I.; Brock, N. L.; Dickschat, J. S.; Junker, C.; Schulz, B.; Stadler, M. Hymenosetin, a 3-decalinoyltetramic acid antibiotic from cultures of the ash dieback pathogen, *Hymenoscyphus pseudoaldibus*. *Phytochemistry.* **2014**, *100*, 86-91.

60 Yang, Y-L.; Lu, C-P.; Chen, M-Y.; Chen, K-Y.; Wu, Y-C.; Wu, S-H. Cytotoxic Polyketides Containing Tetramic Acid Moieties Isolated from the Fungus Myceliophthora Thermophila: Elucidation of the Reltionship between Cytotoxicity and Stereoconfiguration. *Chem. Eur. J.* **2007**, *13*(24), 6985-6991.

61 Dettweiler, M.; Melander, R. J.; Porras, G.; Risener, C.; Marquez, L.; Samarakoon, T.; Melander, C.; Quave, C. L. A Clerodane Diterpene from *Callicarpa americana* Resensitizes Methicillin-Resistant *Staphylococcus aureus* to b-Lactam Antibiotics. *ACS. Infect. Dis.* **2020**, *6*(7), 1667-1673.

62 Jang, K. H.; Nam, S-J.; Locke, J. B.; Kauffmann, C. K.; Beatty, D. S.; Paul, L. A.; Fenical, W. Anthracimycin, a Potent Anthrax Antibiotic from a Marine-Derived Actinomycete. *Angew. Chem. Int. Ed.* **2013**, *52*(30), 7822-7824.

63 Alt, S.; Wilkinson, B. Biosynthesis of the Novel Macrolide Antibiotic Anthracimycin. *ACS. Chem. Biol.* **2015**, *10*(11), 2468-2479.

64 Jungmann, K.; Jansen, R.; Gerth, K.; Huch, V.; Krug, D.; Fenical, W.; Müller, R. Tow of a Kind – The Biosynthetic Pathways of Chlorotonil and Anthracimycin. *ACS. Chem. Biol.* **2015**, *10*(11), 2480-2490.

65 Freeman, J. L.; Brimble, M. A.; Furkert, D. P. A chiral auxiliary-based synthesis of the C5-C17 *trans*-decalin framework of anthracimycin. *Org. Chem. Front.* **2019**, *6*(16), 2954-2963.

66 Davison, E, K.; Freeman, J. L.; Zhang, W.; Wuest, W. M.; Furkert, D. P.; Brimble, M. A. Asymmetric Total Synthesis of the Naturally Occurring Antibiotic Anthracimycin. *Org. Lett.* **2020**, *22*(14), 5550-5554.

67 Ling, T.; Rivas, F.; Theodorakis, E. A. Stereoselective synthesis of the fully functionalized core fragment of terpentecin. *Tetrahedron. Lett.* **2002**, *43*(50), 9019-9022.

68 Turos, E.; Audia, J. E.; Danishefsky, S. J. Total synthesis of the Fusarium toxin equisetin: proof of the stereochemical relationship of the tetramate and terpenoid sectors. *J. Am. Chem. Soc.* **1989**, *111*(21), 8231-8236.

69 Danishefsky, S.; Funk, R. L.; Kerwin Jr., J. F. Claisen rearrangements of lactonic (silyl) enolates: a new route to functionalized cycloalkenes. *J. Am. Chem. Soc.* **1980**, *102*(22), 6889-6891.

70 Tatsuta, K.; Suzuki, Y.; Furuyama, A.; Ikegami, H. The first total synthesis of a tetracyclic antibiotic, (-)-tetrodecamycin. *Tetrahedron. Lett.* **2006**, *21*(22), 3595-3598.

71 Ishiyama, H.; Kozawa, S.; Aoyama, K.; Mikami, Y.; Fromont, J.; Kobayashi, J. Halichonadin F and Cu(I) complex of Halichonadin C from the Sponge *Halichondria* sp. *J. Nat. Prod.* **2008**, *71*(7), 1301-1303.

72 Hack, D.; Blümel, M.; Chauhan, P.; Philipps, A. R.; Enders, D. Catalytic Conia-ene and related reactions. *Chem. Soc. Rev.* **2015**, *44*(15), 6059-6093.

73 Vuagnouz-d'Augustin, M.; Alexakis, A. Copper-Catalyzed Asymmetric Conjugate Addition of Trialkylaluminum Reagents to Trisubstituted Enones: Construction of Chiral Quaternary Centers. *Chem. Eur. J.* **2013**, *13*(34), 9647-9662.

74 Murphy, S. K.; Zeng, M.; Herzon, S. B. Stereoselective Multicomponent Reactions Using Zincate Nucelophiles: β-Dicarbonyl Synthesis and Functionalization. *Org. Lett.* **2016**, *18*(19), 4880-4883.

75 Rahman, S. M. A.; Ohno, H.; Yoshino, H.; Satoh, N.; Tsukaguchi, M.; Murakami, K.; Iwata, C.; Maezaki, N.; Tanaka, T. A model study for the total synthesis of (+)-scopadulin: stereoselective construction of the A/B ring system with desired functionalities. *Tetrahedron.* **2001**, *51*(1), 127-134.

2. Target Based Design and Synthesis of a New Promysalin Analog

2.1. Background

As was mentioned in chapter 1, one of the key contributing factors to bacterial resistance is the widespread administration of broad-spectrum antibiotics. While these antibiotics are highly effective against many infectious pathogens, particularly when the identity of the virulent microbe is unknown, their broad scope of activity also renders them lethal to commensal bacteria as well, wreaking havoc on the host microbiome. Prolonged use of a broad-spectrum antibiotic will kill the infecting pathogen but will also kill much or all of the commensal population, which enables any surviving resistant mutants of the infecting bacteria to grow and repopulate with little competition for vital resources (Fig. 2.01).[1-5] One way that scientists envision minimizing the risks associated with broad-spectrum therapeutics is by the development of narrow-spectrum, or species-specific antibiotics. Contrary to broad-spectrum treatments, a species-specific antibiotic would only eradicate the infecting pathogen, enabling commensal bacteria to survive making it much more difficult for any resistant to freely proliferate (Fig. 2.01).[3] One particularly promising source for species-specific antibiotic compounds is the rhizosphere, the region of soil that directly surrounds the root of a plant. In this environment, bacteria compete with a vast array of microbes for limited resources essential to survival. Thus, one key survival strategy employed by many bacteria inhabiting the rhizosphere is the production of secondary metabolites exclusively toxic to other competing microbial species.[6] These secondary metabolites therefore represent a promising starting point for the discovery of new narrow-spectrum antibiotics with decreased susceptibility to bacterial resistance. Promysalin is one such compound recently isolated from the rhizosphere; I will discuss its synthesis and biological evaluation herein.

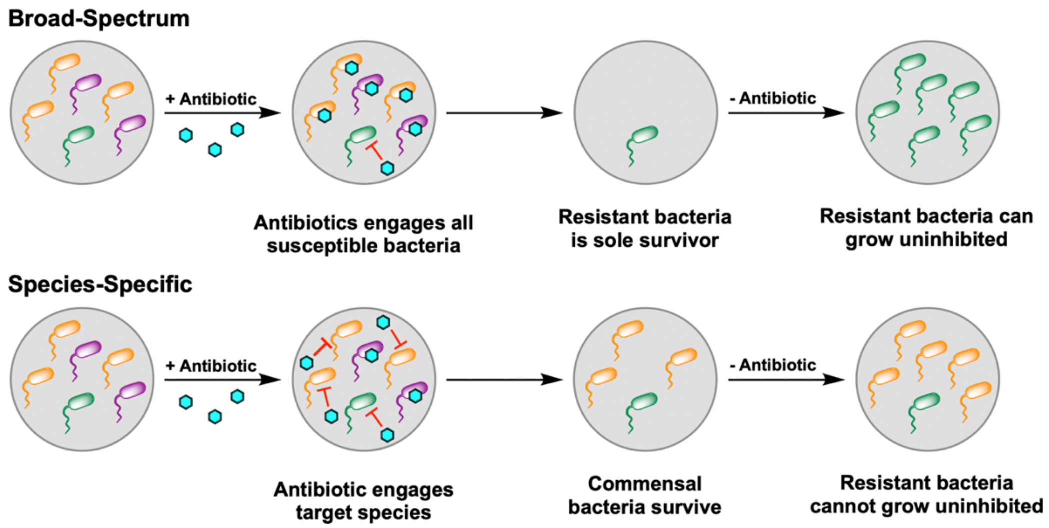
Broad-Spectrum
+ Antibiotic
- Antibiotic
Antibiotics engages all susceptible bacteria
Resistant bacteria is sole survivor
Resistant bacteria can grow uninhibited
Species-Specific
+ Antibiotic
- Antibiotic
Antibiotic engages target species
Commensal bacteria survive
Resistant bacteria cannot grow uninhibited

Figure 2.01. Schematic representation of broad-spectrum and species-specific antibiotics.

2.1.1.Isolation of Promysalin[7]

Promysalin was originally isolated in 2011 from *Pseudomonas putida* RW10S1, an inhabitant of the rhizosphere of rice plants in Sri Lanka. This metabolite was found to promote both swarming and biofilm formation in *P. putida*. In addition, it inhibited the growth of all 83 strains of *P. aeruginosa* tested, with IC_{50} values of 4.1 µM and 67 nM against two readily available laboratory strains, moderately virulent PAO1 and highly virulent PA14, respectively. Interestingly, promysalin was also tested against a panel of 32 other Gram-negative bacteria and was only active against *Azotobacter vinelandii* and was completely inactive against the panel of 9 Gram-positive bacteria including *Staphylococcus aureus* as well as fungus *Candida albicans* and ascomycete *Saccharomyces cerevisiae*. Taken together, this activity was quite promising as it suggested that promysalin could act as a narrow-spectrum antibiotic, which, as previously mentioned, is crucial in the development antibiotics with decreased susceptibility to resistance.

Structurally, promysalin is comprised of three main fragments: salicylate, dehydroproline, and myristic acid (Fig. 2.01). Additionally, there are three stereogenic centers in the molecule, which De Mot and coworkers were unable to decipher from their spectral analysis. Preliminary computational studies of the biosynthetic gene cluster using AntiSMASH aided in deducing the natural L-isomer of the dehydroproline motif (16*S*) however the orientation of the remaining two stereocenters, 2 and 8 remained unknown.[8] The uncertainty of stereoconfiguration of this natural product, as well as its promising biological activity thus prompted our group to take on the synthesis of all four stereoisomers in 2015 in the hopes of identifying the correct structure and confirming the originally reported bioactivity.

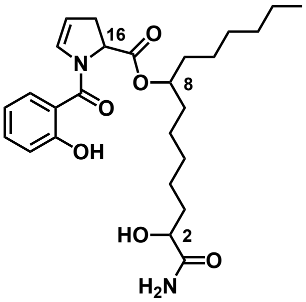

Figure 2.02. Structure of promysalin with undeduced stereochemistry.[7]

2.1.2. Total Synthesis of Promysalin[8]

In 2015, previous members of the Wuest group completed the total synthesis of the four possible stereoisomers of promysalin (Scheme 2.01). In this highly modular route, the natural product was broken into two key fragments: a proline and salicylate-derived carboxylic acid, synthesized in seven steps, and an α-hydroxy myristic acid secondary alcohol synthesized in five steps. The myristic acid side chain was strategically formed via a cross-metathesis reaction wherein each alkene precursor contained one of the stereocenters in question, thereby enabling efficient construction of all four possible stereoisomers. These two building blocks were then coupled in an EDC-mediated esterification and globally deprotected giving the target compounds in a longest linear sequence of nine steps. Once all four compounds were synthesized, their spectroscopic properties and biological activity were compared to the original isolation report, ultimately revealing that the absolute configuration of the natural product is 2*R*, 8*R*, 16*S*.

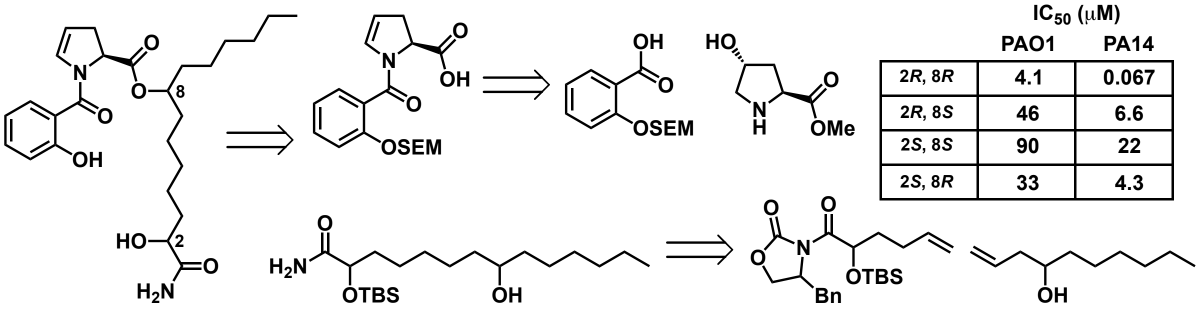

IC_{50} (μM)	PAO1	PA14
2*R*, 8*R*	4.1	0.067
2*R*, 8*S*	46	6.6
2*S*, 8*S*	90	22
2*S*, 8*R*	33	4.3

Scheme 2.01. Retrosynthesis of promysalin and confirmation of biological activity.[8]

2.1.3.SAR Studies[9]

After determining the correct stereoconfiguration and confirming the biological activity of promysalin, previous Wuest group members, primarily Colleen Keohane and Andrew Steele, continued their studies of this natural product by exploiting the modular synthetic route to conduct SAR studies. In this work, the salicylate, proline, and myristic acid portions of the molecule were systematically modified to assess which alterations would enhance activity (Fig. 2.03). Overall, modifications to the salicylate and proline fragments were largely untolerated with the exception of the dehydroproline motif (Fig. 2.03). In contrast, the myristic acid side chain was somewhat more tolerant to manipulations, wherein activity was retained by removing the α-hydroxy motif or by leaving the alkene following cross metathesis intact (Fig. 2.03).

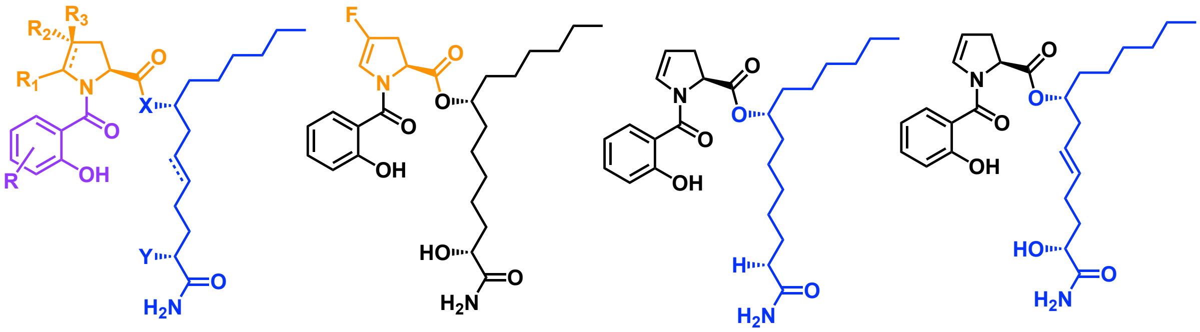

Figure 2.03. Summary of modifications made to the promysalin scaffold and structures of analogs with retained activity.[9]

It was also postulated that the ester of promysalin is cleaved by esterases, and the active compound would be one of these fragments (Fig 2.04), however after testing, neither the carboxylic acid nor the myristic acid fragment displayed activity. Further, the more stable amide analog displayed complete abolishment of activity. Additionally, it had been shown that promysalin was prone to acid-catalyzed cyclization of the phenol onto the proline (Fig. 2.04), however this cyclized product was also inactive. Taken together, these results indicated that the most potent compound is in fact the reported natural product.

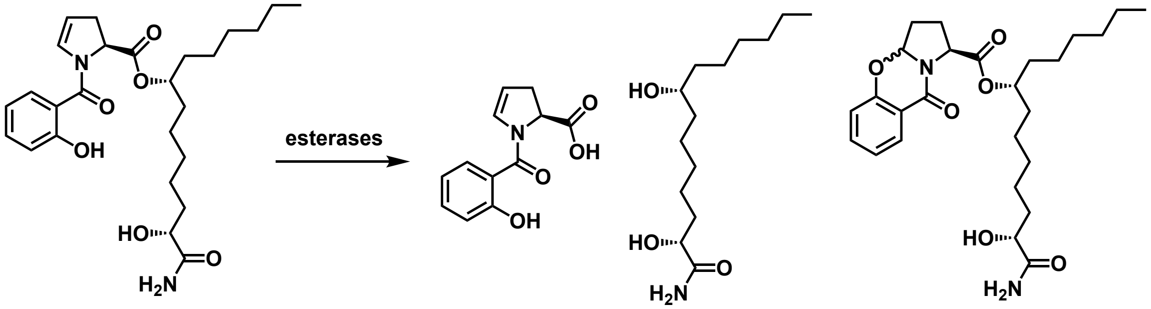

Figure 2.04. Postulated hydrolysis of promysalin by esterases and structure of acid-catalyzed cyclization product.[9]

2.1.4. Target Identification[10]

Next, an affinity-based protein profiling (AfBPP) approach was taken to elucidate any potential intracellular protein target(s) of promysalin (Fig. 2.05). In these studies, a photoaffinity probe was appended to the natural product at the terminal amide, as this was the one position where alteration was tolerated without loss of activity.[11] This probe molecule was incubated with the PA14 strain (more susceptible than PAO1), then irradiated with UV light, wherein the diazirine would react expelling N_2 leaving a reactive carbene to crosslink with the target protein. Copper click reaction between the probe alkyne and biotin-azide, followed by enrichment with avidin, trypsin-digest and labeling, and subsequent LC-MS/MS analysis ultimately identified succinate dehydrogenase C-subunit (SdhC) as the target protein. This target was further validated through in vitro IC_{50} assays against Sdh, as well as through computational molecular docking with the structurally homologous *E. coli* Sdh wherein it was shown that promysalin likely binds the ubiquinone-binding site. Additionally, a promysalin-resistant mutant of PA14, named RO5 was generated via a resistance assay, and sequencing of this mutant revealed an I206V mutation in the ubiquinone binding site interface between SdhB and SdhC, which reduced the amount of hydrophobic contact with promysalin. Taken together, these results all strongly supported that promysalin exerts its activity by binding SdhC thereby preventing the conversion of succinate to fumarate in the tricarboxylic acid cycle and thus interrupting primary carbon metabolism.

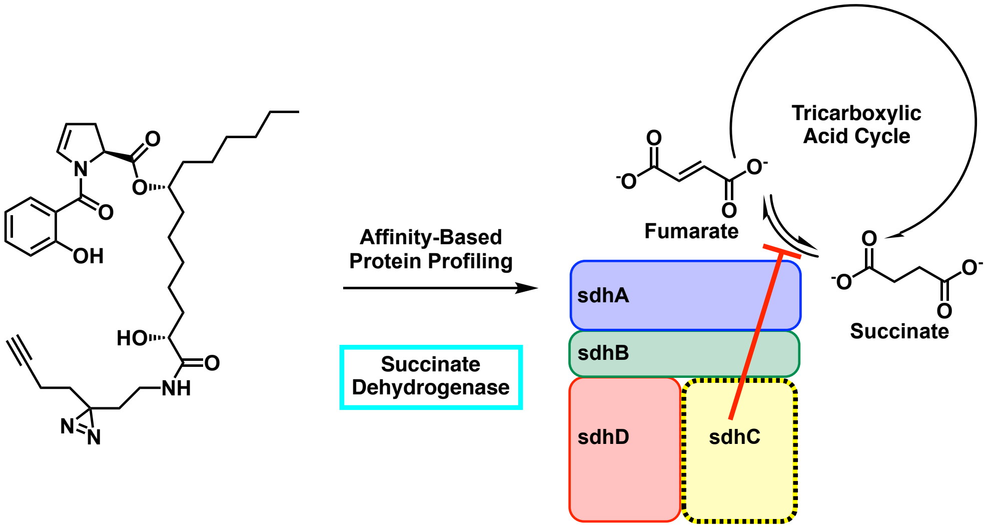

Figure 2.05. Schematic representation of AfBPP approach to identifying the biological target of promysalin.[10]

2.1.5.Species Specificity of Promysalin

While it was exciting to have elucidated the biological target of promysalin, it was quite peculiar that this target is so ubiquitous to nearly all bacteria, thus begging the question, how does promysalin exert its species-specific activity? One possible explanation was that there are subtle differences in the regulation of various pathways within the tricarboxylic acid cycle between *P. aeruginosa* and *P. putida*, and that was the source of species specificity. There are two pathways that *Pseudomonas* can utilize to access fumarate; either through the main TCA pathway converting succinate to fumarate, or by means of the glyoxylate shunt, which converts isocitrate to fumarate directly through a glyoxylate intermediate, bypassing three intermediates, a-ketoglutarate, succinyl-CoA, and succinate (Scheme 2.02).[12]

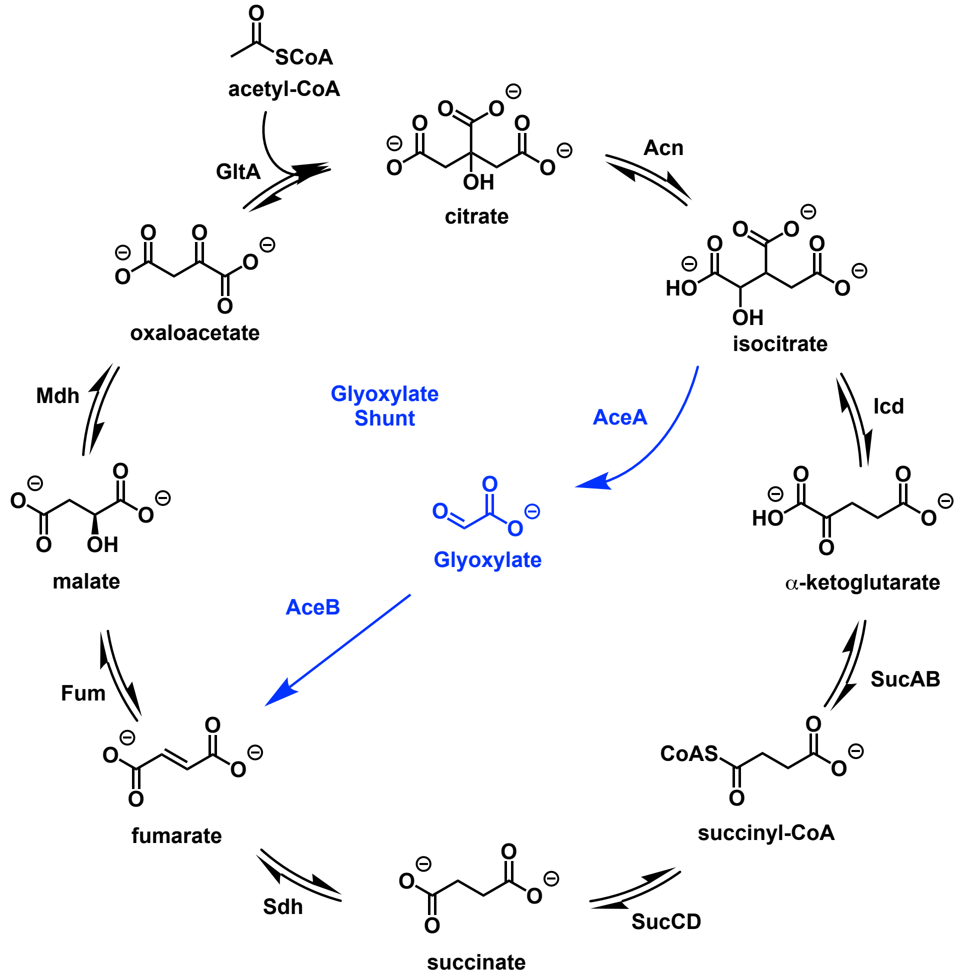
SCoA
acetyl-CoA
GltA
citrate
Acn
isocitrate
Icd
α-ketoglutarate
SucAB
CoAS
succinyl-CoA
SucCD
succinate
Sdh
fumarate
Fum
malate
Mdh
oxaloacetate
Glyoxylate Shunt
AceA
Glyoxylate
AceB

Scheme 2.02. Tricarboxylic acid cycle and glyoxylate shunt used by *Pseudomonads*.[12]

In order to confirm this hypothesis, feeding studies were conducted. To this end, promysalin was incubated with *P. aeruginosa* and the producing strain, *P. putida* in both TSB (nutrient rich) media as well as M9 minimal media which only differs from TSB in terms of carbon source; TSB contains glucose while M9 contains succinate (Fig. 2.06). Unsurprisingly, promysalin inhibited the growth of *P. aeruginosa* (PA14 and PAO1) in both the nutrient rich and the minimal M9 media. Promysalin was inactive against *P. putida* (KT2440 and RW10S1) in nutrient rich media. However, in M9 media, promysalin significantly inhibited the growth of *P. putida*, indicating that when *P. putida* is forced to utilize succinate dehydrogenase to access fumarate, it is unable to do so, further supporting the notion that *P. putida* is more effective at utilizing the glyoxylate shunt pathway. In other words, the reason why promysalin is active against *P. aeruginosa* and not *P. putida* is in fact due to the differences in carbon flux, wherein *P. putida* can much more readily divert carbon flux through the glyoxylate shunt enabling it to survive treatment with promysalin, unlike *P. aeruginosa* which clearly relies more heavily on succinate dehydrogenase.

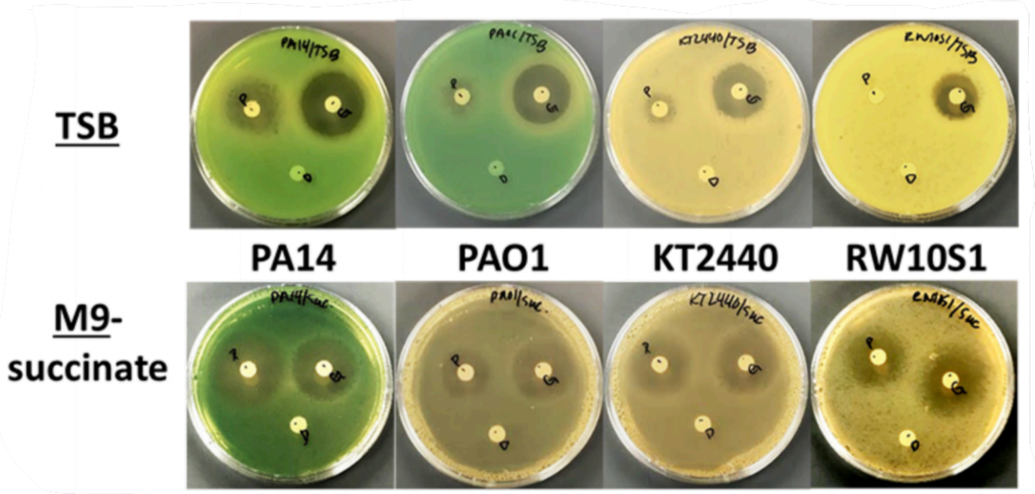

Figure 2.06. Feeding studies of promysalin with *P. aeruginosa* (PA14 and PAO1) and *P. putida* (KT2440 and RW10S1) in TSB (nutrient-rich) and M9 minimal media.[10]

Shapiro J. A.†.; **Kaplan, A. R.**†.; Wuest, W. M. From General to Specific: Can *Pseudomonas* Primary Metabolism Be Exploited for Narrow-Spectrum Antibiotics? *ChemBioChem.* **2019**, *20*(1), 34-39. https://doi.org/10.10002/cbic.201800383

The subtle differences in carbon flux between *P. aeruginosa* and *P. putida* led our group to wonder if there were aspects of primary metabolism that could be exploited to develop species-specific antibiotics. To this end, former postdoctoral researcher Justin Shapiro and I wrote a perspective article discussing these intricacies and their potential for further exploration as antibiotic targets. We discussed instances wherein primary metabolism can be exploited to recapitulate the activity of antibiotics in resistant or tolerant organisms as well as cases of subtle nuances between species in primary metabolism which show promise as antibiotic targets.[12,13] Finally, we discussed two case studies of narrow-spectrum antibiotics targeting Sdh, promysalin and siccanin (Fig. 2.07).[7-10,14] Ultimately, we hoped that this perspective article serves as inspiration for the design and construction of novel narrow-spectrum antibiotics. Writing this perspective did prompt me to consider other fundamental life processes that could function as targets for antibiotics, specifically Fe^{III} acquisition, which will be detailed in full in chapter 3.

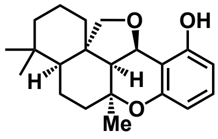

Siccanin

Figure 2.07. Structure of siccanin, a known Sdh inhibitor.[14]

2.2. Side Chain Analogs

Post, S. J.†.; Keohane, C. E.†.; Rossiter, L. M.; **Kaplan, A. R**.; Khowsathit, J.; Matuska, K.; Karanicolas, J.; Wuest, W. M. Target-Based Design of Promysalin Analogues Identifies a New Putative Binding Cleft in Succinate Dehydrogenase. *ACS. Infect. Dis.* **2020**, *6*(6), 1372-1377. https://doi.org/10.1021/acsinfecdis.0c00024

With significant insight into the biological mechanism of promysalin, the next avenue of work hinged on making modifications to the aliphatic side chain to further understand its interactions with Sdh, and in particular, the effect of hydrophobic character on binding and activity. A series of side chain analogs were synthesized by Savannah Post and Colleen Keohane to answer two key questions:

1. Does increased hydrophobicity enhance uptake into cells, and by extension biological activity?
2. Is there specificity associated with carbon chain lengths? Since promysalin binds an enzyme, which should have substrate specificity, will modifications to the side chain abolish binding and activity?

A total of ten analogs with structural modifications summarized in Table 2.01, were synthesized, and evaluated against three different strains of P. aeruginosa, PAO1, PA14, and RO5, the resistant mutant derived from PA14. Shifting the side chain by one carbon on the ester linkage (**11a**, **11b**), adding steric bulk directly adjacent to the ester linkage (**11c**, **11d**), and truncating the side chain (**11e**, **11f**, **11g**), significantly diminished activity. However, elongating the side chain by one and two carbons (**11h**, **11i**) enhanced activity then diminished after adding additional carbon atoms (**11j**).

Table 2.01. Structures of promysalin side chain analogs and their activity against *P. aeruginosa.*

	Structure	PA14 IC_{50} (µM)	PA14 IC_{90} (µM)	PAO1 IC_{50} (µM)	PAO1 IC_{90} (µM)	RO5 IC_{50} (µM)	RO5 IC_{90} (µM)
Connectivity	**(-)-11a** n = 0 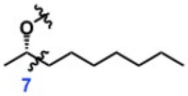	3.1	12	32	190	15	43
	(-)-11b n = 2 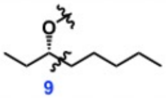	5.7	22	37	130	40	120
Bulky	**(-)-11c** n = 1 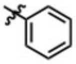	38	140	--	--	--	--
	(-)-11d n = 1 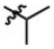	130	200	--	--	--	--
Truncated	**(-)-11e** n = 1 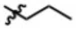	9.4	22	85	150	77	210
	(-)-11f n = 1 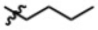	5.7	21	27	>250	49	160
	(-)-11g n = 1 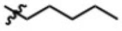	2.5	12	14	30	16	140
	(-)-1 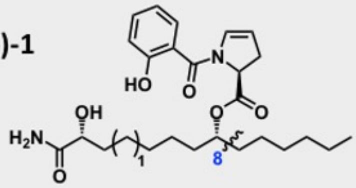	0.065	4.6	6.9	73	2.9	15
Elongated	**(-)-11h** n = 1 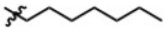	0.026	0.89	1.8	>250	3.7	13
	(-)-11i n = 1 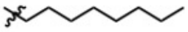	0.035	1.0	1.1	10	1.7	4.4
	(-)-11j n = 1 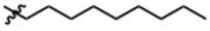	0.15	1.6	3.4	89	1.8	3.8

2.2.1. Computational Analysis

To further understand the origins of activity enhancement of the elongated analogs, we once again looked to our computational collaborators for further insight. Interestingly, these docking studies showed that the side chain of promysalin (green) orients itself towards the edge of the SdhC binding pocket, while the side chain analog elongated by one carbon (orange) adopts a slightly altered conformation wherein the side chain orients itself back into the pocket (Fig. 2.08). We believe that this shift in conformation occurred in order to avoid solvent exposure to this hydrophobic portion of the molecule.

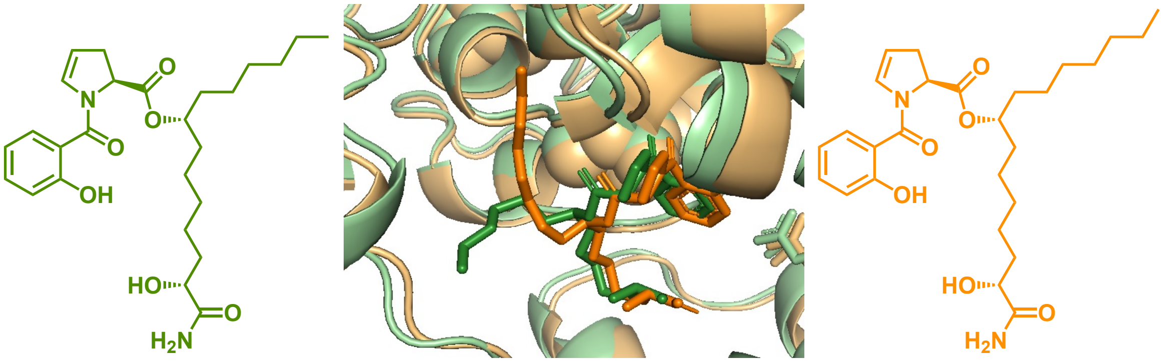

Figure 2.08. Molecular docking of promysalin (green) and extended side chain analog (orange) in the SdhC binding pocket.

2.2.2. Terminal Aryl Analogs

The new conformation of this extended side chain analog places the terminus of this side chain proximal to a tryptophan residue, suggesting that perhaps the binding affinity, and therefore the activity, could be enhanced further by introducing π-stacking interactions with a terminal aryl motif. Our collaborators docked a hypothetical terminal phenyl analog and found that indeed this compound appeared to interact favorably in the SdhC binding pocket with the aryl ring orienting itself directly adjacent to the tryptophan residue (Fig. 2.09). They also docked several other terminal aryl analogs, in the binding pocket which also had favorable interactions. These analogs will be discussed in further in section 2.4.

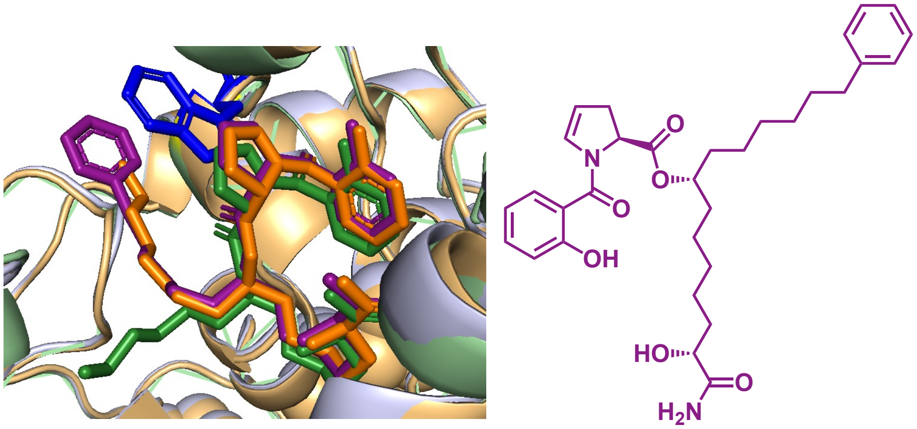
O
N
O
O
OH
HO
O
H₂N

2.01

Figure 2.09. Molecular docking of terminal aryl promysalin analog (purple) in the SdhC binding pocket.

2.3. Compound 2.01

As a proof-of-concept, I elected to evaluate the terminal phenyl analog, compound **2.01**, as an electronically neutral starting point due to the lack of electron-donating or -withdrawing groups. The biological activity of this analog would then guide the design of future analogs with more varied stereoelectronic properties.

2.3.1. Synthesis of 2.01

The objective in the synthesis of this proof-of-concept terminal aryl analog was to deviate from the originally published route as little as possible. To this end, the carboxylic acid fragment, **2.03**, was synthesized in the same fashion as previously reported by means of hydrolyzing methyl ester **2.02** (Scheme 2.03). For the aliphatic side chain, synthesis of the α-hydroxylated amide **2.06** was achieved in three steps as previously described.[8]

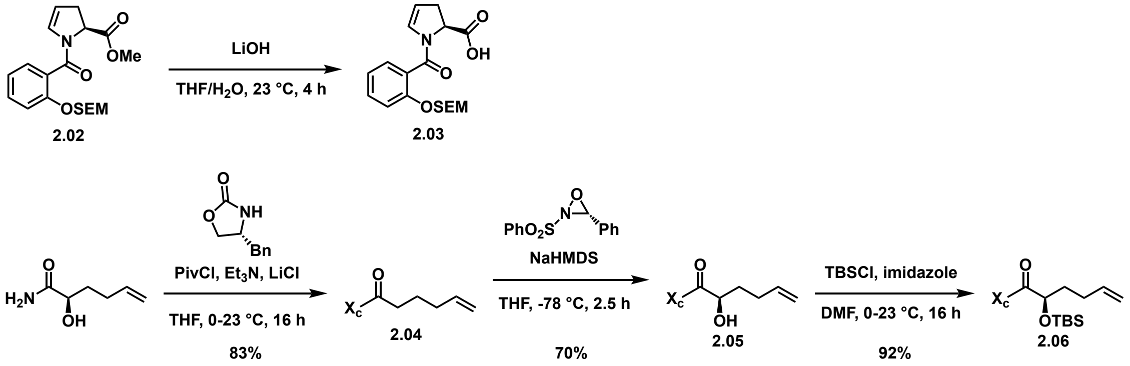
OMe
OSEM
2.02
LiOH
THF/H₂O, 23 °C, 4 h
OH
OSEM
2.03
H₂N
OH
NH
Bn
PivCl, Et₃N, LiCl
THF, 0-23 °C, 16 h
83%
Xc
2.04
PhO₂S
N
Ph
NaHMDS
THF, -78 °C, 2.5 h
70%
Xc
OH
2.05
TBSCl, imidazole
DMF, 0-23 °C, 16 h
92%
Xc
OTBS
2.06

Scheme 2.03. Synthesis of previously reported compounds **2.03** and **2.06**.

In previous work, an asymmetric Keck allylation was used the access a stereoenriched homoallylic alcohol from various aldehyde precursors (Scheme 2.04).[8,9]

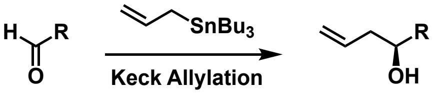

H
R
O
SnBu3
Keck Allylation
R
OH

Scheme 2.04. Asymmetric Keck allylation used to synthesize stereoenriched homoallylic alcohols.[8,9]

Since aldehyde **2.09** was not commercially available, I synthesized this compound in three steps (Scheme 2.05). Cross metathesis between ethyl heptanoate and styrene followed by hydrogenation gave **2.08**, which then underwent reduction with DIBAL affording **2.09**. Next, the aldehyde underwent the aforementioned asymmetric Keck allylation, furnishing the stereoenriched homoallylic alcohol, **2.10**. Cross metathesis with **2.06**, accessed using previously established chemistry, followed by hydrogenation afforded **2.12**. Unfortunately, the final aminolysis reaction to remove the Evans' oxazolidinone and liberate the terminal amide was not successful using previously reported conditions and no conversion was observed by TLC analysis. Resubjecting for a longer reaction time, increasing the amount of ammonia, and changing the ammonia source were also unsuccessful, forcing me explore alternative routes to access **2.13**.

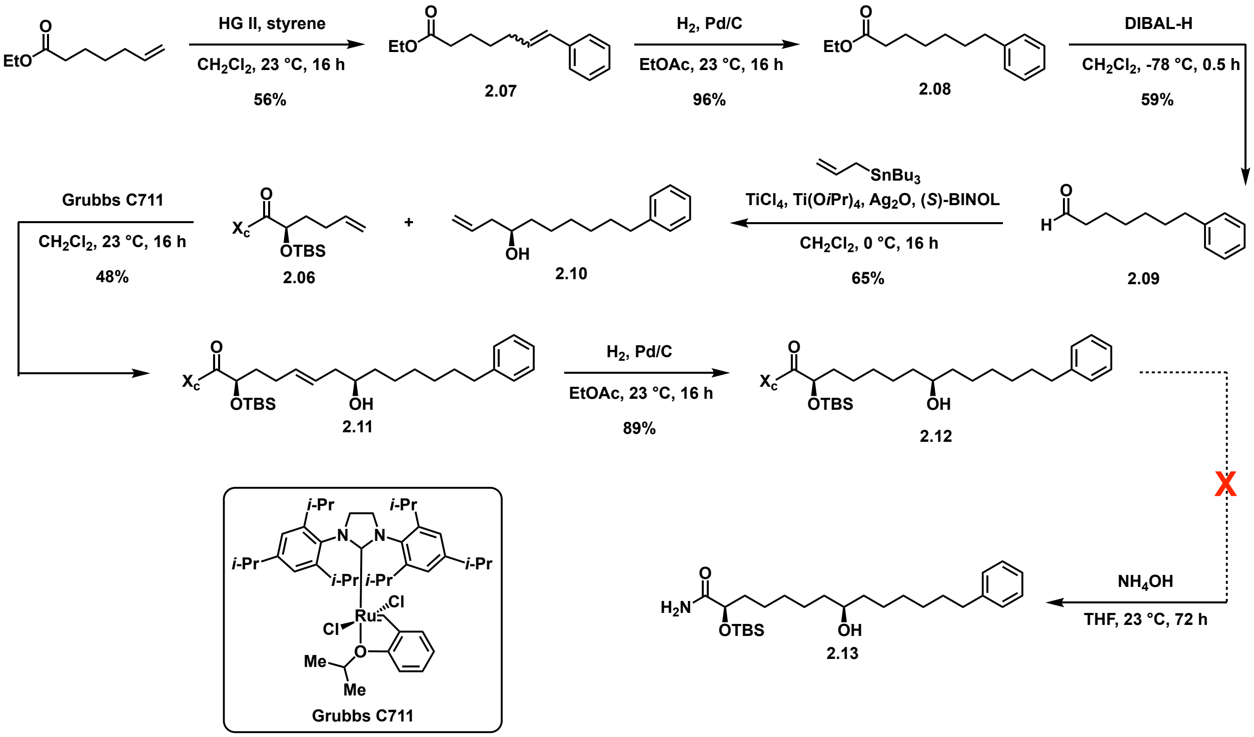

EtO
HG II, styrene
CH2Cl2, 23 °C, 16 h
56%
EtO
2.07
H2, Pd/C
EtOAc, 23 °C, 16 h
96%
EtO
2.08
DIBAL-H
CH2Cl2, -78 °C, 0.5 h
59%
H
2.09
SnBu3
TiCl4, Ti(OiPr)4, Ag2O, (S)-BINOL
CH2Cl2, 0 °C, 16 h
65%
OH
2.10
+
Xc
OTBS
2.06
Grubbs C711
CH2Cl2, 23 °C, 16 h
48%
Xc
OTBS
OH
2.11
H2, Pd/C
EtOAc, 23 °C, 16 h
89%
Xc
OTBS
OH
2.12
X
NH4OH
THF, 23 °C, 72 h
H2N
OTBS
OH
2.13
i-Pr
i-Pr
i-Pr
i-Pr
i-Pr
i-Pr
N
N
Ru
Cl
Cl
O
Me
Me
Grubbs C711

Scheme 2.05. Initial synthetic route to side chain **2.13**.

As a first attempt, I opted for a more indirect method of accessing the terminal amide, wherein the treatment with lithium hydroxide and hydrogen peroxide would remove the oxazolidinone and give rise to carboxylic acid **2.14** which could then undergo amination to **2.03** (Scheme 2.06).[15] However, several attempts at this first reaction did not proceed and returned starting material. Next, I wondered if perhaps the oxazolidinone could be removed prior to cross metathesis which would ultimately shorten the linear route by one step. Aminolysis of **2.06** proceeded more swiftly than the sluggish 72-hour reaction for the full side chains affording **2.14** in 57% yield. However, cross metathesis only yielded small amounts of the dimer of **2.10** and recovery of **2.14**. With those two failed routes, I then pursued another less direct route to **2.13**. Treatment of **2.06** with *n*-butyllithium and benzyl alcohol gave the corresponding benzyl ester **2.16** which then underwent successful cross metathesis with **2.10** to give **2.17** in 62% yield. At this point, I aimed to both remove the benzyl ester and reduce the alkene in a single step via hydrogenation, and the resulting carboxylic acid would then undergo aminolysis to **2.13** as described before. To my surprise, this typically robust reaction was only successful in reducing the alkene and did not remove the benzyl ester in any observable quantity giving compound **2.18** as the exclusive product. A variety of solvents were screened, including methanol to enhance solubility of the hydrogen and increase the rate of reaction. With these failed results, I began to wonder if there was an intramolecular π-stacking interaction that was hindering reactivity of substrates **2.12** and **2.17**, as both of these compounds contain an aromatic motif on each terminus. If this was the case, then performing the hydrogenation in toluene would minimize this intramolecular π-stacking interaction, increasing the accessibility to the benzyl ester. Unfortunately, this was not the case; several attempts of this reaction were made with toluene as the sole solvent and as a cosolvent, and the only product observed in every case was **2.18**.

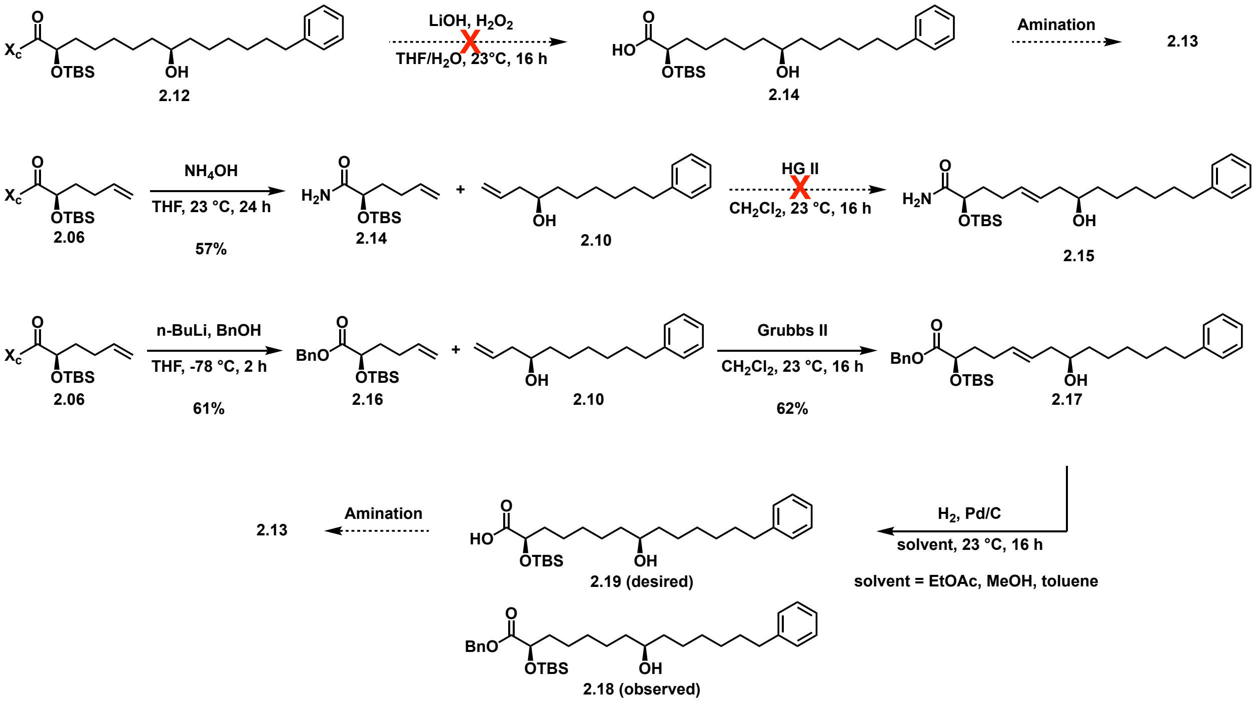

LiOH, H_2O_2
THF/H_2O, 23°C, 16 h
Amination
2.12
2.14
2.13
NH_4OH
THF, 23 °C, 24 h
57%
HG II
CH_2Cl_2, 23 °C, 16 h
2.06
2.14
2.10
2.15
n-BuLi, BnOH
THF, -78 °C, 2 h
61%
Grubbs II
CH_2Cl_2, 23 °C, 16 h
62%
2.16
2.17
H_2, Pd/C
solvent, 23 °C, 16 h
solvent = EtOAc, MeOH, toluene
2.19 (desired)
2.18 (observed)

Scheme 2.06. Failed troubleshooting routes to side chain **2.09**.

At this point, I opted to revisit the cross-metathesis strategy with the free amide (Scheme 2.07). It has been shown that substrates containing nitrogen atoms, particularly unprotected nitrogen atoms, are far less prone to undergo cross metathesis reactions, and can contribute to the degradation of the ruthenium catalyst.[16,17] This led me to wonder if increasing the catalyst loading would facilitate the reaction long enough to generate an appreciable amount of product before entirely poisoning the catalyst and shutting the reaction down. Excitingly, increasing the catalyst loading to 20 mole percent gave **2.15** in 48% yield. Subsequent hydrogenation afforded the desired side chain, **2.19**. Finally, esterification with **2.03**, synthesized using previously published chemistry, followed by global deprotection furnished terminal phenyl analog, **2.01**.[8]

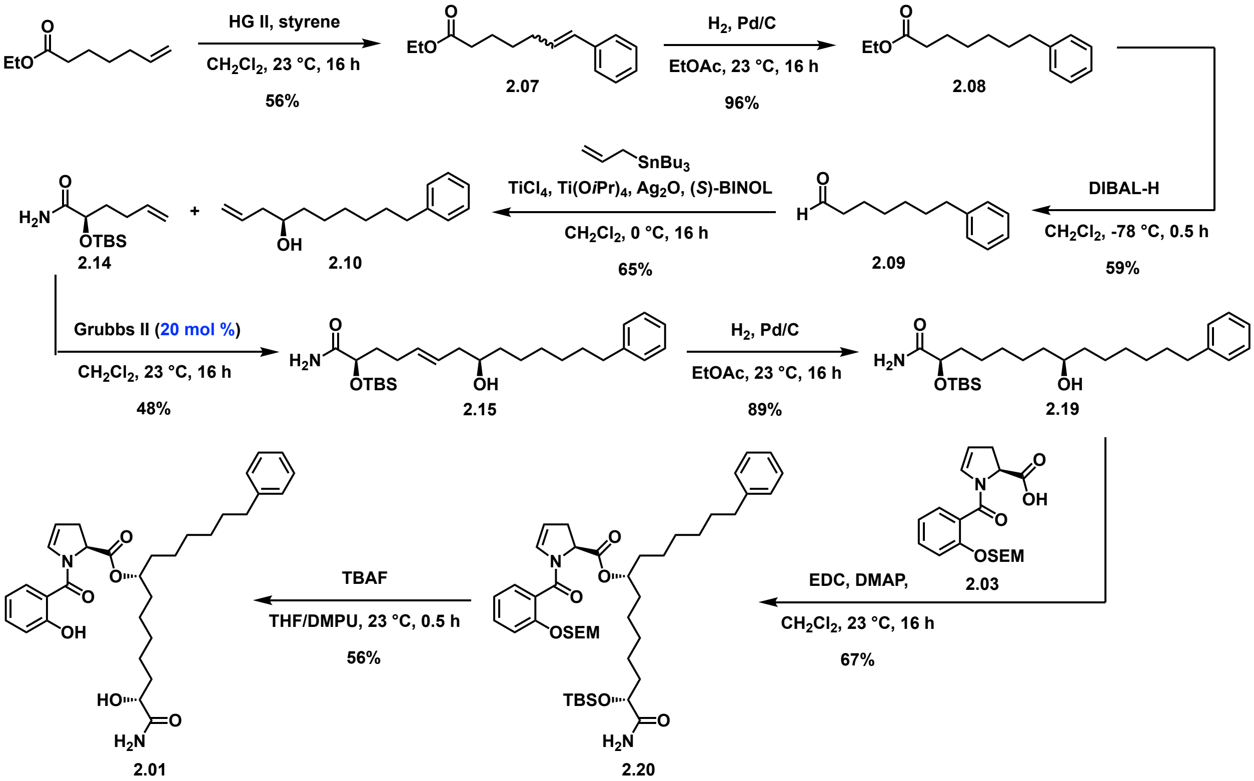
HG II, styrene
CH2Cl2, 23 °C, 16 h
56%
2.07
H2, Pd/C
EtOAc, 23 °C, 16 h
96%
2.08
DIBAL-H
CH2Cl2, -78 °C, 0.5 h
59%
2.09
SnBu3
TiCl4, Ti(OiPr)4, Ag2O, (S)-BINOL
CH2Cl2, 0 °C, 16 h
65%
2.10
2.14
Grubbs II (20 mol %)
CH2Cl2, 23 °C, 16 h
48%
2.15
H2, Pd/C
EtOAc, 23 °C, 16 h
89%
2.19
EDC, DMAP,
2.03
CH2Cl2, 23 °C, 16 h
67%
2.20
TBAF
THF/DMPU, 23 °C, 0.5 h
56%
2.01

Scheme 2.07. Full synthetic route to terminal aryl analog **2.01**.

2.3.2. Biological Evaluation of 2.01

With analog **2.01** in hand, I evaluated its activity against the same three strains previously assessed. Against PAO1, this analog had an IC_{50} of 2.4 μM, which was more active than promysalin and slightly less active than the extended side chain analog. Against PA14, the IC_{50} was 0.75 μM, more than 10-fold higher than the IC_{50} values of promysalin (0.065 μM) and the extended side chain analog (0.035 μM). Interestingly, **2.01** had an IC_{50} value of 1.7 μM against RO5, the mutant derived from PA14, comparable to the values of promysalin (2.9 μM) and the extended side chain analog (1.7 μM). Taken together, this data does indicate that while not remarkably active compared to promysalin or the extended side chain analog, **2.01** serves as an excellent starting point for the design of new terminal aryl analogs.

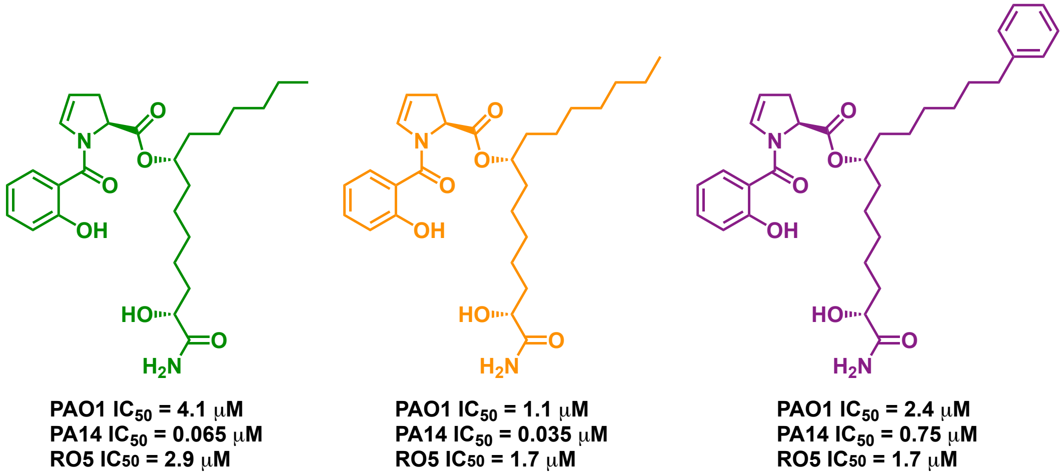

PAO1 IC_{50} = 4.1 μM
PA14 IC_{50} = 0.065 μM
RO5 IC_{50} = 2.9 μM

PAO1 IC_{50} = 1.1 μM
PA14 IC_{50} = 0.035 μM
RO5 IC_{50} = 1.7 μM

PAO1 IC_{50} = 2.4 μM
PA14 IC_{50} = 0.75 μM
RO5 IC_{50} = 1.7 μM

Figure 2.10. Structures and corresponding biological activity of promysalin (green), extended side-chain analog (orange) and terminal aryl analog (purple).

2.4. New Terminal Aryl Analogs

With these promising results of proof-of-principle analog **2.01**, other members of our lab are currently synthesizing a series of terminal aryl analogs with varying stereoelectronic properties. Based on the computations previously discussed, we elected to evaluate the series of analogs shown in figure 2.11. Evaluation of the biological activity of these compounds with varied electronics will then enable assignment of a "Hammett-like" correlation to this series of compounds and give us further insight into their bioactivity and interactions in the SdhC binding pocket.

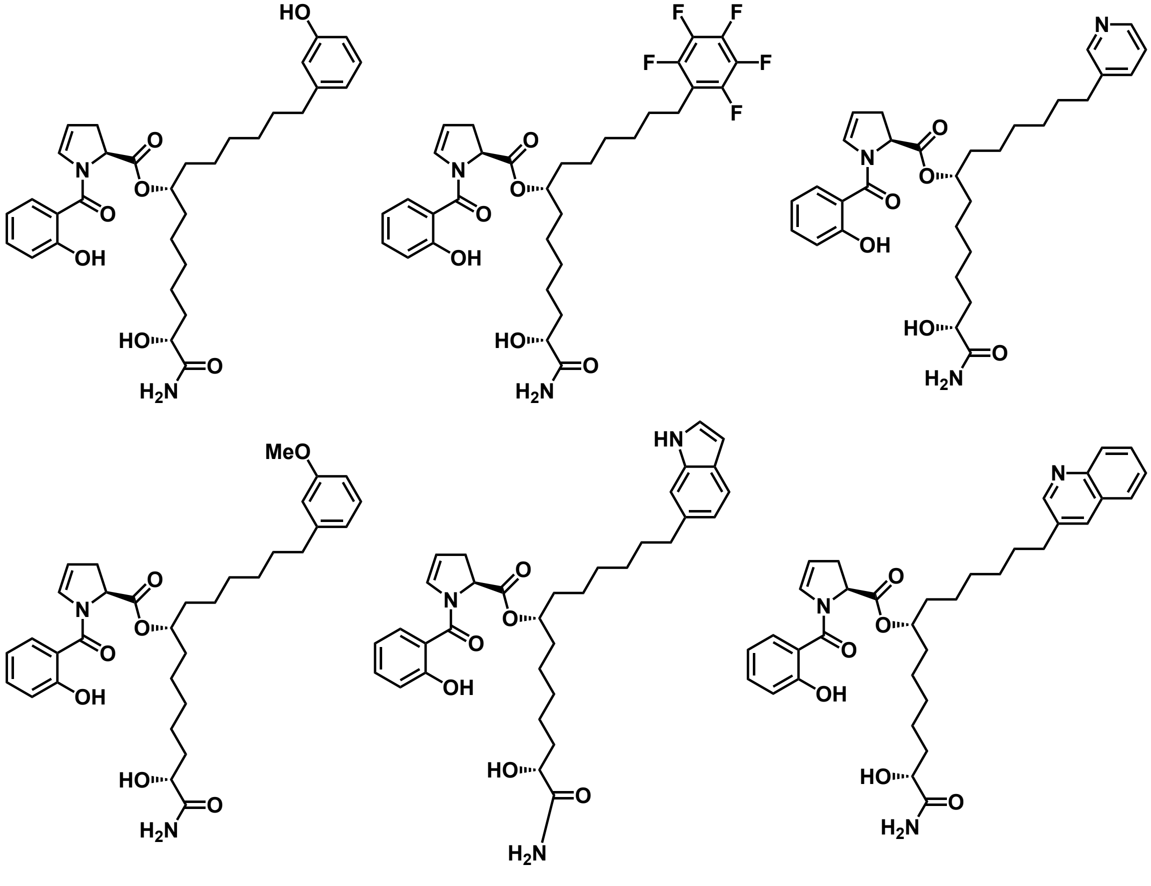

Figure 2.11. Structures of proposed promysalin terminal aryl analogs.

2.5. References

1 Ory, E. M.; Yow, E. M. Broad Spectrum Antibiotics. *JAMA*. **1963**, *185*, 273-279.

2 Leekha, S.; Terrell, C. L.; Edson, R. S. General Principles of Antimicrobial Therapy. *Mayo. Clin. Proc*. **2011**, *86*, 156-167.

3 Garland, M.; Loscher, M.; Bogyo, M. Chemical Strategies to Target Bacterial Virulence. *Chem. Rev*. **2017**, *117*, 4422-4461.

4 Canton, R.; Morosini, M. Emergence and spread of antibiotic resistance following exposure to antibiotics. *FEMS. Microbiol. Rev*. **2011**, *35*, 977-991.

5 Lobanovska, M.; Pilla, G. Penicillin's Discovery and Antibiotic Resistance: Lessons for the Future?. *Yale. J. Biol. Med*. **2017**, *90*, 135-145.

6 Keohane, C. E.; Steele, A. D.; Wuest, W. M. The Rhizosphere Microbiome: A Playground for Natural Product Chemists. *Synlett.* **2015**, *26*, 2739-2744.

7 Li, W.; Estrada-De Los Santos, P.; Matthijs, S.; Xie, G. L.; Busson, R.; Cornelis, P.; Rozenski, J.; De Mot, R. Promysalin, a Salicylate-Containing Pseudomonas Putida Antibiotic, Promotes Surface Colonization and Selectively Targets Other Pseudomonas. *Chem. Biol.* **2011**, *18*, 1320-1330.

8 Steele, A. D.; Knouse, K. W.; Keohane, C. E.; Wuest, W. M. Total Synthesis and Biological Investigation of (-)-Promysalin. *J. Am. Chem. Soc.* **2015**, *137*, 7314-7317.

9 Steele, A. D.; Keohane, C. E.; Knouse, K. W.; Rossiter, S. E.; Williams, S. J.; Wuest, W. M. Diverted Total Synthesis of Promysalin Analogs Demonstrates That an Iron-Binding Motif is Responsible for Its Narrow-Spectrum Antibacterial Activity. *J. Am. Chem. Soc.* **2016**, *138*, 5833-5836.

10 Keohane, C. E.; Steele, A. D.; Fetzer, C.; Khowsathis, J.; Van Tyne, D.; Moynié, L.; Gilmore, M. S.; Karanicolas, J.; Sieber, S. A.; Wuest, W. M. Promysalin Ellicits Species-Specific Inhibition of *Pseudomonas Aeruginosa* by Targeting Succinate Dehydrogenase. *J. Am. Chem. Soc.* **2018**, *140*, 1774-1782.

11 Li, Z.; Hao, P.; Li, L.; Tan, C. Y. J.; Cheng, X.; Chen, G. Y. J.; Sze, S. K.; Shen, H. M.; Yao, S. Q. Design and Synthesis of Minimalist Terminal Alkyne-Containing Diazirine Photo-Crosslinkers and Their Incorporation into Kinase Inhibitors for Cell- and Tissue-Based Proteome Profiling. *Angew. Chemie. Int. Ed.* **2013**, *52*, 8551-8556.

12 Meylan, S.; Porter, C. B. M.; Yang, J. H.; Belenky, P.; Guiterrez, M. A.; Lobritz, M. A.; Park, J.; Kim, S. H.; Moskowitz, S. M.; Collins, J. J. Carbon Sources Tune Antibiotic Susceptibility in *Pseudomonas aeruginosa* via Tricarboxylic Acid Cycle Control. *Cell. Chem. Biol.* **2017**, *24*, 195-206.

13 Nickel, P.; Chavarría, M.; Fuhrer, T.; Sauer, U.; de Lorenzo, V. *Pseudomonas putida* KT2440 Strain Metabolizes Glucose through a Cycle Formed by Enzymes of the Entner-Doudoroff, Embden-Meyerhof-Parnas, and Pentose Phosphate Pathways. *J. Biol. Chem.* **2015**, *290*, 25920-25932.

14 Mogi, T.; Kawakami, T.; Arai, H.; Igarashi, Y.; Matsushita, K.; Mori, M.; Shiomi, K.; Omura, S.; Harada, S.; Kita, K. Siccanin Rediscovered as a Species-Selective Succinate Dehydrogenase Inhibitor. *J. Biochem.* **2009**, *146*, 383-387.

15 Beutner, G. L.; Cohen, B. JM.; DelMonte, A. J.; Dixon, D. D.; Fraunhoffer, K. J.; Glace, A. W.; Lo, E.; Stevens, J. M.; Vanyo, D.; Wilbert, C. Revisting the Cleavage of Evans Oxazolidinones with LiOH/H_2O_2. *Org. Process. Res. Dev.* **2019**, *23*, 1378-1385.

16 Chatterjee, A. K.; Choi, T-L.; Sanders, D. P.; Grubbs, R. H. A General Model for Selectivity in Olefin Cross Metathesis. *J. Am. Chem. Soc.* **2003**, *125*, 11360-11370.

17 Jawiczuk, M.; Marczyk, A.; Trzaskowski, B. Decomposition of Ruthenium Olefin Metathesis Catalyst. *Catalysts.* **2020**, *10*, 887-942.

3. Synthesis and Biological Evaluation of Iron-Binding Bacterial Metabolites

3.1. The Role of Iron in Bacteria

Iron is a nutrient essential to the survival of nearly all living organisms including bacteria, playing a central role in a wide variety of critical biological functions. Iron often times serves as a key cofactor in several metalloenzymes and plays pivotal role in a range of cellular processes including cell growth and proliferation, detoxification, metabolic pathways including respiration, carbon metabolism, and ATP generation, as well as processes as vital as iron transport.[1,2,3] In bacteria, iron is necessary for promoting sufficient growth, particularly in host environments.[4] In fact, it has been shown that iron in the oral cavity can elevate bacterial growth in human serum.[5] However, even more importantly for bacteria, iron plays a key role in bacterial pathogenesis, making its acquisition in host organisms a significant priority.[4,6,7]

3.2. Bacterial Iron Acquisition

Bacteria have adopted strategies to survive in a wide range of environments both aquatic and terrestrial, with one of the most densely populated ones being the rhizosphere, the region directly surrounding the root of a plant. In this environment, bacteria must compete with numerous other species for incredibly limited but vital resources, including iron, as a means for survival.[8] Iron is typically acquired by bacteria in ferric (Fe^{II}) or ferrous (Fe^{III}) forms. However, in aerobic environments, which includes the rhizosphere, iron is most commonly present as a highly insoluble ferric oxide complex (Fe_2O_3). This complex is incredibly stable, thereby limiting the bioavailable Fe^{III} concentration to anywhere in the range of 10^{-9} to 10^{-18} M, at least three orders of magnitude lower than the concentration of 10^{-6} M required for bacterial survival.[2,3,9] Moreover, mammalian host organisms present a unique challenge for bacterial survival. This environment is particularly sparse, as the majority of Fe^{III} is tightly complexed and stored in various circulating proteins including ferretin, heme, and transferrin, limiting the available Fe^{III} concentration to 10^{-24} M.[2,3,10] Therefore, in order to survive in these challenging environments, bacteria have evolved several mechanisms for the acquisition of Fe^{III}.

3.2.1.Methods for Iron Uptake

Bacteria have developed multiple strategies for the highly selective uptake of iron either directly or indirectly. One direct uptake method of iron entails the sequestration of entire complexes of host iron sources including lactoferrin, transferrin, heme, ferretin, and various other metalloproteins.[2,11] This method allows the bacteria to acquire large quantities of Fe^{III} quite efficiently, however this method requires a receptor specific to each iron source, thus limiting the bacteria to only host organisms with Fe^{III} sources that are recognized by bacterial receptors. This major limitation associated with direct uptake is thought to be the reason why there is a much broader distribution of indirect uptake mechanisms among bacteria. One such mechanism is the use of hemophores, which are secreted proteins with the unique function of acquiring heme.[2] Examples include the *hxu* hemophore system in *Haemophilus influenzae*, which uses heme-loaded hemopexin as its iron source, as well as the *has* system utilized by several other Gram-negative bacteria. However, this method is also limited to environments rich in heme; in environments with low heme availability, this iron acquisition method is virtually useless. This then begs the questions: do bacteria have a means of acquiring Fe^{III} that is more generalized to a wide range of environments?

3.2.2.Siderophores

Of all of the Fe^{III} acquisition strategies employed by bacteria, the use of siderophores is the most broadly applied. Siderophores are small molecules that are produced by bacteria under iron-limited conditions. They are released by the bacteria, wherein they chelate extracellular Fe^{III}, forming siderophore-iron complexes. These siderophore-Fe^{III} complexes are then selectively reimported into cells, wherein Fe^{III} is then released from the complex and utilized in various essential cellular processes.[2,9] By a similar mechanism, xenosiderophores can also be taken up by bacteria when complexed with Fe^{III} using similar receptors, the major difference being that xenosiderophores are not natively produced by the bacteria in question.[12] It must be noted that specific transport machinery is required to import the Fe^{III}-chelated complexes into the cell, regardless of whether the siderophore is natively produced by the bacteria or not. Xenosiderophores do represent an excellent alternative for bacteria in highly competitive environments, they allow bacteria to avoid expending large amounts of biosynthetic energy on the production of said siderophores.

Siderophores commonly contain at least one of five structural motifs that enable them to chelate Fe^{III}; hydroxamate, phenolate, catecholate, carboxylate, and oxazoline/thiazoline heterocycles (Fig. 3.01).[2,9,13,14] Many siderophores like enterobactin, desferrioxamine B, and staphyloferrin contain a single iron binding motif. However, it is quite common for siderophores to contain a several of these moieties classifying them as mixed-type siderophores.[2,9] This is best exemplified in siderophores produced by Gram-negative pathogens. *Pseudomonads* combine the phenolate/catecholate moiety with oxazolines/thiazolines, and have been of interest to our research group, particularly in recent years.

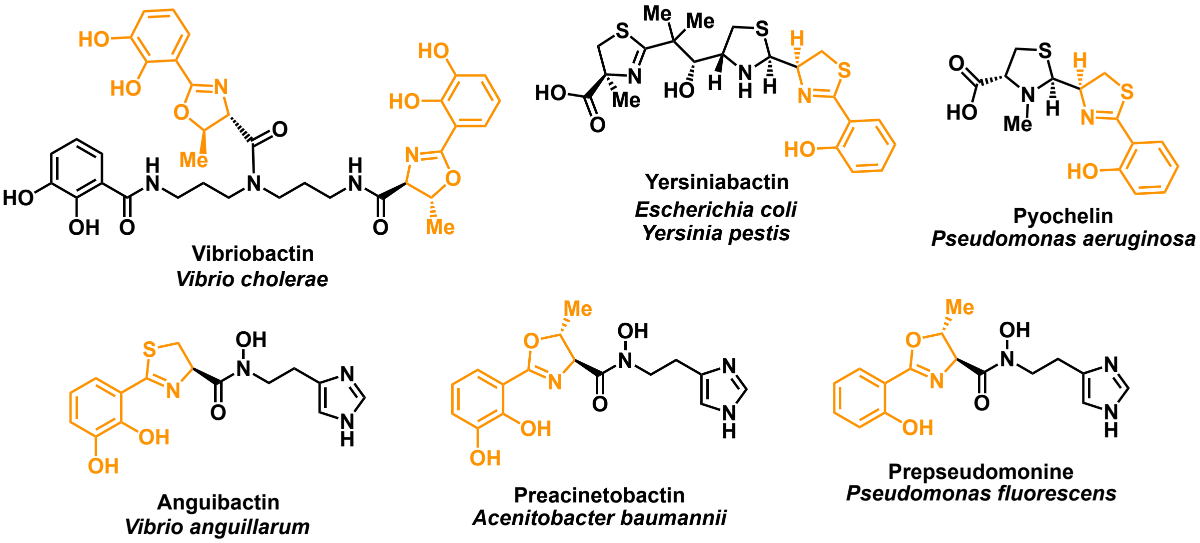

Vibriobactin
Vibrio cholerae

Yersiniabactin
Escherichia coli
Yersinia pestis

Pyochelin
Pseudomonas aeruginosa

Anguibactin
Vibrio anguillarum

Preacinetobactin
Acenitobacter baumannii

Prepseudomonine
Pseudomonas fluorescens

Figure 3.01. Structures of siderophores containing the combination of a phenolate/catecholate motif and an oxazoline/thiazoline (highlighted in orange) and the corresponding producing organisms.[2,9,13,14]

3.3. *Pseudomonas* Metabolites

Pseudomonads produces a wide variety of metabolites including antibiotics and siderophores to gain a competitive advantage in densely populated environments (Fig. 3.02).[15,16] Antibiotic compounds like pyoluteorin, pyrrolnitrin, and 2,4-deacetylphlorglucinol allow *Pseudomonas* to outcompete other microbial species in soil environments like the rhizosphere. Virulence factors like pyocyanin enable the bacteria to infect its host organism. However, the compounds of greatest concern to us are the two siderophores produced by most *Pseudomonads*, pyochelin and pyoverdine.

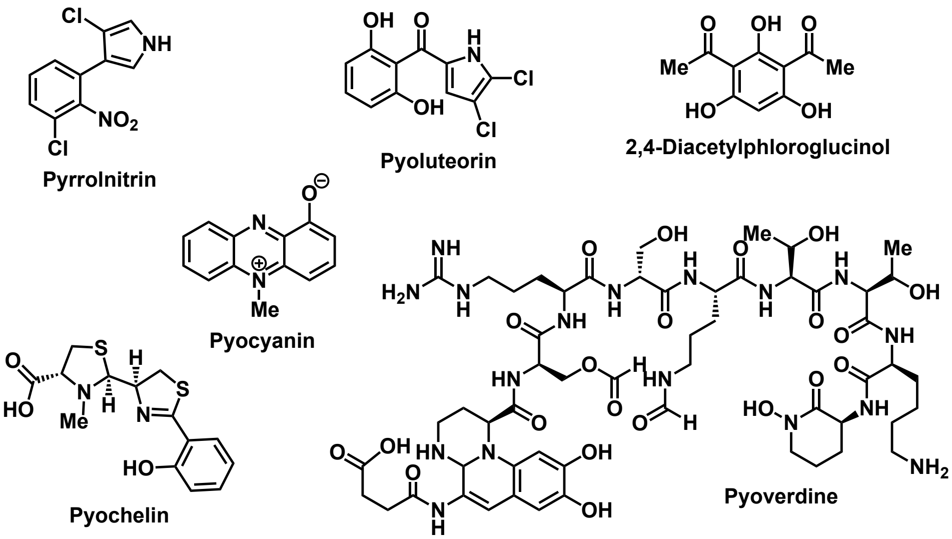

Figure 3.02. Structures of selected *Pseudomonas* metabolites.[15,16]

3.3.1. Pyochelin and Pyoverdine

Similar to other pathogenic bacteria, *P. aeruginosa*, often found in the lungs of cystic fibrosis patients,[17] produces two siderophores with differing affinity for Fe^{III}.[12] Pyoverdine has a higher affinity for Fe^{III} and is therefore the primary siderophore, whereas pyochelin is a lower-affinity secondary siderophore. Production levels of these two siderophores are regulated by the ferric uptake regulatory system, which senses levels of bioavailable extracellular Fe^{III} then promotes transcription of the appropriate biosynthetic machinery.[18] Our lab has had a long-standing interest in pyochelin-like natural products such as ulbactin F[19,20] as well as other Fe^{III}-binding *Pseudomonad* antibiotics including promysalin discussed in the Chapter 2 (Fig. 3.03).[21-25] To this end, I became interested in investigating the physiochemical and biological properties a series of pyochelin biosynthetic shunt products.

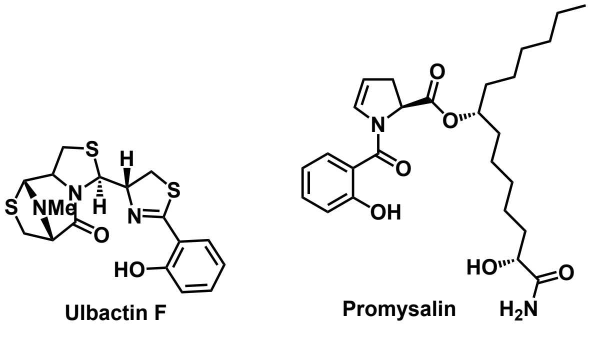

Figure 3.03. Structures of ulbactin F and promysalin.[19,21]

3.3.2.Pyochelin Biosynthesis

The biosynthesis of pyochelin, similar to many siderophores, is conducted via nonribosomal peptide synthetases (Scheme 3.01).[13,14] First, two accessory enzymes, PchA and PchB convert chorismite to salicylate in two steps. Salicylate is then activated by PchD and loaded to PchE at which point it is condensed with one molecule of L-cysteine, cyclized, and epimerized. Next, another molecule of cysteine is incorporated into the scaffold by PchF, with no subsequent epimerization. Finally, the tailoring protein, PchG reduces this second thiazoline to a thiazolidine, which is then *N*-methylated. At this point, pyochelin is released from the biosynthetic machinery and exported to sequester extracellular Fe^{III}.[26,27]

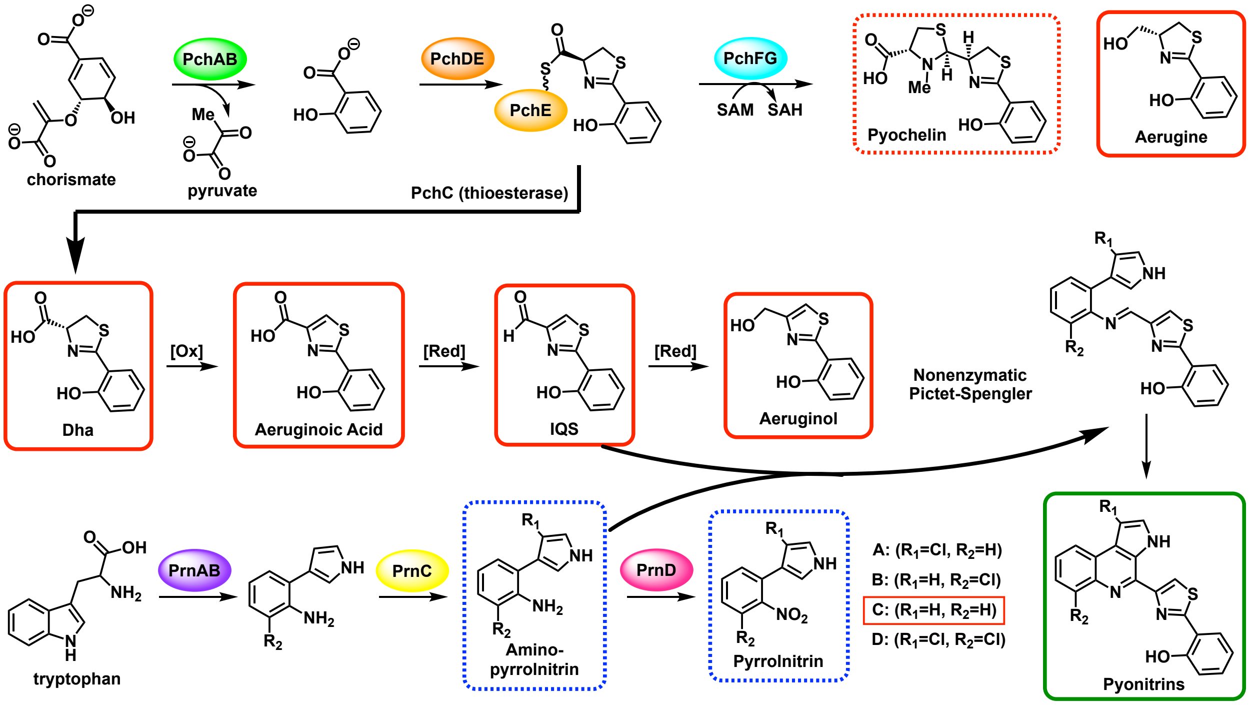
chorismate
PchAB
Me
pyruvate
PchDE
PchE
PchC (thioesterase)
PchFG
SAM
SAH
Pyochelin
Aerugine
Dha
[Ox]
Aeruginoic Acid
[Red]
IQS
[Red]
Aeruginol
Nonenzymatic
Pictet-Spengler
tryptophan
PrnAB
PrnC
Amino-
pyrrolnitrin
PrnD
Pyrrolnitrin
A: (R_1=Cl, R_2=H)
B: (R_1=H, R_2=Cl)
C: (R_1=H, R_2=H)
D: (R_1=Cl, R_2=Cl)
Pyonitrins

Scheme 3.01. Abbreviated biosynthetic pathways to pyochelin and pyrrolnitrin, offshoot pathway to Dha and its redox breakdown to aeruginoic acid, IQS, and aeruginol, structure of aerugine, and postulated spontaneous nonenzymatic Pictet Spengler reaction between IQS and amino pyrrolnitrin to form pyonitrins A-D.[13,14,26-31,41,42]

3.3.3.Pyochelin Biosynthetic Shunt Products

While relatively straightforward, this biosynthetic pathway can be interrupted giving rise to various shunt products (Scheme 3.01). For example, the thioesterase, PchC, can cleave PchE-appended salicylate, resulting in the premature release and accumulation of (*R*)-dihydroaeruginoic acid (Dha). This metabolite can then undergo various redox breakdown processes giving rise to aeruginoic acid, aeruginaldehyde (also known as IQS), and aeruginol.[28,29] Aerugine, is a structurally related metabolite isolated from *P.*

fluorescens, however, it has not been shown to result from this same pathway.[30] Other sources have noted that these metabolites may also be formed by means of other pathways.[31]

The physiochemical and biological properties of pyochelin have been studied extensively and at this point are very well known. However, these same properties are far less studied for the aforementioned simpler biosynthetic shunt products, and in fact are largely unknown. Dha was initially characterized as an antiproliferative compound that acted through an iron-chelating mechanism.[32] However, reports on these iron-chelating properties were not detailed in their accounts of this property. Dha has also been shown to have modest antifungal and antibacterial activity, albeit against a limited scope of microbes.[33] Aeruginoic acid was isolated and synthesized by Yamada and co-workers in 1970, however no further investigations of its bioactivity were conducted.[34] Similarly, aeruginol was isolated from a $CHCl_3$ extract of *P. aeruginosa* and structurally characterized in 1993, with no further evaluation to the best of our knowledge.[35] Aerugine has limited antifungal activity, however, similar to all of the other metabolites described, it has not been further characterized.[30]

3.3.4. IQS and Other *Pseudomonad* Metabolites

IQS has been isolated from several *Pseudomonads* and it has been shown to have modest antifungal activity.[28,36,37] It was recently coined “the fourth quorum sensing molecule” in *P. aeruginosa*, however this has been highly contested, and this claim was ultimately refuted by Cornelis.[38,39] One key structural feature of IQS is the reactive aldehyde motif. Reaction of this aldehyde enables IQS to become incorporated into the scaffolds of several natural products like mindapyrrole B and malleonitrone (Fig. 3.04).[31,40] Recently, Clardy and coworkers discovered the pyonitrins A-D from the extract of *P. protegens*. Careful assessment of the genome ultimately led to the hypothesis that these metabolites arise from a spontaneous nonenzymatic Pictet-Spengler condensation reaction between IQS and aminopyrrolnitrin, a precursor to the known *Pseudomonad* antifungal, pyrrolnitrin (Scheme 3.1).[29,41] This pathway was also recently validated through the biomimetic total synthesis of pyonitrins A-D by MacMillan and co-workers as well as the synthesis of pyonitrin C to be described in this work.[42]

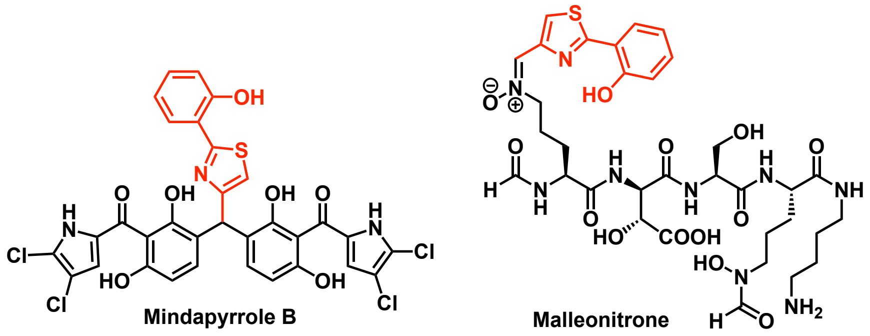

Figure 3.04. Structures of mindapyrrole B and malleonitrone.[23,34]

3.4. Hypothesis for Pyochelin Shunt Metabolites

Overall, there was very limited knowledge of these compounds, which led me to propose a more extensive but directed investigation of their physiochemical and biological properties in the hopes that this would provide further evolutionary insight into their origins. One major question I had was if these metabolites played a role in iron homeostasis in *P. aeruginosa*. As previously mentioned, pyochelin and pyoverdine production is tightly regulated by the Fur system. This system likely evolved to prioritize biosynthetic efforts based on the present environment. Thus, while pyoverdine is far more structurally complex, and therefore biosynthetically taxing to produce, the Fur system will upregulate production of pyoverdine if amounts of bioavailable Fe^{III} are low enough to necessitate the use of this higher affinity siderophore. However, when extracellular levels of Fe^{III} increase, the *Pseudomonas* will then switch over to producing primarily pyochelin, thereby relieving the bacteria of any additional biosynthetic energy. Since Dha has been identified in iron-limited *P. aeruginosa* supernatants, I reasoned that it may function as a simplified secondary siderophore, which was originally proposed by Reimann and coworkers in 2014.[43,44]

Alternatively, these shunt metabolites may have a function similar to escherichelin, a metabolite produced during yersiniabactin biosynthesis in clinical *Escherichia coli* infection (Fig. 3.05).[45-47] This metabolite was originally studied by Mislin and coworkers as an inhibitor of pyochelin mediated Fe^{III} uptake in *P. aeruginosa*.[45] However, despite displaying Fe^{III}-binding capabilities, escherichelin does not support Fe^{III}-dependent *E. coli* growth, and in fact inhibits the growth of pyoverdine-deficient *P. aeruginosa* in Fe^{III}-restricted media. This indicates that unlike its structurally similar counterparts, it is not a siderophore.[45,47] Studies conducted by Henderson and coworkers revealed that although escherichelin is a biosynthetic precursor to both pyochelin and yersiniabactin, its release by *P. aeruginosa* is significantly diminished compared to *E. coli*.[47] Hence, it is likely that escherichelin is released by *E. coli* to inhibit Fe^{III} uptake by competing species. Based on these reports, I posed a second hypothesis that these pyochelin biosynthetic shunt metabolites may also act through an Fe^{III}-starvation mechanism to outcompete other neighboring microbial species.

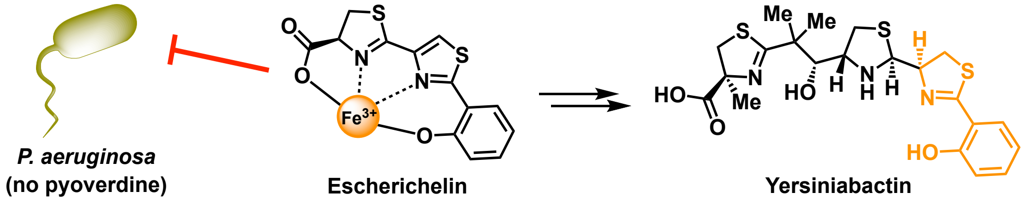

Figure 3.05. Structure of yersiniabactin and its biosynthetic shunt product escheriachelin and its inhibition of the growth of pyoverdine-deficient *P. aeruginosa* growth via an Fe^{III}-binding mechanism.[23,34]

3.5. Investigation of Pyochelin Shunt Metabolites

Kaplan, A. R.†; Musaev, D. G.; Wuest, W. M. Pyochelin Biosynthetic Metabolites Bind Iron and Promote Growth in Pseudomonads Demonstrating Siderophore-like Activity *ACS. Infect. Dis.* **2021**, *7*(3), 544-551. https://doi.org/10.1021/acsinfecdis.0c00897.

With a series of unanswered questions, my goal was to gain insight into the physiochemical and biological properties of pyochelin biosynthetic shunt metabolites in an effort to illuminate their function in *P. aeruginosa* or elsewhere in nature. To this end, I synthesized a library of these metabolites, assessed their Fe^{III}-binding characteristics qualitatively and quantitatively, and performed extensive biological assays on these six compounds to answer the two main questions detailed above.

3.5.1. Synthesis

As shown in Scheme 3.02, Dha (**3.01**) was synthesized in a single step by condensing 2-hydroxybenzonitrile with L-cysteine, as previously described by Mislin.[48,49] Aeruginoic acid (**3.04**) was synthesized in three steps using the synthetic route published by Yamada.[34] First, 2-hydroxybenzamidde was converted to the corresponding thioamide (**3.02**) then condensed with ethyl bromopyruvate giving thiazole (**3.03**). Hydrolysis of the ester then furnished aeruginoic acid (**3.04**) which was then reduced with BH_3•THF to give aeruginol (**3.05**). Next, 2-hydroxybenzonitrile was condensed with L-cysteine methyl ester hydrochloride to afford thiazoline (**3.06**). The methyl ester was then reduced to give aerugine (**3.07**), which was then oxidized directly to IQS (**3.08**) using a Swern oxidation.[48] It is worth noting that IQS (**3.08**) has also been synthesized via a Weinreb amide intermediate wherein the thiazoline is first oxidized to the thiazole and the Weinreb amide is subsequently reduced to the corresponding aldehyde.[42] However, we found it more efficient stepwise to access IQS using the methods serendipitously discovered by Mislin.

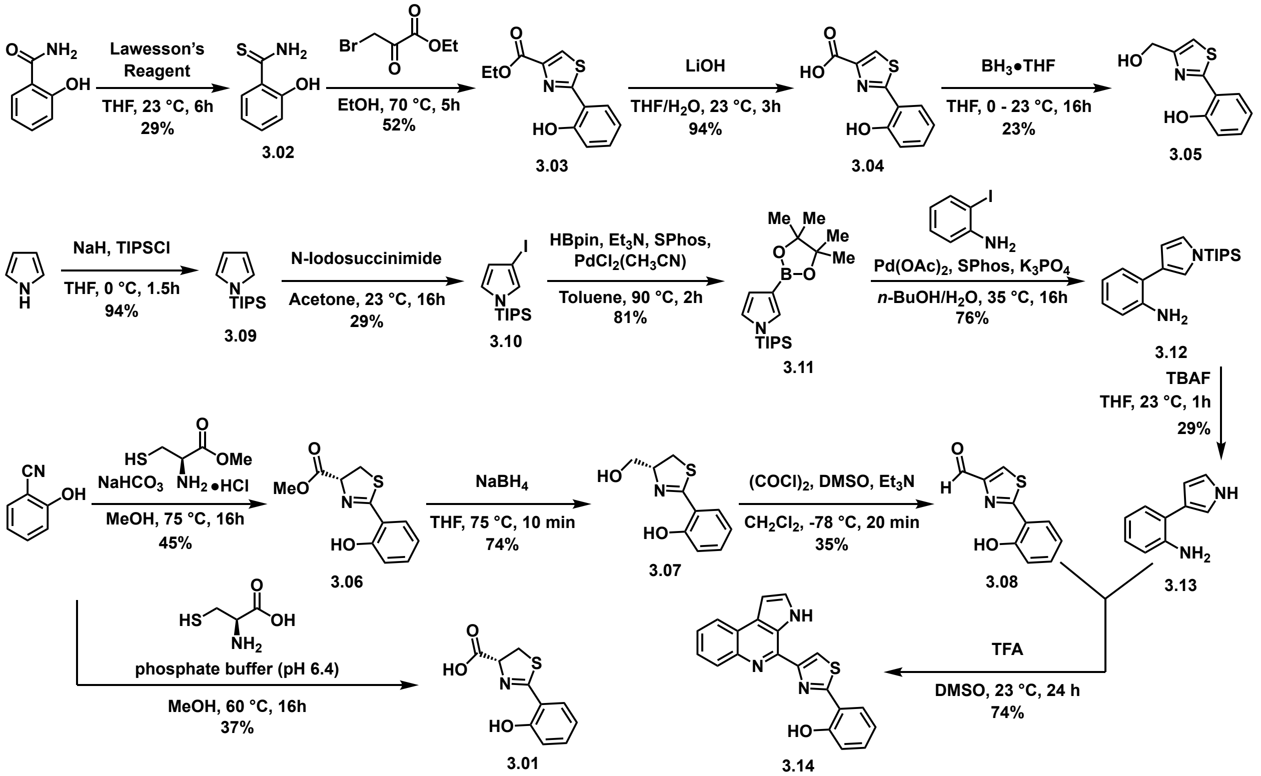

Lawesson's Reagent
THF, 23 °C, 6h
29%
3.02
EtOH, 70 °C, 5h
52%
3.03
LiOH
THF/H2O, 23 °C, 3h
94%
3.04
BH3•THF
THF, 0 - 23 °C, 16h
23%
3.05
NaH, TIPSCl
THF, 0 °C, 1.5h
94%
3.09
N-Iodosuccinimide
Acetone, 23 °C, 16h
29%
3.10
HBpin, Et3N, SPhos, PdCl2(CH3CN)
Toluene, 90 °C, 2h
81%
3.11
Pd(OAc)2, SPhos, K3PO4
n-BuOH/H2O, 35 °C, 16h
76%
3.12
TBAF
THF, 23 °C, 1h
29%
NaHCO3
MeOH, 75 °C, 16h
45%
3.06
NaBH4
THF, 75 °C, 10 min
74%
3.07
(COCl)2, DMSO, Et3N
CH2Cl2, -78 °C, 20 min
35%
3.08
3.13
phosphate buffer (pH 6.4)
MeOH, 60 °C, 16h
37%
3.01
3.14
TFA
DMSO, 23 °C, 24 h
74%

Scheme 3.02. Synthesis of Dha (**3.01**), aeruginoic (**3.04**), IQS (**3.08**), aeruginol (**3.05**), aerugine (**3.07**), pyonitrin C (**3.14**).[34,42,48-50]

With construction of the first five metabolites complete, including IQS (**3.08**), one of the building blocks for pyonitrin C, I then turned my attention to the synthesis of the second precursor, aminopyrrolnitrin (**3.13**).[50] First, pyrrole was protected with TIPS in nearly quantitative yield. This bulky protecting group facilitated regioselective 3-iodination, affording 3-iodopyrrole (**3.10**). Borylation followed by Suzuki-Miyaura coupling to 2-iodoaniline gave **3.12** in 85% yield over two steps. The TIPS group was then removed using TBAF furnishing aminopyrrolnitrin (**3.13**). Penultimate Pictet-Spengler condensation and rearomatization was performed using conditions adapted from MacMillan and co-workers; IQS (**3.08**) and aminopyrrolnitrin (**3.13**) were stirred in a 1% solution of TFA in DMSO for 24 hours affording the desired compound, pyonitrin C (**3.14**).[42] Although the published protocol reported a 72 hour reaction time, I noticed significant formation of a degradation product past this 24 hour mark that was difficult to separate from pyonitrin C (**3.14**), and thus decided to stop the reaction at 24 hours instead of reacting for the full reported 72 hours. Ultimately, this synthetic route does confirm the inherent reactivity these substrates have towards each other supporting the postulated biosynthetic formation of pyonitrins A-D.

3.5.2. Iron-Binding Evaluation

With all six compounds in hand, I began with my assessment of their properties starting with evaluating their Fe^{III}-chelating abilities. I evaluated this qualitatively using a self-designed $FeCl_3$ assay then quantitatively using a fluorescence titration assay.

3.5.2.1. $FeCl_3$ Assay

The purpose of this assay was to detect a colorimetric change upon adding Fe^{III} to a solution of each of the six compounds. If a color change was observed, this would be indicative of an Fe^{III}-binding event. Increasing amounts of a 1 M solution of each compound in methanol was added to a 1 M solution of $FeCl_3$ giving final test concentrations of 0 μM, 125 μM, 250 μM, and 500 μM. In all cases, addition of compound resulted in a change in color from yellow to purple, and in most cases this color change was fairly distinct, indicative of an iron-binding event (Fig. 3.06). Additionally, this color change became more distinct with the addition of increasing amount of compound, indicating a concentration dependence as well. In the case of pyonitrin C (**3.14**), the color change was not as obvious, which would necessitate the fluorescence titration assay further detailed below to confirm an Fe^{III}-binding event.

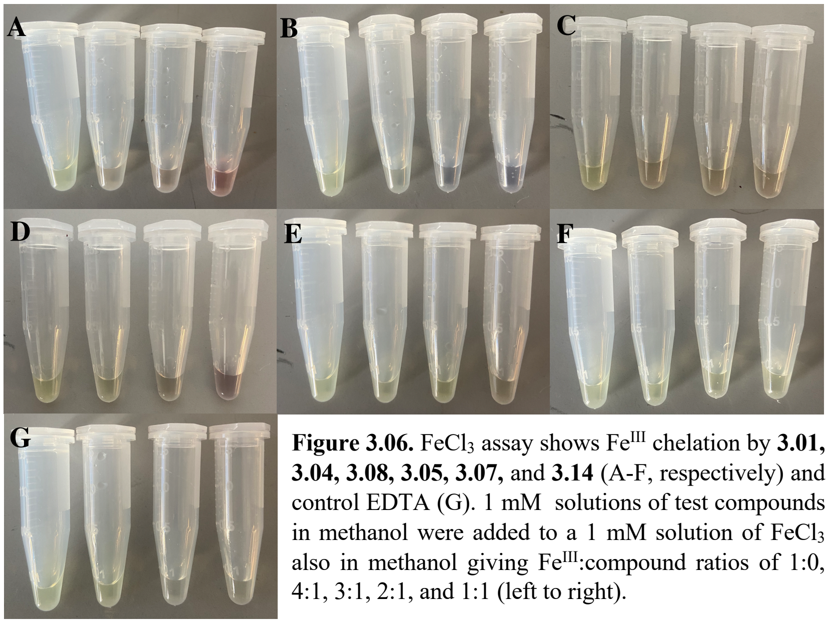

Figure 3.06. $FeCl_3$ assay shows Fe^{III} chelation by **3.01, 3.04, 3.08, 3.05, 3.07,** and **3.14** (A-F, respectively) and control EDTA (G). 1 mM solutions of test compounds in methanol were added to a 1 mM solution of $FeCl_3$ also in methanol giving Fe^{III}:compound ratios of 1:0, 4:1, 3:1, 2:1, and 1:1 (left to right).

3.5.2.2. Fluorescence Titration Assay

The Fe^{III}-chelating properties of all six compounds were then quantified using fluorescence titration experiments. In these experiments, 1.0 equivalents of Fe^{III} were added to a solution of each given compound in methanol in 0.1 equivalent increments, recording an emission spectrum after each addition. Quenching of the emission signal would confirm the previously observed Fe^{III}-binding events. Consistent with the findings from the $FeCl_3$ assay, the emission signals of all six compounds were quenched by the addition of Fe^{III} thus further supporting that these metabolites do bind iron (Fig. 3.07). Dha (**3.01**) and aeruginoic acid (**3.04**) were also titrated with five additional biologically relevant metals: cobalt, copper, magnesium, manganese, and nickel. Contrary to pyochelin, which is known to have affinity for several of these metals, none of these metals quenched the emission signal of either of these compounds, indicating that they both have a specific affinity for Fe^{III} (Fig. 3.08).[51]

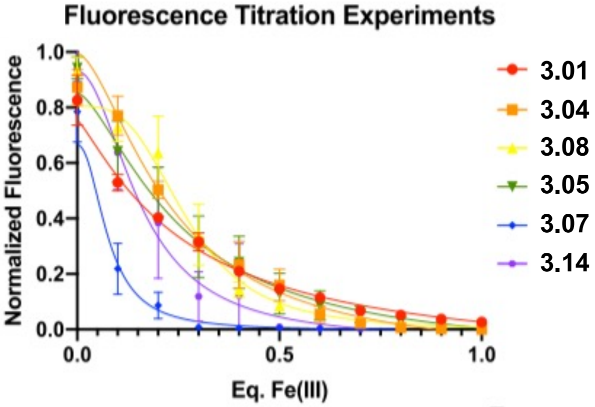

Figure 3.07. Fluorescence titration curves of **3.01**, **3.04**, **3.08**, **3.05**, **3.07**, and **3.14** titrated with 1.0 equivalents of $FeCl_3$. All experiments were performed in triplicate.

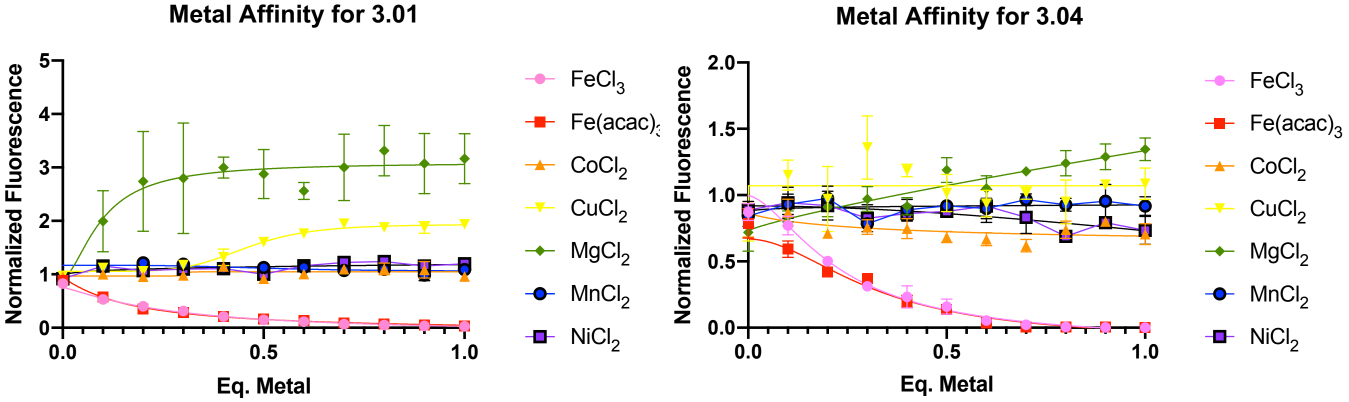

Figure 3.08. Fluorescence titration curves of **3.01** (left) and **3.04** (right) titrated with 1.0 equivalents of $FeCl_3$ $Fe(acac)_3$, $CoCl_2$, $CuCl_2$, $MgCl_2$, $MnCl_2$, and $NiCl_2$. All measurements were taken in methanol.

This data also allowed for quantification of the ligand-to-Fe^{III} binding ratios (L:Fe^{III}), which were deduced in the same manner as previously reported.[52-54] If the emission signal was quenched after the addition of 1.0 equivalents of Fe^{III}, this would be indicative of a 1:1 L:Fe^{III} binding stoichiometry. Further quenching after the addition of 0.5 equivalents of Fe^{III} would be indicative of a 2:1 ratio and after 0.33 equivalents of Fe^{III} a 3:1 ratio. Using the normalized fluorescence titration curves generated from these experiments (Fig. 3.07, raw data shown in supporting information), I deduced the L:Fe^{III} ratios of all six compounds which are summarized in table 3.01.

Table 3.01. Binding stoichiometries and calculated K_d values for **3.01**, **3.04**, **3.08**, **3.05**, **3.07**, **3.14** and pyochelin.[52-54]

Compound	L:Fe^{III}	K_d (μM)
3.01	1:1	111.4
3.04	1:1	206.4
3.08	2:1	174.3
3.05	1:1	54.94
3.07	3:1	16.39
3.14	2:1	80.38
Pyochelin[55-57]	1:1/2:1	2.0-5.0

Based on this data, it was difficult to ascertain any trends associated with this data or why certain compounds bound with a 1:1 stoichiometry while others bound with 2:1 or 3:1 stoichiometry. Based on the values in table 3.01, steric bulk does not appear to play a role, as **3.14**, the largest of the six compounds binds with a 2:1 stoichiometry compared to 1:1 stoichiometries associated with **3.01**, **3.04**, and **3.05**. Electronically, there isn't a clear pattern either. While the two compounds containing carboxylic acids, **3.01** and **3.04**, shared the same L:Fe^{III} ratio of 1:1, this did not hold up with the two primary alcohols, **3.05** and **3.07**, which bound with 1:1 and 3:1 stoichiometries, respectively. Rigidity also did not appear to have a clear influence; while thiazoles **3.04** and **3.05** bound with the same L:Fe^{III} ratio of 1:1, thiazoline **3.01** bound with a 1:1 ratio while **3.07** bound with a 3:1 ratio. In addition, the L:Fe^{III} ratios determined in 3.7.2 also did not show any clear trends, which prompted supplementary computational studies.

It should be noted that these ratios were important in determining the correct stoichiometry to use in the biological experiments discussed in the next section. Unfortunately, the L:Fe^{III} binding stoichiometries determined in table 3.01 could not be explained based on chemical structure intuitions. To this end, I sought out computational insights from Dr. Djamaladdin Musaev to support the experimentally determined L:Fe^{III} ratios (Fig. 3.09, S3.01, S3.02, S3.03). In these studies, the free energy associated with the sequential formation of each complsex was determined. When modeling **3.01**, it was determined that the energy of formation of a 1:1 complex with Fe^{III} was favorable, however the energy associated with addition of a second ligand to form a 2:1 complex with Fe^{III} was not favorable, indicating that a 1:1 complex would likely be the predominant species (Fig. 3.09, S3.01).

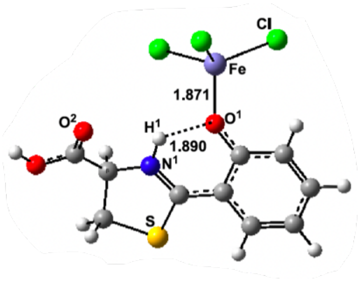

Figure 3.09. Ball-and-stick model of minimal energy structures of **3.01**-FeCl$_3$ complex.

Computations with **3.08** indicated that formation of a 1:1 complex was energetically favorable, and addition of a second ligand to form a 2:1 complex was also energetically favorable, but addition of a third ligand to form a 3:1 complex was not energetically favorable, supporting the experimentally determined 2:1 L:Fe^{III} ratio (Fig. S3.02). Finally, computations with **3.07** indicated that formation of a 1:1 and 2:1 complex was favorable, and addition of a third ligand to form the 3:1 complex was favorable, supporting the experimentally determined 3:1 L:Fe^{III} ratio (Fig. S3.03). It is important to note that this computational work does not by any means serve as definitive results. The purpose of the computational work was never to generate concrete data, but to support the previously determined experimental L:Fe^{III} binding stoichiometries. Notwithstanding, having some computational validation of one example of each L:Fe^{III} ratio, 1:1, 2:1, and 3:1 did provide a level of confidence high enough to move forward with the biological experiments to be discussed in the next section.

This fluorescence titration data was also used to calculate putative dissociation constant (K_d) values for all six compounds. The data was then extrapolated into a binding curve using Prism to calculate predicted K_d values (Fig. 3.10). These values, shown in table 3.01, were slightly higher than the K_d of pyochelin, supporting the notion that these compounds may act as lower-affinity siderophores.[55-57] Of note, these values were approximated in Prism, and serve simply as estimates of the true K_d of each compound.

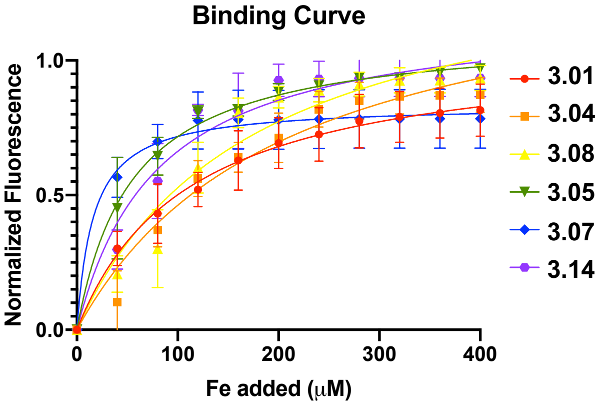

Figure 3.10. Binding curves for **3.01**, **3.04**, **3.08**, **3.05**, **3.07**, and **3.14** derived from fluorescence titration data.

As mentioned previously, the computations used to support the L:Fe^{III} ratios were performed in a sequential manner to determine whether or not addition of each subsequent ligand was energetically favorable. Based on this computational method, it is reasonable to assume that there is likely an equilibrium associated with formation of each complex favoring one L:Fe^{III} stoichiometry over others. With this in mind, putative K_d calculations were conducted in prism with truncated data for 2:1 and 3:1 complexes, however these values were incredibly erratic and thus it was only possible to calculate reasonable K_d values with the full data set from 0 all the way to 1 full equivalent of Fe^{III} added.

3.5.3.Biological Evaluation

With the promising Fe^{III}-binding results, I next sought to perform a biological evaluation of these compounds to gain a better understanding of their *in vivo* ramifications. The guiding question to these investigations was whether or not these metabolites serve as growth promoters, inhibitors, or both.

3.5.3.1. Growth Inhibition Assay

First, I tested these compounds for their ability to impart an iron starvation effect against non-producing bacterial strains. These compounds were evaluated against a panel of clinically relevant species (*Enterococcus faecalis*, *Escherichia coli*, and (methicillin-resistant) *Staphylococcus aureus*) using standard MIC/IC_{50} assay conditions. No growth inhibition was observed against any of these strains. Thus, the conclusion from these experiments is that the iron-binding properties of these compounds are unlikely to play a role in iron starvation as seen in the case of escherichelin.[45-47]

3.5.3.2. Growth Promotion Assay

To test the hypothesis that these compounds promote growth in *Pseudomonas* by means of their Fe^{III}-chelating abilities, I developed a growth promotion assay. Each compound was incubated with both the wild-type *P. aeruginosa* (PAO1) and a double knockout mutant incapable of producing either of its native siderophores, pyoverdine or pyochelin (ΔpvdDΔphcEF). All assays were performed in Fe^{III}-depleted growth media with each compound as both the free ligand as well as a prechelated Fe^{III}-ligand complex using $Fe(acac)_3$ as the Fe^{III} source. If these ligands were to promote growth via an Fe^{III}-binding mechanism, I would expect that the unchelated ligands would have little to no impact on growth of either strain, which was indeed what I observed (Fig. 3.11). With the exception of **3.14**, which may have had some background fluorescence at the wavelength I took readings at, the growth curves of each with each of the remaining five compounds were nearly identical to the DMSO control.

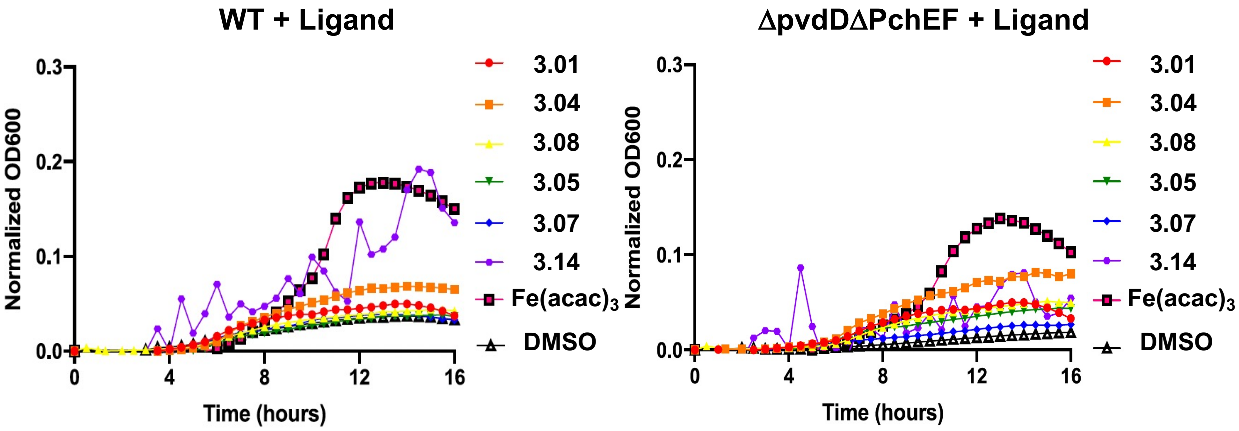

Figure 3.11. Growth curves of PAO1 and ΔpvdDΔpchEF in Fe^{III}-depleted media with 125 μM of free ligand of each test compound. Fe(acac)$_3$ was the positive control and DMSO was the negative control. All experiments were performed in triplicate.

Next, I incubated PAO1 with each of the six compounds prechelated with Fe^{III} and observed a marked enhancement of growth compared to the DMSO control. In fact, in most cases this enhancement of growth was slightly higher than that with the Fe(acac)$_3$ control (Fig. 3.12). However, at this point it was unclear whether or not this growth enhancement arose from direct uptake of these ligand- Fe^{III} complexes or if the native siderophores were stripping the Fe^{III} from these complexes and importing Fe^{III} into the cell in that fashion. This was where the double knockout strain became important. If growth promotion was still observed with this strain, then I would know that these ligand- Fe^{III} complexes were in fact getting directly imported by the bacteria. Excitingly, this was exactly what I observed; all six ligand-Fe^{III} complexes enhanced the growth of the ΔpvdDΔphcEF strain (Fig. 3.12). In fact, this data indicates that for the first to my knowledge, these metabolites do exhibit some siderophore-like properties.

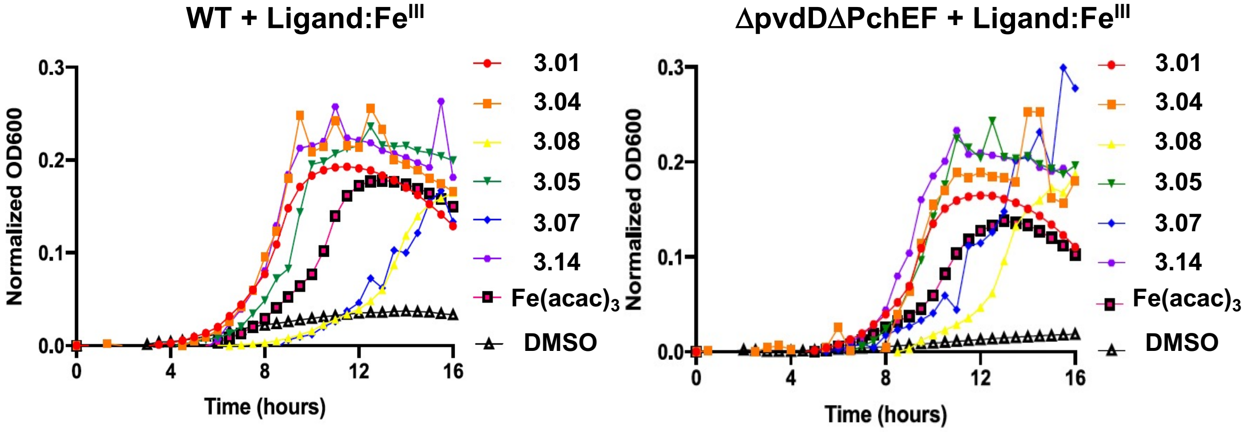

Figure 3.12. Growth curves of PAO1 and ΔpvdDΔpchEF in Fe^{III}-depleted media with 125 μM of ligand:Fe^{III} complex of each test compound. Fe(acac)$_3$ was the positive control and DMSO was the negative control. All experiments were performed in triplicate.

One interesting feature worth noting was the delayed growth curves of **3.08** and **3.07** compared to the other test compounds. One possible explanation for this could be that there was delayed uptake of these two particular complexes possibly due to their 3-dimensional nature. Other factors may have been at play as well; for example, with the exception of pyonitrin C, the other four metabolites contain a phenol -OH and either a carboxylic acid or alcohol -OH group, while IQS only contains the phenol. This difference in hydrogen bonding may lend itself to the delayed growth enhancement. In contrast, **3.07** has both of the aforementioned -OH groups, however as previously mentioned, this metabolite was not found to be implicated in the redox breakdown process giving rise to the other metabolites, and therefore may simply be less easily recognized by the bacteria transporters. Regardless, further work into this structure-activity relationship would be required to determine the reason for this phenomenon.

3.6. Conclusions and Broader Impacts

In this work, I aimed to answer several key questions about the physiochemical properties and biological role(s) of several *Pseudomonad* metabolites arising from the premature release of Dha from the pyochelin biosynthetic machinery. First, their Fe^{III}-binding capabilities were characterized both qualitatively and quantitatively and verified computationally. Next, these Fe^{III}-binding compounds were assessed in multiple biological assays. I found that while these compounds do not inhibit the growth of other pathogenic bacteria by means of an Fe^{III}-starvation mechanism, they do promote the growth of *P. aeruginosa* in Fe^{III}-depleted conditions, indicating for the first time that these metabolites do act in a siderophore-like manner. One key question that still needs to be answered is how these pyochelin biosynthetic shunt metabolites are recognized and imported as Fe^{III}-ligand complexes. Uptake of pyoverdine and pyochelin ferrisiderophore complexes occurs via TonB-dependent receptors.[58] However, it is unclear whether import of the simplified Fe^{III}-ligand complexes is conducted using the same machinery or a different receptor yet to be elucidated. Future work will involve determination of transport machinery, if any, involved in the uptake of these complexes to confirm their role as native siderophores.

One of the key potential broader implications of this work is the potential to utilize these simplified siderophore metabolites in antibiotic-siderophore conjugates as part of a minimalist "Trojan-Horse" strategy.[59] This phenomenon was recently applied to the development of the antibiotic Fetroja® (cefiderocol) approved for use by the FDA in 2019.[60] The scaffold of Fetroja® is comprised of two key features, a combination of two cephalosporin antibiotic structures, ceftazidime and cefepime and an Fe^{III}-binding catechol motif commonly found in many siderophore structures. The combination of an antibiotic scaffold with a common siderophore moiety renders this conjugate antibiotic less susceptible to resistance mechanisms, particularly efflux, as the bacteria has essentially been tricked into thinking this molecule will enable to it harbor essential Fe^{III} thereby rendering the antibiotic itself more effective. While this antibiotic was found to be effective against several Gram-negative pathogens, I wondered if perhaps it would be more effective to design species-specific siderophore-antibiotic conjugates. Species specificity would further decrease susceptibility to resistance for reasons described in greater detail in the previous chapter. Also briefly highlighted in the previous chapter is the benefit of synthetic simplification; by appending a truncated pyochelin metabolite, for example Dha which only takes a single step to synthesize, it is possible to bypass a large amount of synthetic effort to access a Trojan Horse antibiotic with the same level of species specificity. I postulate that using the platform recently developed by the Seiple group, one can systematically design an antibiotic-linker-siderophore conjugate with specificity for *Pseudomonas* or any other Gram-negative pathogens.[61] Future work is focused on this exact task.

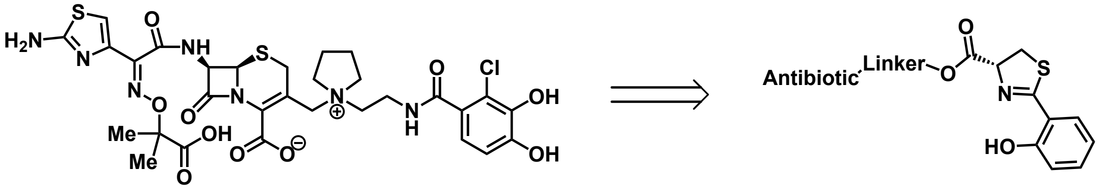

Fetroja ® (cefiderocol)

Species-Specific Trojan Horse Antibiotic

Figure 3.13. Structure of Fetroja® (cefiderocol) and hypothetic species-specific Trojan Horse antibiotic.

3.7. Oxazoline and Oxazole Analogs

Kaplan, A. R.†.; Wuest, W. M. Promiscuous Pseudomonas: Uptake of non-endogenous ligands for iron acqisition. *Tetrahedron. Lett.* **2021**, *75*(6), 153204-153206. https://doi.org/10.1016/j.tetlet.2021.153204.

With these exciting results obtained for the *Pseudomonad* pyochelin shunt metabolites, I wondered if these results were limited to these naturally occurring metabolites, or if perhaps these same siderophore-like properties would be observed with molecules that had been slightly modified. As previously mentioned, oxazolines are highly prevalent Fe^{III}-binding motifs in siderophores, just like their thiazoline counterparts in the series of *Pseudomonad* siderophore-like compounds.[2,9,13,14] Additionally, the previous computational studies showed that the atoms involved in Fe^{III} chelation were likely the phenol -OH group and the heterocyclic nitrogen. This indicates that the sulfur atom is likely not directly involved in any Fe^{III}-binding, and thus could hypothetically be swapped out with another atom, such as oxygen, without drastically altering the overall physiochemical and biological properties of these small molecules. This led me to wonder if I would observe similar siderophore-like properties in oxazoline and oxazole counterparts to the thiazoline and thiazole-containing metabolites. To this end, I synthesized a series of four oxygen-containing counterparts to Dha (**3.01**), aeruginoic acid (**3.04**), aeruginol (**3.05**), and aerugine (**3.07**) and evaluated them in a similar fashion as previously described.

3.7.1.Synthesis

Synthesis of this series of compounds was achieved in a fairly straightforward manner using standard protocols (Scheme 3.03). 2-Hydroxybenzonitrile was converted imidate **3.15**, which was then immediately condensed with L-serine methyl ester hydrochloride giving oxazoline, **3.16**.[62] The methyl ester was then either hydrolyzed to carboxylic acid, **3.17**, or reduced to primary alcohol, **3.18**. Next, the oxazoline methyl ester was desaturated to the corresponding oxazole, **3.19**, using methodology previously developed by Wipf and Williams.[63,64] In the same manner as with the oxazoline methyl ester, 3.16, the oxazole methyl ester was further elaborated to carboxylic acid **3.20**, and primary alcohol, **3.21**.

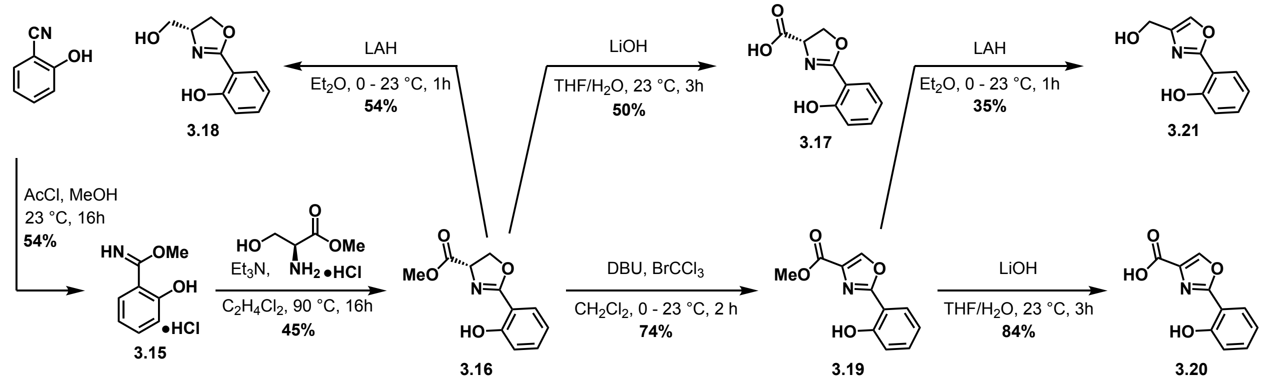

CN
OH
AcCl, MeOH
23 °C, 16h
54%
HN
OMe
OH
•HCl
3.15
HO
O
OMe
Et3N, NH2•HCl
C2H4Cl2, 90 °C, 16h
45%
MeO
O
N
HO
3.16
LAH
Et2O, 0 - 23 °C, 1h
54%
HO
3.18
LiOH
THF/H2O, 23 °C, 3h
50%
3.17
LAH
Et2O, 0 - 23 °C, 1h
35%
3.21
DBU, BrCCl3
CH2Cl2, 0 - 23 °C, 2 h
74%
3.19
LiOH
THF/H2O, 23 °C, 3h
84%
3.20

Scheme 3.03. Synthetic route to compounds **3.17**, **3.18**, **3.20**, **3.21**.[61-64]

3.7.2.Fe^{III}-Binding Properties

With these four compounds in hand, I then moved on to investigating their Fe^{III}-binding characteristics. Qualitative analysis of each compound using the previously described $FeCl_3$ assay revealed that all four compounds displayed an ability to bind Fe^{III}, as indicated by the change in color of the solution from yellow to purple, similar to the previously described results (Fig. 3.14). Additionally, similar to previous results, this bleaching effect was more obvious for some compounds and less obvious for compounds like **3.16**.

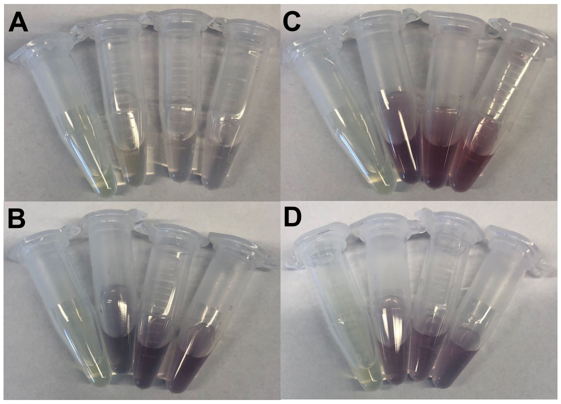

Figure 3.14 $FeCl_3$ assay shows Fe^{III} chelation by compounds **3.17, 3.18, 3.20,** and **3.21** (**A-D**, respectively). 1 mM solutions of test compounds in methanol were added to 1 mM solution of $FeCl_3$ also in methanol giving Fe^{III}:compound ratios of 1:0, 4:1, 3:1, 2:1, and 1:1 (left to right).

Next the Fe^{III}-binding properties of these compounds were quantified using the fluorescence titration assay also described previously. As was found previously, the emission signal of each compound was quenched by the addition of varying amounts of Fe^{III} indicative of an Fe^{III}-binding event. Fluorescence titration curves (Fig. 3.15) and binding curves (Fig. 3.16) were also generated from these experiments and enabled me to deduce the L:Fe^{III} stoichiometries and K_d values shown in Table 3.02. These values were all comparable to the values obtained previously, indicating that they may also have siderophore-like activity. As mentioned previously, it was difficult to assign any definitive trends with respect to chemical structure and L:Fe^{III} stoichiometries, and these four compounds were no exception to that. No clear trend or pattern could be determined based on steric or electronic nature of these compounds. However, as previously mentioned, computational modeling was valuable in supporting these experimentally determined values.

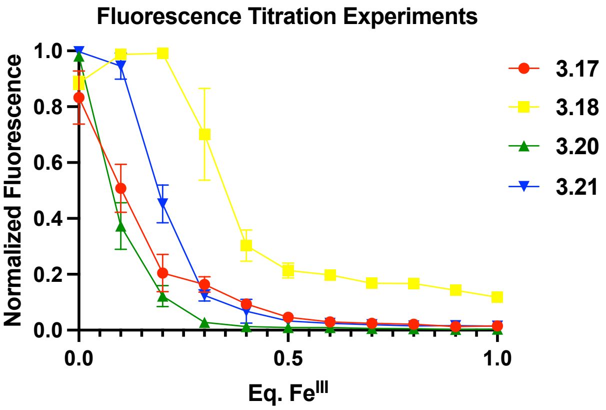

Figure 3.15. Fluorescence titration curves for **3.16**, **3.17**, **3.19**, and **3.20** titrated with 1.0 equivalents of $FeCl_3$. Each titration was performed in triplicate.

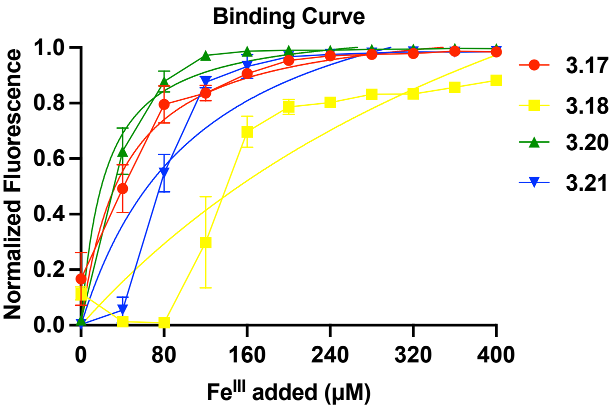

Figure 3.16. Binding curves for **3.16**, **3.17**, **3.19**, and **3.20** which were generated from fluorescence titration data.

Table 3.02. Binding stoichiometries and K_d values for **3.16**, **3.17**, **3.19**, and **3.20**.

Compound	L:Fe^{III}	K_d (μM)
3.17	2:1	40.81
3.18	1:1	553.7
3.20	3:1	23.14
3.21	2:1	113.5

3.7.3.Biological Evaluation

These four compounds were then evaluated in the same assays as the previous work. Just as before, these compounds did not inhibit the growth of the panel of pathogenic bacteria (*Enterococcus faecalis*, *Escherichia coli*, and (methicillin-resistant) *Staphylococcus aureus*). However, when evaluated for growth promoting activity, these compounds behaved virtually the same as the sulfur-containing *Pseudomonas* metabolites. None of the four free ligands promoted *P. aeruginosa* growth in $\mathrm{Fe^{III}}$-depleted growth media. However, all four ligand:$\mathrm{Fe^{III}}$ complexes did promote growth; in fact, the difference in growth of ΔpvdDΔphcEF treated with each ligand:$\mathrm{Fe^{III}}$ complex compared to $\mathrm{Fe(acac)_3}$ was particularly stark.

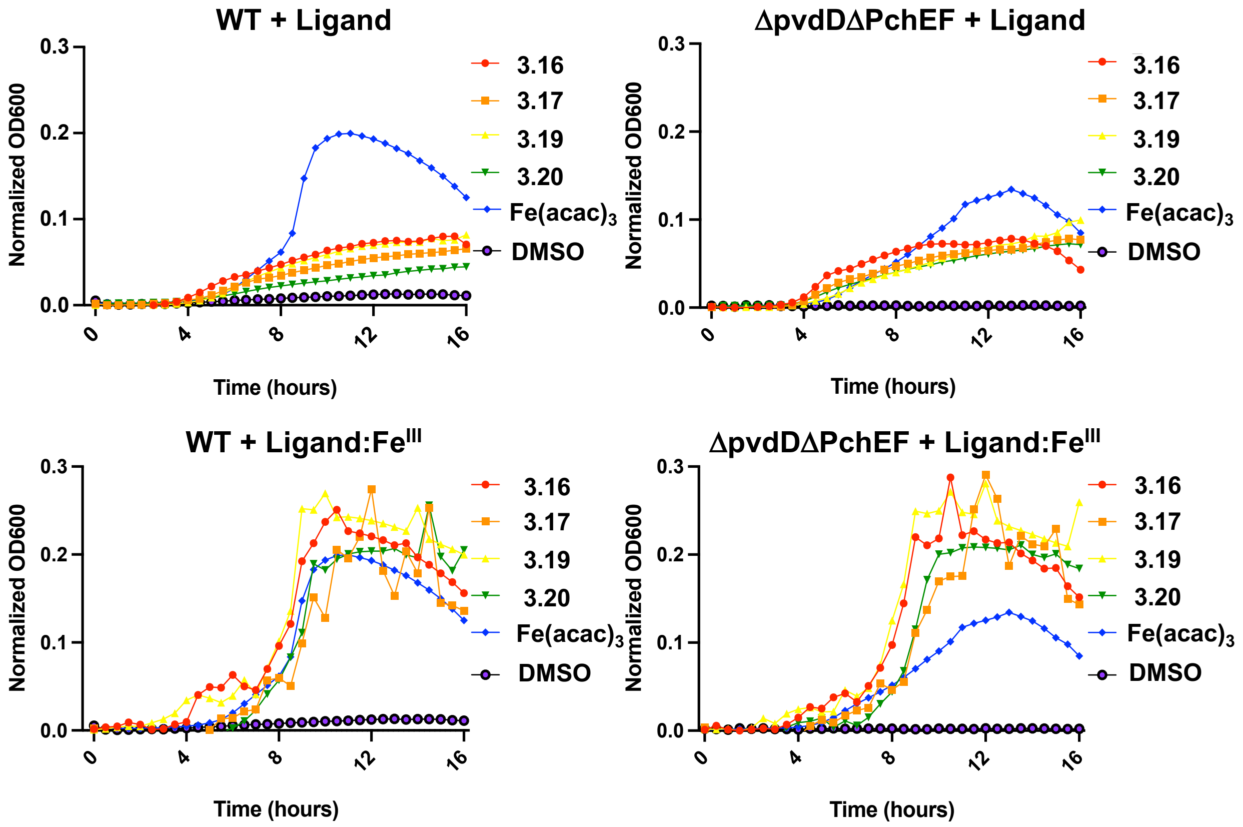

Figure 3.17. Growth curves of PAO1 (left) and ΔpvdDΔpchEF (right) in $\mathrm{Fe^{III}}$-depleted media with 125 μM of free ligand (top) and ligand:$\mathrm{Fe^{III}}$ complex (bottom) of each test compound. $\mathrm{Fe(acac)_3}$ was the positive control and DMSO was the negative control. All experiments were performed in triplicate.

3.7.4.Conclusions

To summarize, experimental results from this work indicated that the oxazoline and oxazole counterparts to the previously studied pyochelin biosynthetic shunt metabolites demonstrated highly similar Fe^{III}-binding and siderophore-like activity. This suggests that *P. aeruginosa* is somewhat promiscuous in its uptake of these simplified siderophore-like complexes. As previously mentioned, further work would be necessary to elucidate the mechanism and possible transport machinery responsible for the import of these complexes. These results led me to wonder if this growth promotion phenomenon is exclusive to *Pseudomonas*, or if it occurs in other pathogenic Gram-negative bacteria like *Acinetobacter baumannii*. My work to investigate this question is discussed in the next section.

3.8. Acinetobacter Siderophores

Kaplan, A. R.†.; Haney, B. A.; Wuest, W. M. Acinetobactin Biosynthetic Intermediate Binds Iron and Displays Uniqe Biiological Profile in *Acinetobacter Baumannii*. *ChemBioChem.* **2022**, *Submitted.*

As I had mentioned above, I was especially interested in seeing if siderophore biosynthetic precursors could impart a growth-promoting effect in *A. baumannii* similar to what I had previously observed in *Pseudomonas*. *A. baumannii* is an opportunistic Gram-negative pathogen and a causative agent in a variety of diseases as common as burn, wound, and urinary tract infections and as serious as pneumonia and sepsis.[65] *A. baumannii*, similar to *P. aeruginosa,* produces multiple siderophores: acinetobactin, which exists in two pH-dependent isomers, fimsbactins, and baumannoferrins (Fig. 3.18).[66-69] The primary siderophore, acinetobactin, was of particular interest due to catechol-oxazoline motifs similar to the phenol-thiazoline in the structure of pyochelin.

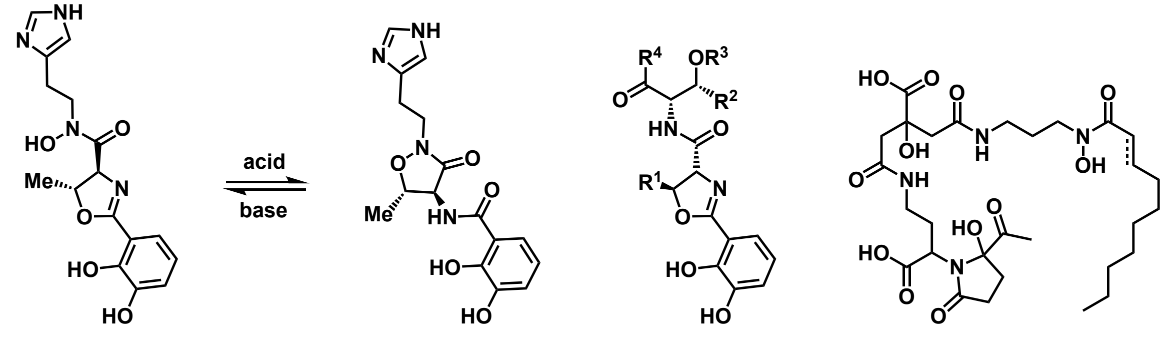

preacinetobactin acinetobactin fimsbactins A-F baumannoferrins A&B

Figure 3.18. Structures of preacinetobactin, acinetobactin, fimsbactins A-F, and baumannoferrins A&B.[63-66]

3.8.1. Acinetobactin Biosynthesis

Similar to pyochelin, the biosynthesis of acinetobactin starts chorismite which gets converted to enzyme-activated 2,3-dihydroxybenzoate. Next, L-threonine undergoes a condensation reaction giving rise to the oxazoline core. Finally, N-hydroxyhistamine is incorporated into the scaffold, which is then released as preacinetobactin, which can freely isomerize to acinetobactin under basic conditions (Scheme 3.04).[69-71] To the best of my knowledge, there are no reports of premature release of the oxazoline precursor, **3.24**. This led me to hypothesize that **3.22** could play a similar role in *A. baumannii*, thereby supporting the notion that this compound can be prematurely released from the acinetobactin biosynthetic machinery. To this end, I investigated this hypothesis alongside an undergraduate in our lab, Brittney Haney, using the same methods as previously described.

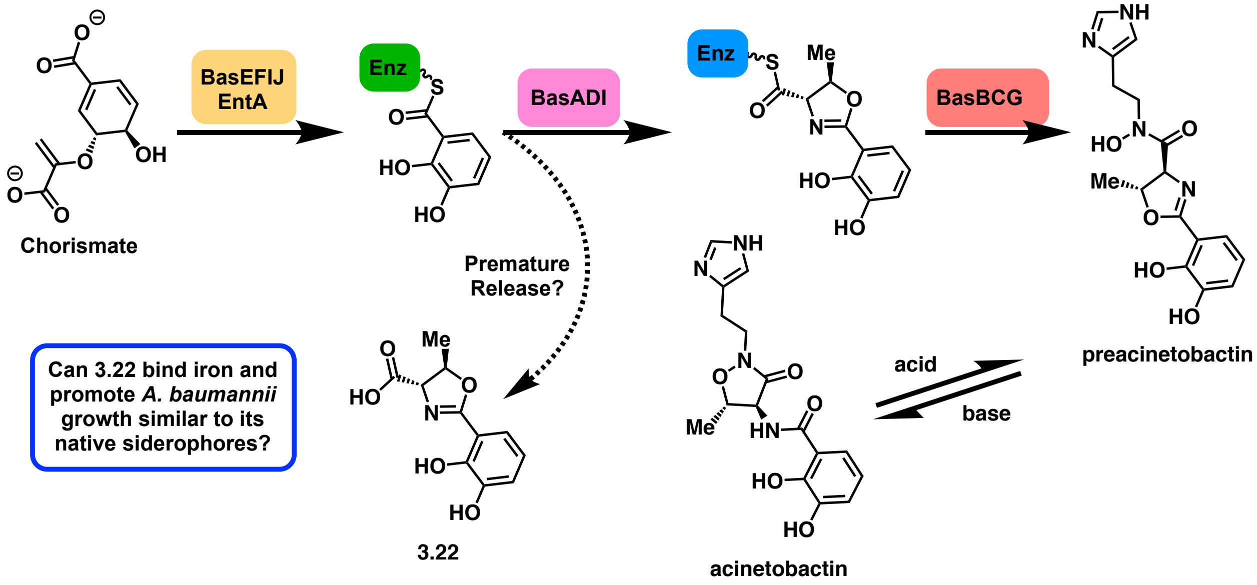
BasEFIJ
EntA
Enz
BasADI
Enz
BasBCG
Me
Chorismate
Premature Release?
Can 3.22 bind iron and promote *A. baumannii* growth similar to its native siderophores?
3.22
acinetobactin
acid
base
preacinetobactin

Scheme 3.04. Abbreviated biosynthetic pathway to preacinetobactin, its pH dependent isomerization to acinetobactin, and the hypothetical premature release of compound **3.22**.[69-71]

3.8.2.Synthesis of 3.22

Synthesis of **3.24** was achieved in a fairly straightforward fashion (Scheme 3.05).[65,72] First, 2,3-dihydroxybenzonitrile was converted to the corresponding imidate, 3.23, which was then condensed with threonine benzyl ester oxalate, furnishing the oxazoline **3.24** in 27% over two steps. Then, hydrogenolysis of the benzyl ester afforded the corresponding carboxylic acid, giving **3.22** in 92% yield over three steps.

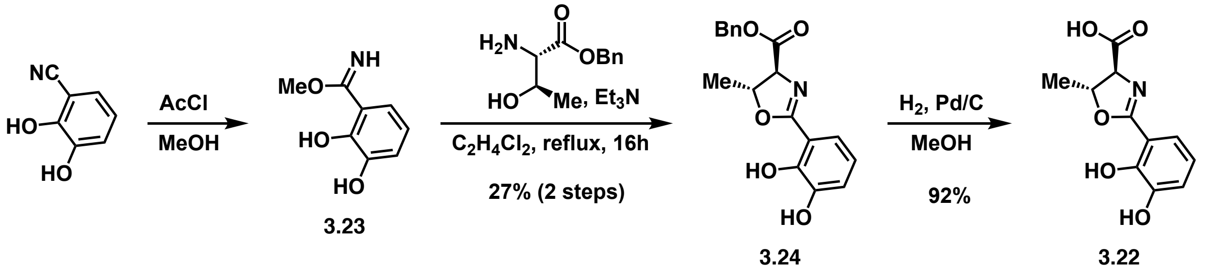
NC
HO
HO
AcCl
MeOH
NH
MeO
HO
HO
3.23
O
H₂N
OBn
HO
Me, Et₃N
C₂H₄Cl₂, reflux, 16h
27% (2 steps)
BnO
O
Me
N
O
HO
HO
3.24
H₂, Pd/C
MeOH
92%
HO
O
Me
N
O
HO
HO
3.22

Scheme 3.05. Synthesis of **3.24** was achieved in three steps.[65,72]

3.8.3.Iron-Binding Properties

Qualitative analysis of **3.22** performed as previously described, showed that **3.22** indeed binds iron, and does so in a concentration-dependent manner (Fig. 3.19).

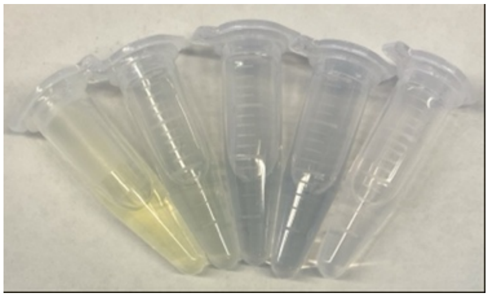

Figure 3.19. $FeCl_3$ assay shows Fe^{III} chelation by **3.22**. A 1 mM solution of compound **3.22** in methanol was added to a 1 mM solution of $FeCl_3$ also in methanol giving **3.22**:$FeCl_3$ ratios of 0:1, 1:1, 2:1, 3:1, and 1:0 (left to right).

Next, Fe^{III}-binding was quantified using the previously described fluorescence titration experiments. As shown in figure 3.20, the emission signal was quenched by the addition of 1.0 equivalents of Fe^{III}, thereby further supporting that **3.22** binds Fe^{III} and does so in a 1:1 L:Fe^{III} stoichiometry. The binding curve resulting from these experiments, shown in figure 3.21, enabled calculation of a predicted K_d value of 73.0 μM. This value is notably higher than experimental values reported for preacinetobactin (1:1 preacinetobactin:Fe^{III} K_d = 763 nM, 2:1 preacinetobactin:Fe^{III} K_d = 83 nM).[73]

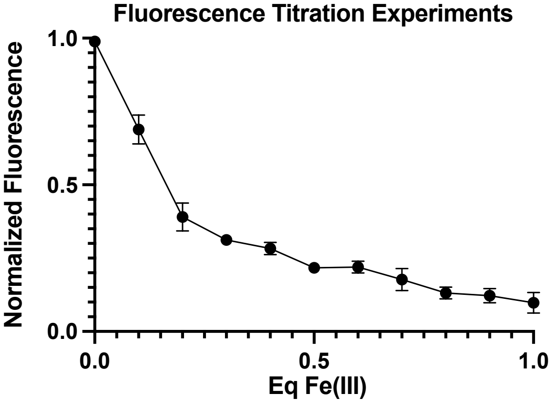

Figure 3.20. Fluorescence titration curve for **3.22** titrated with 1.0 equivalents of $FeCl_3$. Each titration was performed in triplicate.

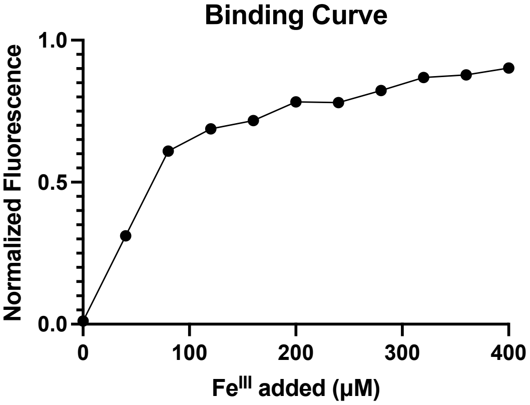

Figure 3.21. Binding curves for **3.22**, which was generated from fluorescence titration data.

3.8.4.Biological Evaluation

Finally, we assessed the effect of **3.22** on the growth of *A. baumannii*. For this work, we utilized the wild-type (ATCC 17978) as well as a complete siderophore biosynthetic knockout mutant (ΔbasGΔbfnLΔfbsE), generously provided by the Skaar lab at Vanderbilt University, incapable of producing any of the three previously mentioned native siderophores. Each strain was incubated with first the free ligand of **3.22** then the **3.22**:Fe^{III} complex in Fe^{III}depleted growth media supplemented with a non-lethal amount of known Fe^{III}-chelator EDTA (32 μM), across a range of concentrations, monitoring growth until stationary phase was reached (Fig. 3.22). For the wild-type, wild-type growth was comparable to the DMSO control at all test concentrations excluding 250 μM, wherein a significant decrease in growth was observed. This decrease was even more drastic with the **3.22**:Fe^{III} complex, for which there was a slight enhancement of growth for all test concentrations compared to DMSO, except at 250 μM , wherein growth was almost entirely inhibited. This peculiar effect was even more drastic with the ΔbasGΔbfnLΔfbsE strain, which did not appear to grow at all with the DMSO control. Also similar to the wild-type, the enhancement of growth compared to DMSO as well as the inhibitory effect at 250 μM was more obvious for the **3.22**:Fe^{III} complex than for **3.22** as the free ligand. Overall, these results suggest a dual role for this hypothetical metabolite in *A. baumannii*: it promotes growth until it reaches a certain concentration threshold, at which point it exerts some degree of toxicity.

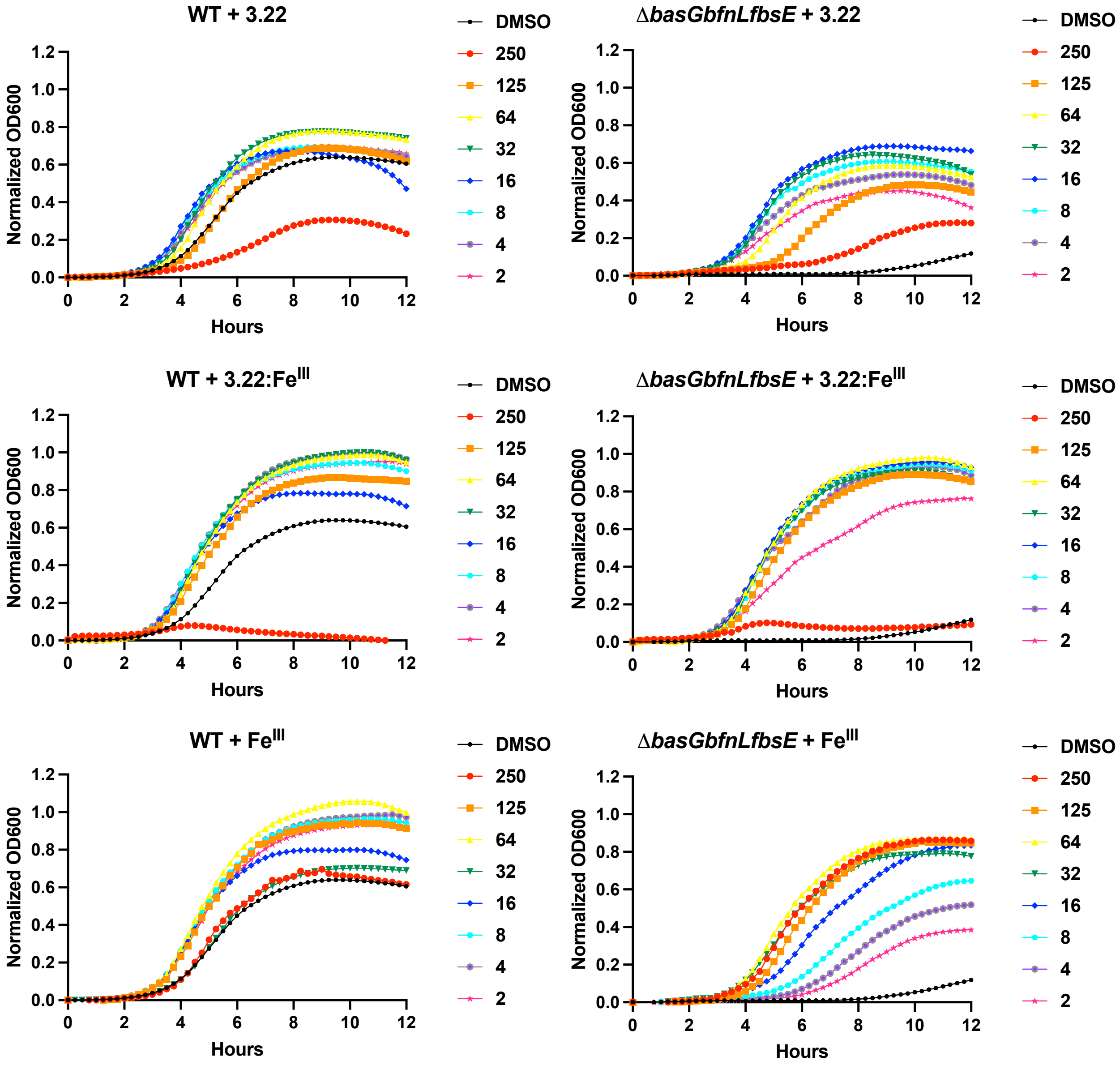

Figure 3.22. Growth curves of *A. baumannii* wild-type strain (left) and ΔbasGΔbfnLΔfbsE strain (right) grown in Fe^{III}-depleted media supplemented with 32 μM EDTA in the presence of free ligand **3.22** (top), **3.22**:Fe^{III} complex (middle), and $FeCl_3$ (bottom). All experiments were performed in triplicate.

We were particularly intrigued by the inhibitory effect that **3.22** seemed to have on *A. baumannii* growth at 250 µM, and therefore probed this further by repeating the same growth assays with the same range of test concentrations but in normal, iron-replete Mueller Hinton broth (Fig. 3.23). For both the wild-type and the ΔbasGΔbfnLΔfbsE strains, there was a clear decrease in growth at 250 µM compared to the other test concentrations. Taken together, these results indicate that **3.22** plays a concentration-dependent dual role in *A. baumannii*, promoting growth at lower concentrations and hindering growth at higher concentrations.

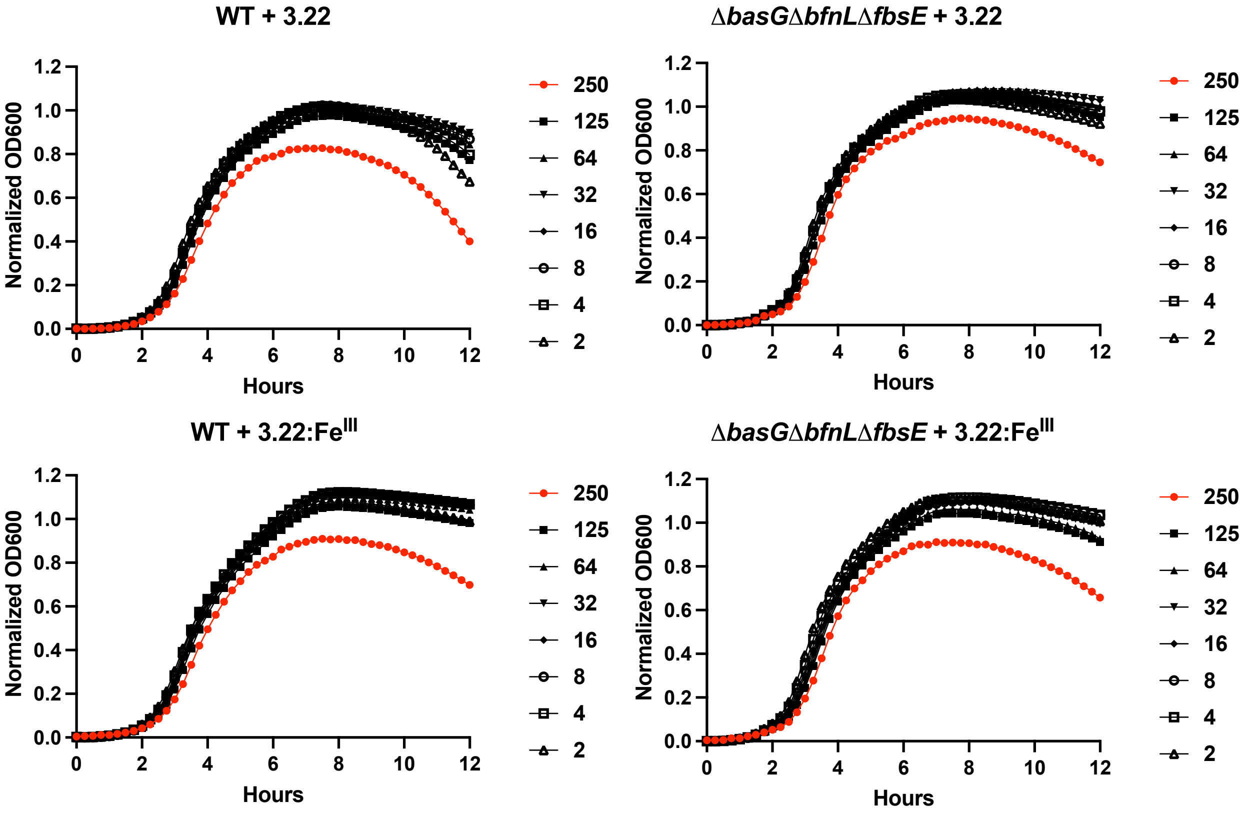

WT + 3.22

Δ***basG***Δ***bfnL***Δ***fbsE* + 3.22**

WT + 3.22:Fe^{III}

Δ***basG***Δ***bfnL***Δ***fbsE* + 3.22:Fe^{III}**

Figure 3.23. Growth curves of *A. baumannii* wild-type strain (left) and ΔbasGΔbfnLΔfbsE (right) grown in MH media in the presence of free ligand **3.22** (top), and **3.22**:Fe^{III} complex (bottom). All experiments were performed in triplicate.

3.8.5.Conclusions

Our evaluation of **3.22** revealed an Fe^{III}-chelation ratio of 1:1 (ligand:Fe^{III}) and a K_d of 73.0 μM. These compounds displayed an intriguing dual effect on growth, with a peculiar difference from the effects observed in *P. aeruginosa*, wherein at lower concentrations, **3.22** enhanced with growth of *A. baumannii*, however at higher concentrations a toxicity effect emerged. It should be noted that previous work by Wencewicz showed that both acinetobactin and fimsbactin alone promote the growth of *A. baumannii*, however in combination, they appear to compete with one another, ultimately inhibiting growth. They also showed these two siderophores compete for binding BauB, an essential periplasmic siderophore-binding protein, giving rise to what they postulated to be apo-siderophore buildup in the periplasm, ultimately leading to Fe^{III} starvation and diminished bacterial growth. While it is possible that this phenomenon could be occurring with the *A. baumannii* wild-type strain in this work, it remains unclear the mechanism behind the growth inhibition observed in the ΔbasGΔbfnLΔfbsE strain in this work as this strain does not produce the native siderophores that would possibly compete with **3.22**. Hence, the question still remains as to what the role of **3.22** is in *A. baumannii*. We hope to elucidate the biological mechanism of **3.22** in *A baumannii*, which will perhaps illuminate knowledge essential for combatting this priority critical pathogen and urgent threat as classified by the World Health Organization and Centers for Disease Control and Prevention.[74-77]

It should be noted that

3.9. References

1 Barry, S. M.; Challis, G. L. Recent advanes in siderophore biosynthesis. *Curr. Opin. Chem. Biol.* **2009**, *13*(2), 205-215.

2 Miethke, M.; Marahiel, M. Siderophore-Based Iron Acquisition and Pathogen Control. *Mol. Bio. Rev.* **2007**, *71*(3), 413-451.

3 Andrews, S. C.; Robinson, A. K.; Rodriguez-Quinones, F. Bacterial iron homeostasis. *FEMS. Microbiol. Rev.* **2003**, *27*(2-3), 215-237.

4 Zughaier, S. M.; Cornelis, P. Editorial: Role of Iron in Bacterial Pathogenesis. *Front. Cell. Infect. Microbiol.* **2018**, *8*(344), 1-2.

5 Cross, J. H.; Bradbury, R. S.; Fulford, A. J.; Jallow, A. T.; Wegmüller, R.; Prentice, A. M.; Cerami, C. Oral iron acutely elevates bacterial growth in human serum. *Sci. Rep.* **2015**, *5*, 16670-16676.

6 Butt, A. T.; Thomas, M. S. Iron Acquisition Mechanisms and Their Role in the Virulence of *Burkholderia* Species. *Front. Cell. Infect. Microbiol.* **2017**, *7*(408), 1-21.

7 Ramakrishnan, G. Iron and Virulence in *Francisella tularensis*. *Front. Cell. Infect. Microbiol.* **2017**, *7*(107), 1-7.

8 Keohane, C. E.; Steele, A. D.; Wuest, W. M. The Rhizosphere Microbiome: A Playground for Natural Product Chemists. *Synlettl.* **2015**, *26*(20), 2739-2744.

9 Khan, A.; Singh, P.; Srivastava, A. Synthesis, nature and utility of universal iron chelator – Siderophore: A review. *Microbiol. Mol. Biol. Rev.* **2011**, *6*(2), 223-249.

10 Parrow, N. L.; Fleming, R. E.; Minnick, M. F. Sequestration and Scavenging of Iron in Infection. *Infect. Immun.* **2013**, *81*(10), 3503-3514.

11 Wandersman, C.; Delepelaire, P. Bacterial iron sources: from siderophores to hemophores. *Annu. Rev. Microbiol.* **2004**, *58*, 611-647.

12 Cornelis, P. Iron uptake and metabolism in pseudomonads *Appl. Microbiol. Biotechnol.* **2010**, *86*(6), 1637-1645.

13 Wuest, W. M.; Sattely, E. S.; Walsh, C. T. Three Siderophores from One Bacterial Enzymatic Assembly Line. *J. Am. Chem. Soc.* **2009**, *131*(14), 5056-5057.

14 Crosa, J. H.; Walsh, C. T. Genetics and Assembly Line Enzymology of Siderophore Biosynthesis in Bacteria. *Microbiol. Mol. Biol. Rev.* **2011**, *6*(2), 223-249.

15 Porras-Alfaro, A.; Bayman, P. Hidden Fungi, Emergent Properties: Endophytes and Microbiomes.

Annu. Rev. Phytopathol. **2011**, *49*, 291-315.

16 Haas, D.; Défago, G. Biological Control of Soil-Borne Pathogens by Flurescent *Pseudomonads*. *Nat. Rev. Microbiol.* **2005**, *3*, 307-319.

17 Bhagirath, A. Y.; Li, Y.; Somayajula, D.; Dadashi, M.; Badr, S.; Duan, K. Cystic Fibrosis Lung Environment and Pseudomonas Aeruginosa Infection. *BMC Pulm. Med.* **2016**, *16*, 17

18 Leoni, L. Ciervo, A.; Orsi, N.; Visca, P. Iron-Regulated Transcription of the *pvdA* Gene in *Pseudomonas aeruginosa*: Effect of Fur and PvdS on Promoter Activity. *J. Bacteriol.* **1996**, *178*(8), 2299-2313.

19 Igarashi, Y.; Asano, D.; Sawamura, M.; In, Y.; Ishida, T.; Imoto, M. Ulbactins F and G, Polycyclic Thiazoline Derivatives with Tumor Cell Migration Inhibitory Activity from *Brevibacillus* sp. *Org. Lett.* **2016**, *18*(7), 1658-1661.

20 Shapiro, J. A.; Morrison, K. R.; Chodisetty, S. S.; Musaev, D. G.; Wuest, W. M. Biologically Inspired Total Synthesis of Ulbactin F, an Iron-Binding Natural Product. *Org. Lett.* **2018**, *20*, 5922-5926.

21 Li, W.; Estrada-de los Sntos, P.; Matthijs, S.; Zie, G-L.; Busson, R.; Cornelis, P.; Roenski, J.; De Mot, R. Promysalin, a Salycylate-Containing *Pseudomonas putida* Antibiotic, Promotes Surface Colonization and Selectively Targets Other *Pseudomonas*. *Chem. Biol.* **2011**, *18*(10), 1320-1330.

22 Steele, A. D.; Knouse, K. W.; Keohane, C. E.; Wuest, W. M. Total Synthesis and Biological Investigation of (-)-Promysalin. *J. Am. Chem. Soc.* **2015**, *137*(23), 7314-7317.

23 Steele, A. D.; Keohane, C. E.; Knouse, K. W.; Rossiter, S. E.; Williams, S. J.; Wuest, W. M. Diverted Total Synthesis of Promysalin Analogs Demonstrates that an Iron-Binding Moif is Responsible for Its Narrow-Spectrum Antibacterial Activity. *J. Am. Chem. Soc.* **2016**, *138*(18), 5833-5836.

24 Keohane, C. E.; Steele, A. D.; Fetzer, C.; Khowsathis, J.; Van Tyne, D.; Moynié, L.; Gilmore, M. S.; Karanicolas, J.; Sieber, S. A.; Wuest, W. M. Promysalin Elicits Species-Selective Inhibition of *Pseudomonas Aeruginosa* by Targeting Succinate Dehydrogenase. *J. Am. Chem. Soc.* **2018**, *140*(5), 1774-1782.

25 Post, S. J.; Keohane, C. E.; Rossiter, L. M.; Kaplan, A. R.; Khowsathis, J.; Matuska, K.; Karanicolas, J.; Wuest, W. M. Target-Based Design of Promysalin Analogues Identifies a New Putative Binding Cleft in Succinate Dehydrogenase. *ACS. Infect. Dis.* **2020**, *6*(6), 1372-1377.

26 Serino, L.; Reimmann, C.; Visca, P.; Beyeler, M.; Chiesa, V. D.; Haas, D. Biosynthesis of Pyochelin and Dihydroaeruginoic Acid Requires the Iron-Regulated *pch*DCBA Operon in *Pseudomonas aeruginosa*. *J. Bacteriol.* **1997**, *179*(1), 248-257.

27 Ronnebaum, T. A.; Lamb, A. L. Nonribosomal peptides for iron acquisition: pyochelin bioynthesis as a case study. *Curr. Opin. Struct. Biol.* **2018**, *53*, 1-11.

28 Ye, L.; Cornelis, L. Y. P.; Guillemyn, K.; Ballet, S.; Christopherson, C.; Hammerich, O. Structure Revision of *N*-Mercapto-4-formylcarbostyril Produced by *Pseudomonaas fluorescens* G308 to 2-(2-Hydroxyphenyl)thiazole-4-carbaldehyde [aeruginaldehyde]. *Nat. Prod. Commun.* **2014**, *9*(6), 789-794.

29 Mevers, E.; Saurí, J.; Helrich, E. J. N.; Henke, M.; Burns, K. J.; Bugni, T. S.; Andes, A.; Curris, C. R.; Clardy, J. Pyonitrins A-D: Chimeric Natural Products Produced by *Pseudomonas Protegens*. *J. Am. Chem. Soc.* **2019**, *141*(43), 17098–17101.

30 Lee, J. Y.; Moon, S. S.; Hwang, B. K. Isolation and Antifungal and Antioomycete Activities of Aerugine Produced by *Pseudomonas fluorescen*s Strain MM-B16. *Appl. Environ. Microbiol.* **2003**, *69*(4), 2023-2031.

31 Trottmann, F.; Franke, J.; Ishida, K.; García-Altares, M.; Hertweck, C. A Pair of Bacterial Siderophores Releases and Traps an Intercellular Signal Molecule: An Unusual Case of Natural Nitron Bioconjugation. *Angew. Chem. Int. Ed.* **2019**, *58*(1), 200-204.

32 Elliott, G. T.; Kelly, K. F.; Bonna, R. L; Wardlaw, T. R.; Burns, E. R. In vitro antiproliferative activity of 2'-(2-hydroxyphenyl)-2'-thiazoline-4'-carboxylic aci and its methyl ester on L1210 and P388 murine neoplasms. *Cancer. Chemother. Pharmacol.* **1988**, *21* (18), 233-236.

33 Carmi, R.; Carmeli, S. (+)-(*S*)-dihydroaeruginoic Acid, an Inhibitor of *Septori tritici* and other phytopathogenic fungi and bacteria, produced by *Pseudomonas fluorescens*. *J. Nat. Prod.* **1994**, *57*(9),1200-1205.

34 Yamada, Y.; Seki, N.; Kitahara, T.; Takahashi, M.; Matsui, M. PThe Structure and Synthesis of Aeruginoic Acid (2-*o*-Hydroxy-phenylthiazole-4-carboxylic Acid). *Agr. Biol. Chem.* **1970**, *34*(5), 780-783.

35 Yang, W.; Dostal, L.; Rosazza, J. P. N. Aeruginol {2-(2'-hydroxyphenyl)-4-hydroxymethylthiazole}, a New Secondary Metabolite from *Pseudomonas aeruginosa*. *J. Nat. Prod.* **1993**, *56*(11), 1993-1994.

36 Bukovits, G. J.; Mohr, N.; , M.; Budzikiewicz, H, Korth, H.; Pulverer, G. 2-Phenylthiazol-Derivate aus *Pseudomonas cepacia. Zeitschrift.fur. Naturforschung.* **1982**, *37b*, 877-880.

37 Fakhouri, W.; Walker, F.; Vogler, B.; Armbruster, W.; Buchenauer, H.. Isolation and identification of *N*-mercapto-4-formylcarbostyril, an antibiotic produced by *Pseudomonas fluorescens*. *Phytochemistry.* **2001**, *58*(8), 1297-1303.

38 Lee, J.; Wu, J.; Deng, Y.; Wang, J.; Wang, C.; Wang, J.; Chang, C.; Dong, Y.; Williams, P.; Zhang, L-H. A cell-cell communication signal integrates quorum sensing and stress response. *Nat. Chem. Biol.* **2013**, *9*(5), 339-343.

39 Cornelis, P. Putting an end to the *Pseudomonas aeruginosa* IQS controversy. *MicrobiologyOpen.* **2019**, *9*(2), 1-2.

40 Lacerna II, N. M.; Miller, B. W.; Lim, A. L.; Tun, J. O.; Robes, J. M. D.; Cleofas, M. J. B.; Lin, Z.; Salvador-Reyes, L. A.; Haygood, M. G.; Schmidt, E. W.; Concepcion, G. P. Mindapyrroles A-C, Pyoluteorin Analogues from a Shipworm-Associated Bacterium. *J. Nat. Prod.* **2019**, *82*(4), 1024-1028.

41 Hammer, P. E.; Hill, D. S.; Lam, S. T.; Van Pée, K-H, Ligon, J. Four Genes from *Pseudomonas fluorescens* That Encode the Biosynthesis of Pyrrolnitrin. *Appl. Environ. Microbiol.* **1997**, *63*(6), 2147-2154.

42 Shingare, R. D.; Aniebok, V.; Lee, H-W.; MacMillan, J. B. Synthesis and Investigation of the Abiotic

Formation of Pyonitrins A-D. *Org. Lett.* **2020**, *22*(4), 1516-1519.

43 Reimmann, C.; Serino, L.; Beyeler, M; Haas, D, Dihydroaeruginoic acid synthetase and pyochelin synthetase, products of the *pchEF* genes, are induced by extracellular pyochelin in *Pseudomonas aeruginosa*. *J. Microbiology.* **1998**, *144*(11),3135-3148.

44 Maspoli, A.; Wenner, N.; Mislin, G. L. A.; Reimmann, C. Functional analysis of pyochelin-/enantiopyochelin-related genes from a pathogenicity island of *Pseudomonas aeruginosa* strain PA14. *Biometals.* **2014**, *27*(3), 559-573.

45 Mislin, G. L. A.; Hoegy, F.; Cobessi, D.; Poole, D. R.; Schlk, I. J. Binding Properties of Pyochelin and Structurally Related Molecules to FptA of *Pseudomonas aeruginosa*. *J. Mol. Biol.* **2006**, *357*(5), 1437-1448.

46 Ahmadi, M. K.; Fawaz, S.; Jones, C. H.; Zhang, G.; Pfeier, B. A. Total Biosynthesis and Diverse Applications of the Nonribosomal Peptide-Polyketide Siderophore Yersiniabactin. *Appl. Environ. Microbiol.* **2015**, *81*(16), 5290-5298.

47 Ohlemacher, S. I.; Giblin, D. E.; d'Avignon, D. A.; Stapleton, A. E.; Trautner, B. W.; Henderson, J. P. Enterobacteria secrete an inhibitor of *Pseudomonas* virulence during clinical bacteriuria. *J. Clin. Invest.* **2017**, *127*(11), 74018-4030.

48 Zamri, A.; Abdallah, A. An Improved Stereocontrolled Synthesis of Pyochelin, Siderophore of *Pseudomonas aeruginosa* and *Burkholderia cepacia*. *Tetrahedron.* **2000**, *56*(2), 249-256.

49 Noël, S.; Guillon, L.; Schalk, I. J.; Mislin, G. L. A. T. Synthesis of Fluorescent Probes Based on the Pyochelin Siderophore Scaffold. *Org Lett.* **2011**, *13*(5), 844-847.

50 Morrison, M. D.; Hanthorn, J. J.; Pratt, D. A. Synthesis of Pyrrolnitrin and Related Halogenated Phenylpyrroles. *Org Lett.* **2009**, *11*(5), 1051-1054.

51 Braud, A.; Hannauer, M.; Mislin, G. L. A.; Schalk, I. J. The *Pseudomonas aeruginosa* Pyochelin-Iron Uptake Pahway and Its Metal Specificity. *J. Bacteriol.* **2009**, *191*(11), 3517-3525.

52 Bohac, T. J.; Shapiro, J. A.; Wencewicz, T. A. Rigid Oxazole Acinetobactin Analog Blocks Siderophore Cycling in *Acinetobacter baumannii*. *ACS. Infect. Dis.* **2017**, *3*, 802-806.

53 Bohac, T. J.; Fang, L.; Giblin, D. E.; Wencewicz, T. A. Fimsbactin and Acinetobactin Compete for the Periplasmic Siderophore Binding Protein BauB in Pathogenic *Acinetobacter baumannii*. *ACS. Chem. Biol.* **2019**, *14*, 674-687.

54 Bohac, T. J.; Fang, L.; Banas, V. S.; Giblin, D. E.; Wencewicz, T. A. Synthetic Mimics of Native Siderophores Dirsupt Iron Trafficking in *Acinetobacter baumannii*. *ACS. Infect. Dis.* **2021**, *7*, 2138-2151.

55 Cox, C. D.; Graham, R. Isolation of an Iron-Binding Compound from *Pseudomonas aeruginosa*. *J. Bacteriol.* **1979**, *137*(1), 357-364.

56 Schlegel, K.; Lex, J.; Taraz, K.; Budzikiewicz, H. The X-Ray Structure of the Pyochelin Fe^{3+} Complex. *Z. Naturforsch. C. J. Biosci.* **2006**, *61*(3-4), 263-266.

57 Tseng, C-F.; Burger, A.; Mislin, G. L. A.; Schalk, I. S.; Yu, S. S-F.; Chan, S. I.; Abdallah, M. A. Bacterial siderophores: the solution stoichiometry and coordination of the Fe(III) complexes of pyochelin and related compounds. *J. Biol. Inorg. Chem.* **2006**, *11*, 419-432.

58 Cornelis, P.; Dingemans, J. *Pseudomonas aeruginosa* adapts its iron uptake strategies in function of the type of infections. *Front. Cell. Infect. Microbiol.* **2013**, *3*(75), 1-7.

59 Cheng, A. V.; Wuest, W. M. Signed, Sealed, Delivered: Conjugate and Prodrug Strategies as Targeted Delivery Vectors for Antibiotics. *ACS. Infect. Dis.* **2019**, *5*(6), 816-828.

60 Zhanel, G. G.; Golden, A. R.; Zelenitsky, S.; Wiebe, K.; Lawrence, C. K.; Adam, H. J.; Idow, T.; Domalaon, R.; Schweizer, F.; Zhanel, M. A.; Lagacé-Wiens, P. R. S.; Walkty, A. J.; Noreddin, A.; Lynch Iii, J. P.; Karlowsky, J. A. Cefiderocol: A Siderophore Cephalosporin with Activity Against Carbepenem-Resistant and Multidrug-Resistant Gram-Negative Bacilli. *Drugs.* **2019**, *79*(3), 271-289.

61 Boyce, J. H, Dang, B.; Ary, B.; Edmonson, Q.; Craik, C. S.; DeGrado, W. F.; Seiple, I. B. Platform to Discover Protease-Activated Antibiotics and Application to Siderophore-Antibiotic Conjugates. *J. Am. Chem. Soc..* **2020**, *142*(51), 21310-21321.

62 Li, L. B.; Dan, W. J.; Tan, F. F.; Cui, L. H.; Yuan, Z. P.; Wu, W. J.; Zhang, J. W. Synthesis and Antibacterial Activities of Yanglingmycin Analogues. *Chem. Pharm. Bull.* **2015**, *63*, 33-37.

63 Phillips, A. J.; Uto, Y.; Wipf, P.; Reno, M. J.; Williams, D. R. Synthesis of Functionalized Oxazolines and Oxazoles with DAST and Deoxo-Fluor. *Org. Lett.* **2000**, *2*, 1165-1168.

64 Moraski, G. C.; Chang, M.; Villegas-Estrada, A.; Franzblau, S. G.; Möllmann, U.; Miller, M. J. Structure-activity relationship of new anti-tuberculosis agents derived from oxazoline and oxazole benzyl esters. *Eur. J. Med. Chem.* **2010**, *45*, 1703-1716.

65 Wong, D.; Nielsen, T. B.; Bonomo, R. A.; Pantapalangkoor, P.; Luna, B.; Spellberg, B. Clinical and pathophysiological overview of *Acinetobacter* infections: A century of challenges. *Clin. Microbiol. Rev.* **2017**, *30*, 409-447.

66 Yamamoto, S.; Okujo, N, Sakakibara, Y. Isolation and structure eludication of acinetobactin., a novel siderophore from *Acinetobacter baumannii*. *Arch. Microbiol.* **1994**, *162*, 249-254.

67 Penwell, W. F.; Degrace, N.; Tentarelli, S.; Gauthier, L.; Gilbert, C. M.; Arivett, B. A.; Miller, A. A.; Durand Reville, T. F.; Joubran, C.; Actic, L. A. Discovery and characterization of new hydroxamate siderophores, baumannoferrin A and B, produced by *Acinetobacter baumannii*. *ChemBioChem.* **2015**, *16*, 1896-1904.

68 Proschak, A.; Lubata, P.; Grün, P.; Löhr, F.; Wilharm, G.; De Berardinis, V.; Bode, H. B. Structure and biosynthesis of fimsbactins A-F, siderophores from *Acinetobacter baumannii* and *Acinetobacter baylyi*. *ChemBioChem.* **2013**, *14*, 633-638.

69 Shapiro, J.; Wencewicz, T. A. Acinetobactin Isomerization Enables Adaptive Iron Acquisition in *Acinetobacter baumannii* through pH-Triggered Siderophore Swapping. *ACS Infect. Dis.* **2016**, *2*, 157-168.

70 Sattely, E. S.; Walsh, C. T. J. A Latent Oxazoline Electrophile for N-O-C Bond Formation in Pseudomonine Biosynthesis. *J. Am. Chem. Soc.* **2008**, *130*, 12282-12284.

71 Wuest, W. M. Sattely, E. S.; Walsh, C. T. J. Three siderophores from one bacterial enzymatic assembly line. *J. Am. Chem. Soc.* **2009**, *131*, 5056-5057.

72 Takeuchi, Y.; Ozaki, S.; Sato, M.; Mimura, K.; Hara, S.; Abe, H.; Nishioka, H.; Harayama, T. Synthesis of Acinetobactin. *Chem. Pharm. Bull.* **2010**, *58*, 1552-1553.

73 Moynié, L.; Serra, I.; Scorciapino, M. A.; Oueis, E.; Page, M. G. P.; Ceccarelli, M.; Naismith, J. H. Preacinetobactin not acinetobactin is essential for iron uptake by the BauA transporter of the pathogen *Acinetobacter baumannii*. *eLife.* **2018**, *7*, 42270-42285.

74 Hamidian, M.; Nigro, S. J. Emergence, molecular mechanisms and global spread of carbapenem-resistant *Acinetobacter baumannii*. *Microb. Genomics.* **2019**, *5*, e000306.

75 Clark, N. M.; Zhanel, G. G.; Lynch, J. P. Emergence of antimicrobial resistance among *Acinetobacter* species: A global threat. *Curr. Opin. Crit. Care.* **2016**, *22*, 491-499.

76 Press WHO. Global priority list of antibiotic-resistant bacteria to guide research, discovery, and development of new antibiotics. Geneva: World Health Organization.

77 CDC. Antibiotic resistance threats in the Untied States. Atlanta, Georgia.

4. Investigation of Quaternary Ammonium Compounds (QACs)

4.1. (Methicillin-Resistant) *Staphylococcus aureus* and Prevention of Infections

As discussed in Chapter 1, (methicillin-resistant) *Staphylococcus aureus* infections are an becoming increasingly difficult to treat, with one major contributing factor being the lifespan of this highly infective pathogen on a range of commonly used surfaces including but not limited to countertops, furniture, and razors.[1] Further, any contact but particular of open wounds with these surfaces can lead to serious MRSA infections if they are not disinfected properly. Some particularly prevalent areas where these infections can spread quite rapidly are various public places, especially athletic and laundry facilities, which often harbor infectious material like blood or puss. Healthcare settings are also highly populated with this surface-born bacteria, creating the threat of bacterial coinfection of immunocompromised patients.[1] Therefore, if we can develop effective disinfecting agents, we can prevent these infections from occurring in the first place, and significantly decrease the number of avoidable serious MRSA infections as well as exposure of this microbe to first-line antibiotics. It is also worth highlighting again the importance of preventative antimicrobial measures in recent years, as increased fatality rates in Covid-19 patients were directly correlated with bacterial coinfection.[2,3] To this end, our lab has been heavily involved in this area of research for the past decade, with efforts increasing recently due to the emergence of the Covid-19 pandemic.

4.2. QAC Background

One class of antimicrobial compounds that show significant promise with respect to surface disinfection are called quaternary ammonium compounds QACs, which are a class of cationic amphiphilic small molecules. Structurally, they are characterized by the presence of at least one cationic nitrogen combined with a significant amount of aliphatic character (Fig. 4.02).[4-6] Their amphiphilic scaffolds lend themselves to several favorable physiochemical properties, giving them a tremendous amount of utility in a variety of products including cationic surfactants, detergents, preservatives, soaps, hair care products, cosmetics, biological stains and dyes, and of particular interest to our lab, in antimicrobials.[6-10] In fact, QACs are found in leading antiseptics in residential, commercial, healthcare, industrial, and agricultural contexts dating as far back as 1916 when their bactericidal activity was first reported.[5,11-13] Additional advantages to QAC usage includes their relatively low toxicity and their structural simplicity, which makes their production particularly facile. Figure 4.01 shows the structures of four common commercial QACs: benzalkonium chloride (BAC), cetylpyridinium chloride (CPC), cetyltrimethylammonium bromide (CTAB), and dialkyldimethylammonium chloride (DDAC), all of which had played a significant role in the disinfection of surfaces in a range of settings.[5]

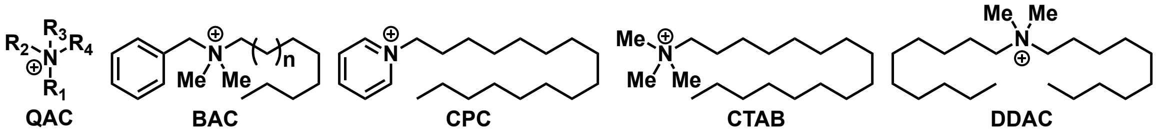

Figure 4.01. Structure of generic QAC and commercial QACs.[5]

Mechanistically, these compounds are thought to act by depolarizing the cell membrane surface via electrostatic interactions between the membrane’s negatively charged phosphate head and positively charged QAC nitrogen. This interaction allows the aliphatic tail(s) to then intercalate into the membrane and interact with the phospholipid lipid tails. Cell death can then result from one of two pathways; either multiple molecules will interact independently with the membrane resulting in the disruption of ion gradients or alternatively they will form aggregates in the membrane causing cell components to leak or pores to form ultimately causing the cell to lyse (Fig. 4.02).[14,15] This membrane-targeting mechanism renders QACs a particularly promising class of disinfecting antimicrobials as their unbiased action ensures that all surface-born bacterial cells including MRSA will be eradicated. It should be noted that QACs can accumulate in the environment due to their relatively low reactivity and hence their high stability. Bacteria in the environment are thus regularly exposed to sublethal doses of QACs, which can promote the development of resistance genes.[16,17]

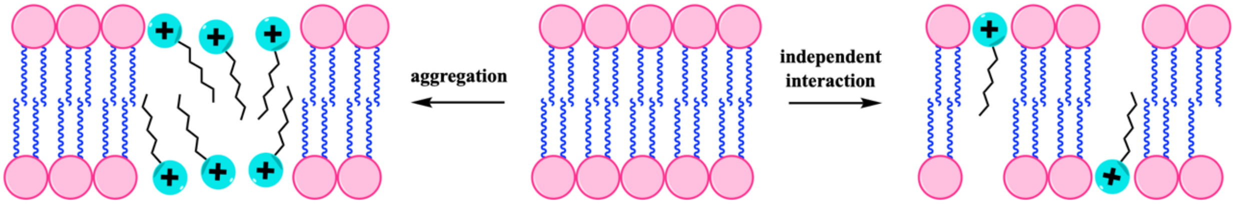

Figure 4.02. Schematic representation of QAC mechanisms of action.[14,15]

4.2.1.Previous Work

As previously mentioned, the design, synthesis, and biological evaluation of QACs has been extensively studied over the last century. Polymeric QACs, or polyQACs, have been used as polymer coatings for medical devices like catheters.[18] Some groups have looked to repurpose known antibiotics like vancomycin and polymyxin B as QACs giving them an additional antibacterial mechanism of action, therefore enhancing their versatility.[17,19-21] Other groups have designed QACs containing easily cleavable amide or ester groups to minimize bioaccumulation and unnecessary exposure to bacteria, thus the risk of acquiring resistance.[22-26]

4.2.1.1. Natural Product Inspired QACs

Interestingly, natural products have also been investigated as QACs (Fig. 4.03). In some cases, the natural product contains a positively charged quaternary nitrogen in the scaffold, as is the case with berberine.[27] In other cases, the natural product contains a latent QAC moiety via resonance and/or pH changes instead of the permanent positively charged nitrogen, as is the case with batzelladine K.[5,28] All of these compounds demonstrated a high degree of antimicrobial activity through QAC-like mechanisms.

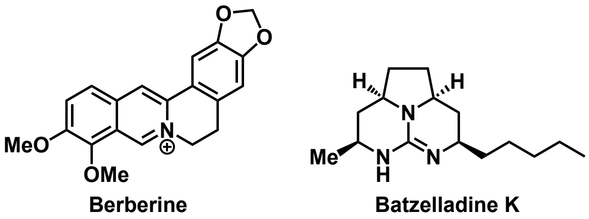

Figure. 4.03. Structures of natural product QACs.[27,28]

To this end, I was inspired to design several series of QACs based off of these two concepts (Fig. 4.04). A series of tricepyridinium-inspired QACs were recently synthesized and evaluated by Wuest lab members undergraduate Michelle Garrison and her graduate mentor Andrew Mahoney.[29,30] Another series currently being synthesized by another Wuest lab undergraduate, Caroline McCormack, are the uncharged and quaternized versions of ianthelliformisamines A-C, with the hypothesis that quaternizing the amine nitrogens of these antimicrobial efflux pump inhibitors will render these QAC analogs both more potent than the natural products as well as less prone to QAC resistance mechanisms.[31] Finally, I was intrigued by the scaffold of the haliclocyclins, which will be discussed in greater detail in sections 4.3-4.7.[32,33]

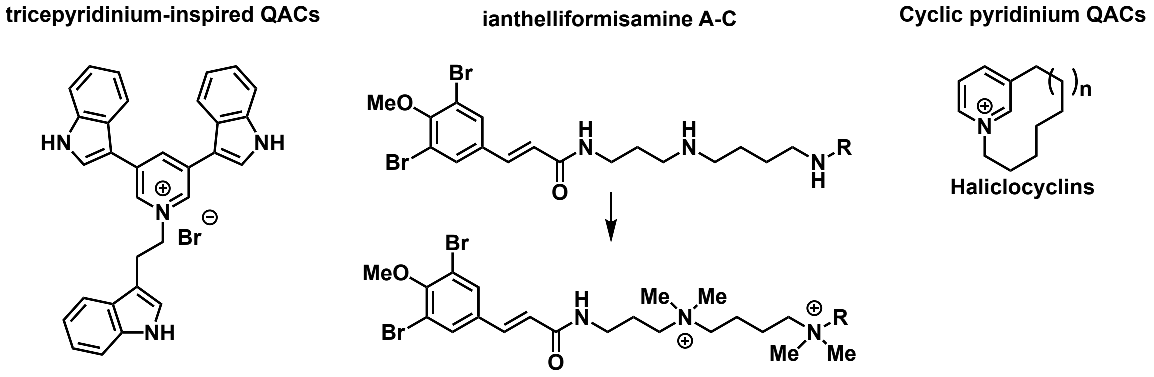
tricepyridinium-inspired QACs

ianthelliformisamine A-C

Cyclic pyridinium QACs

Figure 4.04. Structures of natural product-inspired QACs.[29-33]

4.2.2. Wuest and Minbiole

Since 2014, the Wuest and Minbiole labs have been involved in a collaborative investigation of QACs particularly with respect to their design and structural optimization(Fig. 4.05). Much of the initial work involved designing QACs containing a core structure based on *N.N.N'N'*-tetraethylethylenediamine (TMEDA) and confirming previously established trends associated with alkyl chain length and the number of quaternary centers.[34,35] To this end, a series of monoQACs and bisQACs varying in alkyl chain length and a series of bis-, tris-, and tetraQACs were synthesized and evaluated. Linker length between cationic nitrogens on the bisQACs was also evaluated. TMEDA-12,12 was ultimately identified as the optimized QAC structure from these series and is now used as a positive control in our QAC assays.[36,37] Other series included hybrid QACs combining aspects of BAC and CPC into one QAC as well as amide hybrid QACs to address the previously mentioned issue of bioaccumulation leading to resistance.[38,39]

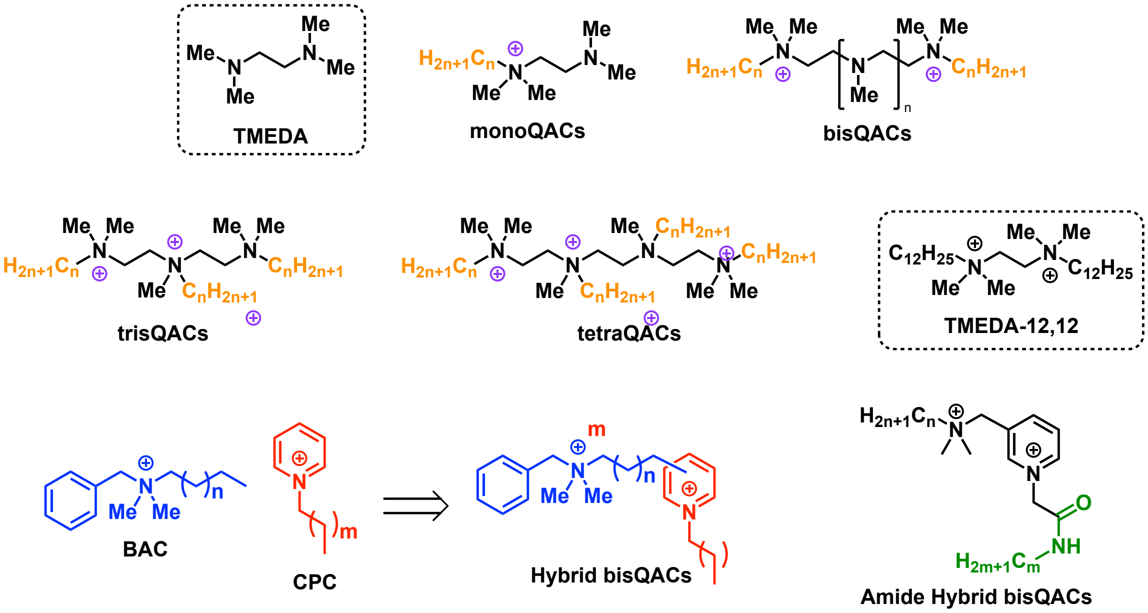
TMEDA
monoQACs
bisQACs
trisQACs
tetraQACs
TMEDA-12,12
BAC
CPC
Hybrid bisQACs
Amide Hybrid bisQACs

Figure 4.05. Summary of initial QAC series synthesized and evaluated by Wuest and Minbiole.[34-39]

4.2.3.Rigidity-Activity QAC Series

Kontos, R. C.; Schallenhammer, S. A.; Bentley, B. S.; Morrison, K. R.; Feliciano, J. A.; Tasca, J. A.; **Kaplan, A. R**.; Bezpalko, M. W.; Kassel, W. S.; Wuest, W. M. Minbiole, K. P. C. An Investigation into Regidity–Activity Relationships in BisQAC Amphiphilic Antiseptics. *ChemMedChem.* **2019**, *14*(1), 83-87. https://doi.org/10.1002/cmdc.201800622

In this work, we sought to investigate the influence of structural rigidity on the biological activity of QACs. The hypothesis at the onset of this work was that the conformational flexibility of QACs would enable them to more easily embed into and disrupt bacterial membranes, making them more active than their more rigid counterparts. To this end, a series of QACs were synthesized (for synthetic details see the reference listed above) with increased conformational rigidity compared to the TMEDA bisQAC, **TMEDA-12,12**. This series included piperazine alkyl and amide bisQACs, as well as DABCO bisQACs (Fig. 4.06).

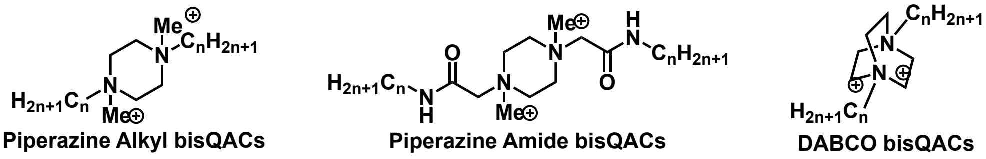
Piperazine Alkyl bisQACs
Piperazine Amide bisQACs
DABCO bisQACs

Figure 4.06. General structures of QACs synthesized in the rigidity-activity series.

Kelly Morrison and I evaluated the antimicrobial activity as well as the toxicity of these compounds using MIC and red blood cell lysis assays, respectively (Table 4.01). To our surprise, the activity trend was the opposite of what we predicted; structural rigidity actually enhanced activity. We rationalized this result by postulating that the rigidity of these molecules forces the alkyl side chains and quaternized amines into a conformation optimized for anchoring and embedding in the bacterial membrane.

Table 4.01. Antimicrobial activity and red blood cell lysis activity of rigidity-activity bisQAC series.

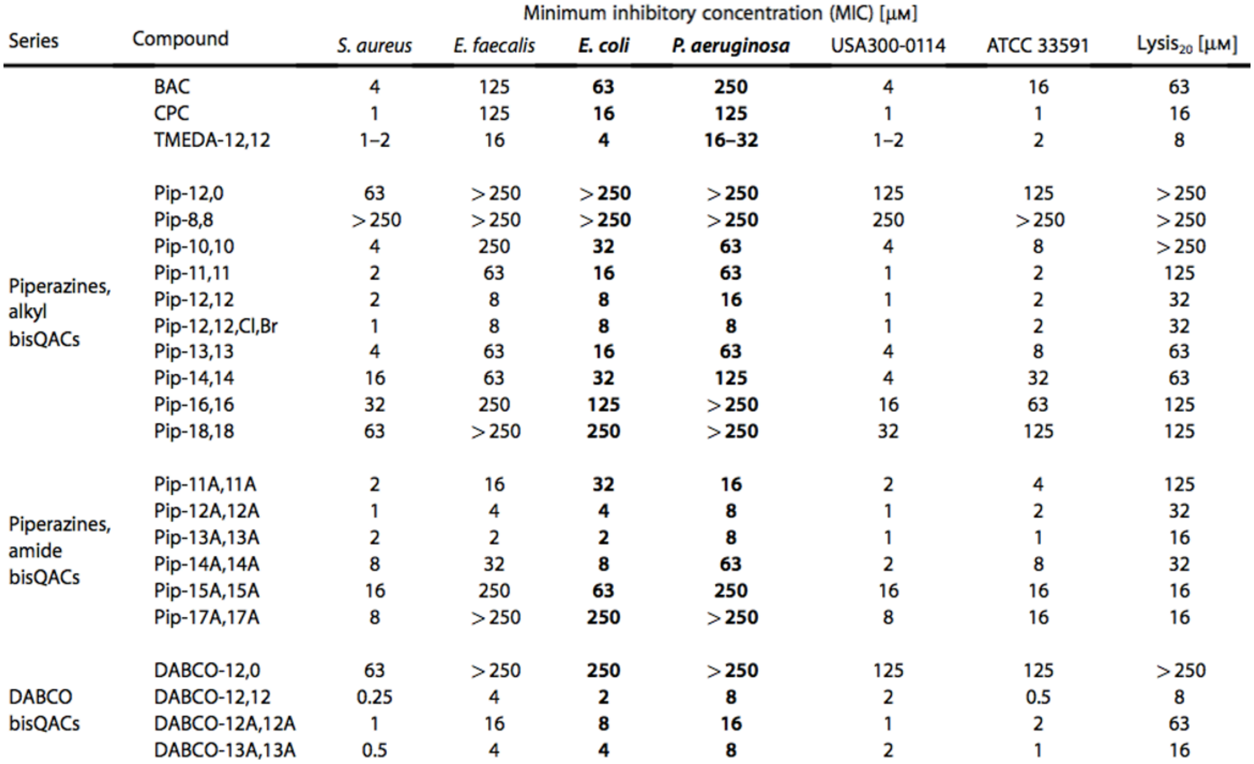

Series	Compound	Minimum inhibitory concentration (MIC) [µM]						
		S. aureus	*E. faecalis*	***E. coli***	***P. aeruginosa***	USA300-0114	ATCC 33591	Lysis_{20} [µM]
	BAC	4	125	**63**	**250**	4	16	63
	CPC	1	125	**16**	**125**	1	1	16
	TMEDA-12,12	1–2	16	**4**	**16–32**	1–2	2	8
Piperazines, alkyl bisQACs	Pip-12,0	63	>250	**>250**	**>250**	125	125	>250
	Pip-8,8	>250	>250	**>250**	**>250**	250	>250	>250
	Pip-10,10	4	250	**32**	**63**	4	8	>250
	Pip-11,11	2	63	**16**	**63**	1	2	125
	Pip-12,12	2	8	**8**	**16**	1	2	32
	Pip-12,12,Cl,Br	1	8	**8**	**8**	1	2	32
	Pip-13,13	4	63	**16**	**63**	4	8	63
	Pip-14,14	16	63	**32**	**125**	4	32	63
	Pip-16,16	32	250	**125**	**>250**	16	63	125
	Pip-18,18	63	>250	**250**	**>250**	32	125	125
Piperazines, amide bisQACs	Pip-11A,11A	2	16	**32**	**16**	2	4	125
	Pip-12A,12A	1	4	**4**	**8**	1	2	32
	Pip-13A,13A	2	2	**2**	**8**	1	1	16
	Pip-14A,14A	8	32	**8**	**63**	2	8	32
	Pip-15A,15A	16	250	**63**	**250**	16	16	16
	Pip-17A,17A	8	>250	**250**	**>250**	8	16	16
DABCO bisQACs	DABCO-12,0	63	>250	**250**	**>250**	125	125	>250
	DABCO-12,12	0.25	4	**2**	**8**	2	0.5	8
	DABCO-12A,12A	1	16	**8**	**16**	1	2	63
	DABCO-13A,13A	0.5	4	**4**	**8**	2	1	16

In conclusion, our investigation of a series of QACs ranging in structural rigidity revealed that the more structurally rigid QACs are more active than their less rigid counterparts. In fact, a 180° angle of separation of the alkyl chains appeared to lend itself to greater antimicrobial activity. To further probe this rigidity-activity relationship, an additional series of pyridine alkyl and amide bisQACs with varied two-carbon linker geometries were investigated (Fig. 4.07).[40] In contrast to the original rigidity-activity series, this acvitiy of this series demonstrated the opposite trend, wherein bisQACs containing more rigid linkers were less active and bisQACs containing less rigid linkers were more active. With these somewhat confusing results, I decided to evaluate another series of pyridine-based QACs detailed further in sections 4.3-4.7.

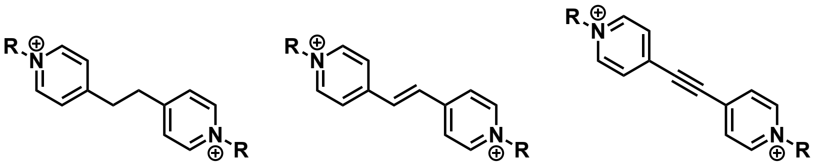

Figure. 4.07. General structures of pyridine alkyl and amide bisQACs with alkane, alkene, and alkyne linkers.[40]

4.3. 3-Alkylpyridine Alkaloids (3-APAs)

It is well known within the scientific community that marine alkaloids are a class of small molecules with unique and interesting molecular scaffolds, often posing challenges to synthetic chemists. Commonly isolated from sponges, these natural products often possess a range of promising biological activity including anticancer and antimicrobial.[41] The *Haliclona* sponges are a highly abundant source of one particular subset of these alkaloids known as 3-alkylpyridine alkaloids (3-APAs). Structurally, these compounds contain at least one pyridinium or tetrahydropyridine moiety, which is typically alkylated at the 1- and/or 3- positions.[42] Some of the more structurally complex examples of these compounds include methylaruguspongine C, halicyclamine A, sarain-1, and manzamine A (Fig. 4.08).[43-46] The biosynthetic and structural diversity of 3-APAs produced by these sponges is well studied in tropical waters. However, differing levels of predation and thus the need to produce chemical defenses in more temperate regions such as that arctic have left the biosynthetic landscape of *Haliclona* sponges in these regions underexplored.[42,47]

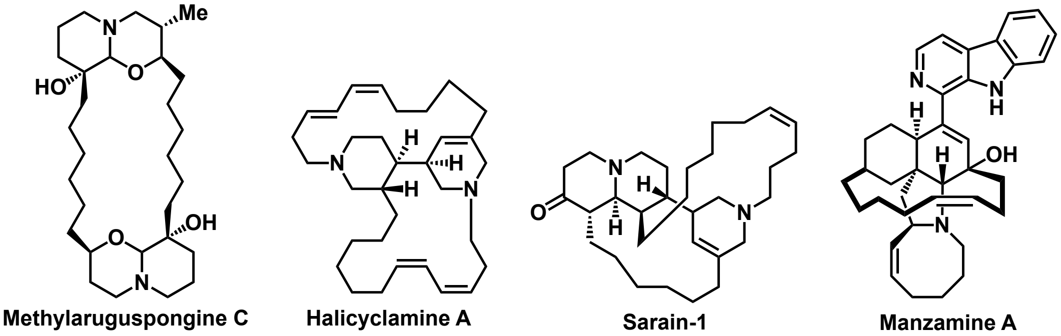

Figure 4.08. Structures of 3-APAs isolated from *Haliclona* sp.

4.3.1.Arctic 3-APAs

One artic sponge that has received a modest amount of attention for its production of 3-APAs is *Haliclona viscosa*. To date, five classes have been isolated; haliclocyclins, cyclostellettamines, haliclamines, viscosamines, and viscosalines (Fig. 4.10).[32,33,48-55] Structurally, these classes differ from each other by the number of pyridines in the scaffold and the oxidation state of said pyridine, while members of each class differ only by the length of the alkyl chain. Interestingly, members of the cyclostellettamine and haliclamine classes closely resemble a common intermediate used in the synthesis of previously mentioned manzamine A and halcyclamine A.[56]

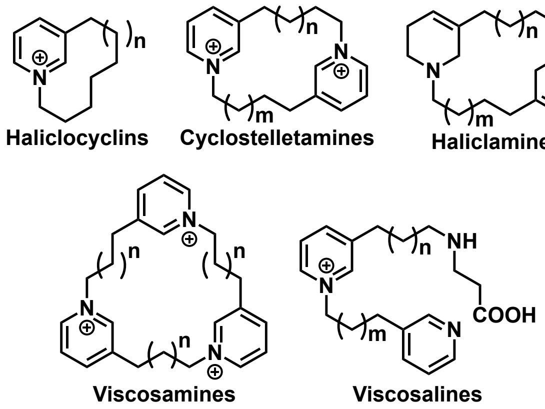

Figure. 4.09. Structures of the five classes of 3-APAs isolated from *Haliclona viscosa*.

4.3.2.Previous Biological and Synthetic Investigations

While these classes of 3-APAs are more structurally simple compared to those shown in figure 4.08, they still possess a comparably broad range of preliminary bioactivity, including epidermal growth factor inhibition, muscarinic acetylcholine receptor antagonistic activity, mouse embryonic fibroblast cytotoxicity, and most importantly, antimicrobial activity.[32,42,57,58] Unfortunately, the extent of these studies were quite limited primarily due to challenges in isolating sufficient quantities of material from the producing organisms, as these sponges are under far less pressure to produce their chemical defense molecules in the much more sparsely populated arctic waters.[47] Moreover, the disc diffusion assays used to evaluate the antimicrobial activity of a small subset of these 3-APAs have since been found to have limited accuracy with cationic compounds due to their slower rates of diffusion through agar.[59]

In addition to a complete lack of material available by isolation, the synthetic studies by other groups involved a fairly lengthy route hinging on the use of a common intermediate, **A**, for the construction of all five 3-APA classes (Scheme 4.01).[32,52,57-62] A total of six transformations are required to convert the starting diacids to **A**, employing both harsh reaction conditions and protection of the primary alcohol for the harsh picoline alkylation step. With this in mind, we wondered if we could perhaps design a more efficient route to **A**, thereby enabling a more streamlined synthesis of any of the five classes of these 3-APAs.

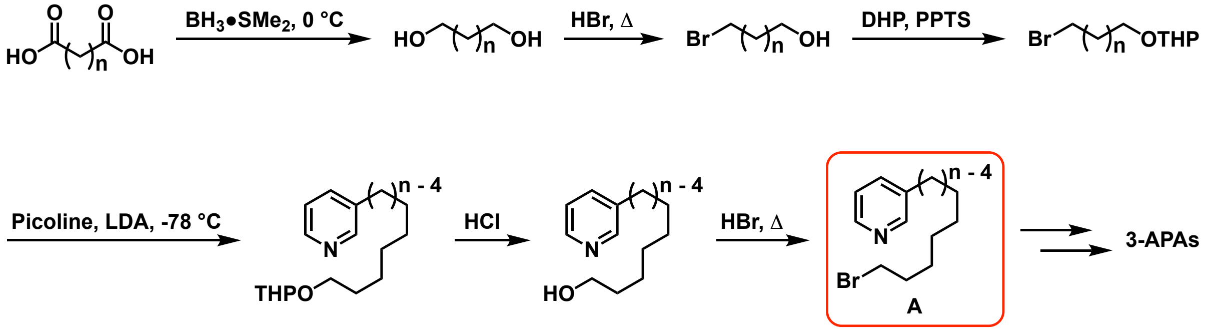

Scheme 4.01. Synthetic route previously employed to access common intermediate **A**.[32,52,57-62]

4.4. Haliclocyclins as QACs

Kaplan, A. R.†.; Schrank, C. L.†.; Wuest, W. M. An Efficient Synthesis of 3-Alkylpyridine Alkaloids Enables Their Biological Evaluation. *ChemMedChem.* **2021**, *16*(16), 2487-2490. https://doi.org/10.10002/cmdc.202100134

Knowing that a small subset of 3-APAs displayed preliminary antimicrobial activity, we wondered if perhaps they were acting through the membrane perturbing mechanism by which QACs act. Additionally, the haliclocyclins are highly similar in structure to CPC, a QAC commonly found in commercial mouthwash with the only difference being the additional alkylation at the 3-position, giving them a macrocyclic conformation. Thus, we decided to synthesize a series of haliclocyclins varying in their aliphatic chain length to further expand on the rigidity-activity series by exploring the effect of macrocyclization on QAC activity.

4.5. Synthesis of Haliclocyclins

We envisioned that methodology recently developed by members of the Jui lab would enable access to desired 3-alkylated pyridine intermediate, **A**, in a single step (Scheme 4.02).[63-65] This process is completely regioselective for the anti-Markovnikov adduct and is tolerant of a wide range of functional groups with a broad scope of halopyridines and alkenes. This reaction was also applied to a modified synthesis of fluopyram, a commercial fungicide produced by Bayer.[65] In addition to decreasing the step count from six steps to one, these fairly mild photocatalytic conditions would also ablate the use of harsh reaction conditions or protecting groups.

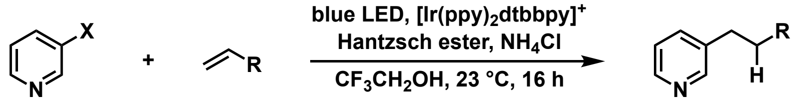

Scheme 4.02. Hydroarylation reaction developed by the Jui group.[63-65]

Synthesis of our nine-compound proof-of-principle macrocyclic pyridine QAC series started with hydroarylation of 3-iodopyridine with terminal bromoalkenes varying in length from 8-16 carbon atoms, affording the desired 3-alkylated adducts **4.05-4.13** (Scheme 4.03). Alkenes **4.01-4.04** were difficult to obtain through commercial sources and were synthesized in one step using a Grignard reaction between 4-pentylmagnesium bromide and corresponding dibromoalkane. We observed that a decrease in yield seemed to be correlated with an increase in alkene chain length. This was likely due to the decrease in solubility of these increasingly nonpolar alkenes. Addition of small amounts of toluene was found to slightly increase solubility in certain instances. However, we did not evaluate less polar solvents as the use of highly polar trifluoroethanol has been shown to be vital for reactivity as it likely functions as a Brönsted acid to give a protonated pyridinium radical intermediate.[64] These adducts were then cyclized using the previously reported Finklestein conditions giving **4.14-4.22** in modest to good yields.

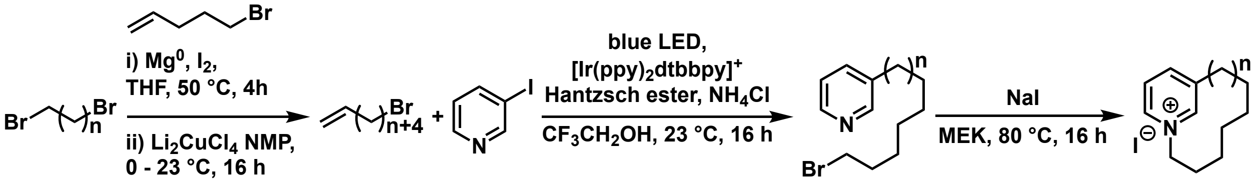

4.01: n = 7 (70%)
4.02: n = 8 (78%)
4.03: n = 9 (72%)
4.04: n = 10 (70%)

4.05: n = 2 (30%)
4.06: n = 3 (36%)
4.07: n = 4 (33%)
4.08: n = 5 (38%)
4.09: n = 6 (27%)

4.10: n = 7 (19%)
4.11: n = 8 (14%)
4.12: n = 9 (6%)
4.13: n = 10 (10%)

4.14: n = 2 (62%)
4.15: n = 3 (94%)
4.16: n = 4 (87%)
4.17: n = 5 (29%)
4.18: n = 6 (93%)

4.19: n = 7 (70%)
4.20: n = 8 (78%)
4.21: n = 9 (72%)
4.22: n = 10 (70%)

Scheme 4.03. Synthesis of haliclocyclins and analogs and corresponding yields.

4.6. Biological Evaluation of Haliclocyclins

With our library of compounds in hand, we then moved on to evaluating their antimicrobial activity, screening them against a panel of seven strains of bacteria, including the highly virulent oral pathogen, *Streptococcus mutans* (Table 4.02). In contrast to previous work on 3-APAs, we performed MIC assays, which are more compatible with this class of compounds than the previously mentioned disc-diffusion assays. These compounds were more active against Gram-positive bacteria, (methicillin-resistant) *S. aureus* and *S. mutans,* than they were against Gram-negative bacteria or *E. faecalis*, generally consistant with previous SAR. Additionally, an increase in activity was loosely correlated with increased aliphatic character, with the most active analog being **4.22** containing 16 aliphatic carbons. Because the best activity was observed at the end of the series, more aliphatic analogs may be necessary to determin the ideal chain length for this class of QACs.

Table 4.02. Minimum inhibitory concentration (MIC) and red blood cell hemolysis (Lysis$_{20}$) values for **4.14-4.22** and positive controls CPC and BAC. CA = community acquired; HA = hospital acquired).

	MIC (µM)							Lysis$_{20}$ (µM)
Compound	*S. aureus*	CA-MRSA	HA-MRSA	*E. faecalis*	*E. coli*	*P. aeruginosa*	*S. mutans*	
4.14	32	32	32	64	32	64	64	2
4.15	32	32	16	64	32	64	125	0.25
4.16	32	32	16	64	32	64	32	0.5
4.17	32	32	32	64	64	64	125	0.125
4.18	32	32	16	125	125	125	64	8
4.19	16	16	8	125	32	125	16	4
4.20	32	32	16	250	64	250	32	16
4.21	32	16	16	250	64	250	32	16
4.22	8	8	8	125	64	125	16	8
CPC	0.5	1	1	250	32	250	1	16
BAC	2	4	4	125	64	125	1	8

A red blood cell lysis assay was also performed to assess the toxicity, and therefore therapeutic potential of these compounds. Generally, these compounds displayed a fairly high toxicity profile as indicated by their low Lysis$_{20}$ values. This was not particularly surprising to us, as there were reports of cytotoxicity of certain 3-APAs against mouse embryonic fibroblasts.[5g] However, this high degree of cytotoxicity along with the diminished activity compared to CPC does leave room for structural optimization.

4.7. Conclusions and Further SAR Efforts

In our investigations of the haliclocyclins, we efficiently synthesized a library of these compounds varying in the number of macrocyclic aliphatic carbons in just two steps. Additionally, we found that these compounds exerted moderate antimicrobial activity against (methicillin-resistant) *S. aureus*, with a loose correlation between increasing activity and increasing aliphatic chain length, consistent with previous QAC SAR. Also consistent with previous QAC findings was the fact that these compounds were not active against Gram-negative bacteria. The data clearly indicated that COC is still the superior QAC, leaving room for improvement on the haliclocyclin scaffold. We therefore envision several ways to optimize this scaffold.

1. **Exchanging the iodine for a chlorine.** While this may not necessarily decrease the MIC with respect to molarity (µM) it would decrease the value with respect to overall mass (µg/mL). Since QAC compounds are commonly used in commercial settings, these analogs would decrease the overall mass of the compound necessary to kill microbes.
2. **Functionalizing the pyridine.** We imagined that it may be possible to decrease the toxicity of these compounds by appending various functional groups to the pyridyl ring. To this end, we decided to synthesize a series of four analogs with 4-methyl, -chloro, -amino, and -carboxy substituents and the 16-carbon chain length. Unfortunately, initial attempts to access these desired hydroarylation products were unsuccessful (Scheme 4.04). We instead isolated starting material and dehalogenated pyridine. The recovery of starting material can be rationalized primarily by the inherently diminished reactivity of 3-halopyridines compared to 2- and 4-halopyridines due to electronic differences. Further, the presence of dehalogenated pyridine is indicative of some reactivity of the starting 3-iodopyridine substrates but due to the low solubility of the 16-carbon alkene substrate, hydroarylation did not proceed in a productive fashion.

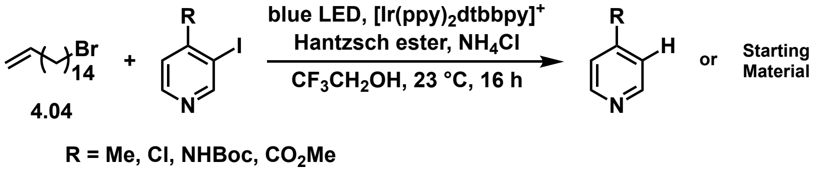

Scheme 4.04. Unsuccessful reactions between functionalized 3-iodopyridines and **4.04**.

To address both of these issues, we are looking to utilize alternative photochemical methods disclosed by the Jui group in 2021, wherein instead of relying on the iridium photocatalyst itself as the radical reductant, a more highly reducing carbon dioxide radical anion ($CO_2^{\bullet-}$) is generated from sodium formate (Scheme 4.05).[66] Not only will this address the issue of diminished reactivity of the 3-halopyridine, the solvent system may aid in solubilizing the longer and less polar alkenes.

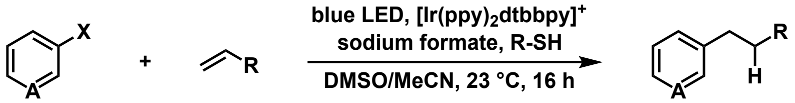

Scheme 4.05. Alternative photocatalytic conditions to access functionalized pyridine analogs.[6]

3. **Increase the number of hydrocarbons in the macrocycle.** Another factor to consider with these macrocyclic QACs is how their structure relates to the membrane-perturbing mechanism previously described. As shown in figure 4.10, CPC contains a 16-hydrocarbon chain which further through the hypothetical membrane drawn than the macrocyclic counterpart containing the same number of aliphatic carbons. Therefore, despite the fact that the aliphatic content is the same for both compounds, the macrocyclic compound may be less active because it cannot puncture as far through the membrane as CPC. Thus, it may be prudent to extend the hydrocarbon chain even in these macrocycles further to assess this hypothesis.

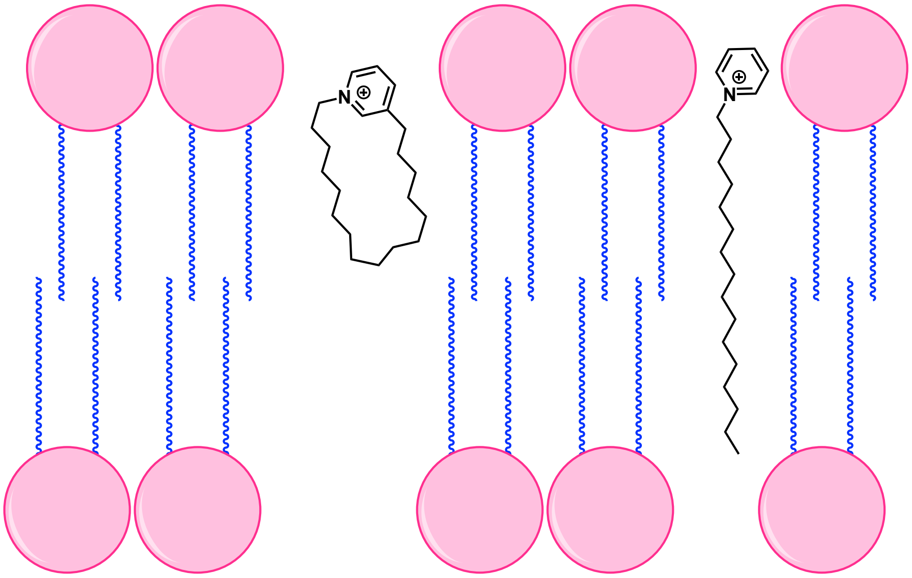

Figure 4.10. CPC and its macrocyclic counterpart interacting with a hypothetical cell membrane.

4. **2-alkylated haliclocyclins analogs**. Another proposed series of analogs hinges on addressing the issues of reactivity of 3-halopyridines and the macrocycle issue. By alkylating at the 2-position instead of the 3-position, the previously discussed issues with inherent reactivity may be mitigated. Additionally, by moving the position of alkylation closer to the pyridyl nitrogen, this may extend the reach of a macrocycle containing the exact same number of hydrocarbons, assuming there is no major conformational difference between these two macrocycles (Fig. 4.11)

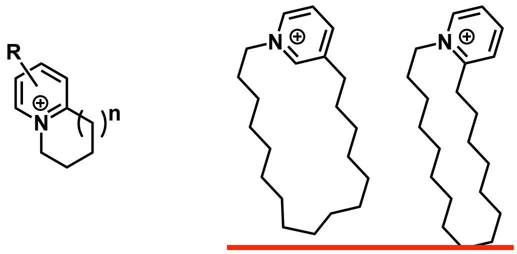

Figure 4.11. Structure of 2-APAs (left) and comparison of 3-APA and 2-APA aliphatic portion lengths.

5. **Change the order of reactions**. Another important factor to consider is the role of trifluoroethanol in the reaction. As previously mentioned, this solvent functions as a Brönsted acid to generate the 3-pyridinium radical species.[62] However, if the pyridyl nitrogen had a permanent positive charge, dramatically altering the polarity of the substrate, this particular solvent would no longer be necessary in the reaction. Thus, it would be possible to utilize a solvent system more accommodating to the highly nonpolar alkenes. Additionally, replacing trifluoroethanol with an eco-friendlier solvent would also be ultimately less taxing on the environment.

4.8. References

1 Cleaning and Disinfection. *Center for Disease Control and Prevention, National Center for Emergy Zoonotic Infectious Diseases (NCEZID), Division of Healthcare Quality Promotion (DHQP)*. 2019.

2 Protonotarious, E.; Mantzana, P.; Meletis, G.; Tychala, A.; Kassomenaki, A.; Vasilaki, O.; Kagkalou, G.; Gkeka, I.; Archonti, M.; Kati, S.; Metallidis, S.; Skoura, L. Microbiological characteristics of bacteremias among COVID-19 hospitalized patients in a tertiary referral hospital in Northern Greece during the second epidemic wave. *FEMS. Microbes*. **2021**, *2*, xtab021.

3 Mahoney, A. R.; Safaee, M. M.; Wuest, W. M.; Furst, A. L. The silent pandemic: Emergent antibiotic resistances following the global response to SARS-CoV-2. *iScience*. **2021**, *24*(4), 102304-102312.

4 Walker, E. B.; Paulson, D. *Quaternary Ammonium Compounds*; Marcel Dekker: New York, 1932; Vol 23.

5 Jennings, M. C.; Minbiole, K. P. C.; Wuest, W. M. Quaternary Ammonium Compounds: An Antimicrobial Mainstay and Platform for Innovation to Address Bacterial Resistance. *ACS. Infect. Dis.* **2015**, *1*, 288-303.

6 Tezel, U.; Pavlostathis, S. G. Role of Quaternary Ammonium Compounds on Antimicrobial Resistance in the Environment. In *Antimicrobial Resistance in the Eivironment*; Keen, P. L.; Montforts, M. H. M. M., Eds.; John Wiley & Sons: New York, 2011; pp 349-387.

7 Reich, C. (1997) Surfactants in Cosmetics. In *Surfactant Science Series;*(Rieger, M.; Rhein, L. D.; Eds.) Marcel Dekker: New York; p 373.

8 Cumming, J. L.; Hawker, D. W.; Nugent, K. W.; Chapman, H. F. (2008) Ecotoxicities of polyquaterniums and their associated polyelectrolyte-surfactant aggregates (PSA) to Gambusia holbrooki. *J. Environment. Sci. Health, Part A: Toxic/Hazard. Subst. Environ. Eng. 43,* 113-117.

9 Codling, C. E.; Maillard, J.; Russell, A. D. Aspects of the antimicrobial mechanisms of action of polyquaterniums and an amidoamine. *J. Antimicrob. Chemother.* **2003**, *51*, 1153-1158.

10 Annual Review of Cosmetic Ingredient Safety Assessments: 2005/2006. *Int. J. Tox.* 2008, 27, 7-142. 10.1080/10915810802032362.

11 Jacobs, W. A.; No Title, *J. Exp. Med.* **1916**, *23*, 563-568.

12 Jacobs, W. A.; No Title, *J. Exp. Med.* **1916**, *23*, 569-576.

13 Jacobs, W. A.; No Title, *J. Exp. Med.* **1916**, *23*, 577-599.

14 Hugo, W. B. The Mode of Action of Antibacterial Agents. *J. Appl. Bact.* **1967**, *30*, 17-50.

15 Goswami, S.; Adhikari, M. D.; Kar, C.; Thiyagarajan, D.; Das, G.; Ramesh, A. Synthetic amphiphiles as therapeutic antibacterials: lessons on bactericidal efficacy and cytotoxicity and potential application as an adjuvant in antimicrobial chemotherapy. *J. Meter. Chem.* **2013**, *1*, 2612-2623.

16 Laxminaryan, R. Antibiotic effectiveness: Balancing conservation against innovation. *Science.* **2014**, *345*, 1299-1301.

17 Morrison, K. R.; Allen, R. A.; Minbiole, K. P. C.; Wuest, W. M. More QACs, more questions: Recent advances in structure activity relationships and hurdles in understanding resistance mechanisms. *Tetrahedron. Lett.* **2019**, *60*, 150935-150947.

18 Uppu, D. S. S. M.; Samaddar, S.; Ghosh, C.; Paramanandham, K.; Shome, B. R.; Haldar, J. Amide Side Chain Amphiphilic Polymers Disrupt Surface Established Bacterial Bio-Films and Protect Mice from Chronic Acinetobacter Baumannii Infection. *Biomaterials.* **2016**, *74*, 131-143.

19 Okano, A.; Nakayama, A.; Wu, K.; Lindsey, E. A.; Schammel, A. W.; Feng, Y.; Collins, K. C.; Boger, D. L. Total Synthesis and Initial Evaluation of [Ψ[C(=S)NH]Tpg4]Vancomycin, [Ψ[=NH)NH]Tpg4]Vancomycin, [Ψ [CH2NH]Tpg4]Vancomycin, and Their (4-Chlorobiphenyl)Methyl Derivatives: Synergistic Binding Pocket and Peripheral Modifications for the Glycopeptide Antibio. *J. Am. Chem. Soc.* **2015**, *137*(10), 3693-3704.

20 Xie, J.; Okano, A.; Pierce, J. G.; James, R. C.; Stamm, S.; Crane, C. M.; Boger, D. J. Total Synthesis of [Ψ [C(=S)NH]Tpg4]Vancomycin Aglycon, [Ψ [C(=NH)NH]Tpg4]Vancomycn Aglycon, and Related Key Compounds: Reengineering Vancomycin for Dual D-Ala-D-Ala and D-Ala-D-Lac Binding. *J. Am. Chem. Soc.* **2012**, *134*(2), 1284-1297.

21 Ongwae, G.; Morrison, K. R.; Allen, R.; Kim, S.; Im, W.; Wuest, W. M.; Pires, M. M. Broadening Activity of Polymyxin by Quaternary Ammonium Grafting. *ACS Infect. Dis.* **2020**, *6*(6), 1427-1435.

22 Geng, Z.; Finn, M. G. Fragmentable Polycationic Materials Based on Anchimeric Assistance. *Chem. Mater.* **2016**, *28*(1), 146-152.

23 Geng, Z.; Finn, M. G. Thiabycyclononane-Based Antimicrobial Polycations. *J. Am. Chem. Soc.* **2017**, *139*(43), 15401-15406.

24 Lindstedt, M.; Allenmark, S.; Thompson, R. A.; Edebo, L. Antimicrobial activity of betaine esters, quaternary ammonium amphiphiles which spontaneously hydrolyze into nontoxic components. *Antimicrob. Agents. Chemother.* **1990**, *34*, 1949-1954.

25 Ahlstrom, B.; Chelminski-Bertilsson, M.; Thompson, R. A.; Edebo, L. Long-Chain Alkanoylchloines, a New Category of Soft Antimicrobial Agents That Are Enzymatically Degradable. *Antimicrob. Agents. Chemother.* **1995**, *39*, 50-55.

26 Boor, N. Soft Drugs. 1. Labile Quaternary Ammonium Salts as Soft Antimicrobials. *J. Med. Chem.* **1980**, *23*, 469-474.

27 Fletcher, M. H.; Jennings, M. C.; Wuest, W. M. Draining the moat: disrupting bacterial biofilms with natural products. *Tetrahedron.* **2014**, *70*, 6373-6383.

28 Hua, H.; Peng, J.; Dunbar, D. C.; Schinazi, R. F.; de Castro Andrews, A. G.; Cuevas, C.; Garcia-Fernandez, L. F.; Kelly, M.; Hamann, M. T. Betzellaine alkaloids from the Caribbean sponge *Monanchora unguifera* and the significant activities against HIV-1 an AIDS opportunistic infectious pathogens. *Tetrahedron.* **2017**, *63*, 11179-11188.

29 Okada, M.; Sugita, T.; Wong, C. P.; Wakimoto, T.; Abe, I. Identification of Pyridinium with Three

Indole Moieties as an Antimicrobial Agent. *J. Nat. Prod.* **2017**, *80*(4), 1205-1209.

30 Garrison, M. A.; Mahoney, A. R.; Wuest, W. M. Tricepyridinium-inspired QACs yield potent antimicrobials and provide insight into QAC resistance. *ChemMedChem.* **2020**, *16*(3), 463-466.

31 Xu, M.; Davis, R. A.; Feng, Y.; Sykes, M. L.; Shelper, T.; Avery, V. M.; Camp, D.; Quinn, R. J. Ianthelliformisamines A-C, Antibacterial Bromotyrosine-Derived Metabolites from the Marine Sponge *Subera ianthelliformis*. *J. Nat. Prod.* **2012**, *75*, 1001-1005.

32 Timm, C.; Volk, C.; Sasse, F.; Köck, M. The first cyclic monomeric 3-alkylpyridinium alkaloid from natural sources: identification, synthesis, and biological activity. *Org. Biomol. Chem.* **2008**, *6*, 4036-4040.

33 Schmit, G.; Timm, C, Köck, M. Haliclocyclin C, a New Monomeric 3-Alkyl Pyridinium Alkaloid from the Arctic Marine Sponge *Haliclona viscosa*. *Z. Naturforsch.* **2011**, *66b*, 745-748.

34 Böttcher, T.; Kolodkin-Gal, I.; Kolter, R.; Losick, R.; Clardy, J. Synthesis and Activity of Biomimetic Biofilm Disrupters. *J. Am. Chem. Soc.* **2013**, *135*, 2927-2930.

35 Kolodkin-Gal, I.; Cao, S.; Chai, L.; Böttcher, T.; Kolter, R.; Clardy, J, Losick, R. A Self-Produced Trigger for Biofilm Disassembly That Targets Exopolysaccharide. *Cell.* **2012**, *149*(3), 4684-4692.

36 Black, J. W.; Jennings, M. C.; Azarewicz, J.; Paniak, T. J.; Grenier, M. C.; Wuest, W. M.; Minboiole, K. P. C. TMEDA-Derived Biscationic Amphiphiles: An Economical Preparation of Potent Antibacterial Agents. *Bioorganic. Med. Chem. Lett.* **2014**, *24*(1), 99-102.

37 Paniak, T. J.; Jennings, M. C.; Shanahan, P. C.; Joyce, M. D.; Santiago, C. N.; Wuest, W. M.; Minbiole, K. P. C. The Antimicrobial Activity of Mono-, Bis-, Tris-, and Tetracationic Amphiphiles Derived from Simple Polyamine Platforms. *Bioorganic. Med. Chem. Lett.* **2014**, *24*(24), 5824-5828.

38 Schallenhammer, S. A.; Duggan, S. M.; Morrison, K. R.; Bentley, B. S.; Wuest, W. M.; Minbiole, K. P. C. Hybrid BisQACs: Potent Biscationic Quaternary Ammonium Compounds Merging the Structure of Two Commercial Antiseptics. *ChemMedChem.* **2017**, *12*(23), 1931-1934.

39 Allen, R. A.; Jennings, M. C.; Mitchell, M. A.; Al-Khalifa, S. E.; Wuest, W. M.; Minbiole, K. P. C. Ester- and Amide-Containing MultiQACs: Exploring Multicationic Soft Antimicrobial Agents. *Bioorganic. Med. Chem. Lett.* **2017**, *27*(10), 2107-2112.

40 Leitgeb, A. J.; Feliciano, J. A.; Sanchez, H.; Allen, R. A.; Morrison, K. R.; Sommers, K. J.; Carden, R. G.; Wuest, W. M.; Minbiole, K. P. C. Further Investigations into Rigidity-Activity Relationships in BisQAC Amphiphilic Antiseptics. *ChemMedChem.* **2020**, *15*(8), 667-670.

41 Carroll, R.; Copp, B. R.; avis, R. A.; Keyzers, R. A.; Prinsep, M. R. Marine natural products. *Nat. Prod. Rep.* **2019**, *36*, 122-173.

42 Köck, M.; Muñoz, J.; Cychon, C.; Timm, C.; Schmidt, G. The Arctic sponge *Haliclona viscosa* as a source of a wide array of 3-alkylpyridine alkaloids. *Phytochem. Rev.* **2013**, *12*, 391-406.

43 Cimino, G.; De Stefano, S.; Scognamigliio, G.; Sodano, G.; Trivellone, E. Sarains: a new class of alkaloids from the marine sponge *Reniera sarai*. *Bull. Soc. Chim. Belg.* **1986**, *72*, 301-303.

44 Sakai, R.; Higa, T. Manzamine, A, a novel antitumor alkaloid from a sponge. *J. Am. Chem. Soc.* **1986**, *108*, 6404-6405.

45 Venkateswarlu, Y.; Venkata Rami Reddy, M.; Venkaeswara Rao, J. Bis-1-oxaquinolizidines from the Sponge *Haliclona exigua*. *J. Nat. Prod.* **1994**, *57*, 1283-1285.

46 Jaspars, M.; Pasupathy, V.; Crews, P. A tetracyclic diamine alkaloid, halicyclamine A, from the marine sponge *Haliclona* sp. *J. Org. Chem.* **1994**, *59*, 3253-3255.

47 Ruzicka, R.; Gleason, D. F. Latitudinal variation in spongivorous fishes and the effectiveness of sponge chemical defenses. *Oecologia.* **2008**, *154*, 785-794.

48 Fusetani, N.; Asai, N.; Matsunaga, S.; Honda, K.; Yasumuro, K. Cyclostellettamines A-F, pyridine alkaloids which inhibit binding of methyl quinuclidinyl benzilate (QNB) to muscarinic acetylcholine receptors, from the marine sponge, *Stelletta maxima*. *Tetraheron. Lett.* **1994**, *35*, 3967-3970.

49 Volk, C. A.; Köck, M. Viscosamine: The first naturally occurring trimeric 3-alkyl pyridinium alkaloid. *Org. Lett.* **2003**, *5*, 3567-3569.

50 Volk, C. A.; Köck, M. Viscosaline: new 3-alkylpyridinium alkaloid from the Arctic sponge *Haliclona viscosa*. *Org. Biomol. Chem.* **2004**, *2*, 1827-1830.

51 Volk, C. A.; Lippert, H.; Lichte, E.; Köck, M. Two New Haliclamines from the Arctic Sponge *Haliclona viscosa*. *Eur. J. Org. Chem.* **2004**, 3154-3158.

52 Grube, A.; Timm, C.; Köck, M. Synthesis and Mass Spectrometric Analysis of Cyclostellettamines H, I, K and L. *Eur. J. Org. Chem.* **2006**, *5*, 1285-1295.

53 Teruya, T.; Kobayashi, K.; Suenaga, K.; Kigoshi, H. Cyclohaliclonamines A-E: Dimeric, Trimeric, Tetrameric, Pentameric, and Hexameric 3-Alkyl Pyridinium Alkaloids from a Marine Sponge *Haliclona* sp. *J. Nat. Prod.* **2006**, *69*, 135-137.

54 Schmidt, G.; Timm, C.; Köck, M. New haliclamines E and F from the Arctic sponge *Haliclona viscosa*. *Org. Biomol. Chem.* **2009**, *7*, 3061-3064.

55 Schmidt, C.; Timme, C.; Grube, A.; Volk, C. A; Köck, M. Viscosalines $B_{1,2}$ and $E_{1,2}$: Challenging New 3-Alkyl Pyridinium Alkaloids from the Marine Sponge *Haliclona viscosa*. *Chem. Eur. J.* **2012**, *18*, 8180-8189.

56 Morimoto, Y.; Yokoe, C. Total synthesis of haliclamine A, a macrocyclic marine alkaloid related to the key biogenetic intermediate of manzamines. *Tetrahedron. Lett.* **1997**, *38*, 8981-8984.

57 Davies-Coleman, M. T.; Faulkner, D. J. A new EGF-active polymeric pyridinium alkaloid from the sponge *Callyspongia fibrosa*. *J. Org. Chem.* **1993**, *58*, 5925-5930.

58 Anan, H.; Seki, N.; Noshiro, O.; Honda, K.; Yasamuro, K.; Ozasa, T.; Fusetaru, N. Total synthesis of cyclostellettamine C, a bispyridinium macrocyclic alkaloid having muscarinic acetylcholine receptor antagonistic activity. *Tetrahedron.* **1996**, *52*, 10849-10869.

59 Piddock, L. J. V. Techniques used for the determination of antimicrobial resistance and sensitivity in bacteria. *J. Appl. Bacteriol.* **2000**, *88*, 784-790.

60 Timm, C.; Mordhorst, T.; Köck, M. Synthesis of 3-alkyl pyridinium alkaloids from the arctic sponge *Haliclona viscosa*. *Mar. Drugs.* **2010**, *8*, 483-497.

61 Baldwin, J. E.; Spring, D. R.; Atkinson, C. E.; Lee, V. Efficient synthesis of the sponge alkaloids cyclostellettamines A-F. *Tetraheron.* **1998**, *54*, 13655-13680.

62 Kaiser, A.; Billot, X.; Gateau-Olesker, A.; Marazano, C.; Das, B. C. Selective entry to the dimeric or oligomeric pyridinium sponge macrocycles via aminopentadienal derivatives. Possible biogenetic relevance with Manzamine Alkaloids. *J. Am. Chem. Soc.* **1998**, *120*, 8026-8034.

63 Boyington, A. J.; Riu, M-L.; Jui, N. T. Anti-Markovnikov Hydroarylation of Unactivated Olefins via Pyridyl Radical Intermediates. *J. Am. Chem. Soc.* **2017**, *139*, 6582-6585.

64 Seath, C. P.; Vogt, D. B.; Boyington, A. J. Jui, N. T. Radical Hydroarylation of Functionalized Olefins and Mechanistic Investigation of Photocatalytic Pyridyl Radical Reactions. *J. Am. Chem. Soc.* **2018**, *140*, 15525-15534.

65 Boyington, A. J.; Seath, C. P.; Zearfoss, A. M.; Xu, Z.; Jui, N. T. Catalytic Strategy for Regioselective Arylethylamine Synthesis. *J. Am. Chem. Soc.* **2019**, *141*, 4147-4153.

66 Hendy, C. M.; Smith, G. C.; Xu, Z.; Lian, T.; Jui, N. T. Radical Chain Reduction via Carbon Dioxide Radical Anion ($CO_2^{\bullet-}$). *J. Am. Chem. Soc.* **2019**, *141*, 4147-4153.

5. Evaluating the Effect of Bromination on Indole-Containing Antibiotics

5.1. Indole as a Bacterial Metabolite

Indole is a naturally occurring metabolite that is used by nearly all organisms in every domain of life. It is produced by means of bacterial tryptophanase (TnaA) which breaks tryptophan into its three constituent molecules, indole, pyruvate, and ammonia (Scheme 5.01).[1-5] TnaA also metabolizes cysteine, thus its expression is regulated by the presence of cysteine or tryptophan, as well as alkaline stress, heme depletion, and cyclic AMP, whereas excess acetate, pyruvate, and glucose tend to decrease TnaA expression and subsequent indole production.[1] Interestingly, this pathway allows indole-producing bacteria to rely exclusively on tryptophan as both a carbon and nitrogen source.[1-3] Indole can also be utilized as a precursor to L-tryptophan in non-indole-producing bacteria by means of tryptophan synthetase, which combines L-serine with indole.[1,4] Indole and tryptophan can also be metabolized by both plants and animals to other indole-containing compounds such as serotonin, melatonin, isatin, indoxyl sulfate, or other hydroxyindoles.[1,2] Indole and related compounds have been shown in the brain, peripheral, tissues, blood, sweat, and urine, with potential influences on various diseases including intestinal inflammation, neurological diseases, diabetes, and bacterial infections, among others.[1-5] In addition, they play a significant role in plant protection and growth, along human health, particularly in the guy where indole has been found at concentration of approximately 250-1100 μM.[2]

Of particular interest to our group are the ramifications that indole and indole-containing metabolites have on microbial communities. Although its exact role is hotly debated, indole is considered by many to be an intercellular signaling molecule affecting a variety of bacterial processes.[6,7] This signaling molecule can modulate spore formation by Gram-positive bacteria, plasmid stability, cell division, antibiotic resistance and tolerance, virulence, and biofilm formation.[6-14] Interestingly, this molecule can have contrasting effects on different species. For example, expression of indole-producing tryptophanase increased biofilm formation and antibiotic resistance in a marine pathogen *Edwardsiella tarda*, while a decrease in biofilm formation and virulence in response to indole was observed in *Vibrio anguillarum*.[15,16] In addition, indole also has been shown to play contrasting roles in bacterial persistence. It was reported to increase the formation of antibiotic-tolerant persister *Escherichia coli* cells in response to oxidative stress and phage shock pathways but can also decrease persister formation via the phosphodiesterase DosP responsible for reducing cyclic adenosine monophosphate levels that are required to activate TnaA, the enzyme responsible for its production.[7,17] Taken together, it is clear that indole is a unique bacterial metabolite with a wide range of biological implications.

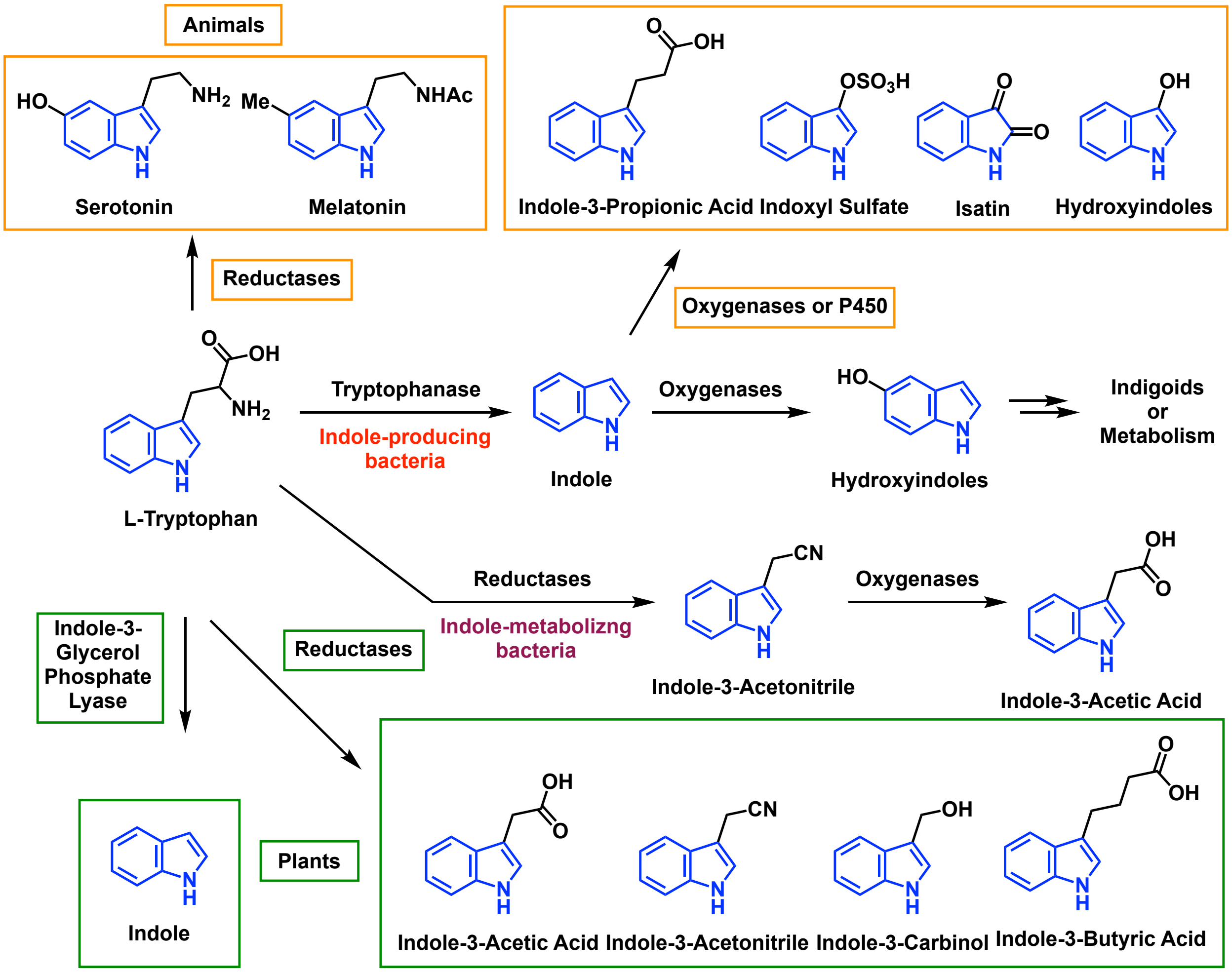
Animals
Serotonin
Melatonin
Indole-3-Propionic Acid
Indoxyl Sulfate
Isatin
Hydroxyindoles
Reductases
Oxygenases or P450
L-Tryptophan
Tryptophanase
Indole-producing bacteria
Indole
Oxygenases
Hydroxyindoles
Indigoids or Metabolism
Reductases
Indole-metabolizng bacteria
Indole-3-Acetonitrile
Oxygenases
Indole-3-Acetic Acid
Indole-3-Glycerol Phosphate Lyase
Reductases
Indole
Plants
Indole-3-Acetic Acid
Indole-3-Acetonitrile
Indole-3-Carbinol
Indole-3-Butyric Acid

Scheme 5.01. Biosynthesis of indole and derivatives in bacteria.[1-5]

5.2. The Potential of Indole-Containing Antibiotics

In addition to indole's abundance in nature, the variety of natural product scaffolds that it is present in and its unique reactivity has led scientists to frequently draw inspiration from indole in areas ranging from antibiotics and other drug discovery to synthetic chemistry and methodology development.[18,19] While all of these areas of research are quite fruitful, the focus of the remainder of this chapter will be on the use of indole-containing compounds in the realm of antibiotic development, particularly as it pertains to eradicating persister cells and bacterial biofilms.

5.2.1.Indole-Containing Anti-Persister Compounds

As mentioned in Chapter 1, persister cells are dormant and metabolically inactive meaning they are not susceptible to traditional antibiotic treatments, presenting a unique challenge in finding persister-targeting antibiotic compounds.[20,21] However, following antibiotic treatment, these cells can revert back to a metabolically active phenotype and then repopulate within the host (Fig. 5.01).[22]

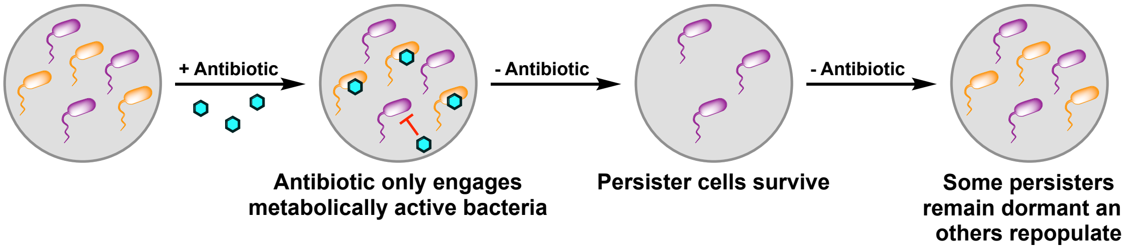
+ Antibiotic
- Antibiotic
- Antibiotic
Antibiotic only engages metabolically active bacteria
Persister cells survive
Some persisters remain dormant and others repopulate

Figure 5.01. Schematic representation of bacterial persistence.[20-22]

To date three main strategies have been employed to combat persister cells: inhibiting the formation of persister cells, direct killing of persister cells while they are dormant, or waking dormant persister cells to their metabolically active state followed by treatment with traditional antibiotics.[23-26] The overwhelming majority of anti-persister compounds identified are involved in direct killing of persister cells, many of which contain indole scaffolds (Fig. 5.02). Simple substituted indigoids were found to have increased persister-killing activity when combined with antibiotics and metals. For example, 5-methylindole combined with tobramycin eradicates MRSA and *S. epidermis* persisters while 5-nitroindole combined with copper and zinc nanoparticles effectively killed *E. coli, P. aeruginosa*, and *Enterobacter tabaci* persister cells.[27,28] 5-nitro-3-phenyl-1*H*-indol-2-yl-methylamine hydrochloride (NPIMA) is effective against *E. coli,* *P. aeruginosa*, and *S. aureus* persister cells, while *N*-[(6-trifluoromethyl)-1*H*-indoly-2-yl)methyl]cyclooctanamine (IMA6) and 74a are active against various *Mycobacterium* persister cells.[29-31] Finally, the synthetic indole-containing compound, nTZDpa eradicates *S. aureus* persister cells and recently underwent extensive SAR optimizations in our lab in collaboration with the Mylonakis group.[32,33]

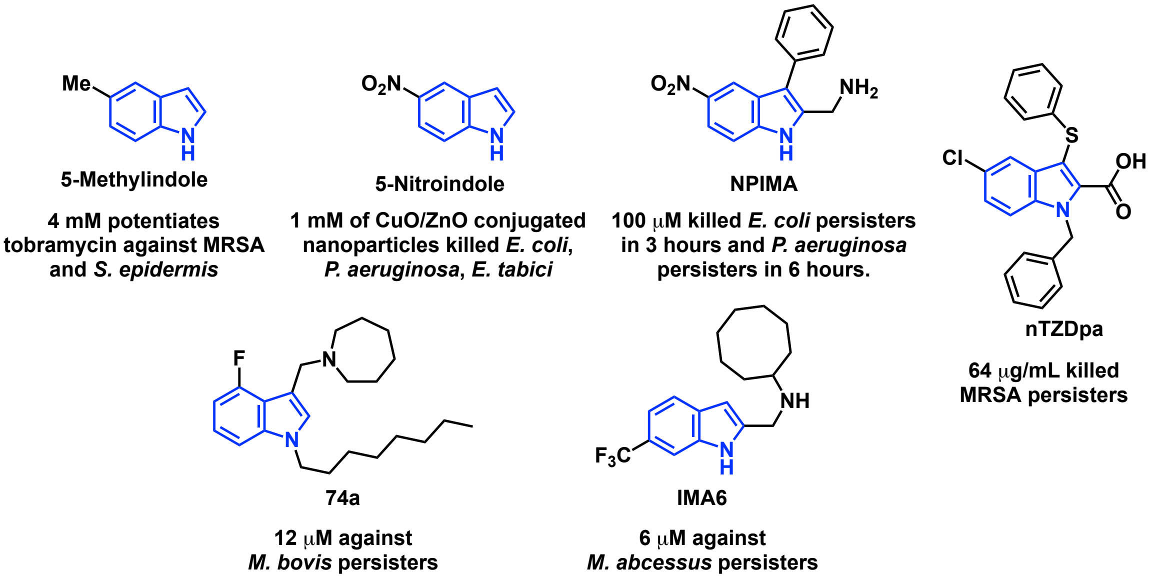

5-Methylindole

4 mM potentiates tobramycin against MRSA and *S. epidermis*

5-Nitroindole

1 mM of CuO/ZnO conjugated nanoparticles killed *E. coli*, *P. aeruginosa*, *E. tabici*

NPIMA

100 μM killed *E. coli* persisters in 3 hours and *P. aeruginosa* persisters in 6 hours.

nTZDpa

64 μg/mL killed MRSA persisters

74a

12 μM against *M. bovis* persisters

IMA6

6 μM against *M. abcessus* persisters

Figure 5.02. Structures of indole-containing anti-persister compounds.[27-33]

5.2.2.Indole-Containing Anti-Biofilm Compounds

In addition to having activity against persister cells, indole-containing compounds have also been found to have noteworthy anti-biofilm activity. Biofilms are a conglomerate of many microbes encapsulated in an exopolysaccharide matrix, often highly enriched with adherent persister cells.[34,35] Accounting for approximately 80% of bacterial infections biofilms are an ideal target for antibiotics.[34] The biofilm phenotype is particularly difficult to target with traditional antibiotics partially due to the higher prevalence of metabolically dormant persister cells but also because of the composition of the exopolysaccharide matrix that is more difficult to penetrate than a planktonic cell.[34,35] Therefore, a significant amount of research has gone into evaluating and optimizing the anti-biofilm properties of various indole-containing compounds. Similar to the anti-persister investigations, simple substituted indoles also exhibited potent antibiofilm activity (Fig. 5.03). Formation of *E. coli* biofilms was significantly diminished by both 5-hydroxyindole and 7-hydroxyindole.[36] Other simple naturally occurring indole metabolites, indole-3-

carboxyaldehyde and indole-3-acetonitrile displayed pronounced inhibition of *E. coli* and *P. aeruginosa* biofilm formation.[37] Recently, two prenylated indole carbaldehyde natural products significantly inhibited the production of *S. aureus* biofilm.[38] Finally, the scaffold of the naturally occurring biofilm inhibitor, oroidin, was elaborated to indole-containing scaffolds, ultimately giving rise to a new hit compound.[39]

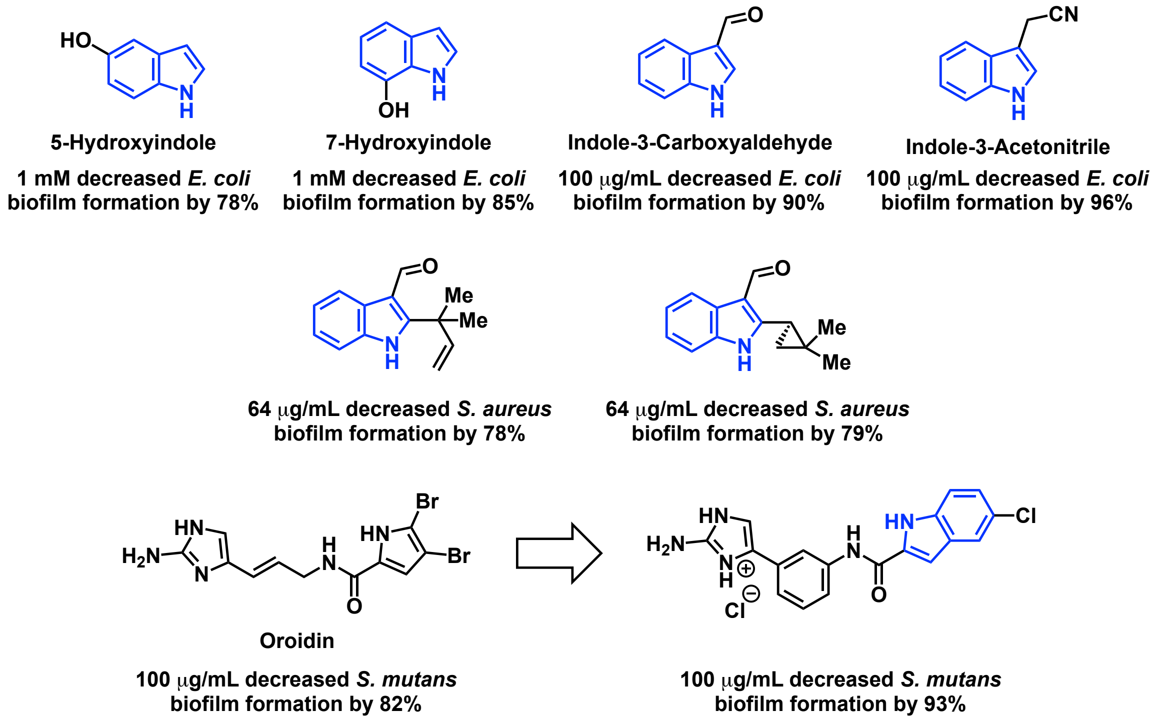

5-Hydroxyindole

1 mM decreased *E. coli* biofilm formation by 78%

7-Hydroxyindole

1 mM decreased *E. coli* biofilm formation by 85%

Indole-3-Carboxyaldehyde

100 μg/mL decreased *E. coli* biofilm formation by 90%

Indole-3-Acetonitrile

100 μg/mL decreased *E. coli* biofilm formation by 96%

64 μg/mL decreased *S. aureus* biofilm formation by 78%

64 μg/mL decreased *S. aureus* biofilm formation by 79%

Oroidin

100 μg/mL decreased *S. mutans* biofilm formation by 82%

100 μg/mL decreased *S. mutans* biofilm formation by 93%

Figure 5.03. Structures of indole-containing anti-biofilm compounds.[36-39]

5.2.2.1. Melander and Coworkers

The Melander group is one of several research groups that has widely explored indole-containing compounds with anti-biofilm activity (Fig. 5.04). In 2011, they investigated a series of desformylflustrabromine (dFBr) analogues and identified compounds that were 10-1000 times more active than indole against *E. coli* or *S. aureus* biofilms.[40] They also synthesized a series of pyrroloindoline triazole-amide hybrid analogues of dihydroflustramine C and evaluated their activity against *A. baumannii*, *E. coli*, and MRSA. In this work, they were able to identify several compounds with low micromolar IC_{50} values against biofilms.[41] Next, investigated another series of dFBr derivatives to act as probes for indole signaling and other biofilm-related events.[42] Finally, in 2018, they reported the synthesis of the marine natural product, meridianin D, and analogues, and their antibiofilm activity against MRSA.[43] They also published two follow-up libraries which displayed anti-biofilm activity against *Mycobacterium smegmatis*.[44,45] Overall, this work showed that derivatization of indole-containing natural product scaffolds is a promising way to develop novel antibiofilm small molecules.

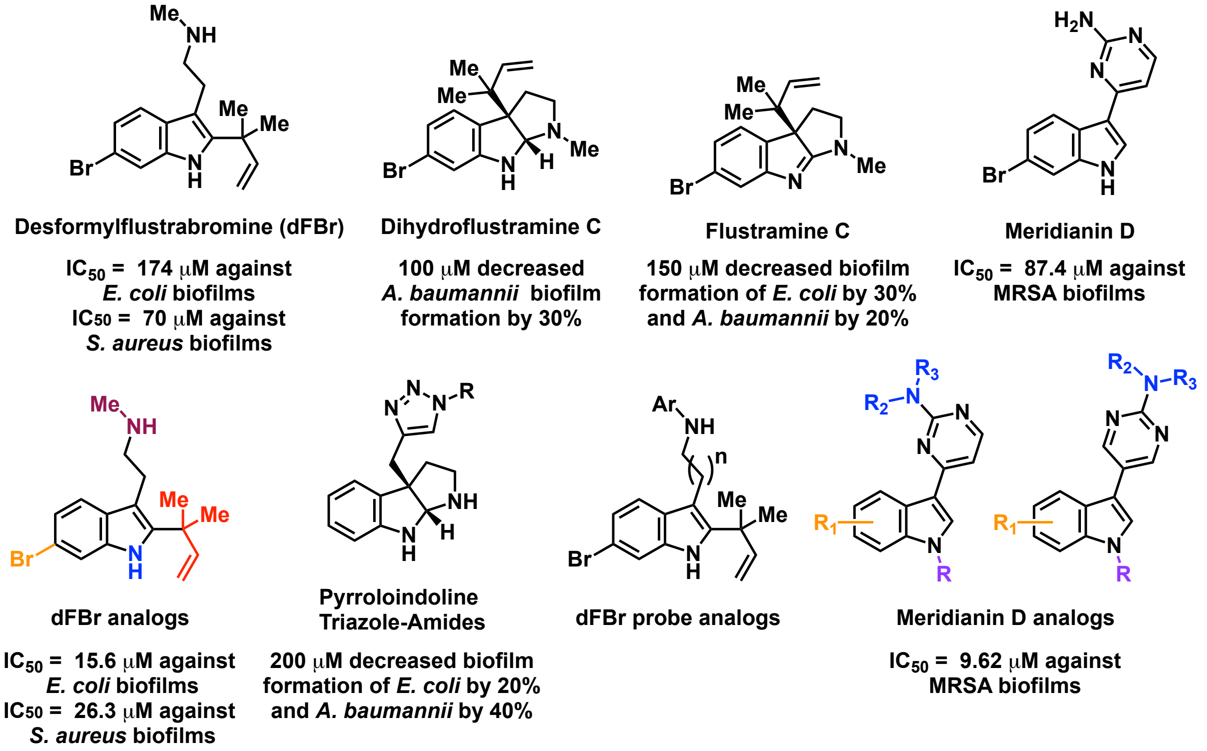

Desformylflustrabromine (dFBr)

IC_{50} = 174 μM against *E. coli* biofilms
IC_{50} = 70 μM against *S. aureus* biofilms

Dihydroflustramine C

100 μM decreased *A. baumannii* biofilm formation by 30%

Flustramine C

150 μM decreased biofilm formation of *E. coli* by 30% and *A. baumannii* by 20%

Meridianin D

IC_{50} = 87.4 μM against MRSA biofilms

dFBr analogs

IC_{50} = 15.6 μM against *E. coli* biofilms
IC_{50} = 26.3 μM against *S. aureus* biofilms

Pyrroloindoline Triazole-Amides

200 μM decreased biofilm formation of *E. coli* by 20% and *A. baumannii* by 40%

dFBr probe analogs

Meridianin D analogs

IC_{50} = 9.62 μM against MRSA biofilms

Figure 5.04. Structures of indole-containing compounds investigated by the Melander group.[40-43]

5.2.3. Halogenated Indole Antibiotics

Indole-containing compounds clearly show a lot of promise in eradicating persister cells and inhibiting bacterial biofilms. Additionally, one frequently observed motif in the scaffolds previously discussed is a halogen. In a recent report by Lee and coworkers, several halogenated indoles were shown to have markedly higher inhibition of *E. coli* persister cells compared to other non-halogenated substituted indoles. Further, 5-iodoindole also inhibited (methicillin-resistant) *S. aureus* persister cells as well as the formation of *E. coli* and *S. aureus* biofilms.[46] A follow-up report demonstrated that 5-iodoindole also dispersed and inhibited formation of *Acinetobacter baumannii* biofilms.[47] Taken together, these reports along with the results obtained from previously mentioned studies that investigated persister-killing and antibiofilm activity of halogenated indole-containing compounds suggest that halogenated indole-containing antibiotics show potential promise in inhibiting bacterial persister cells and biofilms.

5.3. Brominated Bis- and Tris- Indole Antimicrobial Compounds

There have been several reports of brominated bis-indole compounds with a range of reported biological activity, including antiviral and antimicrobial (Fig. 5.05). Hamacanthins A and B were active against *Candida albicans*, *Cryptococcus neoformans*, and *Bacillus subtilis* and both of these natural products have since been synthesized.[48-50] Topsentin alkaloids have varying levels of bromination in their scaffolds and were also isolated in these reports. The biological activity of these compounds was not consistently reported in previous work, however multiple groups have synthesized several of these compounds.[51-54] Notwithstanding, the structural similarities of these brominated bis-indole compounds compared to hamacanthin A and B suggest that they could display other promising biological activity, perhaps antibacterial, anti-biofilm, and/or antipersister activity.

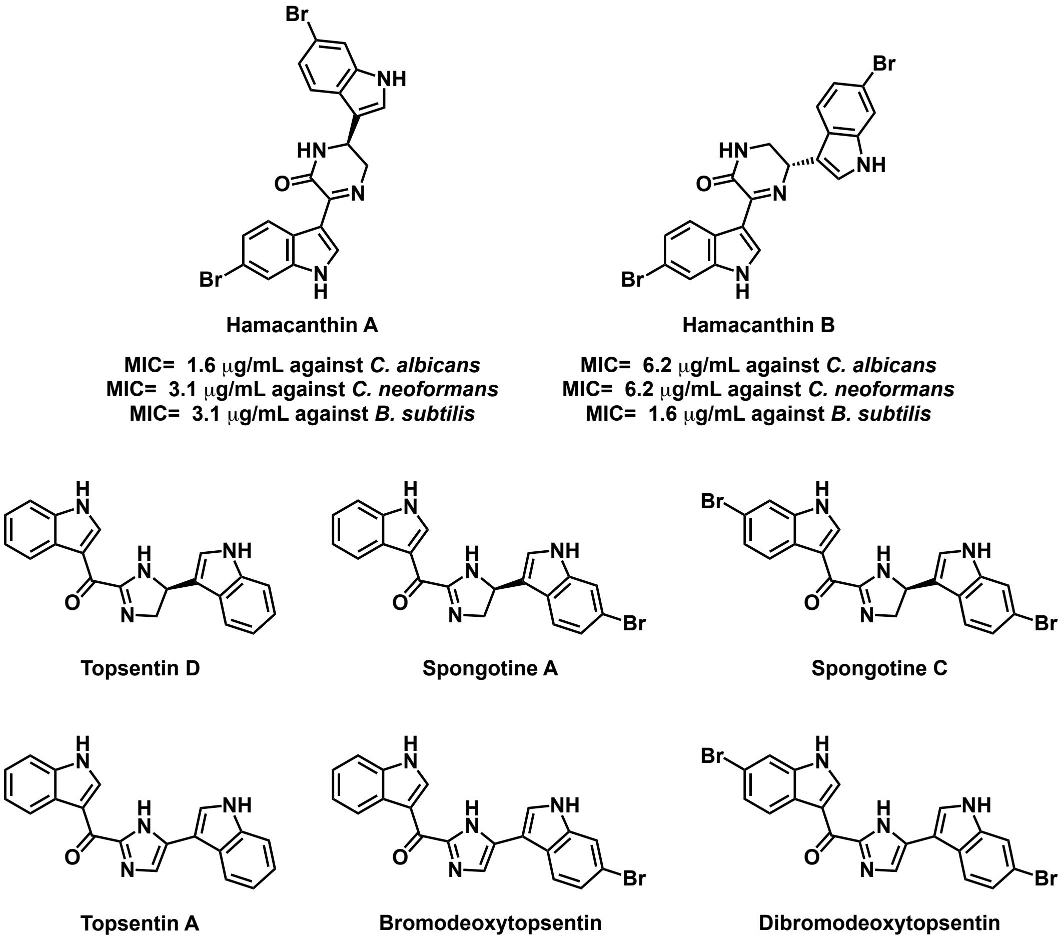
Hamacanthin A

MIC= 1.6 μg/mL against *C. albicans*
MIC= 3.1 μg/mL against *C. neoformans*
MIC= 3.1 μg/mL against *B. subtilis*

Hamacanthin B

MIC= 6.2 μg/mL against *C. albicans*
MIC= 6.2 μg/mL against *C. neoformans*
MIC= 1.6 μg/mL against *B. subtilis*

Topsentin D

Spongotine A

Spongotine C

Topsentin A

Bromodeoxytopsentin

Dibromodeoxytopsentin

Figure 5.05. Structures of bioactive bis-indole compounds.

5.3.1.Isolation and Biological Activity of Tulongicin and Dihydrospongotine C

Recently, Carole Bewley and coworkers reported the isolation of a tris-indole alkaloid, tulongicin, along with three bisindole alkaloids, dihydrospongotine C and previously isolated spongotine C and dibromodeoxytopsentin (Fig. 5.06). These compounds displayed potent activity against *S. aureus* ATCC 29213 with MIC values of 1.1-11 μg/mL. Additionally, these compounds exhibited no cytotoxicity toward control human and monkey cell lines, indicating a promising degree of selectivity towards *S. aureus*.[55] Intrigued by these natural products, labmate Christian Sanchez and I elected to synthesize these natural products along with structural analogues and perform a thorough biological evaluation.

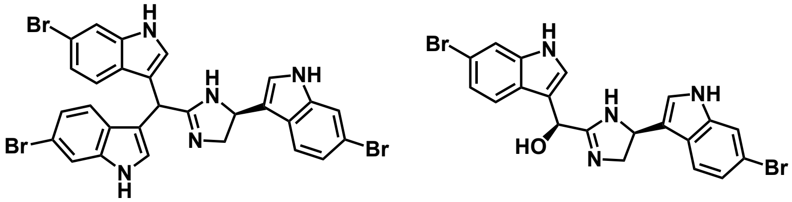

Tulongicin
(1.2 μg/mL)

Dihydrospongotine C
(3.7 μg/mL)

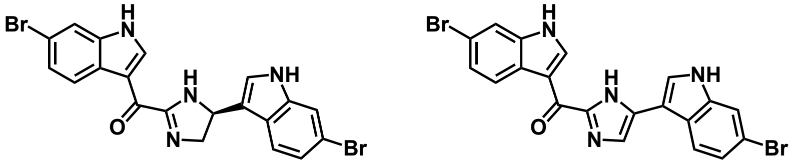

Spongotine C
(1.1 μg/mL)

Dibromodeoxytopsentin
(11 μg/mL)

Figure 5.06. Structures of tulongicin, dihydrospongotine C, spongotine C, and dibromodeoxytopsentin.

5.3.2.Synthetic Library

Based on the activity of the above four natural products and previously established anti-persister and anti-biofilm activity of halogenated indole-containing antibiotics, we decided to synthesize the four natural products as well as their non-brominated counterparts, which would enable us to determine whether or not the natural products have anti-persister or anti-biofilm activity and if/what the influence of bromination is on that activity. We also wanted to synthesize the racemic counterparts of all applicable compounds, which would allow us to determine whether or not the stereocenter affects antibacterial, anti-persister, or antibiofilm activity and give insight into potential mechanisms of action.

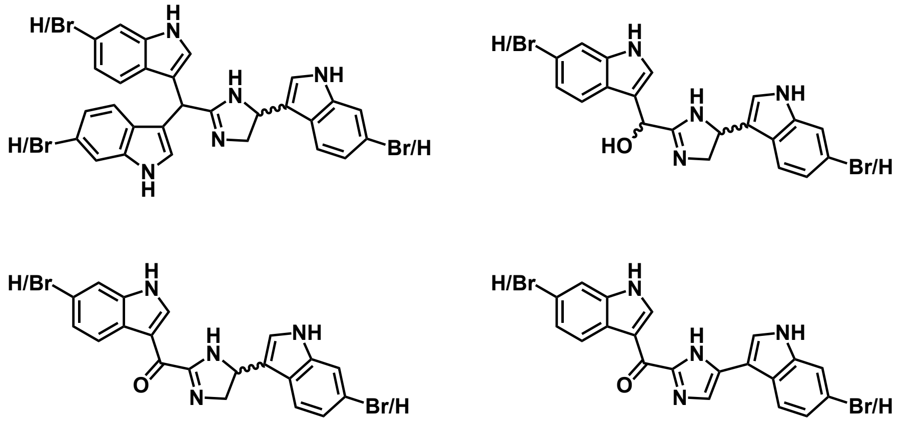
H/Br
H/Br
Br/H
HO
O
N
H
NH

Figure 5.07. Structures of proposed bis- and tris-indole compounds for our synthetic library.

5.3.2.1. Synthesis Outline

Syntheses of the topsentin D, spongotine C, topsentin A and dibromodeoxytopsentin had been previously established, so we elected to employ these previously established strategies (Scheme 5.02).[53,54] To this end, topsentin A and dibromodeoxytopsentin would be constructed via condensation between the corresponding 2-oxoacetaldehyde and ammonium acetate while topsentin D, spongotine C, and their corresponding racemates would arise from condensation between the same 2-oxoacetaldehyde precursor and corresponding 1,2-diamine.[53,54] We then envisioned that the secondary alcohol could be accessed through a simple reduction which would then undergo a deoxygenative substitution reaction with indole or 5-bromoindole to generate the desired tris-indole compounds.

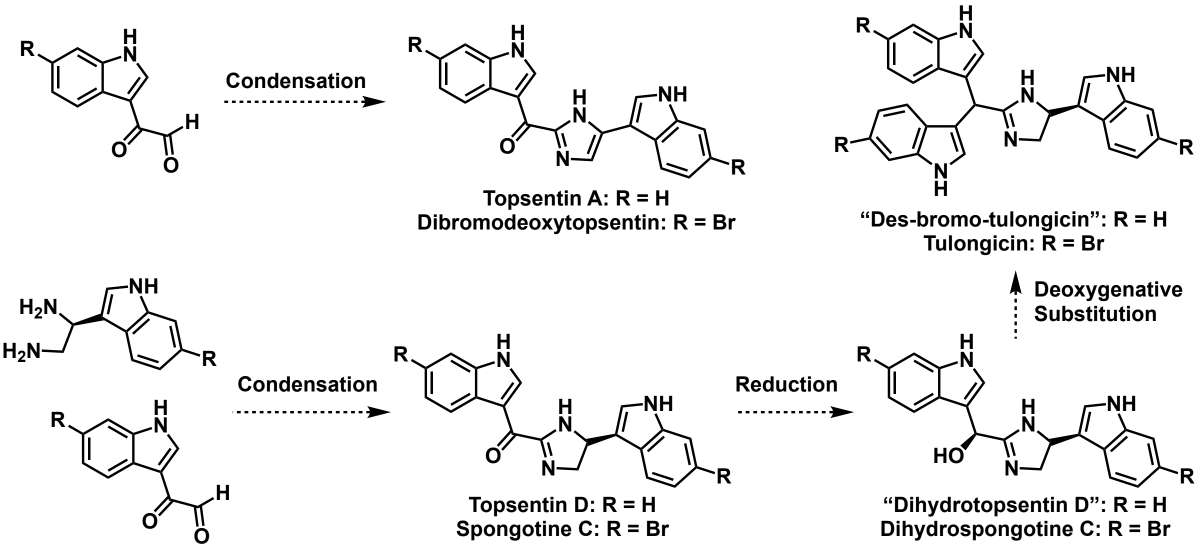
Condensation
Topsentin A: R = H
Dibromodeoxytopsentin: R = Br
"Des-bromo-tulongicin": R = H
Tulongicin: R = Br
Deoxygenative Substitution
Condensation
Reduction
Topsentin D: R = H
Spongotine C: R = Br
"Dihydrotopsentin D": R = H
Dihydrospongotine C: R = Br

Scheme 5.02. General synthetic outline to bis- and tris-indole compounds.[52-54]

5.3.2.2. Forward Synthesis

Synthetic efforts began with construction of the 2-oxaloacetaldehyde and 1,2-diamine building blocks (Scheme 5.03).[52-54] To access the 2-oxaloacetaldehyde building blocks, indole was first treated with oxalyl chloride to give 2-oxoacetyl chlorides **5.01** and **5.02** which were then subsequently reduced with tributyltin hydride, affording 2-oxoacetaldehydes **5.03** and **5.04** in just two steps. This material did not undergo any further purification and was used crude in both condensation reactions described in the next paragraph. Synthesis of the racemic and (*S*)-1,2-diamine building blocks began with tosyl protection of 1*H*-indole-3-carbaldehyde followed by Wittig olefination yielding tosyl vinyl indole **5.06**. Racemic (potassium osmate and *N*-methylmorpholine N-oxide) or asymmetric (methane sulfonamide and AD-mix-β) dihydroxylation of this compound using then gave rise to (*R*/*S*) diol **5.07** and (*R*) diol **5.08**. Mitsunobu reaction afforded diazides **5.09** and **5.10** which then underwent Staudinger reduction to give diamines **5.11** and **5.12**.

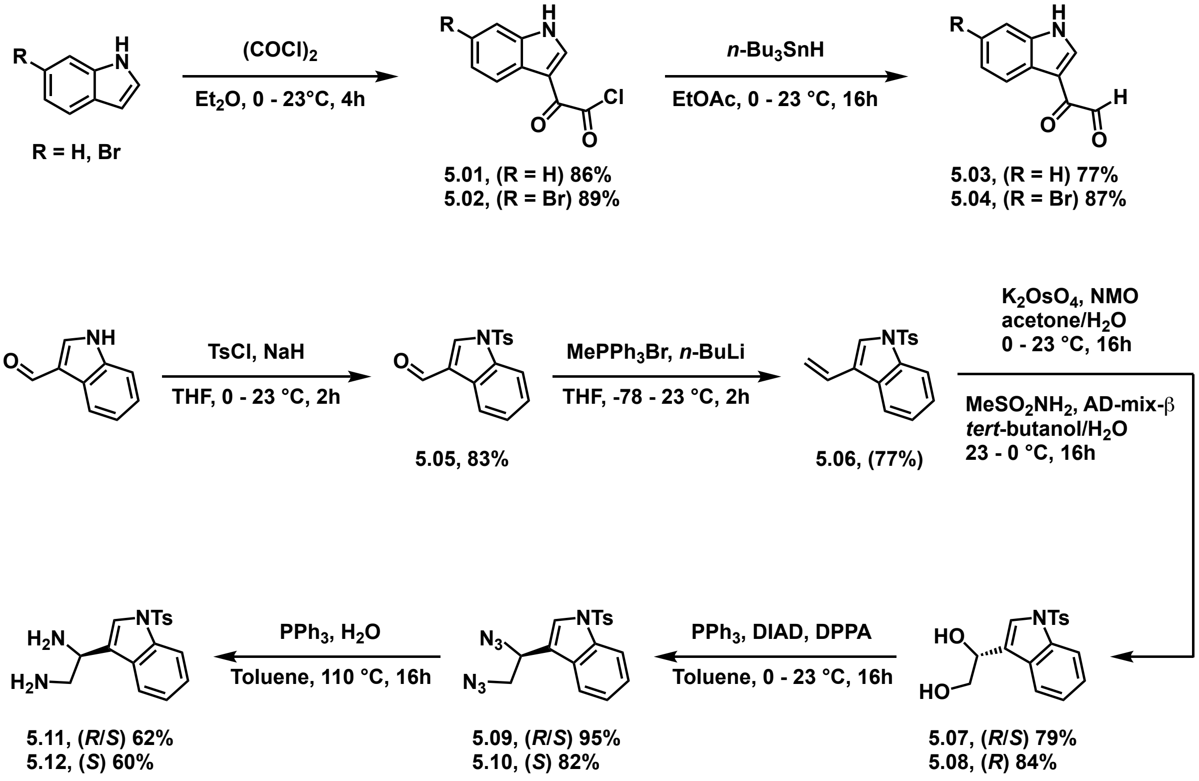
R = H, Br
(COCl)2
Et2O, 0 - 23°C, 4h
5.01, (R = H) 86%
5.02, (R = Br) 89%
n-Bu3SnH
EtOAc, 0 - 23 °C, 16h
5.03, (R = H) 77%
5.04, (R = Br) 87%
TsCl, NaH
THF, 0 - 23 °C, 2h
5.05, 83%
MePPh3Br, n-BuLi
THF, -78 - 23 °C, 2h
5.06, (77%)
K2OsO4, NMO
acetone/H2O
0 - 23 °C, 16h
MeSO2NH2, AD-mix-β
tert-butanol/H2O
23 - 0 °C, 16h
5.07, (R/S) 79%
5.08, (R) 84%
PPh3, DIAD, DPPA
Toluene, 0 - 23 °C, 16h
5.09, (R/S) 95%
5.10, (S) 82%
PPh3, H2O
Toluene, 110 °C, 16h
5.11, (R/S) 62%
5.12, (S) 60%

Scheme 5.03. Synthesis of 2-oxoacetaldehydes **5.03** and **5.04** and 1,2-diamines **5.11** and **5.12**.[52-54]

Synthesis of topsentin A (**5.13**) and dibromodeoxytopsentin (**5.14**) was accomplished by condensing corresponding 2-oxoacetaldehyde precursors **5.03** and **5.04**, respectively, with ammonium acetate in ethanol.[54] Next, the imidazoline scaffold present in the remainder of the compounds was accessed by condensing 2-oxoacetaldehyde **5.03** with diamines **5.11** and **5.12** followed by removal of the tosyl group giving rise to racemic topsentin D, **5.15** and stereoenriched topsentin D, **5.16**.[52-54]

To my surprise, reduction of the carbonyl proved to be more challenging than expected. Treatment with milder reducing agents such as sodium acetoxy borohydride, sodium cyanoborohydride, and sodium borohydride returned starting material only even with heating of the reaction. In contrast, use of stronger reducing agents including lithium borohydride, diisobutyl aluminum hydride, and lithium aluminum hydride led to decomposition of the starting material.

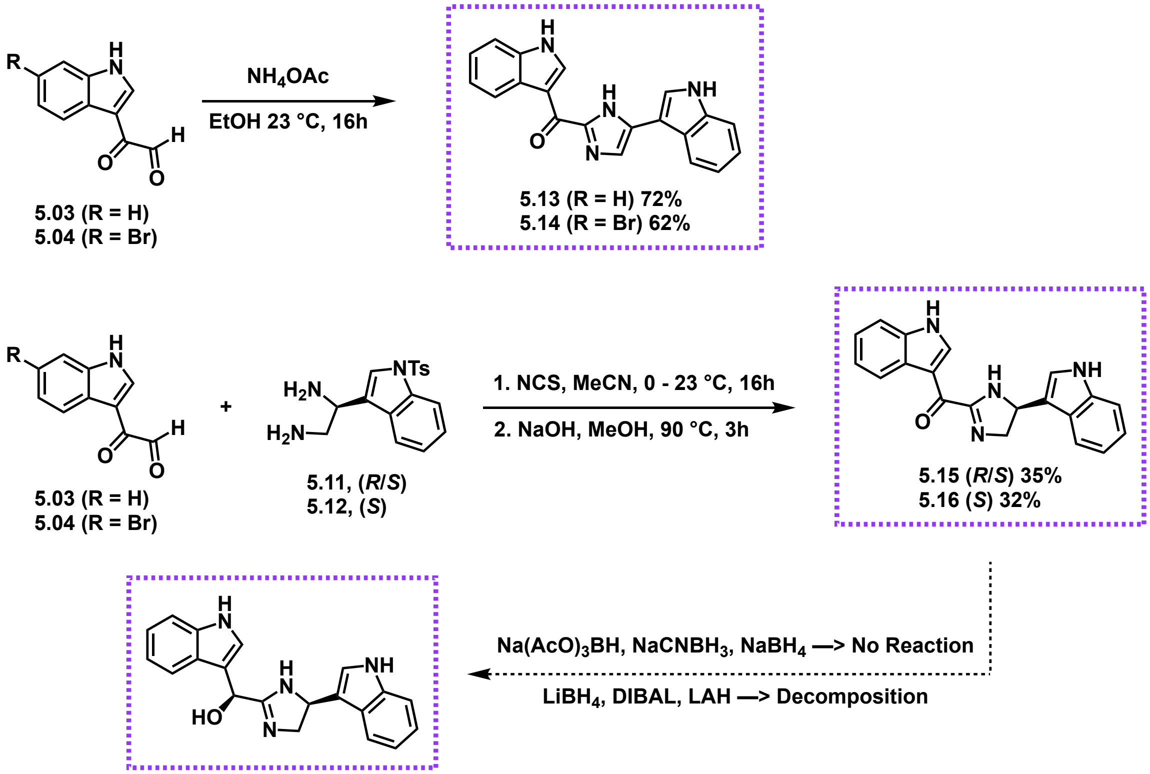

NH_4OAc
EtOH 23 °C, 16h
5.03 (R = H)
5.04 (R = Br)
5.13 (R = H) 72%
5.14 (R = Br) 62%
5.11, (*R*/*S*)
5.12, (*S*)
1. NCS, MeCN, 0 - 23 °C, 16h
2. NaOH, MeOH, 90 °C, 3h
5.03 (R = H)
5.04 (R = Br)
5.15 (*R*/*S*) 35%
5.16 (*S*) 32%
$Na(AcO)_3BH$, $NaCNBH_3$, $NaBH_4$ —> No Reaction
$LiBH_4$, DIBAL, LAH —> Decomposition

Scheme 5.04. Synthesis of library of non-halogenated bis- and tris-indole compounds.

One potential explanation for this could be a lack of reactivity of the carbonyl due to electron donation of the indole nitrogen generating a less electrophilic resonance form (Scheme 5.05). Another question that arose regarding this reduction was the stability of the product. In the report of its isolation, it was shown that treatment of dihydrospongotine C with reagents as mild as potassium carbonate and methyl iodide generated four different products (Scheme 5.05).[55] This led me to believe that the milder reducing agents were simply not reactive enough to reduce this particular ketone while the stronger reducing agents did in fact reduce the ketone to the secondary alcohol, but this product was not stable leading to its rapid decomposition. To this end, Christian Sanchez will attempt this reduction with a tris-tosylated scaffold which will then be deprotected under mild enough conditions to minimize side reactions or decomposition (Scheme 5.05).[56,57] Alternatively, another route being pursued is the condensation of the diamine with a terminal aldehyde instead of the 2-oxoacetaldehyde precursor to generate the imidazoline scaffold followed by benzylic oxidation (Scheme 5.05).[58]

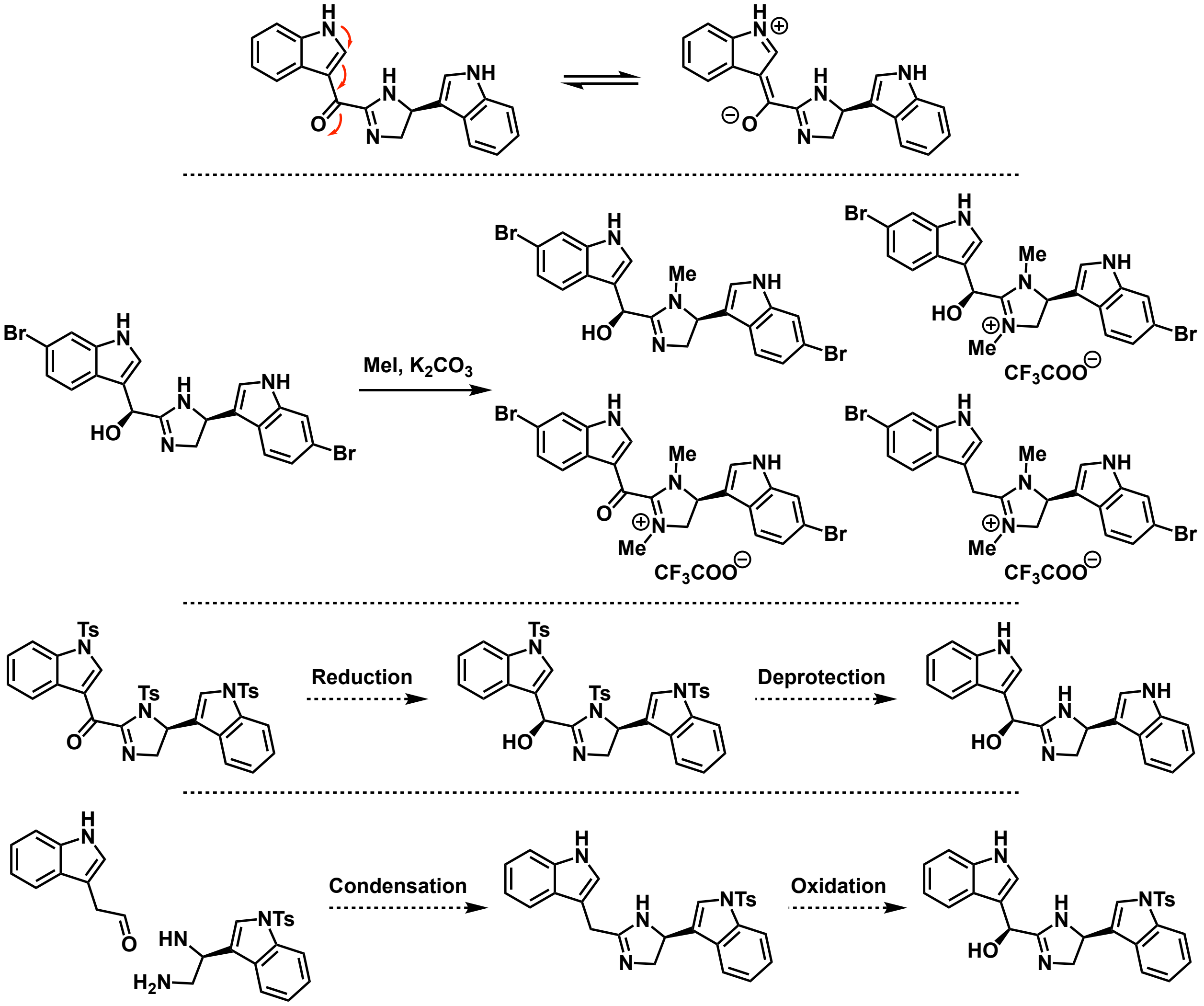

Scheme 5.05. Resonance form of topsentin D, reaction of dihydrospongotine with MeI and K_2CO_3, and alternateive approaches to accessing the secondary alcohol in "dihydrotopsentin D" and dihydrospongotine.[55-58]

5.3.3. Conclusions and Future Directions

In conclusion, I was able to synthesize topsentin A (**5.13**), dibromodeoxytopsentin (**5.14**), topsentin D, (**5.15**) and stereoenriched topsentin D, (**5.16**). In. addition, I attempted to synthesize the secondary alcohol and tris-indole analogs, however initial attempts to reduce the ketone to the corresponding secondary alcohol proved unsuccessful. In the future, Christian Sanchez will lead the efforts on this project by completing the synthesis of the remaining compounds in the library. The secondary alcohol will be accessed using one of the strategies outlined in scheme 5.05 and the tris-indole may be accessed by either a deoxygenative coupling with the carbonyl or a deoxygenative substitution with the secondary alcohol (Scheme 5.06).[59-61] After completing the synthesis of this library, Christian will evaluate the activity of these compounds against *S. aureus* as well as against persister cells.

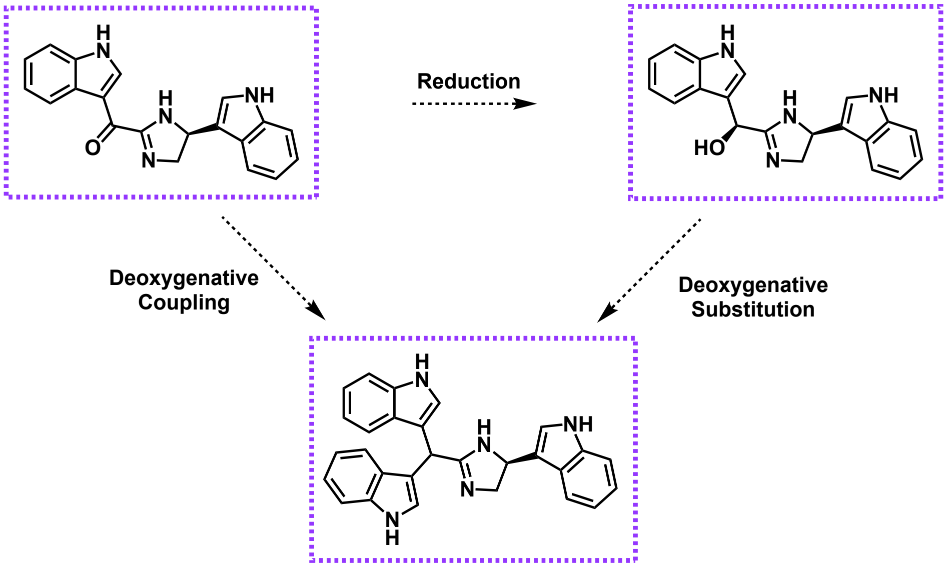

Scheme 5.06. Proposed route to secondary alcohol and tris-indole analogs.[59-61]

5.4. References

1 Kim, J.; Park, W. Indole: a signaling molecule or a mere metabolic byproduct that alters bacterial physiology at a high concentration? *J. Microbiol.* **2015**, *53*(7), 421-428.

2 Lee, J-H.; Wood, T. K.; Lee, J. Roles of Indole as an Interspecies and Interkingdom Signaling Molecule. *Trends. Microbiol.* **2015**, *23*(11), 707-718.

3 Kumar, P.; Lee, J-H.; Lee, J. Diverse roles of microbial indole compounds in eukaryotic systems. *Biol. Rev. Camb. Philos. Soc.* **2021**, *96*(6), 2522-2545.

4 Swamy, K. V.; Khetmalas, M. Indole: A novel signaling molecule and its applications. *Indian. J. Biotechnol.* **2013**, *12*(3), 297-310.

5 Lee, J-H.; Lee, J. Indole as an intercellular signal in microbial communities. *FEMS. Microbiol. Rev.* **2010**, *34*(4), 426-444.

6 Lee, H. H.; Molla, M. N.; Cantor, C. R.; Collins, J. J. Bacterial charity work leads to population-wide resistance. *Nature.* **2010**, *467*(7311), 82-85.

7 Vega, N. M.; Allison, K. R.; Khalil, A. S.; Collins, J. J. Signaling-mediated bacterial persister formation. *Nat. Chem. Biol.* **2012**, *8*(5), 431-433.

8 Stamm, I.; Lottspeich, F.; Plaga, W. The pyruvate kinase of Stigmatella aurantiaca is an indole binding protein and essential for development. *Mol. Microbiol.* **2005**, *56*(5), 1386-1395.

9 Kim, Y-G.; Lee, J-H.; Cho, M. H.; Lee, J. Indole and 3-indolylacetonitrile inhibit spore maturation in *Paenibacillus alvei*. *BMC. Microbiol.* **2011**, *11*, 119-128.

10 Chant, E. L.; Summers, D. K. Indole signalling contributes to the stable maintenance of *Escherichia coli* multicopy plasmids. *Mol. Microbiol.* **2007**, *63*(1), 35-43.

11 Chimerel, C.; Field, C. M.; Piñero-Fernandez, S.; Keyser, U. F.; Summers, D. K. Indole Prevents *Escherichia coli* cell division by modulating membrane potential. *Biochim. Biophys. Acta.* **2012**, *1818*(7), 1590-1594.

12 Bommarius, B.; Anyanful, A.; Izrayelit, Y.; Bhatt, S.; Cartwright, E. Wang, W.; Swimm, A. I.; Benian, G. M.; Schroeder, F. C.; Kalman, D. A Family of Indoles Regulate Virulence and Shiga Toxin Production in Pathogenic *E. coli*. *PLOS. ONE.* **2013**, *8*(1), e54456.

13 Hirakawa, H.; Kodama, T.; Takumi-Kobayashi, A.; Honda, T.; Yamaguchi, A. Secreted indole serves as a signal for expression of type III secretion system translocators in enterohaemorrhagic *Escherichia coli* O157:H7. *Microbiology.* **2009**, *155*(2), 541-550.

14 Di Martino, P.; Fursy, R.; Bret, L.; Sundararaju, B.; Phillips, R. S. Indole can act as an extracellular signal to regulate biofilm formation of *Escherichia coli* and other indole-producing bacteria. *Can. J. Microbiol.* **2003**, *49*(7), 443-449.

15 Han, Y.; Yang, C-L.; Yang, Q.; Qi, Z.; Liu, W.; Xu, Z-H.; Zhu, W-M.; Bossier, P.; Zhang, X-H.

Mutation of tryptophanase gene tnaA in *Edwardsiella tarda* reduces lipopolysaccharide production, antibiotic resistance and virulence. *Environ. Microbiol. Rep.* **2011**, *3*(5), 603-612.

16 Li, X.; Yang, Q.; Dierckens, K.; Milton, D. L.; Defoirdt, T. RpoS and Indole Signaling Control the Virulence of *Vibrio anguillarum* towards Gnotobiotic Sea Bass (*Dicentrarchus labrax*) Larvae. *PLOS. ONE.* **2014**, *9*(10), e111801.

17 Kwan, B. W.; Osbourne, D. O.; Hu, Y.; Benedik, M. J.; Wood, T. K. Phosphodiesterase DosP increases persistence by reducing cAMP which reduces the signal indole. *Biotechnol. Bioeng.* **2015**, *112*(3), 588-600.

18 Corsello, M. A.; Kim, J.; Garg, N. K. Indole diterpenoid natural products as the inspiration for new synthetic methods and strategies. *Chem. Sci.* **2017**, *8*(9), 5836-5844.

19 Norwood IV, V. M.; Huigens III, R. W. Harnessing the Chemistry of the Indole Heterocycle to Drive Discoveries in Biology and Medicine. *ChemBioChem.* **2019**, *20*(18), 2273-2297.

20 Fridman, O.; Goldberg, A.; Ronin, I.; Shoresh, N.; Balaban, N. Q. Optimization of lag time underlies antibiotic tolerance in evolved bacterial populations. *Nature.* **2014**, *513*(7518), 418-421.

21 Trastoy, R.; Manso, T.; Fernández-García, L.; Blasco, L.; Ambroa, A.; Pérez del Molino, M. L.; Bou, G.; García-Contreras, R.; Wood, T. K.; Tomás, M. Mechanisms of Bacterial Tolerance and Persistence in the Gastrointestinal and Respiratory Environments. *Clin. Microbiol. Rev.* **2018**, *31*(4), e00023-18.

22 Petchiappan, A.; Chatterji, D. Antibiotic Resistance: Current Perspectives. *ACS. Omega.* **2017**, *2*(10), 7400-7409.

23 Wood, T. K. Combatting Bacterial Persister Cells. *Biotechnol. Bioeng.* **2016**, *113*(3), 476-483.

24 Song, S.; Wood, T. K. Combatting Persister Cells With Substituted Indoles. *Front. Microbiol.* **2020**, *11*(1565), 1-9.

25 Defraine, V.; Fauvart, M.; Michiels, J. Fighting bacterial persistence: Current and emerging anti-persister strategies and therapeutics. *Drug. Resist. Updat..* **2018**, *38*, 12-26.

26 Khan, F.; Pham, D. T. N.; Tabassum, N.; Oloketuyi, S. F.; Kim, Y-M. Treatment strategies targeting persister cell formation in bacterial pathogens. *Crit. Rev. Microbiol.* **2020**, *46*(6), 665-688.

27 Sun, F.; Bian, M.; Li, Z.; Lv, B.; Gao, Y.; Wang, Y.; Fu, X. 5-Methylindole Potentiates Aminoglycoside Against Gram-Positive Bacteria Indluding *Staphylococcus aureus* Persisters Under Hypoionic Conditions. *Front. Cell. Infect. Microbiol.* **2020**, *10*(84), 1-12.

28 Manoharan, R. K.; Mahalingham, S.; Gangadaran, P.; Ahn, Y. H. Antibacterial and photocatalytic activities of 5-nitroindole capped bimetal nanoparticles against multidrug resistant bacteria *Colloids. Surf. B. Biointerfaces.* **2020**, *188*, 110825.

29 Song, S.; Gong, T.; Yamasaki, R.; Kim, J-S.; Wood, T. K. Identification of a potent indigoid persister antimicrobial by screening dormant cells. *Biotechnol. Bioeng.* **2019**, *116*, 2263-2274.

30 Yam, Y-K.; Alvarex, N.; Go, M-L.; Dick, T. Extreme Drug Tolerance of *Mycobacterium abscessus* “Persisters”. *Front. Microbiol.* **2020**, *11*(359), 1-9.

31 Yang, T.; Moreira, W.; Nyantakyi, S. A.; Chen, H.; Aziz, D. B.; Go, M-L.; Dick, T. Amphiphilic Indole Derivatives as Antimycobacterial Agents: Structure-Activity Relationships and Membrane Targeting Properties. *J. Med. Chem.* **2017**, *60*(7), 2745-2763.

32 Kim, W.; Steele, A. D.; Zhu, W.; Csatary, E. E.; Fricke, N.; Dekarske, M. M.; Jayamani, E.; Pan, W.; Kwon, B.; Sinitsa, E. F.; Rosen, J. L.; Conery, A. L.; Fuchs, B. B.; Vlahovska, P. M.; Ausubel, F. M.; Gao, H.; Wuest, W. M.; Mylonakis, E. Discovery and Optimization of nTZDpa as an Antibiotic Effective Against Bacterial Persisters. *ACS. Infect. Dis.* **2018**, *4*(11), 1540-1545.

33 Kim, W.; Zou, G.; Hari, T. P. A.; Wilt, I. K.; Zhu, W.; Galle, N.; Faizi, H. A.; Hendricks, G. L.; Tori, K.; Pan, W.; Huang, X.; Steele, A. D.; Csatary, E. E.; Dekarske, M. M.; Rosen, J. L.; de Queiroz Ribeiro, N.; Lee, K.; Port, J.; Fuchs, B. B.; Vlahovska, P. M.; Wuest, W. M.; Gao, H.; Ausubel, F. M.; Mylonakis, E. A selective membrane-targeting repurposed antibiotic with activity against methicillin-resistant *Staphylococcus aureus*. *Proc. Nat. Acad. Sci.* **2019**, *116*(33), 16529-16534.

34 Scharnow, A. M.; Solinski, A. E.; Wuest, W. M. Targeting *S. mutans* biofilms: a perspective on preventing dental caries. *Medchemcomm.* **2019**, *10*(7), 1057-1067.

35 Waters, E. M.; Rowe, S. E.; O'Gara, J. P.; Conlon, B. P. Convergence of *Staphylococcus aureus* Persister and Biofilm Research: Can Biofilms Be Defined as Communities of Adherent Persister Cells? *PLoS. Pathog.* **2016**, *12*(12), e1006012.

36 Lee, J.; Bansal, T.; Jayaraman, A.; Bentley, W. E.; Wood, T. K. Enterohemorrhagic Escherichia coli biofilms are inhibited by 7-hydroxyindole and stimulated by isatin. *Appl. Environ. Microbiol.* **2007**, *73*(13), 1071-1078.

37 Lee, J-H.; Cho, M. H.; Lee, J. 3-Indolylacetonitrile Decreases *Escherichia coli* O157:H7 Biofilm Formation and *Pseudomonas aeruginosa* virulence. *Environ. Microbiol.* **2011**, *13*(1), 62-73.

38 Zin, W. W. M.; Buttachon, S.; Dethoup, T.; Pereira, J. A.; Gales, L.; Inácio, A.; Costa, P. M.; Le, M.; Sekeroglu, N.; Silva, A. M. S.; Pinto, M. M. M.; Kijjoa, A. Antibacterial and antibiofilm activities of the metabolites isolated from the culture of the mangrove-derived fungus *Eurotium chevalieri* KUFA 0006. *Phytochemistry.* **2017**, *141*, 86-97.

39 Hodnik, Z.; Łoś, J. M.; Žula, A.; Zidar, N.; Jakopin, Z.; Łoś, M.; Dolenc, M. S.; Ilaš, J.; Węgrzyn, G.; Mašič, L. P.; Kikelj, D. Inhibition of biofilm formation by conformationally constrained indole-based analogues of the marine alkaloid oroidin. *Bioorg. Med. Chem. Lett.* **2014**, *24*(11), 2530-2534.

40 Bunders, C. A.; Minvielle, M. J.; Worthington, R. J.; Ortiz, M.; Cavanagh, J.; Melander, C. Intercepting bacterial indole signaling with flustramine derivatives. *J. Am. Chem. Soc.* **2011**, *133*(50), 20160-20163.

41 Bunders, C.; Cavanagh, J.; Melander, C. Flustramine inspired synthesis and biological evaluation of pyrroloindoline triazole amides as novel inhibitors of bacterial biofilms. *Org. Biomol. Chem.* **2011**, *9*(15), 5476-5481.

42 Minvielle, M. J.; Eguren, K.; Melander, C. Highly active modulators of indole signaling alter pathogenic behaviors in Gram-negative and Gram-positive bacteria. *Chemistry.* **2013**, *19*(51), 17595-17602.

43 Huggins, W. M.; Barker, W. T.; Baker, J. T.; Hahn, N. A.; Melander, R. J.; Melander, C. Meridianin D

Analogues Display Antibiofilm Activity against MRSA and Increase Colistin Efficacy in Gram-Negative Bacteria. *ACS. Med. Chem. Lett.* **2018**, *9*(7), 702-707.

44 Zeiler, M. J.; Melander, R. J.; Melander, C. Second-Generation Meridianin Analogues Inhibit the Formation of *Mycobacterium smegmatis* Biofilms and Sensitize Polymyxin-Resistant Gram-Negative Bacteria to Colistin. *ChemMedChem.* **2020**, *15*(17), 1672-1679.

45 Brackett, S. M.; Cox, K. E.; Barlock, S. L.; Huggins, W. M.; Ackart, D. F.; Bassaraba, R. J.; Melander, R. J.; Melander, C. Meridianin D analogues possess antibiofilm activity against *Mycobacterium smegmatis*. *RSC. Med. Chem.* **2020**, *11*, 92-97.

46 Lee, J-H.; Kim, Y-G.; Gwon, G.; Wood, T. K.; Lee, J. Halogenated indoles eradicate bacterial persister cells and biofilms. *AMB. Expr.* **2016**, *6*(123), 1-12.

47 Raorane, C. J.; Lee, J-H.; Lee, J. Rapid Killing and Biofilm Inhibition of Multidrug-Resistant *Acinetobacter baumannii* Strains and other Microbes by Iodoindoles. *Biomolecules.* **2020**, *10*(8), 1186-1198.

48 Gunasekera, S. P.; McCarthy, P. J.; Kelly-Borges, M. Hamacanthins A and B, New Antifungal Bis Indole Alkaloids from the Deep-Water Marine Sponge, *Hamacantha* Sp. *J. Nat. Prod.* **1994**, *57*(10), 1437-1441.

49 Jiang, B.; Yang, C. G.; Wang, J. Enantioselective synthesis for the (-)-antipode of the pyrazinone marine alkaloid, hamacanthin A. *J. Org. Chem.* **2001**, *66*(14), 4865-4869.

50 Jiang, B.; Yang, C-G.; Wang, Y. Enantioselective synthesis of marine indole alkaloid hamacanthin B. *J. Org. Chem.* **2002**, *67*(4), 1396-1398.

51 Bao, B.; Sun, Q.; Yao, X.; Hong, J.; Lee, C-O.; Cho, H. Y.; Jung, J. H. Bisindole Alkaloids of the Topsentin and Hamacanthin Classes from a Marine Sponge *Spongosorites* sp. *J. Nat. Prod.* **2007**, *70*(1), 2-8.

52 Guinchard, X.; Vallée, Y.; Denis, J-N. Total Synthesis of Marine Sponge Bis(indole) Alkaloids of the Topsentin Class. *J. Org. Chem.* **2007**, *72*(10), 3972-3975.

53 Murai, K.; Morishita, M.; Nakatani, R.; Kubo, O.; Fujioka, H.; Kita, Y. Concise Total Synthesis of (-)-Spongotine A. *J. Org. Chem.* **2007**, *72*(23), 8947-8949.

54 Ji, X.; Wang, Z.; Dong, J.; Liu, Y.; Lu, A.; Wang, Q. Discovery of Topsentin Alkaloids and Their Derivatives as Novel Antiviral and Anti-phytopathogenic Fungus Agents. *J. Argic. Food. Chem.* **2016**, *64*(48), 9143-9151.

55 Liu, H-B.; Lauro, G.; O'Connor, R. D.; Lohith, K.; Kelly, M.; Colin, P.; Bifulco, G.; Bewley, C. A. Tulongicin, an Antibacterial Tri-Indole Alkaloid from a Deep-Water *Topsentia* sp. Sponge. *J. Nat. Prod.* **2017**, *80*(9), 2556-2560.

56 Shohji, N.; Kawaji, T.; Okamoto, S. Ti(O-i-Pr)$_4$/MeSiCl/Mg-Mediated Reductive Cleavage of Sulfonamides and Sulfonates to Amines and Alcohols. *Org. Lett.* **2011**, *13*, 2626-2629.

57 Alonso, E.; Ramón, D. J.; Yus, M. Reductive deprotection of allyl, benzyl and sulfonyl substituted alcohols, amines and amides using a naphthalene-catalysed lithiation. *Tetrahedron.* **1997**, *53*, 14355-

14368.

58 Murafuji, H.; Muto, T.; Goto, M.; Imajo, S.; Sugawara, H.; Oyama, Y.; Minamitsuji, Y.; Miyazaki, S.; Murai, K.; Fujioka, H. Discovery and structure-activity relationship of imidazolinylindole derivatives as kallikrein 7 inhibitors. *J. Nat. Prod.* **2019**, *29*(2), 334-338.

59 Srihari, P.; Bhunia, D. C.; Sreedhar, P.; Mandal, S. S.; Shyam Sunder Reddy, J.; Yadav, J. S. Iodine-catalyzed C- and O-nucleophilic substitution reactions of aryl-propargyl methanols. *Tetrahedron Lett.* **2007**, *48*, 8120-8124.

60 Masuyama, Y.; Hayashi, M.; Suzuki, N. $SnCl_2$-Catalyzed Propargylic Substitution of Propargylic Alcohols with Carbon and Nitrogen Nucleophiles. *Eur. J. Org. Chem.* **2013**, *2013*, 2914-2921.

61 Zhang, Y.; Stephens, D.; Hernandez, G.; Mendoza, R.; Larionov, O. V. Catalytic Diastereo- and Enantioselective Annulations between Transient Nitrosoalkenes and Indoles. *Chem. Eur. J.* **2012**, *18*, 16612-16615.

6. Supporting Information

Target Based Design and Synthesis of a New Promysalin Analog

Synthesis

General Information

All non-aqueous reactions were conducted in flame-dried glassware equipped with a stir bar under an argon atmosphere using HPLC-grade solvents which were dried by passing through activated alumina. Metathesis catalysts were obtained as generous gifts from Materia, Inc. All other chemicals were used as received from Oakwood, TCI America, Sigma-Aldrich, Alfa Aesar, or AK Scientific. Triethylamine was freshly distilled from CaH_2 prior to use. Thin-layer chromatography was performed on 250µm SiliCycle silica gel F-254 plates and visualized by fluorescence and/or staining using potassium permanganate, or vanillin stains. 3 Å molecular sieves were activated in a round-bottom flask under vacuum heating at 120°C in an oil bath overnight. Brine refers to a saturated aqueous solution of sodium chloride, sat. $NaHCO_3$ refers to a saturated aqueous solution of sodium bicarbonate and sat. NH_4Cl refers to saturated aqueous solution of ammonium chloride. Organic solutions were concentrated under reduced pressure on a Buchi Rotavapor R3 rotary evaporator. Chromatographic purification was accomplished using a Biotage® flash chromatography purification system.

^1H NMR and ^{13}C NMR spectra were recorded on a Bruker (600 MHz), Inova (500 MHz), Inova (400 MHz), or VNMR (400 MHz) spectrometer, all from the Emory University NMR facility. ^1H NMR data were reported in terms of chemical shift (δ ppm relative to tetramethylsilane and with the indicated deuterated solvent as the internal reference), multiplicity, described using the following abbreviations: s (singlet), d (doublet), t (triplet), q (quartet), m (multiplet), br (broad), dd (doublet of doublets), dt (doublet of triplets), etc., coupling constant (Hz), and integration. ^{13}C NMR data were reported in terms of chemical shift. Accurate mass spectra were obtained from a Thermo LTQ-FTMS using APCI techniques.

Experimental Procedures and Spectral Data

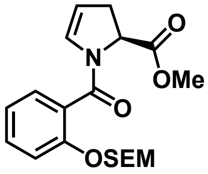

Methyl-(*S*)-1-(2-((2-(trimethylsilyl)ethoxy)methoxy)benzoyl)-2-3-dihydro-1*H*-pyrrole-2-carboxylate 2.02. Generously provided by Savannah J. Post.

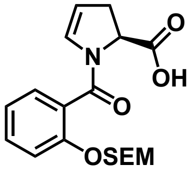

(*S*)-1-(2-((2-(trimethylsilyl)ethoxy)methoxy)benzoyl)-2-3-dihydro-1*H*-pyrrole-2-carboxylic acid 2.03. To a solution of methyl ester **2.02** (114 mg, 0.30 mmol) in 3 mL of THF was added LiOH (127 mg, 3.0 mmol) in 1 mL of H_2O. The solution stirred at ambient temperature for 4 hours. The mixture was then acidified to pH 5, extracted with CH_2Cl_2 (3x), washed with brine (1x), dried over Na_2SO_4, concentrated under reduced pressure, then used immediately in the next step.

*Spectra of this compound matched those previously obtained from our lab.

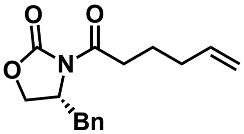

(*R*)-4-benzyl-3-(hex-5-enoyl)oxazolidine-2-one 2.04. Synthesized as previously described.[1] To a solution of **hexenoic acid** (2.00 mL, 25.3 mmol) and triethylamine (9.23 mL, 66.2 mmol) in 120 mL of THF cooled to 0 °C was added pivaloyl chloride (3.12 mL, 25.3 mmol) dropwise and the resulting solution continued to stir at this temperature for 1 hour. Flame-dried lithium chloride (1.18 g, 27.7 mmol) and **(*R*)-4-benzyl-2-oxazolidinone** (4.27 g, 24.1 mmol) were added in one portion, then the solution was warmed to ambient temperature and stirred for 16 hours. The reaction was quenched with sat. $NaHCO_3$, extracted with EtOAc (3x), washed with brine (1x), dried over Na_2SO_4, concentrated under reduced pressure, and purified by column chromatography (0-10% EtOAc/Hexanes) to give the title compound as a clear oil (5.48 g, 83%).

*Spectra of this compound matched those previously obtained from our lab.

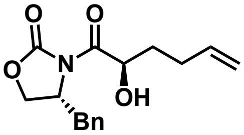

(*R*)-4-benzyl-3-((*R*)-2-hydroxyhex-5-enoyl)oxazolidine-2-one 2.05. To a solution of sodium bis(trimethylsilyl)amide (3.08 mL, 3.08 mmol, 1.0 M solution in THF) in 25 mL of THF cooled to -78 °C was added a solution of **2.04** (700 mg, 2.56 mmol) in 5 mL of THF dropwise. The solution stirred at this same temperature for 1 hour, then a solution of Davis reagent (2-(pheynylsulfonyl)-3-phenyloxaziridine, 805 mg, 3.08 mmol) in 5 mL of THF was added via a syringe pump over 25 minutes at -78 °C. The solution stirred at this temperature for 1 more hour and was then quenched with camphorsulfonic acid. The reaction mixture was then warmed to ambient temperature and deionized water was added, at which point the solution was extracted with EtOAc (3x), dried over Na_2SO_4, concentrated under reduced pressure, and purified by column chromatography (0 – 50% CH_2Cl_2/Hexanes then 0 – 10% EtOAc/Hexanes) giving the title compound as a yellow oil (517 mg, 70% yield).

*Spectra of this compound matched those previously obtained from our lab.

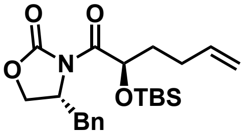

(*R*)-4-benzyl-3-((*R*)-2-((*tert*-butyldimethylsilyl)oxy)hydroxyhex-5-enoyl)oxazolidine-2-one 2.06. To a solution of alcohol **2.05** (506 mg, 1.75 mmol) in 10 mL of DMF cooled to 0 °C was added *tert*-butyldimethylsilyl chloride (395 mg, 2.62 mmol) and imidazole (155 mg, 2.27 mmol), and the solution then warmed to ambient temperature and stirred for 16 hours. The reaction mixture was then poured into deionized H_2O, extracted with a 1:1 mixture of hexanes/EtOAc (4x), washed with deionized H_2O (1x) and brine (1x), dried over Na_2SO_4, concentrated under reduced pressure, and purified by column chromatography (0 – 10% EtOAc/Hexanes) affording the title compound as a white solid (649 mg, 92% yield).

*Spectra of this compound matched those previously obtained from our lab.

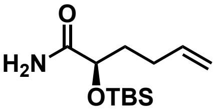

(*R*)-2-((*tert*-butyldimethylsilyl)oxy)hex-5-enamide 2.14. To a solution of oxazolidinone **2.06** (270 mg, 0.668 mmol) in 2 mL of THF was added ammonium hydroxide (2.00 mL, excess). The flask was then tightly sealed and the solution stirred at ambiente temperature for 24 hours. After careful venting, the reaction mixture was concentrated under reduced pressure and azeotroped with methanol, and purified by column chromatography (30% EtOAc/Hexanes) affording the title compound as a white solid (93 mg, 57% yield).

^{1}H NMR (400 MHz, $CDCl_3$) δ 6.53 (s, 1H), 5.81 (dt, *J* = 10.2, 6.6 Hz, 1H), 5.64 (s, 1H), 4.99 (dd, *J* = 3.2, 1.6 Hz, 2H), 4.16 (t, *J* = 5.2 Hz, 1H), 2.22 – 2.06 (m, 2H), 1.92 – 1.74 (m, 2H), 0.93 (s, 9H), 0.11 (s, 3H), 0.09 (s, 3H); **^{13}C NMR** (151 MHz, $CDCl_3$) δ 176.74, 137.99, 115.09, 73.15, 34.59, 28.54, 25.87, 18.15, -4.69, -5.09; **HRMS** Accurate mass (APCI$^+$): Found 244.1725 (-0.93 ppm), $C_{12}H_{26}NO_2{}^{28}Si$ (M+H$^+$) requires 244.17273.

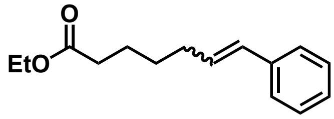

Ethyl (*E*)-7-phenylhept-6-enoate 2.07. A solution of **ethyl heptenoate** (2.00 mL, 11.4 mmol), and **styrene** (2.61 mL, 22.8 mmol), in CH_2Cl_2 (1.0 M) was charged with catalyst C627 (Materia, CAS [301224-40-8]) (**5 mol%**) and stirred at ambient temperature for 16 hours. The solution was then concentrated under reduced pressure and purified by column chromatography (0-5% EtOAc/Hexanes) yielding the title compound as a clear oil (1.49 g, 56% yield).

^{1}H NMR (400 MHz, $CDCl_3$, mixture of E/Z isomers) δ 7.36 – 7.26 (m, 4H), 7.22 – 7.15 (m, 1H), 6.41 – 6.37 (dd, *J* = 15.8, 4.1 Hz, 1H), 6.25-6.15 (dt, *J* = 14.3, 6.9 Hz, 1H), 4.14 (q, *J* = 7.1 Hz, 2H), 2.38-2.30 (t, *J* = 7.5 Hz, 2H), 2.28 – 2.22 (dd, *J* = 13.9, 6.7 Hz, 2H), 1.74-1.64 (m, 2H), 1.56-1.48 (m, 2H), 1.26 (t, *J* = 7.1 Hz, 3H); **^{13}C NMR** (151 MHz, $CDCl_3$) δ 173.79, 137.88, 130.49, 130.30, 128.59, 126.98, 126.06, 60.34, 34.34, 32.76, 28.95, 24.65, 14.38; **HRMS** Accurate mass (APCI$^+$): Found 233.15347 (-0.58 ppm), $C_{15}H_{21}O_2$ (M+H$^+$) requires 233.15361.

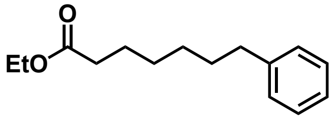

Ethyl 7-phenylheptanoate 2.08. To a solution of alkene **2.07** (1.49 g, 6.41 mmol) in 5 mL of EtOAc vacuum and backfilled with argon 3x at ambient temperature was added 10% Pd/C. The reaction flask was then vacuum and backfilled 3x with H_2 and stirred under H_2 at ambient temperature for 16 hours. The reaction was then filtered through a pad of celite and concentrated under reduced pressure to give the title compound as a clear oil (1.37 g, 91% yield).

^{1}H NMR (400 MHz, $CDCl_3$) δ 7.30 – 7.26 (m, 2H), 7.19 – 7.16 (m, 3H), 4.13 (q, *J* = 7.2 Hz, 2H), 2.60 (t, *J* = 7.5 Hz, 2H), 2.29 (t, *J* = 7.6 Hz, 2H), 1.68 – 1.59 (m, 4H), 1.39-1.33 (m, 4H), 1.26 (t, *J* = 7.2 Hz, 3H); **^{13}C NMR** (151 MHz, $CDCl_3$) δ 173.96, 142.84, 128.52, 128.37, 125.74, 60.30, 36.01, 34.48, 31.41, 29.12, 29.04, 25.04, 14.39; **HRMS** Accurate mass (APCI$^+$): Found 235.16908 (-0.77 ppm), $C_{15}H_{22}O_2$(M+H$^+$) requires 235.16926.

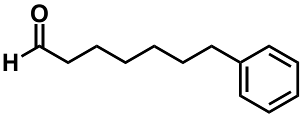

7-phenylheptanal 2.09. To a solution of ethyl ester **2.08** (1.37 g, 5.85 mmol) in 25 mL of CH_2Cl_2 cooled to -78 °C was added DIBAL-H (6.31 mL, 6.31 mmol, 10. M solution in CH_2Cl_2) dropwise. The reaction mixture was stirred for 30 minutes, then quenched with a saturated solution of Rochelle's salt and stirred for 3 hours. This was then extracted with CH_2Cl_2 (3x) washed with 1.0 M HCl (1x), dried over $MgSO_4$, concentrated under reduced pressure, then purified by column chromatography in 5% EtOAc/Hexanes, yielding the title compound as a clear oil (459 mg, 41%).

^{1}H NMR (400 MHz, $CDCl_3$) δ 9.76 (s, 1H), 7.32-7.25 (m, 2H), 7.22 – 7.14 (m, 3H), 2.65-2.57 (m, 2H), 2.45-2.32 (m, 2H), 1.72-1.57 (m, 4H), 1.43-1.29 (m, 4H); **^{13}C NMR** (151 MHz, $CDCl_3$) δ 203.04, 142.79, 128.52, 128.39, 125.77, 43.99, 35.99, 31.37, 29.03, 24.73, 22.13; **HRMS** Accurate mass (ES$^+$): 191.14292 (-0.65 ppm), $C_{13}H_{19}O_5$ (M+H$^+$) requires 191.304.

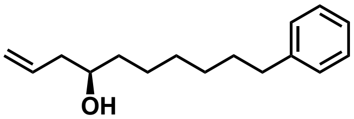

(+)-10-phenyldec-1-en-4-ol 2.10. To 2 mL of CH_2Cl_2 at 0 °C was added $TiCl_4$ (0.12 mL, 0.12 mmol) and Ti(O*iPr*)$_4$ (66 µL, 0.22 mmol), and the solution was warmed to ambient temperature and stirred for 1 hour. Then Ag_2O (56 mg, 0.24 mmol) was added, the flask wrapped in aluminum foil, and the solution stirred 5 hours. Then (S)-BINOL (138 mg, 0.48 mmol) and 2 mL of CH_2Cl_2 was added and the solution stirred another 2 hours. Aldehyde **2.09** (459 mg, 2.41 mmol) and **allyltributylstannane** (0.97 mL, 3.13 mmol) were added, the reaction cooled to 0 °C, and stirred for 16 hours. The reaction was quenched with sat. $NaHCO_3$ followed by celite, and the resulting solution was then vigorously stirred for 4 hours. The organic portion was separated from the aqueous portion, which was extracted with Et_2O (3x). The organic portions were separately washed with a saturated solution of KF (1x each), then combined and washed with brine (1x), dried over Na_2SO_4, and concentrated under reduced pressure. This orange oil was run through a silica plug with Et_2O, concentrated under reduced pressure, and purified by column chromatography (0 – 20% EtOAc/Hexanes) yielding the title compound as a yellow oil (365 mg, 65%).

^{1}H NMR (400 MHz, $CDCl_3$, trace amounts of aldehyde **2.07**) δ 7.32 – 7.25 (m, 2H), 7.22 – 7.15 (m, 3H), 5.89-5.77 (m, 1H), 5.19-5.09 (d, 2H), 3.68-3.60 (m, 1H), 2.65-2.56 (t, *J* = 7.6 Hz 2H), 2.36-2.25 (m, 1H), 2.19-2.08 (m, 1H), 1.69-1.56 (m, 4H), 1.51-1.42 (m, 2H), 1.41-1.29 (m, 6H); **^{13}C NMR** (151 MHz, $CDCl_3$) δ 142.95, 135.02, 128.52, 128.36, 125.71, 118.21, 70.80, 42.06, 36.90, 36.08, 31.55, 29.63, 29.37, 25.72.

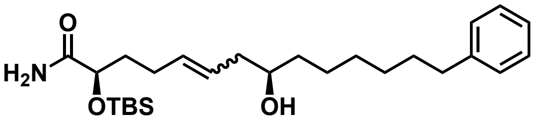

(2*R*,8*R*,*E*)-2-((*tert*-butyldimethylsilyl)oxy)-8-hydroxy-14-phenyltetradec-5-enamide 2.15. A solution of homoallylic alcohol **2.10** (234 mg, 1.01 mmol) and terminal amide **2.06** (82 mg, 0.34 mmol) dissolved in CH_2Cl_2 (1.0 M) was charged with catalyst C848 (Materia, CAS [246047-72-3]) (20 mol%) and stirred at ambient temperature for 16 hours. The solution was then concentrated under reduced pressure and purified by column chromatography (0-50% EtOAc/Hexanes) yielding the title compound as a dark purple oil (72 mg, 48% yield).

^{1}H NMR (400 MHz, $CDCl_3$, mixture of E/Z isomers) δ 7.28-7.24 (m, 2H), 7.21-7.14 (m, 3H), 6.54 (d, *J* = 3.5 Hz, 1H), 5.61 (s, 1H), 5.57-5.39 (m, 2H), 4.16 (t, *J* = 5.0 Hz, 1H), 3.60-3.52 (m, 1H), 2.60 (t, *J* = 7.6 Hz, 2 H), 2.26-1.98 (m, 4H), 1.93-1.82 (m, 1H), 1.81-1.71 (m, 1H), 1.67-1.55 (m, 4H), 1.47-1.21 (m, 10H), 0.93 (s, 9H), 0.11 (s, 3H), 0.10 (s, 3H); **^{13}C NMR** (151 MHz, $CDCl_3$) δ 176.78, 143.00, 133.37, 128.54, 128.36, 126.95, 125.70, 73.07, 71.05, 40.85, 36.91, 36.09, 34.99, 31.58, 29.67, 29.42, 27.42, 25.88, 25.79, 18.15, -4.67, -5.09; **HRMS** Accurate mass (APCI$^+$): Found 448.32399 (-0.34 ppm), $C_{26}H_{46}NO_3{}^{28}Si$ (M+H$^+$) requires 448.32415.

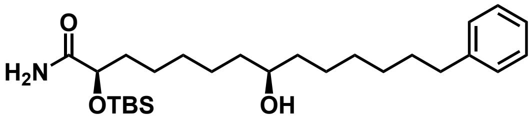

(2*R*,8*R*)-2-((*tert*-butyldimethylsilyl)oxy)-8-hydroxy-14-phenyltetradecanamide 2.19.

To a solution of alkene **2.15** (70 mg, 0.156 mmol) in 2 mL of EtOAc vacuum and backfilled with argon 3x at ambient temperature was added 10% Pd/C. The reaction flask was then vacuum and backfilled 3x with H_2 and stirred under H_2 at ambient temperature for 16 hours. The reaction was then filtered through a pad of celite and concentrated under reduced pressure to give the title compound as a brown oil (62 mg, 89% yield).

^{1}H NMR (400 MHz, $CDCl_3$) δ 7.29 – 7.24 (m, 2H), 7.20 – 7.22-7.16 (m, 3H), 6.54 (s, 1H), 6.13 (s, 1H), 4.13 (t, *J* = 5.1 Hz, 1H), 3.60-3.53 (m, 1H), 2.60 (t, *J* = 7.8 Hz, 2H), 1.81-1.70 (m, 1H), 1.70-1.66 (m, 1H), 1.66-1.56 (m, 3H), 1.47-1.21 (m, 17H), 0.93 (s, 9H), 0.10 (s, 3H), 0.09 (s, 3H); **^{13}C NMR** (151 MHz, $CDCl_3$) δ 177.00, 142.99, 128.54, 128.37, 125.72, 73.61, 72.04, 37.61, 37.53, 36.10, 35.24, 31.58, 31.08, 29.71, 29.43, 25.89, 35.73, 25.63, 24.27, 18.17, -4.67, -5.09; **HRMS** Accurate mass (ES$^+$): Found 450.33928 (-1.14 ppm), $C_{26}H_{48}NO_3{}^{28}Si$ (M+H$^+$) requires 450.3398.

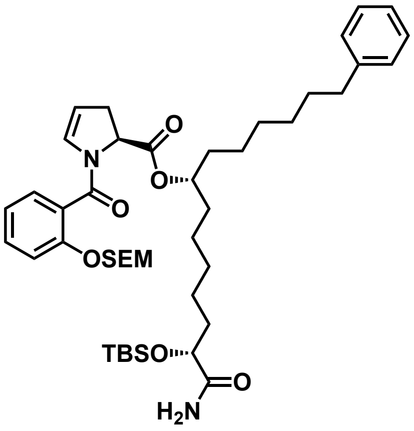

(7*R*,13*R*)-14-amino-13-((*tert*-butyldimethylsilyl)oxy)-14-oxo-1-phenyltetradecan-7-yl (*S*)-1-(2-((2-(trimethylsilyl)ethoxy)methoxy)benzoyl)-2,3-dihydro-1*H*-pyrrole-2-carboxylate 2.20. To a solution of carboxylic acid **2.03** (67 mg, 0.19 mmol) in CH_2Cl_2 (0.2 M) cooled to 0 °C was added N-(3-dimethylaminopropyl)-N'ethylcarbodiimide hydrochloride (47 mg, 0.25 mmol). A solution of alcohol **2.19** (56 mg, 0.12 mmol) and dimethylaminopyridine (15 mg, 0.12 mmol) dissolved in CH_2Cl_2 (0.2 M) was then added at 0 °C, and the resulting solution was stirred at ambient temperature for 16 hours. The reaction mixture was then poured into water, extracted with CH_2Cl_2 (3x), washed with brine (1x), dried over $MgSO_4$, concentrated under reduced pressure, and purified by column chromatography (0 – 50% EtOAc/Hexanes) affording title compound as a yellow oil (66 mg, 67% yield).

^{1}H NMR (400 MHz, $CDCl_3$) δ 7.44-3.37 (m, 2H), 7.31 (t, *J* = 7.5 Hz, 3H), 7.22 (t, *J* = 7.9 Hz, 3H), 7.08 (t, *J* = 7.4 Hz, 1 H), 6.57 (m, 1H), 6.21 (m, 1H), 5.67 (d, *J* = 4.0 Hz, 1H), 5.27 (q, *J* = 7.1 Hz, 2H), 5.08-5.04 (m, 1H), 5.04-4.97 (m, 1H), 4.17 (t, *J* = 4.9 Hz, 1H), 3.79 (t, *J* = 12.6 Hz, 2H), 3.22-3.10 (m, 1H), 2.76-2.67 (m, 1H), 2.63 (t, *J* = 11.7 Hz, 2H), 1.85-1.76 (m, 2H), 1.76-1.69 (m, 1H), 1.69-1.54 (m, 6H), 1.50-1.24 (m, 14H), 0.96 (s, 9H), 0.13 (s, 3H), 0.12 (s, 3H), 0.04 (s, 9H); **^{13}C NMR** (151 MHz, $CDCl_3$) δ 176.93, 170.79, 164.97, 153.86, 142.94, 131.22, 131.06, 129.01, 128.51, 128.34, 126.02, 125.68, 121.98, 115.27, 108.32, 93.38, 75.40, 73.60, 66.63, 58.22, 36.04, 35.13, 34.42, 34.10, 34.06, 31.53, 29.50, 29.31, 25.88, 25.29, 25.06, 24.13, 18.17, 18.15, -1.27, -4.70, -5.13; **HRMS** Accurate mass (APCI$^+$): Found 795.47917 (-0.33 ppm), $C_{44}H_{71}N_2O_7{}^{28}Si_2$ (M+H$^+$) requires 795.47943.

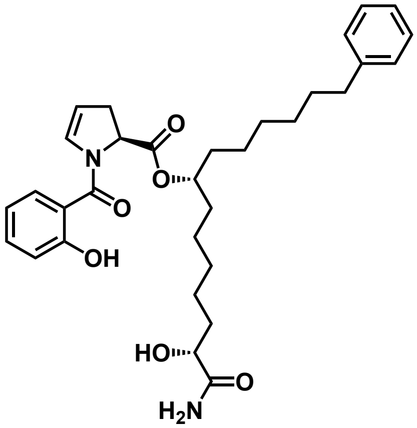

(7*R*,13*R*)-14-amino-13-hydroxy-14-oxo-1-phenyltetradecan-7-yl (*S*)-1-(2-hydroxybenzoyl)-2,3-dihydro-1*H*-pyrrole-2-carboxylate 2.01. To a solution of protected **2.20** (9 mg, 0.011 mmol) in N,N'-dimethylpropyleneurea (1:1 v/v TBAF, dried over 3 Å molecular sieves, 0.05 M) was added tetrabutylammonium fluoride (1.0 M solution in THF dried over 3 Å molecular sieves for 2 days), 0.216 mL, 0.216 mmol) dropwise at ambient temperature. The resulting solution then stirred for 2 additional hours at ambient temperature and was then quenched with sat. NH_4Cl. The mixture was then extracted with Et_2O (5x), washed with sat. NH_4Cl (5x) and brine (1x), dried over Na_2SO_4, concentrated under reduced pressure, and purified by column chromatography (0 – 5% MeOH/CH_2Cl_2) furnishing the title compound as a colorless oil (3 mg, 56% yield).

^{1}H NMR (400 MHz, $CDCl_3$) δ 9.54 (s, 1H), 7.42-7.35 (m, 3H), 7.31-7.24 (m, 3H), 7.21-7.25 (m, 2H), 6.99 (d, *J* = 7.3 Hz, 1H), 6.91 (t, *J* = 7.3 Hz, 1H), 6.99 (s, 1H), 6.91 (s, 1H), 5.31- 5.23 (m, 2H), 5.06-4.96 (m, 2 H), 4.14-4.08 (m, 1H), 3.30 (s, 1H), 3.12 (m, 1H), 2.70 (m, 1H), 2.61-2.55 (m, 3H), 1.86-1.75 (m 1H), 1.72-1.11 (m, 17H); **^{13}C NMR** (151 MHz, $CDCl_3$) δ 176.75, 171.30, 158.13, 142.91, 133.54, 130.85, 128.54, 128.39, 128.30, 125.75, 119.41, 118.05, 117.66, 111.10, 75.94, 71.42, 59.38, 41.18, 36.04, 34.53, 34.35, 34.18, 31.49, 29.85, 29.40, 29.26, 28.36, 25.47, 28.84, 24.56; **HRMS** Accurate mass (ES$^+$): Found 551.31102 (-0.99 ppm), $C_{32}H_{43}N_2O_6$ (M+H$^+$) requires 551.31156.

^{1}H NMR and ^{13}C NMR Spectra

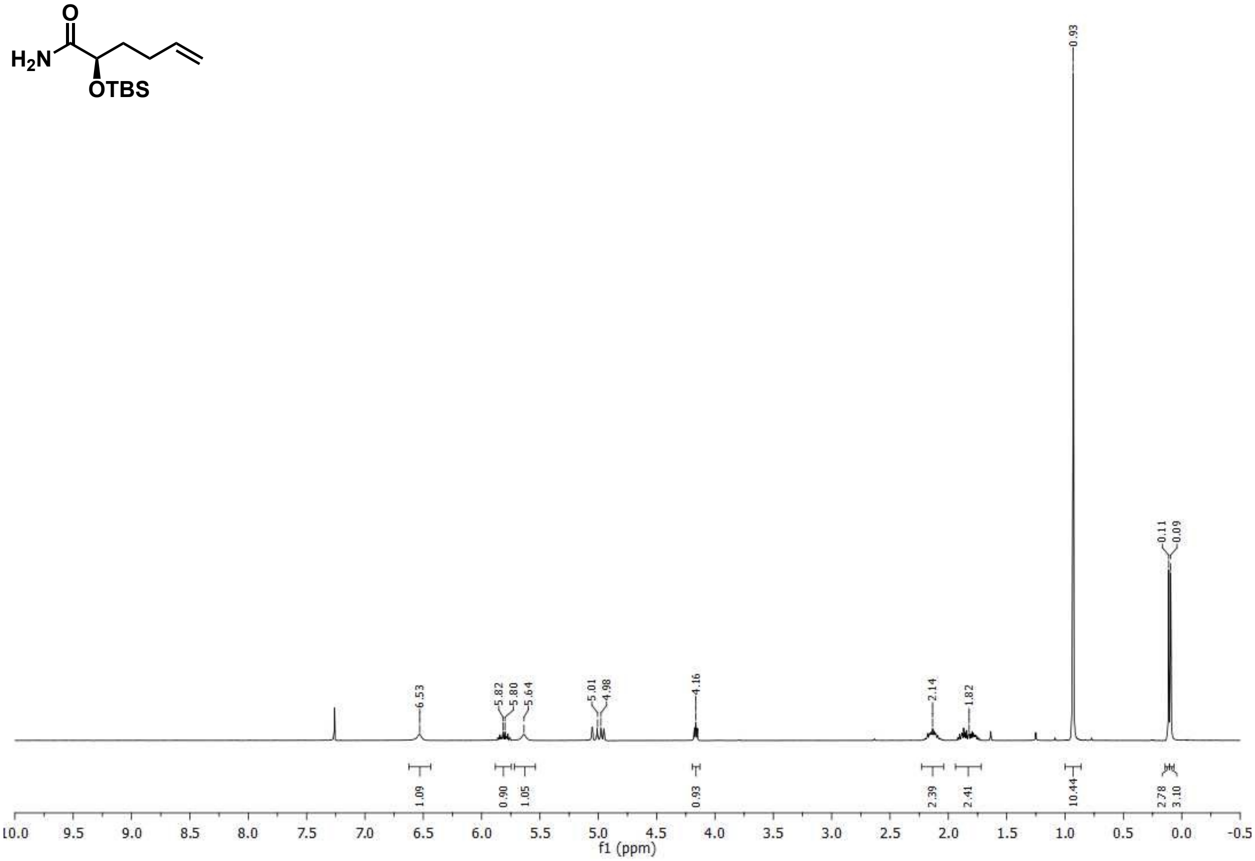

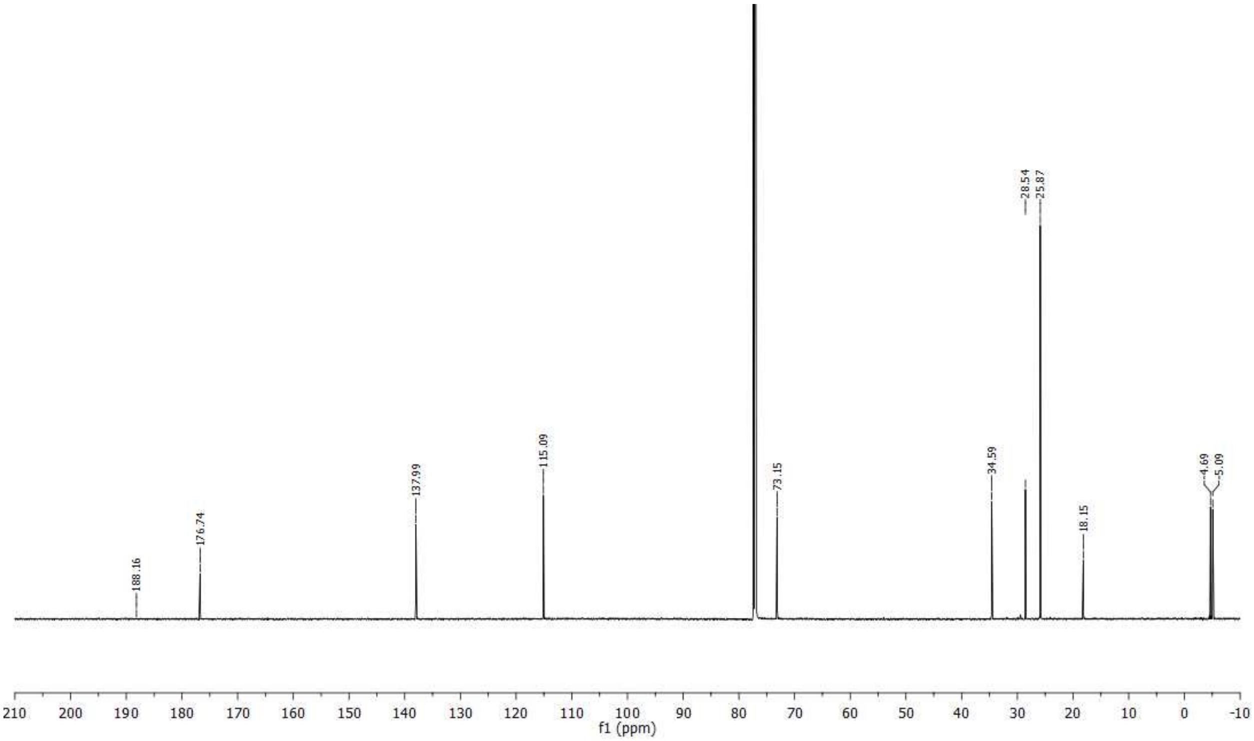

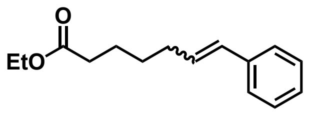
O
EtO

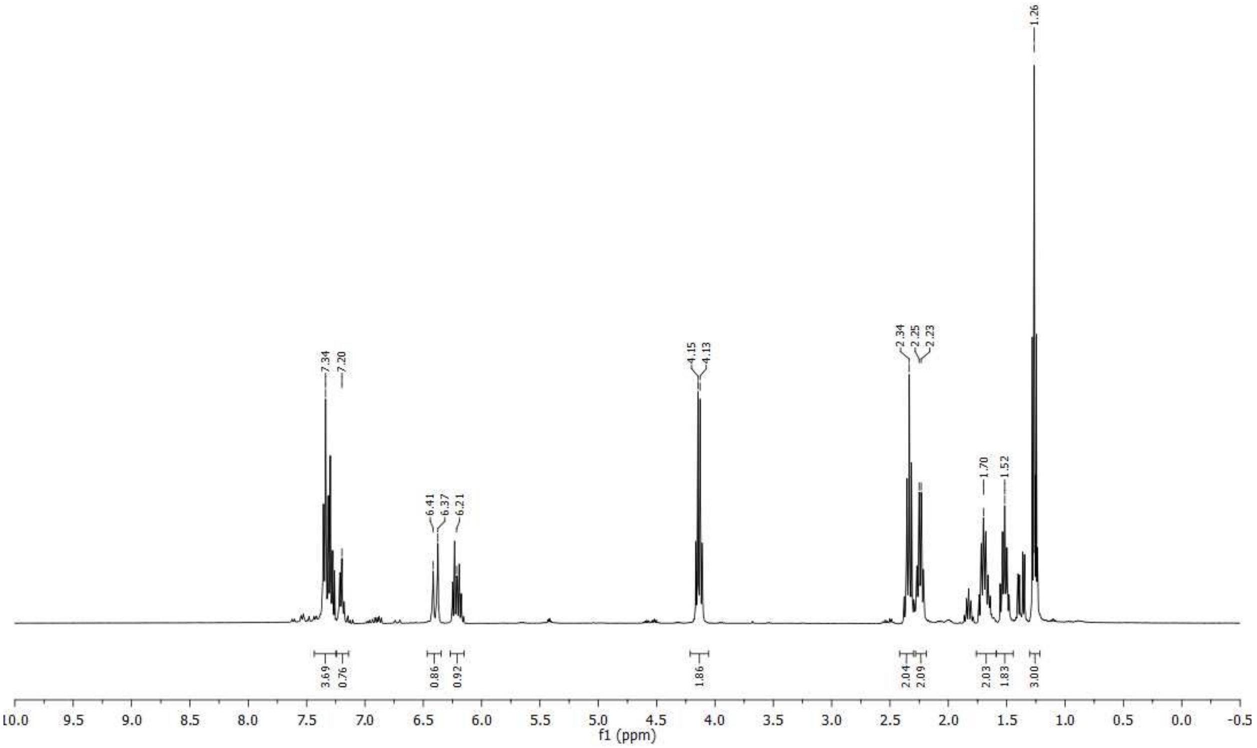
7.34
7.20
6.41
6.37
6.21
4.15
4.13
2.34
2.25
2.23
1.70
1.52
1.26
3.69
0.76
0.86
0.92
1.86
2.04
2.09
2.03
1.83
3.00
10.0
9.5
9.0
8.5
8.0
7.5
7.0
6.5
6.0
5.5
5.0
4.5
4.0
3.5
3.0
2.5
2.0
1.5
1.0
0.5
0.0
-0.5
f1 (ppm)

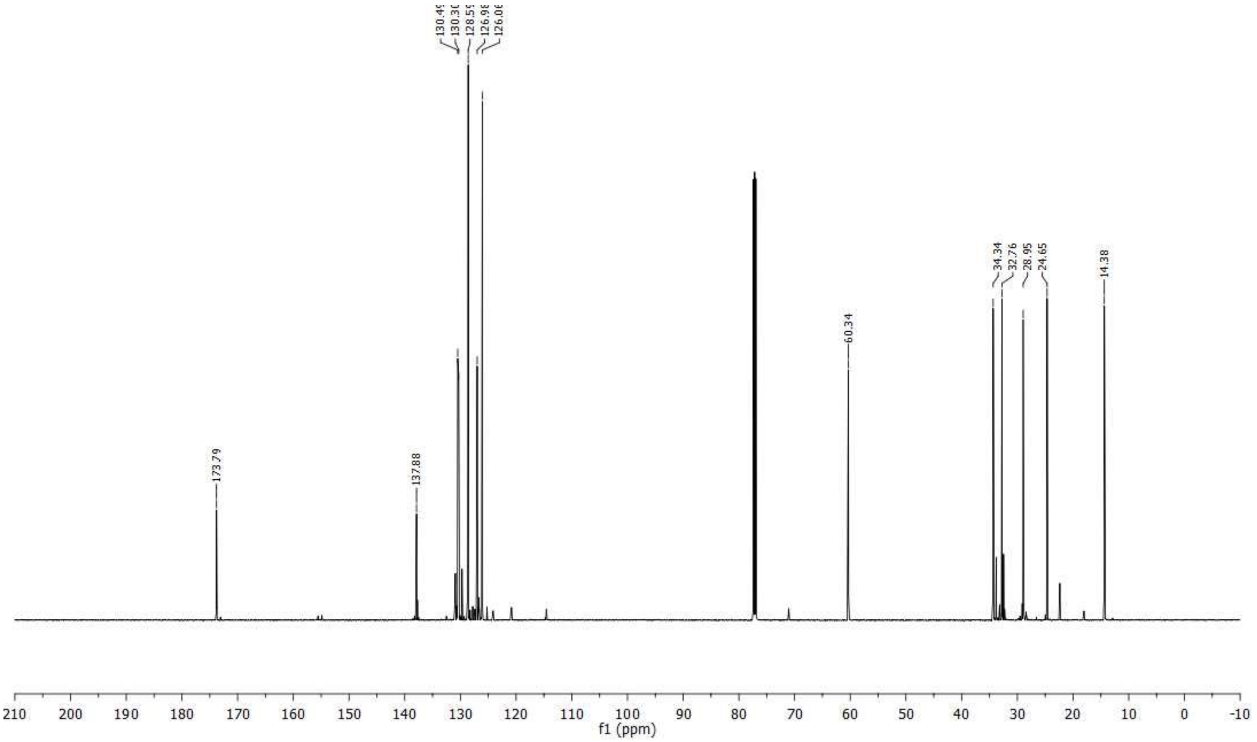
130.49
130.30
128.59
126.98
126.08
173.79
137.88
60.34
34.34
32.76
28.95
24.65
14.38
210
200
190
180
170
160
150
140
130
120
110
100
90
80
70
60
50
40
30
20
10
0
-10
f1 (ppm)

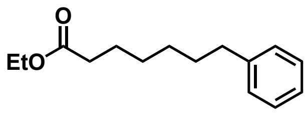

O
EtO

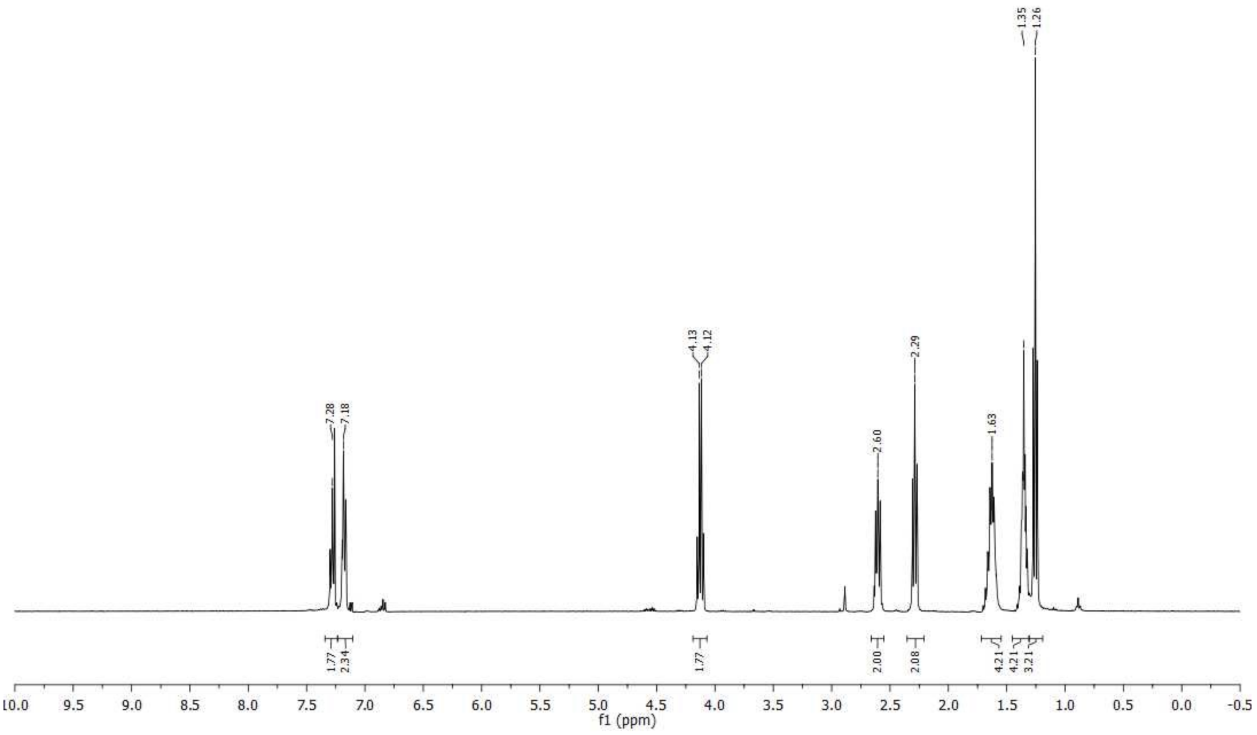

7.28
7.18
4.13
4.12
2.60
2.29
1.63
1.35
1.26
1.77
2.34
1.77
2.00
2.08
4.21
4.21
3.21
10.0
9.5
9.0
8.5
8.0
7.5
7.0
6.5
6.0
5.5
5.0
4.5
4.0
3.5
3.0
2.5
2.0
1.5
1.0
0.5
0.0
-0.5
f1 (ppm)

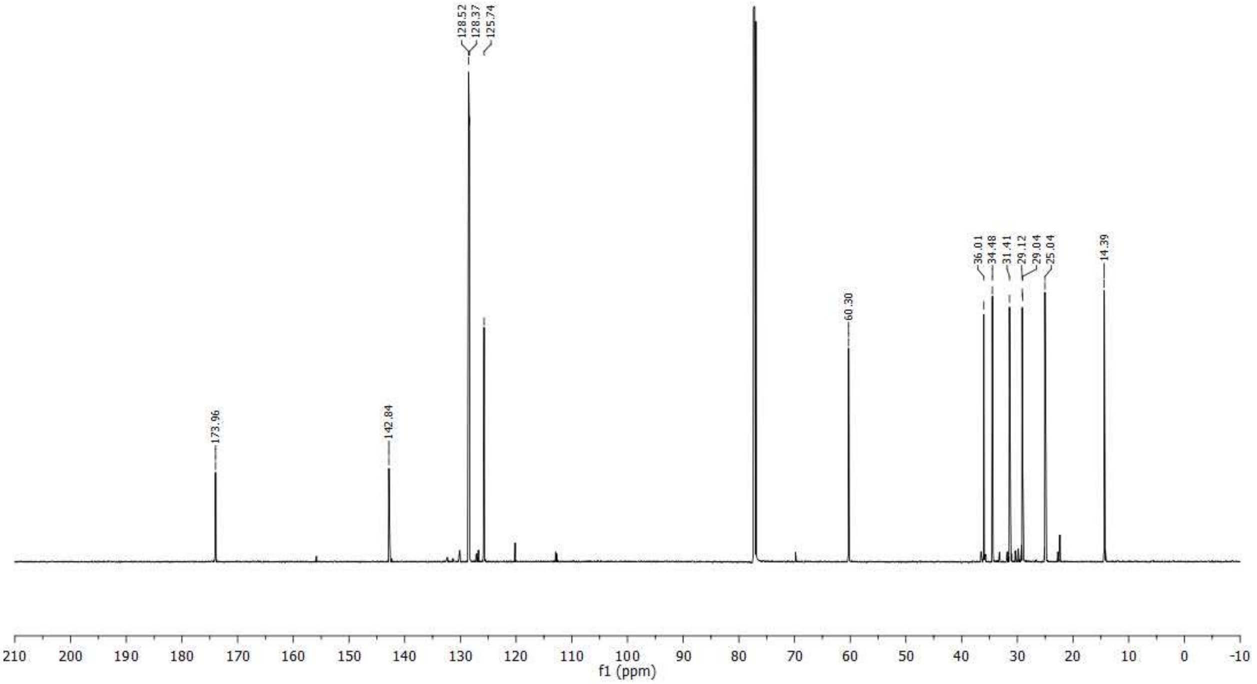

173.96
142.84
128.52
128.37
125.74
60.30
36.01
34.48
31.41
29.12
29.04
25.04
14.39
210
200
190
180
170
160
150
140
130
120
110
100
90
80
70
60
50
40
30
20
10
0
-10
f1 (ppm)

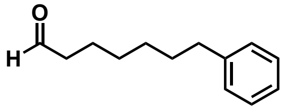
O
H

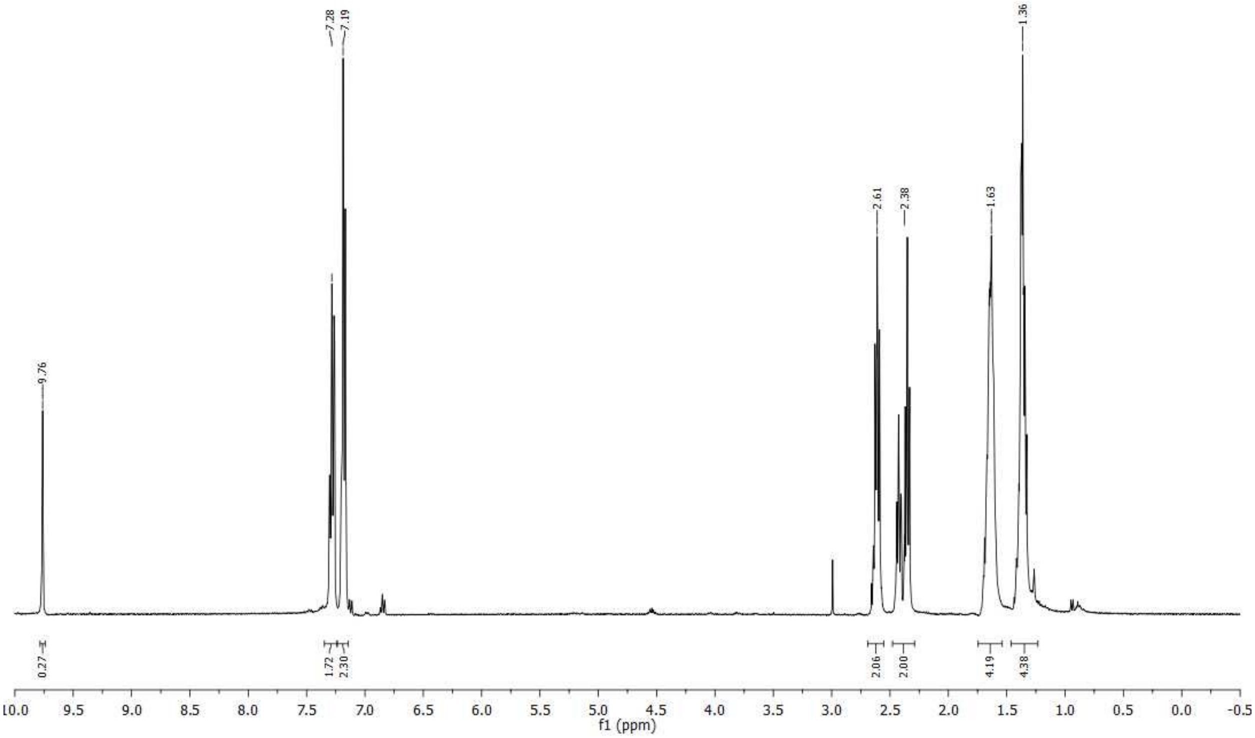
9.76
7.28
7.19
2.61
2.38
1.63
1.36
0.27
1.72
2.30
2.06
2.00
4.19
4.38
10.0
9.5
9.0
8.5
8.0
7.5
7.0
6.5
6.0
5.5
5.0
4.5
4.0
3.5
3.0
2.5
2.0
1.5
1.0
0.5
0.0
-0.5
f1 (ppm)

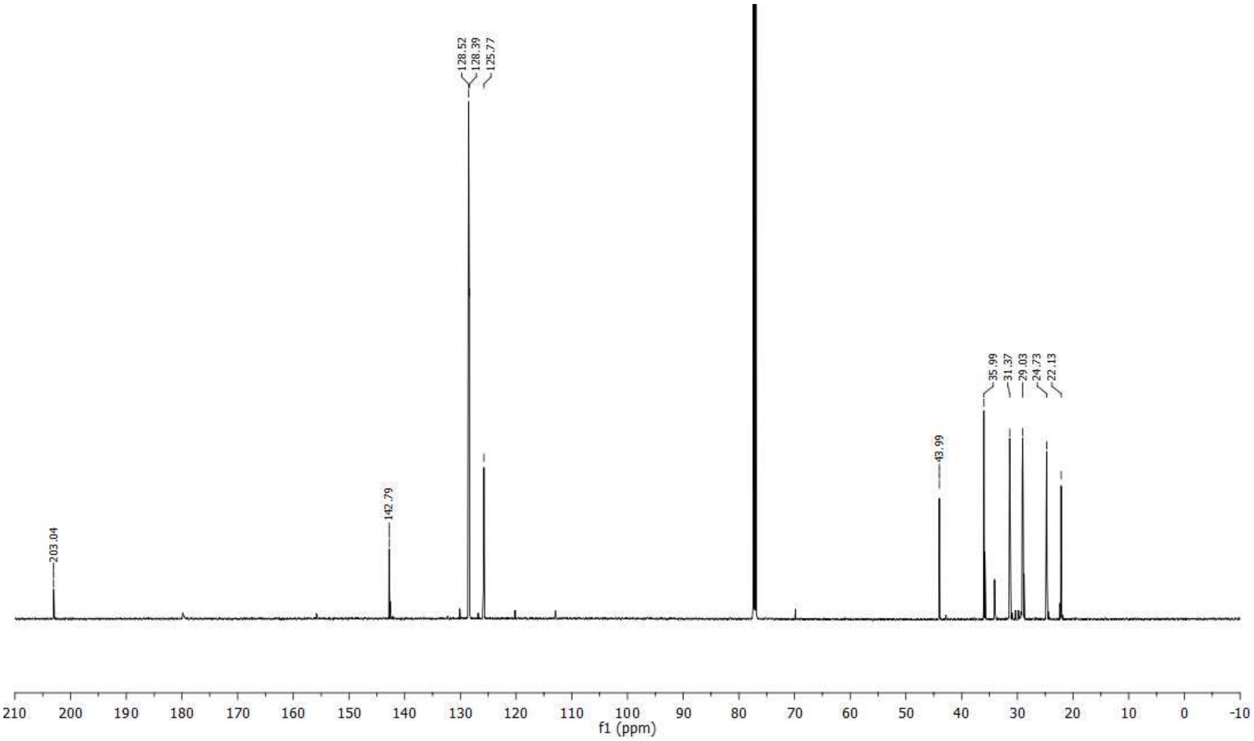
203.04
142.79
128.52
128.39
125.77
43.99
35.99
31.37
29.03
24.73
22.13
210
200
190
180
170
160
150
140
130
120
110
100
90
80
70
60
50
40
30
20
10
0
-10
f1 (ppm)

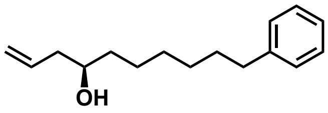
OH

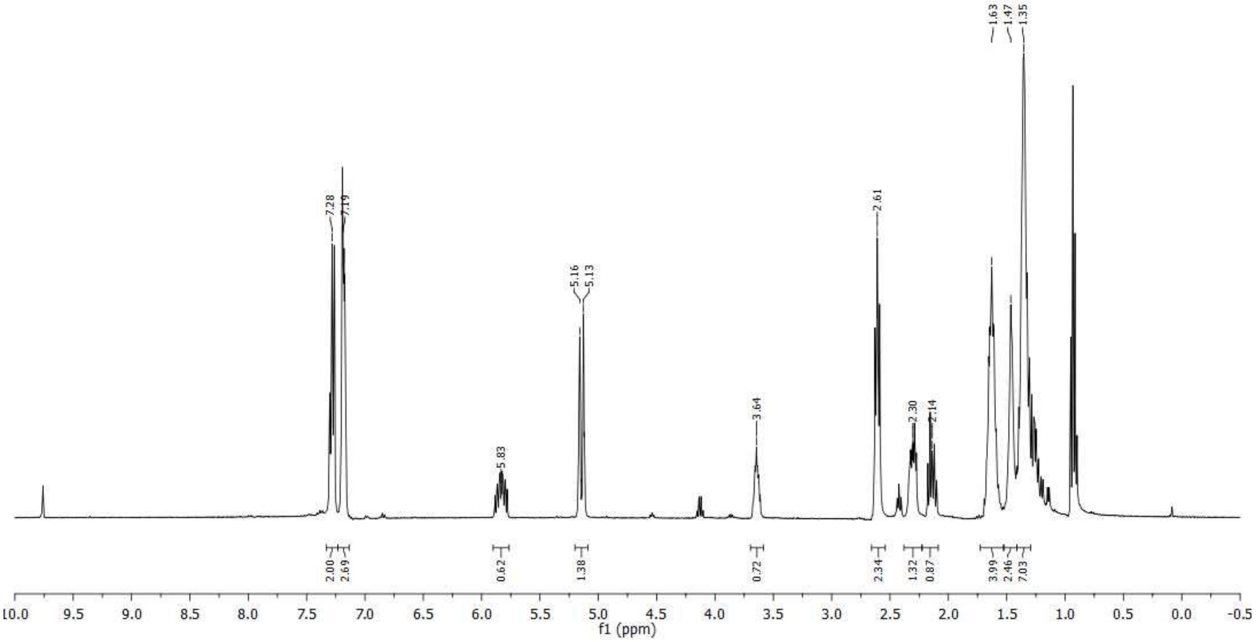
7.28
7.19
5.83
5.16
5.13
3.64
2.61
2.30
2.14
1.63
1.47
1.35
2.00
2.69
0.62
1.38
0.72
2.34
1.32
0.87
3.99
2.46
7.03
10.0
9.5
9.0
8.5
8.0
7.5
7.0
6.5
6.0
5.5
5.0
4.5
4.0
3.5
3.0
2.5
2.0
1.5
1.0
0.5
0.0
-0.5
f1 (ppm)

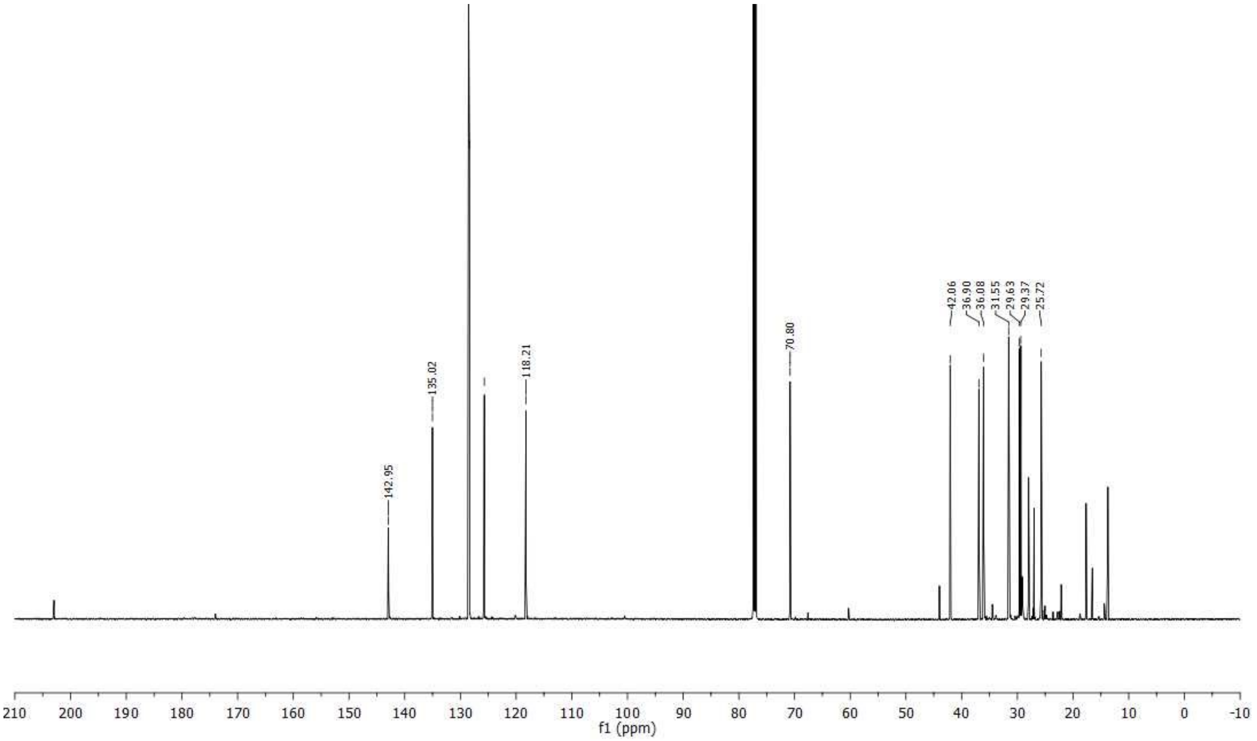
142.95
135.02
118.21
70.80
42.06
36.90
36.08
31.55
29.63
29.37
25.72
210
200
190
180
170
160
150
140
130
120
110
100
90
80
70
60
50
40
30
20
10
0
-10
f1 (ppm)

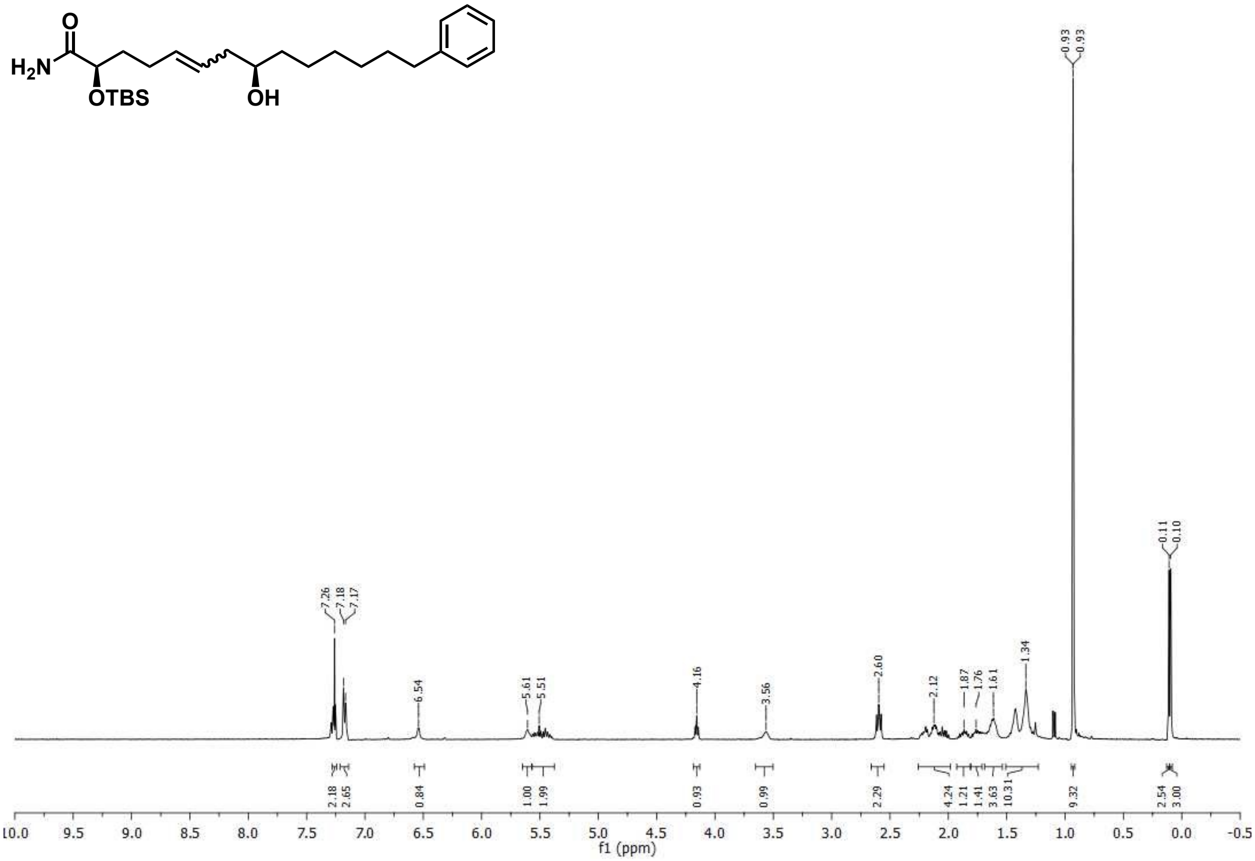
H2N
O
OTBS
OH
7.26
7.18
7.17
6.54
5.61
5.51
4.16
3.56
2.60
2.12
1.87
1.76
1.61
1.34
0.93
0.93
0.11
0.10
2.18
2.65
0.84
1.00
1.99
0.93
0.99
2.29
4.24
1.21
1.41
3.63
10.31
9.32
2.54
3.00
10.0 9.5 9.0 8.5 8.0 7.5 7.0 6.5 6.0 5.5 5.0 4.5 4.0 3.5 3.0 2.5 2.0 1.5 1.0 0.5 0.0 -0.5
f1 (ppm)

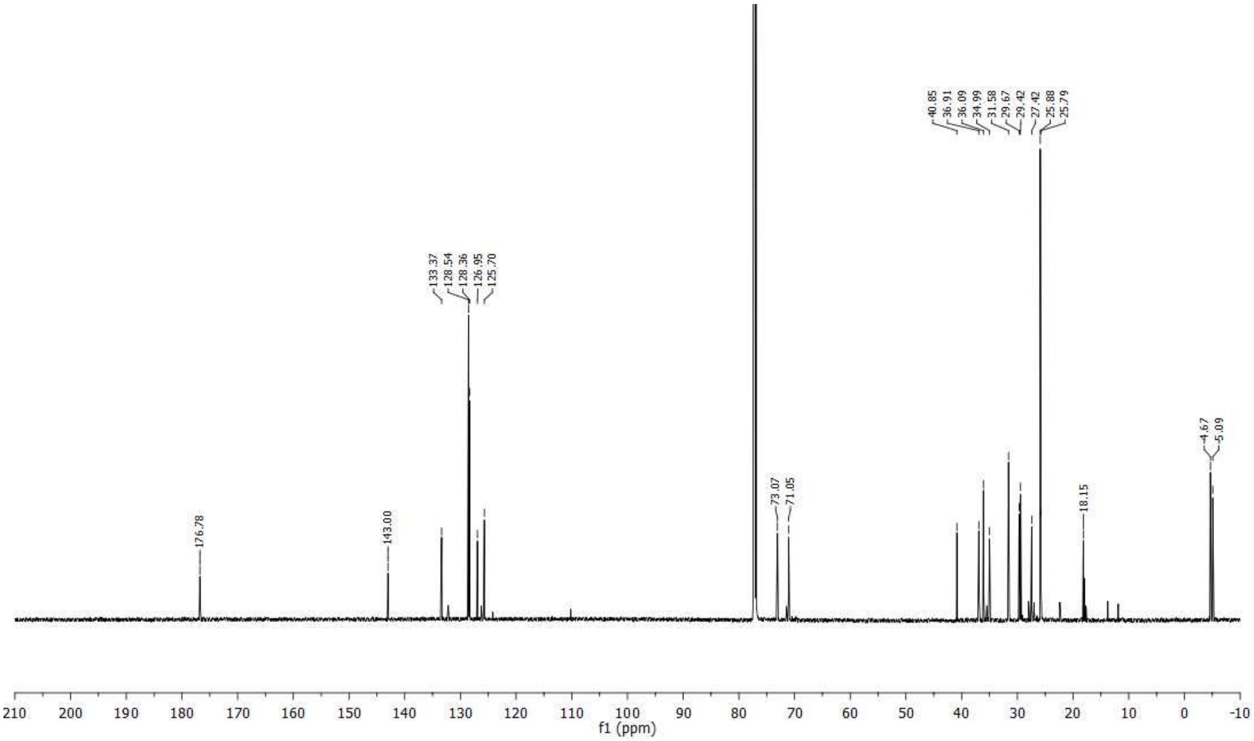
176.78
143.00
133.37
128.54
128.36
126.95
125.70
73.07
71.05
40.85
36.91
36.09
34.99
31.58
29.67
29.42
27.42
25.88
25.79
18.15
-4.67
-5.09
210 200 190 180 170 160 150 140 130 120 110 100 90 80 70 60 50 40 30 20 10 0 -10
f1 (ppm)

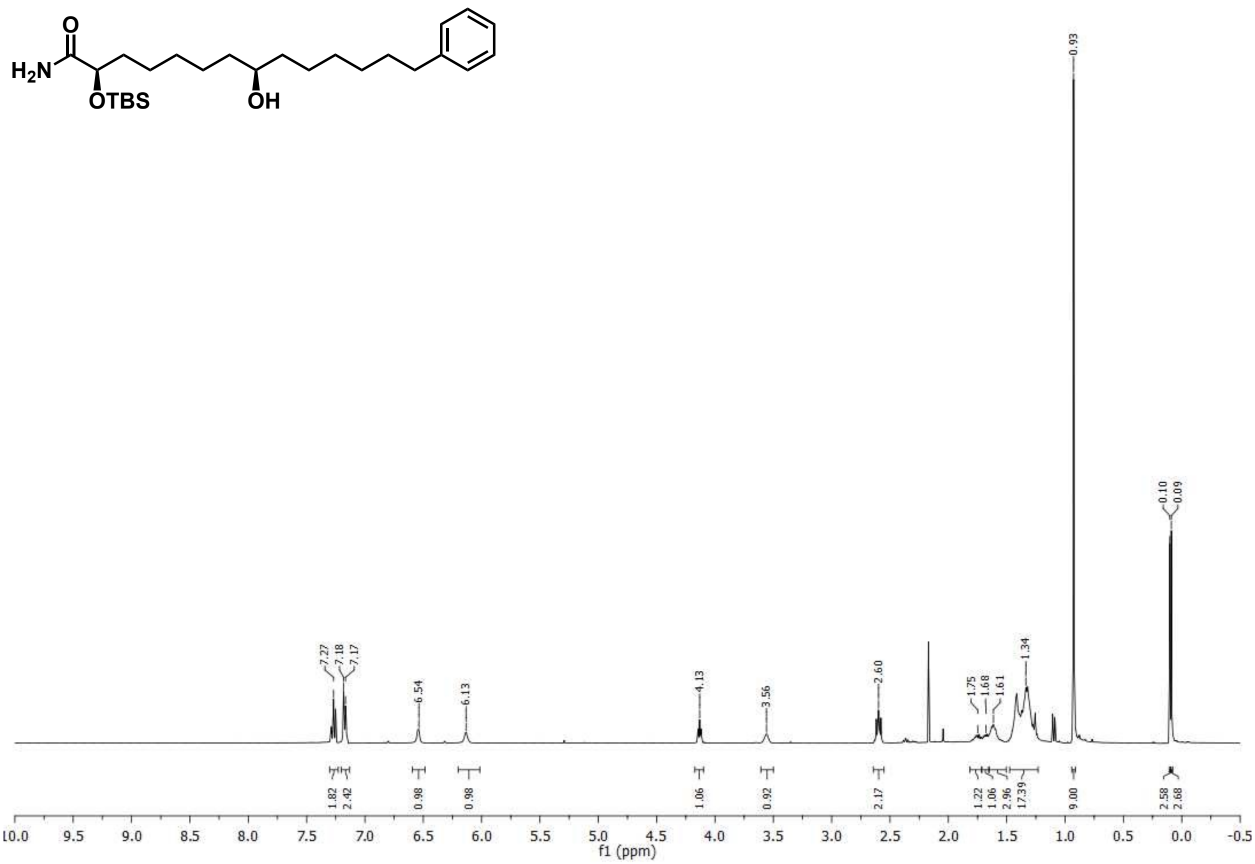
O
H2N
OTBS
OH
7.27
7.18
7.17
6.54
6.13
4.13
3.56
2.60
1.75
1.68
1.61
1.34
0.93
0.10
0.09
1.82
2.42
0.98
0.98
1.06
0.92
2.17
1.22
1.06
2.96
17.39
9.00
2.58
2.68
10.0 9.5 9.0 8.5 8.0 7.5 7.0 6.5 6.0 5.5 5.0 4.5 4.0 3.5 3.0 2.5 2.0 1.5 1.0 0.5 0.0 -0.5
f1 (ppm)

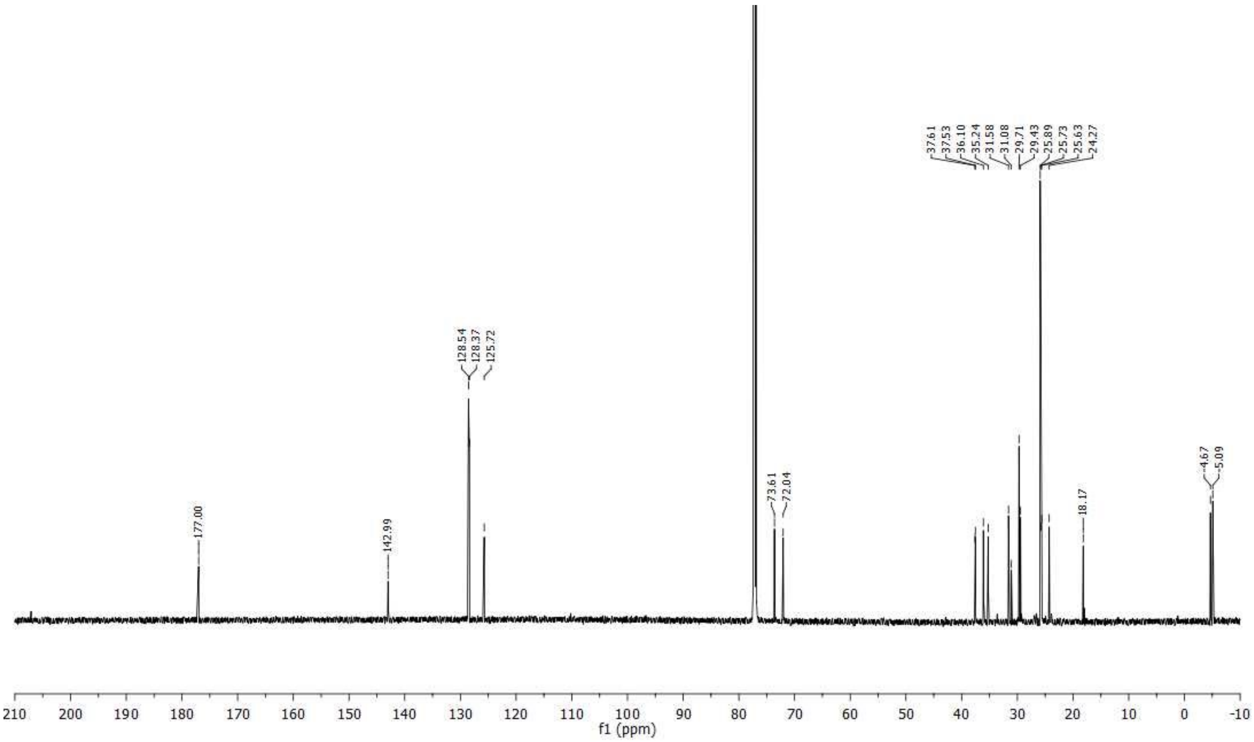
177.00
142.99
128.54
128.37
125.72
73.61
72.04
37.61
37.53
36.10
35.24
31.58
31.08
29.71
29.43
25.89
25.73
25.63
24.27
18.17
-4.67
-5.09
210 200 190 180 170 160 150 140 130 120 110 100 90 80 70 60 50 40 30 20 10 0 -10
f1 (ppm)

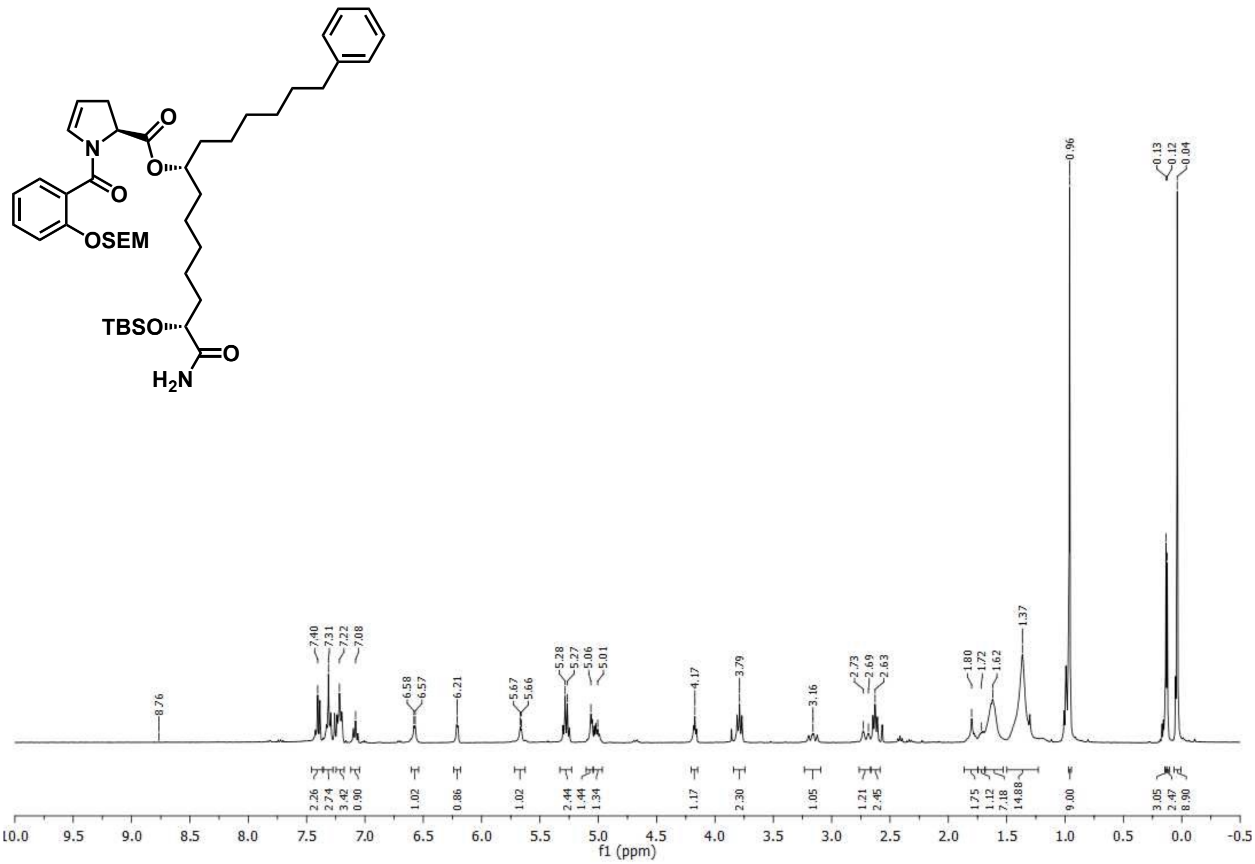
O
N
O
O
OSEM
TBSO
O
H2N
8.76
7.40
7.31
7.22
7.08
6.58
6.57
6.21
5.67
5.66
5.28
5.27
5.06
5.01
4.17
3.79
3.16
2.73
2.69
2.63
1.80
1.72
1.62
1.37
0.96
0.13
0.12
0.04
2.26
2.74
3.42
0.90
1.02
0.86
1.02
2.44
1.44
1.34
1.17
2.30
1.05
1.21
2.45
1.75
1.12
7.18
14.88
9.00
3.05
2.47
8.90
10.0
9.5
9.0
8.5
8.0
7.5
7.0
6.5
6.0
5.5
5.0
4.5
4.0
3.5
3.0
2.5
2.0
1.5
1.0
0.5
0.0
-0.5
f1 (ppm)

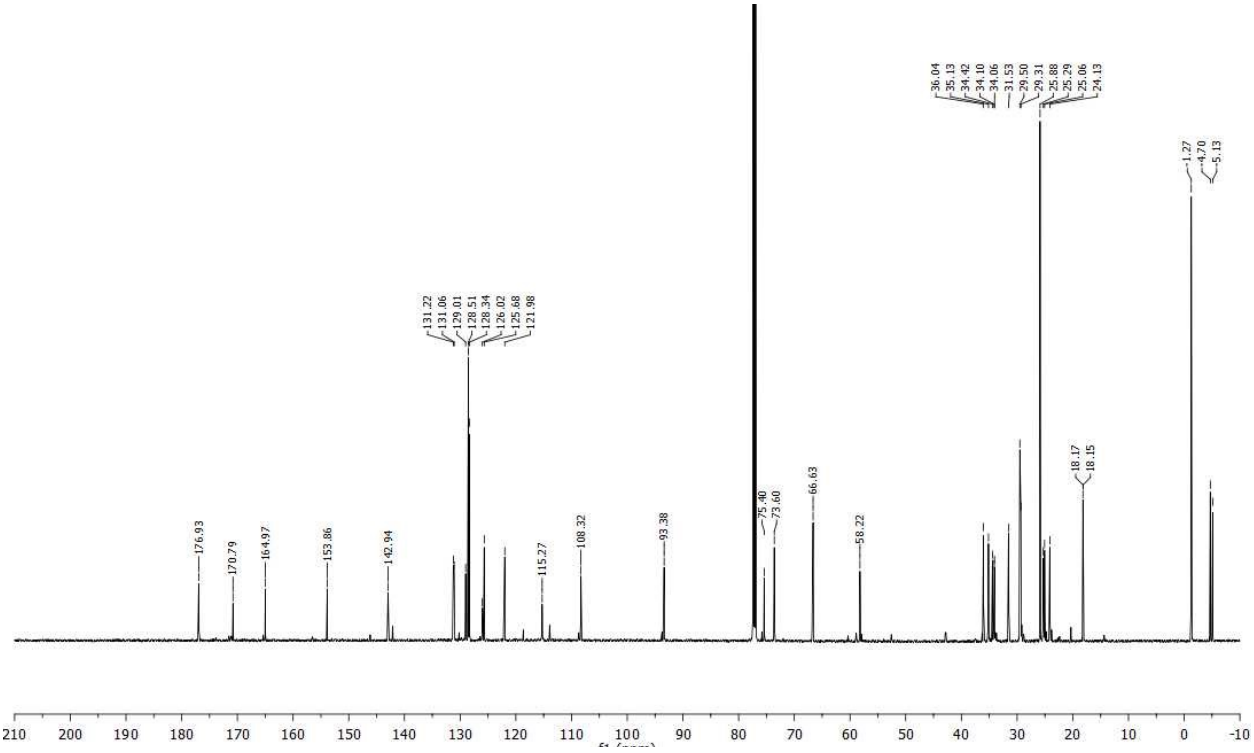
176.93
170.79
164.97
153.86
142.94
131.22
131.06
129.01
128.51
128.34
126.02
125.68
121.98
115.27
108.32
93.38
75.40
73.60
66.63
58.22
36.04
35.13
34.42
34.10
34.06
31.53
29.50
29.31
25.88
25.29
25.06
24.13
18.17
18.15
-1.27
-4.70
-5.13
210
200
190
180
170
160
150
140
130
120
110
100
90
80
70
60
50
40
30
20
10
0
-10

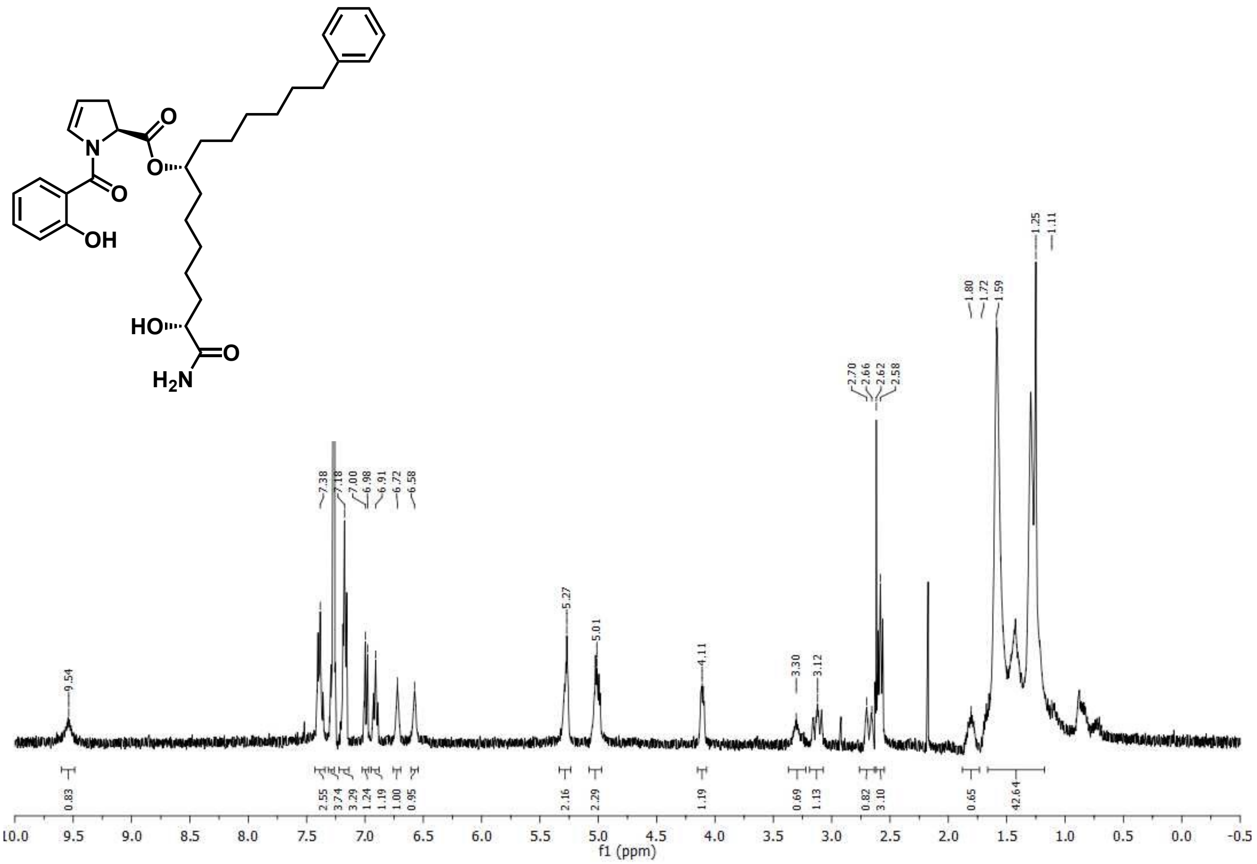
O
N
O
O
OH
HO
O
H₂N
9.54
7.38
7.18
7.00
6.98
6.91
6.72
6.58
5.27
5.01
4.11
3.30
3.12
2.70
2.66
2.62
2.58
1.80
1.72
1.59
1.25
1.11
0.83
2.55
3.74
3.29
1.24
1.19
1.00
0.95
2.16
2.29
1.19
0.69
1.13
0.82
3.10
0.65
42.64
10.0
9.5
9.0
8.5
8.0
7.5
7.0
6.5
6.0
5.5
5.0
4.5
4.0
3.5
3.0
2.5
2.0
1.5
1.0
0.5
0.0
-0.5
f1 (ppm)

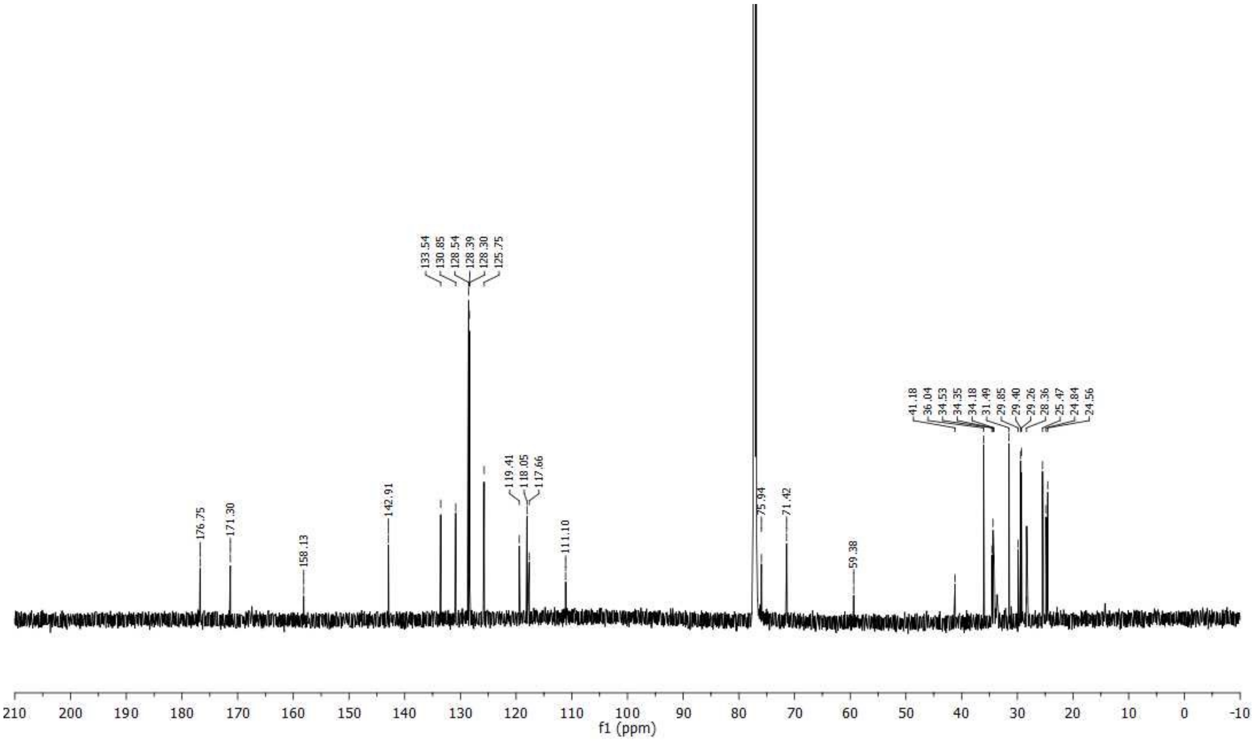
176.75
171.30
158.13
142.91
133.54
130.85
128.54
128.39
128.30
125.75
119.41
118.05
117.66
111.10
75.94
71.42
59.38
41.18
36.04
34.53
34.35
34.18
31.49
29.85
29.40
29.26
28.36
25.47
24.84
24.56
210
200
190
180
170
160
150
140
130
120
110
100
90
80
70
60
50
40
30
20
10
0
-10
f1 (ppm)

Biology

Bacterial Strains and Culture Conditions

P. aeruginosa PAO1 was acquired from Prof. Bettina A. Buttaro (Lewis Katz School of Medicine, Temple University) and *P. aeruginosa* PA14 was acquired from Prof. Joanna B. Goldberg (School of Medicine, Emory University). *P. aeruginosa* RO5 was obtained via resistance selection assay from PA14 in our laboratory.[2] All three strains were grown from a freezer stock overnight (16-24 hours) with shaking at 37 °C, 200 rpm in Trypticase Soy Broth (TSB) media (5 mL).

IC_{50} Assay

Compounds were dissolved in DMSO to give 10 mM stock solutions, which were serially diluted in flat-bottom 96-well microtiter plates yielding 24 test concentrations ranging from 500 μM to 0.030 μM. Controls were prepared by dissolving in 10% DMSO/90% H_2O to 1mM stock solutions and serially diluting in the same manner as for test compounds. The positive control used in all cases was gentamicin and the negative control was a solution of 10% DMSO/90% H_2O. Overnight cultures were diluted 1:100 in 5 mL of fresh media and grown at 37 °C, 200 rpm to an OD_{600} (measured on a Molecular Devices SpectraMax iD3 plate reader) reading of ~0.32. Bacteria were then diluted to a concentration of 0.004 according to the following equation: (x μL regrow culture)*(OD reading) = (0.004)*(volume of diluted bacteria culture needed). Then 100 μL was inoculated into each well of plate already containing 100 μL of compound solution, giving final test concentrations of 250 μM to 0.015 μM. Plates were then incubated statically at 37 °C for 24 hours. OD_{600} readings were taken at this point, and IC_{50} and IC_{90} values were calculated by fitting OD readings vs. concentrations with a four-parameter logistic model. Compounds were tested in triplicate from three separate overnight cultures and averaged. IC_{50} values were calculated in prism by Savannah J. Post.

Computational pose prediction for promysalin analogs

To build structural models of promysalin analog in complex with succinate dehydrogenase (Sdh), we used a very similar protocol to that described in our earlier study.[2] Previously, we used the protein structure extracted from PDB ID 2WU5,[3] and used the ROCS software to overlay low energy conformers of promysalin onto carboxin inhibitor in the active site. From here, the model was refined using a gradient-based full atom minimization in Rosetta.[4] Finally, models were ranked on the bases of the protein-ligand interaction energy.

For the present study, we took advantage of the fact that diversity in the analogs was restricted to the alkyl chain. We therefore fixed the shared promysalin substructure in the active conformation from our previous study, rather than build low-energy conformers from scratch. We built conformers using the OMEGA software,[5,6] with the following command line:

```
omega2 -in input_file.smi -out output_file.sdf.gz -prefix ligand_name -warts -maxconfs 1000000 -rms 0.01 –fixfile original_promysalin_model.pdb
```

Because structural diversity in the conformers was limited to the alkyl chain (i.e., the part of the chemical structure that was varied in this study), the number of conformers generated was much less than would be required if all internal degrees of freedom in the compound were explicitly modeled:

Analog	Number of conformers generated
(-)-11d	3
(-)-11e	8
(-)-11f	18
(-)-11g	36
(-)-1	113
(-)-11h	117
(-)-11i	178
(-)-11j	261
(-)-12	305

Having built these conformers, we replicated our earlier pipeline exactly, with the sole exception that we aligned each promysalin analog to our previous model of the promysalin/Sdh complex (rather than to carboxin from 2WU5). The resulting models were then refined and ranked using Rosetta, exactly as in our previous study.

*Computational work was performed by Jittasak Khowsathit and John Karanicolas.

References

1 Kaliapan, K. P.; Ravikumar, V. *J. Org. Chem.* **2007**, *72*, 6116-6126.

2 Keohane, C. E.; Steele, A. D.; Fetzer, C.; Khowsathit, J.; Van Tyne, D.; Moynié, L.; Gilmore, M. S.; Karanicolas, J.; Sieber, S. A.; Wuest, W. M. *J. Am. Chem. Soc.* **2018**, *140*, 1774-1782.

3 Ruprecht, J.; Yankovskaya, V.; Maklashina, E.; Iwata, S.; Cecchini, G. *J. Biol. Chem.* **2009**, *284*, 29836-29846.

4 Leaver-Fay, A.; Tyka, M.; Lewis, S. M.; Lange, O. F.; Thompson, J.; Jacak, R.; Kaufman, K.; Renfrew, P. D.; Smith, C. A.; Sheffler, W.; Davis, I. W.; Cooper, S.; Treuille, A.; Mandell, D. J.; Richter, F.; Ban, Y. E.; Fleishman, S. J.; Corn, J. E.; Kim, D. E.; Lyskov, S.; Berrondo, M.; Mentzer, S.; Popovic, Z.; Havranek, J. J.; Karanicolas, J.; Das, R.; Meiler, J.; Kortemme, T.; Gray, J. J.; Kuhlman, B.; Baker, D.; Bradley, P. *Methods. Enzymol.* **2011**, *487*, 545-574.

5 Hawkins, P. C. D.; Skillman, A. G.; Warren, G. L.; Ellingson, B. A.; Stahl, M. T. *J. Chem. Inf. Model.* **2010**, *50*, 572-584.

6 Hawkins, P. C. D.; Nicholls, A. *J. Chem. Inf. Model.* **2012**, *52*, 2919-2936.

Synthesis and Biological Evaluation of Iron-Binding *Pseudomonad* Metabolites

Synthesis

General Information

All non-aqueous reactions were conducted in flame-dried glassware equipped with a stir bar under an argon atmosphere using HPLC-grade solvents which were dried by passing through activated alumina. Reagents were purchased from Oakwood, TCI America, Sigma-Aldrich, Alfa Aesar, and AK Scientific. Triethylamine was freshly distilled from CaH_2 prior to use. Thin-layer chromatography was performed on 250μm SiliCycle silica gel F-254 plates and visualized by fluorescence and/or staining using potassium permanganate, or vanillin stains. Brine refers to a saturated aqueous solution of sodium chloride, sat. $NaHCO_3$ refers to a saturated aqueous solution of sodium bicarbonate and sat. NH_4Cl refers to saturated aqueous solution of ammonium chloride. Organic solutions were concentrated under reduced pressure on a Buchi Rotavapor R3 rotary evaporator. Chromatographic purification was accomplished using a Biotage® flash chromatography purification system.

^1H NMR and ^{13}C NMR spectra were recorded on a Bruker (600 MHz), Inova (500 MHz), Inova (400 MHz), or VNMR (400 MHz) spectrometer, all from the Emory University NMR facility. ^1H NMR data were reported in terms of chemical shift (δ ppm relative to tetramethylsilane and with the indicated deuterated solvent as the internal reference), multiplicity, described using the following abbreviations: s (singlet), d (doublet), t (triplet), q (quartet), m (multiplet), br (broad), dd (doublet of doublets), dt (doublet of triplets), etc., coupling constant (Hz), and integration. ^{13}C NMR data were reported in terms of chemical shift. Accurate mass spectra were obtained from a Thermo LTQ-FTMS using APCI techniques.

Experimental Procedures and Spectral Data

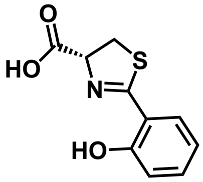

(*R*)-2-(2-hydroxyphenyl)-4,5-dihydrothiazole-4-carboxylic acid 3.01: Synthesized as previously described.[1,2] A solution of **2-hydroxybenzonitrile** (2.00 g, 16.8 mmol) and **L-cysteine** (4.07 g, 33.6 mmol) in 75 mL of MeOH and 75 mL of 0.1 M phosphate buffer was heated to 60 °C and stirred for 16 hours at a pH of 6.4. The reaction mixture was then concentrated under reduced pressure, redissolved in deionized water, and acidified to a pH of 1.0. This solution was then extracted with EtOAc (3x), washed with sat. $NaHCO_3$ (1x) and brine (1x), dried over Na_2SO_4, and concentrated under reduced pressure, yielding a yellow solid (1.37 g, 37%).

^{1}H NMR (500 MHz, $(CD_3)_2CO$) δ 7.48 (dd, *J* = 7.8, 1.7 Hz, 1H), 7.44 (dddd, *J* = 8.3, 7.3, 1.7 Hz, 1H), 6.98 (dd, *J* = 8.3, 1.0 Hz, 1H), 6.95 (dddd, *J* = 8.2, 7.3, 1.4), 5.55 (dd, *J* = 9.3, 7.8 Hz, 1H), 3.77 (m, 2H), 2.82 (br s, 1H); **^{13}C NMR** (151 MHz, $(CD_3)_2CO$) δ 174.47, 171.32, 160.09, 134.44, 131.53, 119.90, 117.87, 116.87, 77.58, 34.15; **HRMS** (APCI$^+$): Found 224.03741 (-0.81 ppm), $C_{10}H_{10}NO_3S$ (M+H) requires 224.03759.

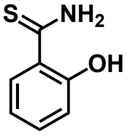

2-hydroxythiobenzamide 3.02: A solution of **2-hydroxybenzamide** (2.00 g, 14.6 mmol) and Lawesson's reagent (4.73 g, 11.7 mmol) in 150 mL of THF was stirred at ambient temperature for 6 hours. The reaction mixture was then concentrated under reduced pressure and purified by column chromatography (0-30% EtOAc/Hexanes) yielding a yellow solid (642 mg, 29%).

^{1}H NMR (600 MHz, $(CD_3)_2CO$) δ 11.91 (br s, 1H), 9.12 (br s, 2H), 7.82, (dd, *J* = 8.1, 1.7 Hz, 1H), 7.41 (ddd, *J* = 8.3, 7.2, 1.7 Hz, 1H), 6.97 (dd, *J* = 8.3, 1.3 Hz, 1H), 6.89 (ddd, *J* = 8.3, 7.2, 1.3 Hz, 1H); **^{13}C NMR** (151 MHz, $(CD_3)_2CO$) δ 198.90, 160.42, 134.83, 127.34, 121.34, 119.69, 119.61; **HRMS** (APCI$^+$): Found 154.03202 (-0.59 ppm), C_7H_8NOS (M+H) requires 154.03211.

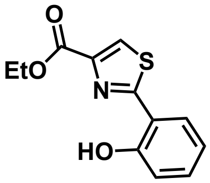

Ethyl 2-(2-hydroxyphenyl)thiazole-4-carboxylate 3.03: Synthesized as previously described.[3] A solution of **ethyl bromopyruvate** (0.632 mL, 5.03 mmol) and thioamide **3.02** (642 mg, 4.19 mmol) in 35 mL of EtOH was heated to 70 °C and stirred 5 hours. The reaction mixture was concentrated under reduced pressure and purified by column chromatography (0-20% EtOAc/Hexanes) yielding a faint yellow solid (540 mg, 52%).

^{1}H NMR (600 MHz, $CDCl_3$) δ 11.91 (s, 1H), 8.10 (s, 1H), 7.61 (d, *J* = 7.9 Hz, 1H), 7.36 (t, *J* = 7.8 Hz, 1H), 7.10 (d, *J* = 8.3 Hz, 1H), 6.93 (t, *J* = 7.5 Hz, 1H), 4.43 (q, *J* = 6.2 Hz, 2H), 1.42 (t, *J* = 7.2 Hz, 3H); **^{13}C NMR** (151 MHz, $CDCl_3$) δ 169.57, 160.68, 157.20, 146.24, 132.66, 127.46, 125.14, 119.67, 118.26, 116.43, 61.74, 14.44; **HRMS** (APCI$^+$): Found 250.05333 (+0.36 ppm), $C_{12}H_{12}NO_3S$ (M+H) requires 250.05324.

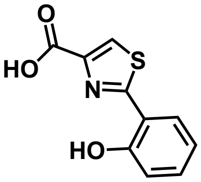

2-(2-hydroxyphenyl)thiazole-4-carboxylic acid 3.04: Synthesized as previously described.[3] To a solution of ester **3.03** (450 mg, 1.81 mmol) in 24 mL of THF/H_2O (1:1) was added a 1.0 M solution of lithium hydroxide (173 mg, 7.23 mmol) in deionized water and the solution stirred at ambient temperature for 3 hours. The reaction mixture was concentrated under reduced pressure, redissolved in minimal EtOAc, and acidified with 2.0 M HCl until a solid precipitated. This was then extracted with EtOAc (3x), washed with brine (1x), and concentrated under reduced pressure to a pale-yellow solid (375 mg, 94%). **^{1}H NMR** (500 MHz, $(CD_3)_2CO$) δ 11.79 (s, 1H), 8.47 (s, 1H), 7.84 (d, *J* = 7.9 Hz, 1H), 7.41 (t, *J* = 7.8 Hz 1H), 7.05 (d, *J* = 8.3 Hz, 1H), 7.00 (t, *J* = 7.0 Hz, 1H), 2.85 (br s, 1H); **^{13}C NMR** (151 MHz, $(CD_3)_2CO$) δ 169.68, 161.44, 157.70, 146.85, 133.32, 128.55, 127.64, 120.64, 118.46, 117.50; **HRMS** (APCI$^+$): Found 222.02195 (+0.04 ppm), $C_{10}H_8NO_3S$ (M+H) requires 222.02194.

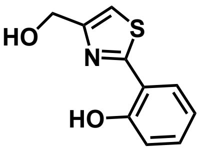

2-(4-(hydroxymethyl)thiazol-2-yl)phenol 3.05: To a solution of carboxylic acid **3.04** (84.1 mg, 0.380 mmol) in 2.0 mL of THF cooled to 0 °C was added 1.0 M borane-tetrahydrofuran complex (1.14 mL, 1.14 mmol). The solution stirred overnight at ambient temperature, after which 1.0 M HCl was added. The solution was extracted with EtOAc (2x), washed with brine (1x), dried over Na_2SO_4, concentrated under reduced pressure, and purified by column chromatography (50% EtOAc/Hexanes) yielding a yellow solid (18.5 mg, 23%).

^{1}H NMR (500 MHz, $CDCl_3$) δ 12.00 (br s, 1H), 7.63 (dd, *J* = 7.6, 1.4 Hz, 1H), 7.32 (ddd, *J* = 7.9, 7.3, 1.0 Hz, 2H), 7.18 (t, *J* = 1.0 Hz, 1H), 7.06 (dd, *J* = 8.3, 0.7 Hz, 1H), 6.91 (ddd, *J* = 7.8, 7.2, 1.2 Hz, 1H), 4.84 (d, *J* = 1.0 Hz, 1H); **^{13}C NMR** (151 MHz, $CDCl_3$) δ169.93, 156.85, 155.35, 132.04, 127.35, 119.64, 117.93, 116.97, 113.01, 61.09; **HRMS** (APCI$^+$): Found 208.04261 (-0.07 ppm), $C_{10}H_{10}NO_2S$ (M+H) requires 208.04268.

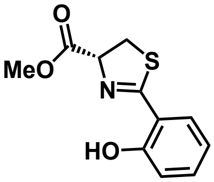

Methyl (*R*)-2-(2-hydroxyphenyl)-4,5-dihydrothiazole-4-carboxylate 3.06: Synthesized as previously described.[4] A solution of **2-hydroxybenzonitrile** (2.38 g, 20.0 mmol), **L-cysteine methyl ester hydrochloride** (13.7 g, 80.0 mmol), and $NaHCO_3$ (2.12 g, 20.0 mmol) in 20 mL of MeOH was refluxed for 16 hours. The reaction was cooled to ambient temperature, quenched with deionized water, extracted with Et_2O (3x), washed with brine (1x), dried over Na_2SO_4, concentrated under reduced pressure, and purified by column chromatography (0-50% EtOAc/hexanes) giving a yellow oil (4.24 g, 89%). **^{1}H NMR** (500 MHz, $CDCl_3$) δ 11.82 (s, 1H), 7.50 (d, *J* = 9.4 Hz, 1H), 7.44 (t, *J* = 8.5 Hz, 1H), 7.01 (d, *J* = 8.3 Hz, 1H), 6.88 (t, *J* = 7.7 Hz, 1H), 5.15 (t, *J* = 3.6 Hz, 1H), 4.07 (m, 2H), 3.88 (s, 3H); **^{13}C NMR** (151 MHz, $CDCl_3$) δ 169.81, 169.23, 161.80, 135.06, 126.05, 119.14, 118.81, 113.64, 53.49, 53.31, 44.96; **HRMS** (APCI$^+$): Found 238.05309 (-0.63 ppm), $C_{11}H_{12}NO_3S$ (M+H) requires 238.05324.

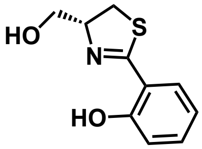

(*R*)-2-(4-(hydroxymethyl)-4,5-dihydrothiazol-2-yl)phenol 3.07: Synthesized as previously described.[1] A solution of **3.06** (331 mg, 1.39 mmol), and sodium borohydride (137 mg, 3.61 mmol) in 4.0 mL of THF was stirred at reflux for 10 minutes before addition of 1.0 mL of MeOH. After being cooled to ambient temperature, 0.3 mL of deionized water was added, and the solution stirred another 10 minutes, followed by the addition of 0.5 mL of deionized water. The reaction mixture was then extracted with Et_2O (3x), washed with brine (1x), dried over Na_2SO_4, concentrated under reduced pressure, and purified by column chromatography (5% $MeOH/CH_2Cl_2$) yielding a yellow oil (216 mg, 74%).

^{1}H NMR (500 MHz, CD_3OD) δ 7.41 (dd, *J* = 7.9, 1.6 Hz, 1H), 7.34 (ddd, *J* = 8.4, 7.2, 1.6 Hz, 1H), 6.93 (d, *J* = 8.4, 1.2 Hz, 1H), 6.87 (ddd, *J* = 8.0, 7.0, 1.3 Hz, 1H), 4.82 (m, 1H), 3.79 (dd, *J* = 5.6, 1.2 Hz, 2H), 3.46 (m, 1H) 3.31 (m, 1H); **^{13}C NMR** (151 MHz, CD_3OD) δ 173.57, 160.18, 134.05, 131.60, 119.94, 117.80, 117.56, 79.48, 64.22, 33.69; **HRMS** (APCI$^+$): Found 210.05815 (-0.84 ppm), $C_{10}H_{12}NO_2S$ (M+H) requires 210.05833.

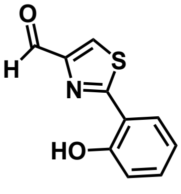

2-(2-hydroxyphenyl)thiazole-4-carbaldehyde 3.08: Synthesized as previously described.[1] To a solution of oxalyl chloride (6.30 mL, 12.6 mmol) and dimethylsulfoxide (1.55 mL, 21.8 mmol) in 180 mL of CH_2Cl_2 cooled to -78 °C was added a solution of **3.07** (1.20 g, 5.73 mmol) in 20 mL of CH_2Cl_2 dropwise via syringe pump over 20 minutes. Triethylamine (9.60 mL, 68.8 mmol) was then added. The reaction mixture was then warmed to ambient temperature and quenched with deionized water. The organic layer was then washed with brine (1x), dried over Na_2SO_4, concentrated under reduced pressure, and purified by column chromatography (100% CH_2Cl_2) affording a yellow solid (414 gm, 35%).

^{1}H NMR (600 MHz, $CDCl_3$) δ 11.61 (s, 1H), 10.06 (s, 1H), 8.13 (s, 1H), 7.63 (dd, *J* = 7.8, 1.6 Hz, 1H), 7.38 (ddd, *J* = 8.8, 7.3, 1.6 Hz, 1H), 7.10 (dd, *J* = 8.4, 1.2 Hz, 1H), 6.95 (ddd, *J* = 7.8, 7.2, 1.6 Hz, 1H); **^{13}C NMR** (151 MHz, $CDCl_3$) δ 183.52, 170.60, 157.02, 153.71, 133.02, 127.72, 125.28, 119.93, 118.31, 116.18; **HRMS** (APCI$^+$): Found 206.0273 (+1.32 ppm), $C_{10}H_8NO_2S$ (M+H) requires 206.02703.

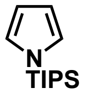

1-(triisopropylsilyl)-1*H*-pyrrole 3.09: To a suspension of sodium hydride (632 mg, 15.9 mmol) in 25 mL of THF cooled to 0 °C was added **1*H*-pyrrole** (1.00 mL, 14.4 mmol). Triisopropylsilyl chloride (3.08mL, 14.4 mmol) was added and the solution stirred for 1.5 hours. The reaction was quenched with iced deionized water, extracted with Et_2O (3x), washed with brine (1x), dried over Na_2SO_4, and concentrated under reduced pressure to a brown oil, which was used without further purification (3.20 g, >99%).

^{1}H NMR (400 MHz, $CDCl_3$) δ 6.80 (t, *J* = 2.0 Hz, 2H), 6.32 (t, *J* = 2.0 Hz, 2H), 1.53-1.38 (hept, *J* = 7.5 Hz, 3H), 1.10 (d, *J* = 7.4 Hz, 18H); **^{13}C NMR** (151 MHz, $CDCl_3$) δ 124.11, 110.17, 17.93, 11.85. **HRMS** (APCI$^+$): Found 224.18309 (+0.84 ppm), $C_{13}H_{26}NSi$ (M+H) requires 224.1829.

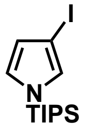

3-iodo-1-(triisopropylsilyl)-1*H*-pyrrole 3.10: Synthesized as previously described.[5] To a solution of **3.09** (3.14 g, 13.5 mmol) in 30 mL of acetone was added N-iodosuccinimide (3.03 g, 13.5 mmol). The reaction was covered with aluminum foil and stirred at ambient temperature for 16 hours, then was concentrated under reduced pressure and purified by column chromatography (20% EtOAc/hexanes) yielding a clear oil (3.32 g, 70%).

^{1}H NMR (600 MHz, $CDCl_3$) δ 6.80 (t, *J* = 1.2 Hz, 1H), 6.67 (t, *J* = 2.5 Hz, 1H), 6.37 (dd, *J* = 2.8, 1.4 Hz, 1H), 1.42 (hept, *J* = 7.5 Hz, 3H), 1.09 (d, *J* = 7.5 Hz, 18H); **^{13}C NMR** (151 MHz, $CDCl_3$) δ 128.85, 125.85, 117.67, 17.86, 11.72 (carbon adjacent to iodine was not detected); **HRMS** (APCI$^+$): Found 349.07999 (+1.26 ppm), $C_{13}H_{25}NISi$ (M+H) requires 350.07955.

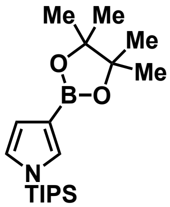

3-(4,4,5,5-tetramethyl-1,3,2-diozaborolan-2-y)-1-(triisopropylsilyl)-1*H*-pyrrole 3.11: Synthesized as previously described.[5] A round-bottomed flask was charged with $PdCl_2(CH_3CN)_2$ (63 mg, 0.24 mmol), and Sphos (297 mg, 0.72 mmol). A solution of **3.10 (**2.81 g, 8.04 mmol) in 25 mL of toluene was then added, followed by degassed triethylamine (2.80 mL, 20.1 mmol) and pinacolborane (1.40 mL, 9.65 mmol). The reaction was stirred at 90 °C for 2 hours, after which it was filtered through a plug of alumina with EtOAc and concentrated under reduced pressure. In order to minimize product decomposition, column chromatography was performed immediately (5% EtOAc/hexanes, treated with 5% triethylamine) to give an orange oil which was used immediately in the next step and assuming quantitative yield.

^{1}H NMR (600 MHz, $CDCl_3$) δ 7.24 (t, *J* = 1.2 Hz, 1H), 6.81 (t, *J* = 2.5 Hz, 1H), 6.62 (dd, *J* = 2.7, 1.3 Hz, 1H), 1.47 (hept, *J* = 7.5 Hz, 3H), 1.09 (d, *J* = 7.5 Hz, 18H); **^{13}C NMR** (151 MHz, $CDCl_3$) δ 133.78, 125.06, 115.76, 82.82, 24.99, 17.93, 11.80 (carbon adjacent to boron was not detected); **HRMS** (APCI$^+$): Found 349.27219 (+1.29 ppm), $C_{19}H_{37}NO_2BSi$ (M+H) requires 349.27174.

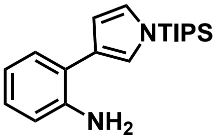

2-(1-(triisopropylsilyl)-1*H*-pyrrol-3-yl)aniline 3.12: Synthesized as previously described.[4,5] A round-bottom flask was charged with **2-iodoaniline** (1.43 g, 6.70 mmol), $Pd(OAc)_2$ (75 mg, 0.34 mmol), SPhos (275 mg, 0.67 mmol), and potassium phosphate tribasic (2.84 g, 13.4 mmol). A solution of **3.11** (2.81 g, 8.04 mmol) in 20 mL of a 2.5:1 solution of degassed *n*-butanol and deionized water was then added, and the reaction stirred at 35 °C for 16 hours. The reaction mixture was then filtered through a pad of celite, concentrated under reduced pressure, and purified by column chromatography (0-5% EtOAc/hexanes, treated with 5% triethylamine) furnishing a yellow oil (1.78 g, 85% over 2 steps).

^{1}H NMR (600 MHz, $(CD_3)_2CO$) δ 7.17 (dd, J = 7.6, 1.7 Hz, 1H), 7.04 (s, 1H), 6.94 (m, 2H), 6.75 (d, J = 8.0 Hz, 1H), 6.63 (td, J = 7.4 1.3 Hz, 1H), 6.50z (dd, J = 2.8, 1.5 Hz, 1H), 4.44 (br s, 2H), 1.57 (hept, *J* = 7.5 Hz, 3H), 1.15 (d, *J* = 7.6 Hz, 18H); **^{13}C NMR** (151 MHz, $(CD_3)_2CO$) δ 145.69, 130.10, 127.44, 125.53, 122.75, 122.65, 118.20, 116.04, 115.82, 111.48, 18.21, 12.36; **HRMS** (APCI$^+$): Found 315.22537 (+0.86 ppm), $C_{19}H_{31}N_2Si$ (M+H) requires 315.2251.

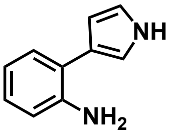

2-(1*H*-pyrrol-3-yl)aniline 3.13: Synthesized as previously described.[4,5] To a solution of **3.12** (628 mg, 2.00 mmol) in 4 mL of THF was added tetrabutylammonium fluoride (4.00 mL, 4.00 mmol, 1.0 M solution in THF) and the reaction stirred at ambient temperature for 1 hour. The reaction mixture was quenched with sat. NH_4Cl, extracted with EtOAc (3x), washed with brine (1x), dried over Na_2SO_4, concentrated under reduced pressure, and purified by column chromatography (0-50% EtOAc/hexanes, treated with 5% triethylamine) yielding a brown oil (131 mg, 41%).

^{1}H NMR (600 MHz, $(CD_3)_2CO$) δ 10.20 (br s, 1H), 7.16 (dd, *J* = 7.6, 1.6 Hz, 1H), 7.01 (dd, *J* = 4.1, 1.8 Hz, 1H), 6.93 (td, *J* = 7.6, 1.6, 1H), 6.88 (dd, *J* = 4.7, 2.6 Hz, 1H), 6.75 (dd, *J* = 7.9, 1.3 Hz, 1H), 6.62 (td, *J* = 7.4, 1.3 Hz, 1H), 6.34 (dd, *J* = 4.2, 2.6 Hz, 1H), 4.46 (br s, 2H); **^{13}C NMR** (151 MHz, $(CD_3)_2CO$) δ 145.69, 130.06, 127.20, 123.01 122.62, 119.16, 118.11, 116.79, 115.93, 108.48; **HRMS** (APCI$^+$): Found 159.09198 (+1.89 ppm), $C_{10}H_{11}N_2$ (M+H) requires 159.09198.

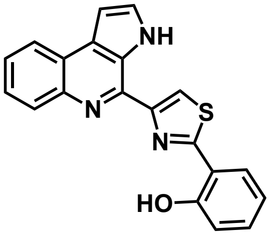

2-(4-3*H*-pyrrolo[2,3-*c*]quinolin-4-yl)thiazol-2-yl)phenol 3.14: Synthesized as previously described.[4,5] A solution of **3.13** (39 mg, 0.25 mmol) and **3.08** (51 mg, 0.25 mmol) in 2.5 mL of a 1% trifluoroacetic acid in dimethylsulfoxide was stirred at ambient temperature for 24 hours. The reaction was then quenched with sat. $NaHCO_3$, extracted with EtOAc (3x), washed with brine (1x), dried over Na_2SO_4, and concentrated under reduced pressure and purified by column chromatography (20% CH_2Cl_2/EtOAc) furnishing a dark yellow solid (42 mg, 50%).

^{1}H NMR (600 MHz, $(CD_3)_2SO$) δ 11.59 (s, 1H), 8.71 (d, *J* = 7.9 Hz, 1H), 8.65 (s, 1H), 8.33 (d, *J* = 7.6 Hz, 1H), 8.09 (dd, *J* = 7.9 Hz, 1H), 7.79 (t, *J* = 2.8 Hz, 1H), 7.59 (m, 2H), 7.37 (t, *J* = 7.7 Hz, 1H), 7.25 (dd, *J* = 2.5 Hz, 1H), 7.10 (d, *J* = 8.2 Hz, 1H), 7.05 (t, *J* = 7.6 Hz, 1H); **^{13}C NMR** (151 MHz, $CDCl_3$) δ 163.42, 153.15, 141,87, 139.21, 131.05, 129.36, 129.05, 128.61, 128.39, 126.00, 125.49, 123.23, 123.10, 120.34, 119.52, 116.40, 110.76; **HRMS** (APCI$^+$): Found 344.08511 (-0.29 ppm), $C_{20}H_{24}N_3OS$ (M$^+$) requires 344.08521.

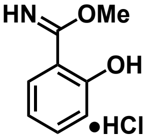

Methyl 2-hydroxybenzimidate hydrochloride 3.15: Synthesized as previously described.[6] To a solution of **2-hydroxybenzonitrile** (4.00 g, 33.6 mmol) in 16 mL of MeOH was added acetyl chloride (19.1 mL, 269 mmol) dropwise. The solution stirred at ambient temperature for 16 hours, and a precipitate formed. The reaction mixture was filtered and rinsed with EtOAc. The resulting white solid was used without further purification (3.39 g, 54%).

^{1}H NMR (600 MHz, CD_3OD) δ 7.95 (d, *J* = 8.1 Hz, 1H), 7.65 (t, *J* = 7.8 Hz, 1H), 7.10 (m, 2H), 4.33 (s, 3H). **^{13}C NMR** (151 MHz, CD_3OD) δ 172.70, 160.48, 138.89, 131.76, 121.69, 118.15, 111.89, 59.54; **HRMS** (APCI$^+$): Found 152.07502 (-0.56 ppm), $C_8H_{10}NO_2$ (M+H) requires 152.07061.

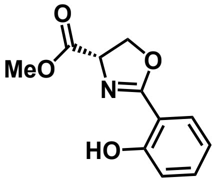

Methyl (*S*)-2-(2-hydroxyphenyl)-4,5-dihydrooxazole-4-carboxylate 3.16: Synthesized as previously described.[6] To a solution of **3.15** (3.39 g, 18.1 mmol) and **L-serine methyl ester hydrochloride** (2.81 g, 18.1 mmol) in 300 mL of $C_2H_4Cl_2$ was added triethylamine (2.31 mL, 18.1 mmol). The solution was stirred at reflux for 16 hours, then cooled to ambient temperature and the solids filtered off. The pink solution was washed with sat. $NaHCO_3$ (1x), dried over Na_2SO_4, concentrated under reduced pressure, and purified by column chromatography (100% CH_2Cl_2) yielding a clear oil (1.78 g, 45%).

^{1}H NMR (600 MHz, $CDCl_3$) δ 11.67 (s, 1H), 7.65 (d, *J* = 7.9 Hz, 1H), 7.39 (t, *J* = 7.8 Hz, 1H), 7.02 (d, *J* = 8.4 Hz, 1H), 6.87 (t, *J* = 7.0 Hz, 1H), 4.97 (t, *J* = 9.0 Hz, 1H), 4.67 (t, *J* = 8.1 Hz, 1H), 4.56 (t, *J* = 9.6 Hz, 1H), 3.80 (s, 3H); **^{13}C NMR** (151 MHz, $CDCl_3$) δ 171.06, 167.65, 160.03, 134.11, 128.45, 118.90, 117.02, 110.14, 69.00, 67.29, 52.88; **$[\alpha]^{20}_D$** +69.6 (c = 1.14 in $CHCl_3$); **HRMS** (APCI$^+$): Found 222.07576 (-1.46 ppm), $C_{11}H_{12}NO_4$ (M+H) requires 222.07608.

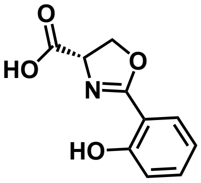

(S)-2-(2-hydroxyphenyl)-4,5-dihydrooxazole-4-carboxylic acid 3.17: To a solution of methyl ester **3.16** (219 mg, 0.992 mmol) in 8.0 mL of THF/H_2O (1:1) was added a 1.0 M solution of lithium hydroxide (95 mg, 3.97 mmol) in deionized water and the solution stirred at ambient temperature for 2 hours. The reaction mixture was concentrated under reduced pressure, redissolved in minimal EtOAc, and then acidified with 1.0 M HCl until a solid precipitated. This was then extracted with EtOAc (3x), washed with brine (1x), and concentrated under reduced pressure to give an orange foam (103 mg, 50%).

^{1}H NMR (600 MHz, $(CD_3)_2CO$) δ 11.49 (br s, 1H), 7.59 (d, *J* = 9.3 Hz, 1H), 7.36 (t, *J* = 7.1 Hz, 1H), 6.89 (d, *J* = 8.3 Hz, 1H), 6.84 (t, *J* = 7.6 Hz, 1H), 5.02 (t, *J* = 8.9 Hz, 1H), 4.65 (d, *J* = 8.9 Hz, 2H); **^{13}C NMR** (151 MHz, $(CD_3)_2CO$) δ 171.85, 167.89, 160.77, 134.86, 129.08, 119.71, 117.50, 111.02, 70.14, 67.90; **HRMS** (APCI$^+$): Found 208.06013 (-1.46 ppm), $C_{10}H_{10}NO_4$ (M+H) requires 208.06043.

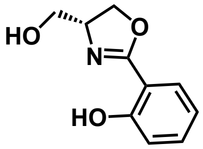

(*R*)-2-(4-(hydroxymethyl)-4,5-dihydrooxazol-2-yl)phenol 3.18: Synthesized as previously described.[1] To a solution of methyl ester **3.16** (221 mg, 1.00 mmol) in 10.0 mL of Et_2O cooled to 0 °C was added LAH (52.8 mg, 1.40 mmol). The solution was stirred at ambient temperature for 1 hour, quenched with MeOH, diluted with EtOAc, and vigorously stirred with a saturated solution of Rochelle's salt at ambient temperature for 2 hours. This was then extracted with EtOAc (3x), washed with sat. $NaHCO_3$ (1x) then brine (1x), dried over Na_2SO_4, concentrated under reduced pressure, and purified by column chromatography (0-5% MeOH/CH_2Cl_2). The resulting off-white solid was then redissolved in CH_2Cl_2, run through a pipette column of activated charcoal, and concentrated under reduced pressure to afford a white solid (21.7 mg, 54%).

^{1}H NMR (600 MHz, $CDCl_3$) δ 11.95 (br s, 1H), 7.65 (d, *J* = 7.9 Hz, 1H), 7.38 (t, *J* = 7.8 Hz, 1H), 7.01 (d, *J* = 8.3 Hz, 1H), 6.87 (t, *J* = 7.6 Hz, 1H), 4.49 (m, 2H), 4.35 (t, *J* = 6.5 Hz, 1H), 3.88 (d, *J* = 11.9 Hz, 1H), 3.71 (d, J = 11.2 Hz, 1H); **^{13}C NMR** (151 MHz, $CDCl_3$) δ 167.08, 159.94, 133.80, 128.36, 118.93, 116.89, 110.54, 68.71, 67.04, 64.11; **HRMS** (APCI$^+$): Found 194.08103 (-0.72 ppm), $C_{10}H_{12}NO_3$ (M+H) requires 194.08117.

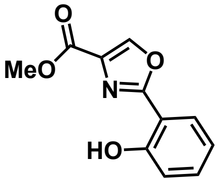

Methyl 2-(2-hydroxyphenyl)oxazole-4-carboxylate 3.19: Synthesized as previously described.[7,8] To a solution of oxazoline **3.16** (972 mg, 4.39 mmol) in 25 mL of CH_2Cl_2 cooled to 0 °C was added 1,8-diazabicyclo(5.4.0)undece7-ene (1.97 mL, 13.2 mmol) dropwise. Bromotrichloromethane (1.30 mL, 13.2 mmol) was then slowly added, and the solution stirred at 0 °C for 1 hour. The solution was warmed to ambient temperature and stirred an additional hour, at which point a solution of 10% $NaHCO_3$ was added. The solution was then extracted with CH_2Cl_2 (2x), washed with sat. $NaHCO_3$ (1x) and brine (1x), dried over Na_2SO_4, concentrated under reduced pressure, and purified by column chromatography in 20% EtOAc/Hexanes yielding a white solid (709 mg, 74%).

^{1}H NMR (600 MHz, $CDCl_3$) δ 10.65 (s, 1H), 8.25 (s, 1H), 7.83 (d, *J* = 7.9 Hz, 1H), 7.41 (t, *J* = 7.8 Hz, 1H), 7.10 (d, *J* = 8.3 Hz, 1H), 6.97 (t, *J* = 7.6 Hz, 1H), 3.94 (s, 3H); **^{13}C NMR** (151 MHz, $CDCl_3$) δ 162.15, 161.06, 157.63, 142.59, 133.43, 132.97, 126.41, 119.76, 117.70, 110.31, 52.40; **HRMS** (APCI$^+$): Found 220.06152 (-0.05 ppm), $C_{11}H_{10}NO_4$ (M+H) requires 220.06153.

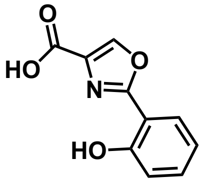

2-(2-hydroxyphenyl)oxazole-4-carboxylic acid 3.20: To a solution of methyl ester **3.19** (223 mg, 1.02 mmol) in 8.0 mL of THF/H_2O (1:1) was added a 1.0 M solution of lithium hydroxide (97 mg, 4.07 mmol) in deionized water then stirred at ambient temperature for 2 hours. The reaction mixture was concentrated under reduced pressure, redissolved in minimal EtOAc, and acidified with 1.0 M HCl until a solid precipitated. This was then extracted with EtOAc (3x), washed with brine (1x), and concentrated under reduced pressure to give a white solid (175 mg, 84%).

^{1}H NMR (600 MHz, CD_3OD) δ 8.55 (s, 1H), 7.84 (d, *J* = 7.9 Hz, 1H), 7.41 (t, *J* = 7.8 Hz, 1H), 7.04 (d, *J* = 8.3 Hz, 1H), 6.98 (t, *J* = 7.6 Hz, 1H); **^{13}C NMR** (151 MHz, CD_3OD) δ 163.68, 163.13, 158.50, 144.77, 134.37, 134.26, 127.51, 120.79, 118.25, 111.49; **HRMS** (APCI$^+$): Found 206.04477 (-0.07 ppm), $C_{10}H_8NO_4$ (M+H) requires 206.04478.

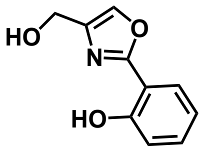

2-(4-(hydroxymethyl)oxazol-2-yl)phenol 3.21: To a solution of methyl ester **3.19** (238 mg, 1.08 mmol) in 10.0 mL of Et_2O cooled to 0 °C was added lithium aluminum hydride (45.2 mg, 1.19 mmol). The solution was stirred at ambient temperature for 1 hour, quenched with MeOH, diluted with EtOAc, and vigorously stirred with a saturated solution of Rochelle's salt at ambient temperature for 2 hours. This was then extracted with EtOAc (3x), washed with sat. $NaHCO_3$ (1x) then brine (1x), dried over Na_2SO_4, concentrated under reduced pressure, and purified by column chromatography (0-50% EtOAc/Hexanes). The resulting off-white solid was redissolved in CH_2Cl_2, run through a pipette column of activated charcoal, and concentrated under reduced pressure to afford a white solid (71.6 mg, 35%).

^{1}H NMR (500 MHz, $CDCl_3$) δ 10.99 (br s, 1H), 7.81 (d, *J* = 7.9 Hz, 1H), 7.63 (s, 1H), 7.36 (t, *J* = 7.0 Hz, 1H), 7.07 (d, *J* = 9.3 Hz, 1H), 6.94 (t, *J* = 7.0 Hz, 1H), 4.68 (s, 2H); **^{13}C NMR** (151 MHz, $CDCl_3$) δ 161.89, 157.24, 139.99, 134.08, 132.67, 126.15, 119.65, 117.31, 111.09, 57.02; **HRMS** (APCI$^+$): Found 192.06554 (+0.11 ppm), $C_{10}H_{10}NO_3$ (M+H) requires 192.06552.

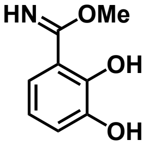

Methyl 2,3-dihydroxybenzimidate 3.22: Synthesized as previously described.[9,10] To a solution of **2,3-dihydroxybenzonitrile** (675 mg, 5.00 mmol) in 10 mL of MeOH was added acetyl chloride (11.4 mL, 160 mmol) dropwise. The solution stirred at ambient temperature for 48 hours, then quenched with sat. $NaHCO_3$. This solution was then extracted with Et_2O (3x), washed with brine (1x), dried over $MgSO_4$, and concentrated under reduced pressure to a yellow solid, used crude.

^{1}H NMR (500 MHz, $(CD_3)_2SO$)) δ 9.04 (br s, 1H), 8.70 (br s, 1H), 7.11 (d, *J* = 8.1 Hz, 1H), 6.82 (d, *J* = 7.7 Hz, 1H), 6.54 (t, *J* = 7.9 Hz, 2H), 3.86 (s, 3H). **^{13}C NMR** (151 MHz, $(CD_3)_2SO$)) δ 165.94, 152.63, 146.42, 122.54, 117.38, 115.91, 112.51, 53.25; **HRMS** (APCI$^+$): Found 168.06541 (-0.67 ppm), $C_8H_{10}NO_3$ (M+H) requires 168.06552.

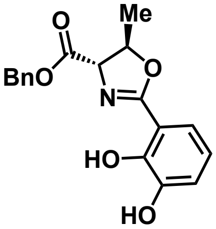

Benzyl (4*S*, 5*R*)-2-(2,3-dihydroxyphenyl)-5-methyl-4,5-dihydrooxazole-4-carboxylate 3.23: Synthesized as previously described.[9,10] To a solution of crude **3.22** (835 mg, 5.00 mmol) and **L-threonine benzyl ester oxalate** (2.34 g, 6.00 mmol) in 100 mL of $C_2H_4Cl_2$ was added triethylamine (1.74 mL, 12.5 mmol). The solution refluxed for 16 hours, then cooled to ambient temperature and concentrated under reduced pressure. This was redissolved in 5% citric acid, extracted with EtOAc (3x), washed with brine, dried over Na_2SO_4, concentrated under reduced pressure, and purified by column chromatography (50% EtOAc/Hexanes) furnishing a viscous purple oil (436 mg, 27% over 2 steps).

^{1}H NMR (500 MHz, $(CD_3)_2SO$)) δ 11.93 (br s, 1H), 9.29 (br s, 1H), 7.42 – 7.35 (m, 5H), 7.08 (dd, *J* = 7.9, 1.6 Hz, 1H), 6.99 (dd, *J* = 7.9, 1.6 Hz, 1H), 6.75 (t, *J* = 7.9 Hz, 1H), 5.22 (d, *J* = 4.3 Hz, 2H), 5.05 (p, *J* = 6.4 Hz, 1H), 4.79 (d, *J* = 6.7 Hz, 1H), 1.48 (d, *J* = 6.4 Hz, 3H); **^{13}C NMR** (151 MHz, $CDCl_3$) δ 169.88, 166.51, 156.60, 148.40, 145.78, 142.53, 135.66, 128.50, 128.02, 127.92, 126.60, 126.41, 78.49, 72.41, 66.41, 62.90, 20.33; **HRMS** (APCI$^+$): Found 328.11748 (-1.42 ppm), $C_{18}H_{18}NO_5$ (M+H) requires 328.11795.

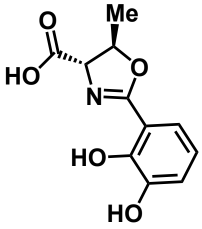

(4*S*, 5*R*)-2-(2,3-Dihydroxyphenyl)-5-methyl-4,5-dihydrooxazole-4-carboxylic acid 3.24: Synthesized as previously described.[9,10] To a solution of **3.23** (436 mg, 1.33 mmol) in 20 mL of MeOH was added 10% Pd/C (13.3 mg, 0.133 mmol) under a hydrogen atmosphere. The solution stirred at ambient temperature for 1 hour at which point the reaction mixture was filtered through a sterile filter. concentrated by rotary evaporation and purified by running through a plug of C18 silica with a 1:1 mixture of MeCN/H_2O yielding a viscous dark purple oil (292 mg, 92%).

^{1}H NMR (600 MHz, $(CD_3)_2SO$)) δ 7.06 (d, *J* = 7.9 Hz, 1H), 6.97 (d, *J* = 7.8 Hz, 1H), 6.73 (t, *J* = 7.9 Hz, 1H), 4.96 (p, *J* = 6.4 Hz, 1H), 4.55 (d, *J* = 7.0 Hz, 1H), 1.45 (d, *J* = 6.4 Hz, 3H); **^{13}C NMR** (151 MHz, $(CD_3)_2SO$)) δ 171.98, 167.78, 149.35, 147.49, 146.03, 119.03, 118.62, 116.89, 66.21, 58.26, 20.66; **HRMS** (APCI$^+$): Found 238.07066 (-1.41 ppm), $C_{11}H_{12}NO_5$ (M+H) requires 238.071.

^{1}H NMR and ^{13}C NMR Spectra

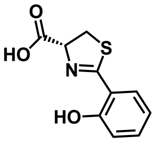

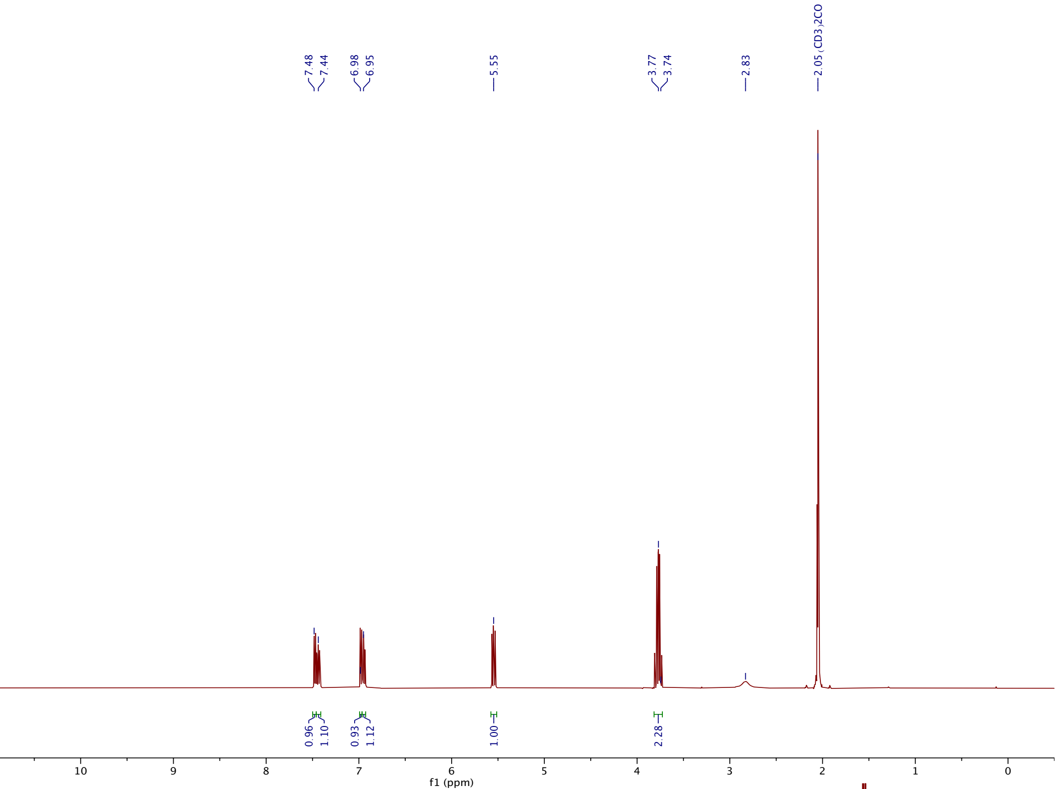

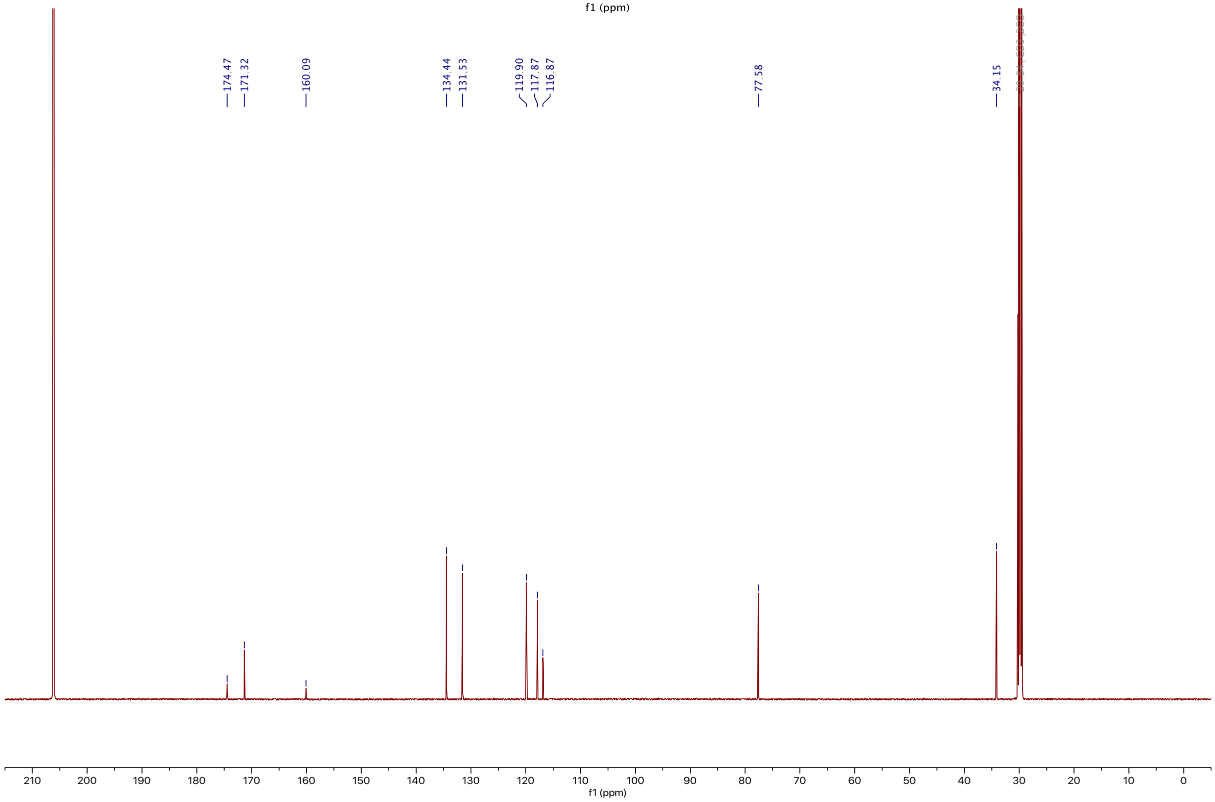

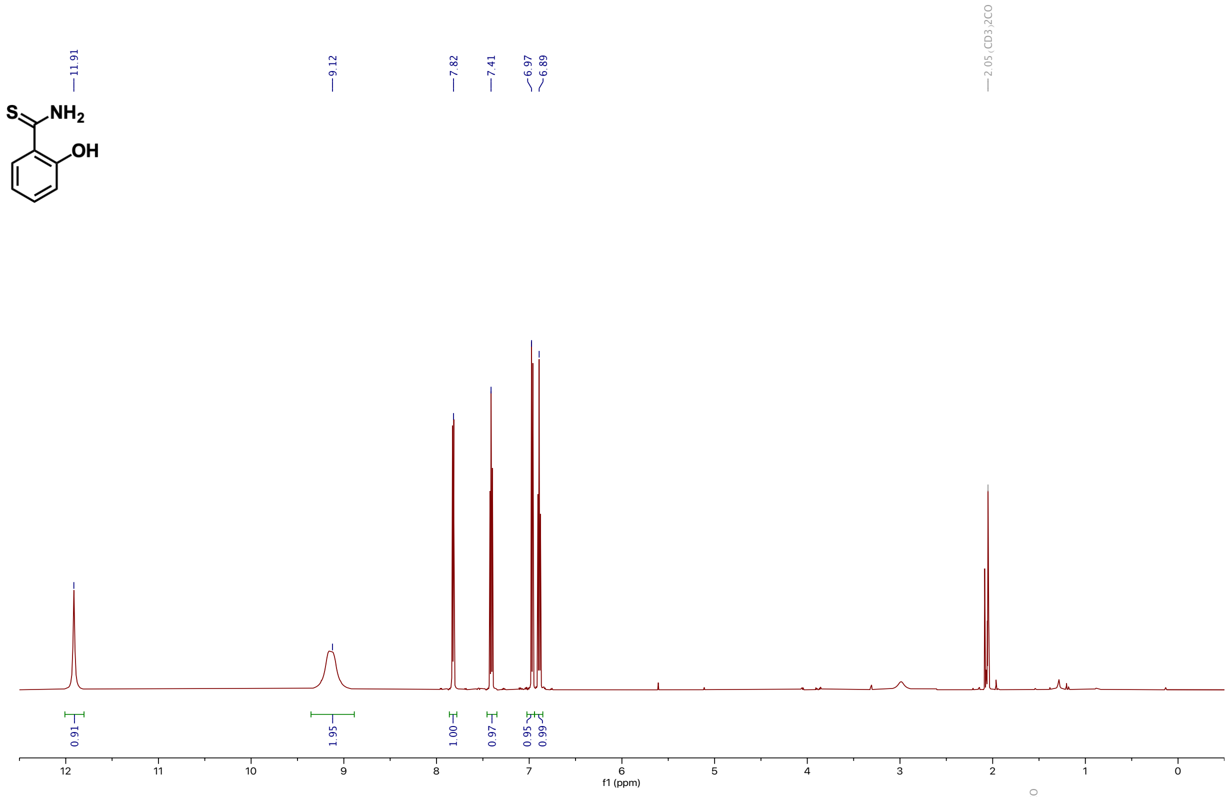
S
NH2
OH
11.91
9.12
7.82
7.41
6.97
6.89
2.05, CD3,2CO
0.91
1.95
1.00
0.97
0.95
0.99
12
11
10
9
8
7
6
5
4
3
2
1
0
f1 (ppm)

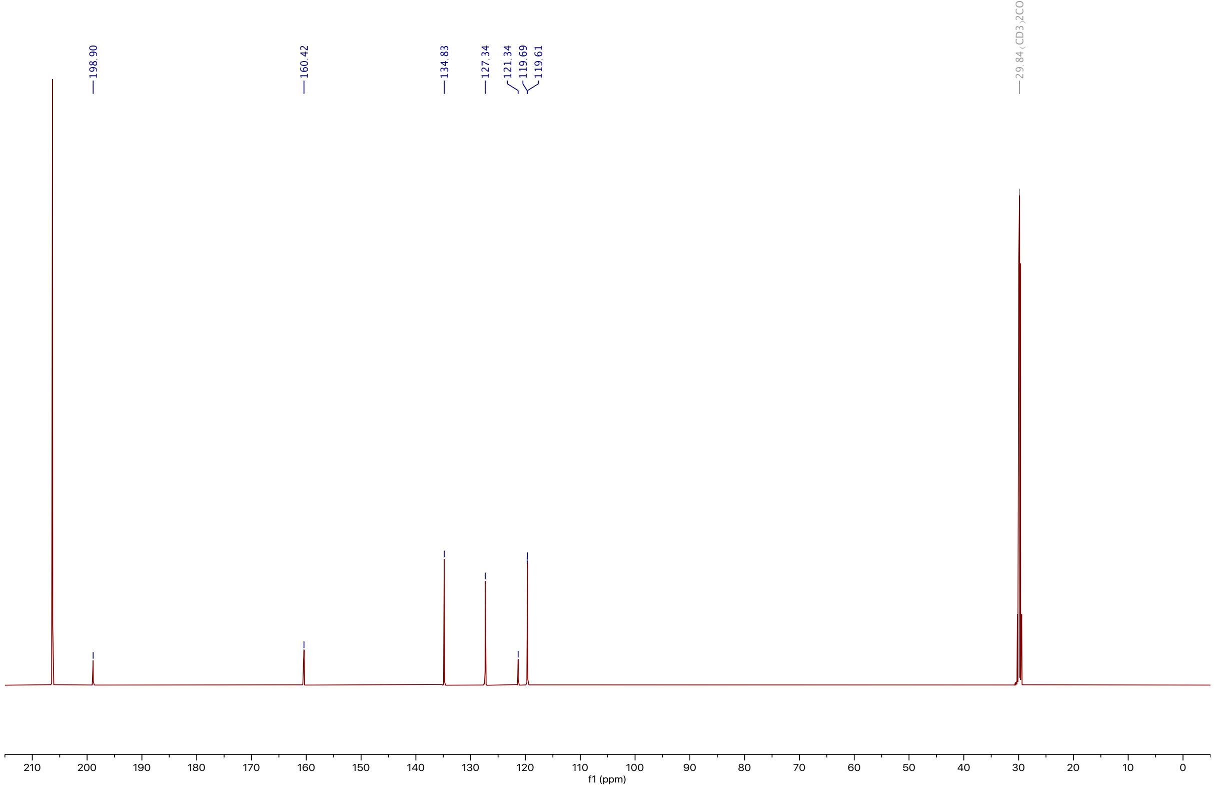
198.90
160.42
134.83
127.34
121.34
119.69
119.61
29.84, CD3,2CO
210
200
190
180
170
160
150
140
130
120
110
100
90
80
70
60
50
40
30
20
10
0
f1 (ppm)

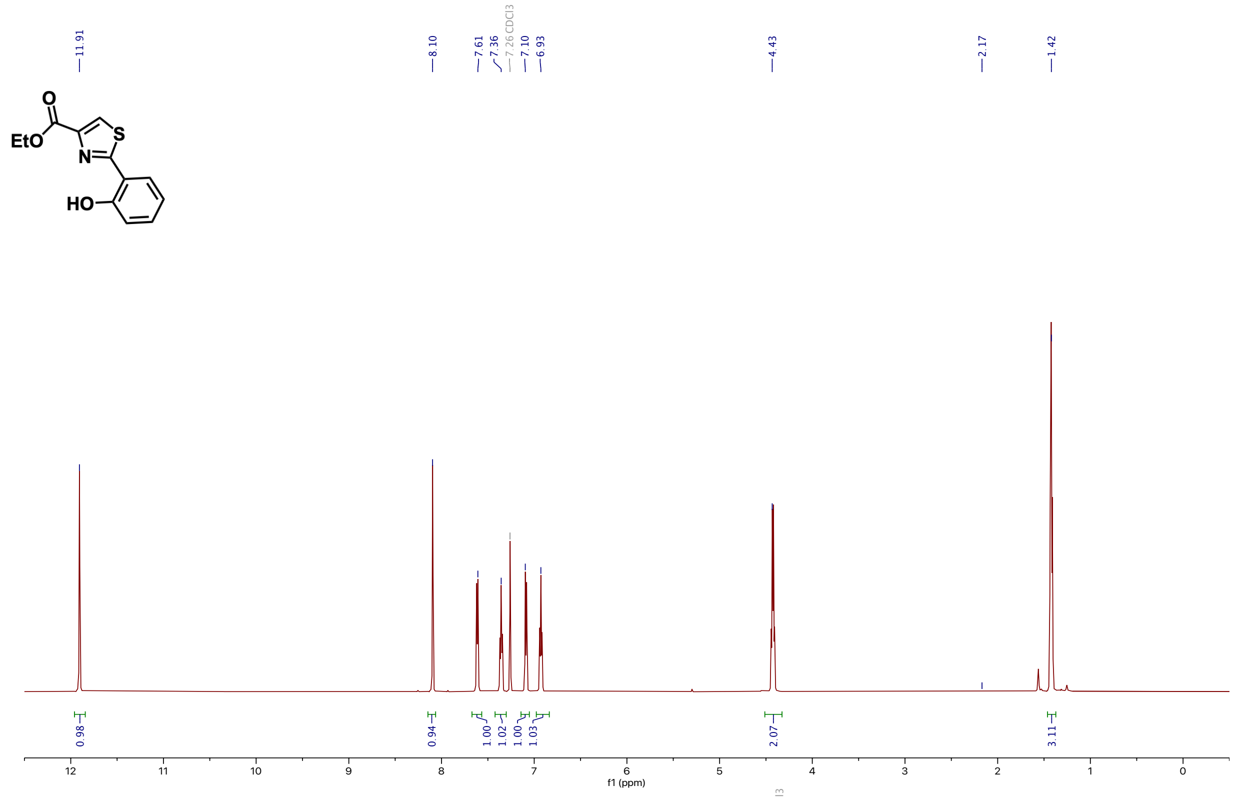

11.91
8.10
7.61
7.36
7.26 CDCl3
7.10
6.93
4.43
2.17
1.42
EtO
O
S
N
HO
0.98
0.94
1.00
1.02
1.00
1.03
2.07
3.11
12
11
10
9
8
7
6
5
4
3
2
1
0
f1 (ppm)

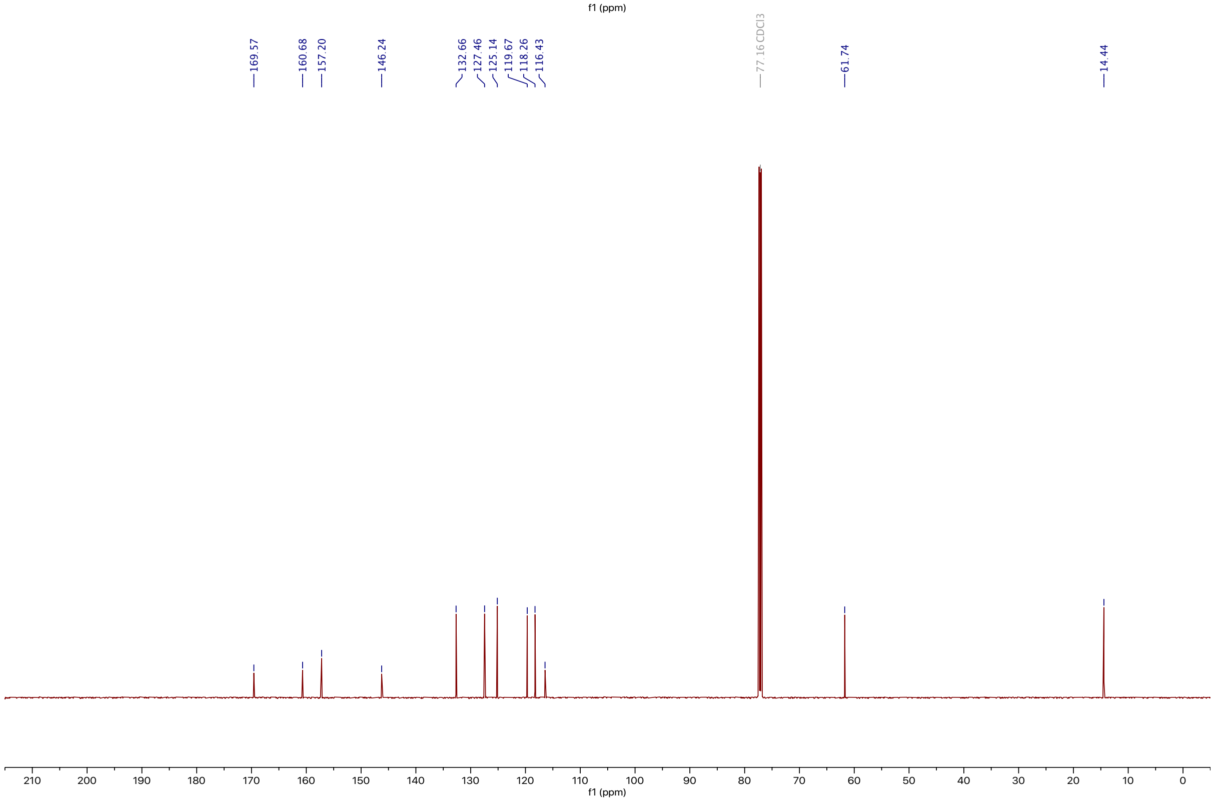

169.57
160.68
157.20
146.24
132.66
127.46
125.14
119.67
118.26
116.43
77.16 CDCl3
61.74
14.44
210
200
190
180
170
160
150
140
130
120
110
100
90
80
70
60
50
40
30
20
10
0
f1 (ppm)

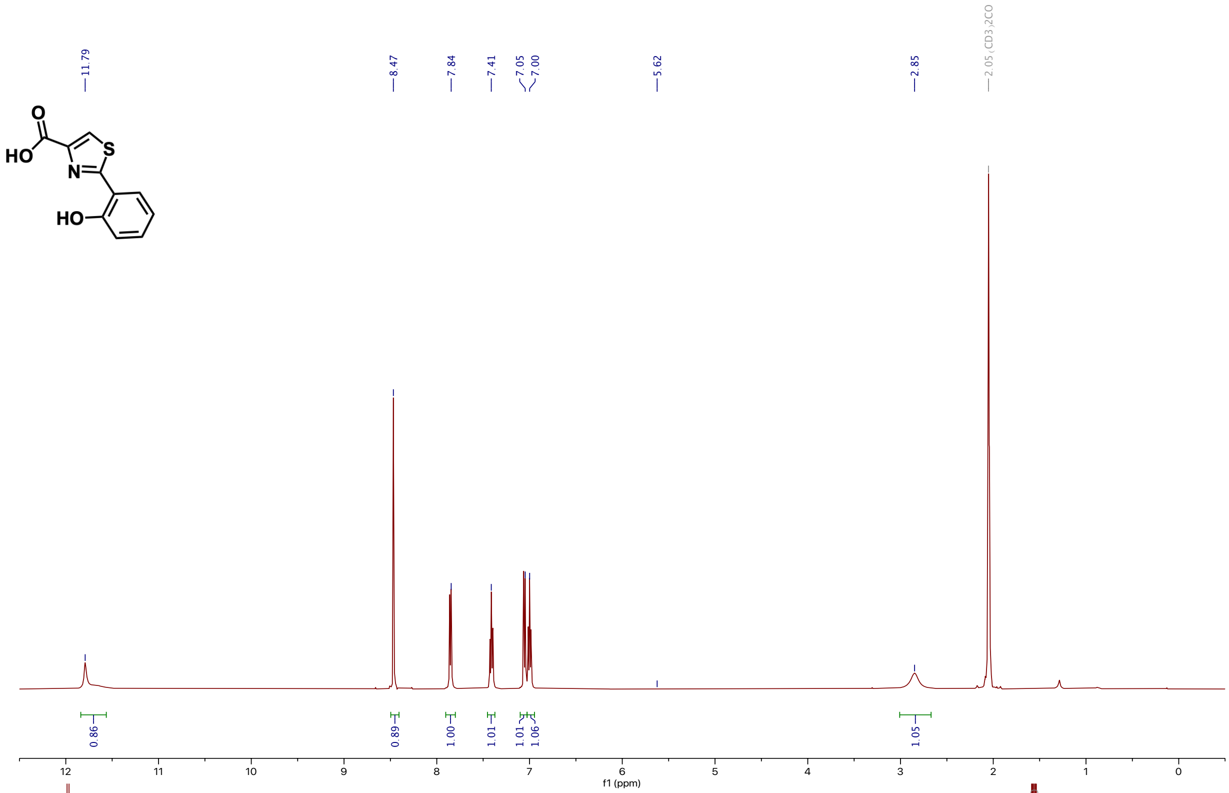
11.79
8.47
7.84
7.41
7.05
7.00
5.62
2.85
2.05, CD3,2CO
HO
O
S
N
HO
0.86
0.89
1.00
1.01
1.01
1.06
1.05
12
11
10
9
8
7
6
5
4
3
2
1
0
f1 (ppm)

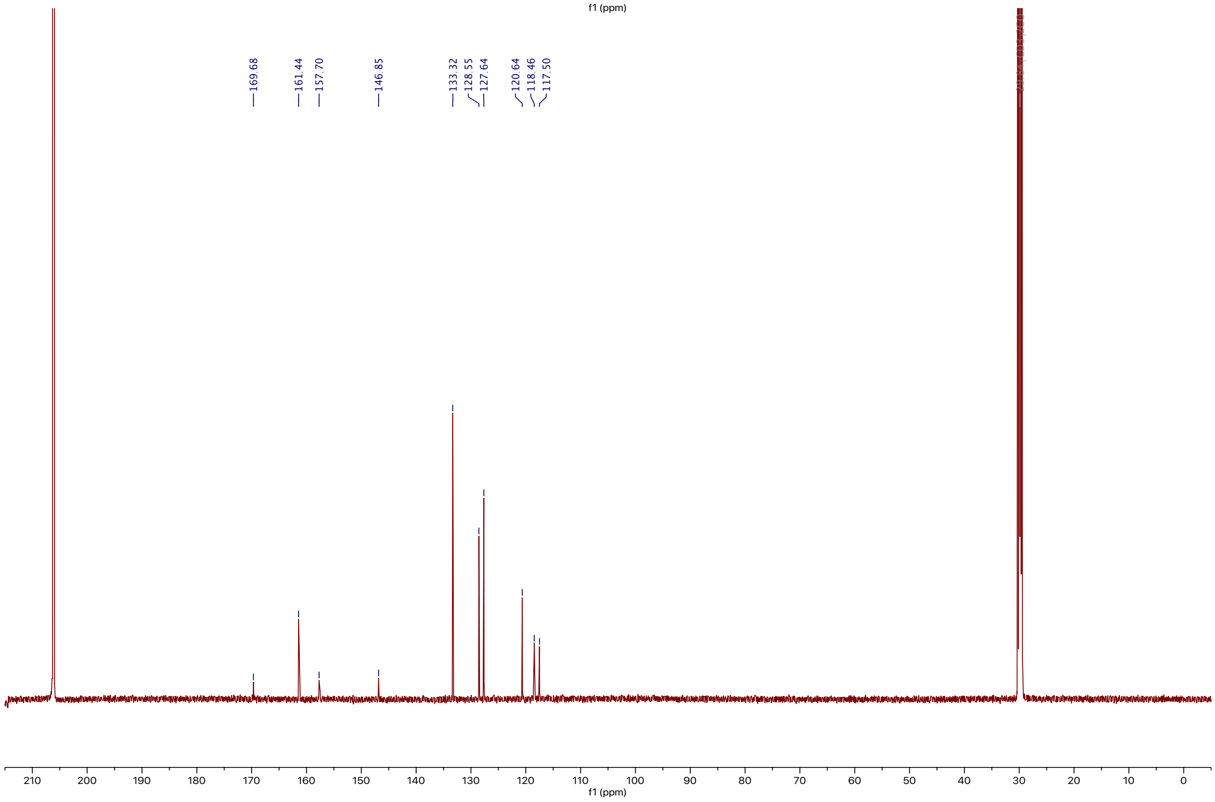
169.68
161.44
157.70
146.85
133.32
128.55
127.64
120.64
118.46
117.50
210
200
190
180
170
160
150
140
130
120
110
100
90
80
70
60
50
40
30
20
10
0
f1 (ppm)

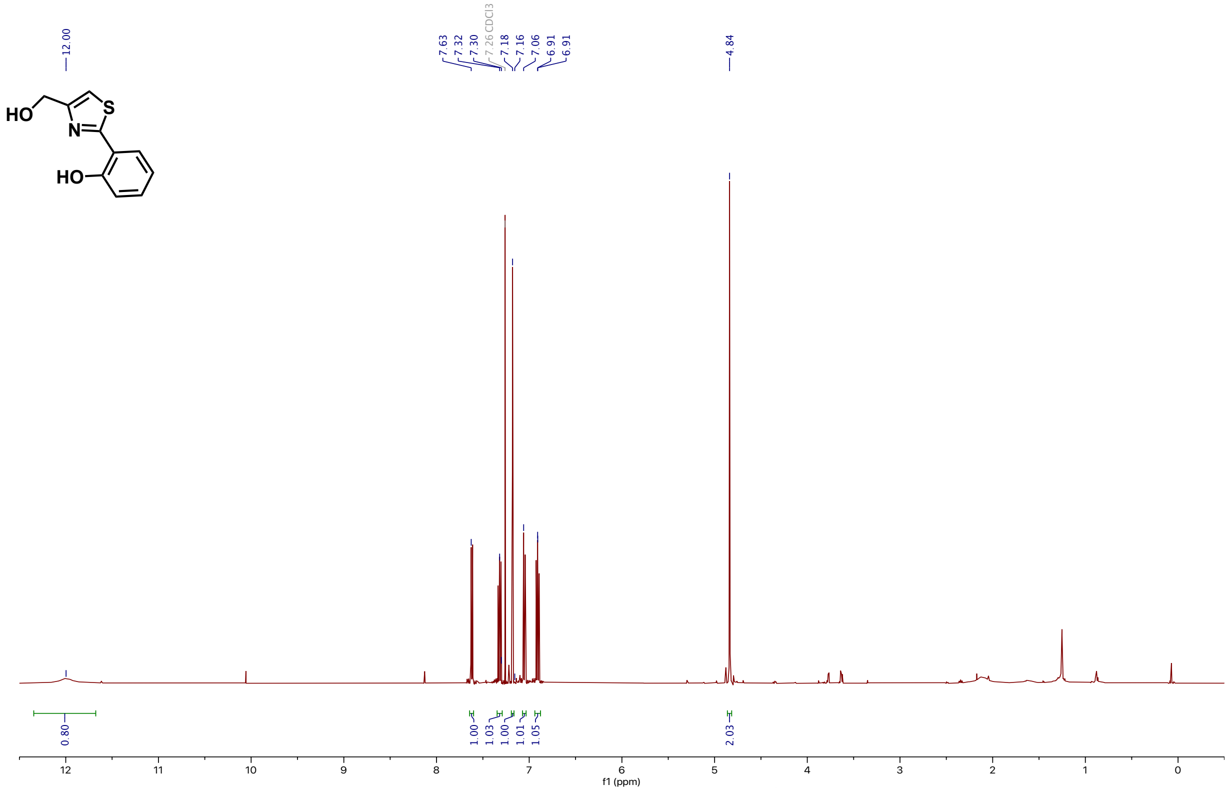
HO
S
N
HO
12.00
7.63
7.32
7.30
7.26 CDCl3
7.18
7.16
7.06
6.91
6.91
4.84
0.80
1.00
1.03
1.00
1.01
1.05
2.03
12
11
10
9
8
7
6
5
4
3
2
1
0
f1 (ppm)

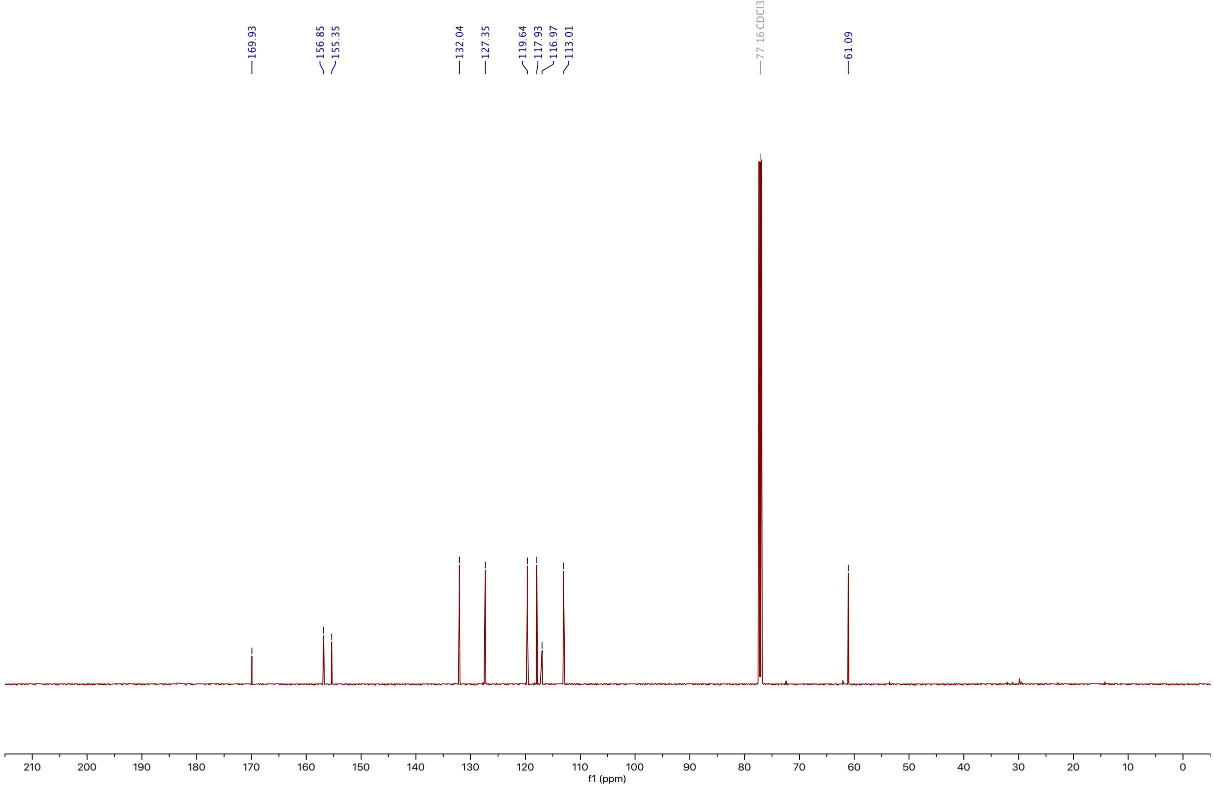
169.93
156.85
155.35
132.04
127.35
119.64
117.93
116.97
113.01
77.16 CDCl3
61.09
210
200
190
180
170
160
150
140
130
120
110
100
90
80
70
60
50
40
30
20
10
0
f1 (ppm)

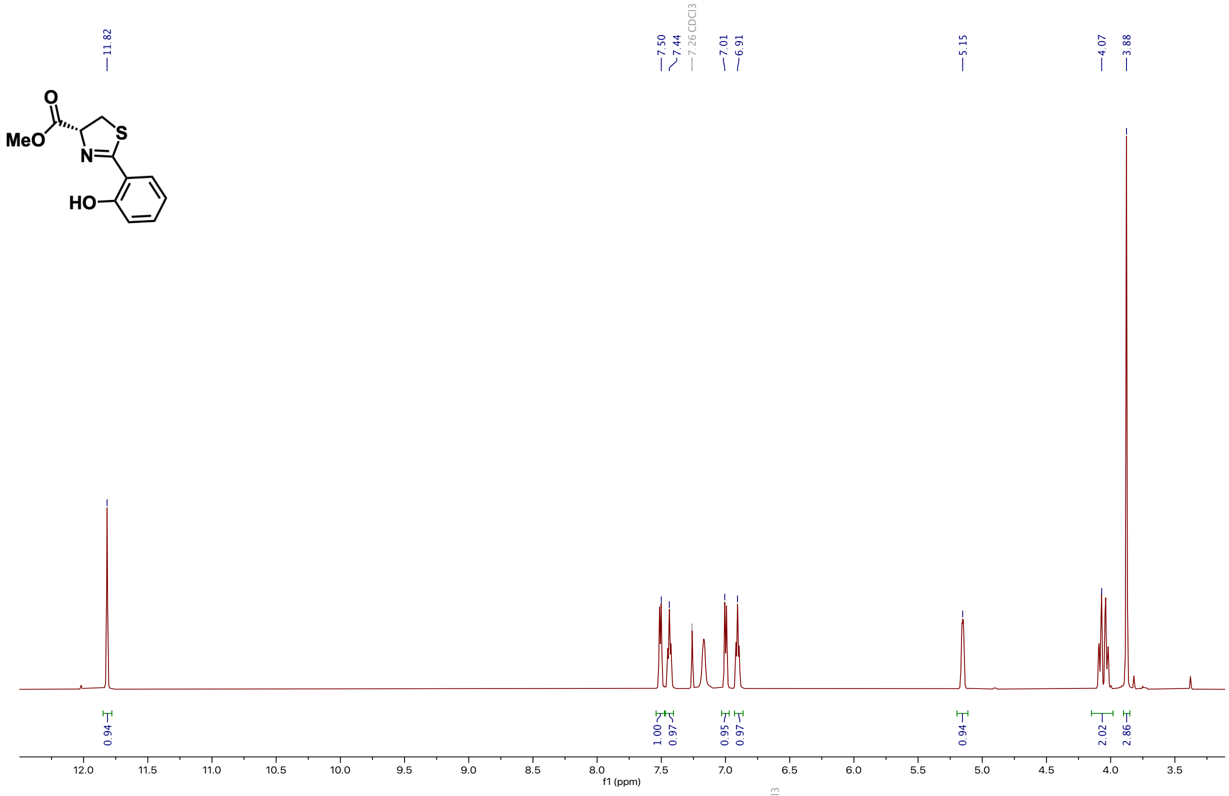
O
MeO
S
N
HO
11.82
7.50
7.44
7.26 CDCl3
7.01
6.91
5.15
4.07
3.88
0.94
1.00
0.97
0.95
0.97
0.94
2.02
2.86
12.0
11.5
11.0
10.5
10.0
9.5
9.0
8.5
8.0
7.5
7.0
6.5
6.0
5.5
5.0
4.5
4.0
3.5
f1 (ppm)

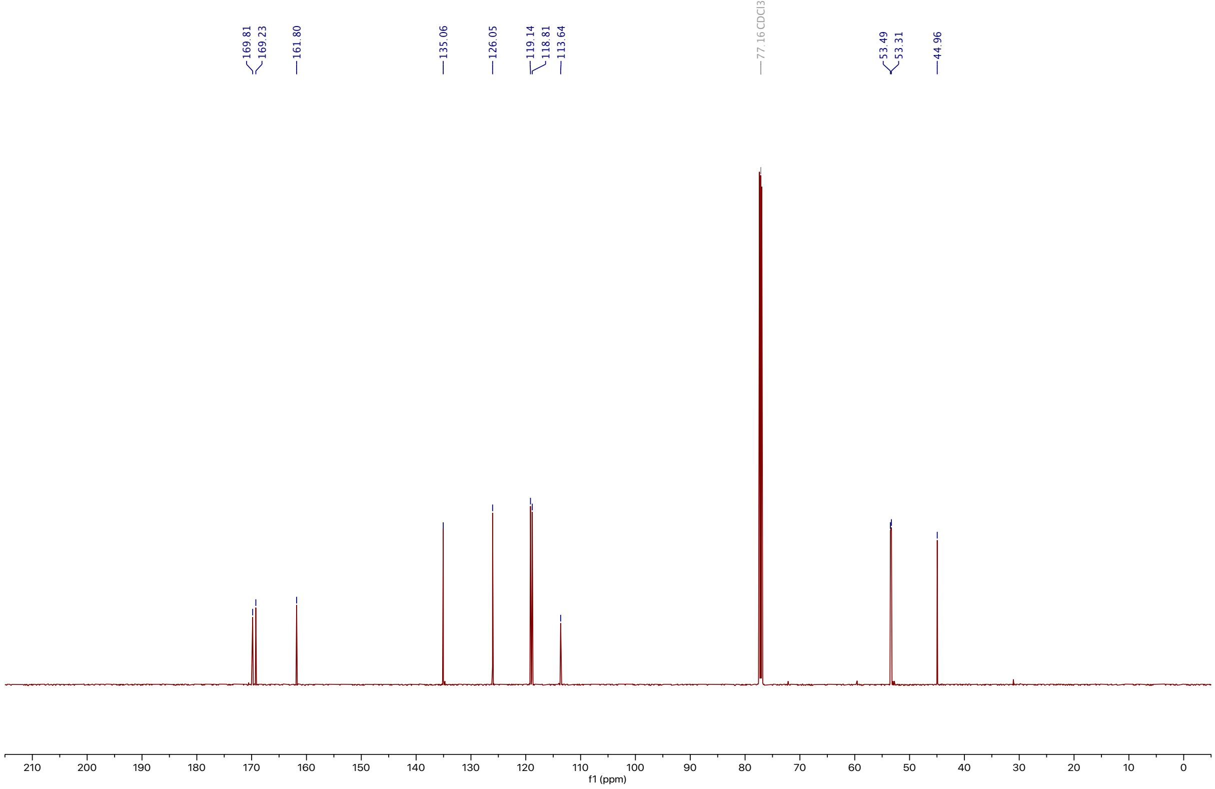
169.81
169.23
161.80
135.06
126.05
119.14
118.81
113.64
77.16 CDCl3
53.49
53.31
44.96
210
200
190
180
170
160
150
140
130
120
110
100
90
80
70
60
50
40
30
20
10
0
f1 (ppm)

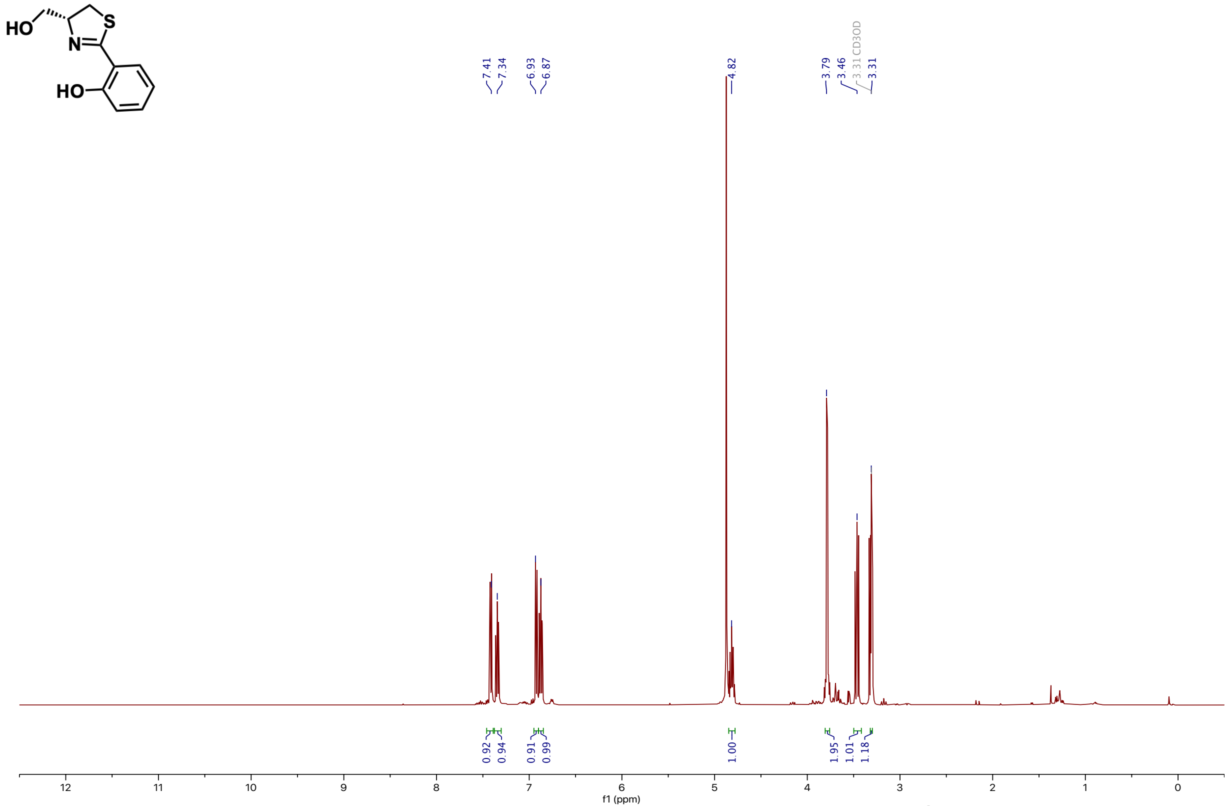

HO
S
N
HO
7.41
7.34
6.93
6.87
4.82
3.79
3.46
3.31 CD3OD
3.31
0.92
0.94
0.91
0.99
1.00
1.95
1.01
1.18
12
11
10
9
8
7
6
5
4
3
2
1
0
f1 (ppm)

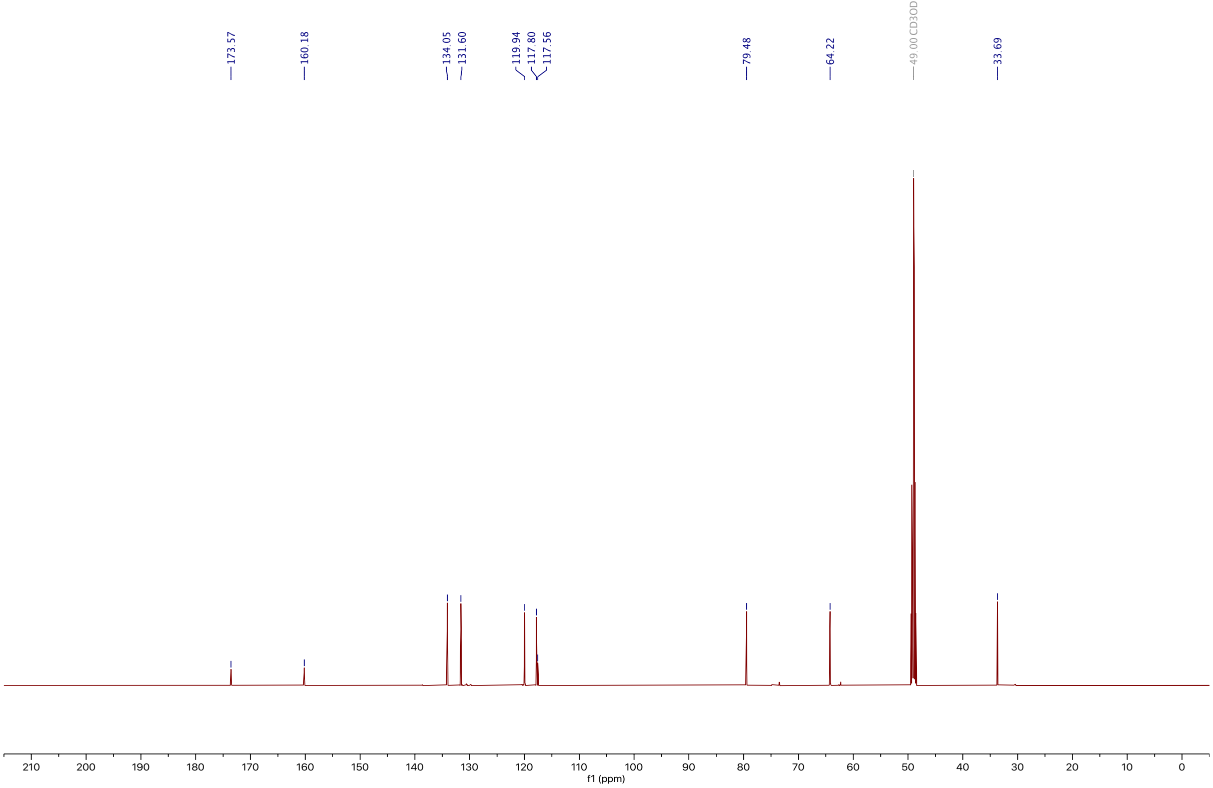

173.57
160.18
134.05
131.60
119.94
117.80
117.56
79.48
64.22
49.00 CD3OD
33.69
210
200
190
180
170
160
150
140
130
120
110
100
90
80
70
60
50
40
30
20
10
0
f1 (ppm)

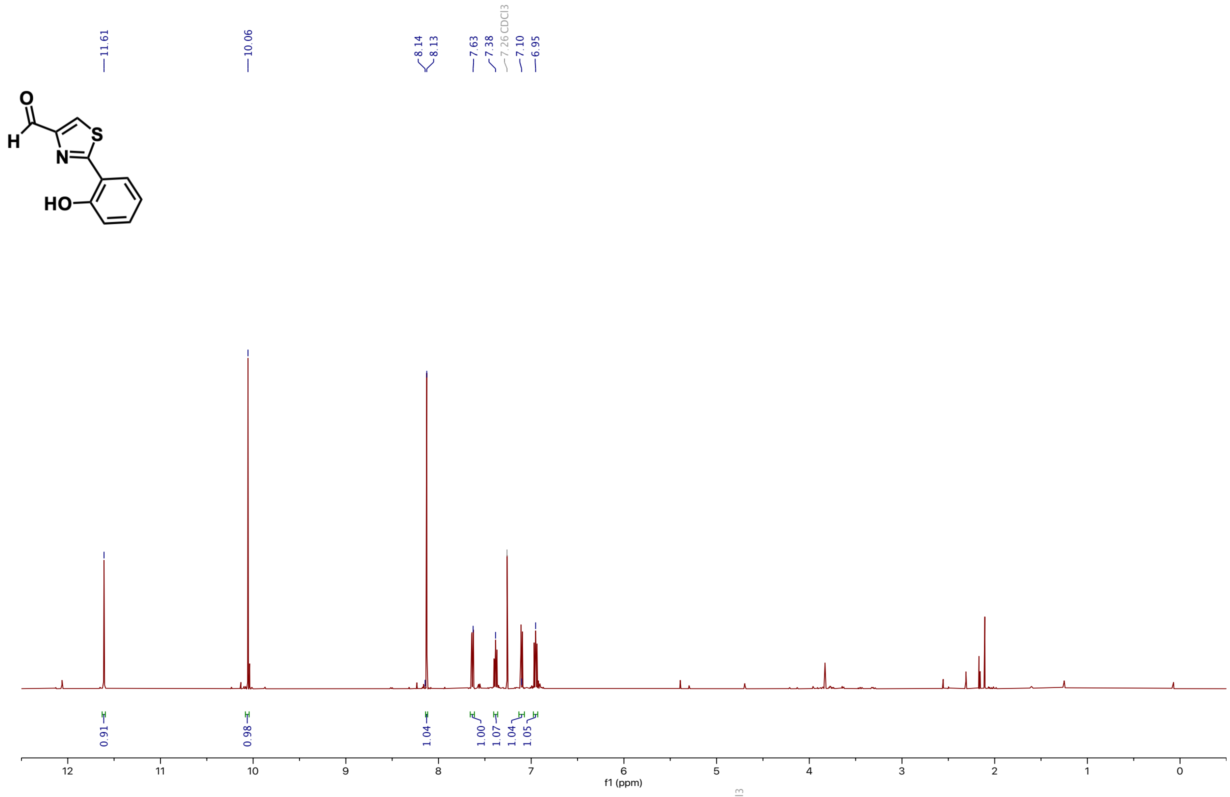
11.61
10.06
8.14
8.13
7.63
7.38
7.26 CDCl3
7.10
6.95
O
H
S
N
HO
0.91
0.98
1.04
1.00
1.07
1.04
1.05
12
11
10
9
8
7
6
5
4
3
2
1
0
f1 (ppm)

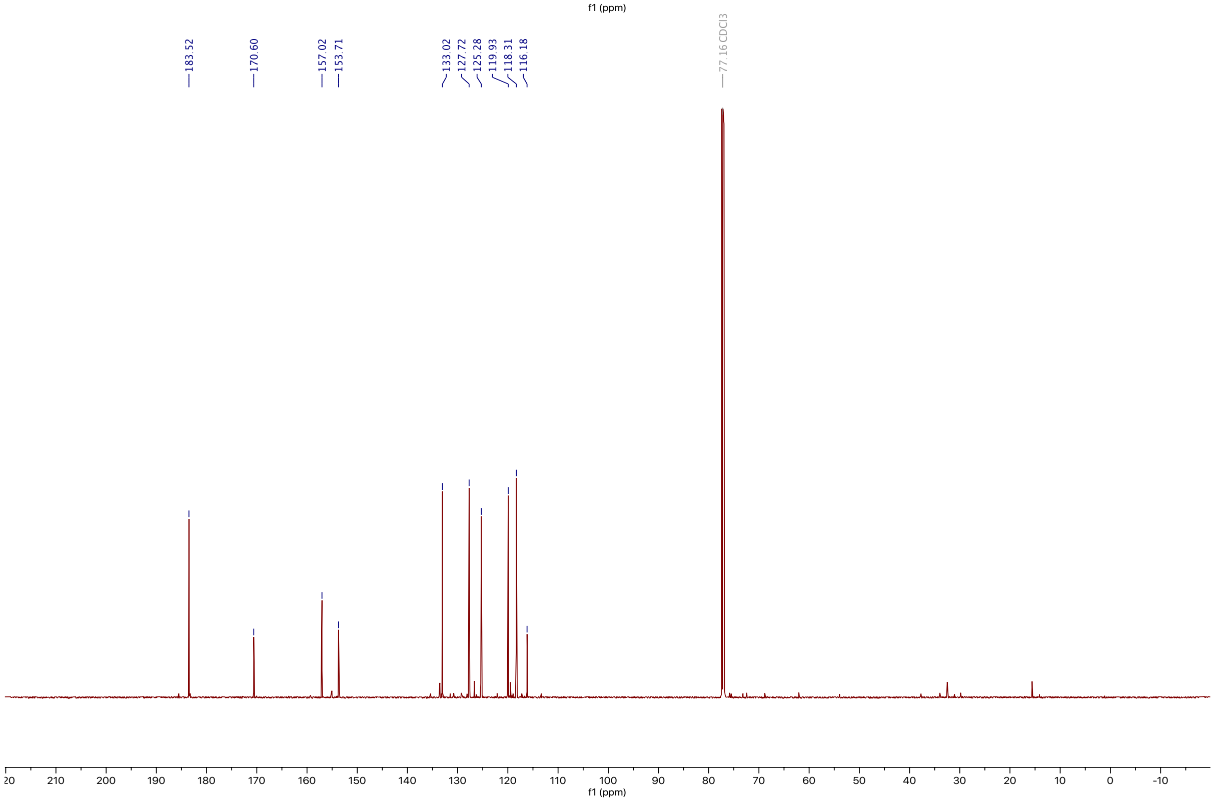
183.52
170.60
157.02
153.71
133.02
127.72
125.28
119.93
118.31
116.18
77.16 CDCl3
20
210
200
190
180
170
160
150
140
130
120
110
100
90
80
70
60
50
40
30
20
10
0
-10
f1 (ppm)

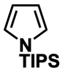
N
TIPS

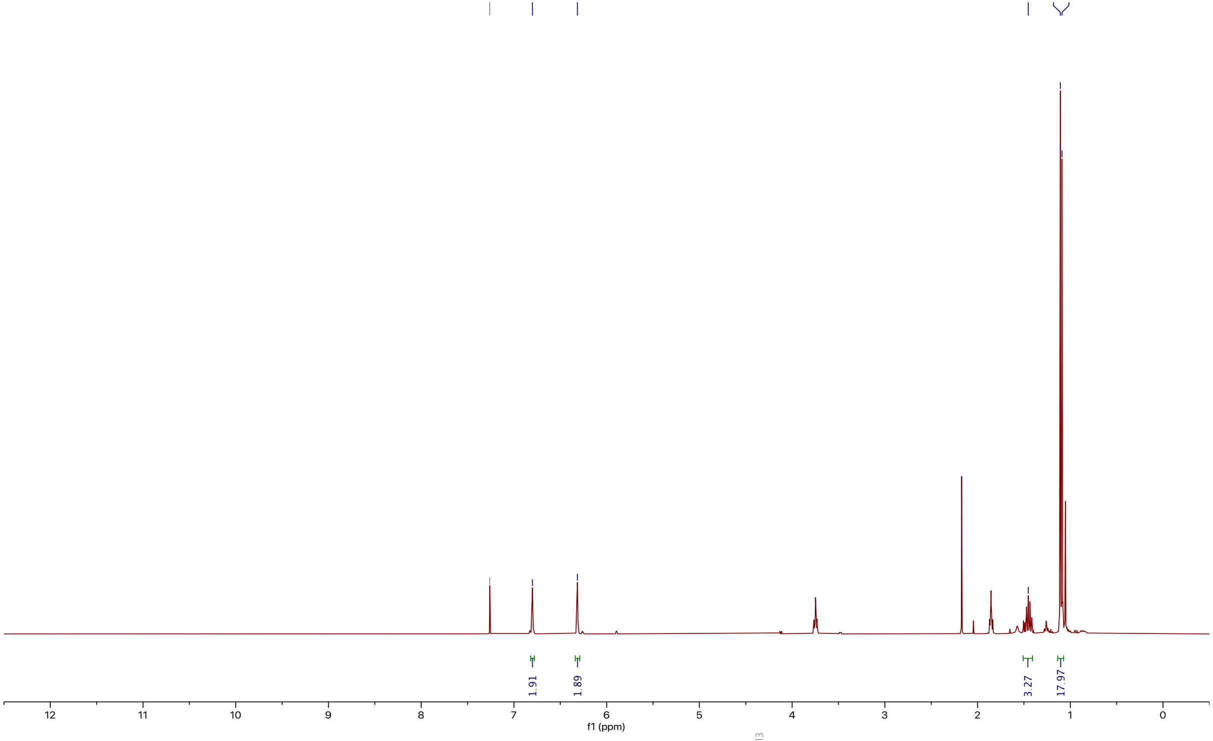
7.26 CDCl3
6.80
6.32
1.45
1.11
1.09
1.91
1.89
3.27
17.97
12
11
10
9
8
7
6
5
4
3
2
1
0
f1 (ppm)

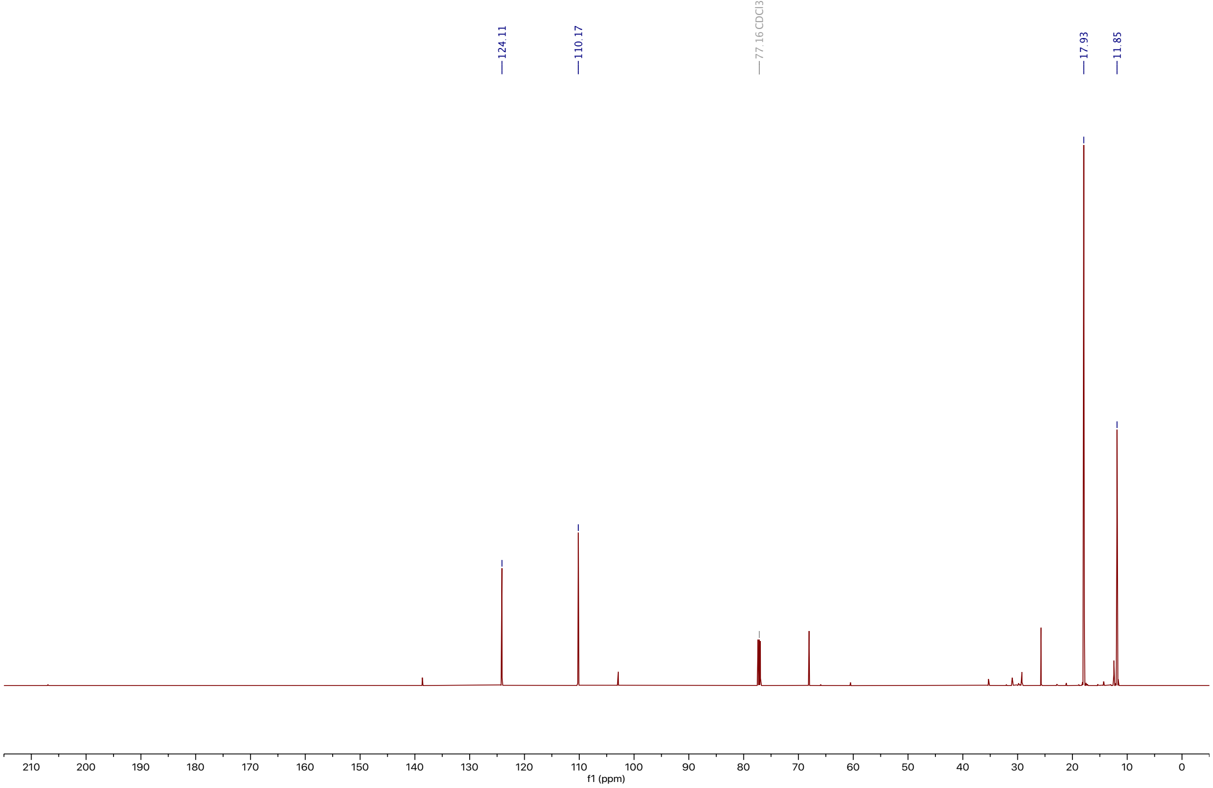
124.11
110.17
77.16 CDCl3
17.93
11.85
210
200
190
180
170
160
150
140
130
120
110
100
90
80
70
60
50
40
30
20
10
0
f1 (ppm)

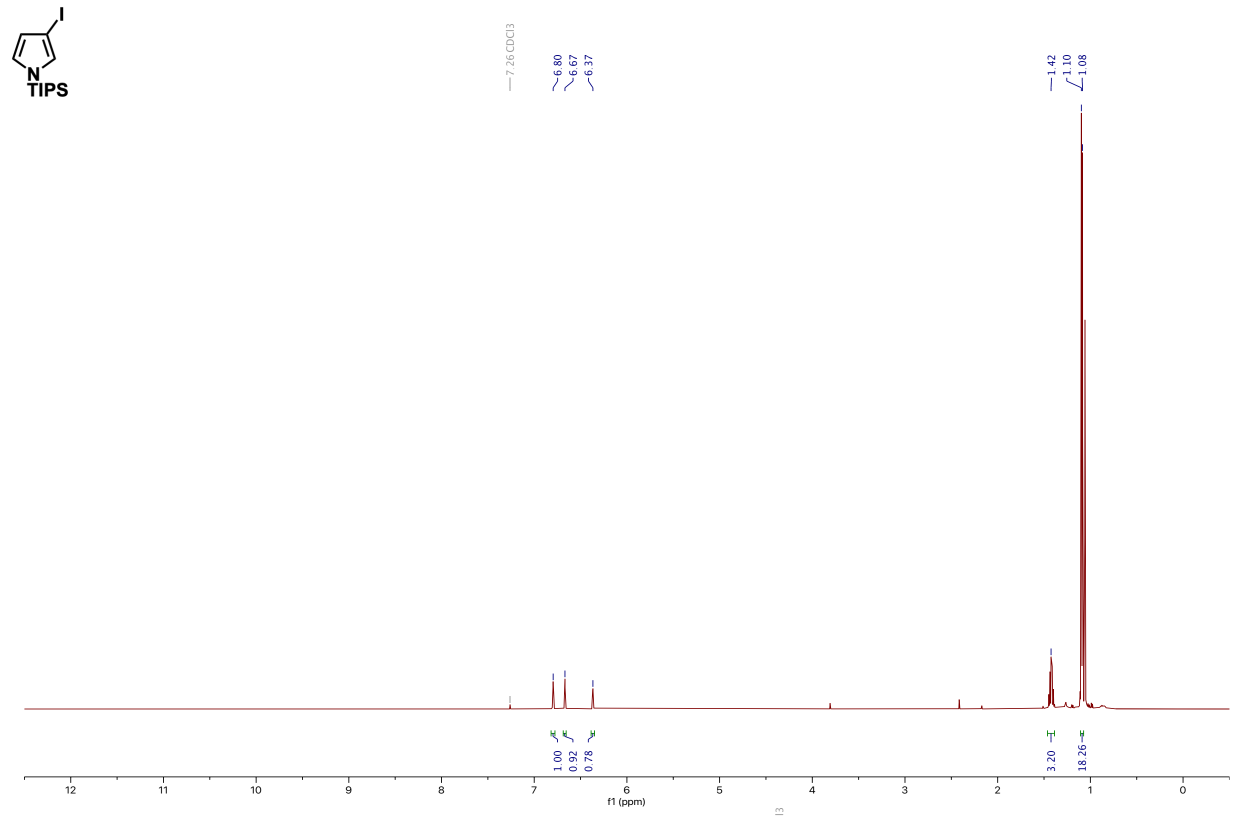
I
N
TIPS
7.26 CDCl3
6.80
6.67
6.37
1.42
1.10
1.08
1.00
0.92
0.78
3.20
18.26
12
11
10
9
8
7
6
5
4
3
2
1
0
f1 (ppm)

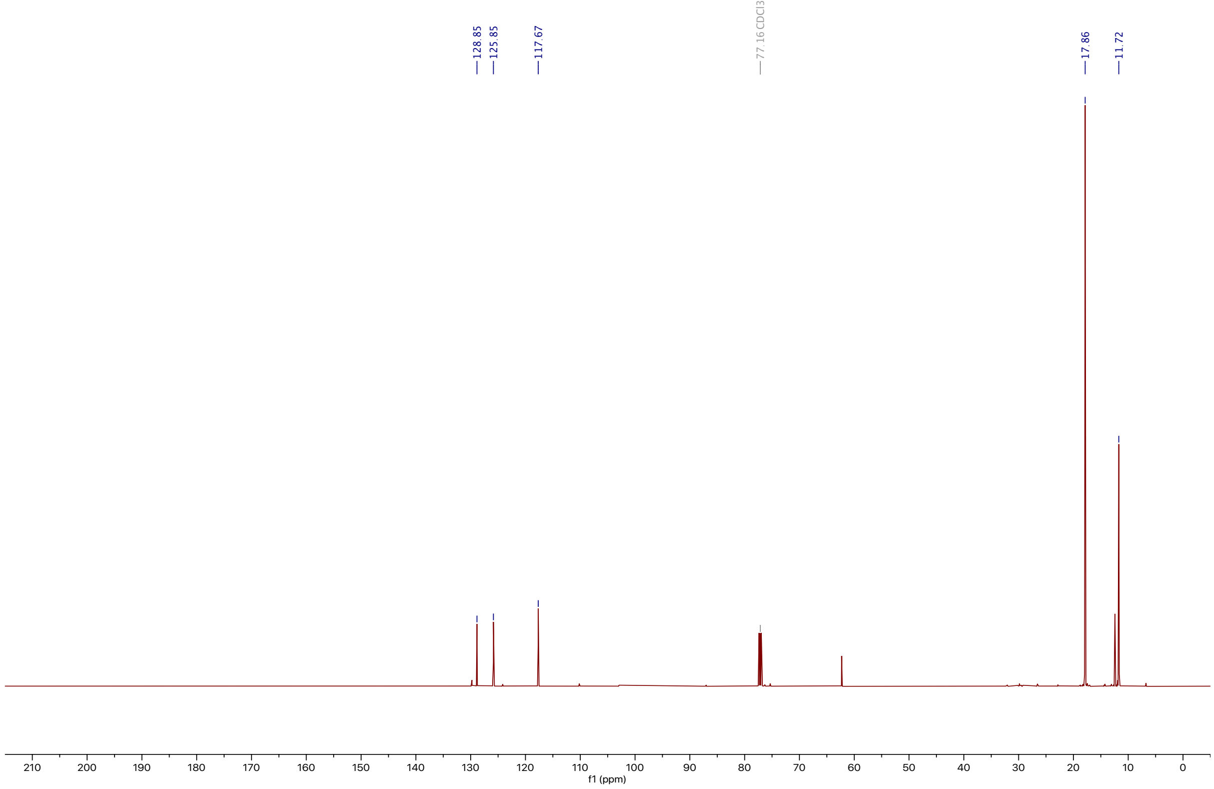
128.85
125.85
117.67
77.16 CDCl3
17.86
11.72
210
200
190
180
170
160
150
140
130
120
110
100
90
80
70
60
50
40
30
20
10
0
f1 (ppm)

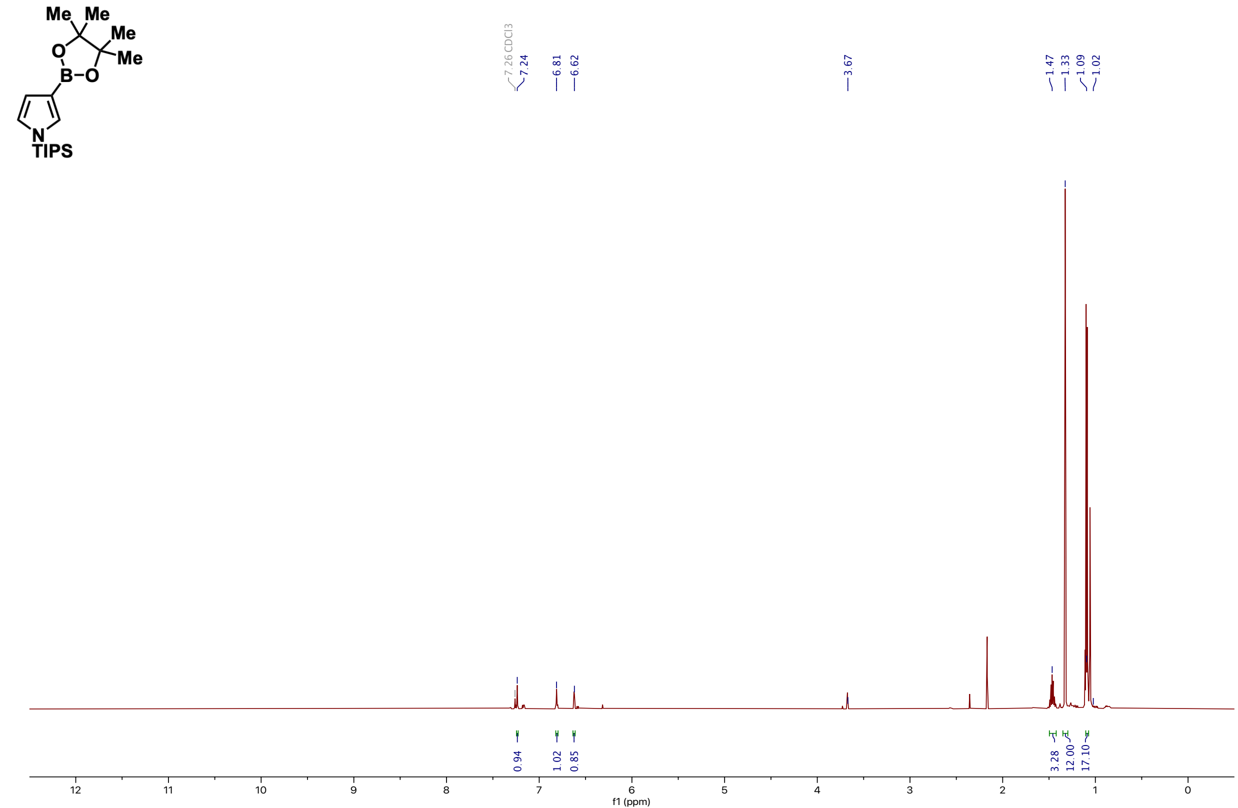
Me
Me
Me
Me
O
B
O
N
TIPS
7.26 CDCl3
7.24
6.81
6.62
3.67
1.47
1.33
1.09
1.02
0.94
1.02
0.85
3.28
12.00
17.10
12
11
10
9
8
7
6
5
4
3
2
1
0
f1 (ppm)

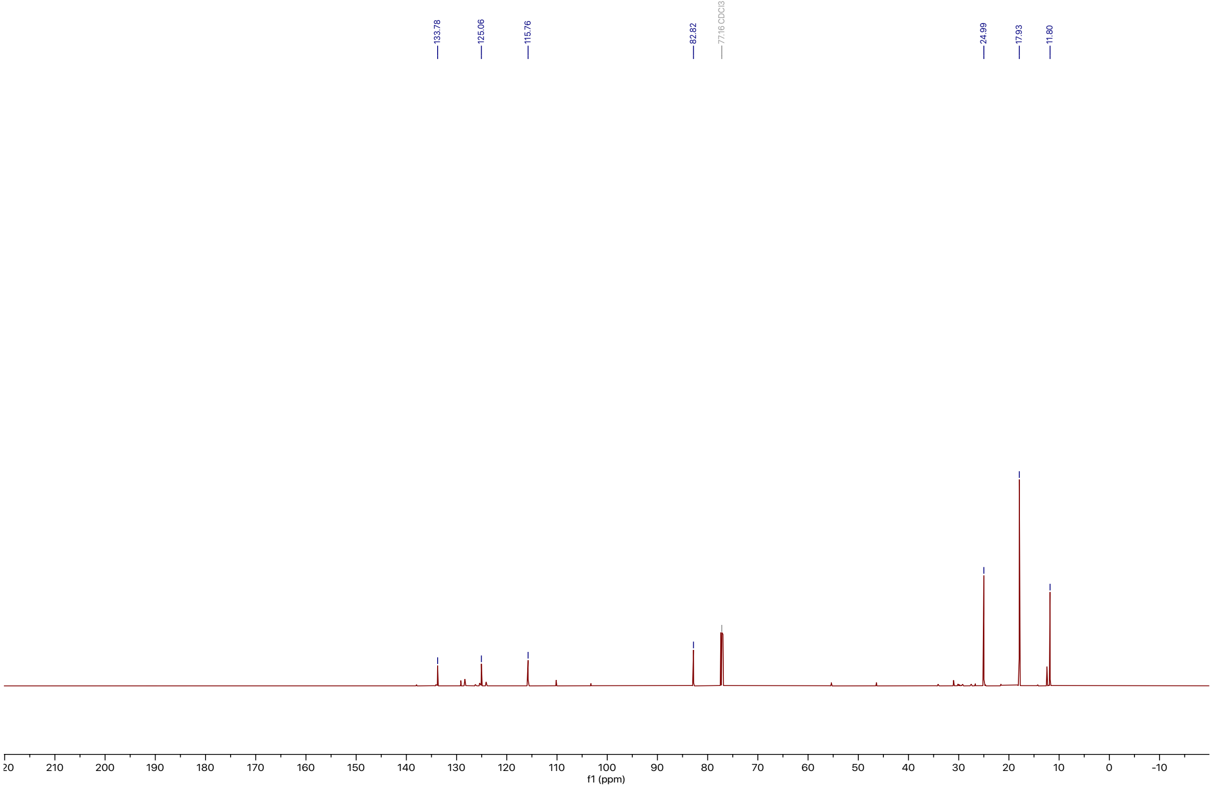
133.78
125.06
115.76
82.82
77.16 CDCl3
24.99
17.93
11.80
220
210
200
190
180
170
160
150
140
130
120
110
100
90
80
70
60
50
40
30
20
10
0
-10
f1 (ppm)

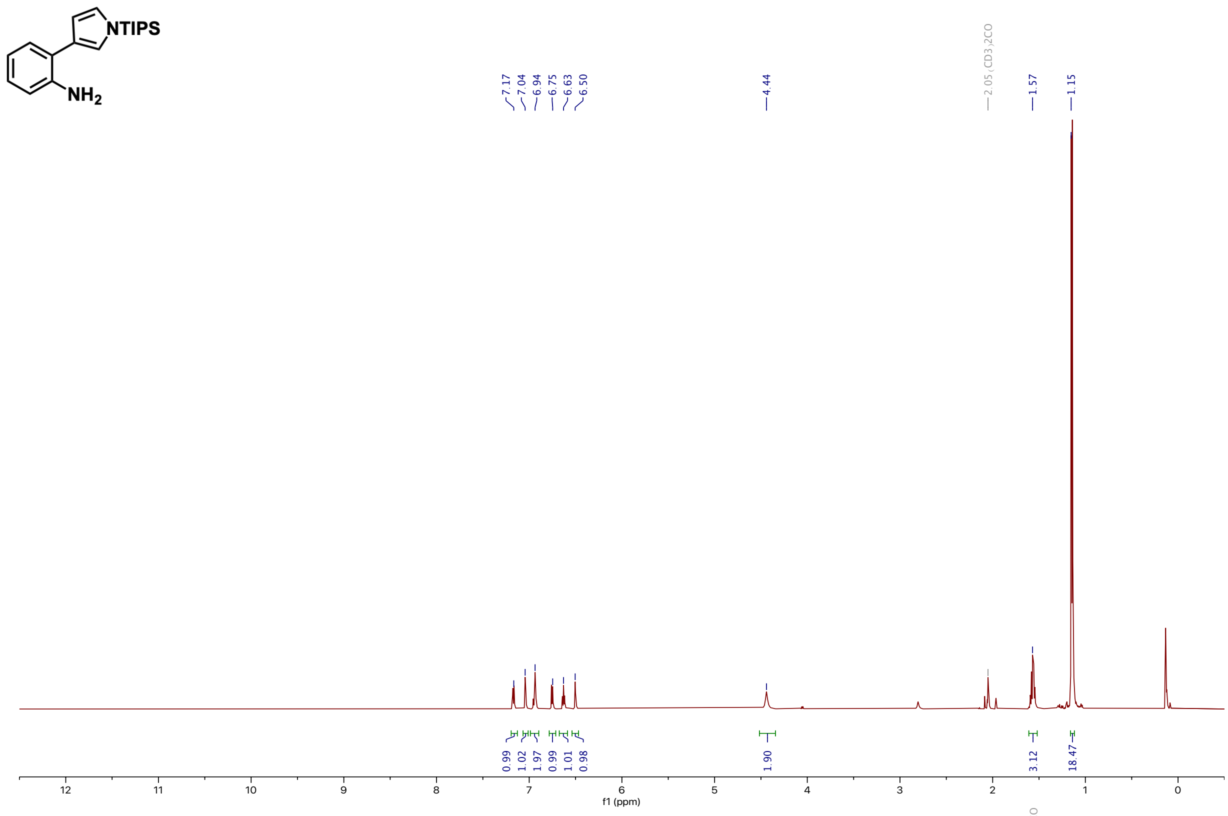
NTIPS
NH2
7.17
7.04
6.94
6.75
6.63
6.50
4.44
2.05, CD3,2CO
1.57
1.15
0.99
1.02
1.97
0.99
1.01
0.98
1.90
3.12
18.47
12
11
10
9
8
7
6
5
4
3
2
1
0
f1 (ppm)

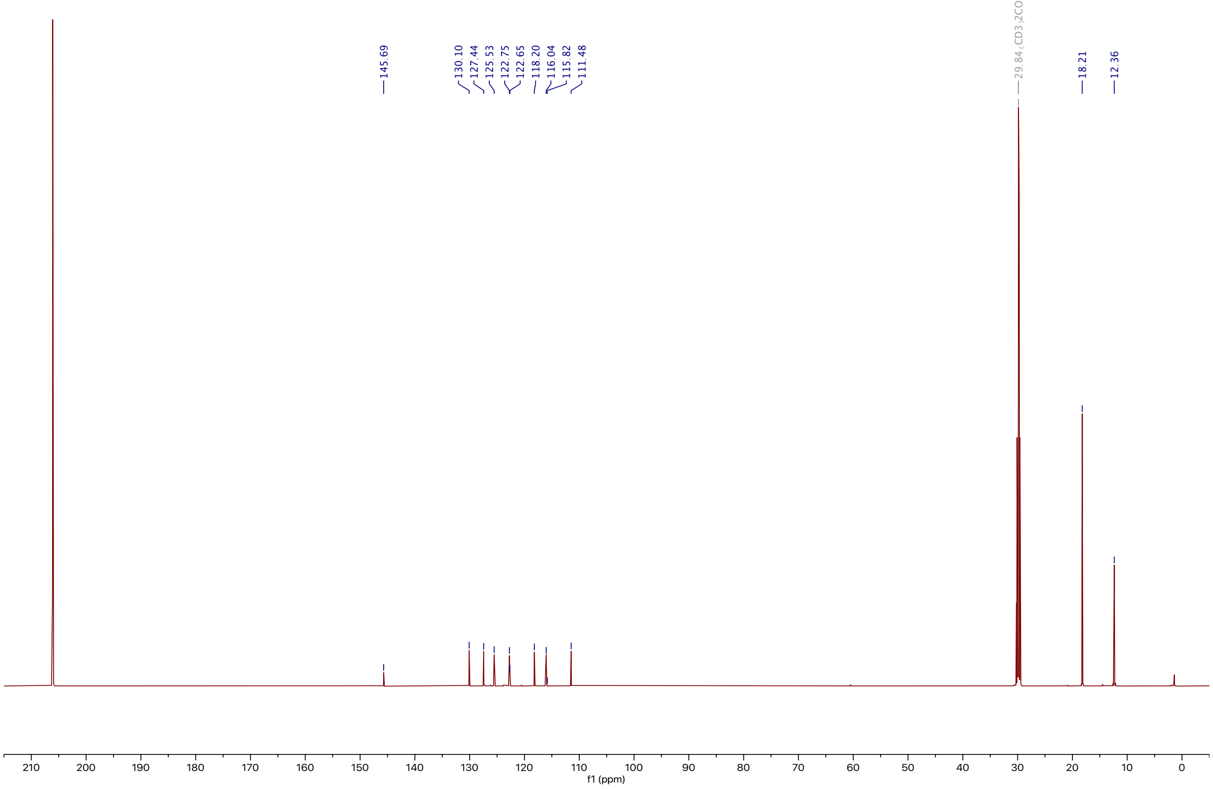
145.69
130.10
127.44
125.53
122.75
122.65
118.20
116.04
115.82
111.48
29.84, CD3,2CO
18.21
12.36
210
200
190
180
170
160
150
140
130
120
110
100
90
80
70
60
50
40
30
20
10
0
f1 (ppm)

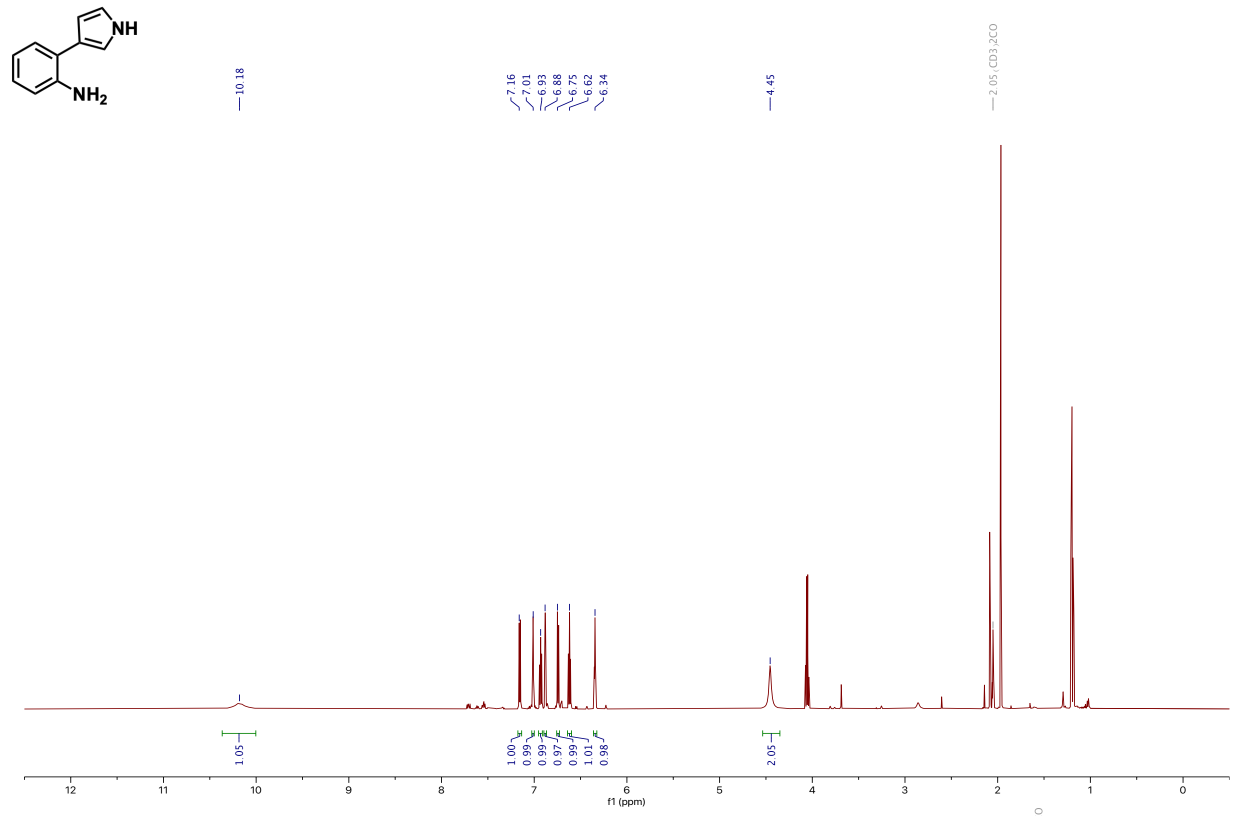
NH
NH2
10.18
7.16
7.01
6.93
6.88
6.75
6.62
6.34
4.45
2.05, CD3,2CO
1.05
1.00
0.99
0.99
0.97
0.99
1.01
0.98
2.05
12
11
10
9
8
7
6
5
4
3
2
1
0
f1 (ppm)

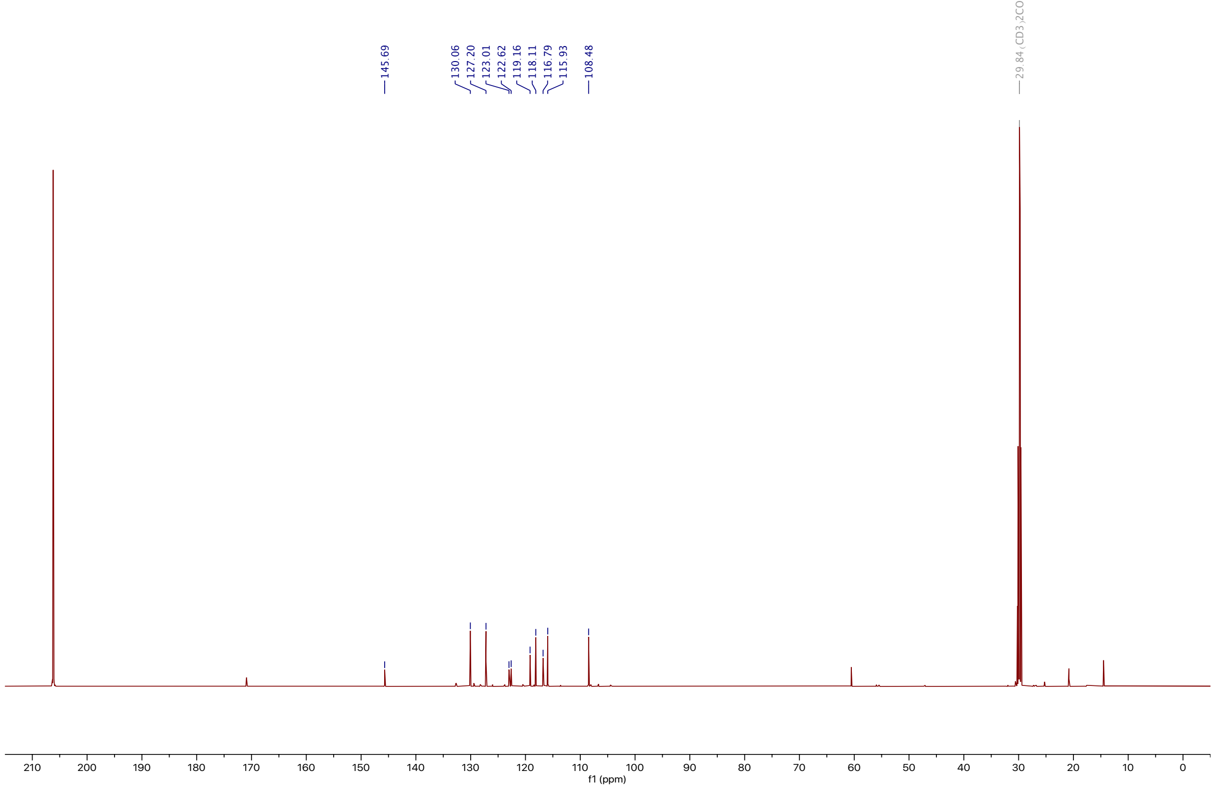
145.69
130.06
127.20
123.01
122.62
119.16
118.11
116.79
115.93
108.48
29.84, CD3,2CO
210
200
190
180
170
160
150
140
130
120
110
100
90
80
70
60
50
40
30
20
10
0
f1 (ppm)

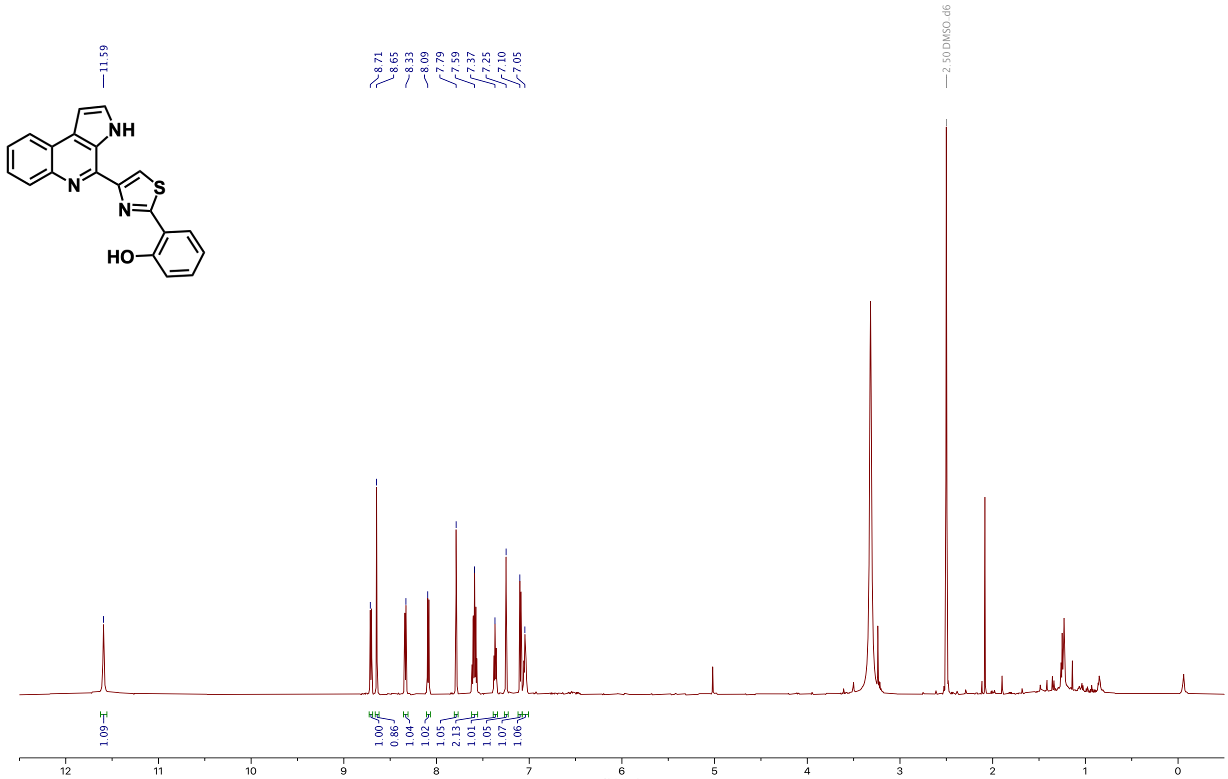
11.59
8.71
8.65
8.33
8.09
7.79
7.59
7.37
7.25
7.10
7.05
2.50 DMSO-d6
NH
N
S
N
HO
1.09
1.00
0.86
1.04
1.02
1.05
2.13
1.01
1.05
1.07
1.06
12
11
10
9
8
7
6
5
4
3
2
1
0
f1 (ppm)

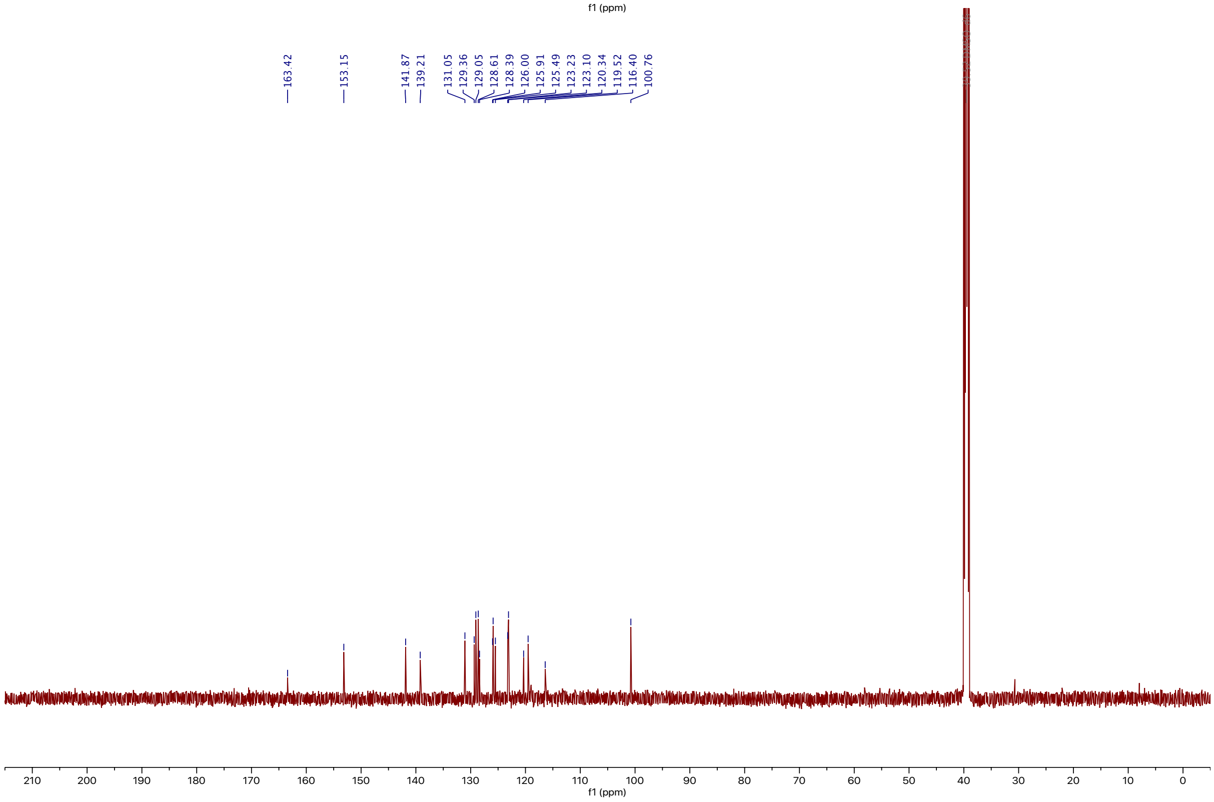
163.42
153.15
141.87
139.21
131.05
129.36
129.05
128.61
128.39
126.00
125.91
125.49
123.23
123.10
120.34
119.52
116.40
100.76
210
200
190
180
170
160
150
140
130
120
110
100
90
80
70
60
50
40
30
20
10
0
f1 (ppm)

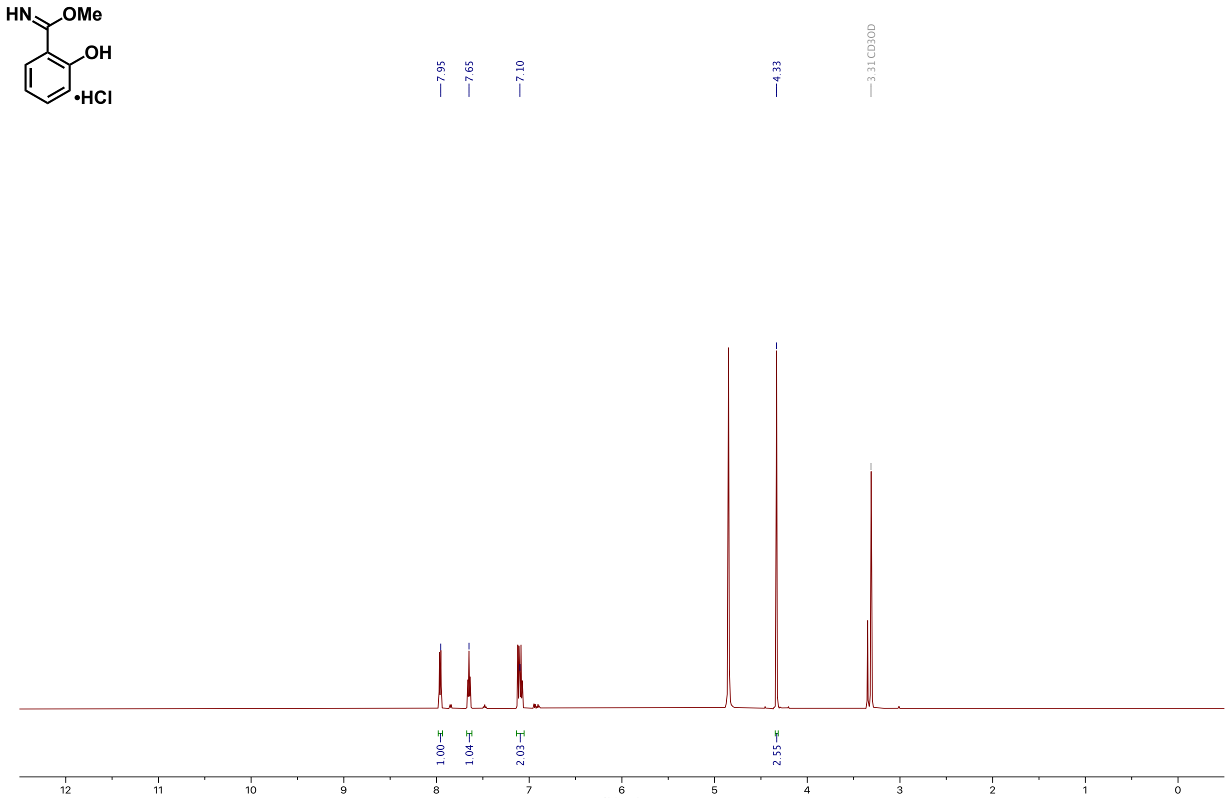
HN
OMe
OH
•HCl
7.95
7.65
7.10
4.33
3.31 CD3OD
1.00
1.04
2.03
2.55
12
11
10
9
8
7
6
5
4
3
2
1
0
f1 (ppm)

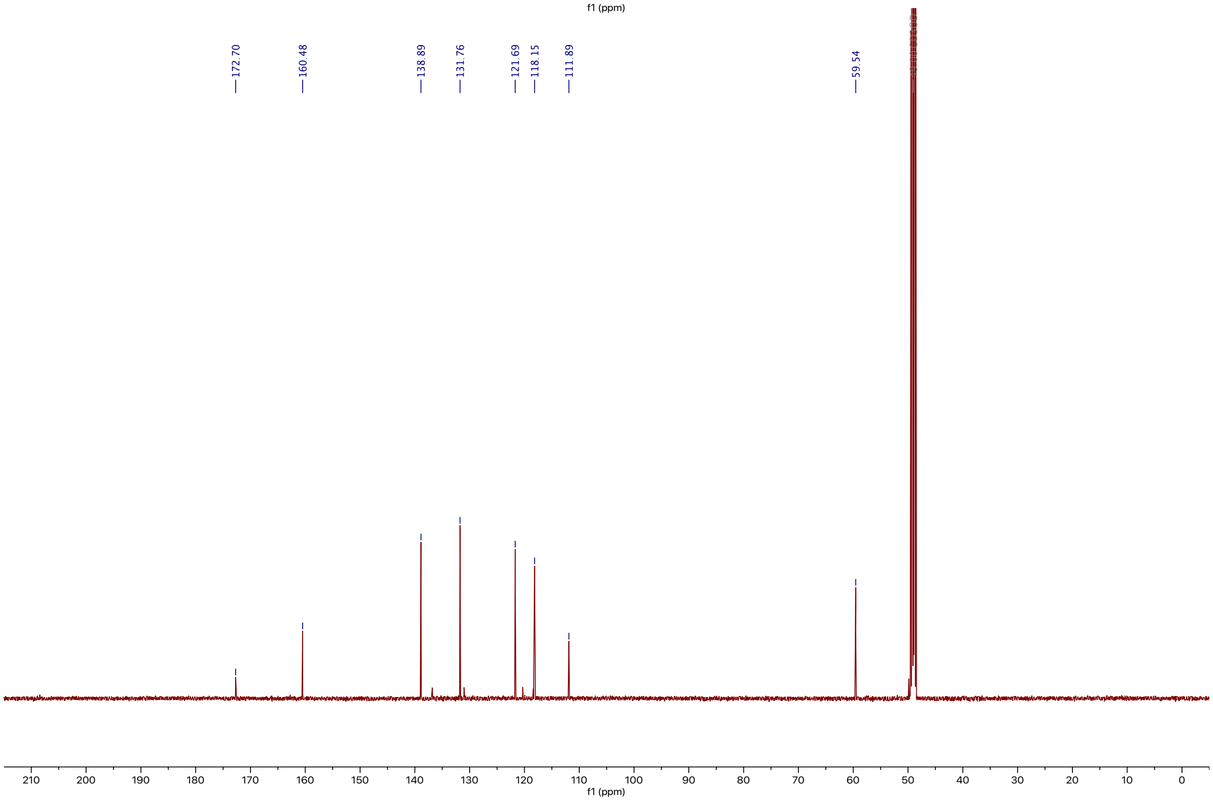
172.70
160.48
138.89
131.76
121.69
118.15
111.89
59.54
210
200
190
180
170
160
150
140
130
120
110
100
90
80
70
60
50
40
30
20
10
0
f1 (ppm)

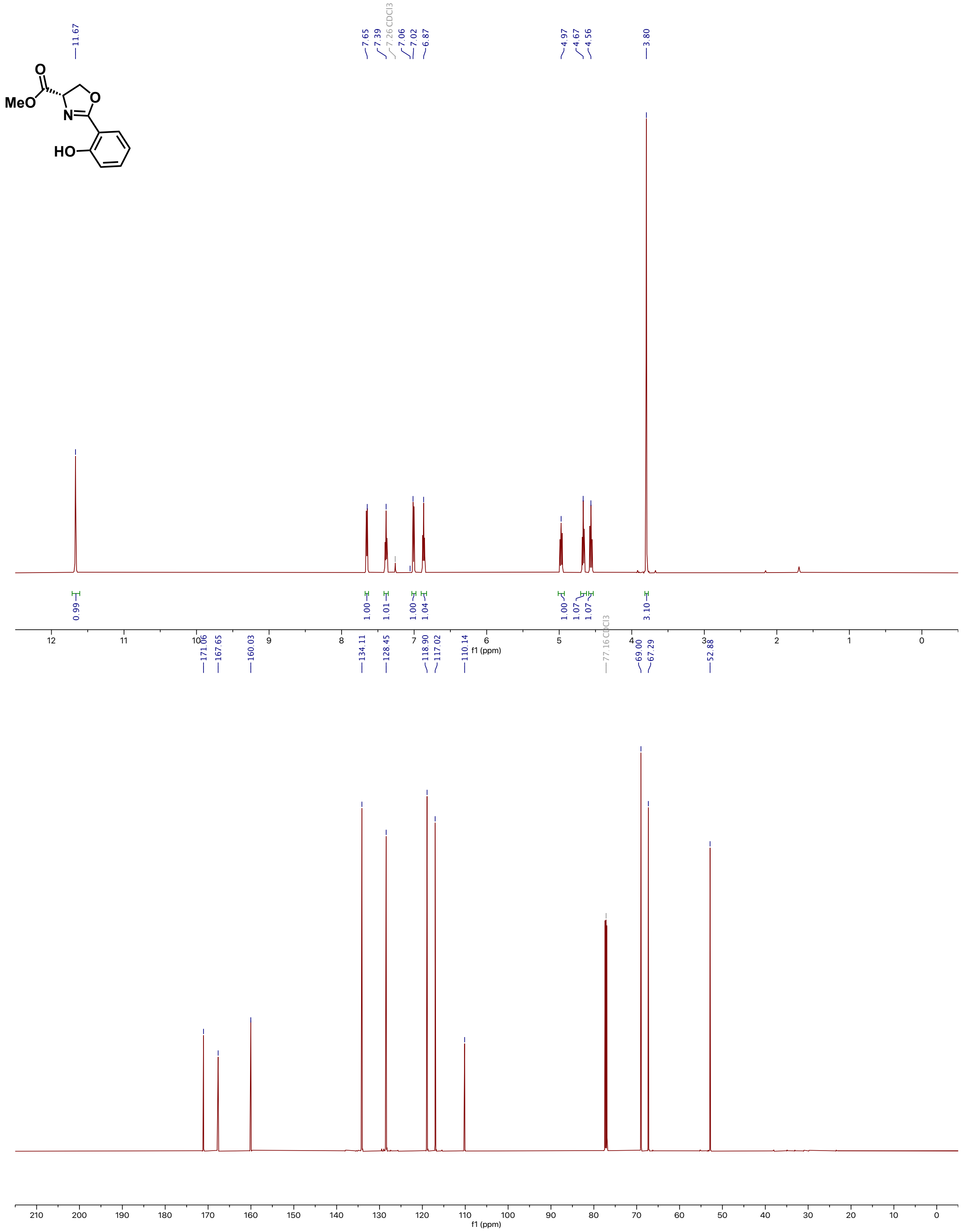
MeO
O
N
O
HO
11.67
7.65
7.39
7.26 CDCl3
7.06
7.02
6.87
4.97
4.67
4.56
3.80
0.99
1.00
1.01
1.00
1.04
1.00
1.07
1.07
3.10
12
11
10
9
8
7
6
5
4
3
2
1
0
f1 (ppm)
171.06
167.65
160.03
134.11
128.45
118.90
117.02
110.14
77.16 CDCl3
69.00
67.29
52.88
210
200
190
180
170
160
150
140
130
120
110
100
90
80
70
60
50
40
30
20
10
0
f1 (ppm)

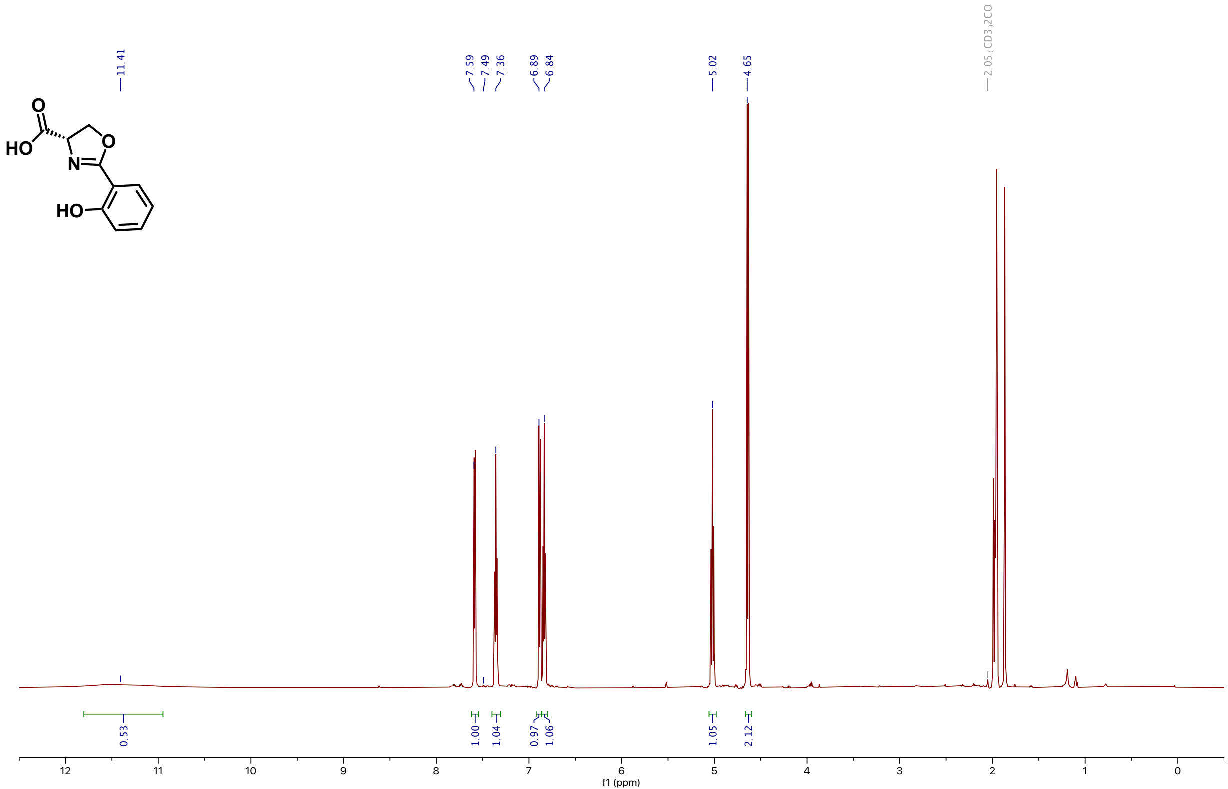
O
HO
N
O
HO
11.41
7.59
7.49
7.36
6.89
6.84
5.02
4.65
2.05,CD3,2CO
0.53
1.00
1.04
0.97
1.06
1.05
2.12
12
11
10
9
8
7
6
5
4
3
2
1
0
f1 (ppm)

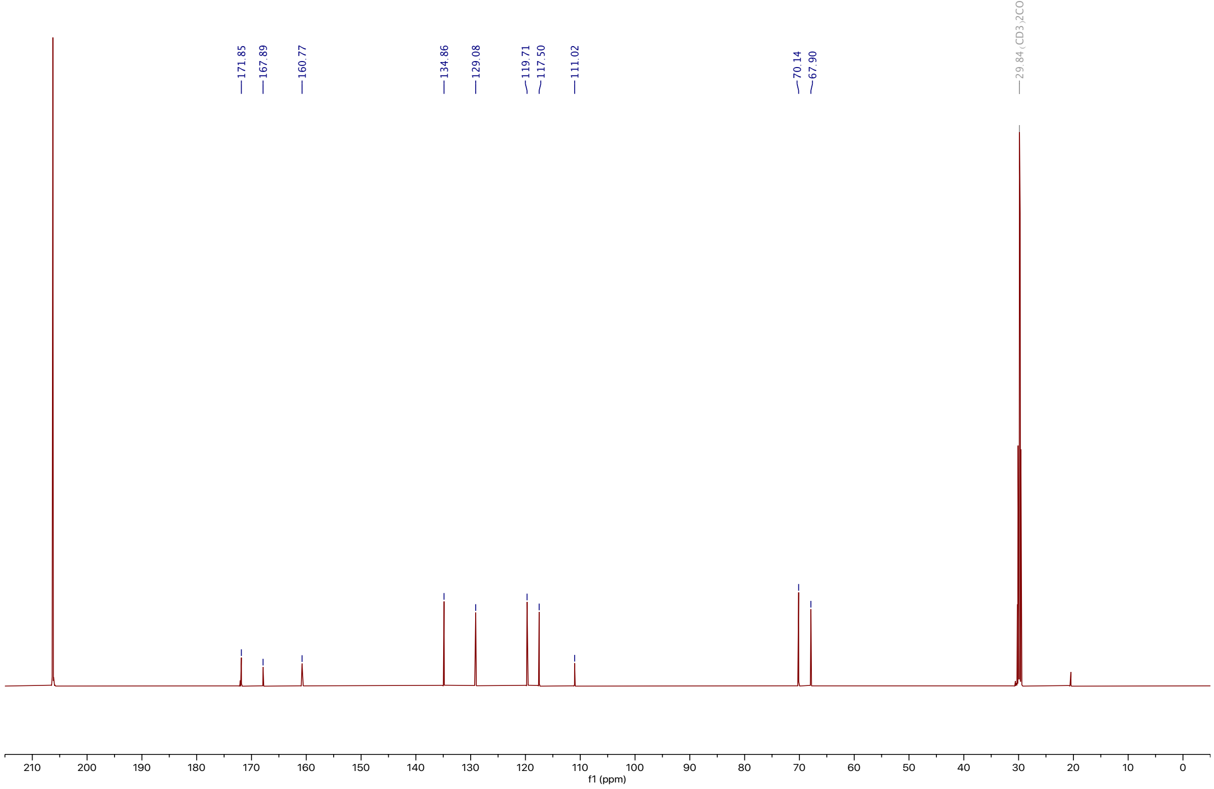
171.85
167.89
160.77
134.86
129.08
119.71
117.50
111.02
70.14
67.90
29.84,CD3,2CO
210
200
190
180
170
160
150
140
130
120
110
100
90
80
70
60
50
40
30
20
10
0
f1 (ppm)

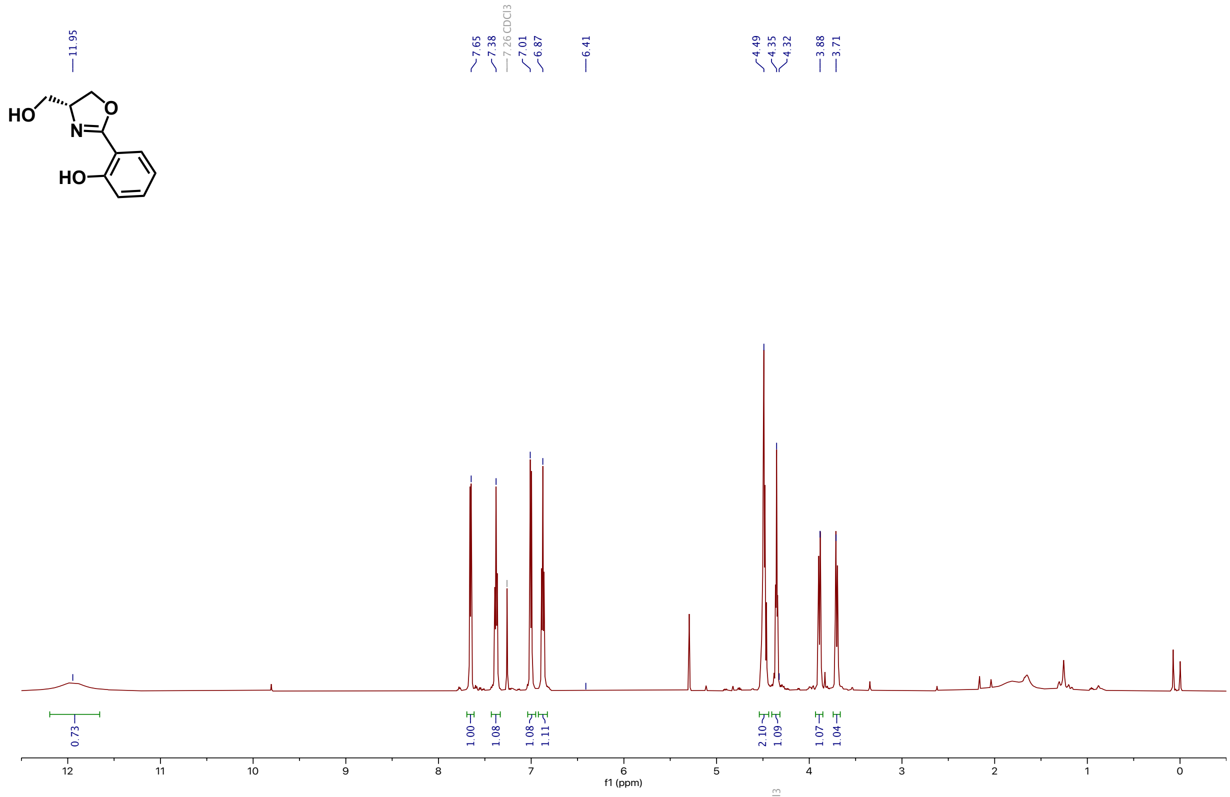
11.95
7.65
7.38
7.26 CDCl3
7.01
6.87
6.41
4.49
4.35
4.32
3.88
3.71
HO
N
O
HO
0.73
1.00
1.08
1.08
1.11
2.10
1.09
1.07
1.04
12
11
10
9
8
7
6
5
4
3
2
1
0
f1 (ppm)

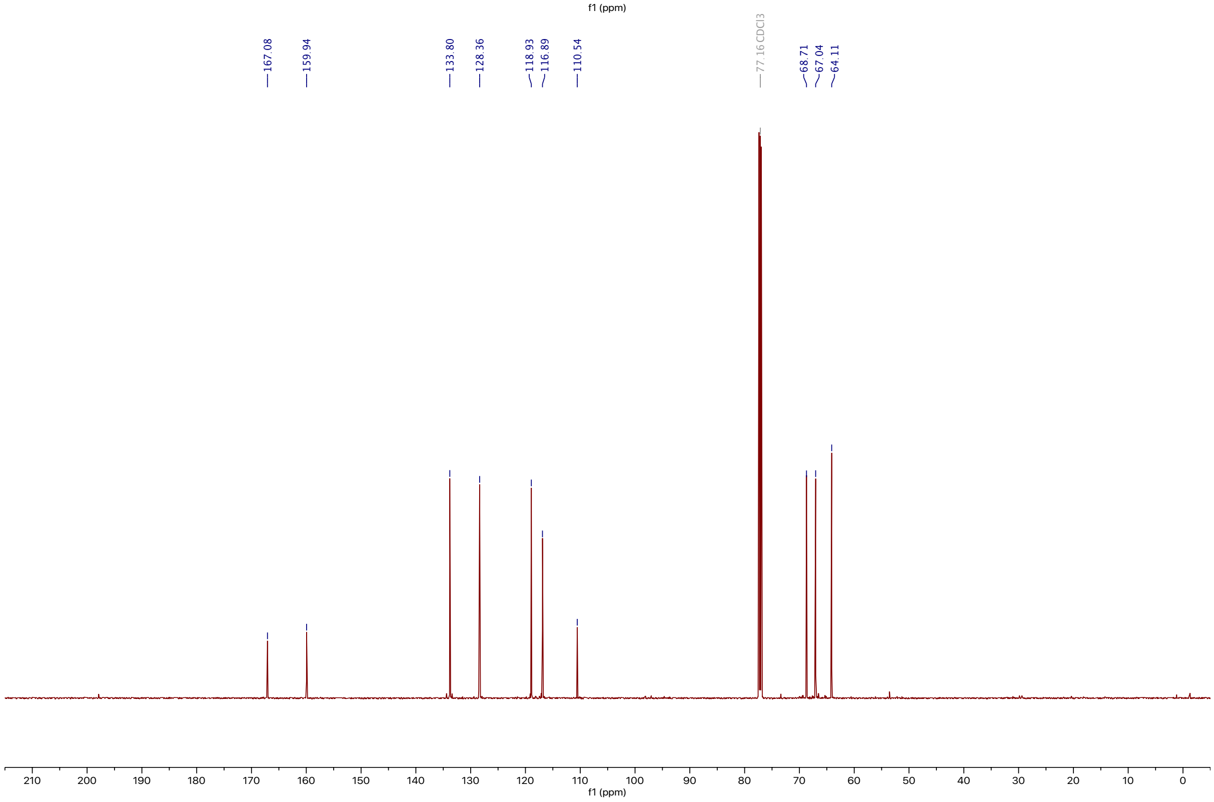
167.08
159.94
133.80
128.36
118.93
116.89
110.54
77.16 CDCl3
68.71
67.04
64.11
210
200
190
180
170
160
150
140
130
120
110
100
90
80
70
60
50
40
30
20
10
0
f1 (ppm)

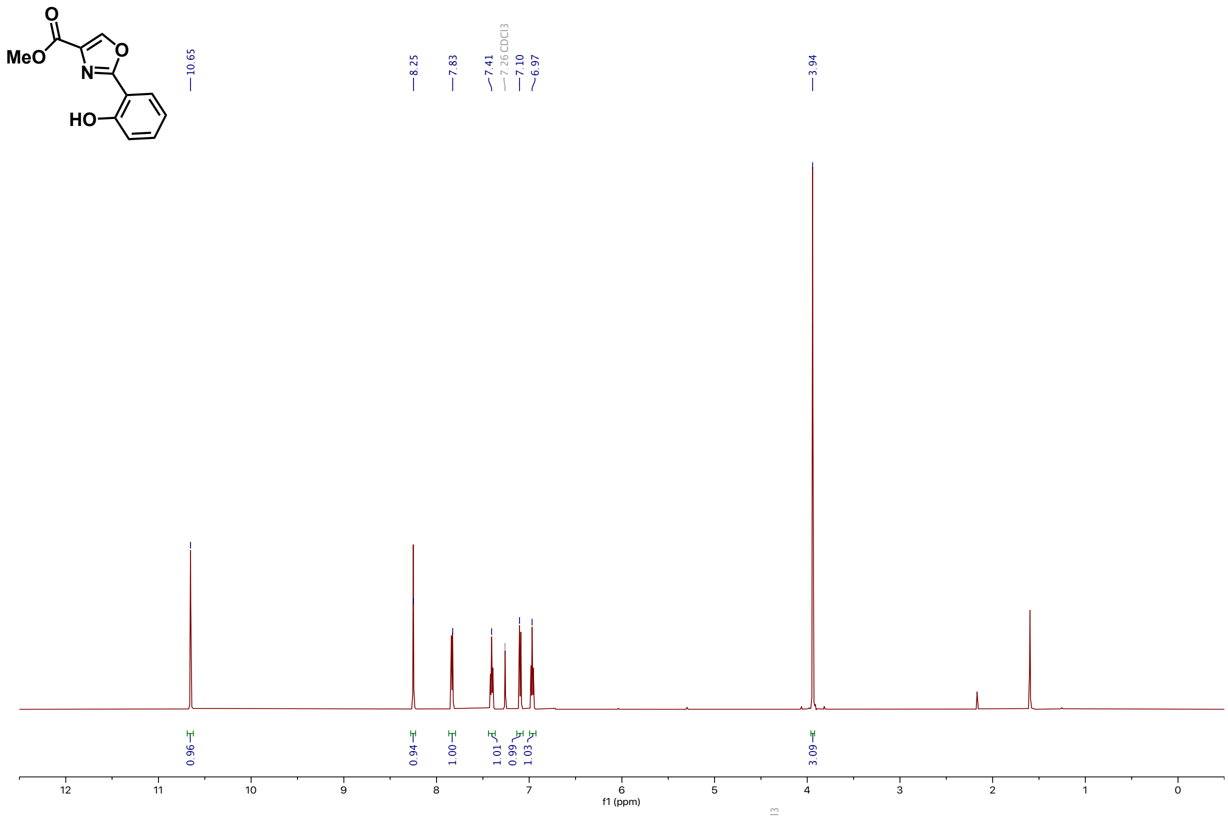
O
MeO
N
O
HO
10.65
8.25
7.83
7.41
7.26 CDCl3
7.10
6.97
3.94
0.96
0.94
1.00
1.01
0.99
1.03
3.09
12
11
10
9
8
7
6
5
4
3
2
1
0
f1 (ppm)

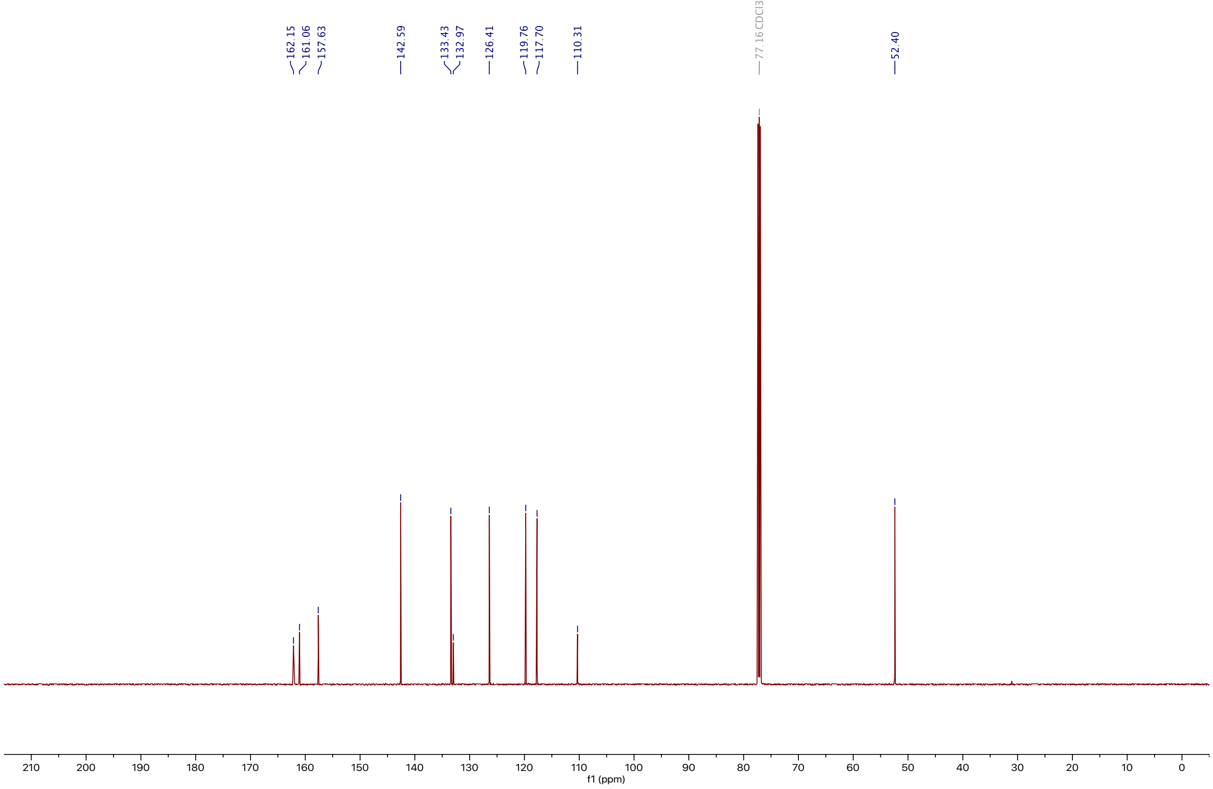
162.15
161.06
157.63
142.59
133.43
132.97
126.41
119.76
117.70
110.31
77.16 CDCl3
52.40
210
200
190
180
170
160
150
140
130
120
110
100
90
80
70
60
50
40
30
20
10
0
f1 (ppm)

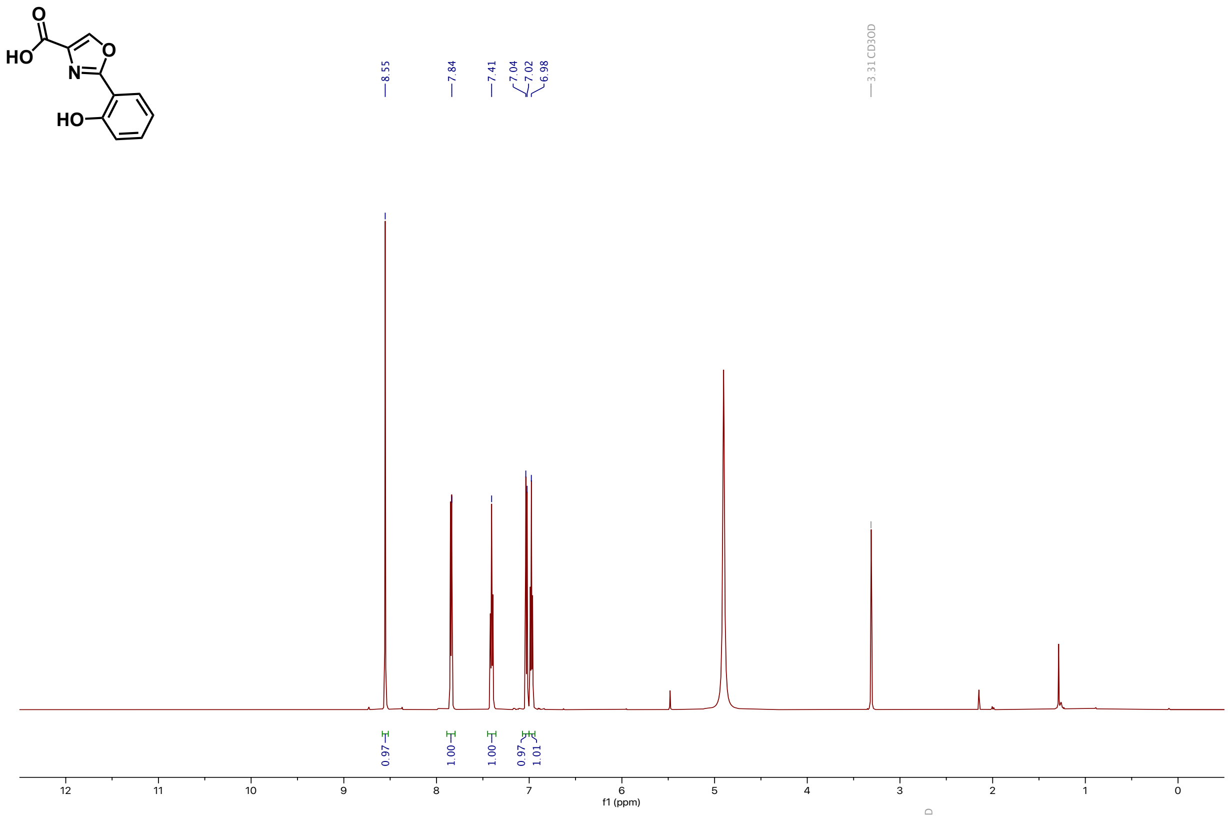
HO
O
O
N
HO
8.55
7.84
7.41
7.04
7.02
6.98
3.31 CD3OD
0.97
1.00
1.00
0.97
1.01
12
11
10
9
8
7
6
5
4
3
2
1
0
f1 (ppm)

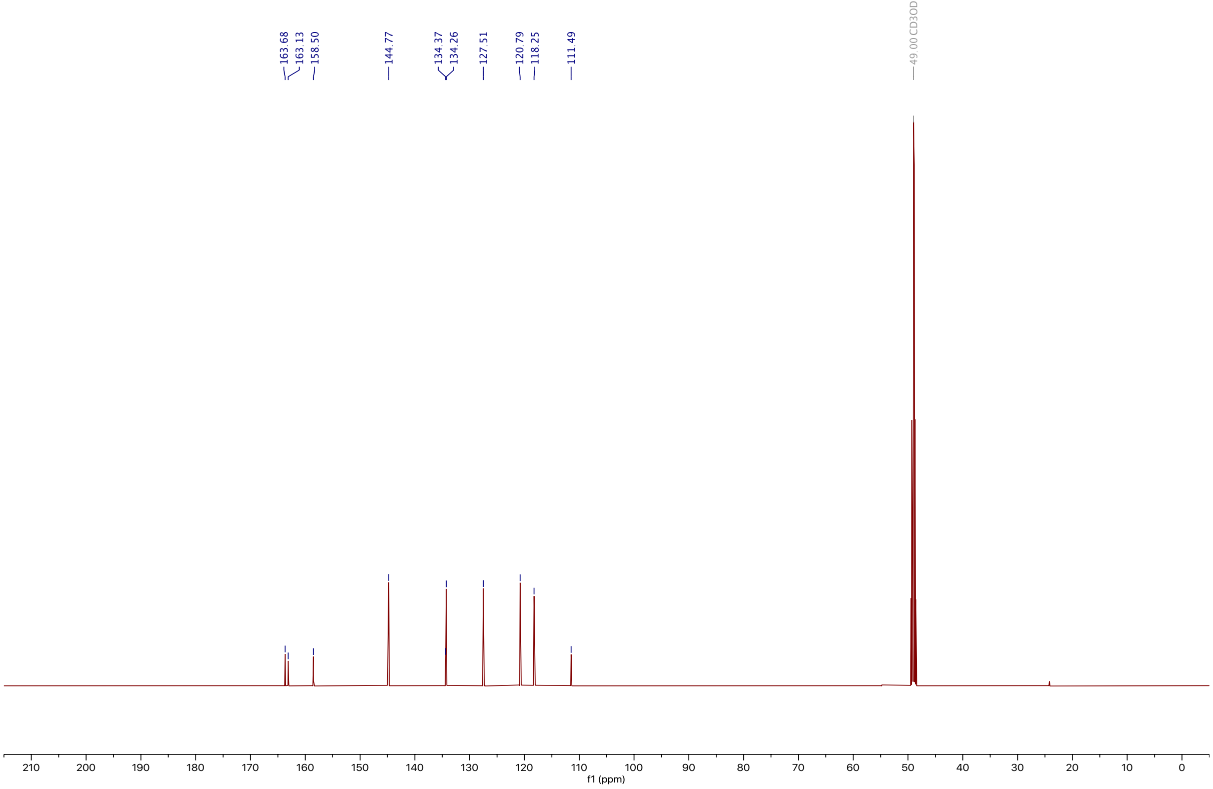
163.68
163.13
158.50
144.77
134.37
134.26
127.51
120.79
118.25
111.49
49.00 CD3OD
210
200
190
180
170
160
150
140
130
120
110
100
90
80
70
60
50
40
30
20
10
0
f1 (ppm)

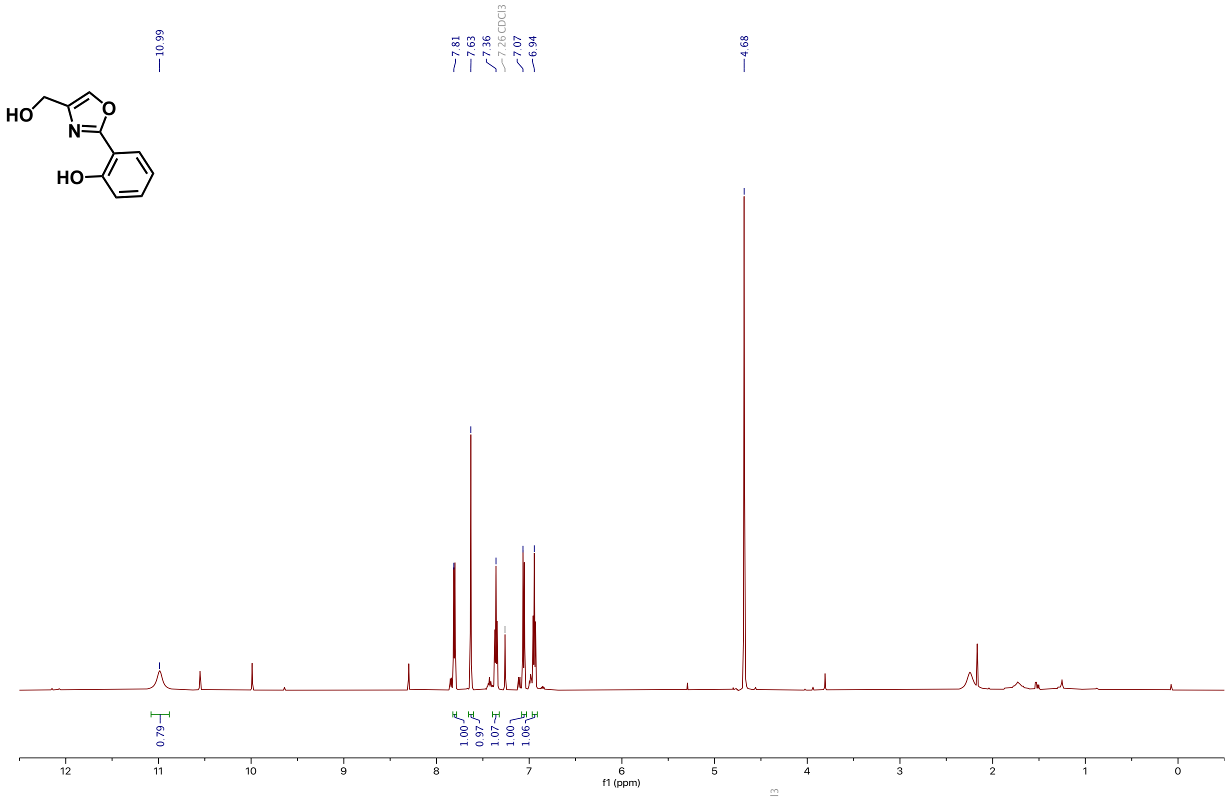
HO
O
N
HO
10.99
7.81
7.63
7.36
7.26 CDCl3
7.07
6.94
4.68
0.79
1.00
0.97
1.07
1.00
1.06
12
11
10
9
8
7
6
5
4
3
2
1
0
f1 (ppm)

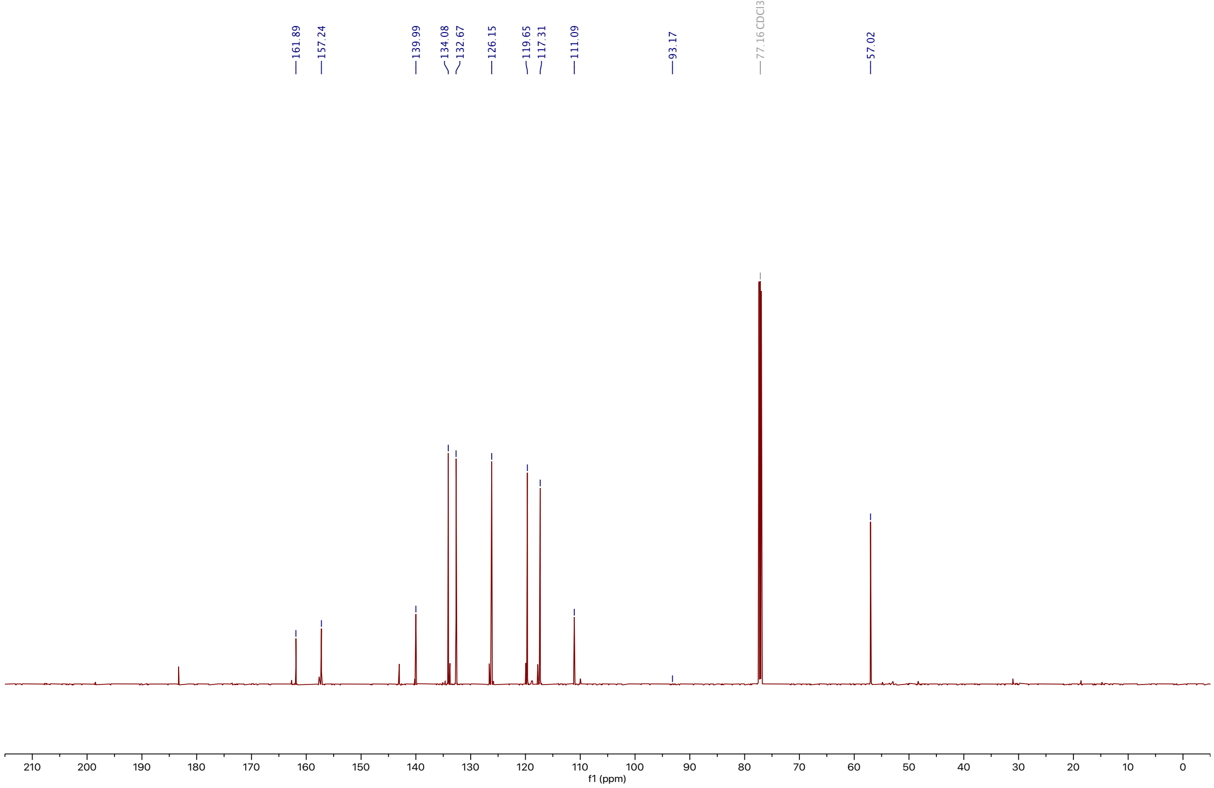
161.89
157.24
139.99
134.08
132.67
126.15
119.65
117.31
111.09
93.17
77.16 CDCl3
57.02
210
200
190
180
170
160
150
140
130
120
110
100
90
80
70
60
50
40
30
20
10
0
f1 (ppm)

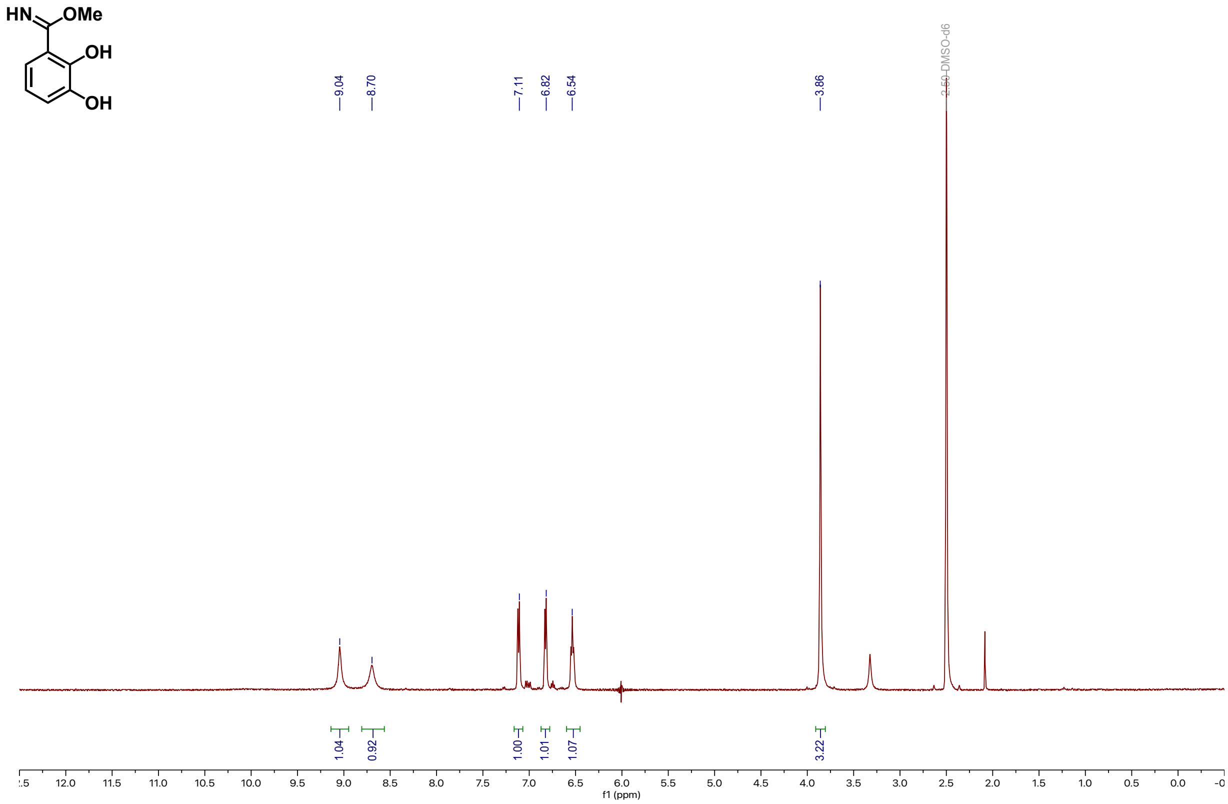
HN
OMe
OH
OH
9.04
8.70
7.11
6.82
6.54
3.86
2.50-DMSO-d6
1.04
0.92
1.00
1.01
1.07
3.22
12.0
11.5
11.0
10.5
10.0
9.5
9.0
8.5
8.0
7.5
7.0
6.5
6.0
5.5
5.0
4.5
4.0
3.5
3.0
2.5
2.0
1.5
1.0
0.5
0.0
f1 (ppm)

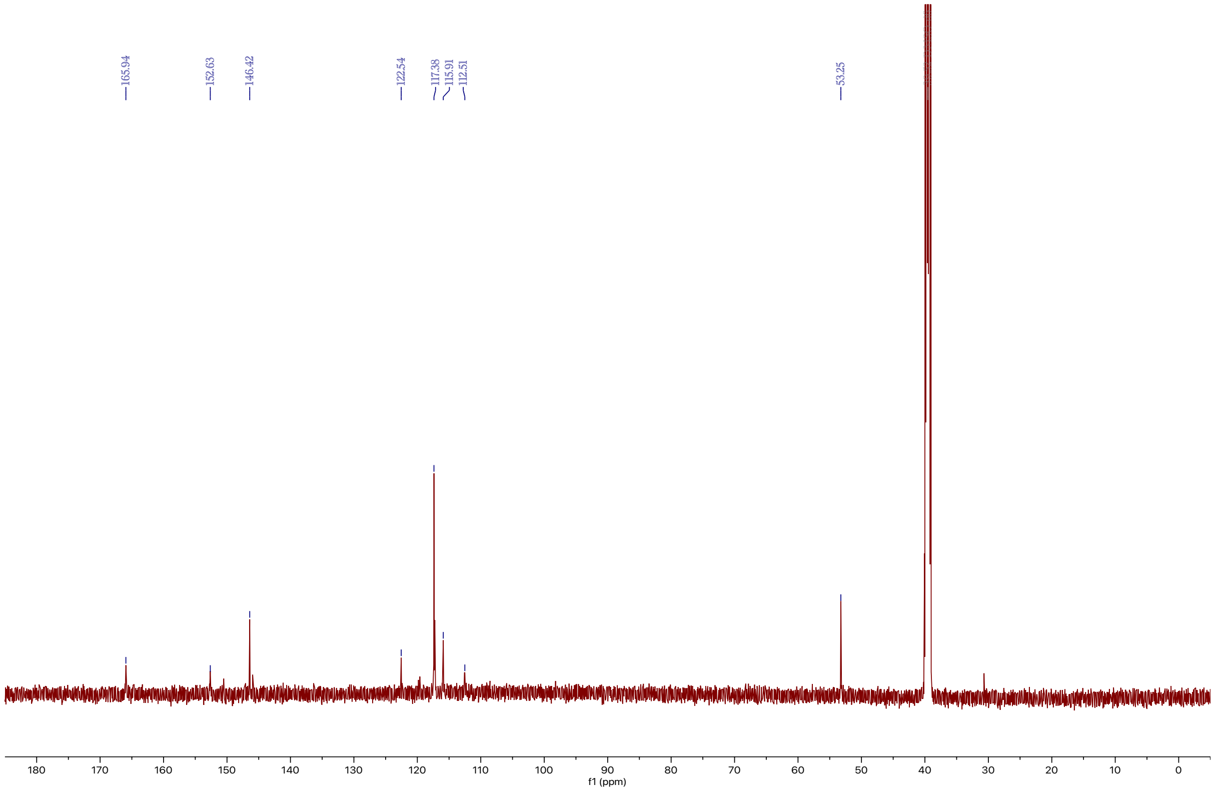
165.94
152.63
146.42
122.54
117.38
115.91
112.51
53.25
180
170
160
150
140
130
120
110
100
90
80
70
60
50
40
30
20
10
0
f1 (ppm)

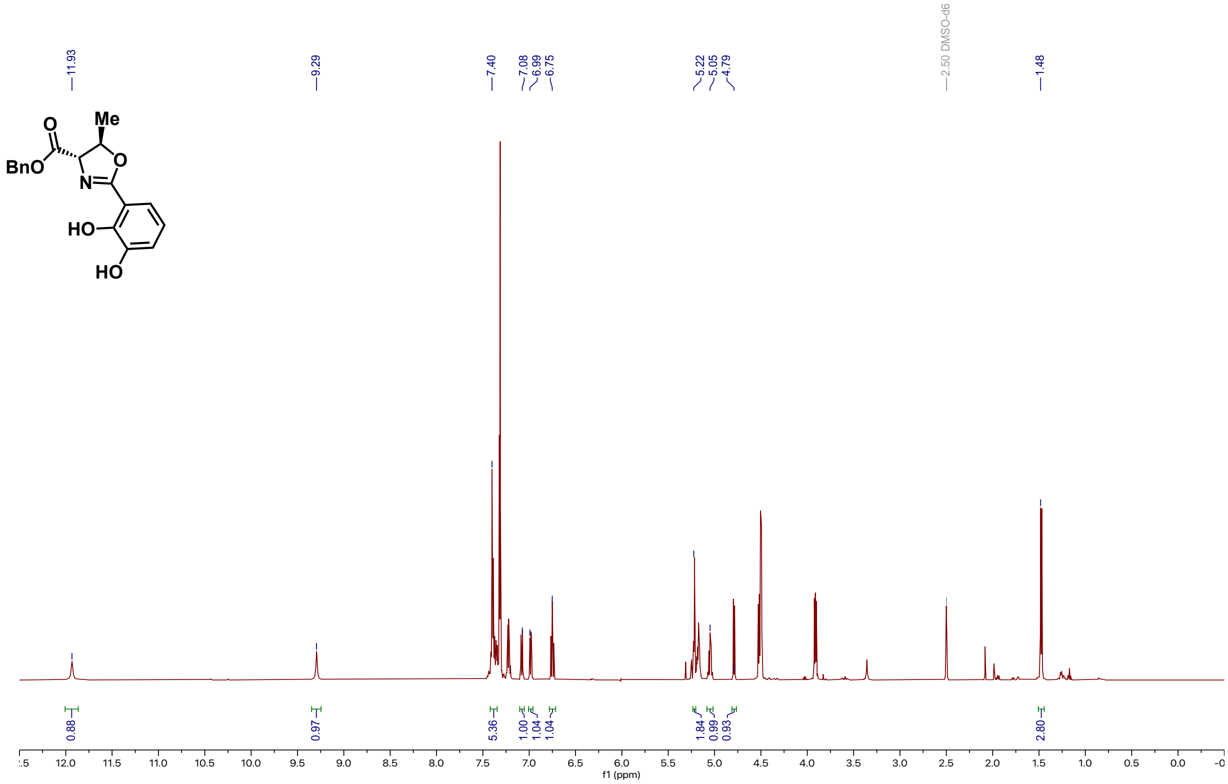

11.93
9.29
7.40
7.08
6.99
6.75
5.22
5.05
4.79
2.50 DMSO-d6
1.48
O
Me
BnO
O
N
HO
HO
0.88
0.97
5.36
1.00
1.04
1.04
1.84
0.99
0.93
2.80
12.0
11.5
11.0
10.5
10.0
9.5
9.0
8.5
8.0
7.5
7.0
6.5
6.0
5.5
5.0
4.5
4.0
3.5
3.0
2.5
2.0
1.5
1.0
0.5
0.0
f1 (ppm)

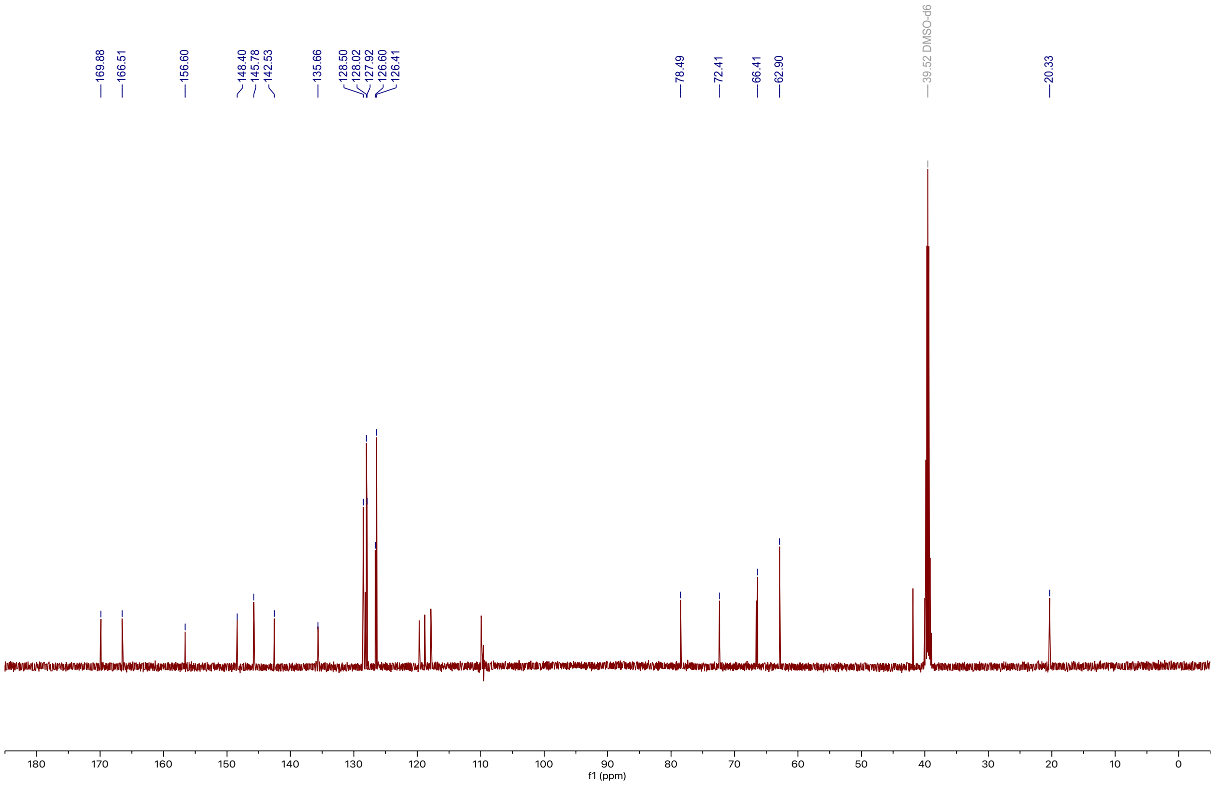

169.88
166.51
156.60
148.40
145.78
142.53
135.66
128.50
128.02
127.92
126.60
126.41
78.49
72.41
66.41
62.90
39.52 DMSO-d6
20.33
180
170
160
150
140
130
120
110
100
90
80
70
60
50
40
30
20
10
0
f1 (ppm)

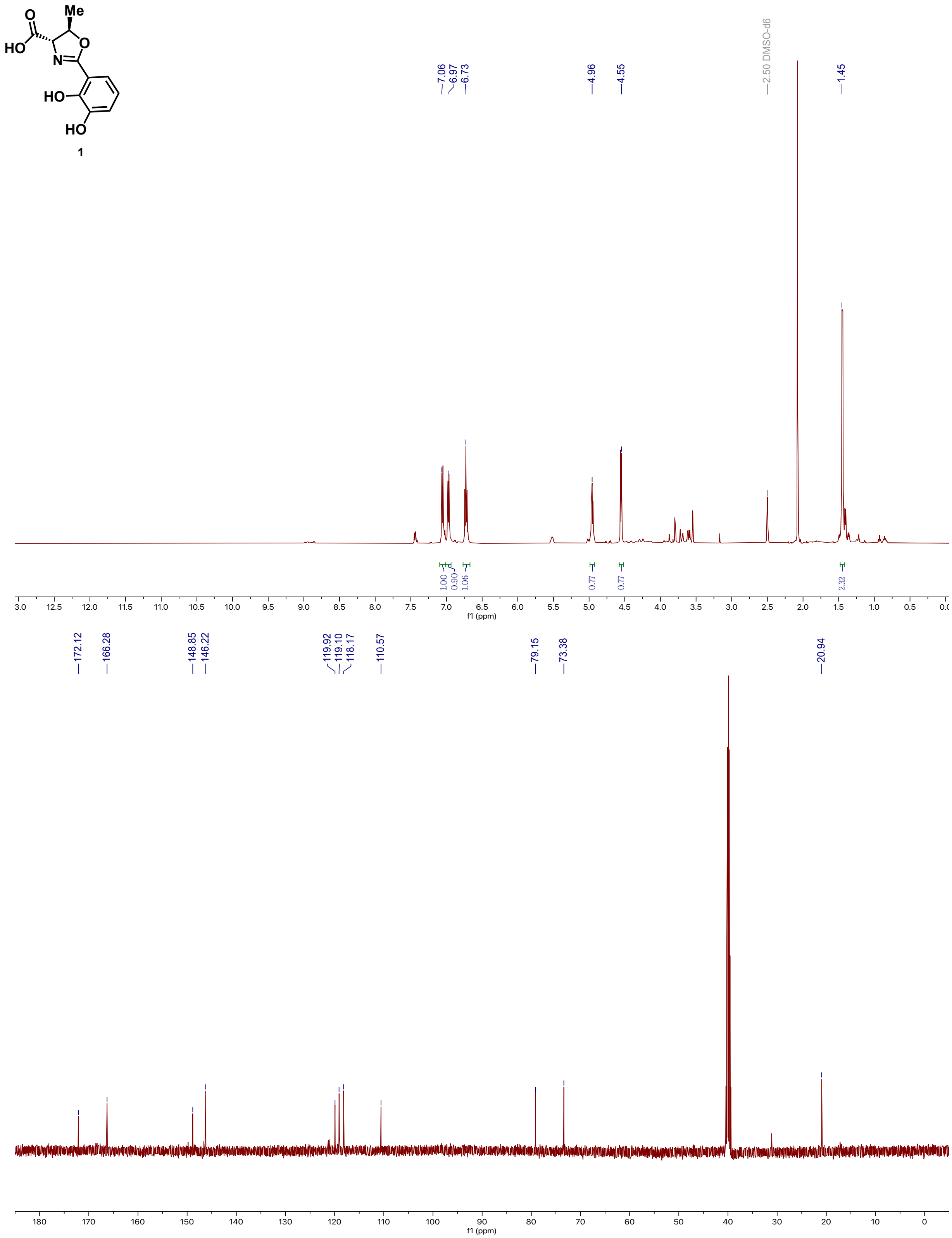

1

Me
O
HO
N
O
HO
HO
7.06
6.97
6.73
4.96
4.55
2.50 DMSO-d6
1.45
1.00
0.90
1.06
0.77
0.77
2.32
3.0
12.5
12.0
11.5
11.0
10.5
10.0
9.5
9.0
8.5
8.0
7.5
7.0
6.5
6.0
5.5
5.0
4.5
4.0
3.5
3.0
2.5
2.0
1.5
1.0
0.5
0.(
f1 (ppm)
172.12
166.28
148.85
146.22
119.92
119.10
118.17
110.57
79.15
73.38
20.94
180
170
160
150
140
130
120
110
100
90
80
70
60
50
40
30
20
10
0
f1 (ppm)

Metal Chelation Assays

$FeCl_3$ Titration Assay

To a 1 mM stock solution of $FeCl_3$ in methanol was added specified volumes of a 1 mM solution of each compound in methanol giving the following range of test concentrations: 0 μM, 125 μM, 250 μM, and 500 μM. The positive control was EDTA and was prepared and tested in the same manner as test compounds.

Fluorescence Titration Assays

Fluorescence measurements were recorded on a FluoroMax spectrophotometer (Horiba Scientific, Edison, New Jersey). These measurements were taken in a quartz fluorescence cuvette with a 1 cm pathlength, a 258-550 nm integration range, and a 2 nm excitation and emission slit width. Fluorescence titrations were all performed in methanol. An emission spectrum of 350 μL of a 400 μM stock solution of compound was recorded ($\lambda_{excitation}$ = wavelength of maximum absorbance (λ_{max}), integration time = 1 second, accumulations = 10). Solutions had varying emission signals and parameters were adjusted accordingly by reducing integration time and/or accumulations. A 10 mM stock solution of metal was added in 1.4 μL portions, the solution gently mixed, and the emission spectrum recorded after each addition. Fluorescence titration curves were generated by plotting equivalents of metal (x-axis) against emission peak (y-axis). Ligand-to-iron binding stoichiometries were determined by dividing the concentration of ligand by the concentration of metal in solution when the emission signal is initially quenched. K_d values were determined using a nonlinear regression curve fit, one site – specific binding analysis in prism.

Extended Data

Raw fluorescence titration curves of all compounds tested in the *Pseudomonas* work (**3.01**, **3.04**, **3.05**, **3.07**, **3.08**, **3.14**, **3.17**, **3.18**, **3.20**, **3.21**). It should be noted that normalization of the curves made it appear as though **3.21** binds Fe^{III} with 2:1 ratio, however from the raw fluorescence titration curve, it appears as though **3.21** binds Fe^{III} with a 1:1 ratio. Because a 2:1 ratio was assumed for this compound, this would ensure that the amount of Fe^{III} used to generate the 2:1 complex would not result in an excess of Fe^{III} in solution resulting in enhanced growth due to excess free Fe^{III} and the growth enhancement observed was in fact due to uptake of the ligand:Fe^{III} complex.

3.01

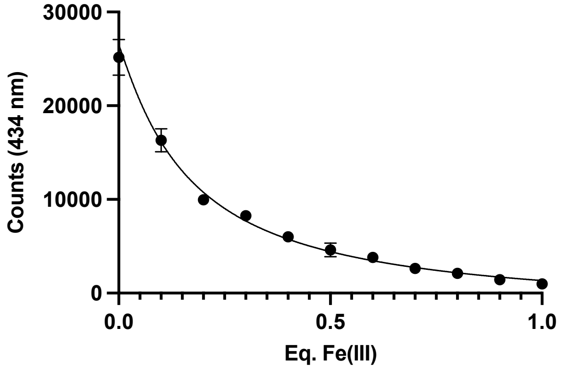

3.04

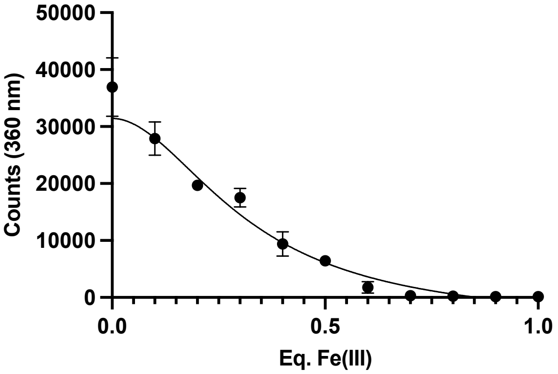

3.05

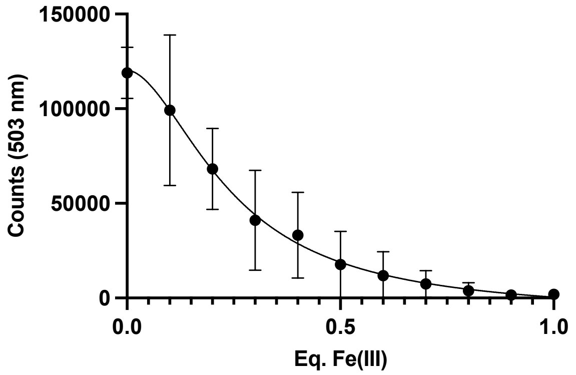

3.07

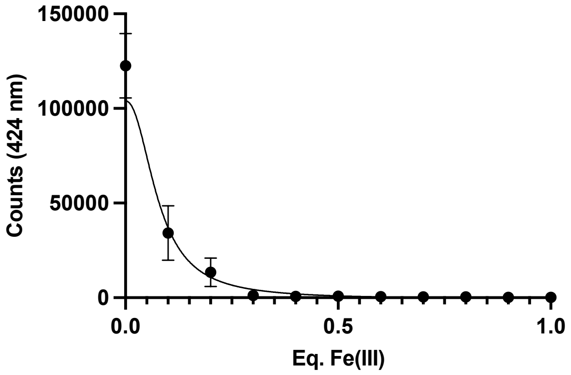

3.08

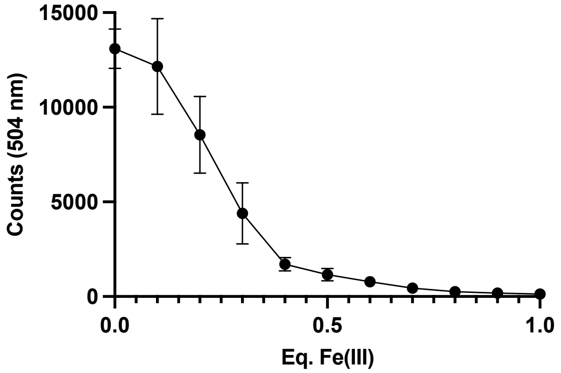

3.14

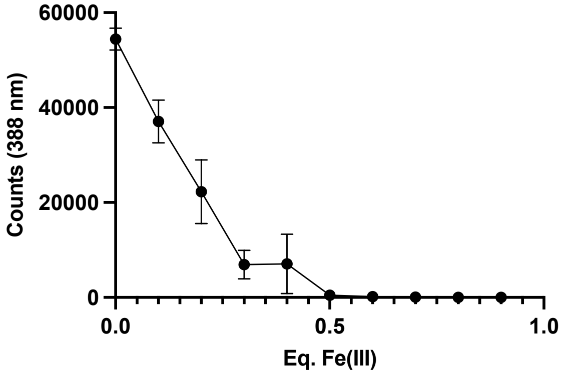

3.17

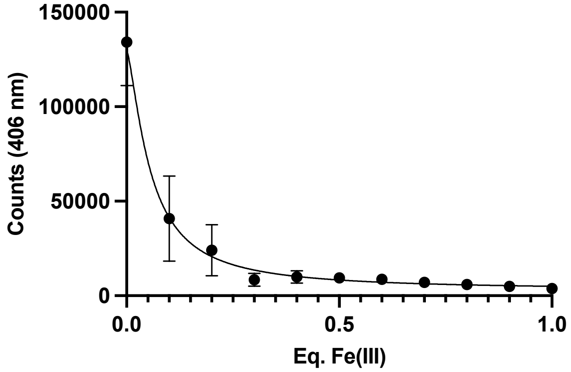

3.18

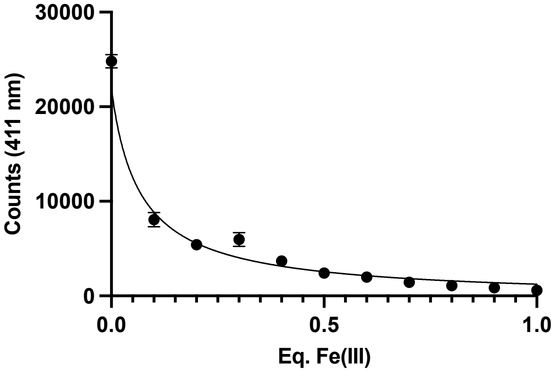

3.20

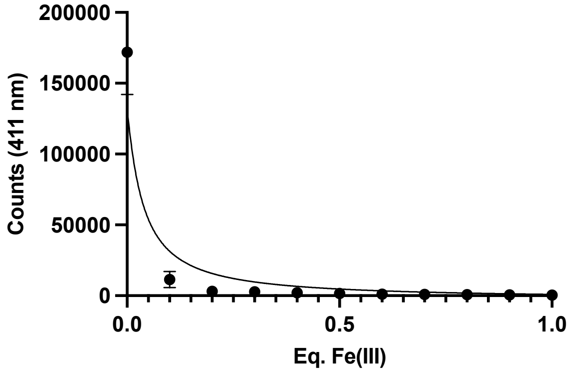

3.21

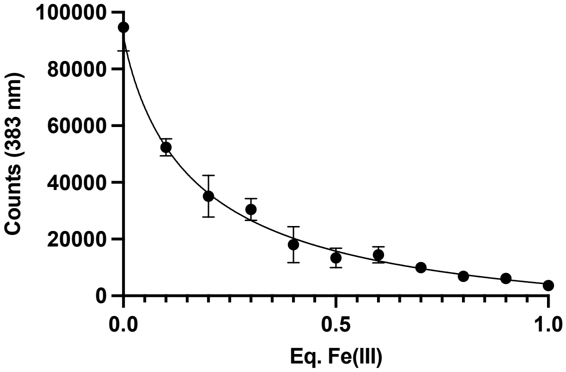

Computational Analysis

Computational Procedures and Supplemental Description

Geometry optimizations and frequency calculations for all reported structures were performed with the Gaussian 09 suite of programs[11] at the B3LYP-D3(BJ)/[6-31G(d,p) + Lanl2dz (Fe)]. Frequency analysis was used to characterize each minimum with zero imaginary frequencies. Thus, here we used the B3LYP[12,13,14] density functional with Grimme's empirical dispersion-correction (D3)[15,16] and Becke-Johnson (BJ)'s damping schemes.[17] Bulk solvent effects were incorporated in all calculations (including the geometry optimization and frequency calculations) at the self-consistent reaction field polarizable continuum model (IEF-PCM)[18] level. As a solvent we chose water. The Gibbs free energies are calculated at 298.15 K temperature and 1 atm. pressure.

The Fe-binding modes for **1**, **3**, and **5** were evaluated computationally. These extensive DFT calculations indicate that coordination of **1**, **3**, and **5** to the Fe(III)-center is favorable with free energies of coordination of 20.8, 23.9, and 24.4 kcal/mol, respectively (S6, S7, S8). The subsequent second ligand coordination is unfavorable by 11.0 and 0.8 kcal/mol for **1** and **3**, respectively, and favorable by 4.4 kcal/mol for **5**. We also calculated adducts (**1-H**)$_2$FeCl(**1**), (**3-H**)$_2$FeCl(**3**), (**5-H**)$_2$FeCl(**5**); (**1-H**, **3-H,** and **5-H** stands for deprotonated **1**, **3,** and **5,** respectively), which can be formed by reaction of three molecules of **1**, **3**, and **5**, and dissociation of two HCl molecules. (**3-H**)$_2$FeCl(**3**) + 2(HCl) and (**5-H**)$_2$FeCl(**5**) + 2(HCl) is favorable by 1.7 and 16.3 kcal/mol, respectively relative to the dissociation limit, and (**1-H**)$_2$FeCl(**1**) + 2(HCl) is highly unfavorable by 14.9 kcal/mol, indicating that it is possible for **3** and **5** to have at least a 2:1 binding ratio while **1** likely binds with 1:1 ratio. Consistent with our experimental findings, these computational data indicate that the Fe(III)-center can coordinate up to two or three IQS (**3**) and aerugine (**5**) molecules, while it may only coordinate one Dha (**1**) molecule. Of note, the data for **3** are slightly contradictory, however the absolute value of both calculated energies are fairly low, so it is also highly likely that both the 1:1 and 2:1 species exist in equilibrium.

* Computational studies were performed by Djamaladdin G. Musaev.

Supporting Figures

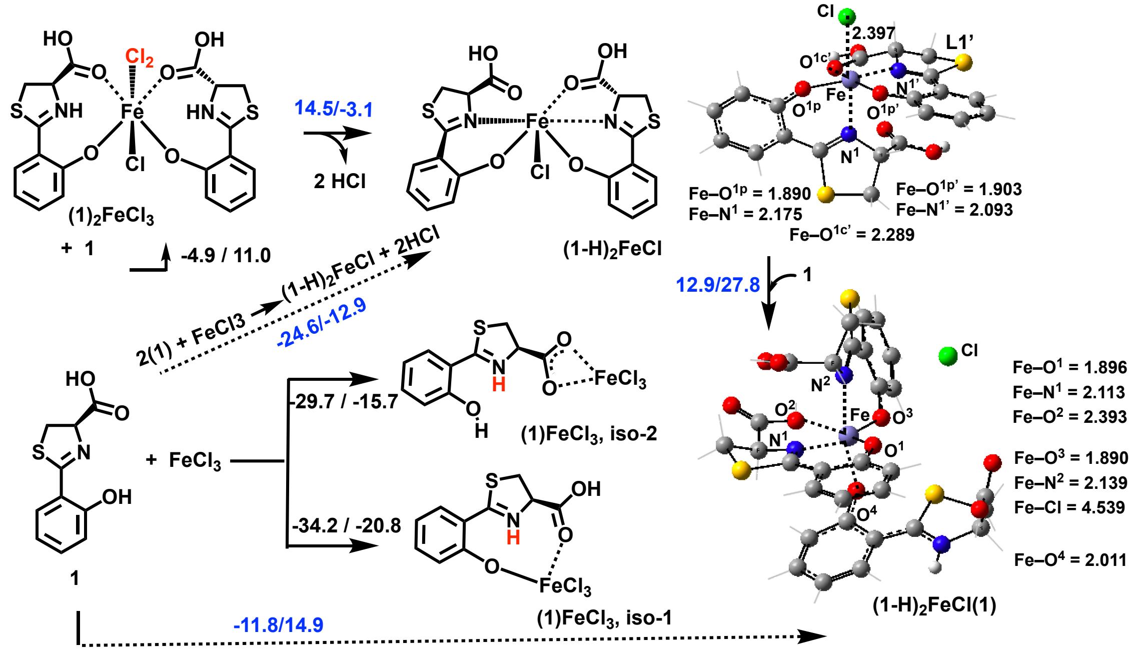

HO
OH
Cl2
Fe
Cl
(1)2FeCl3
+ 1
14.5/-3.1
2 HCl
(1-H)2FeCl
-4.9 / 11.0
2(1) + FeCl3
(1-H)2FeCl + 2HCl
-24.6/-12.9
Cl
2.397
L1'
O1c'
Fe
O1p
O1p'
N1'
N1
Fe–O1p = 1.890
Fe–N1 = 2.175
Fe–O1p' = 1.903
Fe–N1' = 2.093
Fe–O1c' = 2.289
12.9/27.8
1
+ FeCl3
-29.7 / -15.7
(1)FeCl3, iso-2
-34.2 / -20.8
(1)FeCl3, iso-1
1
-11.8/14.9
N2
O2
N1
O3
O1
O4
Fe–O1 = 1.896
Fe–N1 = 2.113
Fe–O2 = 2.393
Fe–O3 = 1.890
Fe–N2 = 2.139
Fe–Cl = 4.539
Fe–O4 = 2.011
(1-H)2FeCl(1)

Figure S3.01. The pathways for formation of and calculated (**1**)FeCl3, iso-1, (**1**)FeCl3, iso-2, (**1**)2FeCl3, and (**1-H**)2FeCl adducts (distances are in Å). ***1** corresponds to **3.01**.

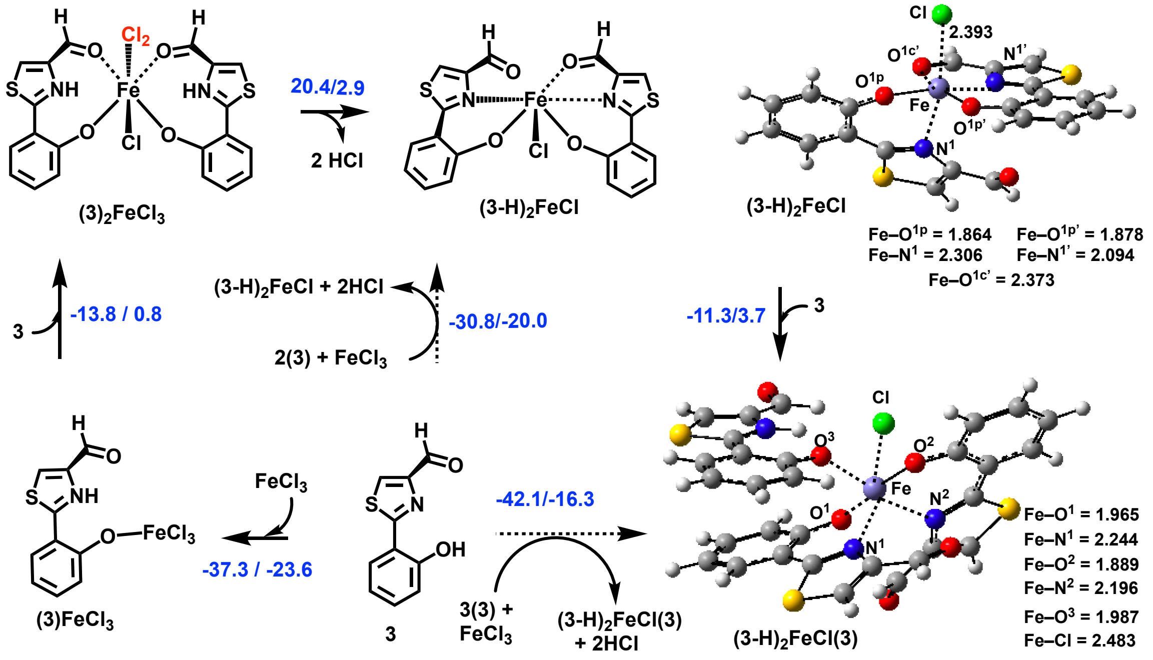

H
Cl2
Fe
Cl
(3)2FeCl3
20.4/2.9
2 HCl
(3-H)2FeCl
Cl
2.393
O1c'
N1'
O1p
Fe
O1p'
N1
(3-H)2FeCl
Fe–O1p = 1.864
Fe–N1 = 2.306
Fe–O1p' = 1.878
Fe–N1' = 2.094
Fe–O1c' = 2.373
3
-13.8 / 0.8
(3-H)2FeCl + 2HCl
-30.8/-20.0
2(3) + FeCl3
-11.3/3.7
3
(3)FeCl3
FeCl3
-37.3 / -23.6
3
-42.1/-16.3
3(3) + FeCl3
(3-H)2FeCl(3) + 2HCl
Cl
O3
O2
Fe
O1
N2
N1
Fe–O1 = 1.965
Fe–N1 = 2.244
Fe–O2 = 1.889
Fe–N2 = 2.196
Fe–O3 = 1.987
Fe–Cl = 2.483
(3-H)2FeCl(3)

Figure S3.02. The pathways for formation of and calculated (**3**)FeCl3, iso-1, (**3**)FeCl3, iso-2, (**3**)2FeCl3, and (**3-H**)2FeCl adducts (distances are in Å). * **3** corresponds to **3.08**.

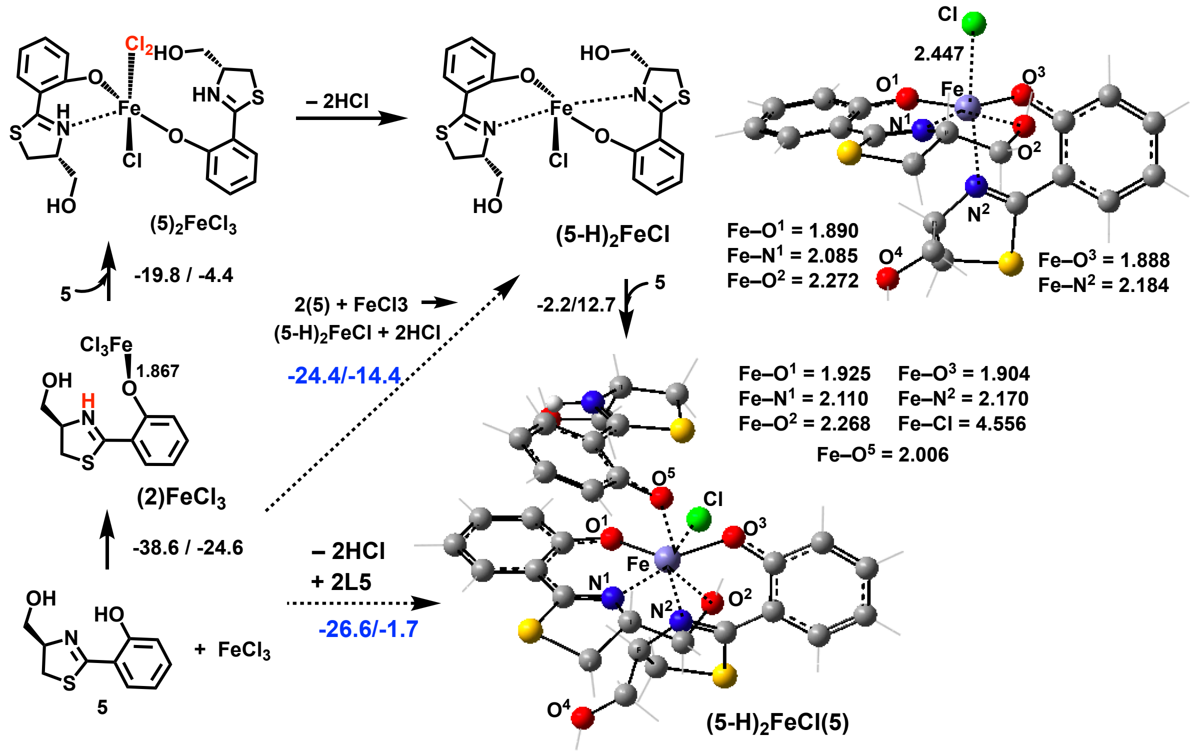

Cl2
HO
Fe
O
HN
S
H
N
S
O
Cl
HO
(5)2FeCl3
– 2HCl
HO
Fe
N
S
S
N
O
Cl
HO
(5-H)2FeCl
Cl
2.447
O1
Fe
O3
N1
O2
N2
O4
Fe–O1 = 1.890
Fe–N1 = 2.085
Fe–O2 = 2.272
Fe–O3 = 1.888
Fe–N2 = 2.184
5
-19.8 / -4.4
2(5) + FeCl3
(5-H)2FeCl + 2HCl
-24.4/-14.4
-2.2/12.7
5
Cl3Fe
1.867
O
OH
H
N
S
(2)FeCl3
-38.6 / -24.6
OH
HO
N
S
+ FeCl3
5
– 2HCl
+ 2L5
-26.6/-1.7
Fe–O1 = 1.925
Fe–N1 = 2.110
Fe–O2 = 2.268
Fe–O3 = 1.904
Fe–N2 = 2.170
Fe–Cl = 4.556
Fe–O5 = 2.006
O5
Cl
O1
O3
Fe
N1
N2
O2
O4
(5-H)2FeCl(5)

Figure S3.03. The pathways for formation of and calculated (**5**)FeCl$_3$, iso-1, (**5**)FeCl$_3$, iso-2, (**5**)$_2$FeCl$_3$, and (**5-H**)$_2$FeCl adducts (distances are in Å). ***5** corresponds to **3.07**.

Pseudomonas etc. Biology

Bacterial strains and culture conditions

P. aeruginosa (PAO1), methicillin-susceptible *Staphylococcus aureus* MSSA (SH1000), community-acquired methicillin-resistant *Staphylococcus aureus* CA-MRSA (USA300-0114), hospital-acquired methicillin-resistant *Staphylococcus aureus* HA-MRSA (ATCC 33591), and *Enterococcus faecalis* (OG1RF), *Escherichia coli* (MC4100) were acquired as a gift from Prof. Bettina Buttaro (Lewis Katz School of Medicine, Temple University). *P. putida* KT2440, and *P. fluorescens* WCS385 were acquired as gifts from Prof. George O'Toole (Geisel School of Medicine, Dartmouth College). *P. syringae* pathovar *actinidiae* BAA-2502 was acquired from ATCC. *P. aeruginosa* ΔPvdDΔPchEF (PAO1 ΔPvdDΔPchEF) was acquired as a gift from Prof. Stephen P Diggle (School of Biology, Georgia Institute of Technology). For the growth assay, both strains PAO1 and PAO1 ΔPvdDΔPchEF were grown from freezer stocks for 16 hours at 200 rpm in 5 mL of MOPS buffered media at 37 °C. For the IC_{50} assay, all bacterial strains were grown from freezer stocks for 16 hours at 200 rpm in 10 mL of media (Mueller-Hinton Broth for SH1000, OR1RF, MC4100, Todd Hewitt Broth for USA300-0114 and ATCC 33591, Trypticase Soy Broth for PAO1 and KT2440, Miller's LB Broth for WCS385, and Nutrient Broth Media) at 37 °C (SH1000, OR1RF, MC4100, USA300-0114, ATCC 33591, and PAO1) or 30 °C (KT2440, WCS385, and BAA-2502).

Growth Assay

Compounds were dissolved in 10% DMSO/90% H_2O to give 1 mM stock solutions, which were diluted to a concentration of 250 μM. Overnight cultures were diluted to 1:50 in 5 mL of fresh media and grown at 37 °C, 200 rpm to an OD_{600} reading of 0.25. Bacteria were then diluted in MOPS media or iron-depleted MOPS media to a concentration of 0.004 according to the following equations: (x μL regrow culture)*(OD_{600} reading) = (0.004)*(volume of diluted bacteria culture needed). Then 100 μL of this diluted bacteria culture was inoculated into each well of a flat-bottom 96-well plate (Corning 3370), giving a final test concentration of 125 μM. Plates were then incubated with some shaking at 37 °C until bacteria reached the stationary phase up to 20 hours and OD_{600} readings were taken every hour. Compounds were tested in triplicate from three separate overnight cultures and averaged.

IC_{50} Assay

Compounds were dissolved in 10% DMSO/90% H_2O to give 1 mM stock solutions, which were serially diluted yielding twelve starting test concentrations ranging from 500 μM to 2.5 μM. Controls were prepared by dissolving in 10% DMSO/90% H_2O to 1mM stock solutions and serially diluting in the same manner as for test compounds. The positive control used in all cases was gentamicin and the negative control was a solution of 10% DMSO/90% H_2O. Overnight cultures were diluted 1:100 in 5 mL of corresponding fresh media and grown at 200 rpm at 37 °C (SH1000, OR1RF, MC4100, USA300-0114, ATCC 33591, KT2440) or 30 °C (WCS385, and BAA-2502) to a predetermined OD_{600} value reflecting exponential growth. Bacteria were then diluted to a concentration of 0.004 according to the following equation: (x μL regrow culture)*(OD reading) = (0.004)*(volume of diluted bacteria culture needed). Then 100 μL was inoculated into each well of a flat-bottom 96-well plate (Corning 3370) already containing 100 μL of compound solution, giving final test concentrations of 250 μM to 1.25 μM. Plates were then incubated statically at 37 °C (SH1000, OR1RF, MC4100, USA300-0114, ATCC 33591, KT2440) or 30 °C (WCS385, and BAA-2502) for 24 hours. OD_{600} readings were taken at this point, and IC_{50} values were calculated by fitting OD readings vs. concentrations with a four-parameter logistic model. Compounds were tested in triplicate from three separate overnight cultures and averaged.

Acinetobacter Biology

Bacterial Strains and Culture Conditions

Acinetobacter baumannii wild type (ATCC 17978) and complete siderophore biosynthetic mutant (Δ*basGbfnLfbsE*; production of all three native siderophores, acinetobactin, baumannoferrin, and fimsbactins disrupted) were acquired as generous gifts from Prof. Eric Skaar (Vanderbilt University Medical Center).[19] Strains were grown from freezer stocks for 16 hours at 200 rpm in 5 mL of Tris-minimal succinate (TMS) media (recipe on next page)[20] or MH broth at 37 °C.

Growth Assay

Compounds were dissolved in 10% DMSO/90% H_2O to give 1 mM stock solutions, which were serially diluted yielding twelve starting test concentrations ranging from 500 μM to 2.5 μM. Controls were prepared in the same manner as for test compounds; the positive control was $FeCl_3$, and the negative control was a solution of 10% DMSO/90% H_2O. Overnight cultures were diluted to 1:100 in 5 mL of fresh media and grown at 37 °C, 200 rpm to an OD_{600} reading of 0.60. Bacteria were then diluted to a concentration of 0.004 according to the following equations: (xx μL regrow culture)*(OD_{600} reading) = (0.004)*(volume of diluted bacteria culture needed) in either TMS media supplemented with 32 μM ethylenediaminetetraacetic acid (EDTA) for iron-depleted conditions or in MH broth for normal growth conditions. Then 100 μL of this diluted bacteria culture was inoculated into each well of a flat-bottom 96-well plate (Corning 3370), giving final test concentrations of 125 μM to 1.25 μM. Plates were then incubated with shaking at 37 °C until bacteria reached the stationary phase up to 12 hours with OD_{600} readings being taken every 15 minutes. Compounds were tested in triplicate from three separate overnight cultures and averaged.

TMS Media Recipe (per 1 L):

25X Tris minimal salts stock (per 1 L):

- 145 g NaCl
- 92.5 g KCl
- 27.5 g NH_4Cl
- 3.55 g Na_2SO_4
- 6.8 g KH_2PO_4

20 ml of 25X Tris minimal salts stock, 12.1 g of Tris base, 16.6 g of succinate, and 50 mL of a 20% casamino acids solution was added to 800 ml of deionized water. The pH was adjusted to 7.4 with a 1M solution of HCl, and the resulting solution was autoclaved. Next 2 ml of tryptophan (10 mg/ml) and 1 ml volumes of cysteine (22 mg/ml), thiamine (16.9 mg/ml), nicotinic acid (1.23 mg/ml), pantothenic acid (0.5 mg/ml), biotin (0.01 mg/ml) $MgCl_2$ (95.3 mg/ml), and $CaCl_2$ (11.1 mg/ml) were added to the solution. For media for overnight and regrow cultures, $FeCl_3$ was also added at this time to a concentration of 50 μM. The volume was then adjusted to 1 liter with sterilized deionized water.

Supplementary Figures

The growth media was supplemented with a non-toxic amount of EDTA (32 μM) in order to prevent sequestration of any trace iron by either the native siderophores in the wild type or by compound **1** itself. Additionally, the 1:1 ligand-Fe^{III} complex of **1** was titrated with EDTA to resemble the EDTA-to-compound **1** ratios at 2, 4, 8, 16, 32, and 64 μM (Fig. S2). The bleaching effect of EDTA on the dark purple ligand-Fe^{III} complex indicates that the growth enhancement observed is likely not due to chelation of compound **1** with trace iron.

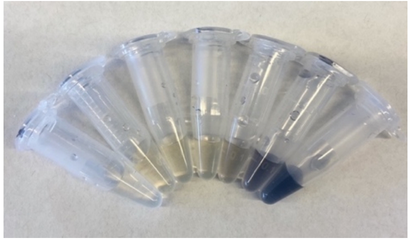

Figure S2. Titration of EDTA with **1**. To a 1 mM solution of **1** in 10% DMSO/90% H_2O was added a 20 mM solution of EDTA in 10% DMSO/90% H_2O giving EDTA:**1** ratios of 0:1, 0.5:1, 1:1, 2:1, 4:1, 8:1, and 16:1 (right to left). The bleaching of the purple solution containing **1** (far right) upon addition of EDTA appears to be concentration dependent.

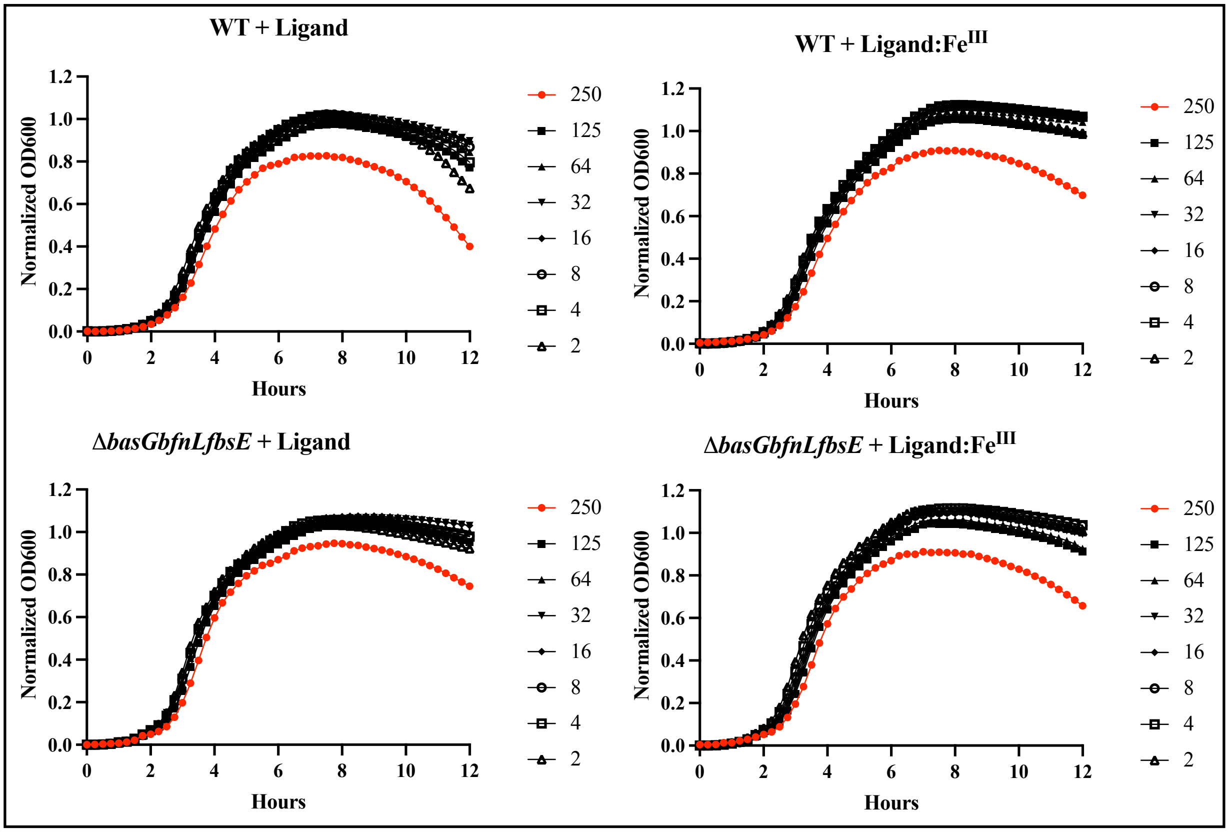

Figure S3. Growth curves of *A. baumannii* wild type strain in MH media in the presence of free ligand (top left) and ligand:Fe^{III} complex (top right) and triple mutant strain Δ*basGbfnLfbsE* (incapable of producing native siderophores) also grown in MH media in the presence of free ligand (bottom left), ligand:Fe^{III} complex (bottom right).

References

1 Noël, S.; Guillon, L.; Schalk, I. J.; Mislin, G. L. A. T. *Org. Lett.* **2011**, *13*, 844-847.

2 Zamri, A.; Abdallah, A. *Tetrahedron.* **2000**, *56*, 249-256.

3 Yamada, Y.; Seki, N.; Kitahara, T.; Matsui, M. *Agr. Biol. Chem.* **1970**, *34*, 780-783.

4 Shingare, R. D.; Aniebok, V.; Lee, H-W.; MacMillan, J. B. *Org. Lett.* **2020**, *22*, 1516-1519.

5 Morrison, M. D.; Hanthorn, J. J.; Pratt, D. A. *Org. Lett.* **2009**, *11*, 1051-1054.

6 Li, L. B.; Dan, W. J.; Tan, F. F.; Cui, L. H.; Yuan, Z. P.; Wu, W. J.; Zhang, J. W. *Chem. Pharm. Bull.* **2015**, *63*, 33-37.

7 Phillips, A. J.; Uto, Y.; Wipf, P.; Reno, M. J.; Williams, D. R. *Org. Lett.* **2000**, *2*, 1165-1168.

8 Moraski, G. C.; Chang, M.; Villegas-Estrada, A.; Franzblau, S. G.; Möllmann, U.; Miller, M. J. *Eur. J. Med. Chem.* **2010**, *45*, 1703-1716.

9 Takeuchi, Y.; Ozaki, S.; Satoh, M.; Mimura, K.; Hara, S.; Abe, H.; Nishioka, H.; Harayama, T. *Chem. Pharm. Bull.* **2010**, *58*, 1552-1553.

10 Shapiro, J. A.; Wencewicz, T. A. *ACS. Infect. Dis.* **2016**, *2*, 157-168.

11 Frisch, M. J. T., G. W.; Schlegel, H. B.; Scuseria, G. E.; Robb, M. A.; Cheeseman, J. R.; Scalmani, G.; Barone, V.; Mennucci, B.; Petersson, G. A.; Nakatsuji, H.; Caricato, M.; Li, X.; Hratchian, H. P.; Izmaylov, A. F.; Bloino, J.; Zheng, G.; Sonnenberg, J. L.; Hada, M.; Ehara, M.; Toyota, K.; Fukuda, R.; Hasegawa, J.; Ishida, M.; Nakajima, T.; Honda, Y.; Kitao, O.; Nakai, H.; Vreven, T.; Montgomery, J. A., Jr.; Peralta, J. E.; Ogliaro, F.; Bearpark, M.; Heyd, J. J.; Brothers, E.; Kudin, K. N.; Staroverov, V. N.; Kobayashi, R.; Normand, J.; Raghavachari, K.; Rendell, A.; Burant, J. C.; Iyengar, S. S.; Tomasi, J.; Cossi, M.; Rega, N.; Millam, M. J.; Klene, M.; Knox, J. E.; *et al.*; *Gaussian 09, Revision D.01*, Gaussian, Inc., Wallingford CT, **2009**.

12 Becke, A. D. *Phys. Rev. A.* **1988,** *38*, 3098-3100.

13 Lee, C.; Yang, W.; Parr, R. G. *Phys. Rev. B.* **1988,** *37*, 785-789.

14 Becke, A. D. *J. Chem. Phys.* **1993,** *98*, 1372-1377.

15 Grimme, S.; Antony, J.; Ehrlich, S.; Krieg, H. *J. Chem. Phys*. **2010**, *132*, 154104.

16 Grimme, S.; Hansen, A.; Brandenburg, J. G.; Bannwarth, C.*Chem. Rev.* **2016**, *116*, 5105-5154.

17 Becke, A. D.; Johnson, E. R. *J. Chem. Phys.* **2005**, *122*, 154104.

18 Cancès, E.; Mennucci, B.; Tomasi, J. *J. Chem. Phys.* **1997,** *107*, 3032-3041.

19 Sheldon, J. R.; Skaar, E. P. *PLoS. Pathog.* **2020**, *16*, e1008995.

20 Sebulsky, M. T.; Speziali, C. D.; Shilton, B. H.; Edgell, D. R.; Heinrichs, D. E. *J. Biol. Chem.* **2004**, *279*, 53152-53159.

Synthesis and Biological Investigation of Quaternary Ammonium Compounds

Synthesis

General Information

All reactions were conducted in flame-dried glassware equipped with a stir bar under an argon atmosphere. HPLC-grade tetrahydrofuran (THF) was dried by passing through activated alumina. Reagents were purchased from Oakwood, Fischer Scientific, TCI Chemicals, Sigma-Aldrich, Millipore Sigma, and Combi Blocks. Triethylamine was freshly distilled from CaH_2 prior to use. Thin-layer chromatography was performed on 250μm SiliCycle silica gel F-254 plates and visualized by fluorescence and/or staining using potassium permanganate, or vanillin stains. Brine refers to saturated aqueous solution of sodium chloride, sat. $NaHCO_3$ refers to a saturated aqueous solution of sodium bicarbonate and sat. NH_4Cl refers to saturated aqueous solution of ammonium chloride. Organic solutions were concentrated under reduced pressure on a Buchi Rotavapor R3 rotary evaporator. Chromatographic purification was accomplished using a Biotage® flash chromatography purification system or C18 silica.

^{1}H NMR and ^{13}C NMR spectra were recorded on a Bruker (600 MHz), Inova (600 MHz), Inova (500 MHz), Bruker (400 MHz), Inova (400 MHz), or VNMR (400 MHz) spectrometer, all from the Emory University NMR facility. ^{1}H NMR data were reported in terms of chemical shift (δ ppm relative to tetramethylsilane and with the indicated deuterated solvent as the internal reference), multiplicity, described using the following abbreviations: s (singlet), d (doublet), t (triplet), q (quartet), m (multiplet), br (broad), dd (doublet of doublets), dt (doublet of triplets), etc, coupling constant (Hz), and integration. ^{13}C NMR data were reported in terms of chemical shift. Accurate mass spectra were obtained from a Thermo LTQ-FTMS using APCI techniques.

Experimental Procedures and Spectral Data

General Procedure A: Grignard Addition. Procedure based on previously described.[1] To a 1.3 M solution of Mg^0 (1.0 equiv) in THF was added a catalytic amount of iodine, giving an orange solution. **5-bromopentene** (0.5 equiv) was then added dropwise. The resulting clear solution was then heated to 50 °C, stirred 4 hours. This Grignard solution was then cooled to room temperature before use. To a separate flask cooled to 0 °C was added dibromoalkane (1.0 equiv), followed by a 0.1 M solution of dilithiumtetrachlorocuprate in THF (0.0125 equiv), then THF, and lastly N-methylpyrrolidinone (2.0 equiv). The Grignard solution was then added dropwise, and the resulting solution was warmed to room temperature and stirred for 16 hours. The reaction was then quenched with sat. NH_4Cl, extracted with Et_2O (3x), washed with brine (1x), dried over $MgSO_4$, concentrated under reduced pressure, and purified by column chromatography (100% hexanes).

General Procedure B: Hydroarylation. Procedure based on previously described.[2] An oven-dried 30 mL screw-top test tube was charged with corresponding **3-iodopyridine** (1.0 equiv), Hantzsch ester (1.3 equiv), solid NH_4Cl (2.0 equiv), photoredox catalyst $Ir[ppy]_2dtbbpy{\bullet}PF_6$ (1.0 mol %) and alkenes (if solid, 5.0 equiv). The atmosphere was exchanged three times by applying vacuum then backfilling with argon. Alkene (if liquid, 5.0 equiv) was added in a solution of degassed 2,2,2-trifluoroethanol if prepared or directly followed by degassed 2,2,2-trifluoroethanol if purchased commercially to give a 0.1 M reaction solution relative to the corresponding starting 3-iodopyridine. The resulting solution was stirred for 16 hours under irradiation with a blue LED (Hydrofarm PowerPAR 15-watt LED Bulb-Blue). The reaction was then quenched with sat. $NaHCO_3$, extracted with EtOAc (3x), washed with brine (1x), dried over Na_2SO_4, concentrated under reduced pressure, and purified by flash column chromatography (0 – 20% EtOAc/hexanes).

General Procedure C: Cyclization. Procedure based on previously described.[3] A solution of alkylpyridine (1.0 equiv) and NaI (1.2 equiv) in a 1:1 mixture of butanone/methanol (0.5 M) and stirred at 80 °C for 16 hours. The resulting solution was then concentrated under reduced pressure and purified using reverse phase flash column chromatography (40% MeCN/H_2O).

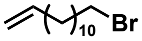

13-Bromo-1-tridecene 4.01. Following **general procedure A**, **1,8-dibromooctane** (1.84 mL, 10.0 mmol) yielded the title compound as a clear oil (2.25 g, 87%).

^{1}H NMR (600 MHz, CDCl$_3$) δ 5.81 (ddt, *J* = 16.9, 10.2, 6.6 Hz, 1H), 4.99 (dq, *J* = 17.1, 1.7 Hz, 1H), 4.93 (ddt, *J* = 10.2, 2.4, 1.3 Hz, 1H), 3.41 (t, *J* = 6.9 Hz, 2H), 2.04 (q, *J* = 7.2 Hz, 2H), 1.85 (dt, *J* = 14.4, 7.2 Hz, 2H), 1.40 (m, 4H), 1.33 – 1.24 (m, 14H). **^{13}C NMR** (151 MHz, CDCl$_3$) δ 139.40, 114.25, 34.20, 33.96, 33.00, 29.69, 29.66, 29.62, 29.58, 29.28, 29.09, 29.91, 28.33. **HRMS** Accurate mass (APCI$^+$): Found 257.08921, $C_{13}H_{22}Br$ (M+H-2H$_2^+$) requires 257.08994.

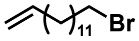

14-Bromo-1-tetradecene 4.02. Following **general procedure A**, **1,9-dibromononane** (2.03 mL, 10.0 mmol) yielded the title compound as a clear oil (2.61 g, 95%).

^{1}H NMR (600 MHz, CDCl$_3$) δ 5.81 (ddt, *J* = 17.0, 10.3, 6.7 Hz, 1H), 4.99 (dq, *J* = 17.1, 1.7 Hz), 4.93 (ddt, *J* = 10.2, 2.5, 1.5 Hz), 3.41 (t, *J* = 6.9 Hz, 2H), 2.04 (q, *J* = 6.7 Hz, 2H), 1.85 (dt, *J* = 14.6, 7.0 Hz, 2H), 1.40 (m, 4H), 1.33 – 1.24 (m, 14H). **^{13}C NMR** (151 MHz, CDCl$_3$) δ 139.42, 114.24, 34.20, 33.97, 33.00, 29.74, 29.73, 29.68, 29.64, 29.58, 29.30, 29.10, 28.92, 28.33. **HRMS** Accurate mass (APCI$^+$): Found 271.10488, $C_{14}H_{24}Br$ (M+H-2H$_2^+$) requires 271.1056.

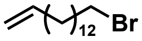

15-Bromo-1-pentadecene 4.03. Following **general procedure A**, 1**,10-dibromodecane** (2.25 mL 10.0 mmol) yielded the title compound as a clear oil (1.84 g, 64%).

^{1}H NMR (600 MHz, CDCl$_3$) δ 5.81 (ddt, *J* = 16.9, 10.2, 6.6 Hz, 1H), 4.99 (dq, *J* = 17.1, 1.7 Hz, 1H), 4.93 (ddt, *J* = 10.2, 2.6, 1.5 Hz, 1H), 3.41 (t, *J* = 6.9 Hz, 2H), 2.04 (q, *J* = 6.7 Hz, 2H), 1.85 (dt, *J* = 14.6, 7.0 Hz, 2H), 1.85 (dt, *J* = 14.5, 7.0 Hz, 2H), 1.40 (m, 4H), 1.32 – 1.24 (m, 16H). **^{13}C NMR** (151 MHz, CDCl$_3$) δ 139.42, 114.23, 34.20, 33.97, 33.00, 29.77, 29.75, 29.68, 29.65, 29.59, 29.30, 29.10, 28.92, 28.33. **HRMS** Accurate mass (APCI$^+$): Found 285.12054, $C_{15}H_{26}Br$ (M+H-2H$_2^+$) requires 285.12124.

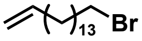

16-Bromo-1-hexadecene 4.04. Following **general procedure A**, **1,11-dibromoundecane** (1.70 mL, 7.23 mmol) yielded the title compound as a clear oil (1.74 g, 57%).

^{1}H NMR (400 MHz, CDCl3) δ 5.81 (ddt, *J* = 16.9, 10.1, 6.7 Hz, 1H), 4.99 (dq, *J* = 17.2, 1.8 Hz, 1H), 4.93 (ddt, *J* = 10.2, 2.6, 1.4 Hz, 1H), 3.41 (t, *J* = 6.9 Hz, 2H), 2.04 (q, *J* = 6.7 Hz, 2H), 1.85 (dt, *J* = 14.6, 7.0 Hz, 2H), 1.40 (m, 4H), 1.33 – 1.23 (m, 18H). **^{13}C NMR** (151 MHz, CDCl$_3$) δ 139.42, 114.22, 34.19, 33.97, 33.00, 29.79, 29.76, 29.69, 29.66, 29.59, 29.31, 29.10, 28.33. **HRMS** Accurate mass (APCI$^+$): Found 303.1686, $C_{16}H_{32}Br$ (M+H$^+$) requires 303.16819.

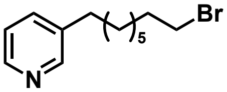

3-(8-bromooctyl)pyridine 4.05. Following **general procedure B**, **8-bromooctene** (950 mg, 5.00 mmol) yielded the title compound as a yellow oil (80 mg, 30%).

^{1}H NMR (600 MHz, CDCl$_3$) δ 8.43 (m, 2H), 7.49 (dt, *J* = 7.6, 2.0 Hz, 1H), 7.20 (dd, *J* = 7.8, 4.8 Hz, 1H), 3.40 (t, *J* = 6.9 Hz, 2H), 2.60 (t, *J* = 7.8 Hz, 2H), 1.84 (p, *J* = 7.0 Hz, 2H), 1.62 (m, 2H), 1.41 (m, 2H), 1.36 – 1.27 (m, 10H). **^{13}C NMR** (151 MHz, CDCl$_3$) δ 150.04, 147.29, 138.04, 135.97, 123.41, 34.12, 33.13, 32.91, 31.21, 29.34, 29.15, 28.79, 28.25. **HRMS** Accurate mass (APCI$^+$): Found 270.08447, $C_{13}H_{21}N^{79}Br$ (M+H) requires 270.08519.

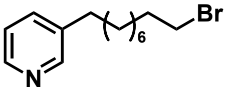

3-(9-bromononyl)pyridine 4.06. Following **general procedure B**, **9-bromononene** (1.02 g, 5.00 mmol) yielded the title compound as a yellow oil (102 mg, 36%).

^{1}H NMR (600 MHz, CDCl$_3$) δ 8.42 (m, 2H), 7.48 (dt, *J* = 7.8, 2.0 Hz, 1H), 7.20 (dd, *J* = 7.7, 4.8 Hz, 1H), 3.40 (t, *J* = 6.9 Hz, 2H), 2.60 (t, *J* = 7.7 Hz, 2H), 1.84 (p, *J* = 7.2 Hz, 2H), 1.61 (p, *J* = 7.5 Hz, 2H), 1.42 (m, 2H), 1.37 – 1.17 (m, 14H). **^{13}C NMR** (151 MHz, CDCl$_3$) δ 150.05, 147.28, 138.07, 135.95, 123.39, 34.16, 33.14, 32.93, 31.23, 29.44, 29.41, 28.84, 28.26. **HRMS** Accurate mass (APCI$^+$): Found 284.10005, $C_{14}H_{23}N^{79}Br$ (M+H) requires 284.10084.

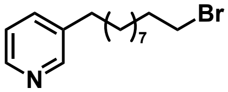

3-(10-bromodecyl)pyridine 4.07. Following **general procedure B**, **10-bromodecene** (1.09 g, 5.00 mmol) yielded the title compound as a yellow oil (99 mg, 33%).

^{1}H NMR (600 MHz, $CDCl_3$) δ 8.42 (m, 2H), 7.48 (dt, *J* = 7.8, 2.0 Hz, 1H), 7.19 (ddd, *J* = 7.7, 4.8, 1.0 Hz, 1H), 3.40 (t, *J* = 6.9 Hz, 2H), 2.59 (t, *J* = 7.7 Hz, 2H), 1.84 (p, *J* = 7.2 Hz, 2H), 1.61 (p, *J* = 7.5 Hz, 2H), 1.41 (m, 2H), 1.36 – 1.19 (m, 14H). **^{13}C NMR** (151 MHz, $CDCl_3$) δ 150.08, 147.29, 138.08, 135.92, 123.37, 34.17, 33.14, 32.95, 31.24, 29.53, 29.51, 29.47, 29.24, 28.86, 28.28. **HRMS** Accurate mass (APCI$^+$): Found 298.11575, $C_{15}H_{25}N^{79}Br$ (M+H) requires 298.11649.

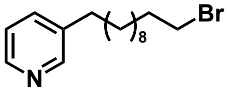

3-(11-bromoundecyl)pyridine 4.08. Following **general procedure B**, **11-bromoundecene** (1.10 mL, 5.00 mmol) yielded the title compound as a yellow oil (114 mg, 38%).

^{1}H NMR (600 MHz, $CDCl_3$) δ 8.42 (m, 2H), 7.48 (dt, *J* = 7.8, 2.1 Hz, 1H), 7.19 (ddd, *J* = 7.8, 4.8, 1.0 Hz, 1H), 3.40 (t, *J* = 6.9 Hz, 2H), 2.59 (t, *J* = 7.8 Hz, 2H), 1.85 (p, *J* = 7.4 Hz, 2H), 1.62 (p, *J* = 7.5 Hz, 2H), 1.42 (m, 2H), 1.35 – 1.20 (m, 16H). **^{13}C NMR** (151 MHz, $CDCl_3$) δ 150.08, 147.28, 138.09, 135.91, 132.35, 34.18, 33.14, 32.95, 31.25, 29.60, 29.52, 29.50, 29.47, 29.25, 28.86, 28.28. **HRMS** Accurate mass (APCI$^+$): Found 312.13132, $C_{16}H_{27}N^{79}Br$ (M+H) requires 312.13214.

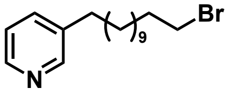

3-(12-bromododecyl)pyridine 4.09. Following **general procedure B**, **12-bromododecene** (1.23 g, 5.00 mmol) yielded the title compound as a yellow oil (87 mg, 27%).

^{1}H NMR (600 MHz, $CDCl_3$) δ 8.43 (m, 2H), 7.48 (dt, *J* = 7.8, 2.0 Hz, 1H), 7.20 (ddd, *J* = 7.8, 4.8, 0.9 Hz, 1H), 3.40 (t, *J* = 6.9 Hz, 2H), 2.60 (t, *J* = 7.7 Hz, 2H), 1.85 (p, *J* = 7.0 Hz, 2H), 1.62 (p, *J* = 7.4 Hz, 2H), 1.42 (p, *J* = 7.3 Hz, 2H), 1.35 – 1.23 (m, 17H). **^{13}C NMR** (151 MHz, $CDCl_3$) δ 150.10, 147.30, 138.13, 135.93, 123.37, 33.17, 32.98, 31.28, 29.69, 29.65, 29.64, 29.56, 29.54, 29.29, 28.90, 28.32, 24.52. **HRMS** Accurate mass (APCI$^+$): Found 326.14688, $C_{17}H_{29}N^{79}Br$ (M+H) requires 326.14779.

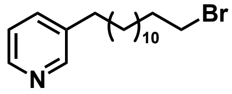

3-(13-bromotridecyl)pyridine 4.10. Following **general procedure B**, **4.01** (1.31 g, 5.00 mmol) yielded the title compound as a yellow oil (65 mg, 19%).

^{1}H NMR (600 MHz, CDCl$_3$) δ 8.43 (m, 2H), 7.49 (d, *J* = 7.8 Hz, 1H), 7.20 (dd, *J* = 7.8, 4.7 Hz, 1H), 3.41 (t, *J* = 6.9 Hz, 2H), 2.60 (t, *J* = 7.7 Hz, 2H), 1.85 (p, *J* = 6.9 Hz, 2H), 1.61 (p, *J* = 7.4 Hz, 2H), 1.42 (p, *J* = 7.4 Hz, 2H), 1.35 – 1.23 (m, 16H). **^{13}C NMR** (151 MHz, CDCl$_3$) δ 150.06, 147.25, 138.16, 135.99, 123.39, 34.21, 33.17, 32.99, 31.29, 29.74, 29.72, 29.67, 29.66, 29.57, 29.55, 29.30, 28.91, 28.32. **HRMS** Accurate mass (APCl$^+$): Found 340.16338, $C_{18}H_{31}NBr$ (M+H) requires 340.16344.

*Synthesized by Cassie L. Schrank

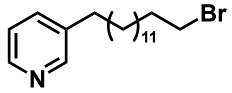

3-(14-bromotetradecyl)pyridine 4.11. Following **general procedure B**, **4.02** (1.38 g, 5.00 mmol) yielded the title compound as a yellow oil (48 mg, 14%).

^{1}H NMR (600 MHz, CDCl$_3$) δ 8.43 (m, 2H), 7.49 (d, *J* = 7.8 Hz, 1H), 7.20 (dd, *J* = 7.7, 4.8 Hz, 1H), 3.40 (t, *J* = 6.9 Hz, 2H), 2.60 (t, *J* = 7.7 Hz, 2H), 1.85 (p, *J* = 7.0 Hz, 2H), 1.61 (m, 10H), 1.42 (p, *J* = 7.3 Hz, 2H), 1.34 – 1.21 (m, 18H). **^{13}C NMR** (151 MHz, CDCl$_3$) δ 149.98, 147.18, 138.21, 136.05 123.41, 34.22, 33.17, 32.99, 31.28, 29.76, 29.73, 29.67, 29.58, 29.55, 29.30, 28.91, 28.32. **HRMS** Accurate mass (APCl$^+$): Found 354.17871, $C_{19}H_{33}NBr$ (M+H) requires 354.17909.

*Synthesized by Cassie L. Schrank

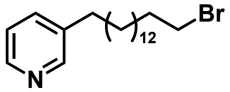

3-(15-bromopentadecyl)pyridine 4.12. Following **general procedure B**, **4.03** (1.45 g, 5.00 mmol) yielded the title compound as a yellow oil (22 mg, 6%).

^{1}H NMR (600 MHz, CDCl$_3$) δ 8.44 (m, 2H), 7.50 (d, *J* = 7.8 Hz, 1H), 7.21 (dd, *J* = 7.8, 4.8 Hz, 1H), 3.41 (t, *J* = 6.9 Hz, 2H), 2.60 (t, *J* = 7.7 Hz, 2H), 1.85 (p, *J* = 7.0 Hz, 2H), 1.61 (p, *J* = 7.5 Hz, 2H), 1.42 (p, *J* = 7.2 Hz, 2H), 1.35 – 1.22 (m, 20H). **^{13}C NMR** (151 MHz, CDCl$_3$) δ 149.97, 147.16, 138.23, 136.08, 123.42, 34.22, 33.18, 32.99, 31.28, 29.78, 29.76, 29.69, 29.59, 29.56, 29.30, 28.92, 28.33. **HRMS** Accurate mass (APCl$^+$): Found 368.1947, $C_{20}H_{35}NBr$ (M+H) requires 368.19474.

*Synthesized by Cassie L. Schrank

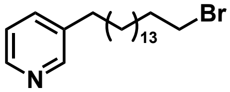

3-(16-bromoheadecyl)pyridine 4.13. Following **general procedure B**, **4.04** (1.52 g, 5.00 mmol) yielded the title compound as a yellow oil (38 mg, 10%).

^{1}H NMR (600 MHz, CDCl$_3$) δ 8.44 (m, 2H), 7.51 (d, *J* = 7.9 Hz, 1H), 7.22 (dd, *J* = 7.8, 4.7 Hz, 1H), 3.41 (t, *J* = 6.9 Hz, 2H), 2.61 (t, *J* = 7.7 Hz, 2H), 1.85 (p, *J* = 6.9 Hz, 2H), 1.62 (p, *J* = 7.4 Hz, 2H), 1.42 (p, *J* = 7.3 Hz, 2H), 1.36 – 1.21 (m, 22H). **^{13}C NMR** (151 MHz, CDCl$_3$) δ 149.77, 146.97, 138.34, 136.27, 123.48, 34.22, 33.17, 33.00, 31.27, 29.79, 29.78, 29.76, 29.69, 29.59, 29.56, 29.30, 28.33. **HRMS** Accurate mass (APCl$^+$): Found 382.21034, $C_{21}H_{37}NBr$ (M+H) requires 382.21039.

*Synthesized by Cassie L. Schrank

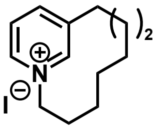

Cyclic pyridinium 4.14. Following **general procedure C**, **4.05** (68 mg, 0.25 mmol) yielded the title compound as a yellow solid (50 mg, 62%).

^{1}HNMR (600 MHz, CD_3OD) δ 9.10 (m, 1H), 8.92 (m, 1H), 8.50 (m, 1H), 8.03 (m, 1H), 4.68 (t, *J* = 7.6 H, 2H), 2.91 (t, *J* = 7.8 Hz, 2H), 2.06 (m 2H), 1.76 (t, *J* = 7.7 Hz, 2H), 1.45-1.21 (m, 12H). **^{13}C NMR** (151 MHz, CD_3OD) δ 146.73, 145.65, 145.33, 143.36, 128.97, 125.15, 62.81, 33.46, 32.54, 31.44, 29.97, 29.86, 29.79, 27.03. **HRMS** Accurate mass (APCI$^+$): Found 318.0704, $C_{13}H_{21}N^{127}I$ (M+H) requires 318.07132.

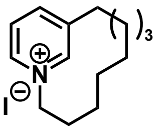

Cyclic pyridinium 4.15. Following **general procedure C**, **4.06** (84 mg, 0.30 mmol) yielded the title compound as a yellow solid (93 mg, 94%).

^{1}HNMR (600 MHz, CD_3OD) δ 9.12 (m, 1H), 8.94 (m, 1H), 8.51 (m, 1H), 8.04 (m, 1H), 4.69 (m, 2H), 2.91 (t, *J* = 8.0 Hz, 2H), 2.06 (m 2H), 1.75 (t, *J* = 7.1 Hz, 2H), 1.47-1.22 (m, 14H). **^{13}C NMR** (151 MHz, CD_3OD) δ 146.76, 145.65, 145.34, 143.34, 128.97, 62.81, 33.47, 32.55, 31.49, 30.19, 30.09, 29.94, 29.91, 27.04. **HRMS** Accurate mass (APCI$^+$): Found 332.08594, $C_{14}H_{23}N^{127}I$ (M+H) requires 332.08697.

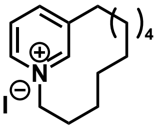

Cyclic pyridinium 4.16. Following **general procedure C**, **4.07** (83 mg, 0.28 mmol) yielded the title compound as a yellow solid (84 mg, 87%).

^{1}HNMR (600 MHz, CD_3OD) δ 9.11 (m, 1H), 8.93 (m, 1H), 8.51 (m, 1H), 8.04 (m, 1H), 4.68 (m, 2H), 2.91 (t, *J* = 7.2 Hz, 2H), 2.06 (m 2H), 1.75 (t, *J* = 7.2 Hz, 2H), 1.46-1.22 (m, 16H). **^{13}C NMR** (151 MHz, CD_3OD) δ 146.73, 145.64, 145.31, 143.33, 128.97, 62.80, 33.47, 32.56, 31.53, 30.41, 30.33, 30.23, 30.01, 29.97, 27.07. **HRMS** Accurate mass (APCI$^+$): Found 346.10164, $C_{15}H_{25}N^{127}I$ (M+H) requires 346.10262.

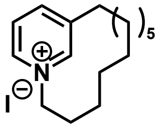

Cyclic pyridinium 4.17. Following **general procedure C**, **4.08** (102 mg, 0.33 mmol) yielded the title compound as a yellow solid (34 mg, 29%).

^{1}HNMR (600 MHz, CD_3OD) δ 9.10 (m, 1H), 8.93 (m, 1H), 8.50 (m, 1H), 8.04 (m, 1H), 4.69 (m, 2H), 2.91 (t, *J* = 7.7 Hz, 2H), 2.05 (m 2H), 1.75 (t, *J* = 6.6 Hz, 2H), 1.48-1.20 (m, 18H). **^{13}C NMR** (151 MHz, CD_3OD) δ 146.71, 145.63, 145.31, 143.33, 128.97, 62.82, 33.47, 32.56, 31.54, 30.52, 30.46, 30.39, 30.31, 30.04, 30.01, 27.09. **HRMS** Accurate mass (APCI$^+$): Found 360.11716, $C_{16}H_{27}N^{127}I$ (M+H) requires 360.11827.

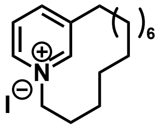

Cyclic pyridinium 4.18. Following **general procedure C**, **4.09** (32 mg, 0.10 mmol) yielded the title compound as a yellow solid (34 mg, 93%).

^{1}HNMR (600 MHz, CD_3OD) δ 9.08 (m, 1H), 8.91 (m, 1H), 8.49 (m, 1H), 8.04 (m, 1H), 4.67 (m, 2H), 2.91 (t, *J* = 8.0 Hz, 2H), 2.06 (m 2H), 1.75 (t, *J* = 7.1 Hz, 2H), 1.47-1.22 (m, 20H). **^{13}C NMR** (151 MHz, CD_3OD) δ 146.73, 145.32, 143.33, 141.98, 129.93, 62.67, 33.49, 32.55, 31.56, 30.59, 30.56, 30.51, 30.45, 30.35, 30.06, 27.11, 24.52. **HRMS** Accurate mass (APCI$^+$): Found 374.13289, $C_{17}H_{29}N^{127}I$ (M+H) requires 374.13392.

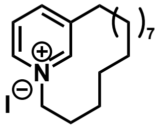

Cyclic pyridinium 4.19. Following **general procedure C**, **4.10** (57 mg, 0.17 mmol) yielded the title compound as a yellow solid (45 mg, 70%).

^{1}H NMR (600 MHz, CD_3OD) δ 9.10 (m, 1H), 8.93 (m, 1H), 8.50 (m, 1H), 8.04 (m, 1H), 4.68 (m, 2H), 2.91 (t, *J* = 7.2 Hz, 2H), 2.04 (m, 2H), 1.75 (t, *J* = 7.2 Hz, 2H), 1.42 – 1.21 (m, 18H). **^{13}C NMR** (151 MHz, CD_3OD) δ 146.71, 145.61, 145.28, 143.32, 128.98, 62.80, 34.81, 33.46, 32.53, 31.53, 30.61, 30.56, 30.51, 30.43, 30.35, 30.09, 27.07. **HRMS** Accurate mass (APCI$^+$): Found 388.14961, $C_{18}H_{31}NI$ (M+H) requires 388.14957.

*Synthesized by Cassie L. Schrank

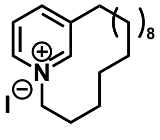

Cyclic pyridinium 4.20. Following **general procedure C**, **4.11** (44 mg, 0.12 mmol) yielded the title compound as a yellow solid (38 mg, 78%).

^{1}H NMR (600 MHz, CD_3OD) δ 9.05 (m, 1H), 8.91 (m, 1H), 8.49 (m, 1H), 8.04 (m, 1H), 4.68 (m, 2H), 2.91 (t, *J* = 8.0 Hz, 2H), 2.04 (m, 2H), 1.75 (t, *J* = 7.4 Hz, 2H), 1.45 – 1.20 (m, 20H). **^{13}C NMR** (151 MHz, CD_3OD) δ 146.71, 145.65, 145.29, 143.33, 129.00, 62.85, 34.84, 33.48, 32.53, 31.55, 30.67, 30.59, 30.56, 30.46, 30.38, 30.32, 30.12, 30.05, 27.10. **HRMS** Accurate mass (APCI$^+$): Found 402.16553, $C_{19}H_{33}NI$ (M+H) requires 402.16522.

*Synthesized by Cassie L. Schrank

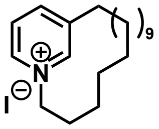

Cyclic pyridinium 4.21. Following **general procedure C**, **4.12** (19 mg, 0.05 mmol) yielded the title compound as a yellow solid (15 mg, 72%).

^{1}**H NMR** (600 MHz, CD_3OD) δ 9.05 (m, 1H), 8.89 (m, 1H), 8.48 (m, 1H), 8.03 (m, 1H), 4.66 (m, 2H), 2.91 (t, *J* = 8.0 Hz, 2H), 2.04 (m, 2H), 1.75 (t, *J* = 6.6 Hz, 2H), 1.41 – 1.25 (m, 22H). ^{13}**C NMR** (151 MHz, CD_3OD) δ 146.70, 145.68 145.30, 143.33, 128.99, 62.88, 34.85, 33.50, 32.52, 31.55, 30.72, 30.69, 30.61, 30.58, 30.48, 30.39, 30.33, 30.13, 30.06, 27.11. **HRMS** Accurate mass ($APCI^+$): Found 416.18112, $C_{20}H_{35}NI$ (M+H) requires 416.18087.

*Synthesized by Cassie L. Schrank

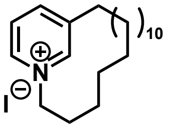

Cyclic pyridinium 4.22. Following **general procedure C**, **4.13** (26 mg, 0.07 mmol) yielded the title compound as a yellow solid (21 mg, 70%).

^{1}**H NMR** (600 MHz, CD_3OD) δ 9.01 (m, 1H), 8.88 (m, 1H), 8.47 (m, 1H), 8.03 (m, 1H), 4.65 (m, 2H), 2.90 (t, *J* = 8.2 Hz, 2H), 2.04 (m, 2H), 1.75 (t, *J* = 7.4 Hz, 2H), 1.40 – 1.25 (m, 24H). ^{13}**C NMR** (151 MHz, CD_3OD) δ 146.71, 145.71, 145.29, 143.34, 129.00, 62.91, 34.86, 33.51, 32.53, 31.57, 30.77, 30.73, 30.64, 30.61, 30.51, 30.47, 30.43, 30.35, 30.14, 30.08, 27.14. **HRMS** Accurate mass ($APCI^+$): Found 430.197, $C_{21}H_{37}NI$ (M+H) requires 430.19652.8.4.

*Synthesized by Cassie L. Schrank

Appendix: ^{1}H NMR and ^{13}C NMR Spectra

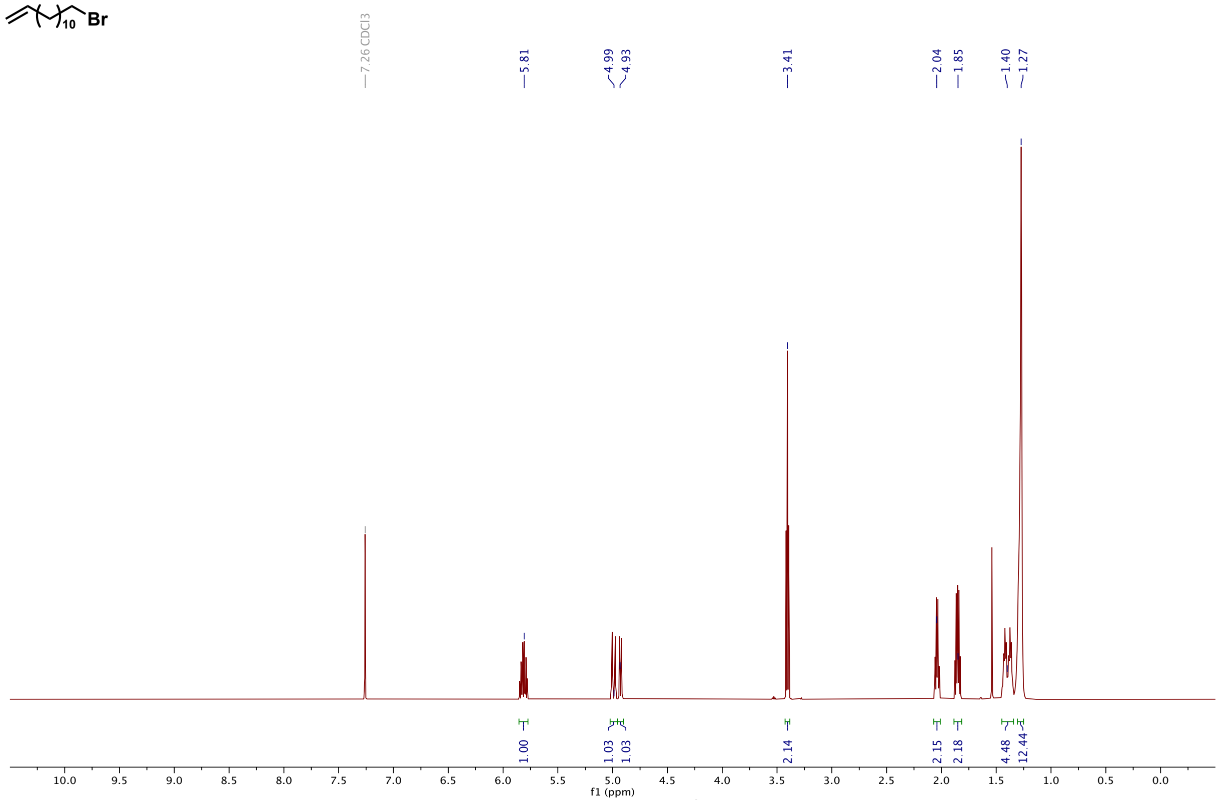

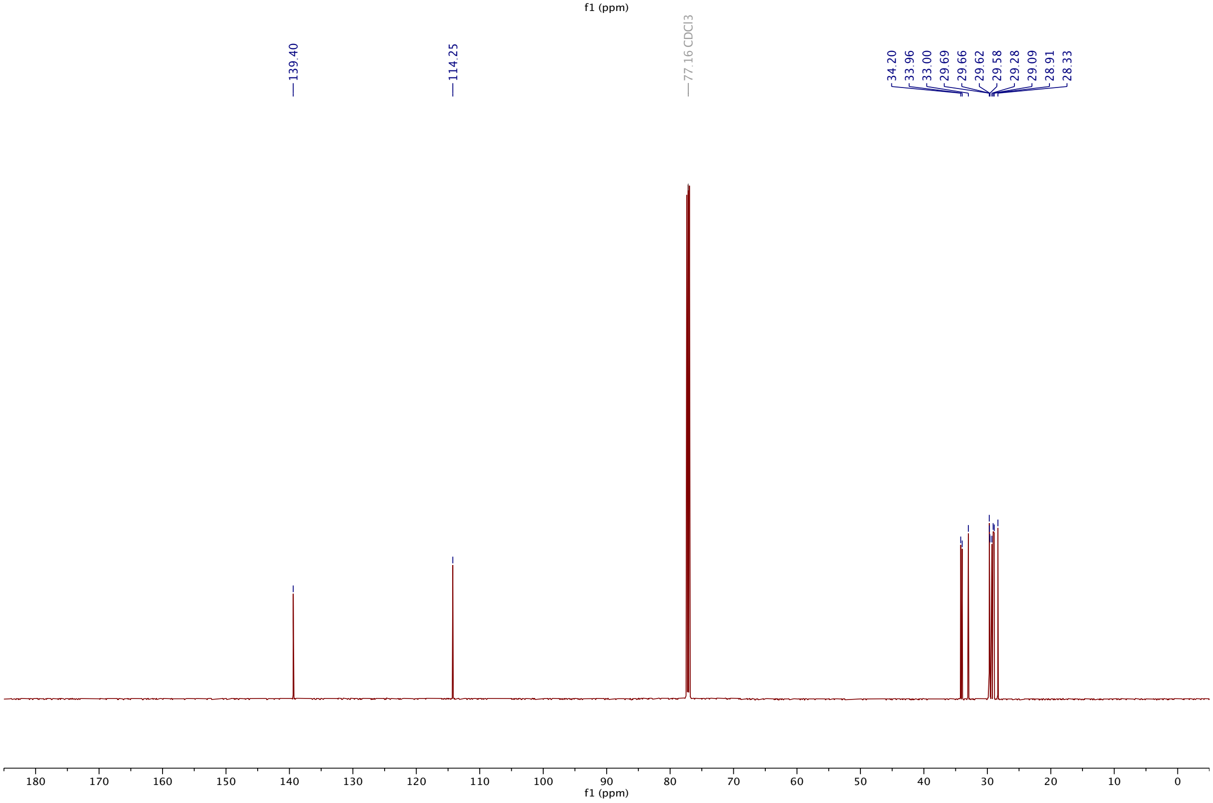

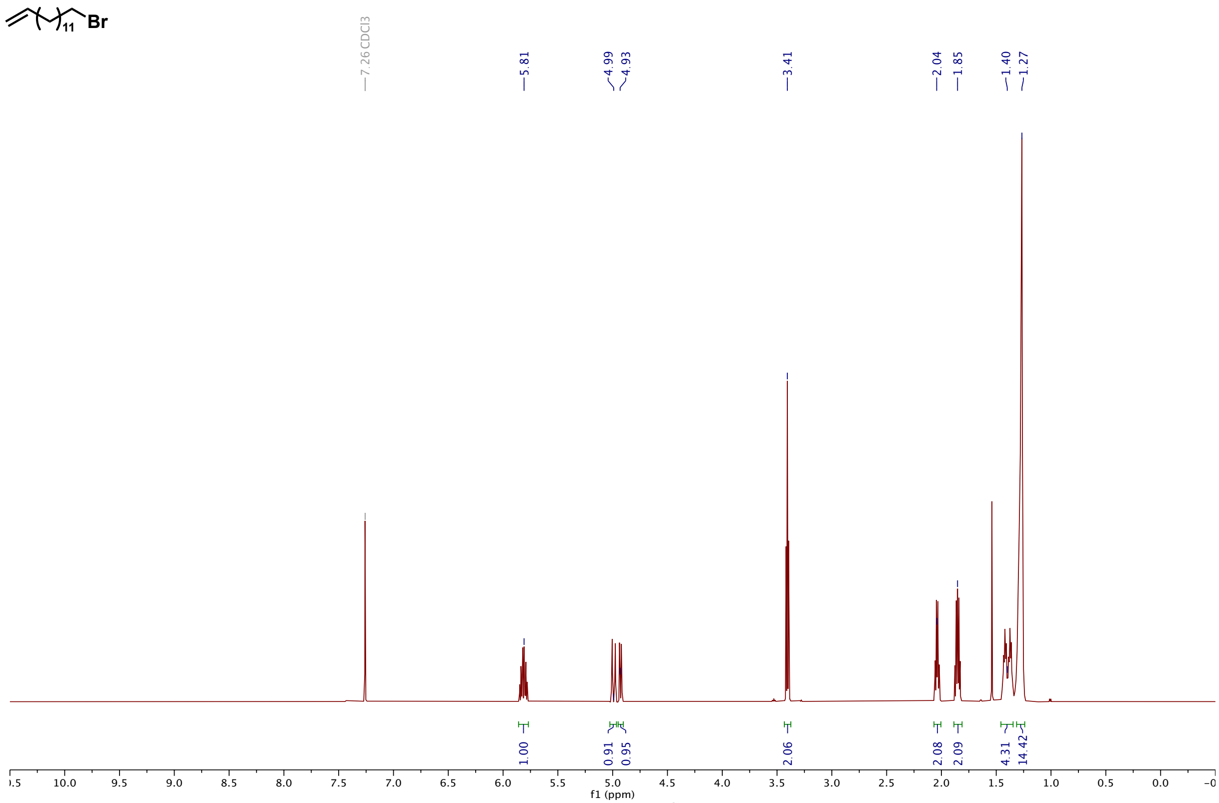
Br
11
7.26 CDCl3
5.81
4.99
4.93
3.41
2.04
1.85
1.40
1.27
1.00
0.91
0.95
2.06
2.08
2.09
4.31
14.42
10.0
9.5
9.0
8.5
8.0
7.5
7.0
6.5
6.0
5.5
5.0
4.5
4.0
3.5
3.0
2.5
2.0
1.5
1.0
0.5
0.0
f1 (ppm)

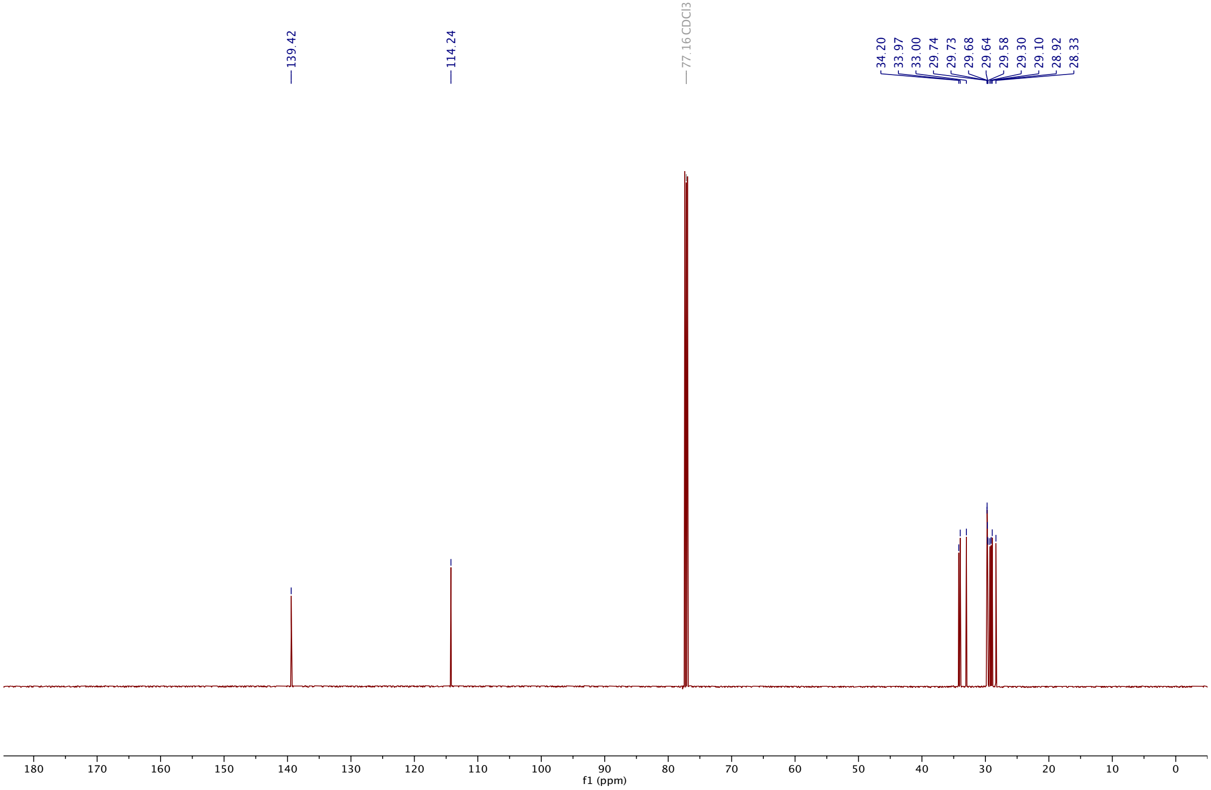
139.42
114.24
77.16 CDCl3
34.20
33.97
33.00
29.74
29.73
29.68
29.64
29.58
29.30
29.10
28.92
28.33
180
170
160
150
140
130
120
110
100
90
80
70
60
50
40
30
20
10
0
f1 (ppm)

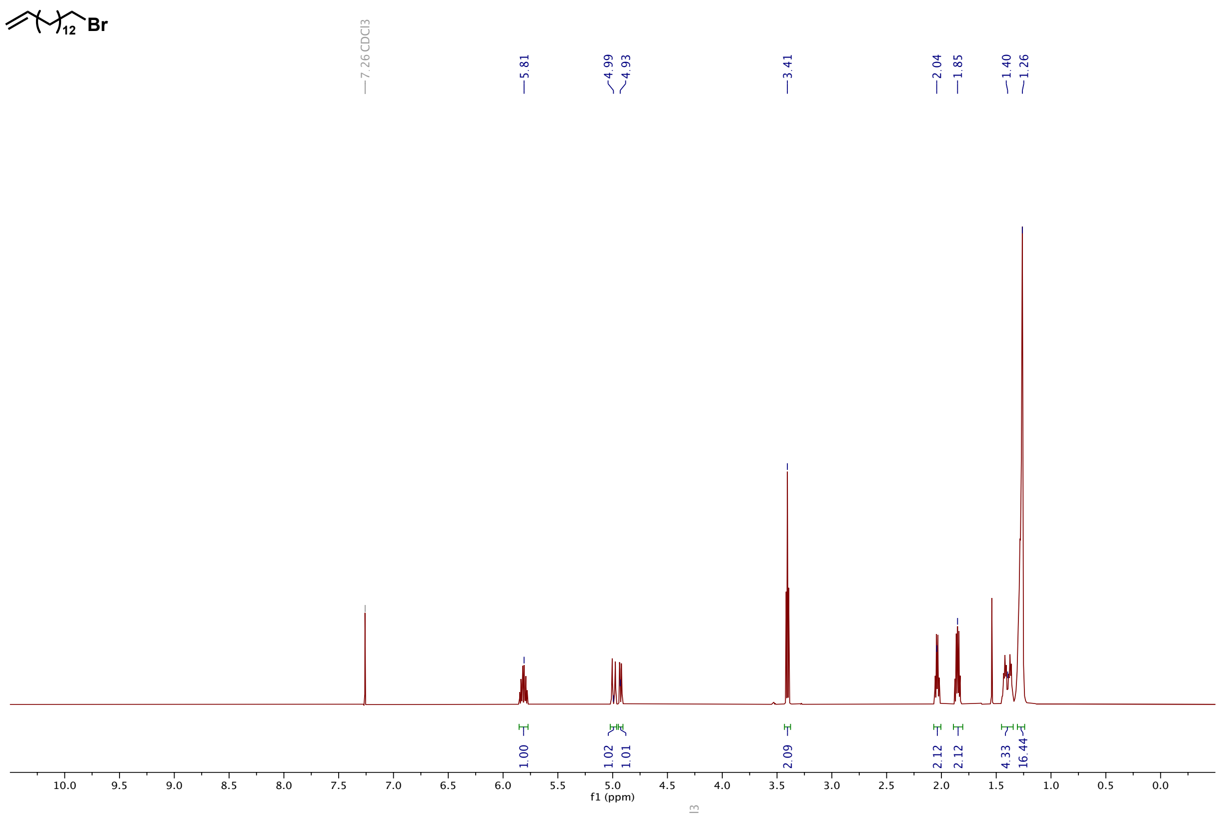
12
Br
7.26 CDCl3
5.81
4.99
4.93
3.41
2.04
1.85
1.40
1.26
1.00
1.02
1.01
2.09
2.12
2.12
4.33
16.44
10.0
9.5
9.0
8.5
8.0
7.5
7.0
6.5
6.0
5.5
5.0
4.5
4.0
3.5
3.0
2.5
2.0
1.5
1.0
0.5
0.0
f1 (ppm)

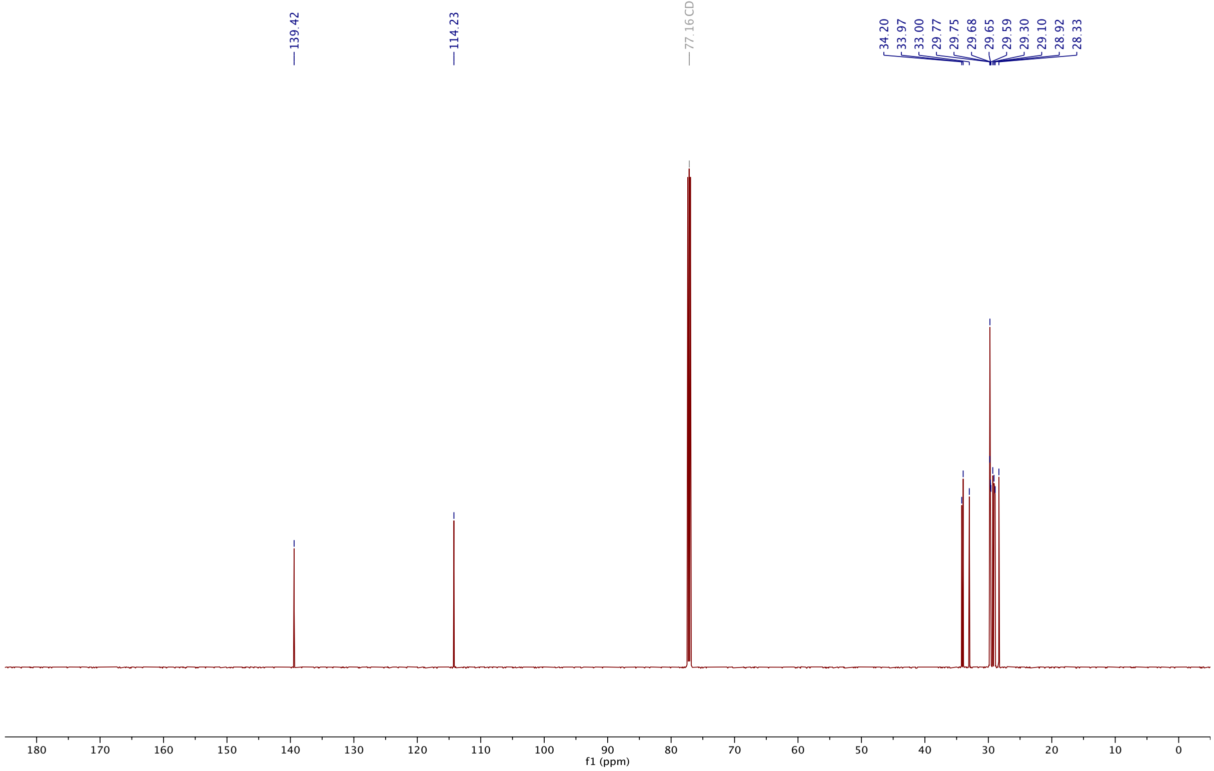
139.42
114.23
77.16 CDCl3
34.20
33.97
33.00
29.77
29.75
29.68
29.65
29.59
29.30
29.10
28.92
28.33
180
170
160
150
140
130
120
110
100
90
80
70
60
50
40
30
20
10
0
f1 (ppm)

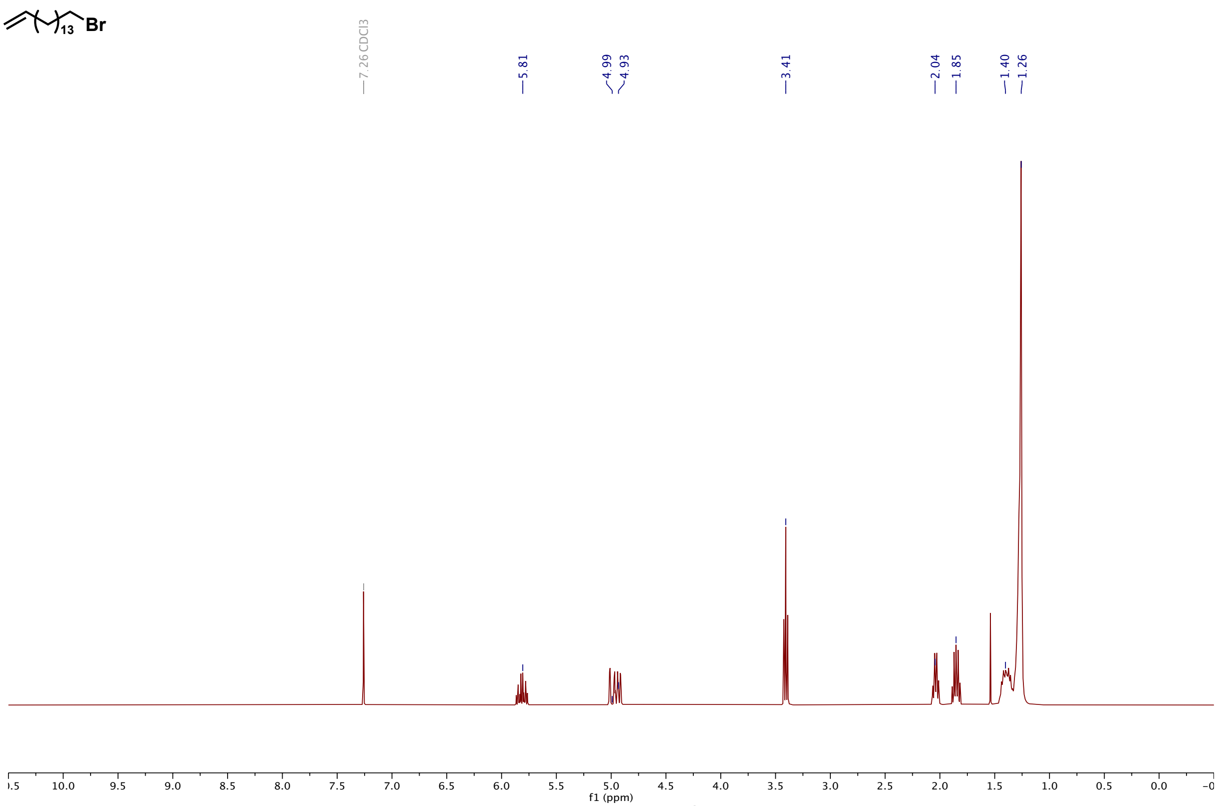

13
Br
7.26 CDCl3
5.81
4.99
4.93
3.41
2.04
1.85
1.40
1.26
.5
10.0
9.5
9.0
8.5
8.0
7.5
7.0
6.5
6.0
5.5
5.0
4.5
4.0
3.5
3.0
2.5
2.0
1.5
1.0
0.5
0.0
–0
f1 (ppm)

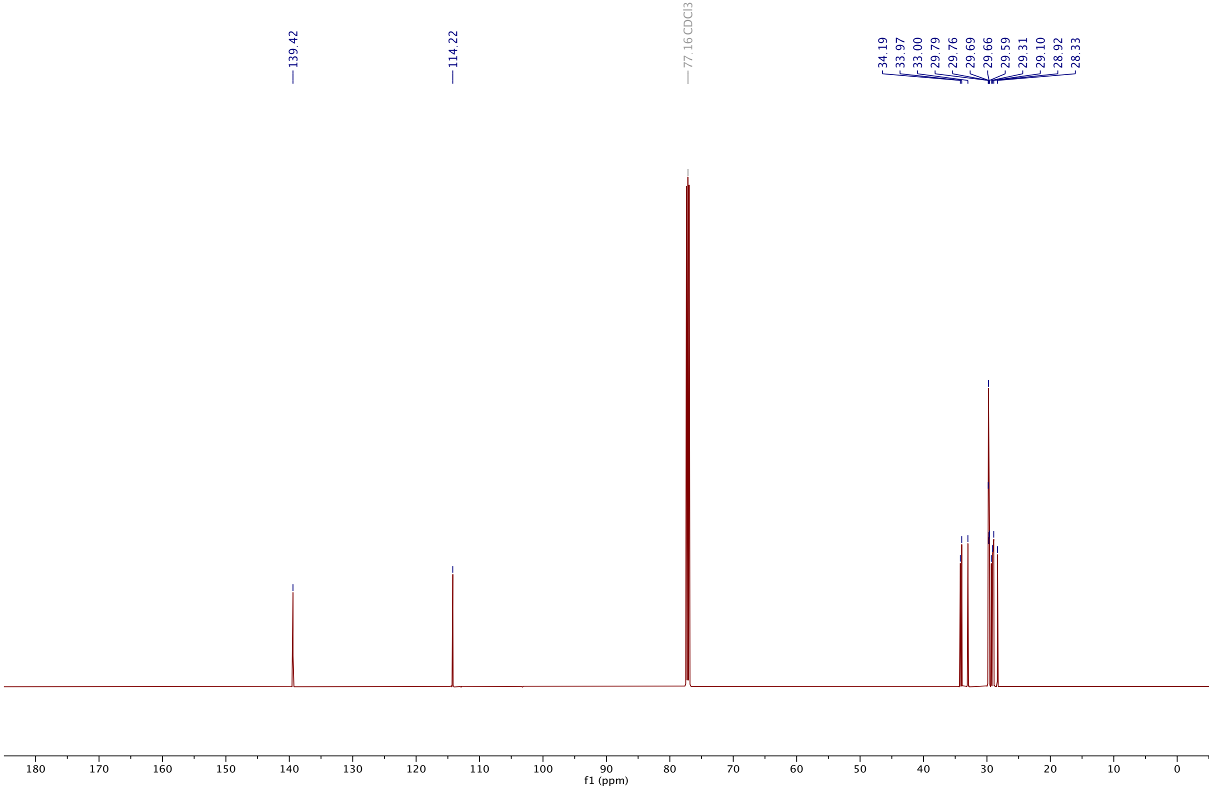

139.42
114.22
77.16 CDCl3
34.19
33.97
33.00
29.79
29.76
29.69
29.66
29.59
29.31
29.10
28.92
28.33
180
170
160
150
140
130
120
110
100
90
80
70
60
50
40
30
20
10
0
f1 (ppm)

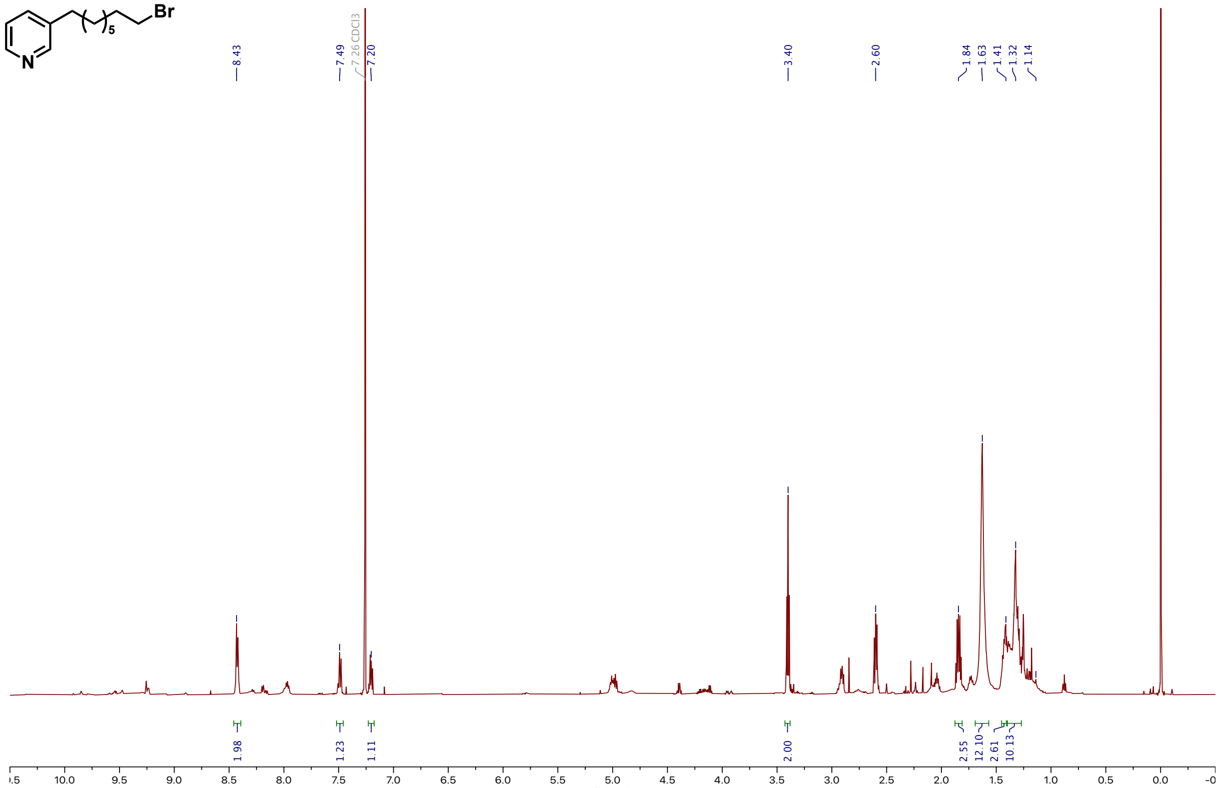
Br
5
N
8.43
7.49
7.26 CDCl3
7.20
3.40
2.60
1.84
1.63
1.41
1.32
1.14
1.98
1.23
1.11
2.00
2.55
12.10
2.61
10.13
10.0
9.5
9.0
8.5
8.0
7.5
7.0
6.5
6.0
5.5
5.0
4.5
4.0
3.5
3.0
2.5
2.0
1.5
1.0
0.5
0.0
f1 (ppm)

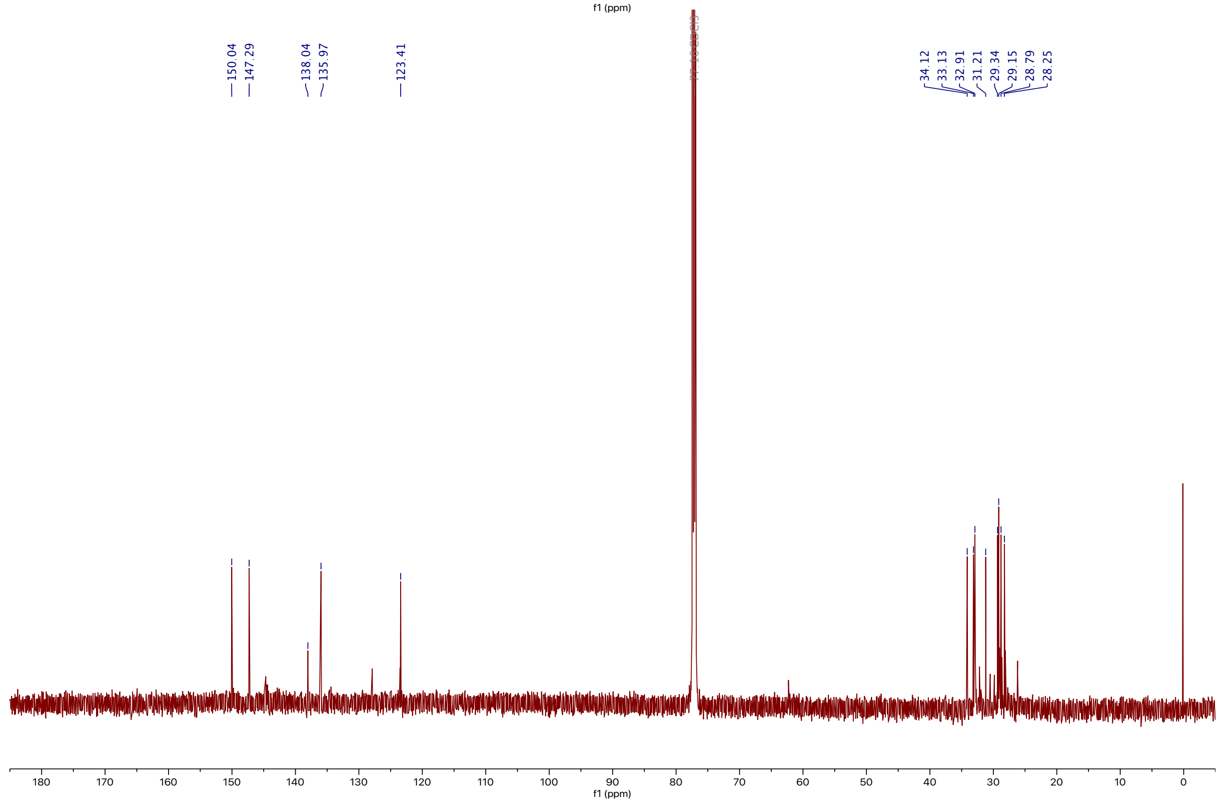
150.04
147.29
138.04
135.97
123.41
34.12
33.13
32.91
31.21
29.34
29.15
28.79
28.25
180
170
160
150
140
130
120
110
100
90
80
70
60
50
40
30
20
10
0
f1 (ppm)

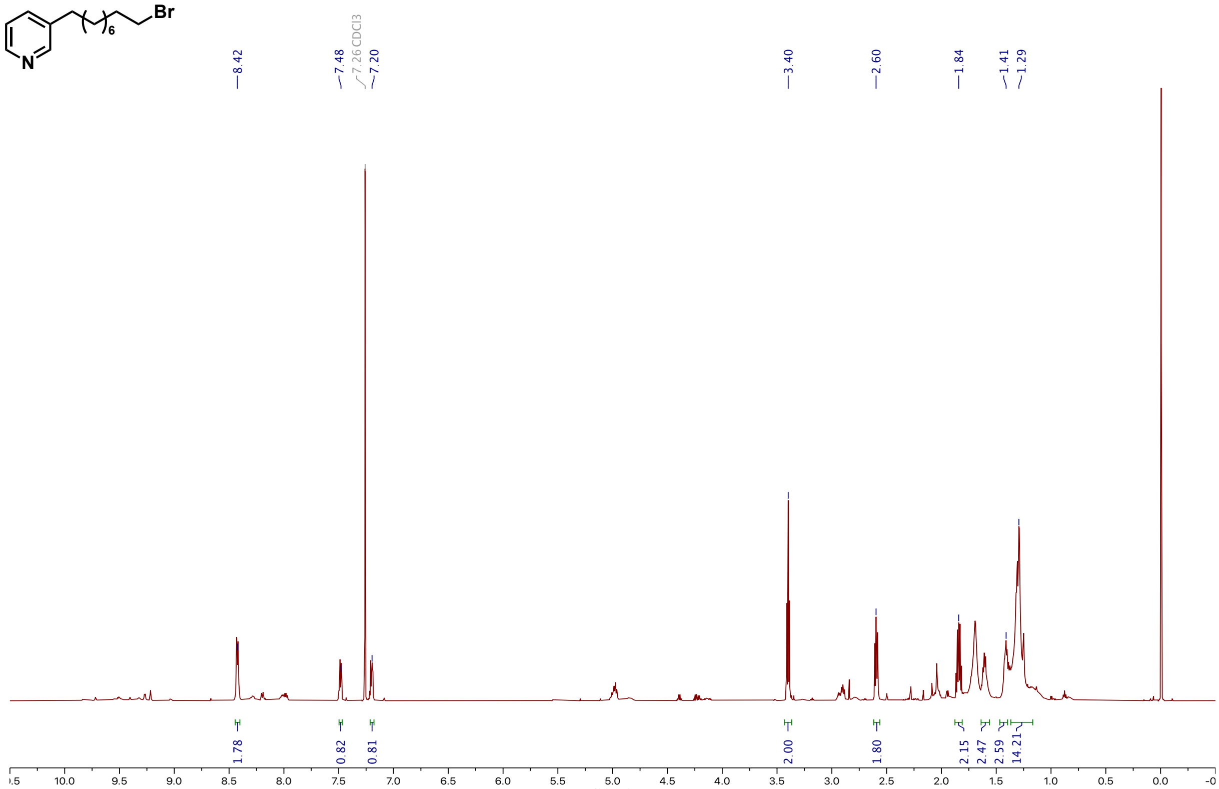

N
Br
6
8.42
7.48
7.26 CDCl3
7.20
3.40
2.60
1.84
1.41
1.29
1.78
0.82
0.81
2.00
1.80
2.15
2.47
2.59
14.21
10.0
9.5
9.0
8.5
8.0
7.5
7.0
6.5
6.0
5.5
5.0
4.5
4.0
3.5
3.0
2.5
2.0
1.5
1.0
0.5
0.0
f1 (ppm)

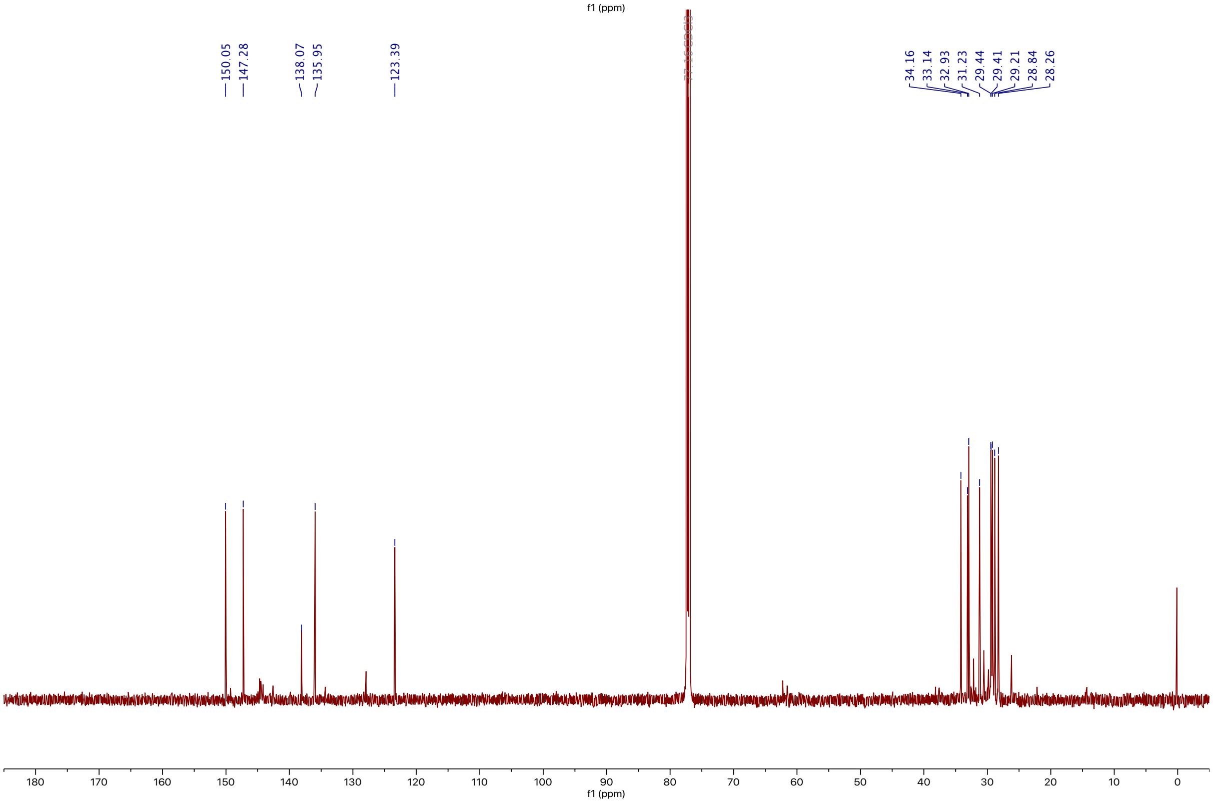

150.05
147.28
138.07
135.95
123.39
34.16
33.14
32.93
31.23
29.44
29.41
29.21
28.84
28.26
180
170
160
150
140
130
120
110
100
90
80
70
60
50
40
30
20
10
0
f1 (ppm)

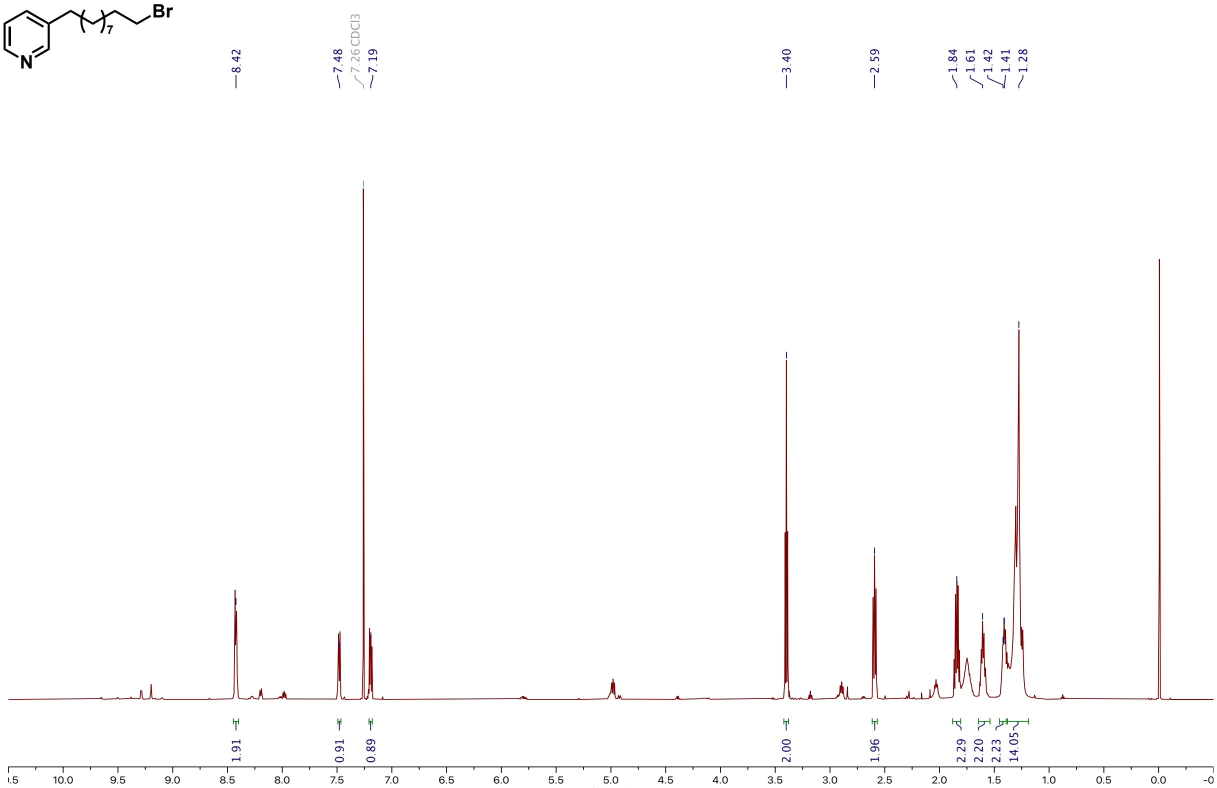
Br
N
7
8.42
7.48
7.26 CDCl3
7.19
3.40
2.59
1.84
1.61
1.42
1.41
1.28
1.91
0.91
0.89
2.00
1.96
2.29
2.20
2.23
14.05
10.0
9.5
9.0
8.5
8.0
7.5
7.0
6.5
6.0
5.5
5.0
4.5
4.0
3.5
3.0
2.5
2.0
1.5
1.0
0.5
0.0
f1 (ppm)

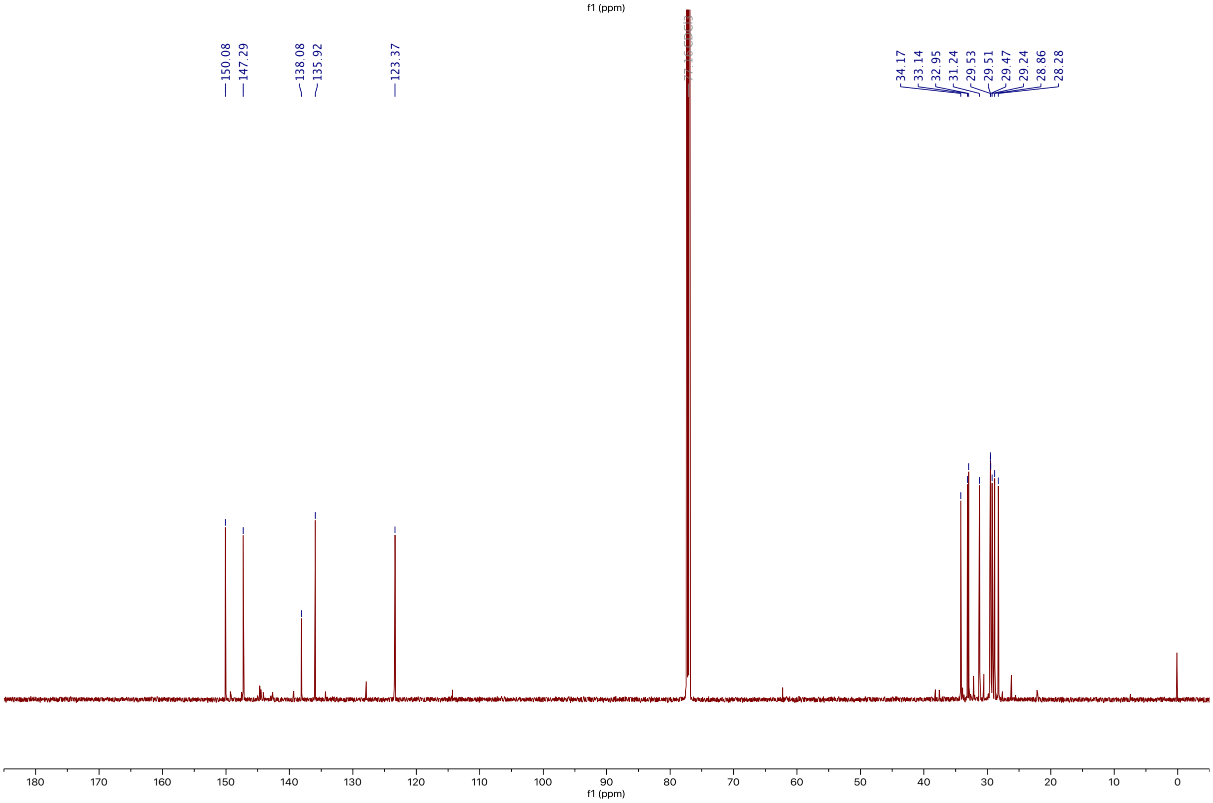
150.08
147.29
138.08
135.92
123.37
34.17
33.14
32.95
31.24
29.53
29.51
29.47
29.24
28.86
28.28
180
170
160
150
140
130
120
110
100
90
80
70
60
50
40
30
20
10
0
f1 (ppm)

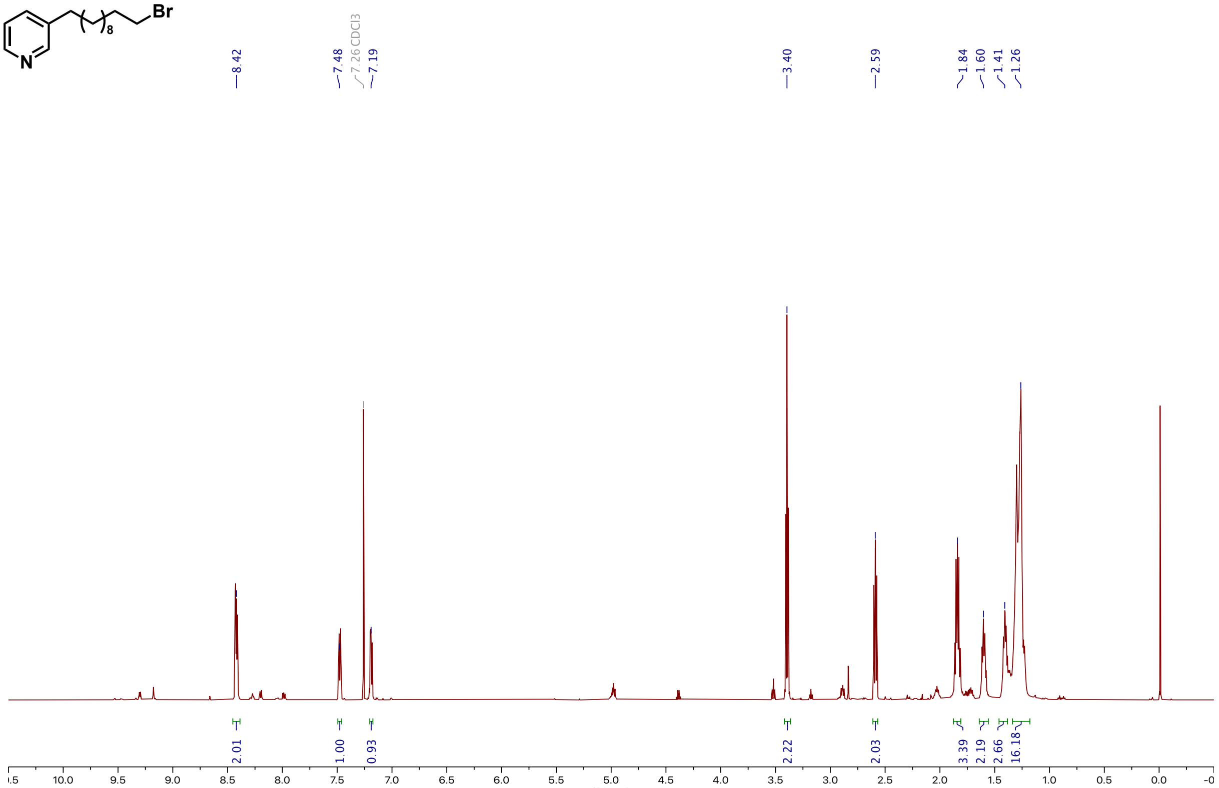
Br
N
8
8.42
7.48
7.26 CDCl3
7.19
3.40
2.59
1.84
1.60
1.41
1.26
2.01
1.00
0.93
2.22
2.03
3.39
2.19
2.66
16.18
10.0
9.5
9.0
8.5
8.0
7.5
7.0
6.5
6.0
5.5
5.0
4.5
4.0
3.5
3.0
2.5
2.0
1.5
1.0
0.5
0.0
f1 (ppm)

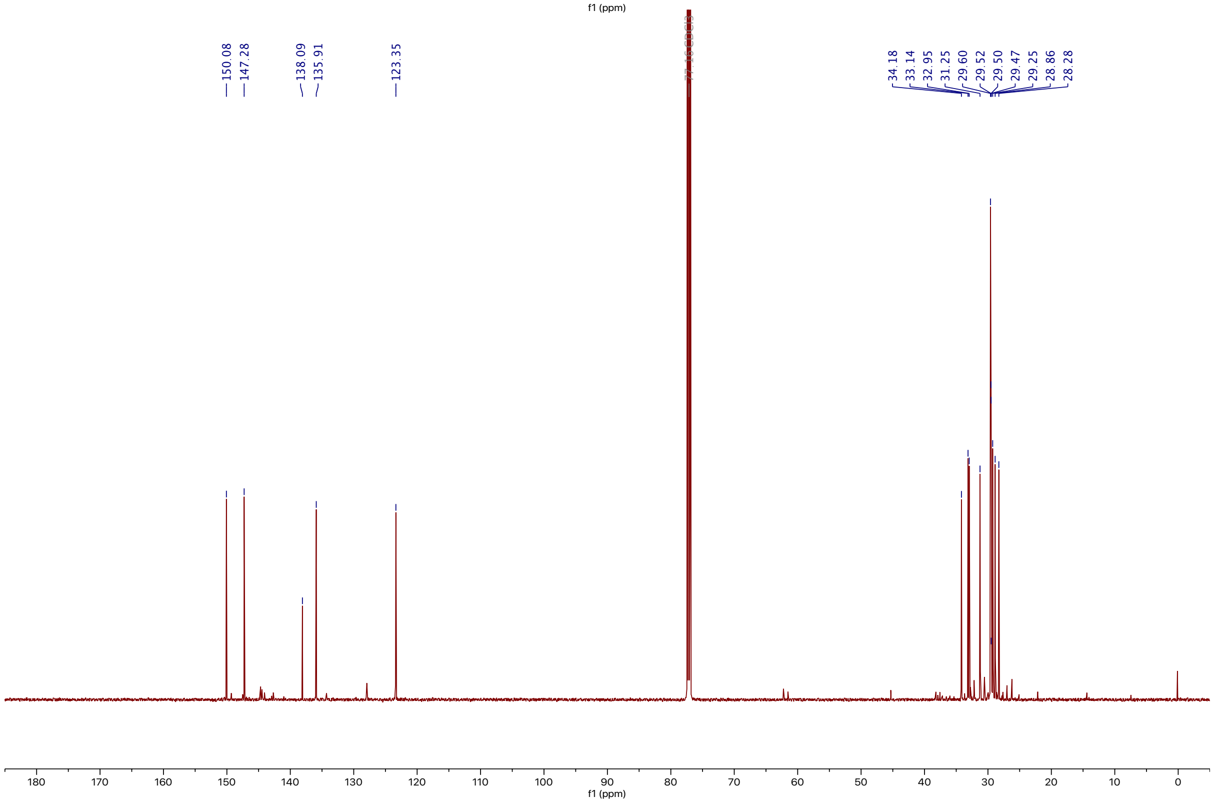
150.08
147.28
138.09
135.91
123.35
77.16 CDCl3
34.18
33.14
32.95
31.25
29.60
29.52
29.50
29.47
29.25
28.86
28.28
180
170
160
150
140
130
120
110
100
90
80
70
60
50
40
30
20
10
0
f1 (ppm)

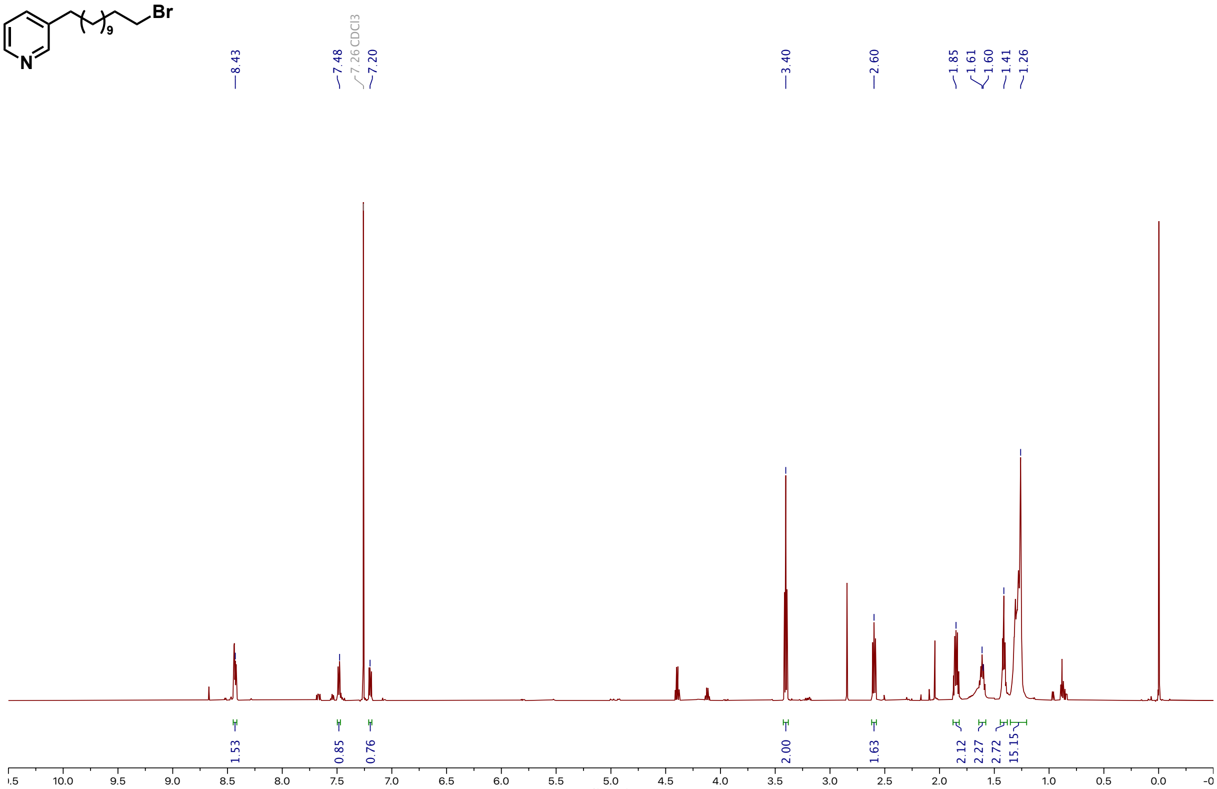
Br
N
9
8.43
7.48
7.26 CDCl3
7.20
3.40
2.60
1.85
1.61
1.60
1.41
1.26
1.53
0.85
0.76
2.00
1.63
2.12
2.27
2.72
15.15
10.0
9.5
9.0
8.5
8.0
7.5
7.0
6.5
6.0
5.5
5.0
4.5
4.0
3.5
3.0
2.5
2.0
1.5
1.0
0.5
0.0
f1 (ppm)

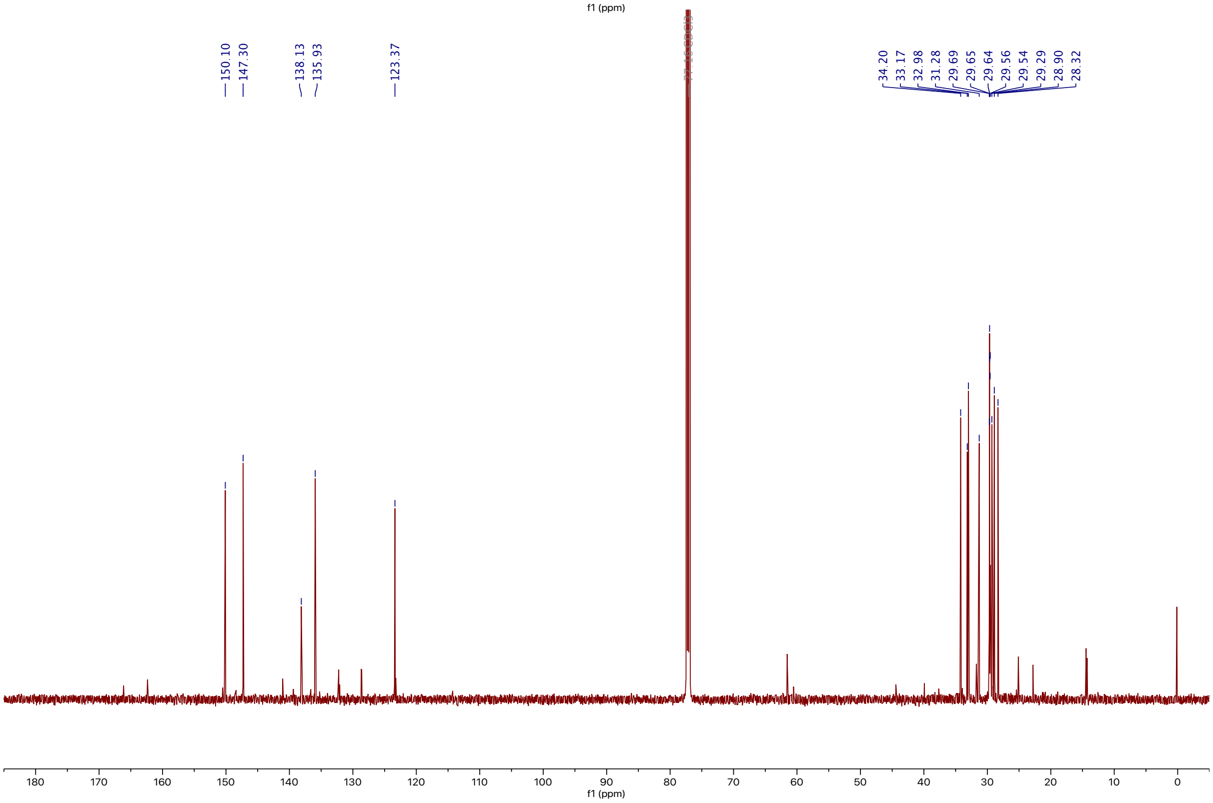
150.10
147.30
138.13
135.93
123.37
34.20
33.17
32.98
31.28
29.69
29.65
29.64
29.56
29.54
29.29
28.90
28.32
180
170
160
150
140
130
120
110
100
90
80
70
60
50
40
30
20
10
0
f1 (ppm)

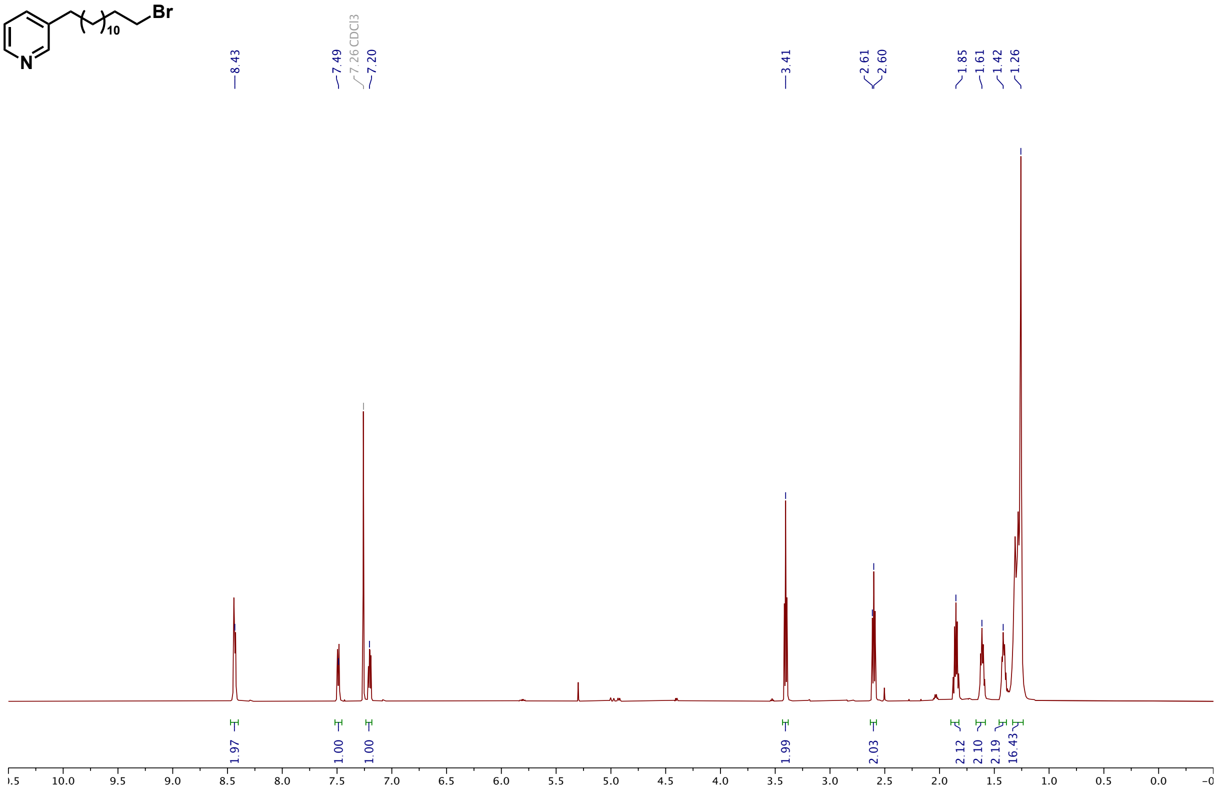
Br
N
10
8.43
7.49
7.26 CDCl3
7.20
3.41
2.61
2.60
1.85
1.61
1.42
1.26
1.97
1.00
1.00
1.99
2.03
2.12
2.10
2.19
16.43
10.0
9.5
9.0
8.5
8.0
7.5
7.0
6.5
6.0
5.5
5.0
4.5
4.0
3.5
3.0
2.5
2.0
1.5
1.0
0.5
0.0
f1 (ppm)

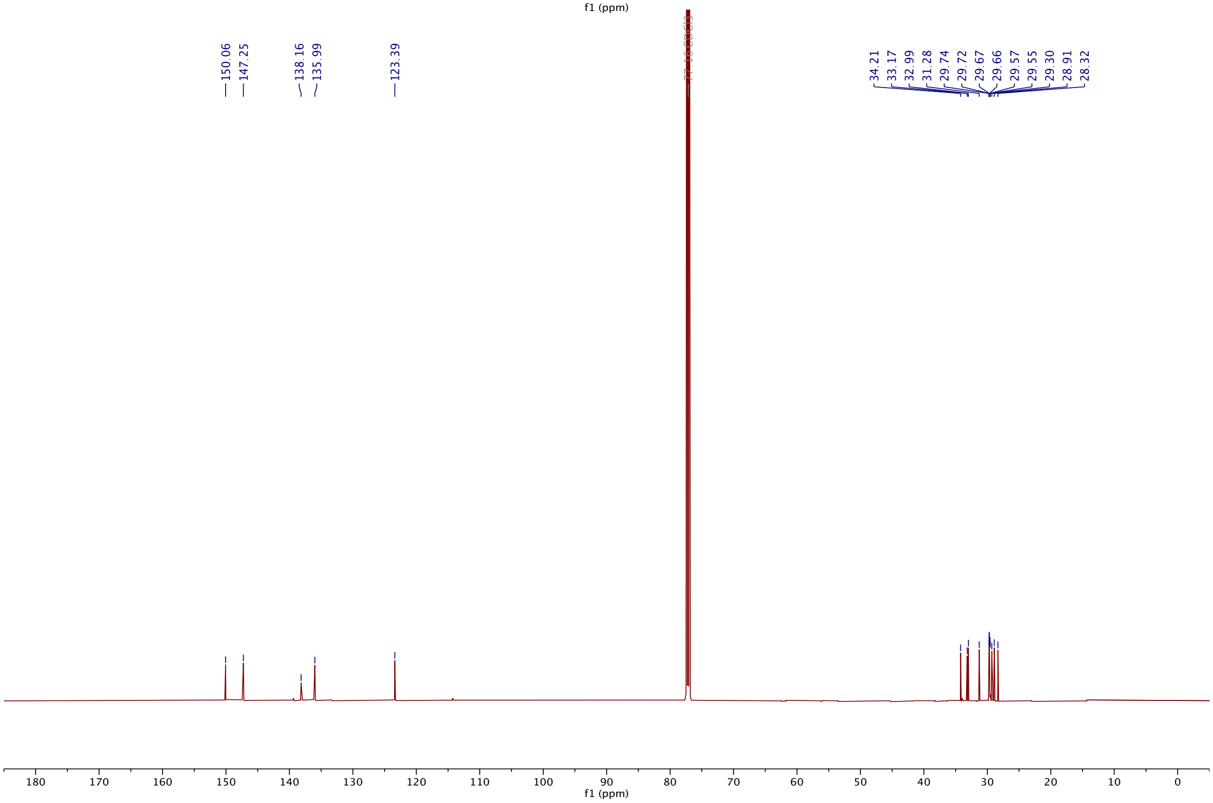
150.06
147.25
138.16
135.99
123.39
77.16 CDCl3
34.21
33.17
32.99
31.28
29.74
29.72
29.67
29.66
29.57
29.55
29.30
28.91
28.32
180
170
160
150
140
130
120
110
100
90
80
70
60
50
40
30
20
10
0
f1 (ppm)

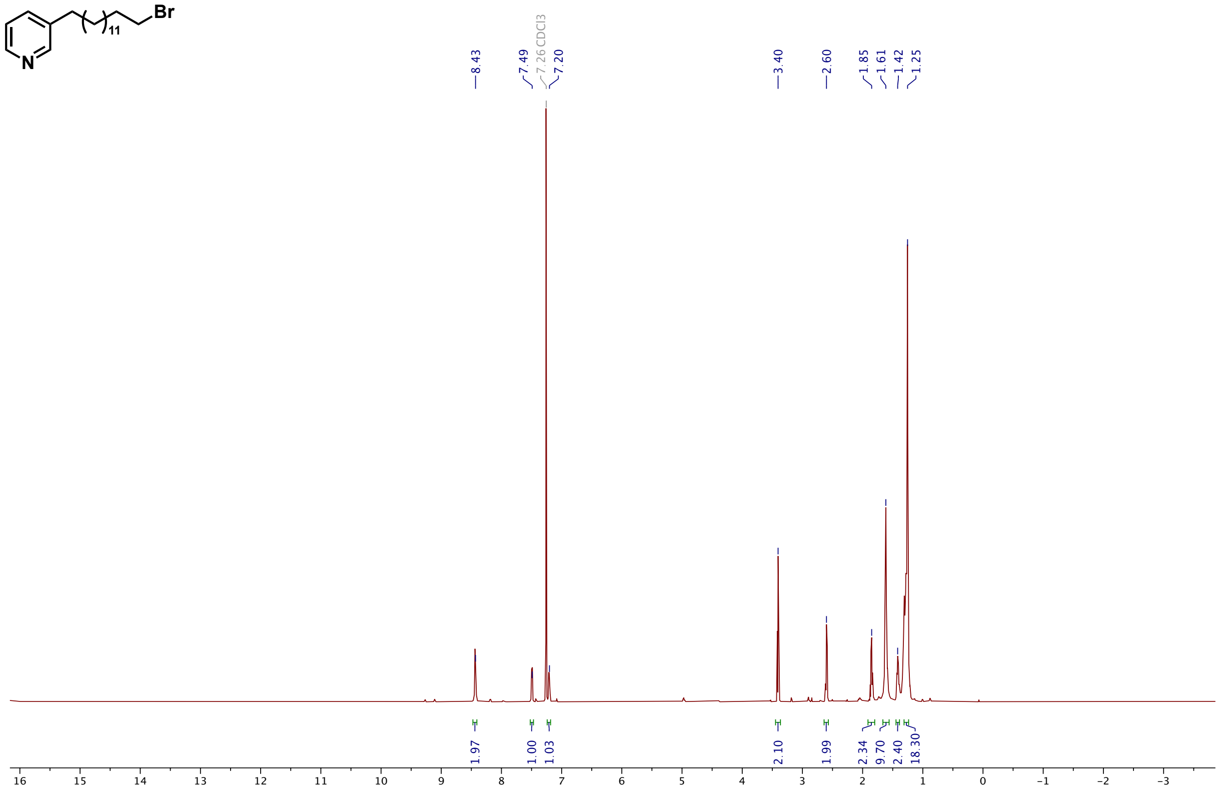
Br
N
11
8.43
7.49
7.26 CDCl3
7.20
3.40
2.60
1.85
1.61
1.42
1.25
1.97
1.00
1.03
2.10
1.99
2.34
9.70
2.40
18.30
16 15 14 13 12 11 10 9 8 7 6 5 4 3 2 1 0 −1 −2 −3
f1 (ppm)

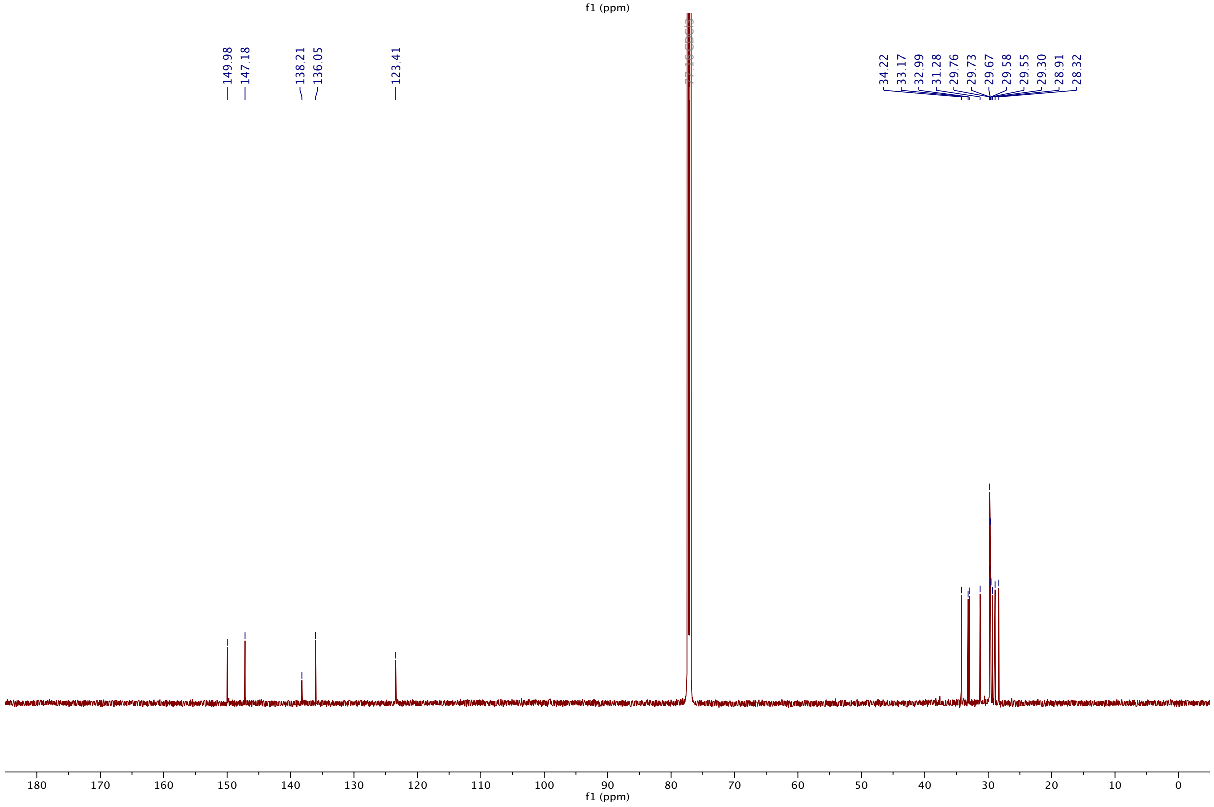
149.98
147.18
138.21
136.05
123.41
34.22
33.17
32.99
31.28
29.76
29.73
29.67
29.58
29.55
29.30
28.91
28.32
180 170 160 150 140 130 120 110 100 90 80 70 60 50 40 30 20 10 0
f1 (ppm)

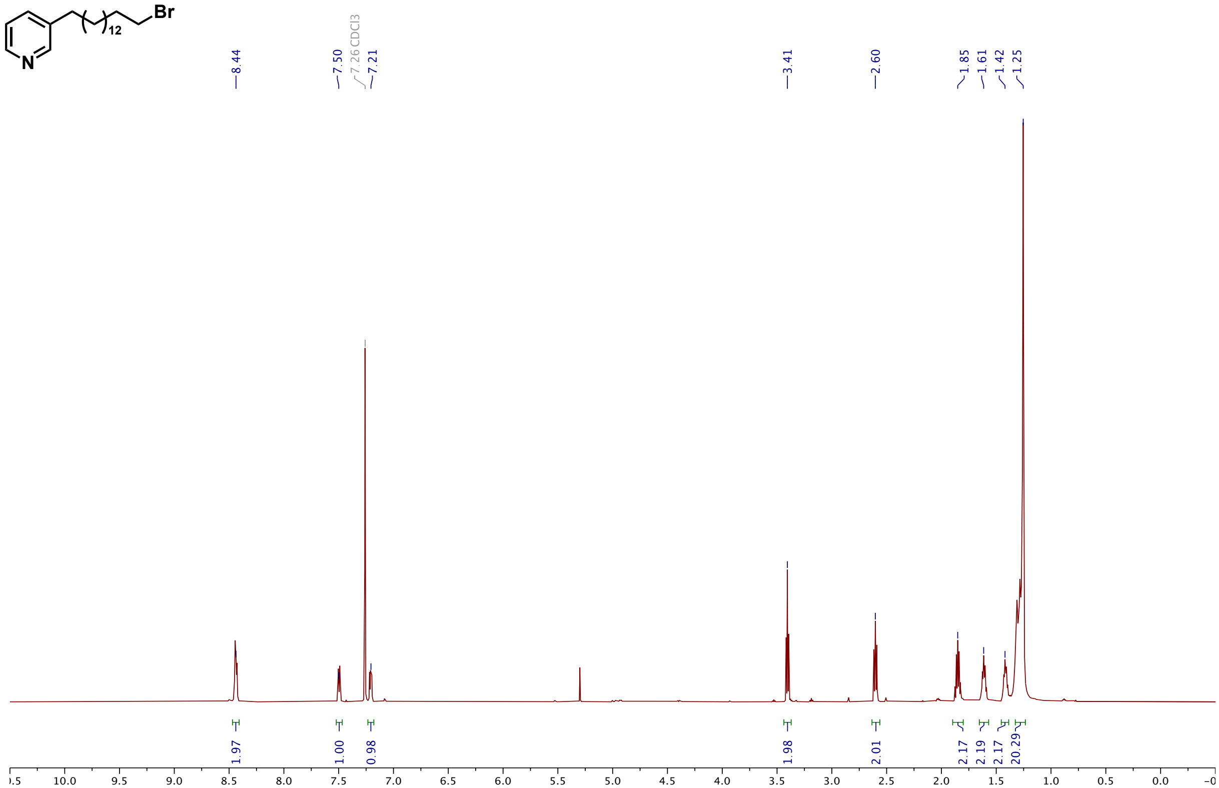
N
12
Br
8.44
7.50
7.26 CDCl3
7.21
3.41
2.60
1.85
1.61
1.42
1.25
1.97
1.00
0.98
1.98
2.01
2.17
2.19
2.17
20.29
10.0
9.5
9.0
8.5
8.0
7.5
7.0
6.5
6.0
5.5
5.0
4.5
4.0
3.5
3.0
2.5
2.0
1.5
1.0
0.5
0.0
f1 (ppm)

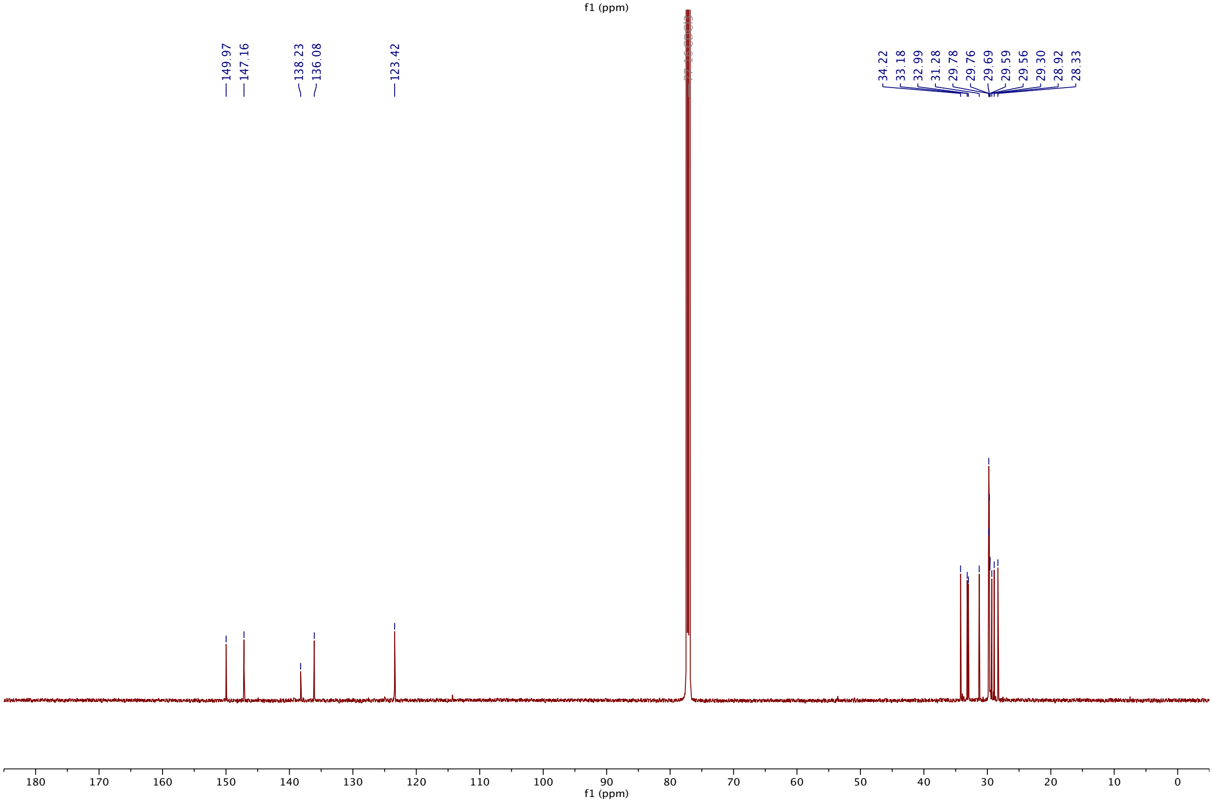
149.97
147.16
138.23
136.08
123.42
77.16 CDCl3
34.22
33.18
32.99
31.28
29.78
29.76
29.69
29.59
29.56
29.30
28.92
28.33
180
170
160
150
140
130
120
110
100
90
80
70
60
50
40
30
20
10
0
f1 (ppm)

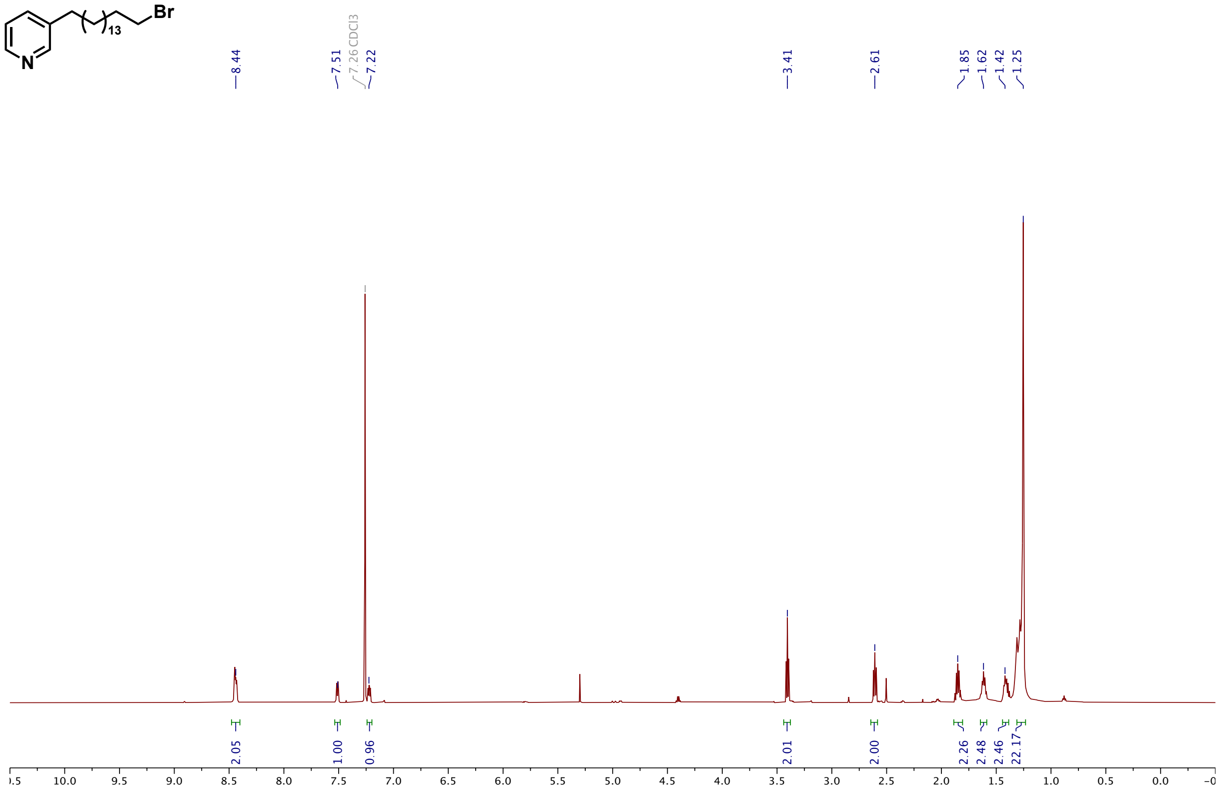
Br
N
13
8.44
7.51
7.26 CDCl3
7.22
3.41
2.61
1.85
1.62
1.42
1.25
2.05
1.00
0.96
2.01
2.00
2.26
2.48
2.46
22.17
10.0
9.5
9.0
8.5
8.0
7.5
7.0
6.5
6.0
5.5
5.0
4.5
4.0
3.5
3.0
2.5
2.0
1.5
1.0
0.5
0.0
f1 (ppm)

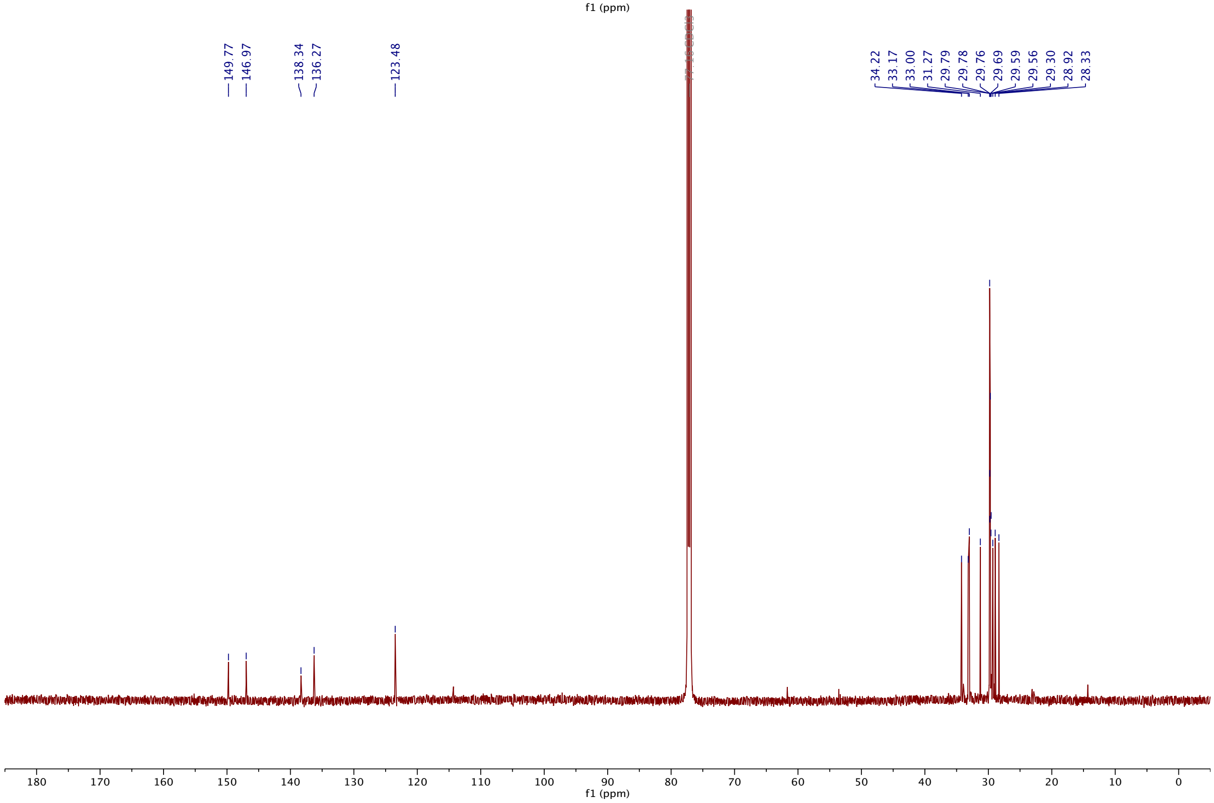
149.77
146.97
138.34
136.27
123.48
34.22
33.17
33.00
31.27
29.79
29.78
29.76
29.69
29.59
29.56
29.30
28.92
28.33
180
170
160
150
140
130
120
110
100
90
80
70
60
50
40
30
20
10
0
f1 (ppm)

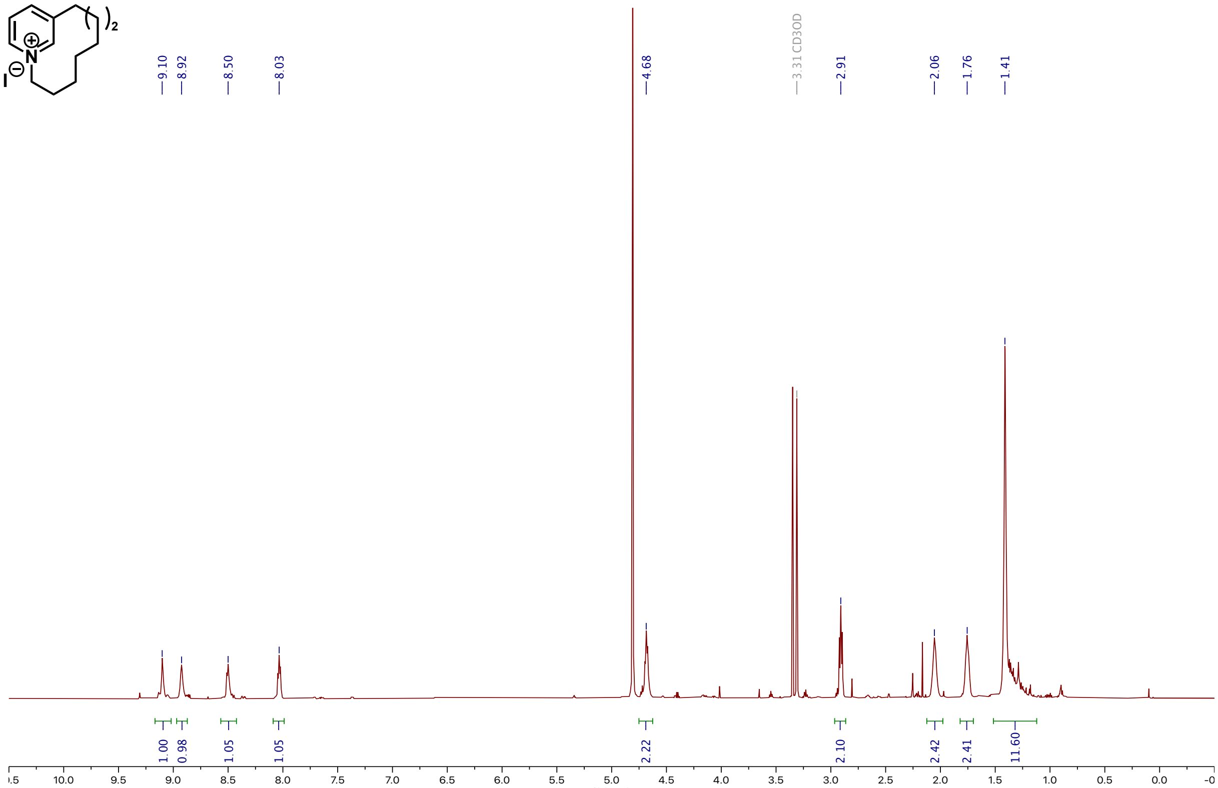
I
N
)2
9.10
8.92
8.50
8.03
4.68
3.31 CD3OD
2.91
2.06
1.76
1.41
1.00
0.98
1.05
1.05
2.22
2.10
2.42
2.41
11.60
10.0
9.5
9.0
8.5
8.0
7.5
7.0
6.5
6.0
5.5
5.0
4.5
4.0
3.5
3.0
2.5
2.0
1.5
1.0
0.5
0.0
f1 (ppm)

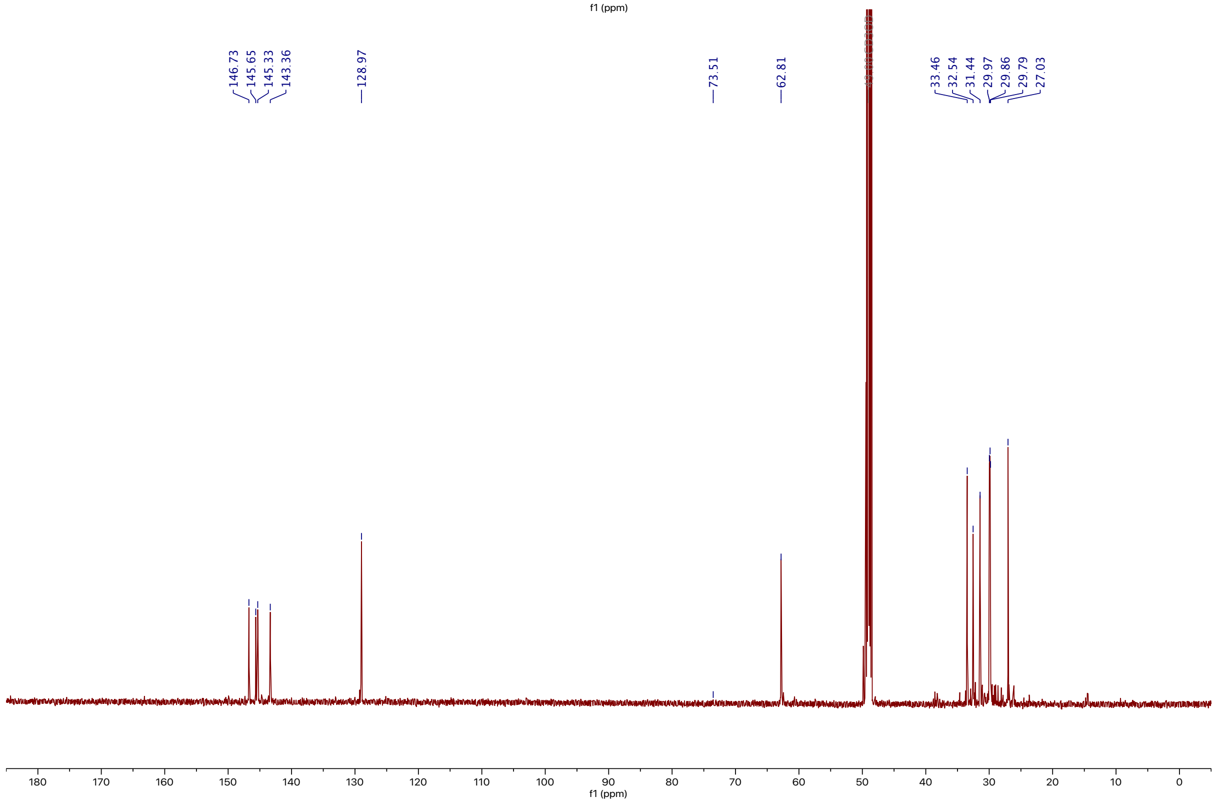
146.73
145.65
145.33
143.36
128.97
73.51
62.81
33.46
32.54
31.44
29.97
29.86
29.79
27.03
180
170
160
150
140
130
120
110
100
90
80
70
60
50
40
30
20
10
0
f1 (ppm)

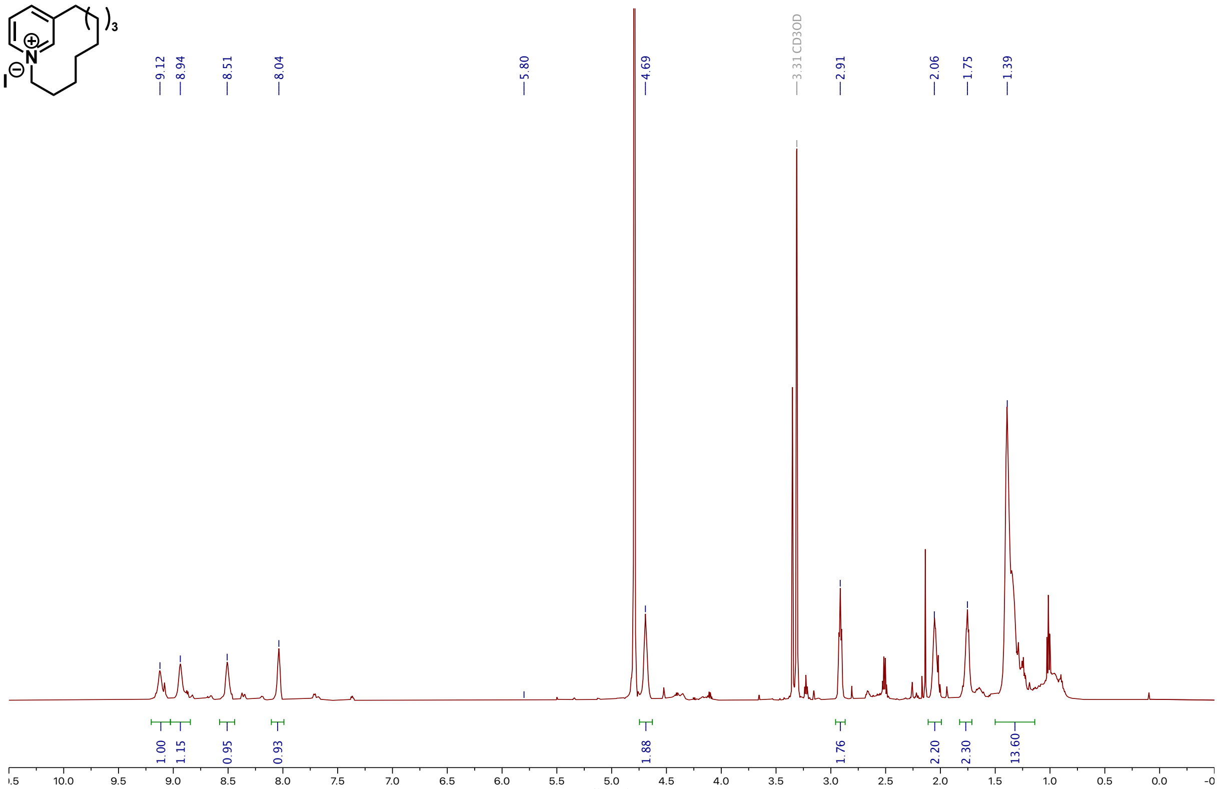
I
N
3
9.12
8.94
8.51
8.04
5.80
4.69
3.31 CD3OD
2.91
2.06
1.75
1.39
1.00
1.15
0.95
0.93
1.88
1.76
2.20
2.30
13.60
10.5
10.0
9.5
9.0
8.5
8.0
7.5
7.0
6.5
6.0
5.5
5.0
4.5
4.0
3.5
3.0
2.5
2.0
1.5
1.0
0.5
0.0
-0
f1 (ppm)

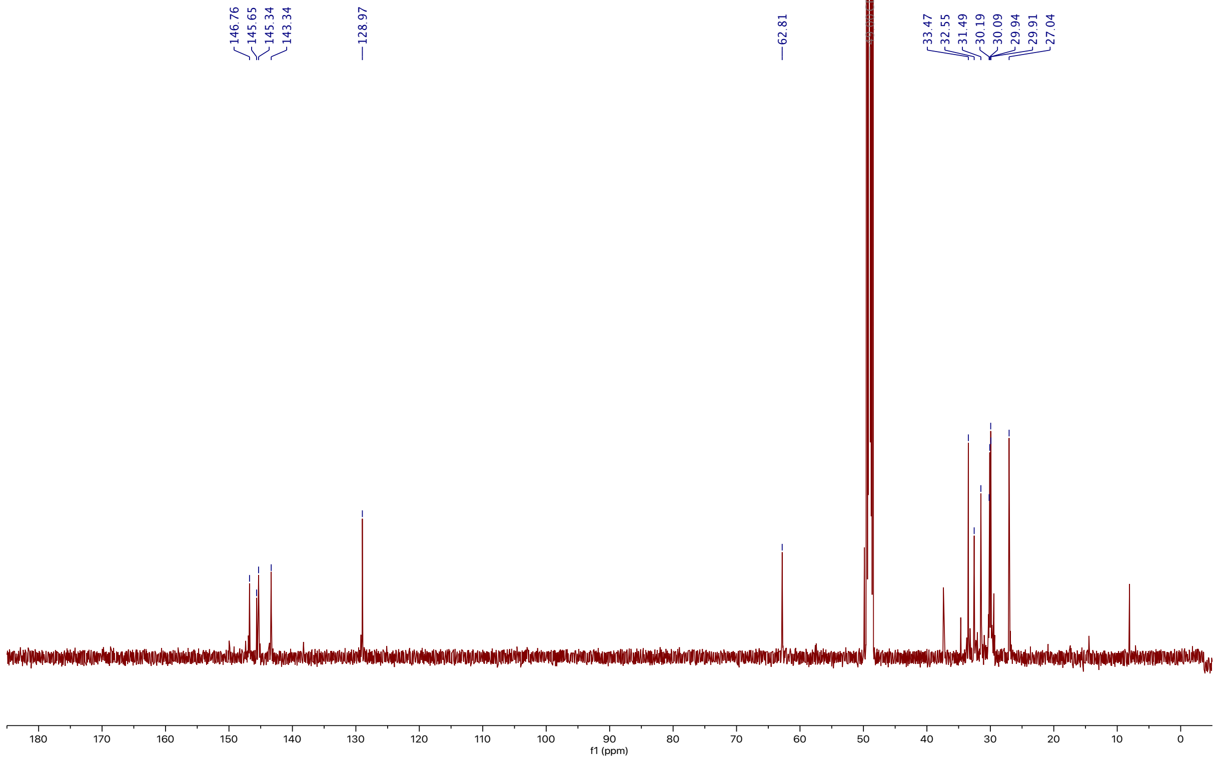
146.76
145.65
145.34
143.34
128.97
62.81
33.47
32.55
31.49
30.19
30.09
29.94
29.91
27.04
180
170
160
150
140
130
120
110
100
90
80
70
60
50
40
30
20
10
0
f1 (ppm)

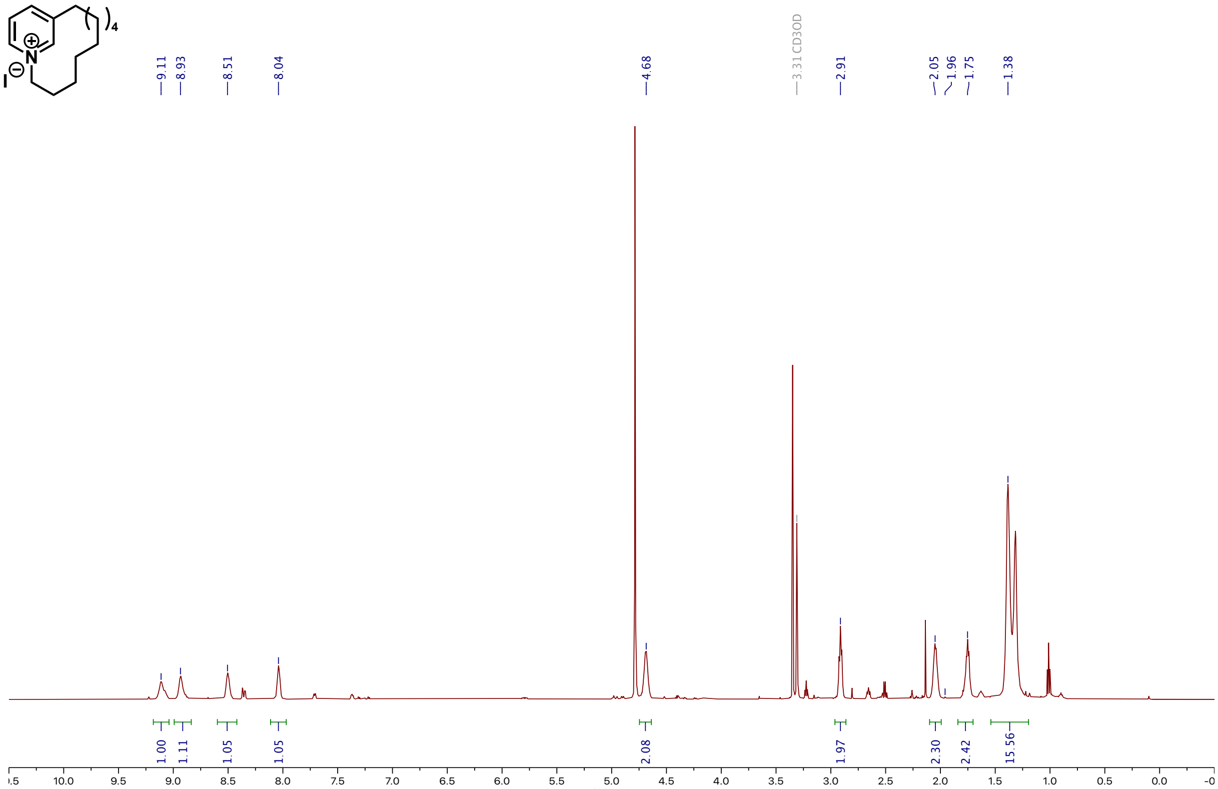
4
I
N
9.11
8.93
8.51
8.04
4.68
3.31 CD3OD
2.91
2.05
1.96
1.75
1.38
1.00
1.11
1.05
1.05
2.08
1.97
2.30
2.42
15.56
10.0
9.5
9.0
8.5
8.0
7.5
7.0
6.5
6.0
5.5
5.0
4.5
4.0
3.5
3.0
2.5
2.0
1.5
1.0
0.5
0.0
f1 (ppm)

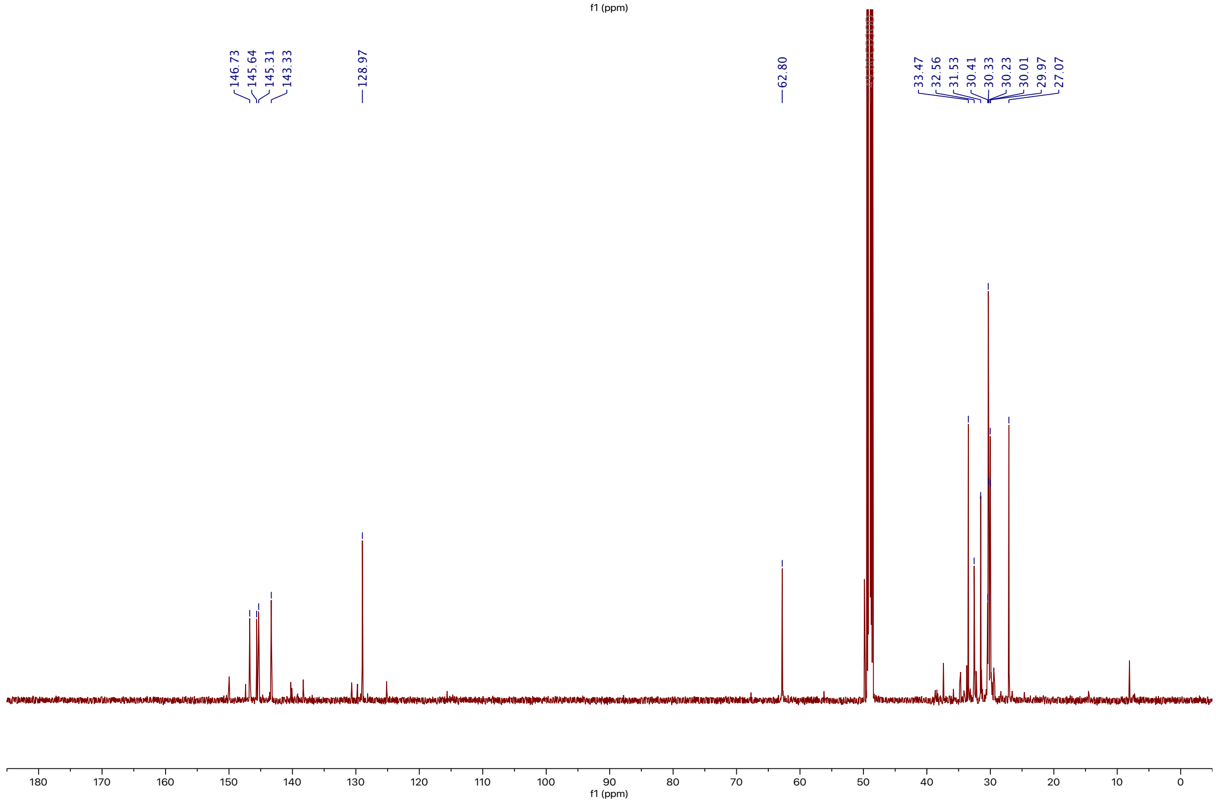
146.73
145.64
145.31
143.33
128.97
62.80
33.47
32.56
31.53
30.41
30.33
30.23
30.01
29.97
27.07
180
170
160
150
140
130
120
110
100
90
80
70
60
50
40
30
20
10
0
f1 (ppm)

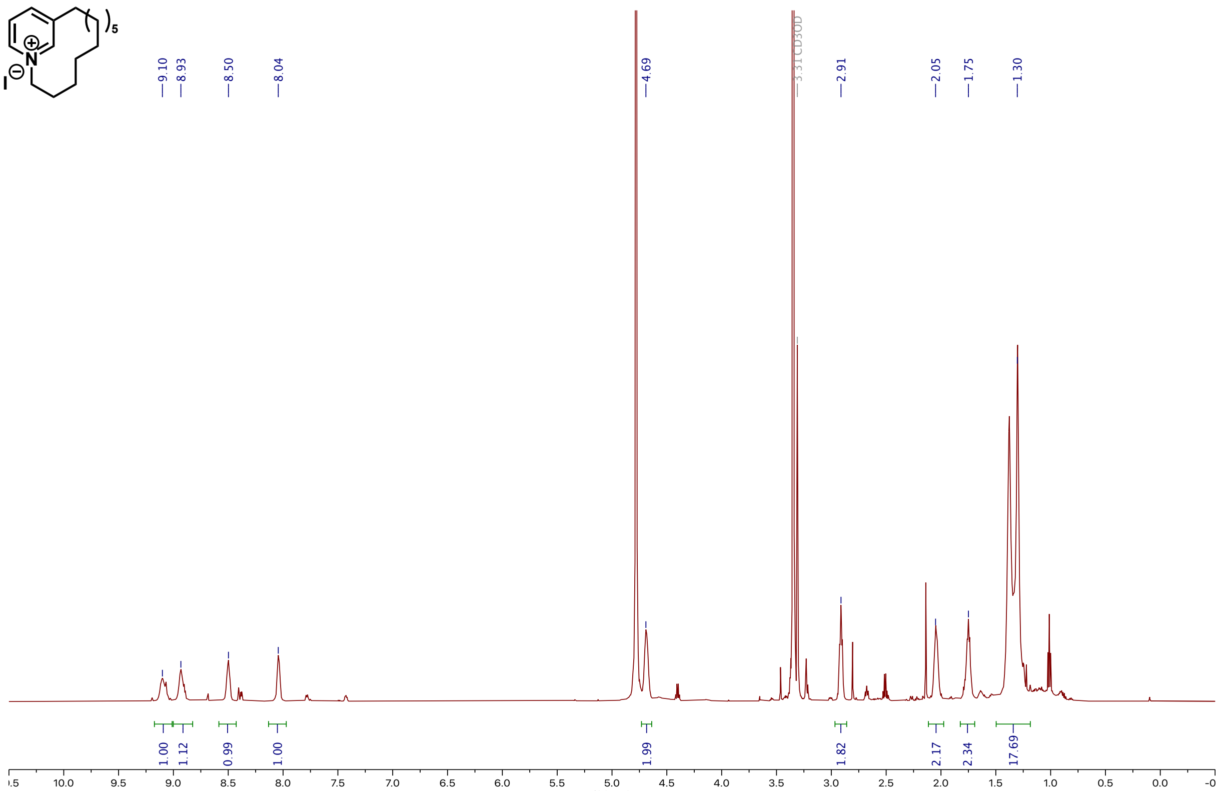

N
I
5
9.10
8.93
8.50
8.04
4.69
3.31 CD3OD
2.91
2.05
1.75
1.30
1.00
1.12
0.99
1.00
1.99
1.82
2.17
2.34
17.69
10.0
9.5
9.0
8.5
8.0
7.5
7.0
6.5
6.0
5.5
5.0
4.5
4.0
3.5
3.0
2.5
2.0
1.5
1.0
0.5
0.0
f1 (ppm)

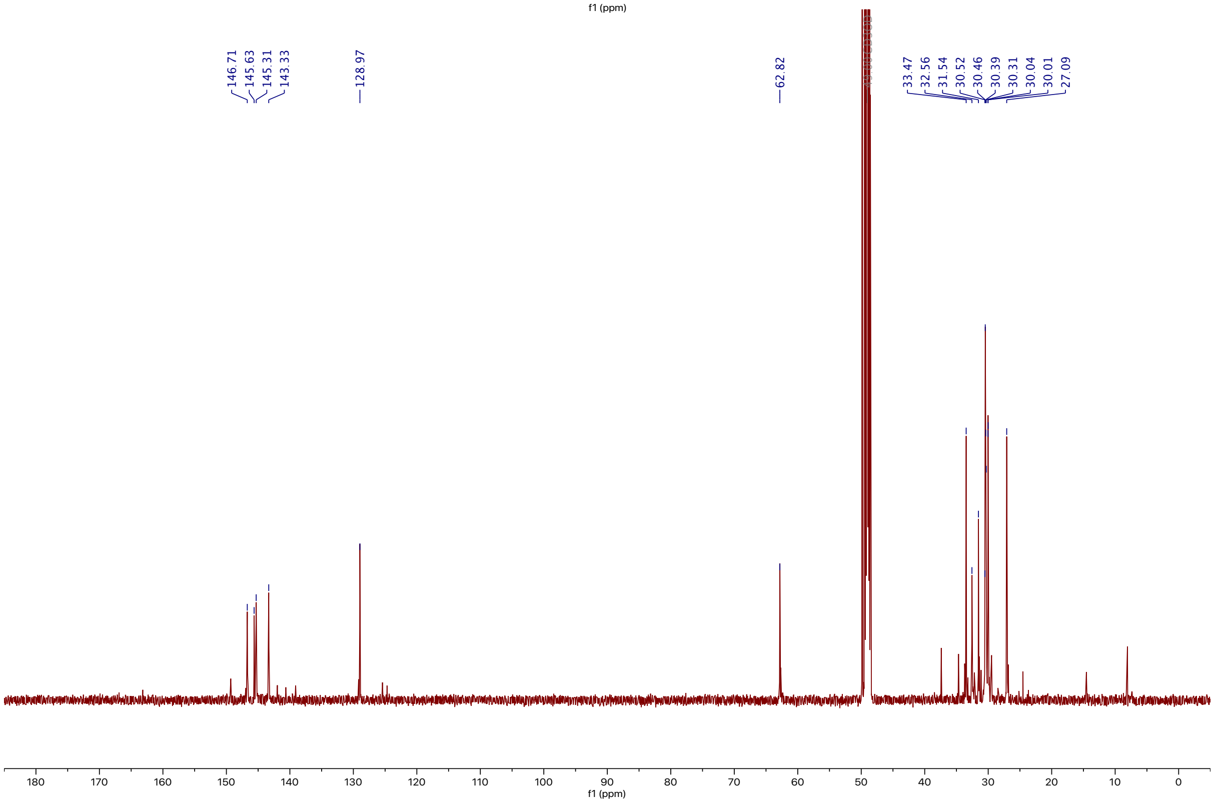

146.71
145.63
145.31
143.33
128.97
62.82
33.47
32.56
31.54
30.52
30.46
30.39
30.31
30.04
30.01
27.09
180
170
160
150
140
130
120
110
100
90
80
70
60
50
40
30
20
10
0
f1 (ppm)

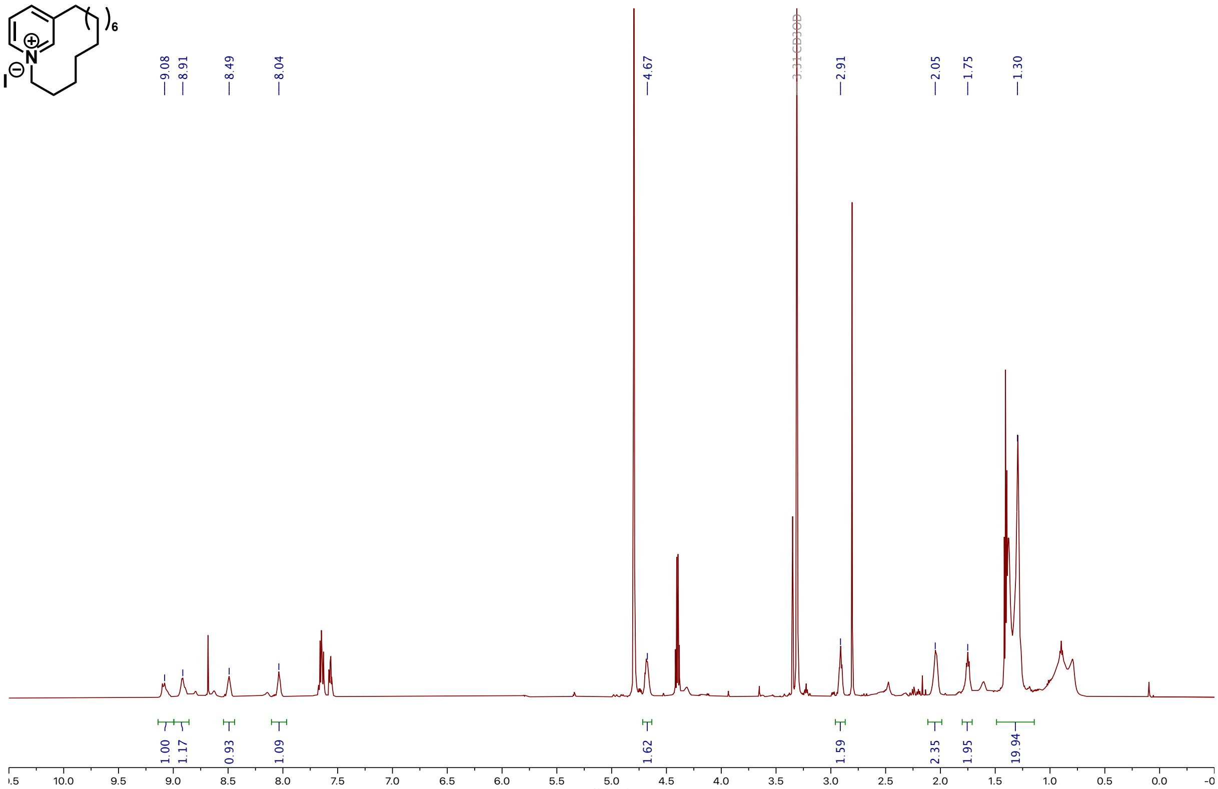
6
I
N
9.08
8.91
8.49
8.04
4.67
3.31 CD3OD
2.91
2.05
1.75
1.30
1.00
1.17
0.93
1.09
1.62
1.59
2.35
1.95
19.94
10.0
9.5
9.0
8.5
8.0
7.5
7.0
6.5
6.0
5.5
5.0
4.5
4.0
3.5
3.0
2.5
2.0
1.5
1.0
0.5
0.0
f1 (ppm)

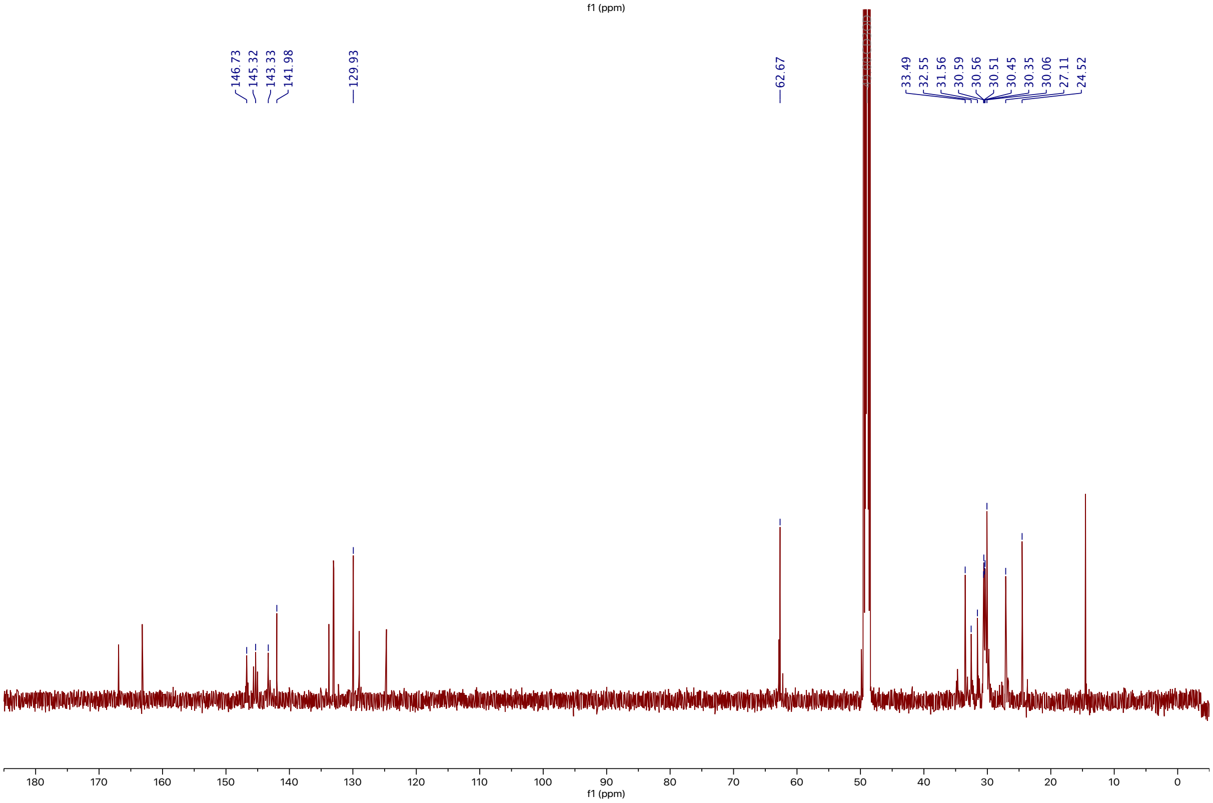
146.73
145.32
143.33
141.98
129.93
62.67
33.49
32.55
31.56
30.59
30.56
30.51
30.45
30.35
30.06
27.11
24.52
180
170
160
150
140
130
120
110
100
90
80
70
60
50
40
30
20
10
0
f1 (ppm)

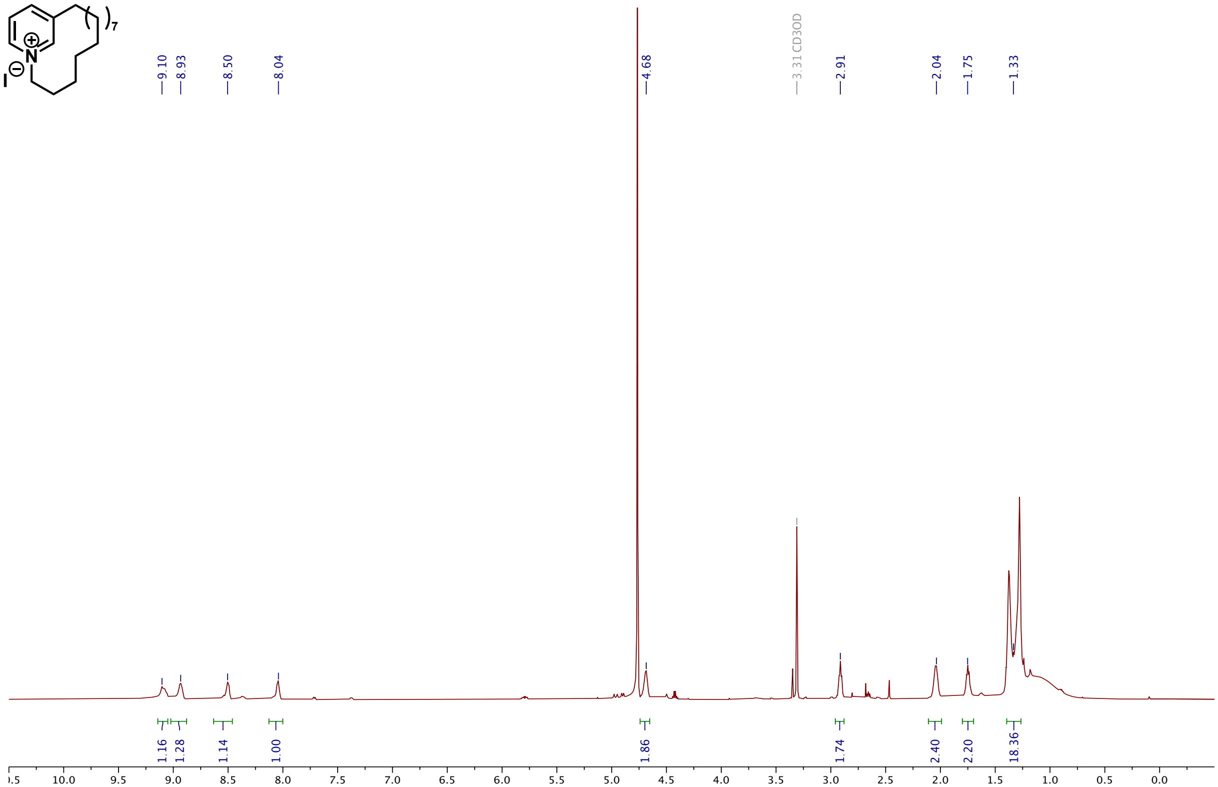

I
N
7
9.10
8.93
8.50
8.04
4.68
3.31 CD3OD
2.91
2.04
1.75
1.33
1.16
1.28
1.14
1.00
1.86
1.74
2.40
2.20
18.36
10.0
9.5
9.0
8.5
8.0
7.5
7.0
6.5
6.0
5.5
5.0
4.5
4.0
3.5
3.0
2.5
2.0
1.5
1.0
0.5
0.0
f1 (ppm)

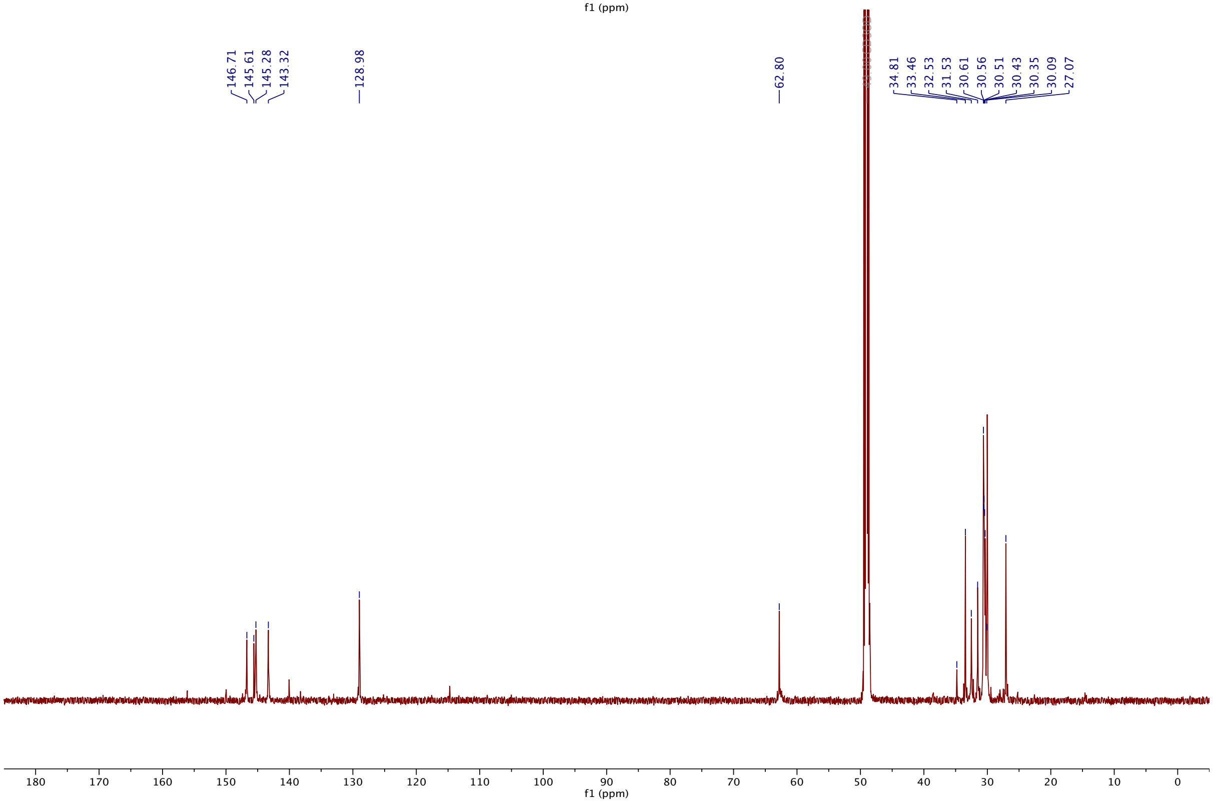

146.71
145.61
145.28
143.32
128.98
62.80
34.81
33.46
32.53
31.53
30.61
30.56
30.51
30.43
30.35
30.09
27.07
180
170
160
150
140
130
120
110
100
90
80
70
60
50
40
30
20
10
0
f1 (ppm)

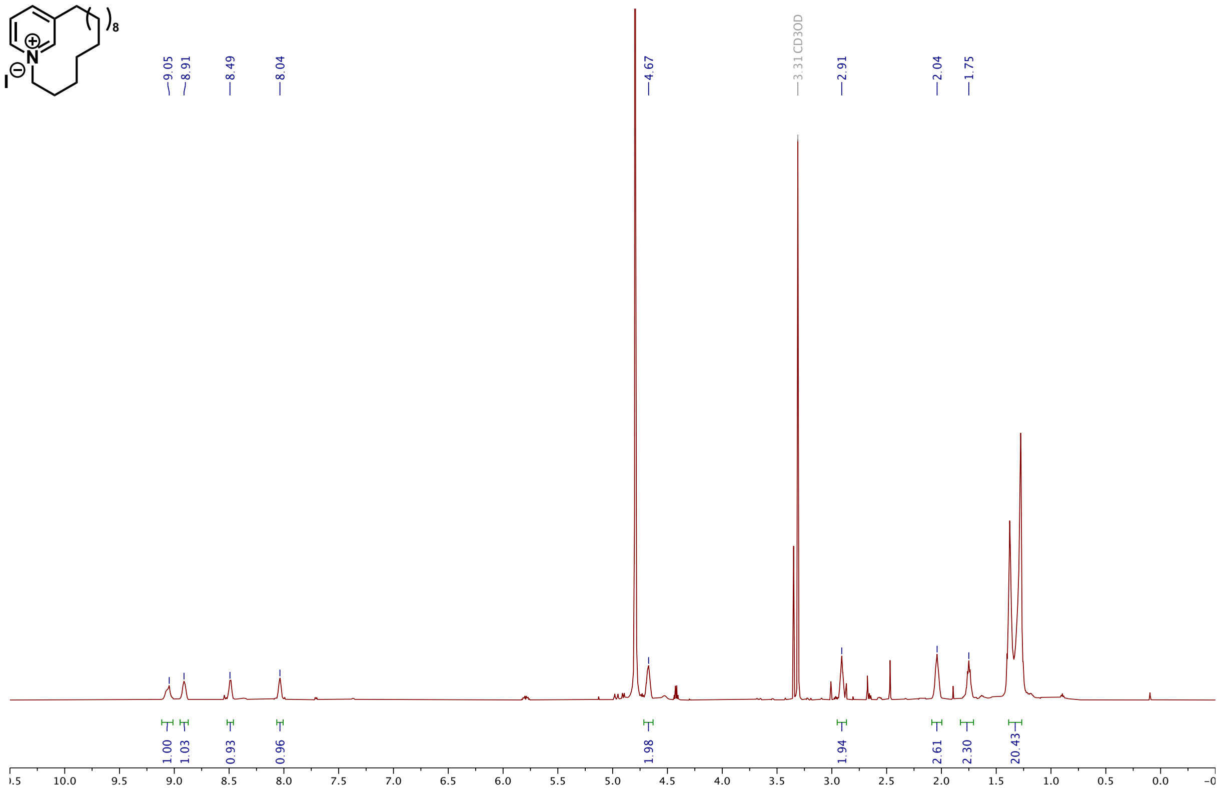
N
I
8
9.05
8.91
8.49
8.04
4.67
3.31 CD3OD
2.91
2.04
1.75
1.00
1.03
0.93
0.96
1.98
1.94
2.61
2.30
20.43
10.0
9.5
9.0
8.5
8.0
7.5
7.0
6.5
6.0
5.5
5.0
4.5
4.0
3.5
3.0
2.5
2.0
1.5
1.0
0.5
0.0
f1 (ppm)

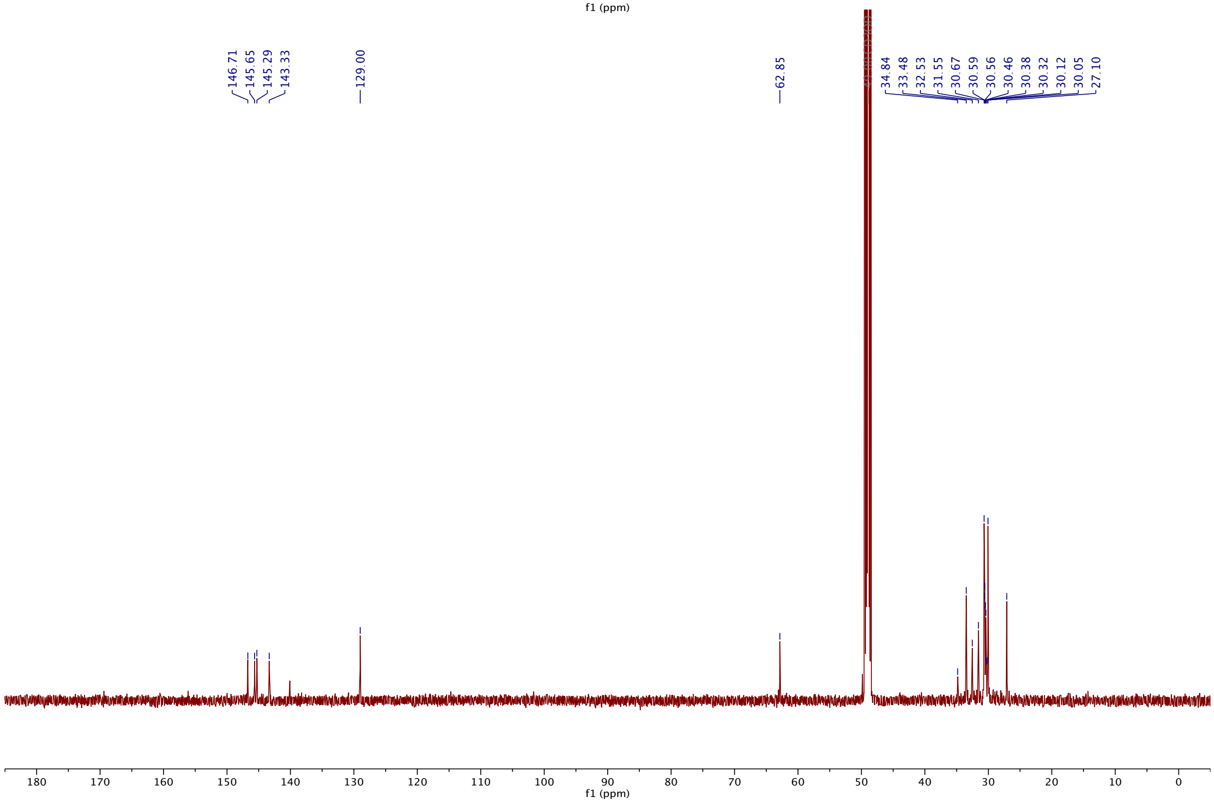
146.71
145.65
145.29
143.33
129.00
62.85
34.84
33.48
32.53
31.55
30.67
30.59
30.56
30.46
30.38
30.32
30.12
30.05
27.10
180
170
160
150
140
130
120
110
100
90
80
70
60
50
40
30
20
10
0
f1 (ppm)

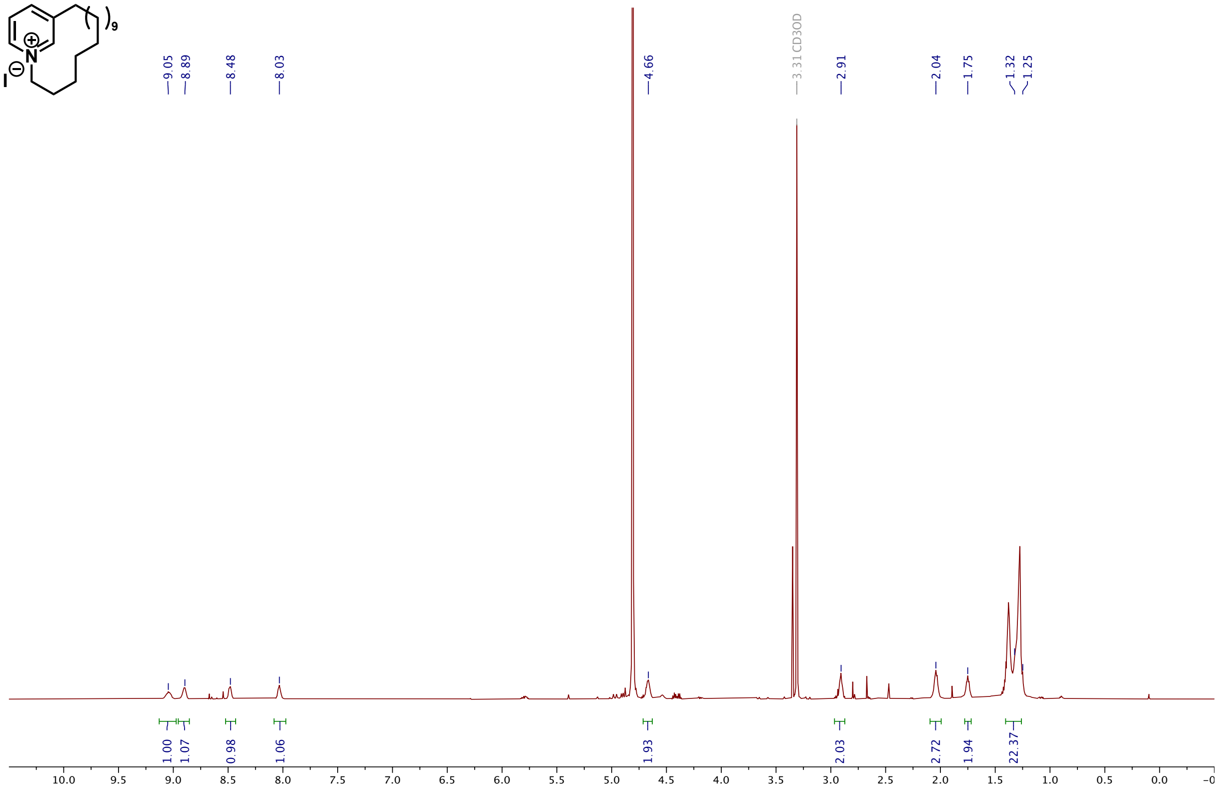
I
N
9
9.05
8.89
8.48
8.03
4.66
3.31 CD3OD
2.91
2.04
1.75
1.32
1.25
1.00
1.07
0.98
1.06
1.93
2.03
2.72
1.94
22.37
10.0
9.5
9.0
8.5
8.0
7.5
7.0
6.5
6.0
5.5
5.0
4.5
4.0
3.5
3.0
2.5
2.0
1.5
1.0
0.5
0.0
f1 (ppm)

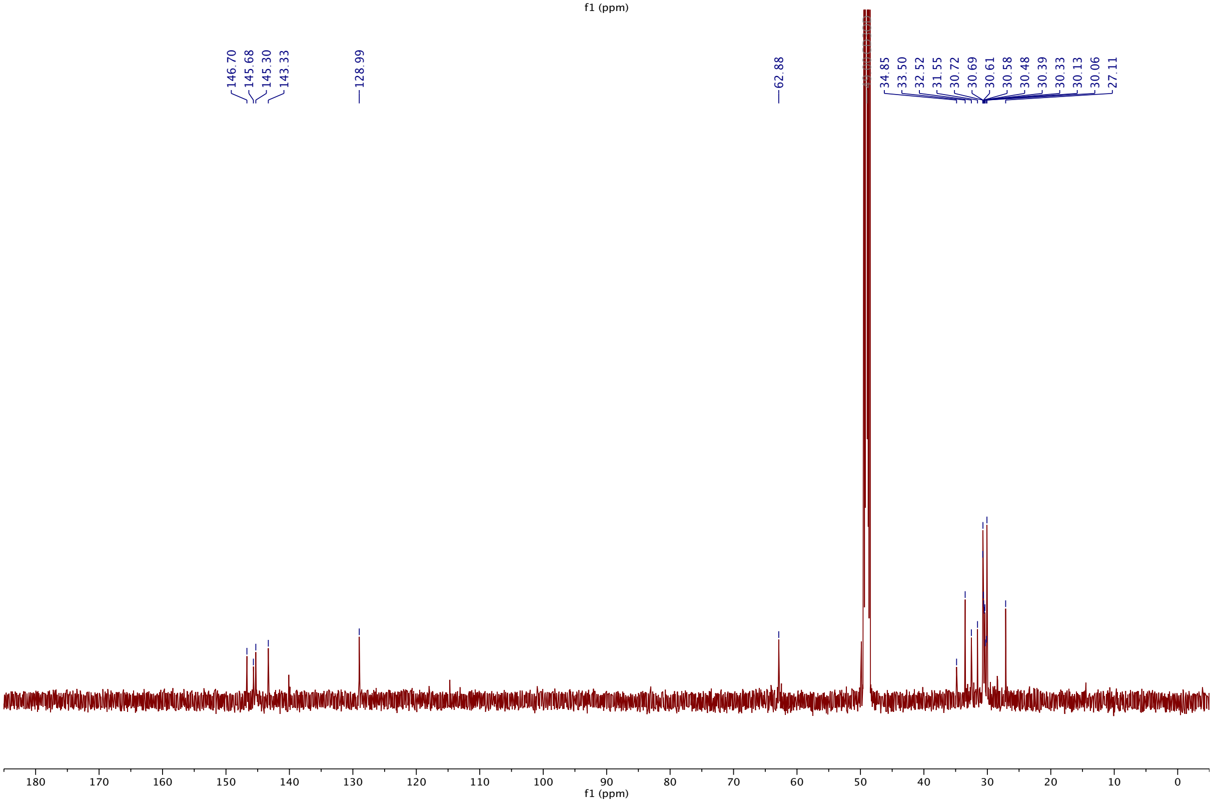
146.70
145.68
145.30
143.33
128.99
62.88
34.85
33.50
32.52
31.55
30.72
30.69
30.61
30.58
30.48
30.39
30.33
30.13
30.06
27.11
180
170
160
150
140
130
120
110
100
90
80
70
60
50
40
30
20
10
0
f1 (ppm)

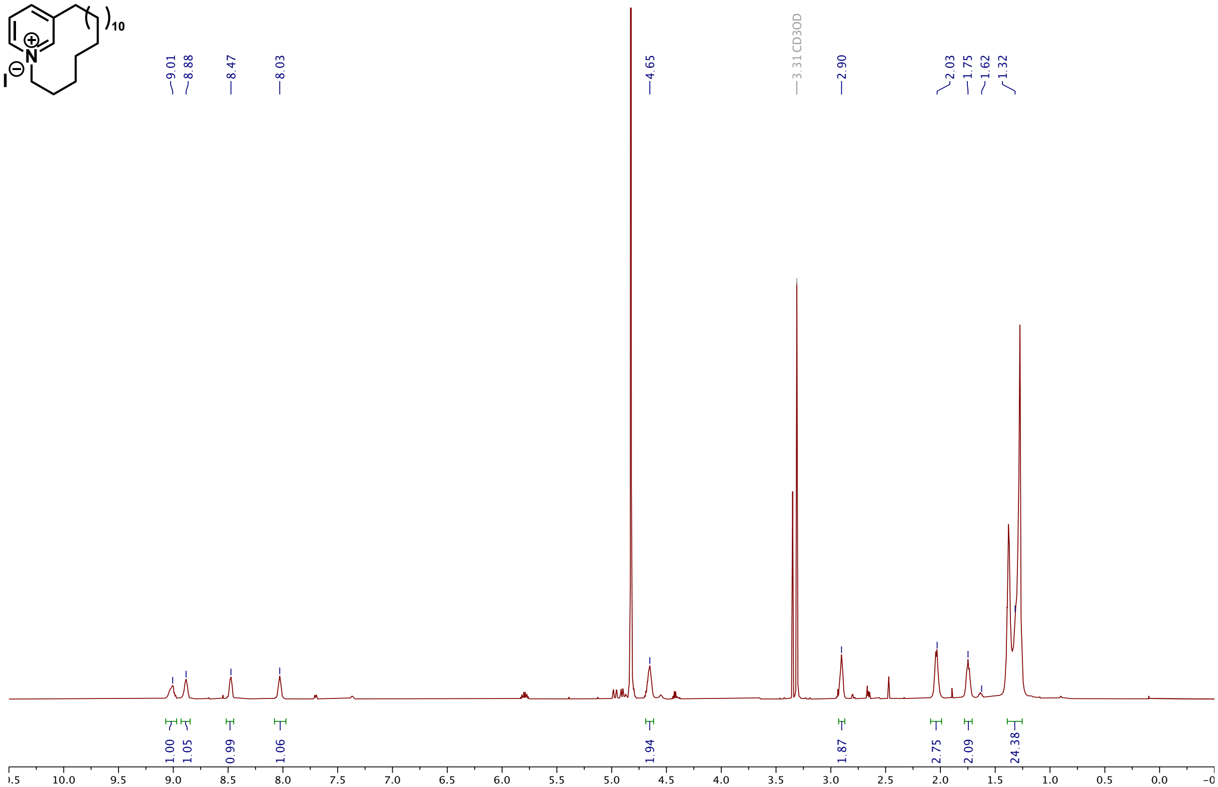
10
I
9.01
8.88
8.47
8.03
4.65
3.31 CD3OD
2.90
2.03
1.75
1.62
1.32
1.00
1.05
0.99
1.06
1.94
1.87
2.75
2.09
24.38
f1 (ppm)

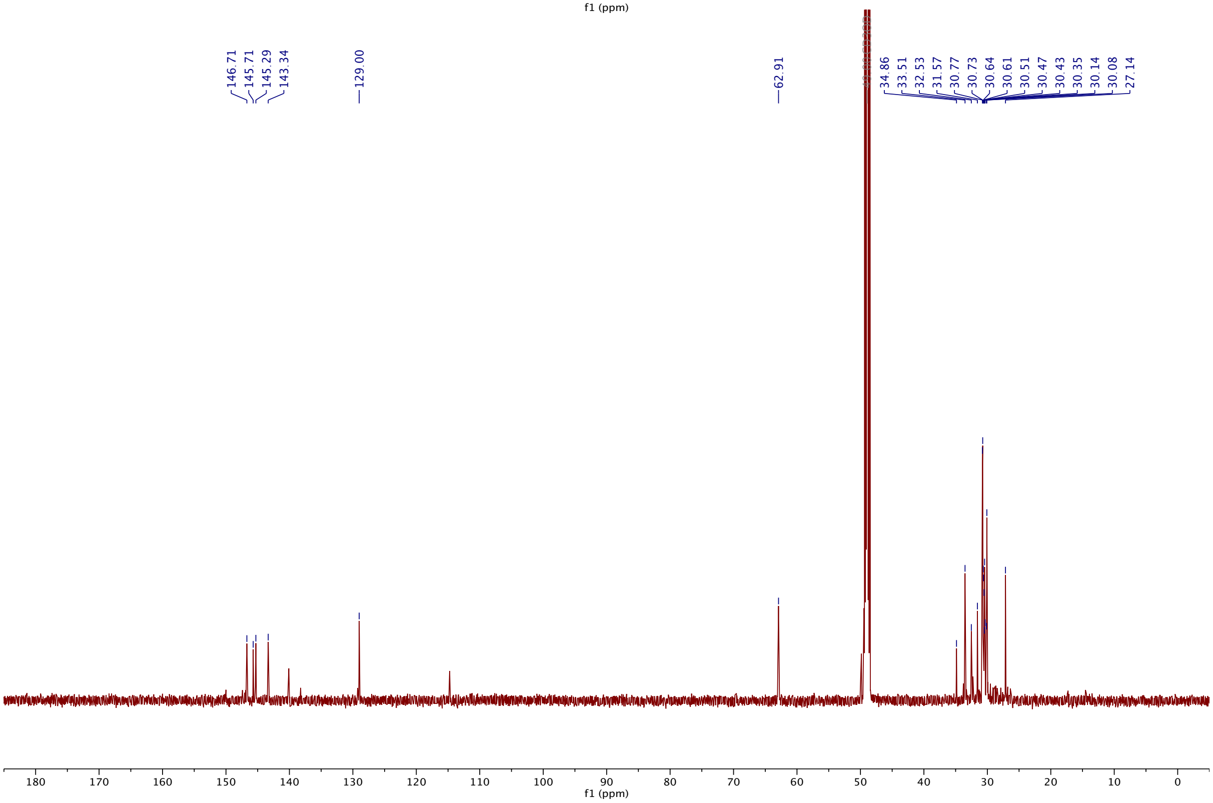
146.71
145.71
145.29
143.34
129.00
62.91
34.86
33.51
32.53
31.57
30.77
30.73
30.64
30.61
30.51
30.47
30.43
30.35
30.14
30.08
27.14
f1 (ppm)

Biology

Bacterial Strains and Culture Conditions

Bacterial strains were acquired as generous gifts from Prof. Bettina Buttaro (Lewis Katz School of Medicine, Temple University). Bacterial cultures of methicillin-susceptible *Staphylococcus aureus* MSSA (SH1000), community-acquired methicillin-resistant *Staphylococcus aureus* CA-MRSA (USA300-0114), hospital-acquired methicillin-resistant *Staphylococcus aureus* HA-MRSA (ATCC 33591), *Enterococcus faecalis* (OG1RF), *Escherichia coli* (MC4100), *Pseudomonas aeruginosa* (PAO1) were grown from freezer stocks for 16 hours at 37 °C, 200 rpm in 10 mL of media (Mueller-Hinton for SH1000, OG1RF, MC4100, and PAO1, Todd Hewitt Broth for USA300-0114 and ATCC 33591). Bacterial cultures of *Streptococcus mutans* (UA159) were grown from a freshly streaked Petri dish containing Todd Hewitt Broth agar for 16 hours at 37 °C statically with 5% CO_2 in 10 mL of media (Todd Hewitt Broth with 5% sucrose)

MIC Assay

Compounds were dissolved in 10% DMSO/90% H_2O to give 1 mM stock solutions, which were serially diluted yielding twelve starting test concentrations ranging from 500 μM to 2.5 μM. Overnight cultures were diluted 1:100 in 5 mL of corresponding fresh media and grown at 37 °C, 200 rpm to predetermined OD_{600} reflecting exponential growth with the exception of UA159 which was grown statically in a CO_2 incubator as described. Bacteria were then diluted in corresponding media to a concentration of 0.004 according to the following equations: (x mL regrow culture)*(OD_{600} reading) = (0.004)*(volume of diluted bacteria culture needed). Then 100 μL was inoculated into each well of U-bottom 96-well plate (BD Biosciences, BD351177)) already containing 100 mL of compound solution, giving final test concentrations of 250 μM to 1.25 μM. Plates were then incubated statically at 37 °C for 72 hours according to previously described growth conditions. The MIC was determined as the concentration of compound completely inhibiting bacterial growth visible to the naked eye based on the highest value of three independent experiments. Aqueous controls included DMSO as a negative control and benzalkonium chloride and cetylpyridinium chloride as positive controls. MIC values are reported as the highest minimum compound concentration required to completely inhibit growth across three independent trials.

Hemolysis Assay

Compounds were dissolved in 10% DMSO/90% H_2O to give 1 mM stock solutions, which were serially diluted with phosphate-buffered saline (PBS) yielding twelve starting test concentrations ranging from 500 μM to 2.5 μM. 1.5 mL of defibrinated sheep blood (Hemostat Labs: DSB030) was centrifuged at 10,000 rpm for 10 minutes. The supernatant was removed, and the blood resuspended in 1 mL of (PBS) and centrifuged again as described above. This process was repeated until the supernatant appeared clear to the naked eye. The clear supernatant was then removed, and the cells resuspended once more in 1 mL of PBS, then diluted 1:20 with PBS. 100 μL was then aliquoted into each well of a U-bottom 96-well plate (BD Biosciences, BD351177) containing the serially diluted compounds giving final test concentrations of 250 μM to 1.25 μM. The plate was then incubated at 37 °C with shaking at 200 rpm for 1 hour after which it was centrifuged at 10,000 rpm for 10 minutes. 100 mL of supernatant from each sample was then transferred to a flat-bottom 96-well plate (Corning 3370) and absorbance measurements taken at 540 nm using a plate reader. The positive control was TritonX (1% by volume, 100% lysis marker) and the negative control was sterile PBS (0% lysis marker). $Lysis_{20}$ values are reported as the lowest minimum concentration required to lyse 20% of red blood cells across three independent trials.

References

1 W. Qu, K. Ploessl, H. Truong, M-P. Kung, H. F. Kung, *Bioorg. Med. Chem. Lett.* **2009**, *19*, 3382-3385.

2 A. J. Boyington, M-L. Y. Riu, N. T. Jui, *J. Am. Chem. Soc.* **2017**, *139*, 6582-6585.

3 C. Timm, T. Mordhorst, M. Köck, *Mar. Drugs.* **2010**, *8*, 483-497.

Evaluating the Effect of Bromination on Indole-Containing Antibiotics

Synthesis

Instrumentation and General Information

All non-aqueous reactions were conducted in flame-dried glassware equipped with a stir bar under an argon atmosphere using HPLC-grade solvents which were dried by passing through activated alumina. Reagents were purchased from Oakwood, TCI America, Sigma-Aldrich, Alfa Aesar, and AK Scientific. Thin-layer chromatography was performed on 250μm SiliCycle silica gel F-254 plates and visualized by fluorescence and/or staining using potassium permanganate, or vanillin stains. Brine refers to saturated aqueous solution of sodium chloride, sat. $NaHCO_3$ refers to a saturated aqueous solution of sodium bicarbonate, sat. $Na_2S_2O_3$ refers to a saturated aqueous solution of sodium thiosulfate and sat. NH_4Cl refers to saturated aqueous solution of ammonium chloride. Organic solutions were concentrated under reduced pressure on a Buchi Rotavapor R3 rotary evaporator. Chromatographic purification was accomplished using a Biotage® flash chromatography purification system or on C18 silica.

^{1}H NMR and ^{13}C NMR spectra were recorded on a Bruker (600 MHz), Inova (500 MHz), Inova (400 MHz), or VNMR (400 MHz) spectrometer, all from the Emory University NMR facility. ^{1}H NMR data were reported in terms of chemical shift (δ ppm relative to tetramethylsilane and with the indicated deuterated solvent as the internal reference), multiplicity, described using the following abbreviations: s (singlet), d (doublet), t (triplet), q (quartet), m (multiplet), br (broad), dd (doublet of doublets), dt (doublet of triplets), etc., coupling constant (Hz), and integration. ^{13}C NMR data were reported in terms of chemical shift. Accurate mass spectra were obtained from a Thermo LTQ-FTMS using APCI techniques. Specific rotations were obtained using a Perkin Elmer Model 341 Polarimeter with a Na/HaI lamp set to 598 nm and a path length of 1 dm. Samples were dissolved in chloroform or acetone, and the polarimeter was zeroed to the solvent before taking each measurement.

Experimental Procedures and Spectral Data

General Procedure A: To a 0.5 M solution of indole (1.00 eq) in Et_2O cooled to 0 °C was added oxalyl chloride (2.0 M in CH_2Cl_2, 1.15 eq) dropwise over 30 minutes. The solution was then stirred for 3 hours at 0 °C then 1 hour at ambient temperature. The reaction mixture was then filtered, and the solid precipitate was washed with Et_2O, dried under vacuum, and used in the next step without further purification.

General Procedure B: To a 1.0 M solution of crude oxoacetyl chloride (1.00 eq) in EtOAc cooled to 0 °C was added a 0.75 M solution of tributyltin hydride in EtOAc. The resulting solution was stirred at 0 °C for 30 minutes then warmed to ambient temperature and stirred an additional 16 hours. Hexane was added and the resulting powder was then collected by filtration. This solid was then washed with a large amount of hexane, dried under vacuum, and used in the next step without further purification.

General Procedure C: To a 0.1 M solution of indole-3-carbaldehyde (1.00 eq) in THF cooled to 0 °C was added NaH (1.20 eq) and the resulting solution stirred at this temperature for 1 hour. Then TsCl (1.05 eq) was added, and the solution then warmed to ambient temperature and stirred for 3 hours. The reaction was quenched with deionized H_2O, extracted with EtOAc (3x), washed with brine (1x), dried over $MgSO_4$, concentrated under reduced pressure, and purified by column chromatography (10-20% EtOAc/hexanes).

General Procedure D: To a 0.1 M solution of methyltriphenylphosphonium bromide (1.30 eq) in THF cooled to 0 °C was added *n*-BuLi (2.0 M in hexane, 1.30 eq) dropwise, and the resulting dark yellow solution stirred for 1 hour at this temperature. The reaction was then cooled to -78 °C and a 1.0 M solution of 1-tosyl-indole (1.00 eq) was then added dropwise. The solution was then warmed to ambient temperature and stirred for 1 hour. The reaction mixture was quenched with sat. NH_4Cl, extracted with EtOAc (3x), washed with brine (1x), dried over $MgSO_4$, concentrated under reduced pressure, and purified by column chromatography (0-20 % EtOAc/hexanes).

General Procedure E: To a 0.1 M solution of alkene (1.00 eq) in 5:1 acetone/H_2O cooled to 0 °C was added K_2OsO_4 (cat.) and NMO (2.0 eq) and the resulting solution was then warmed to ambient temperature and stirred for an additional 16 hours. The reaction was quenched with sat. $NaHCO_3$, extracted with EtOAc (3x), washed with brine (1x), dried over $MgSO_4$, concentrated under reduced pressure, and purified by column chromatography (50-80% EtOAc/hexanes).

General Procedure F: A 0.1 M solution of methane sulfonamide (1.00 eq) and AD-mix-β (1.20 eq) in 1:1 *t*-butyl alcohol/water was stirred at ambient temperature until dissolved. The solution then stirred at 0 °C and stirred until a precipitate formed. Alkene (1.00 eq) was then added, and the solution stirred for 16 hours, quenched with sat. Na_2SO_3 and stirred for an additional hour. The mixture was extracted with EtOAc (3x), washed with brine (1x), dried over $MgSO_4$, concentrated under reduced pressure, and purified by column chromatography (50-80% EtOAc/hexanes).

General Procedure G: To a 0.6 M solution of diol (1.00 eq) in toluene cooled to 0 °C was added PPh_3 (3.00 eq), diethyl azodicarboxylate (3.00 eq), and diphenylphosphoryl azide (3.00 eq). The resulting solution stirred at ambient temperature 16 hours. The solution was then concentrated under reduced pressure and purified by column chromatography (0-5% EtOAc/hexanes).

General Procedure H: To a 0.1 M solution of diazide (1.00 eq) in toluene at ambient temperature was added PPh_3. The resulting solution was then heated under reflux for 30 minutes, then cooled to ambient temperature. H_2O was then added, and the reaction mixture was heated under reflux for 16 hours. The reaction was then cooled to ambient temperature and extracted with 5% HCl. The aqueous phase was washed with Et_2O to get rid of excess PPh_3. The aqueous phase was then basified with 10% NaOH to a pH of 10, extracted with EtOAc (5x), dried over $MgSO_4$, concentrated under reduced pressure, and used in the next step without any further purification.

General Procedure I: To a 0.1 M solution of ketoaldehyde (1.00 eq) in EtOH was added ammonium acetate (7.00 eq) and the solution stirred for 20 hours at ambient temperature. The reaction mixture was then concentrated and recrystallized from CH_2Cl_2. This recrystallized solid was then purified by column chromatography on C18 silica in 30% MeOH/H_2O.

General Procedure J: To a 0.07 M solution of oxoacetaldehyde (1.00 eq) in acetonitrile was added a 0.09 M solution of 1,2-diamine (1.10 eq) in acetonitrile at 0 °C to give a final reaction concentration of 0.04 M. The solution stirred 30 minutes at 0 °C, then N-chlorosuccinimide was added. The reaction was then warmed to ambient temperature and stirred for 16 hours. The reaction mixture was then quenched with $Na_2S_2O_3$ and concentrated, after which $NaHCO_3$ was added followed by filtration. The residue was then resuspended in MeOH and 2 M NaOH (15.0 eq) and heated at 90 °C for 2 hours, then quenched with deionized H_2O. The mixture was then extracted with EtOAc (3x), washed with brine (1x), dried over $MgSO_4$, concentrated under reduced pressure, then purified by column chromatography (0-50% EtOAc/CH_2Cl_2).

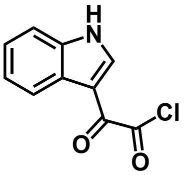

2-(1*H*-indol-3-yl)-2-oxoacetyl chloride 5.01: Following **General Procedure A**, **1*H*-indole** (1.17 g, 10.0 mmol) yielded the title compound as a yellow solid (1.79 g, 86%).

^{1}H NMR (600 MHz, $(CD_3)_2SO$) δ 12.39 (s, 1H), 8.41 (d, *J* = 3.6 Hz, 1H), 8.18 (d, *J* = 6.6 Hz, 1H), 7.55 (dd, *J* = 6.8, 1.5 Hz, 1H), 7.31-7.23 (m, 2H); **^{13}C NMR** (151 MHz, $(CD_3)_2SO$) δ 180.69, 165.16, 137.94, 136.68, 125.54, 123.66, 122.67, 121.11, 112.69, 112.30; **HRMS** (APCI$^+$): Found 208.01647 (+2.36 ppm), $C_{10}H_7NO_2{}^{35}Cl$ (M+H) requires 208.01598.

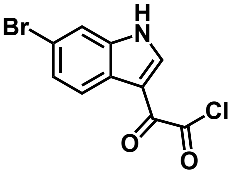

2-(6-bromo-1*H*-indol-3-yl)-2-oxoacetyl chloride 5.02: Following **General Procedure A**, **6-bromo-1*H*-indole** (1.96 g, 10.0 mmol) yielded the title compound a yellow solid (2.53 g, 89%).

^{1}H NMR (600 MHz, $(CD_3)_2SO$) δ 12.47 (s, 1H), 8.45 (d, *J* = 3.7 Hz, 1H), 8.10 (t, *J* = 8.4 Hz, 1H), 7.74 (d, *J* = 1.8 Hz, 1H), 7.41 (d, *J* = 8.4 Hz, 1H); **^{13}C NMR** (151 MHz, $(CD_3)_2SO$) δ 180.65, 164.79, 138.73, 137.58, 125.54, 124.64, 122.75, 116.13, 115.40, 112.26; **HRMS** (APCI$^+$): Found 285.92707 (+0.57 ppm), $C_{10}H_6NO_2{}^{79}Br^{35}Cl$ (M+H) requires 285.9265.

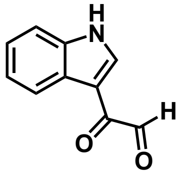

2-(1*H*-indol-3-yl)-2-oxoacetaldehyde 5.03: Following **General Procedure B**, **5.01** (1.79 g, 8.65 mmol) yielded the title compound as a yellow solid (1.15 g, 77%).

^{1}H NMR (600 MHz, $(CD_3)_2SO$) δ 12.35 (s, 1H), 9.58 (s, 1H), 8.42 (d, *J* = 3.3 Hz, 1H), 8.18 (d, *J* = 7.3 Hz, 1H), 7.54 (dd, *J* = 6.8, 1.5 Hz, 1H), 7.27 (pd, *J* = 7.2, 1.5 Hz, 2H); **^{13}C NMR** (151 MHz, $(CD_3)_2SO$) δ 180.76, 165.22, 137.95, 136.67, 125.57, 123.66, 122.67, 121.11, 112.68, 112.31; **HRMS** (APCI$^+$): Found 174.05542 (+0.46 ppm), $C_{10}H_8NO_2$ (M+H) requires 174.05496.

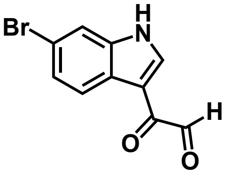

2-(6-bromo-1*H*-indol-3-yl)-2-oxoacetaldehyde 5.04: Following **General Procedure B**, **5.02** (2.53 g, 8.88 mmol) yielded the title compound as a green-yellow solid (1.92 g, 87%).

^{1}H NMR (600 MHz, $(CD_3)_2SO$) δ 12.41 (s, 1H), 9.53 (s, 1H), 8.45 (d, *J* = 3.2 Hz, 1H), 8.10 (t, *J* = 8.5 Hz, 1H), 7.74 (d, *J* = 1.8, 0.6 Hz, 1H), 7.41 (dd, *J* = 8.5, 1.8 Hz, 1H); **^{13}C NMR** (151 MHz, $(CD_3)_2SO$) δ 180.75, 164.88, 138.75, 137.57, 125.55, 124.63, 122.75, 116.14, 115.39, 112.27; **HRMS** (APCI$^+$): Found 251.96599 (+2.07 ppm), $C_{10}H_7NO_2{}^{79}Br$ (M+H) requires 251.96547.

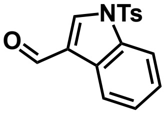

1-tosyl-1*H*-indole-3-carbaldehyde 5.05: Following **General Procedure C**, **1*H*-indole-3-carbaldehyde** (2.18 g, 15.0 mmol) yielded the title compound as an off-white solid (3.73 g, 83%).

^{1}H NMR (400 MHz, $CDCl_3$) δ 10.09 (s, 1H), 8.27-8.24 (m, 1H), 7.95 (dt, *J* = 8.3, 1.2 Hz, 1H), 7.89-7.81 (m, 2H), 7.44-7.33 (m, 2H), 2.37 (s, 3H); **^{13}C NMR** (101 MHz, $CDCl_3$) δ 185.52, 146.31, 136.38, 130.46, 127.37, 126.44, 126.40, 125.19, 122.74, 122.47, 113.37, 21.81; **HRMS** (APCI$^+$): Found 300.06905 (+0.53 ppm), $C_{16}H_{14}NO_3{}^{32}S$ (M+H) requires 300.06889.

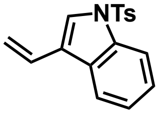

1-tosyl-3-vinyl-1*H*-indole 5.06: Following **General Procedure D**, **5.05** (3.73 g, 12.5 mmol) yielded the title compound as an off-white solid (2.87 g, 77%).

^{1}H NMR (400 MHz, $CDCl_3$) δ 7.99 (dt, *J* = 8.2, 1.0 Hz, 1H), 7.79-7.72 (m, 3H), 7.60 (s, 1H), 7.36-7.27 (m, 1H), 7.25-7.18 (m, 2H), 6.77 (ddd, *J* = 17.9, 11.4, 0.8 Hz, 1H), 5.79 (dd, *J* = 17.9, 1.6, Hz, 1H), 5.35 (dd, *J* = 11.3, 1.2, Hz, 1H); **^{13}C NMR** (101 MHz, $CDCl_3$) δ 145.18, 135.60, 135.21, 130.06, 129.12, 127.69, 126.99, 125.04, 124.20, 123.64, 121.06, 120.55, 115.47, 113.85, 21.72; **HRMS** (APCI$^+$): Found 298.08951 (-0.40 ppm), $C_{17}H_{16}NO_2{}^{32}S$ (M+H) requires 298.08963.

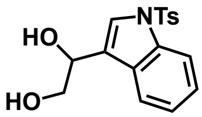

1-(1-tosyl-1*H*-indol-3-yl)ethane-1,2-diol 5.07: Following **General Procedure E**, **5.06** (1.49 g, 5.00 mmol) yielded the title compound as a white solid (1.31 g, 79%).

^{1}H NMR (400 MHz, CDCl$_3$) δ 7.97 (dt, J = 8.3, 0.9 Hz, 1H), 7.80-7.72 (m, 2H), 7.60 (d, J = 1.0 Hz, 1H), 7.58-7.55 (m, 1H), 7.32 (ddd, J = 8.4, 7.2, 1.3 Hz, 1H), 7.26-7.15 (m, 3H) 5.05 (ddd, J = 7.7, 3.5, 1.0 Hz, 1H), 3.92-3.74 (m, 2H), 2.31 (s, 3H); **^{13}C NMR** (101 MHz, CDCl$_3$) δ 145.24, 135.39, 135.15, 130.15, 130.06, 128.86, 126.99, 125.09, 123.62, 123.42, 122.01, 120.16, 113/87, 68.70, 66.58, 21.69; **HRMS** (APCI$^-$): Found 330.08031 (-0.75 ppm), $C_{17}H_{16}NO_4{}^{32}S$ (M-H) requires 330.08055.

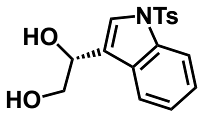

(*R*)- 1-(1-tosyl-1*H*-indol-3-yl)ethane-1,2-diol 5.08: Following **General Procedure F**, **5.06** (3.56 g, 12.0 mmol) yielded the title compound as a white solid (3.34 g, 84%).

^{1}H NMR (400 MHz, CDCl$_3$) δ 7.98 (dt, J = 8.3, 0.9 Hz, 1H), 7.81-7.73 (m, 2H), 7.60 (t, J = 1.4 Hz, 1H), 7.58 (dd, J = 1.3, 0.8 Hz, 1H), 7.33 (ddd, J = 8.4, 7.2, 1.3 Hz, 1H), 7.27-7.17 (m, 3H) 5.06 (ddd, J = 7.6, 3.6, 1.0 Hz, 1H), 3.94-3.77 (m, 2H), 2.33 (s, 3H); **^{13}C NMR** (101 MHz, CDCl$_3$) δ 145.25, 135.42, 135.20, 130.08, 128.85, 127.01, 125.11, 123.63, 123.43, 121.99, 120.16, 113.90, 68.72, 66.59, 21.71; **HRMS** (APCI$^-$): Found 330.08015 (-0.40 ppm), $C_{17}H_{16}NO_4{}^{32}S$ (M-H) requires 330.08055.

*Optical rotation of sample matched reported optical rotation; **$[\alpha]^{25}_{D}$** - 45.5 (c = 1.03 in CHCl$_3$).

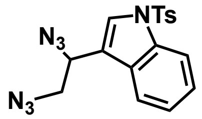

3-(1,2-diazidoethyl)-1-tosyl-1*H*-indole 5.09: Following **General Procedure G**, **5.07** (828 mg, 2.50 mmol) yielded the title compound a clear oil (904 mg, 95%).

^{1}H NMR (400 MHz, CDCl$_3$) δ 7.99 (dt, J = 8.3, 0.9 Hz, 1H), 7.78-7.76 (m, 2H), 7.65 (s, 1H), 7.57 (dd, J = 7.9, 0.9 Hz, 1H), 7.58-7.51 (m, 1H), 7.41-7.34 (m, 5H), 7.30-7.22 (m, 9H), 4.87 (ddd, J = 7.6, 5.0, 0.9 Hz, 1H), 3.67-3.60-3 (m, 2fH), 2.35 (s, 3H); **^{13}C NMR** (101 MHz, CDCl$_3$) δ 145.42, 128.24, 126.91, 126.19, 125.67, 125.52, 124.73, 123.74, 119.64, 117.48, 115.39, 114.00, 58.28, 54.51, 21.60; **HRMS** (ESI$^+$): Found 404.0901 (+0.21 ppm), $C_{17}H_{15}N_7O_2{}^{32}S^{23}Na$ (M+Na) requires 404.09001.

*Sample was carried through with residual triphenylphosphine.

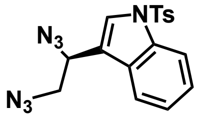

(*S*)-3-diazidoethyl)-1-tosyl-1*H*-indole 5.10: Following **General Procedure G**, **5.08** (1.99g, 6.00 mmol) yielded the title compound as a clear oil (1.88 g, 82%).

^{1}H NMR (500 MHz, $CDCl_3$) δ 7.99 (dt, *J* = 8.4, 1.0 Hz, 1H), 7.78-7.74 (m, 2H), 7.66 (s, 1H), 7.56 (dd, *J* = 7.9, 1.0 Hz, 1H), 7.58-7.51 (m, 1H), 7.39-7.31 (m, 3H), 7.28-7.18 (m, 6H), 4.86 (ddd, *J* = 7.6, 5.0, 0.9 Hz, 1H), 3.66-3.57-3 (m, 2fH), 2.35 (s, 3H); **^{13}C NMR** (126 MHz, $CDCl_3$) δ 145.45, 128.31, 126.95, 126.20, 125.69, 125.56, 124.80, 123.78, 119.68, 117.55, 115.42, 114.06, 58.34, 54.59, 21.62; **HRMS** (APCI$^-$): Found 380.09284 (-1.79 ppm), $C_{17}H_{14}N_7O_2{}^{32}S$ (M-H) requires 380.09352.

*Sample was carried through with residual triphenylphosphine.

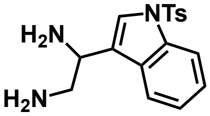

1-(1-tosyl-1*H*-indol-3-yl)ethane-1,2-diamine 5.11: Following **General Procedure H**, **5.09** (618 mg, 1.62 mmol) yielded the title compound as a yellow foam (329 mg, 62%).

^{1}H NMR (600 MHz, $CDCl_3$) δ 7.98 (d, *J* = 9.7 Hz, 1H), 7.78-7.74 (m, 2H), 7.58 (d, *J* = 7.7 Hz, 1H), 7.55 (s, 1H), 7.30 (q, *J* = 7.7 Hz, 1H), 7.25-7.18 (m, 3H), 4.61 (t, *J* = 6.8 Hz, 0.5H), 4.28 (t, *J* = 5.4 Hz, 0.5H), 3.13 (dd, *J* = 12.8, 4.2 Hz, 1H), 2.94 (dd, *J* = 12.7, 7.4 Hz, 1H), 2.45 (br s, 4H), 2.33 (s, 3H); **^{13}C NMR** (151 MHz, $CDCl_3$) δ 145.12, 135.65, 135.31, 130.04, 129.25, 127.00, 125.06, 123.33, 123.06, 120.08, 119.99, 114.01, 50.08, 47.50, 21.69; **HRMS** (ESI$^+$): Found 353.13189 (+2.27 ppm), $C_{17}H_{20}N_3O_2\ {}^{32}S^{23}Na$ (M+H+Na) requires 353.41436.

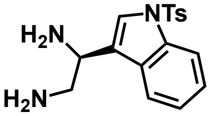

(*S*)-1-(1-tosyl-1*H*-indol-3-yl)ethane-1,2-diamine 5.12: Following **General Procedure H**, **5.10** (1.64 g, 4.30 mmol) yielded the title compound as a yellow foam (852 mg, 60%).

^{1}H NMR (500 MHz, $CDCl_3$) δ 7.98 (d, *J* = 8.3 Hz, 1H), 7.78-7.72 (m, 2H), 7.56 (d, *J* = 7.8 Hz, 1H), 7.54 (s, 1H), 7.32-7.28 (m, 1H), 7.23-7.17 (m, 3H), 4.23 (t, *J* = 5.6 Hz, 1H), 3.10-3.04 (m, 1H), 2.93-2.87 (m, 1H), 2.31 (s, 3H); **^{13}C NMR** (126 MHz, $CDCl_3$) δ 145.06, 135.65, 130.00, 129.35, 126.94, 124.98, 123.26, 123.00, 120.00, 113.99, 50.53, 47.88, 21.66; **HRMS** (APCI$^-$): Found 328.11246 (-0.19 ppm), $C_{17}H_{18}N_3O_2{}^{32}S$ (M-H) requires 328.11252.

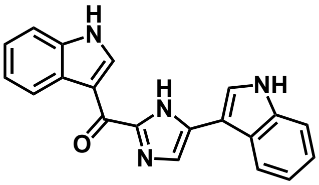

(5-(1-*H*-indol-3-yl)-1*H*-imidazol-2-yl)(1*H*-indol-3-yl)methanone (Topsentin A) 5.13: Following **General Procedure I**, **2-(1*H*-indol-3-yl)-2-oxoacetaldehyde (X)** (173 mg, 1.00 mmol) yielded the title compound as a yellow solid (118 mg, 72%).

^{1}H NMR (600 MHz, $(CD_3)_2SO$) δ 12.51 (br s, 1H), 11.65 (br s, 1H), 8.88 (s, 1H), 8.33 (d, *J* = 6.0 Hz, 1H), 8.11 (s, 1H), 8.03 (*d*, J = 5.2 Hz 1H), 8.02 (s, 1H), 7.60 (d, *J* = 7.0 Hz, 1H), 7.51 (d, *J* = 7.8 Hz 1H), 7.34-7.29 (m, 2H), 7.23 (t, *J* = 7.5 Hz, 1H), 7.19 (t, *J* = 7.4 Hz, 1H); **HRMS** ($APCI^+$): Found 327.1243 (+0.82 ppm), $C_{20}H_{15}N_4O$ (M+H) requires 327.12404.

*Further HPLC purification required for biological experiments.

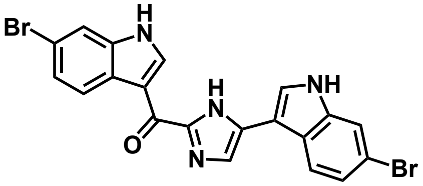

(6-bromo-1*H*-indol-3-yl)(5-(6-bromo-1*H*-indol-3-yl)-1*H*-imidazol-2-yl)methanone (Dibromodeoxytopsentin) 5.14: Following **General Procedure I**, **2-(6-bromo-1*H*-indol-3-yl)-2-oxoacetaldehyde (X)** (250 mg, 1.00 mmol) yielded the title compound as a yellow solid (150 mg, 62%).

^{1}H NMR (600 MHz, $(CD_3)_2SO$) δ 12.49 (br s, 1H), 11.69 (br s, 1H), 8.95 (s, 1H), 8.25 (d, *J* = 8.4 Hz, 1H), 8.08 (s, 1H), 8.01-7.99 (m, 2H), 7.79 (s, 1H), 7.69 (s, 1H), 7.44 (d, *J* = 8.4 Hz, 1H), 7.29 (d, *J* = 8.5 Hz, 1H); **HRMS** ($APCI^+$): Found 482.94596 (+1.85 ppm), $C_{20}H_{13}N_4O^{79}Br_2$ (M+H) requires 482.94506.

*Further HPLC purification required for biological experiments.

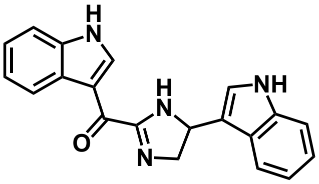

5-(1*H*-indol-3-yl)-4,5-dihydro-1*H*-imidazol-2-yl)(1*H*-indol-3-yl)methanone (Topsentin D) 5.15: Following **General Procedure J**, **2-(1*H*-indol-3-yl)-2-oxoacetaldehyde (5.03)** (434 mg, 2.51 mmol) and **1-(1-tosyl-1*H*-indol-3-yl)ethane-1,2-diamine (5.11)** (907 mg, 2.76 mmol) yielded the title compound as a dark yellow solid (319 mg, 35%).

^{1}H NMR (400 MHz, CD_3OD) δ 8.50 (s, 1H), 8.34-8.28 (m, 1H), 7.63 (d, *J* = 7.9 Hz, 1H), 7.49-7.44 (m, 1H), 7.38 (d, *J* = 8.1 Hz, 1H), 7.29-7.24 (m, 2H), 7.12 (ddd, *J* = 8.3, 7.1, 1.3 Hz, 1H), 7.02 (ddd, *J* = 8.1, 7.1, 1.1 Hz, 1H), 5.47 (dd, *J* = 11.4, 8.5 Hz, 1H), 4.25 (t, *J* = 11.8 Hz, 1H), 3.92 (dd, *J* = 12.2, 8.6 Hz, 1H); **^{13}C NMR** (101 MHz, CD_3OD) δ 181.89, 164.60, 139.39, 138.85, 138.43, 127.44, 126.82, 124.91, 123.84, 123.41, 122.96, 122.71, 120.04, 119.90, 118.07, 115.84, 113.15, 112.63, 56.04, 29.53; **HRMS** (APCI$^-$): Found 329.13981 (+0.12 ppm), $C_{20}H_{17}N_4O$ (M+H) requires 329.13969.

*Further HPLC purification required for biological experiments.

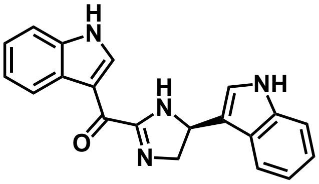

(*S*)-5-(1*H*-indol-3-yl)-4,5-dihydro-1*H*-imidazol-2-yl)(1*H*-indol-3-yl)methanone (Topsentin D) 5.16: Following **General Procedure J**, **2-(1*H*-indol-3-yl)-2-oxoacetyl chloride (5.03)** (788 mg, 1.63 mmol) yielded the title compound as an off-white solid (26 mg, 32%).

^{1}H NMR (400 MHz, CD_3OD) δ 8.49 (s, 1H), 8.33-8.29 (m, 1H), 7.63 (d, *J* = 7.9 Hz, 1H), 7.49-7.44 (m, 1H), 7.38 (d, *J* = 8.1 Hz, 1H), 7.29-7.24 (m, 2H), 7.12 (ddd, *J* = 8.3, 7.1, 1.3 Hz, 1H), 7.02 (ddd, *J* = 8.1, 7.1, 1.1 Hz, 1H), 5.47 (dd, *J* = 11.4, 8.5 Hz, 1H), 4.25 (t, *J* = 11.8 Hz, 1H), 3.92 (dd, *J* = 12.1, 8.5 Hz, 1H); **^{13}C NMR** (101 MHz, CD_3OD) δ 181.56, 164.54, 139.39, 138.84, 138.44, 127.39, 126.77, 124.95, 123.88, 123.49, 122.95, 122.73, 120.08, 119.86, 117.86, 115.81, 113.17, 112.65, 61.53, 20.85; **HRMS** (APCI$^-$): Found 328.11246 (-0.19 ppm), $C_{20}H_{15}N_4O$ (M-H) requires 328.11252.

*Yield based on using 120 mg of tosylated precursor.

*Further HPLC purification required for biological experiments.

^{1}H NMR and ^{13}C NMR Spectra

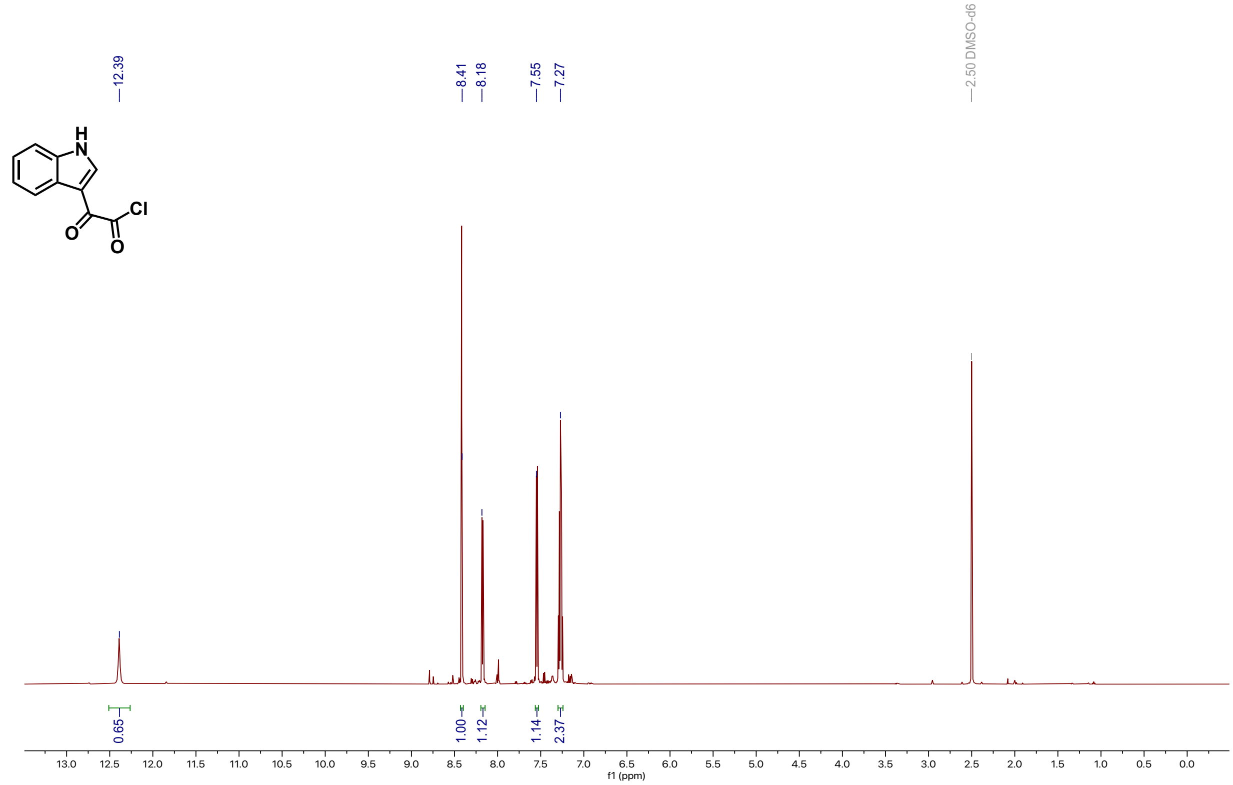

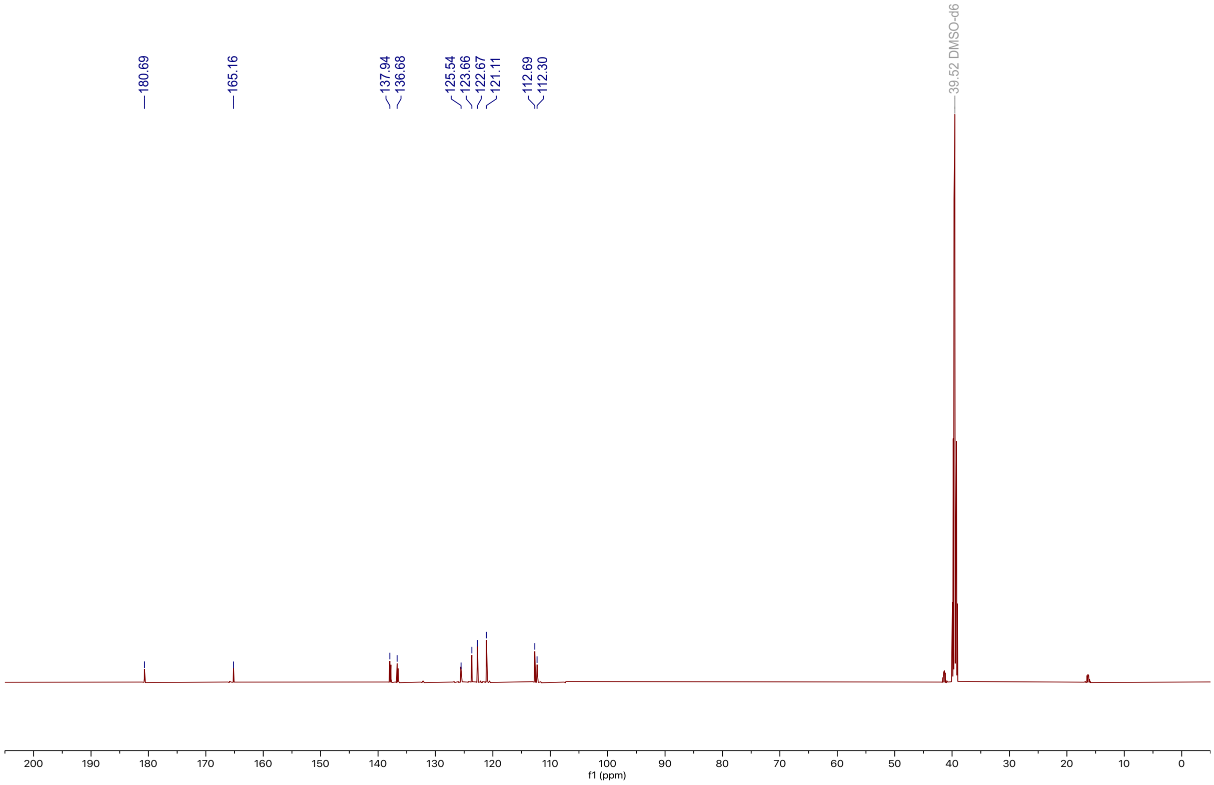

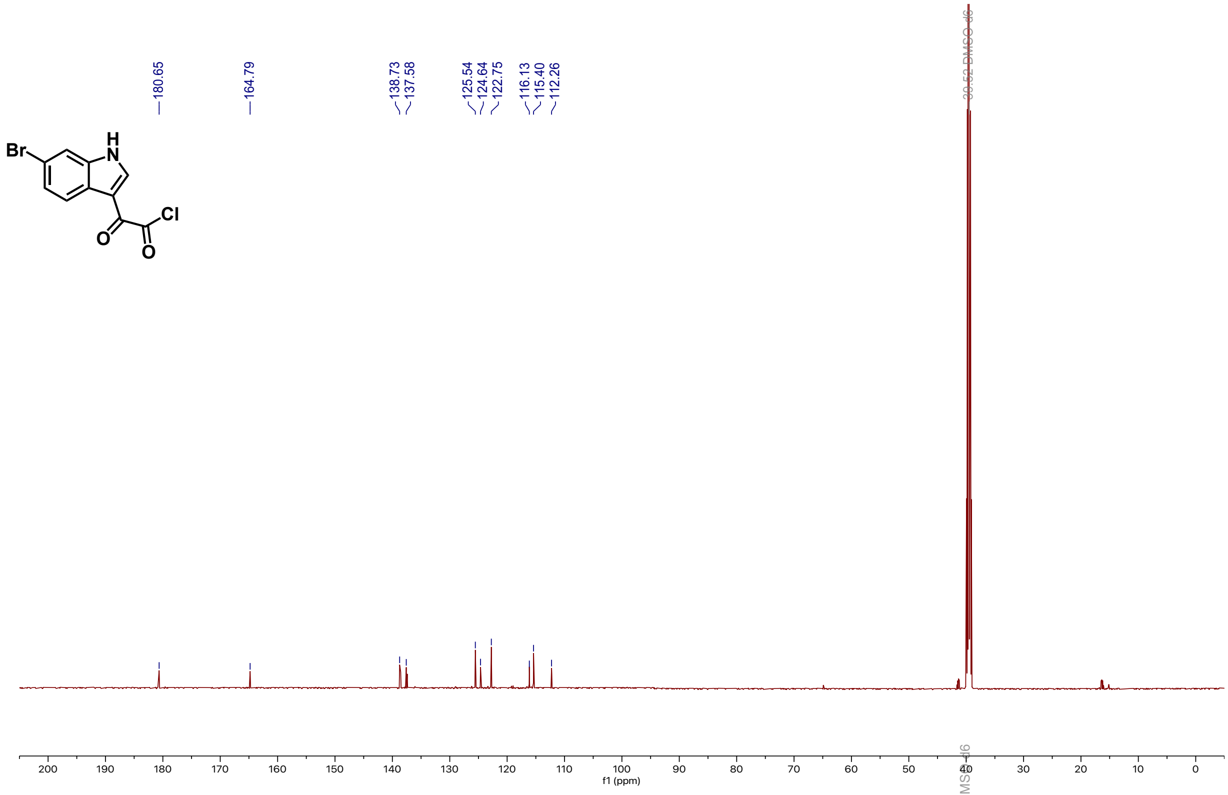

Br
H
N
Cl
O
O
180.65
164.79
138.73
137.58
125.54
124.64
122.75
116.13
115.40
112.26
39.52 DMSO-d6
200
190
180
170
160
150
140
130
120
110
100
90
80
70
60
50
40
30
20
10
0
f1 (ppm)

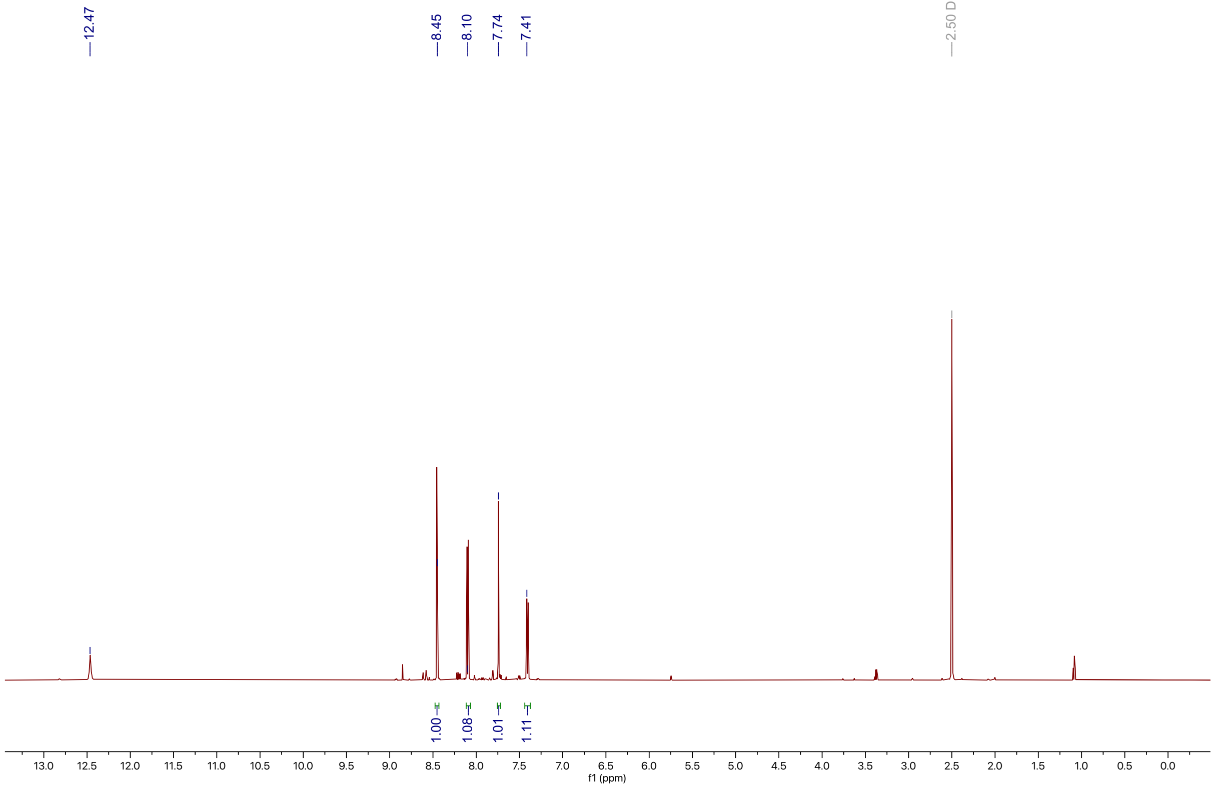

12.47
8.45
8.10
7.74
7.41
2.50 DMSO-d6
1.00
1.08
1.01
1.11
13.0
12.5
12.0
11.5
11.0
10.5
10.0
9.5
9.0
8.5
8.0
7.5
7.0
6.5
6.0
5.5
5.0
4.5
4.0
3.5
3.0
2.5
2.0
1.5
1.0
0.5
0.0
f1 (ppm)

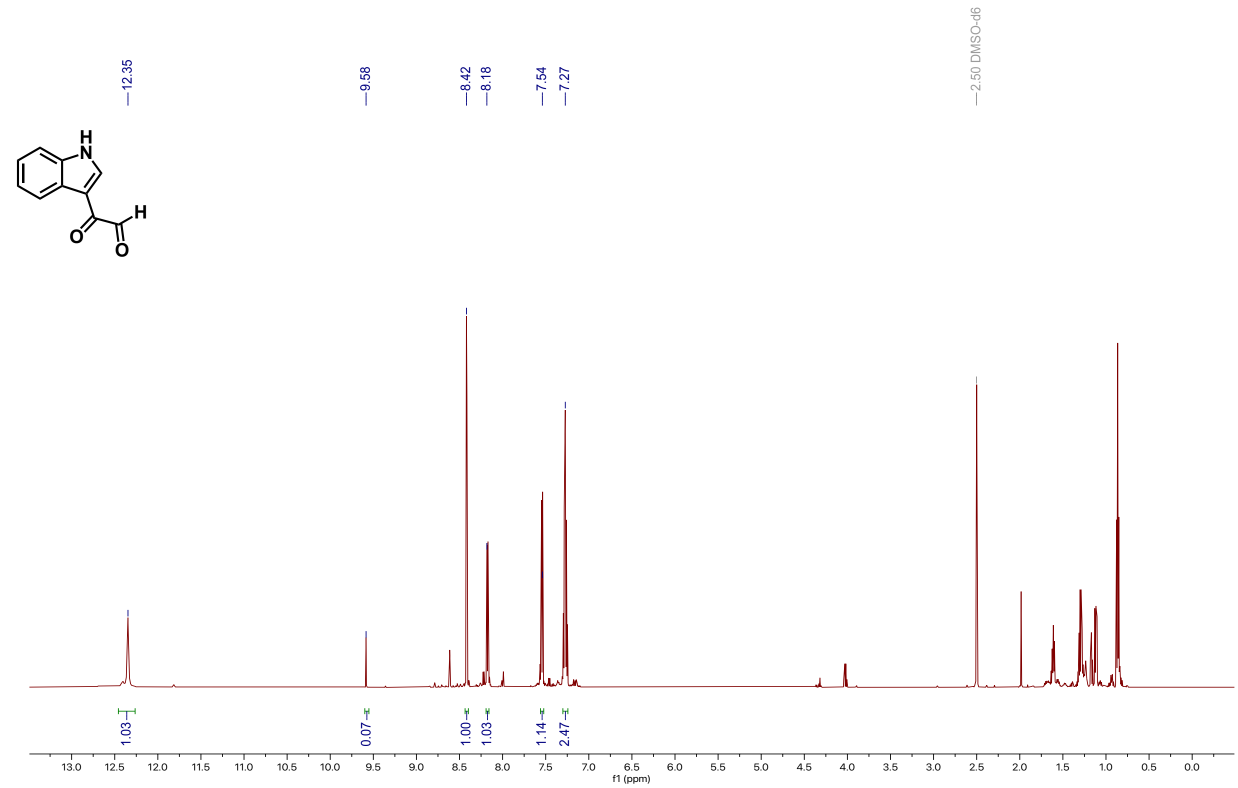
H
N
O
H
O
12.35
9.58
8.42
8.18
7.54
7.27
2.50 DMSO-d6
1.03
0.07
1.00
1.03
1.14
2.47
13.0 12.5 12.0 11.5 11.0 10.5 10.0 9.5 9.0 8.5 8.0 7.5 7.0 6.5 6.0 5.5 5.0 4.5 4.0 3.5 3.0 2.5 2.0 1.5 1.0 0.5 0.0
f1 (ppm)

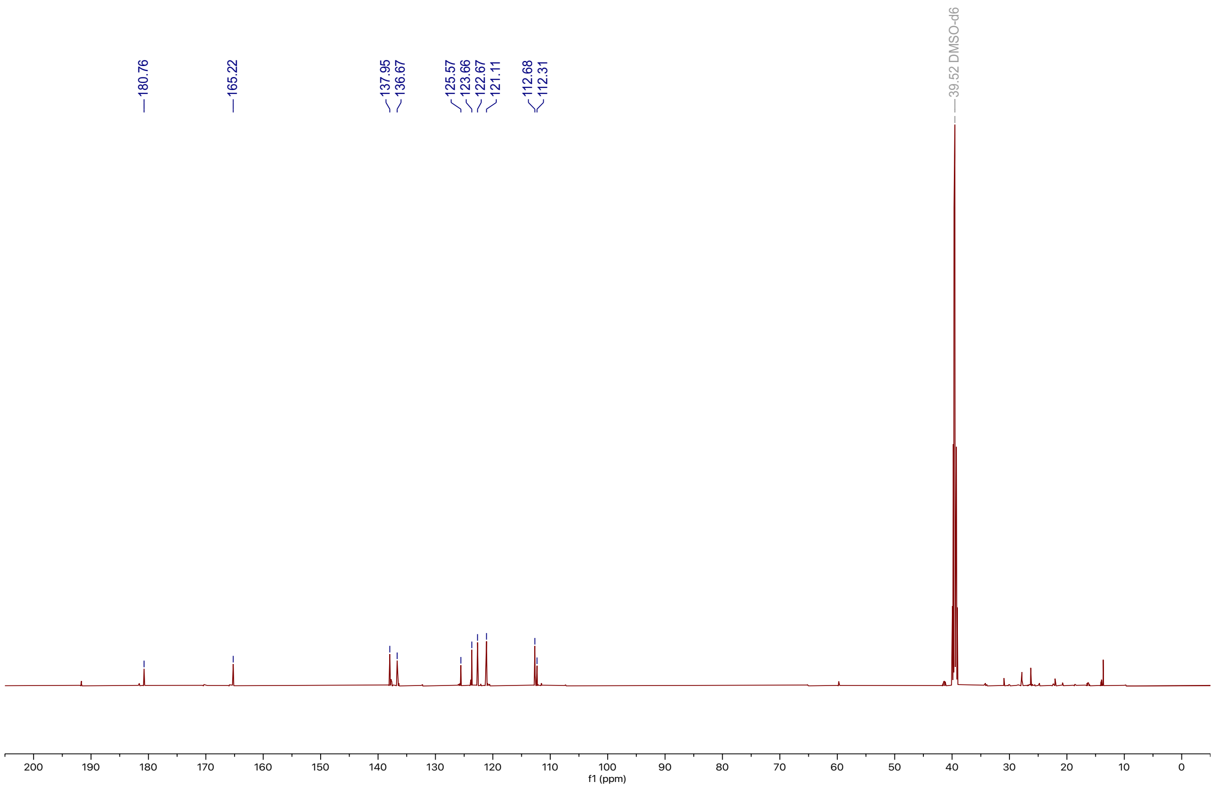
180.76
165.22
137.95
136.67
125.57
123.66
122.67
121.11
112.68
112.31
39.52 DMSO-d6
200 190 180 170 160 150 140 130 120 110 100 90 80 70 60 50 40 30 20 10 0
f1 (ppm)

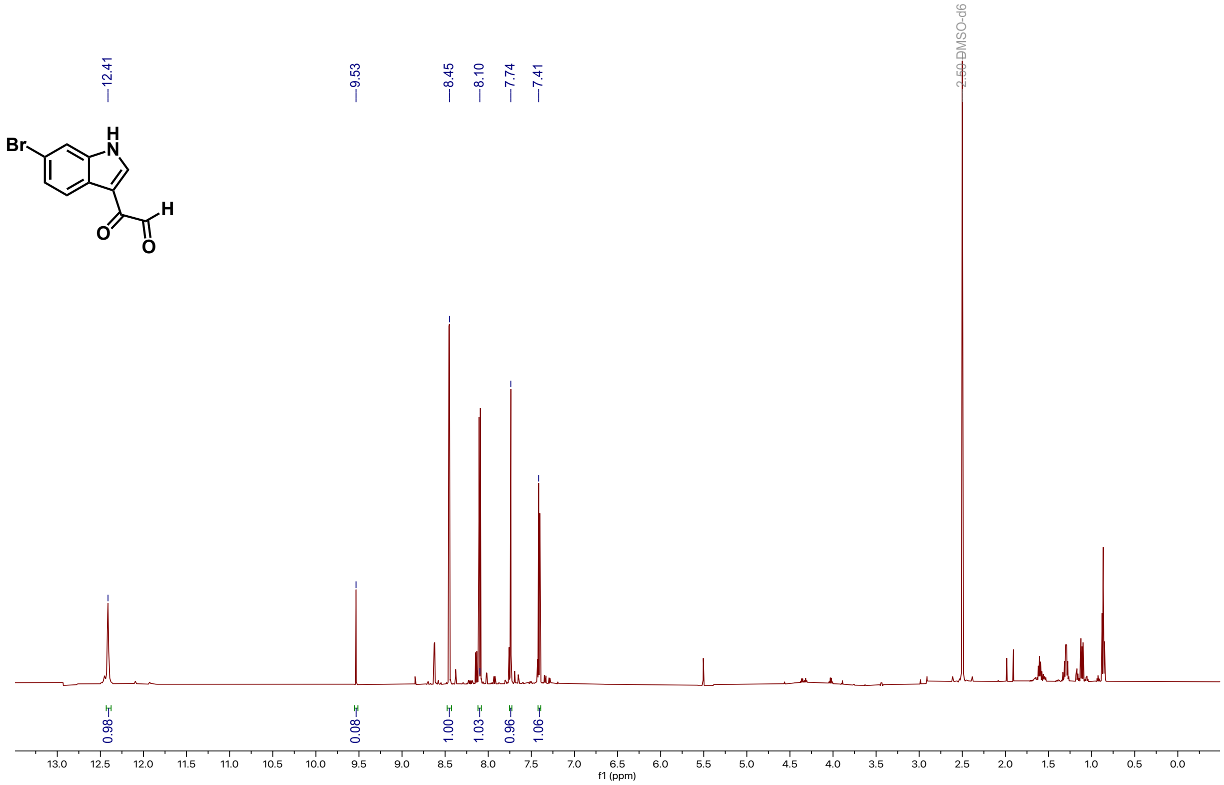
12.41
9.53
8.45
8.10
7.74
7.41
2.50 DMSO-d6
Br
H
N
O
H
O
0.98
0.08
1.00
1.03
0.96
1.06
13.0 12.5 12.0 11.5 11.0 10.5 10.0 9.5 9.0 8.5 8.0 7.5 7.0 6.5 6.0 5.5 5.0 4.5 4.0 3.5 3.0 2.5 2.0 1.5 1.0 0.5 0.0
f1 (ppm)

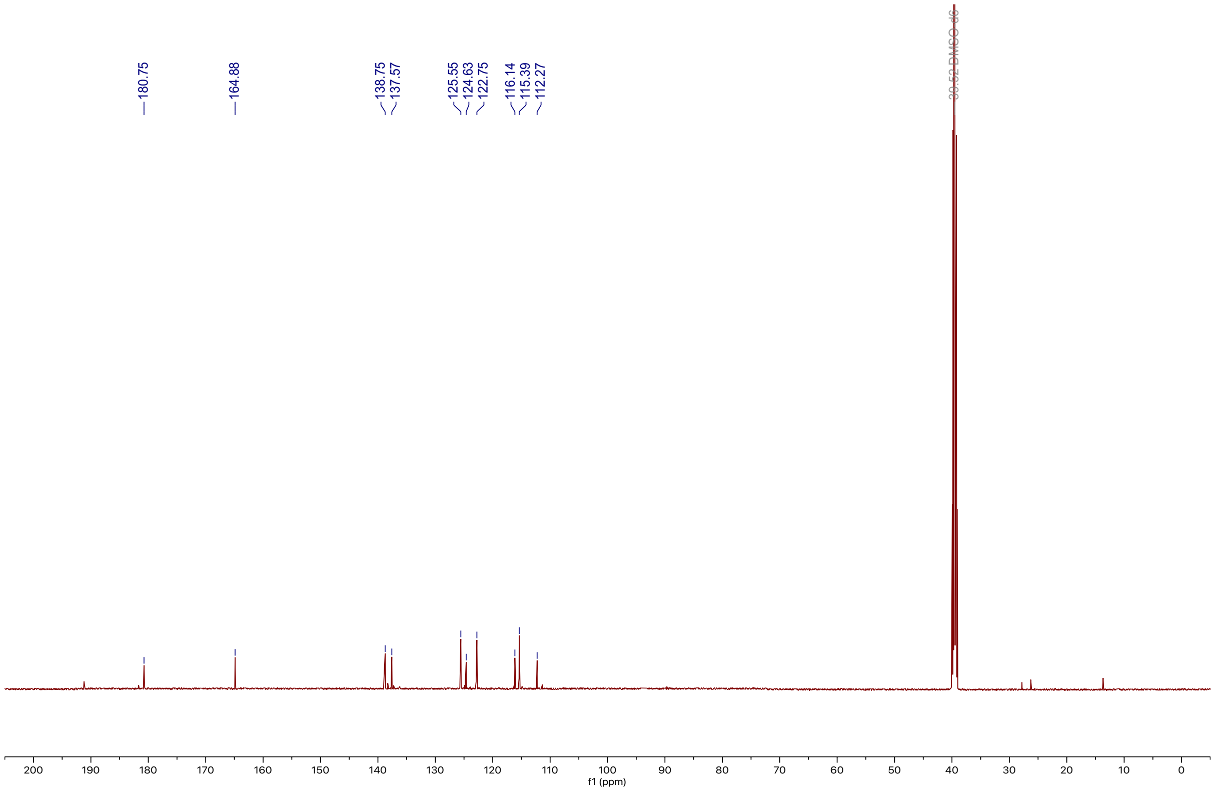
180.75
164.88
138.75
137.57
125.55
124.63
122.75
116.14
115.39
112.27
39.52 DMSO-d6
200 190 180 170 160 150 140 130 120 110 100 90 80 70 60 50 40 30 20 10 0
f1 (ppm)

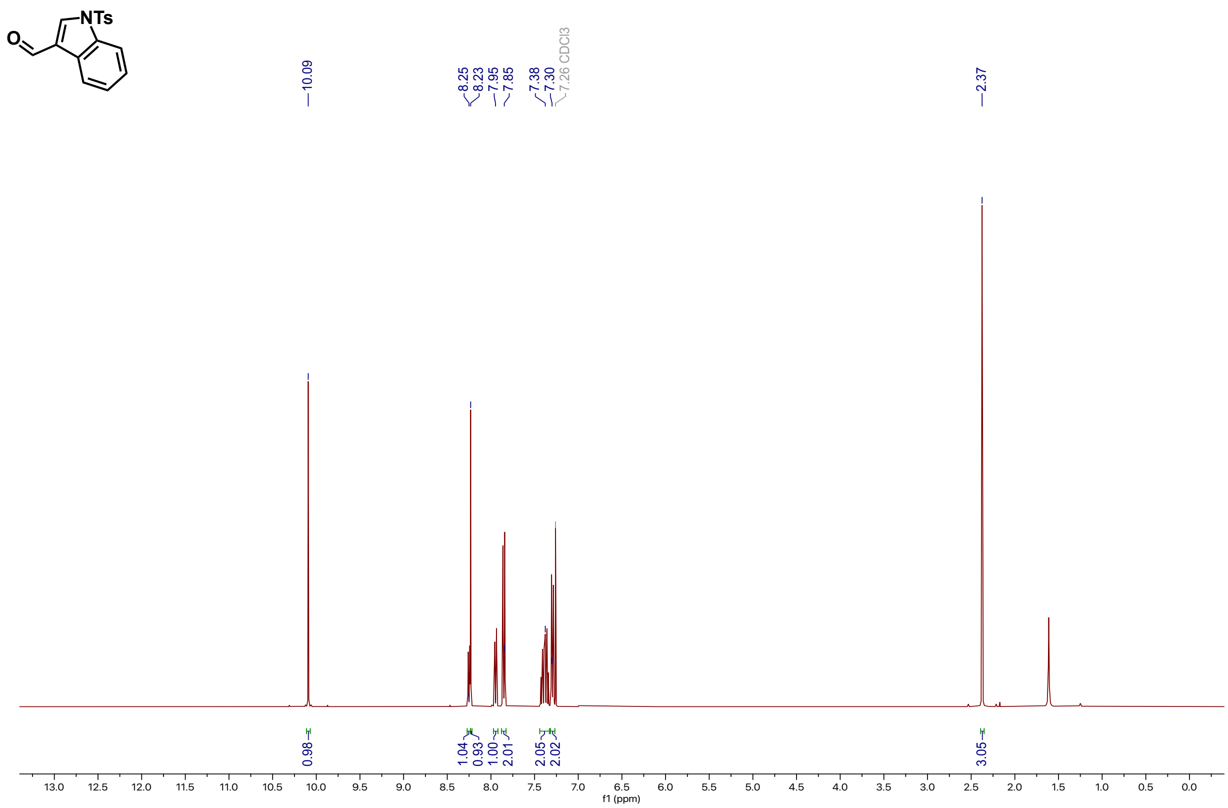
O
NTs
10.09
8.25
8.23
7.95
7.85
7.38
7.30
7.26 CDCl3
2.37
0.98
1.04
0.93
1.00
2.01
2.05
2.02
3.05
13.0
12.5
12.0
11.5
11.0
10.5
10.0
9.5
9.0
8.5
8.0
7.5
7.0
6.5
6.0
5.5
5.0
4.5
4.0
3.5
3.0
2.5
2.0
1.5
1.0
0.5
0.0
f1 (ppm)

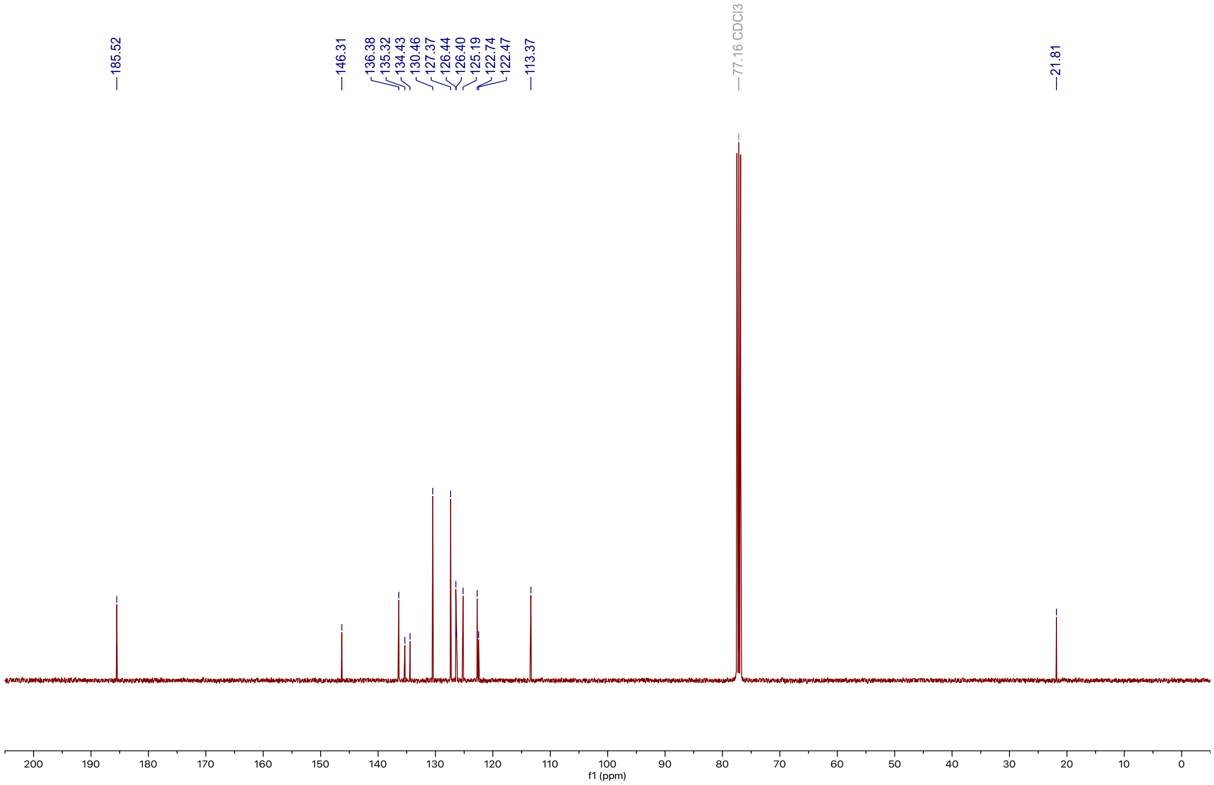
185.52
146.31
136.38
135.32
134.43
130.46
127.37
126.44
126.40
125.19
122.74
122.47
113.37
77.16 CDCl3
21.81
200
190
180
170
160
150
140
130
120
110
100
90
80
70
60
50
40
30
20
10
0
f1 (ppm)

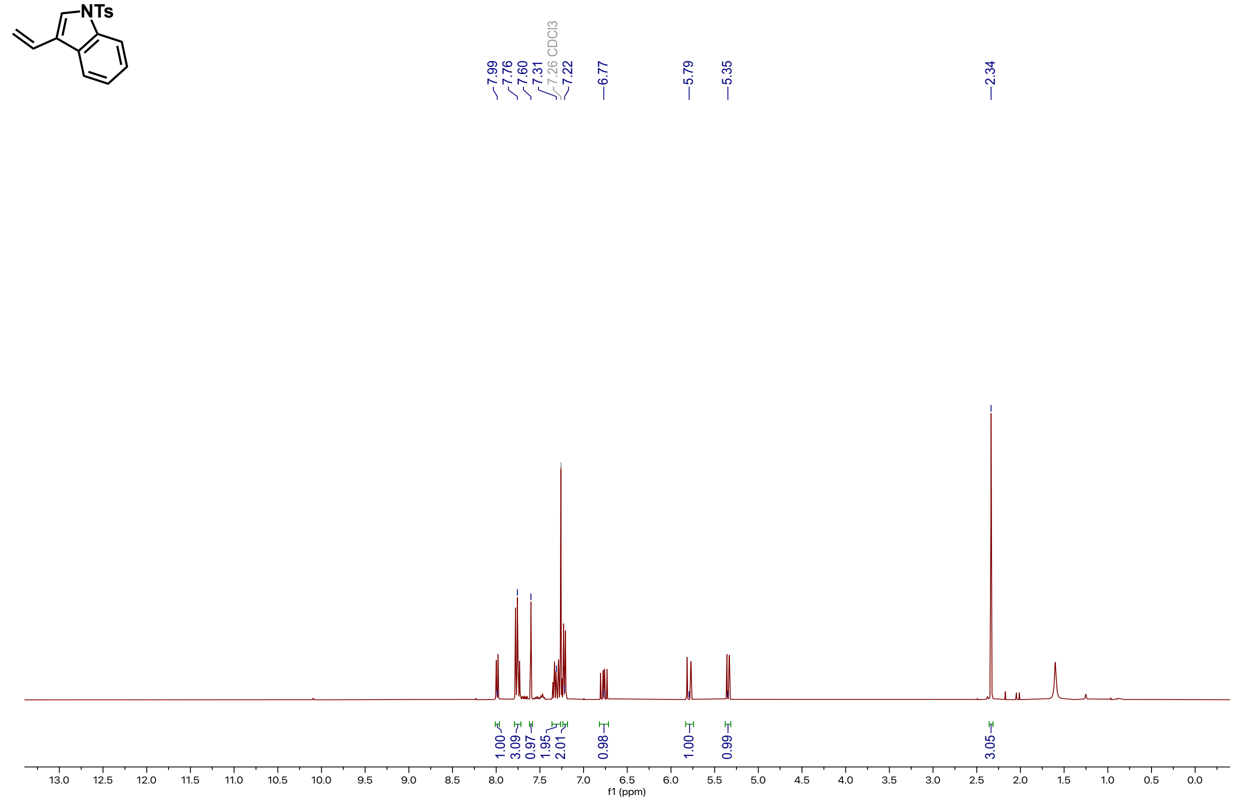
NTs
7.99
7.76
7.60
7.31
7.26 CDCl3
7.22
6.77
5.79
5.35
2.34
1.00
3.09
0.97
1.95
2.01
0.98
1.00
0.99
3.05
13.0 12.5 12.0 11.5 11.0 10.5 10.0 9.5 9.0 8.5 8.0 7.5 7.0 6.5 6.0 5.5 5.0 4.5 4.0 3.5 3.0 2.5 2.0 1.5 1.0 0.5 0.0
f1 (ppm)

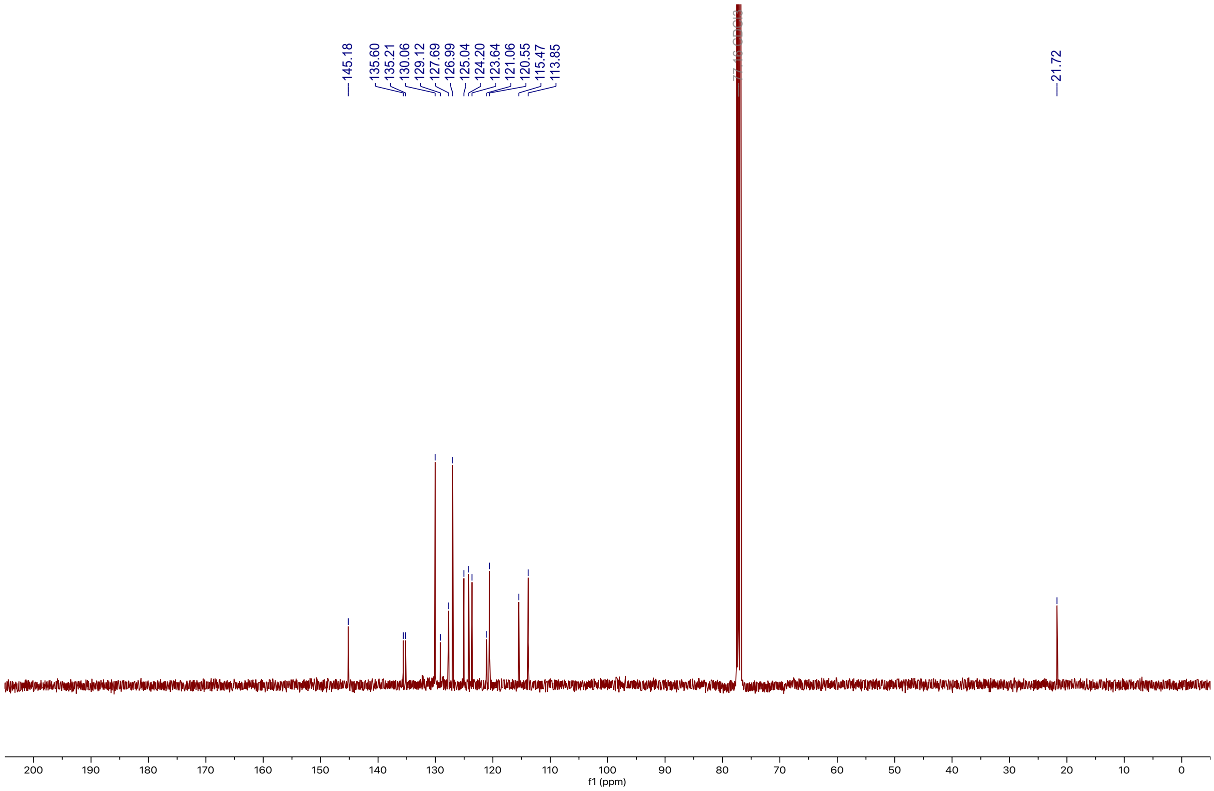
145.18
135.60
135.21
130.06
129.12
127.69
126.99
125.04
124.20
123.64
121.06
120.55
115.47
113.85
77.16 CDCl3
21.72
200 190 180 170 160 150 140 130 120 110 100 90 80 70 60 50 40 30 20 10 0
f1 (ppm)

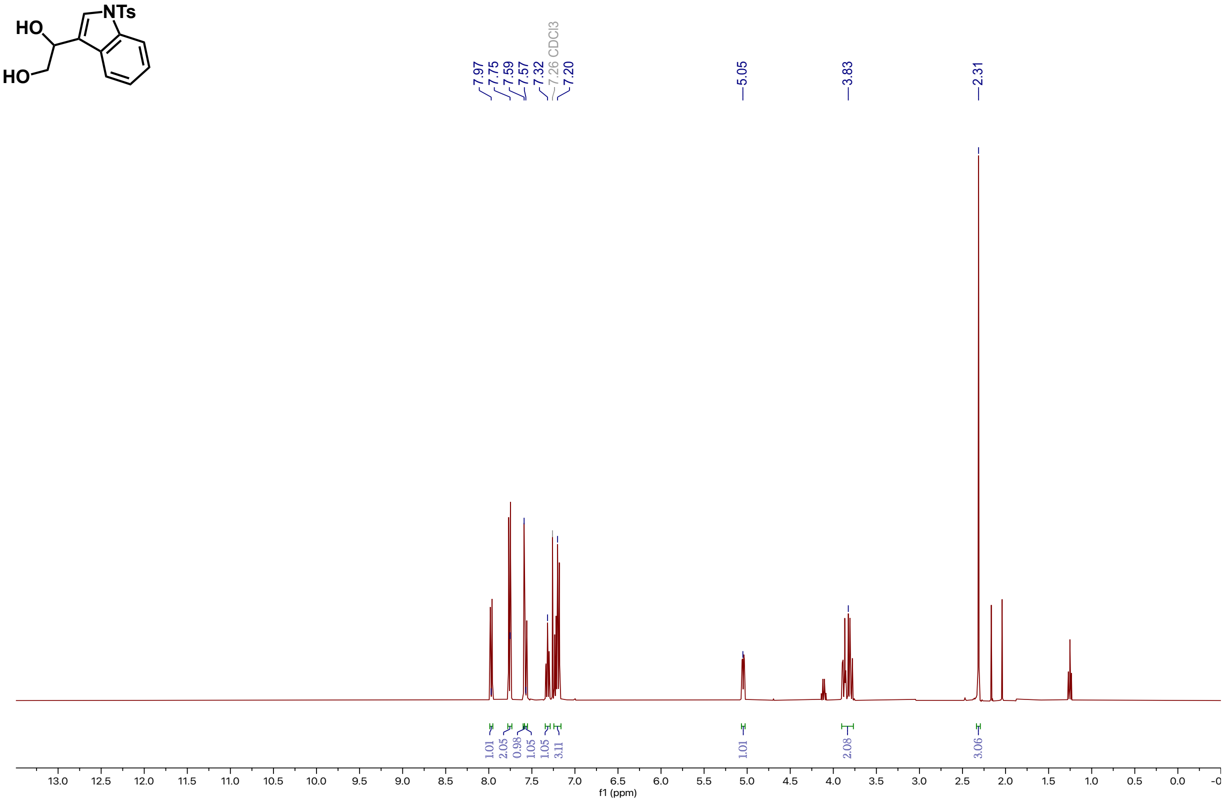
HO
HO
NTs

7.97
7.75
7.59
7.57
7.32
7.26 CDCl3
7.20
5.05
3.83
2.31
1.01
2.05
0.98
1.05
1.05
3.11
1.01
2.08
3.06
13.0
12.5
12.0
11.5
11.0
10.5
10.0
9.5
9.0
8.5
8.0
7.5
7.0
6.5
6.0
5.5
5.0
4.5
4.0
3.5
3.0
2.5
2.0
1.5
1.0
0.5
0.0
f1 (ppm)

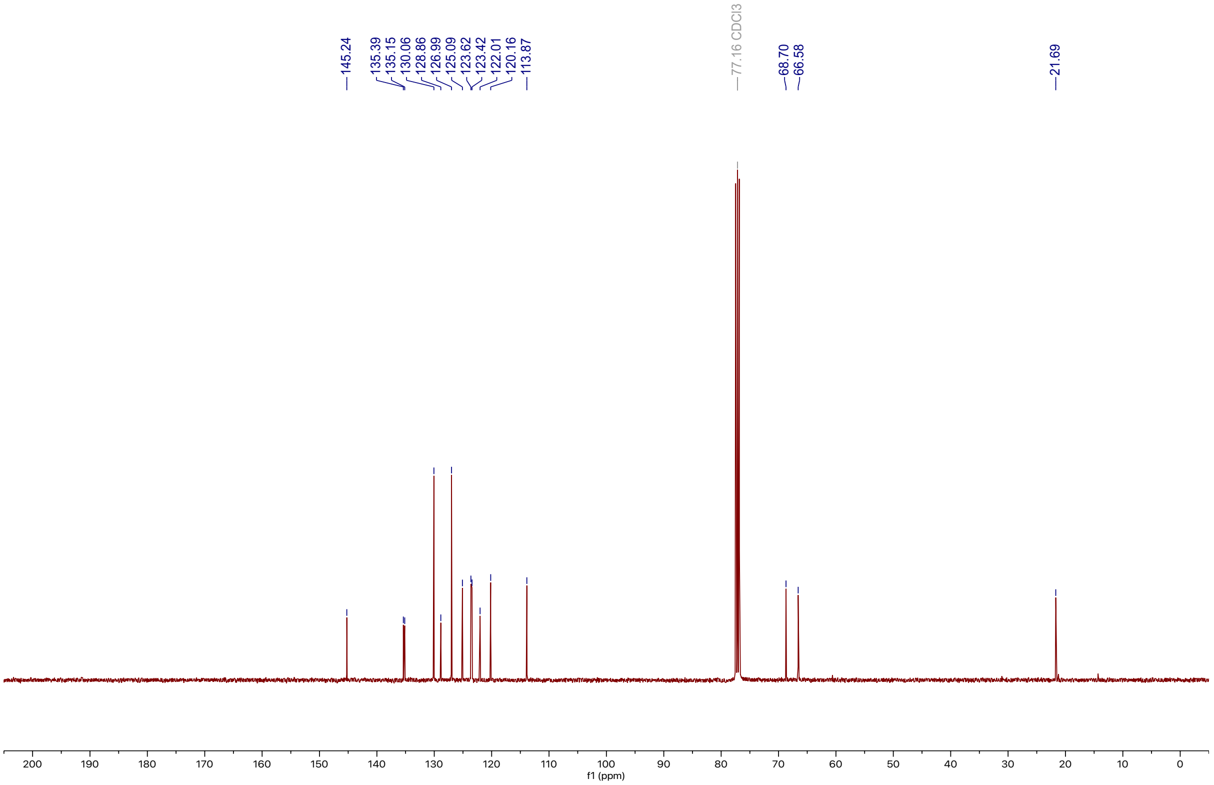
145.24
135.39
135.15
130.06
128.86
126.99
125.09
123.62
123.42
122.01
120.16
113.87
77.16 CDCl3
68.70
66.58
21.69
200
190
180
170
160
150
140
130
120
110
100
90
80
70
60
50
40
30
20
10
0
f1 (ppm)

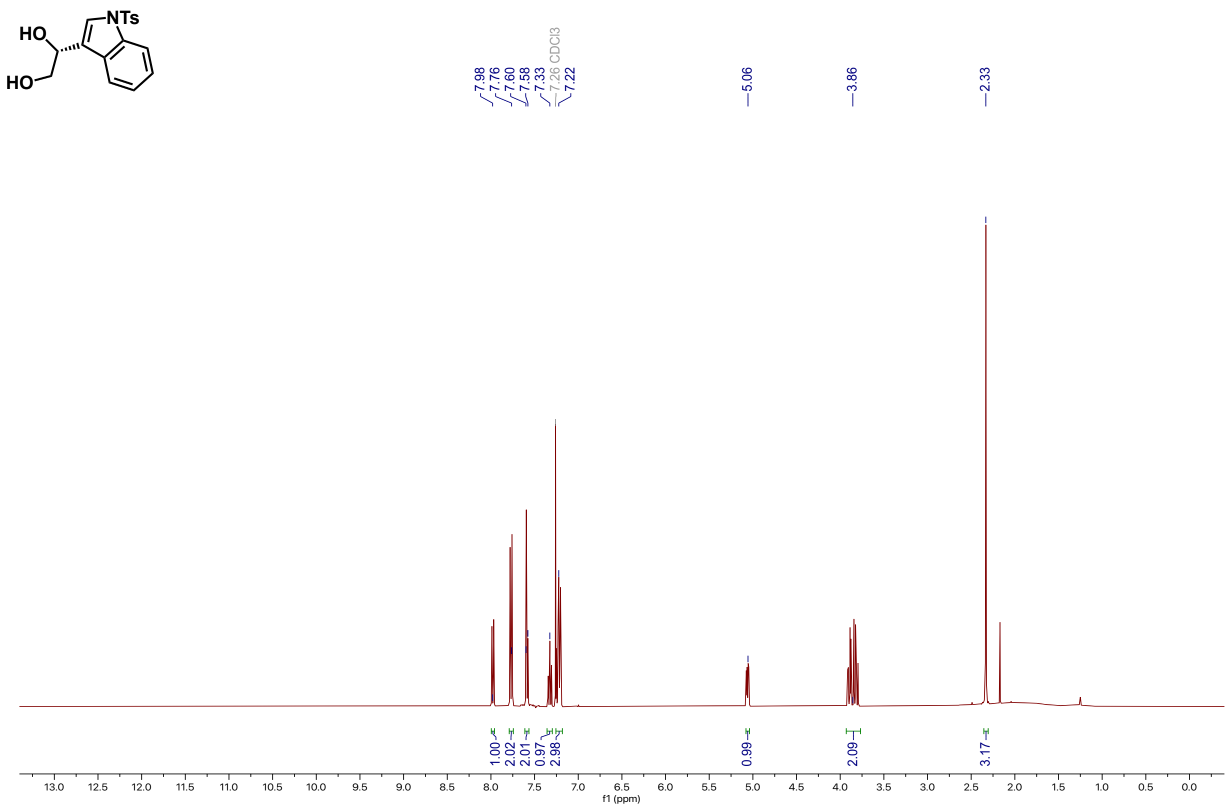
HO
NTs
HO
7.98
7.76
7.60
7.58
7.33
7.26 CDCl3
7.22
5.06
3.86
2.33
1.00
2.02
2.01
0.97
2.98
0.99
2.09
3.17
13.0 12.5 12.0 11.5 11.0 10.5 10.0 9.5 9.0 8.5 8.0 7.5 7.0 6.5 6.0 5.5 5.0 4.5 4.0 3.5 3.0 2.5 2.0 1.5 1.0 0.5 0.0
f1 (ppm)

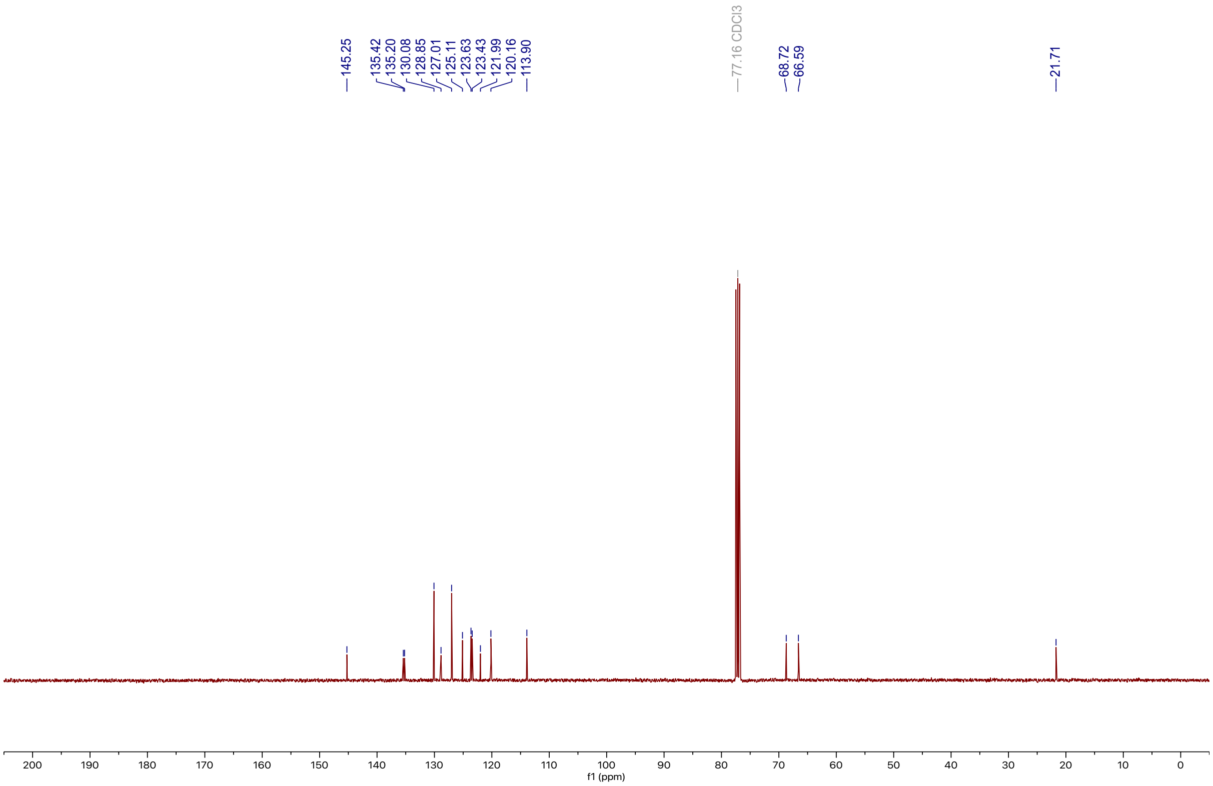
145.25
135.42
135.20
130.08
128.85
127.01
125.11
123.63
123.43
121.99
120.16
113.90
77.16 CDCl3
68.72
66.59
21.71
200 190 180 170 160 150 140 130 120 110 100 90 80 70 60 50 40 30 20 10 0
f1 (ppm)

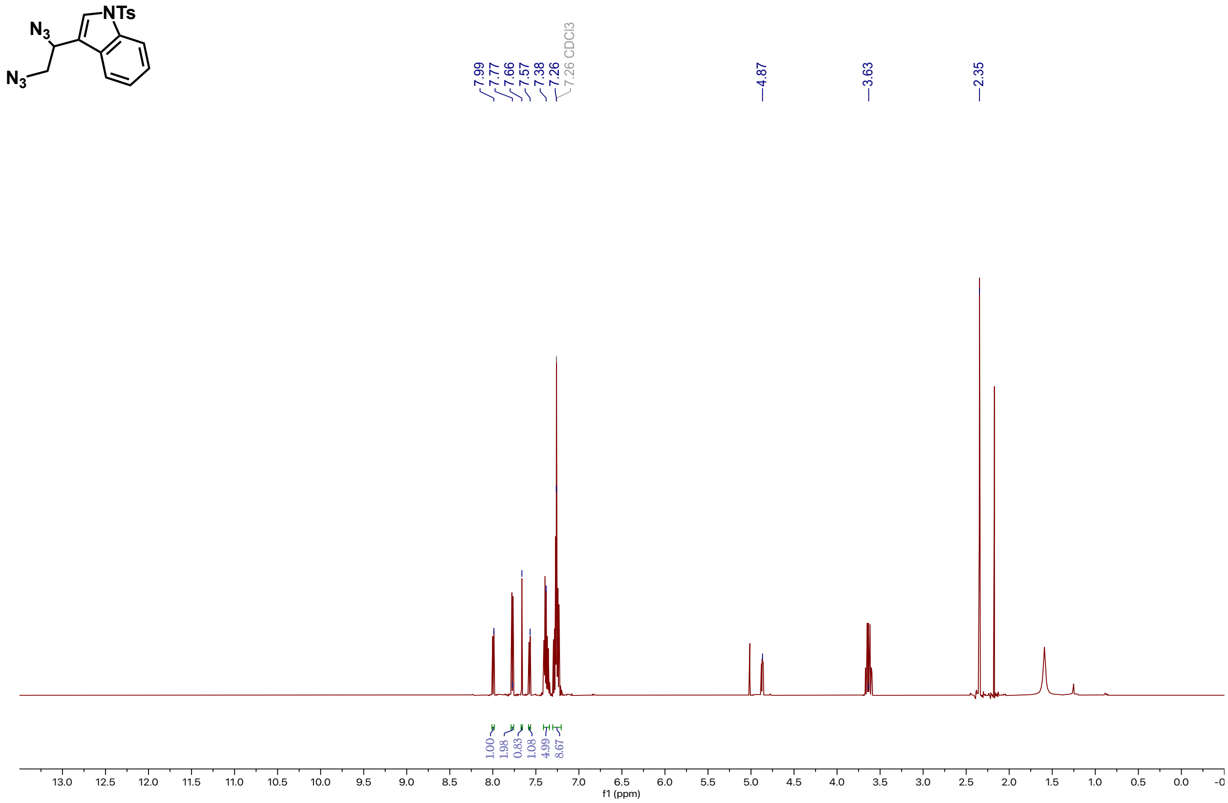
N3
N3
NTs
7.99
7.77
7.66
7.57
7.38
7.26
7.26 CDCl3
4.87
3.63
2.35
1.00
1.98
0.83
1.08
4.99
8.67
13.0
12.5
12.0
11.5
11.0
10.5
10.0
9.5
9.0
8.5
8.0
7.5
7.0
6.5
6.0
5.5
5.0
4.5
4.0
3.5
3.0
2.5
2.0
1.5
1.0
0.5
0.0
f1 (ppm)

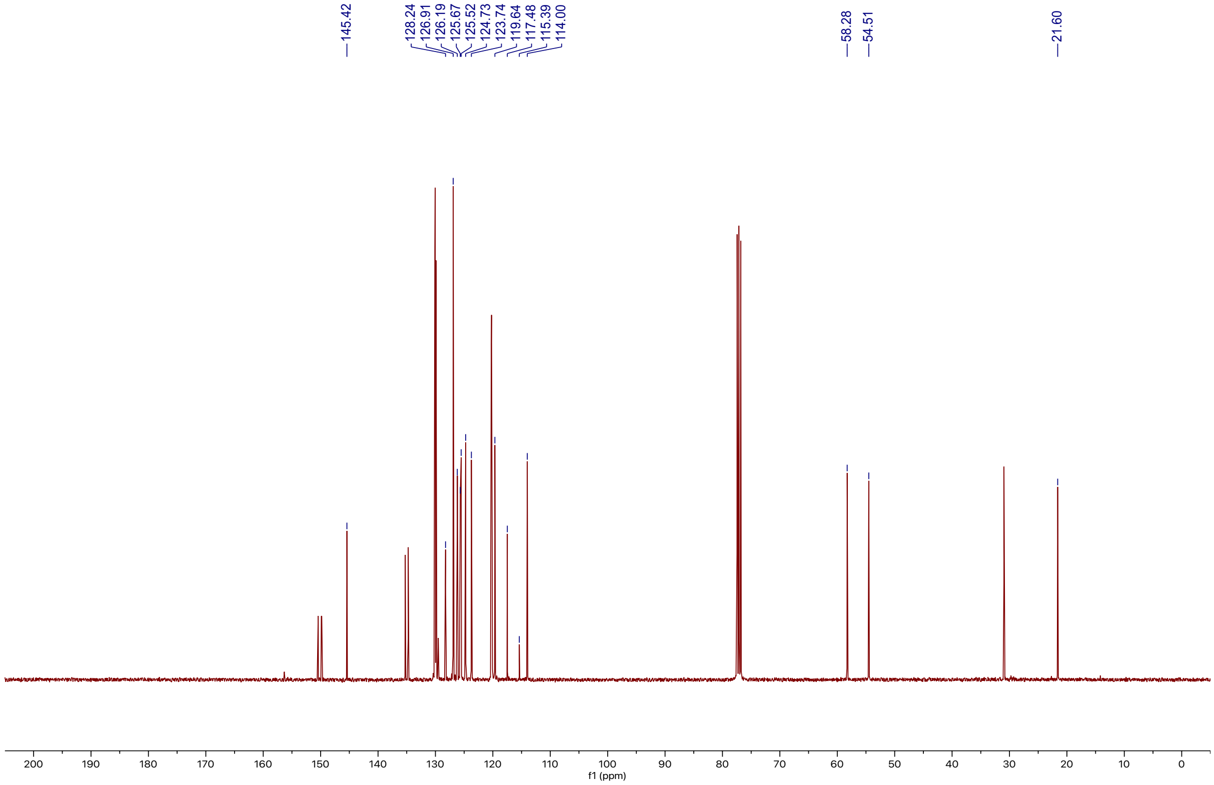
145.42
128.24
126.91
126.19
125.67
125.52
124.73
123.74
119.64
117.48
115.39
114.00
58.28
54.51
21.60
200
190
180
170
160
150
140
130
120
110
100
90
80
70
60
50
40
30
20
10
0
f1 (ppm)

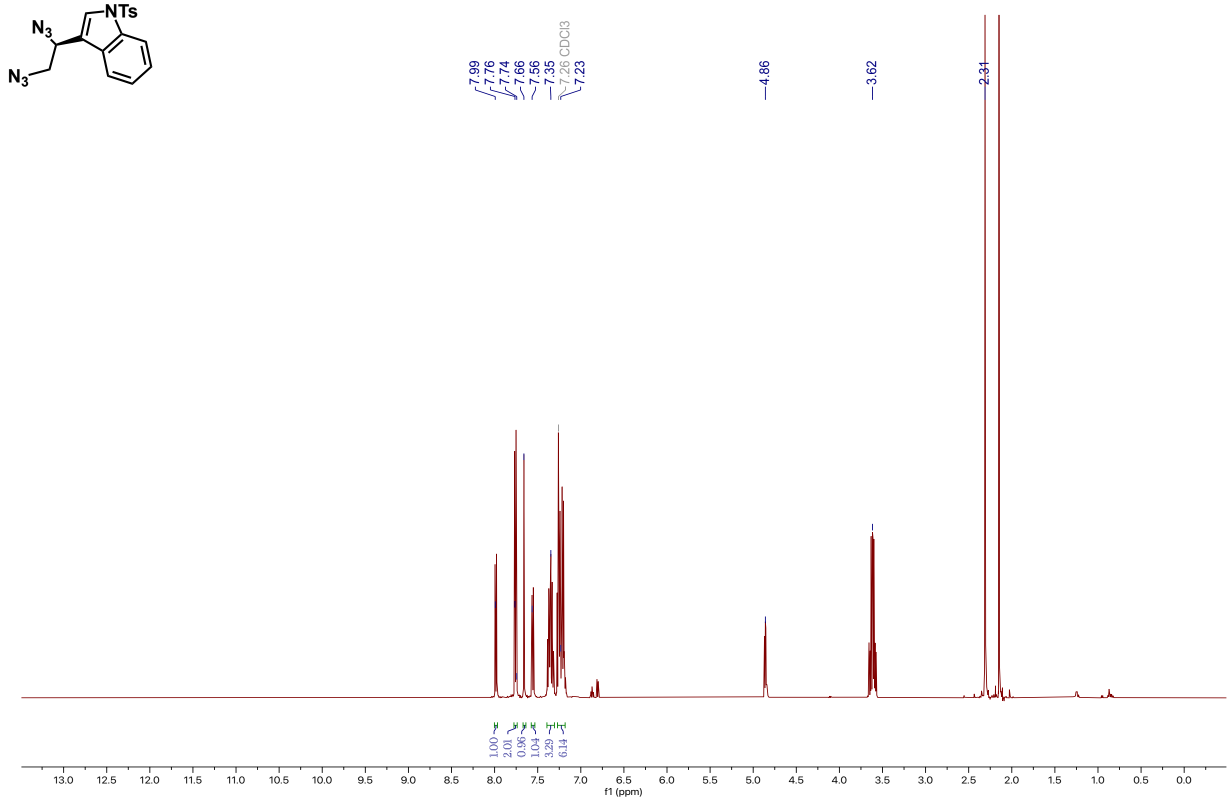
N3
NTs
N3
7.99
7.76
7.74
7.66
7.56
7.35
7.26 CDCl3
7.23
4.86
3.62
2.31
1.00
2.01
0.96
1.04
3.29
6.14
13.0
12.5
12.0
11.5
11.0
10.5
10.0
9.5
9.0
8.5
8.0
7.5
7.0
6.5
6.0
5.5
5.0
4.5
4.0
3.5
3.0
2.5
2.0
1.5
1.0
0.5
0.0
f1 (ppm)

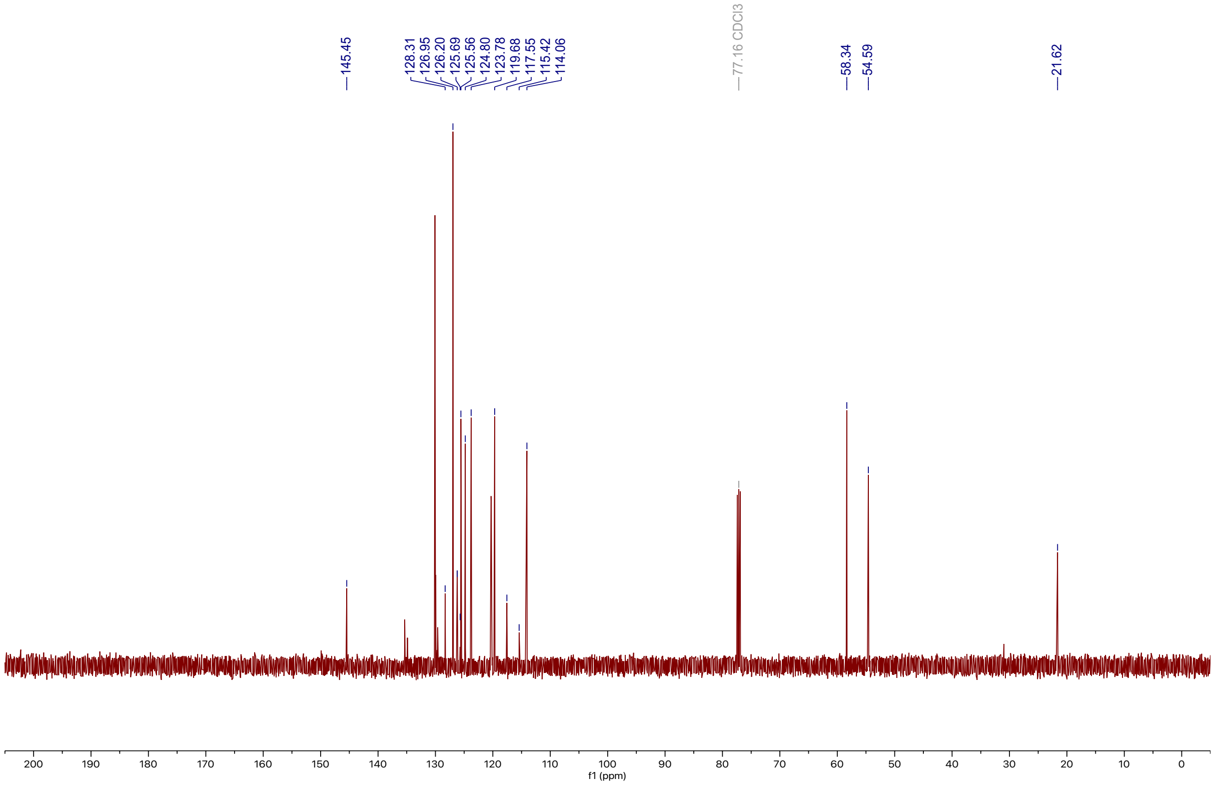
145.45
128.31
126.95
126.20
125.69
125.56
124.80
123.78
119.68
117.55
115.42
114.06
77.16 CDCl3
58.34
54.59
21.62
200
190
180
170
160
150
140
130
120
110
100
90
80
70
60
50
40
30
20
10
0
f1 (ppm)

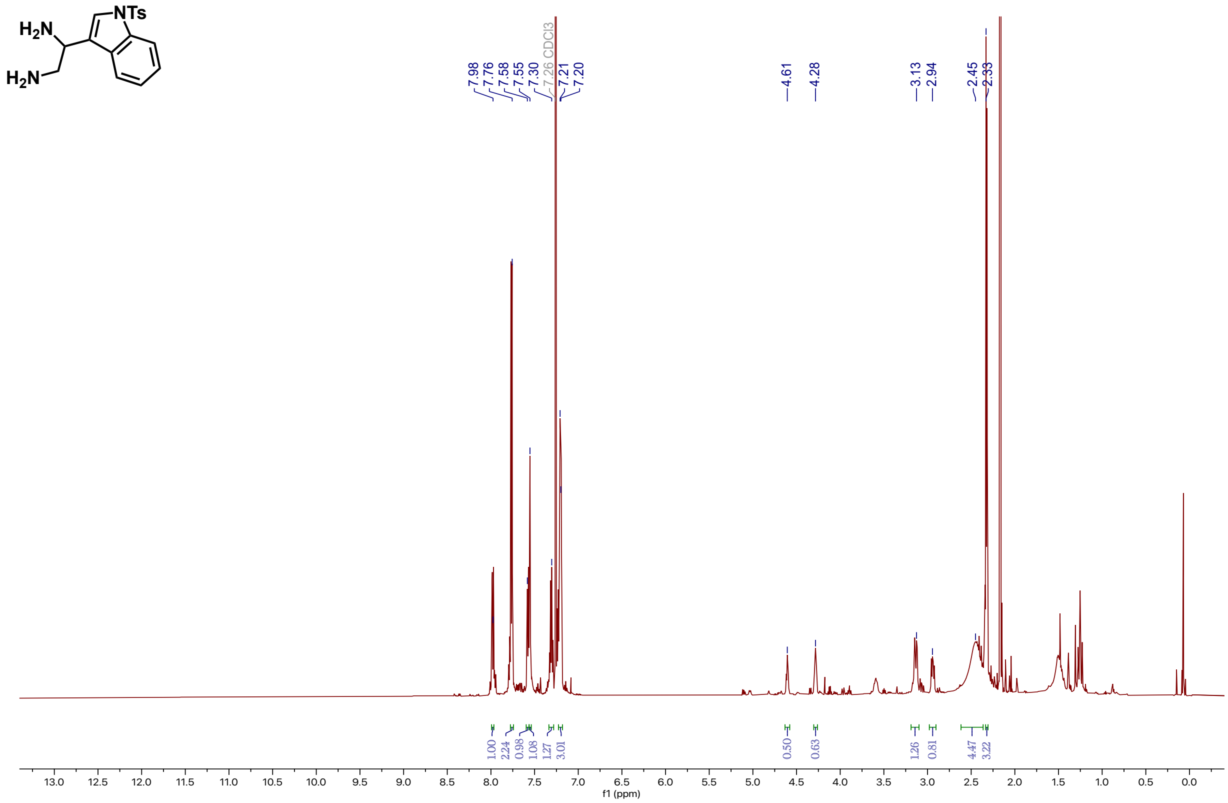
H2N
H2N
NTs
7.98
7.76
7.58
7.55
7.30
7.26 CDCl3
7.21
7.20
4.61
4.28
3.13
2.94
2.45
2.33
1.00
2.24
0.98
1.08
1.27
3.01
0.50
0.63
1.26
0.81
4.47
3.22
13.0
12.5
12.0
11.5
11.0
10.5
10.0
9.5
9.0
8.5
8.0
7.5
7.0
6.5
6.0
5.5
5.0
4.5
4.0
3.5
3.0
2.5
2.0
1.5
1.0
0.5
0.0
f1 (ppm)

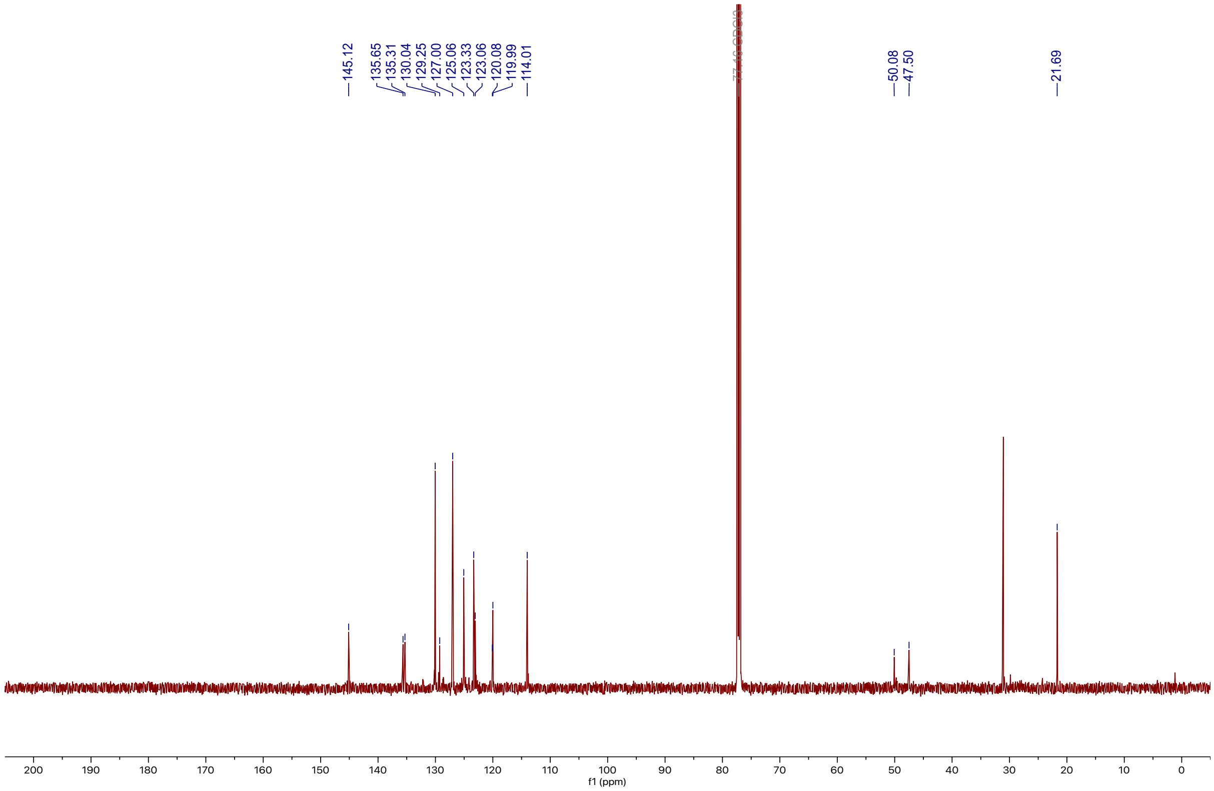
145.12
135.65
135.31
130.04
129.25
127.00
125.06
123.33
123.06
120.08
119.99
114.01
77.16 CDCl3
50.08
47.50
21.69
200
190
180
170
160
150
140
130
120
110
100
90
80
70
60
50
40
30
20
10
0
f1 (ppm)

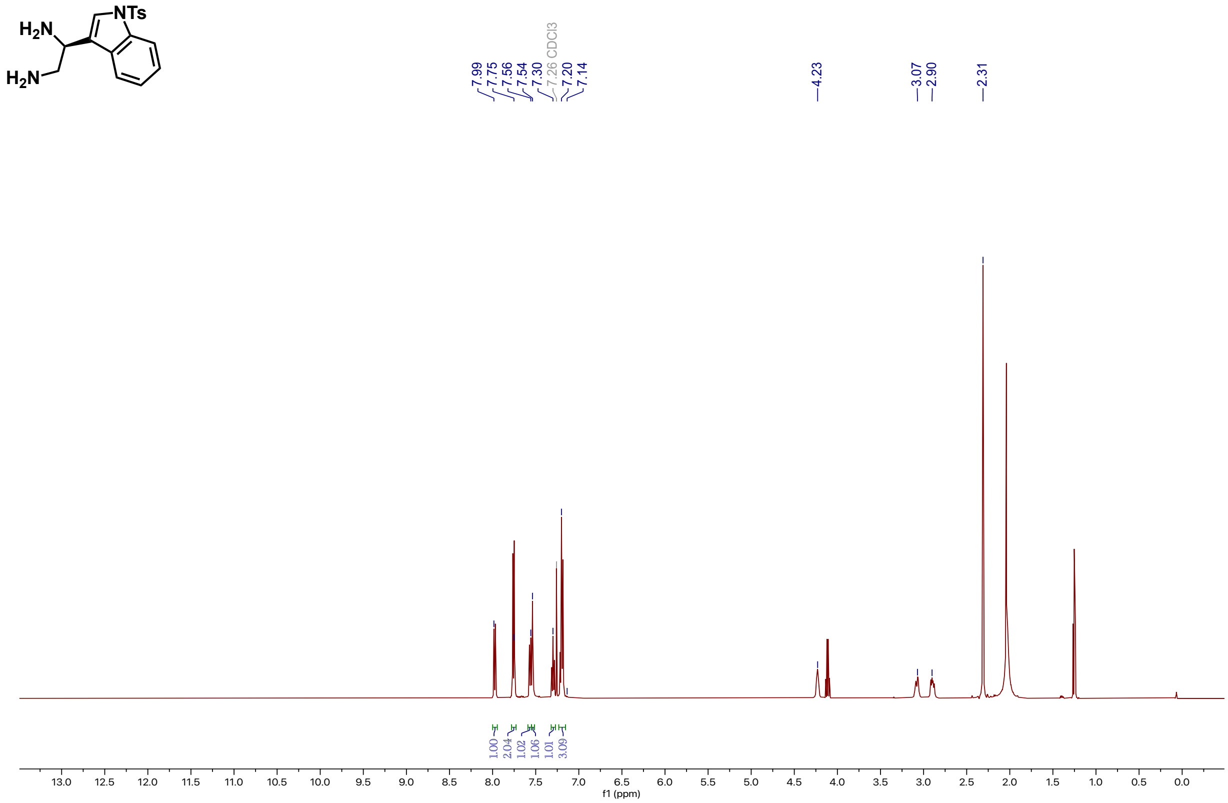
H2N
H2N
NTs
7.99
7.75
7.56
7.54
7.30
7.26 CDCl3
7.20
7.14
4.23
3.07
2.90
2.31
1.00
2.04
1.02
1.06
1.01
3.09
13.0
12.5
12.0
11.5
11.0
10.5
10.0
9.5
9.0
8.5
8.0
7.5
7.0
6.5
6.0
5.5
5.0
4.5
4.0
3.5
3.0
2.5
2.0
1.5
1.0
0.5
0.0
f1 (ppm)

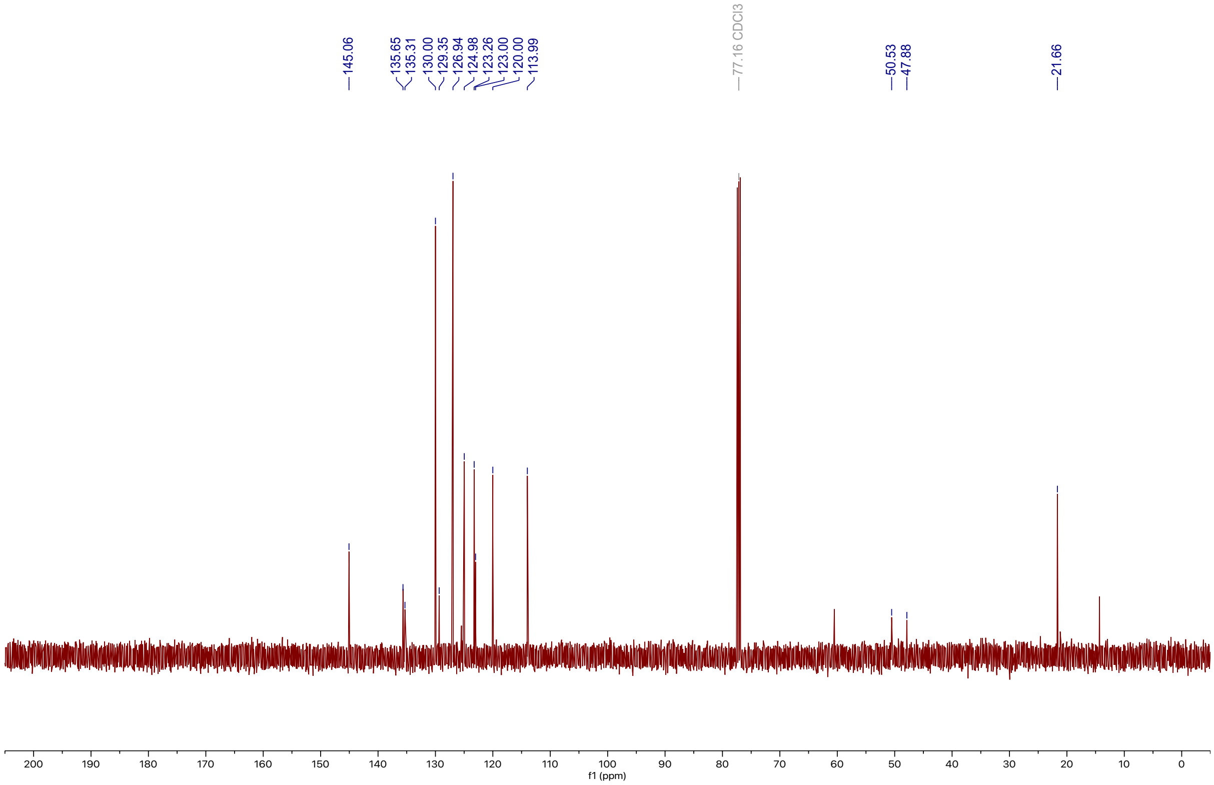
145.06
135.65
135.31
130.00
129.35
126.94
124.98
123.26
123.00
120.00
113.99
77.16 CDCl3
50.53
47.88
21.66
200
190
180
170
160
150
140
130
120
110
100
90
80
70
60
50
40
30
20
10
0
f1 (ppm)

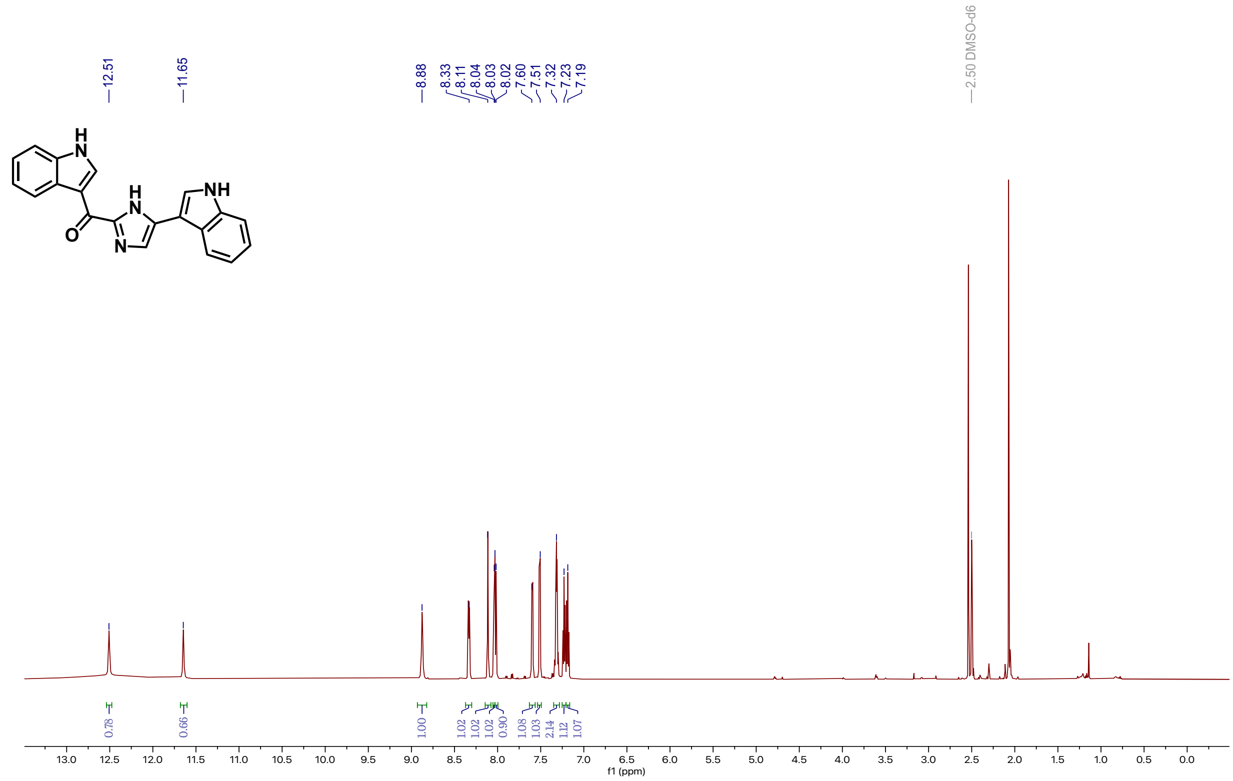
12.51
11.65
8.88
8.33
8.11
8.04
8.03
8.02
7.60
7.51
7.32
7.23
7.19
2.50 DMSO-d6
0.78
0.66
1.00
1.02
1.02
1.02
0.90
1.08
1.03
2.14
1.12
1.07
13.0
12.5
12.0
11.5
11.0
10.5
10.0
9.5
9.0
8.5
8.0
7.5
7.0
6.5
6.0
5.5
5.0
4.5
4.0
3.5
3.0
2.5
2.0
1.5
1.0
0.5
0.0
f1 (ppm)
H
N
H
N
NH
O
N

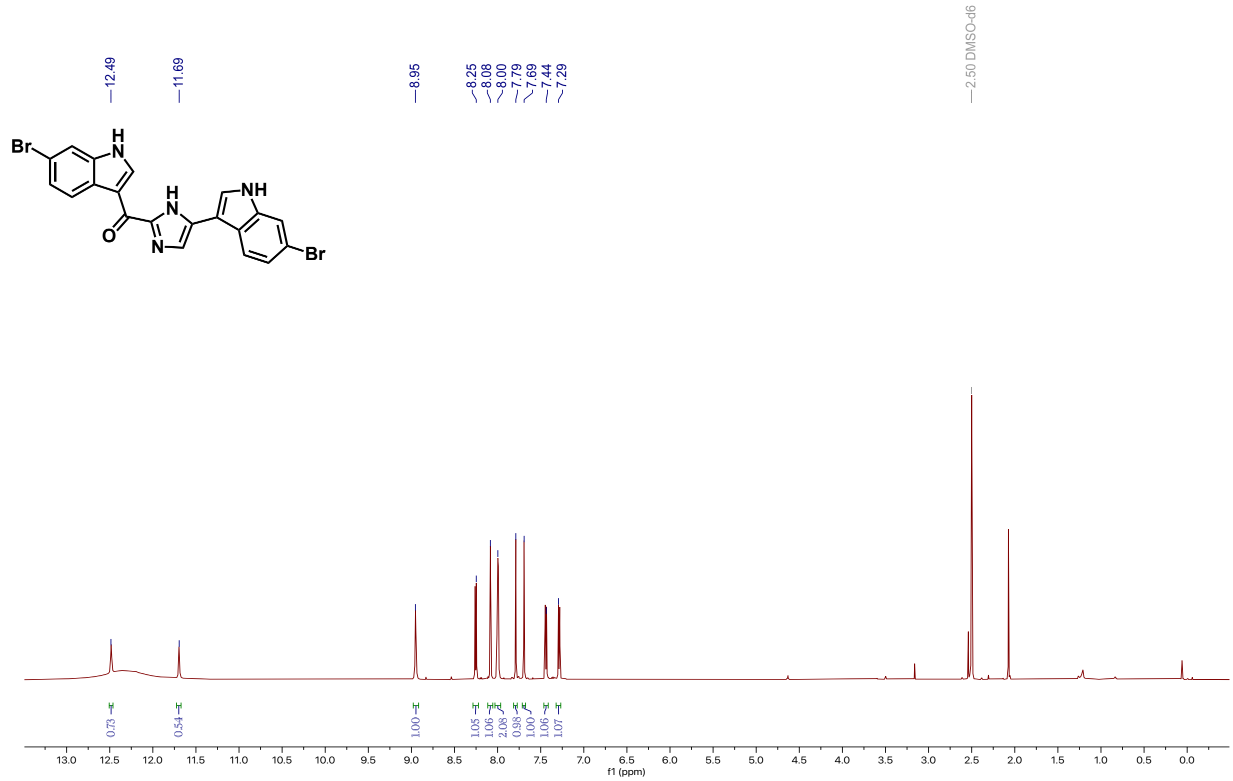
12.49
11.69
8.95
8.25
8.08
8.00
7.79
7.69
7.44
7.29
2.50 DMSO-d6
Br
H
N
H
N
NH
O
N
Br
0.73
0.54
1.00
1.05
1.06
2.08
0.98
1.00
1.06
1.07
13.0
12.5
12.0
11.5
11.0
10.5
10.0
9.5
9.0
8.5
8.0
7.5
7.0
6.5
6.0
5.5
5.0
4.5
4.0
3.5
3.0
2.5
2.0
1.5
1.0
0.5
0.0
f1 (ppm)

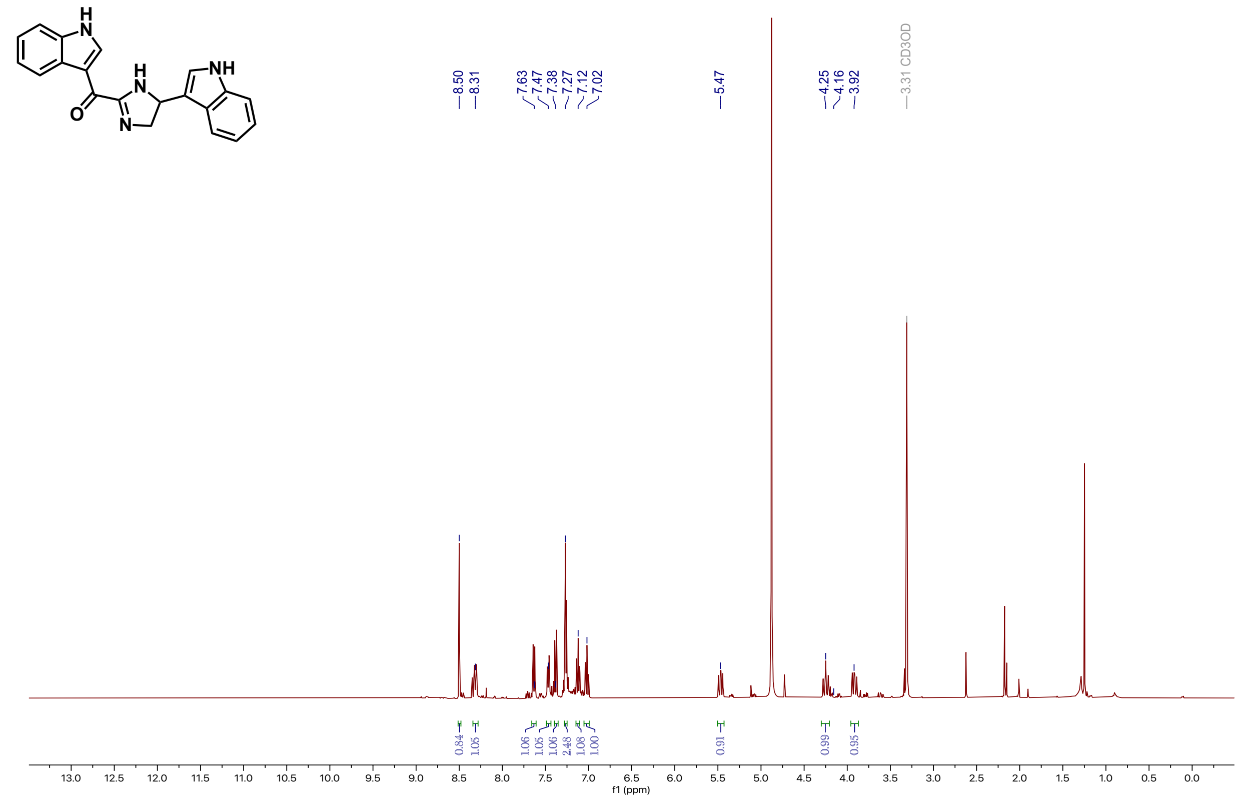
H
N
O
H
N
N
NH
8.50
8.31
7.63
7.47
7.38
7.27
7.12
7.02
5.47
4.25
4.16
3.92
3.31 CD3OD
0.84
1.05
1.06
1.05
1.06
2.48
1.08
1.00
0.91
0.99
0.95
13.0 12.5 12.0 11.5 11.0 10.5 10.0 9.5 9.0 8.5 8.0 7.5 7.0 6.5 6.0 5.5 5.0 4.5 4.0 3.5 3.0 2.5 2.0 1.5 1.0 0.5 0.0
f1 (ppm)

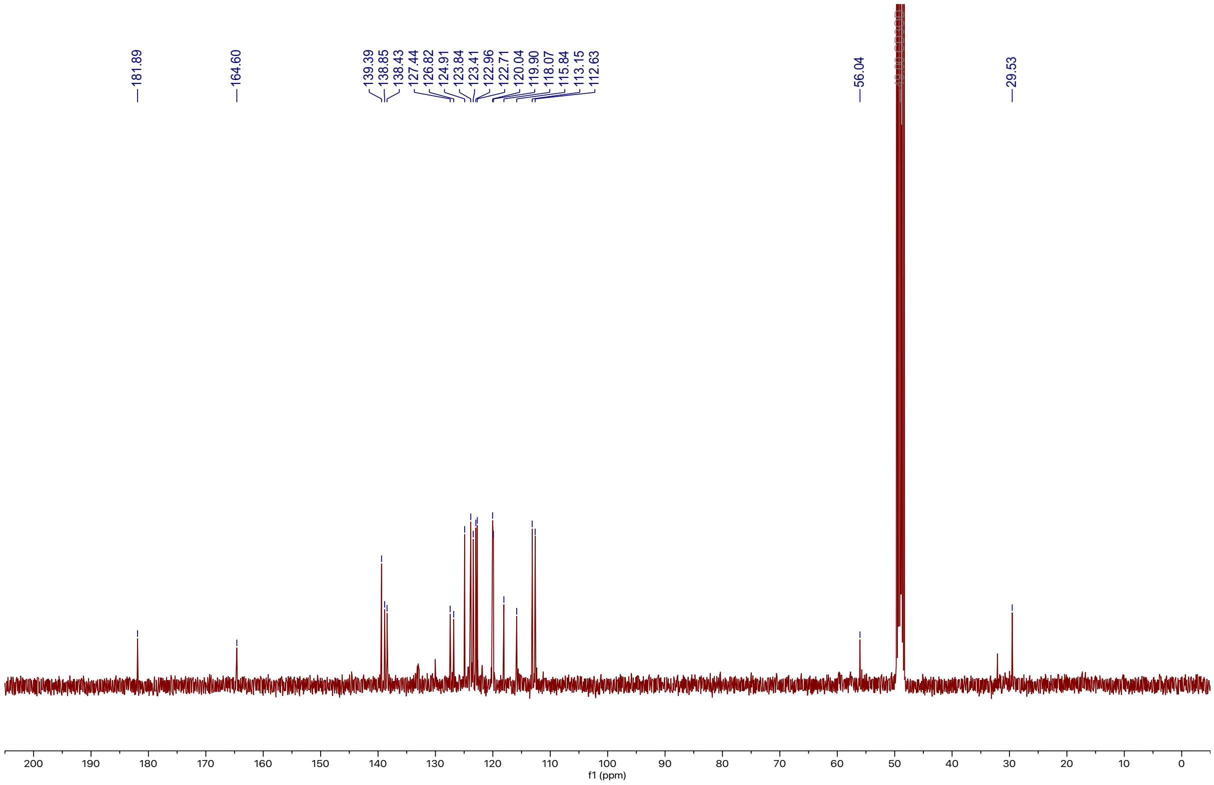
181.89
164.60
139.39
138.85
138.43
127.44
126.82
124.91
123.84
123.41
122.96
122.71
120.04
119.90
118.07
115.84
113.15
112.63
56.04
29.53
200 190 180 170 160 150 140 130 120 110 100 90 80 70 60 50 40 30 20 10 0
f1 (ppm)

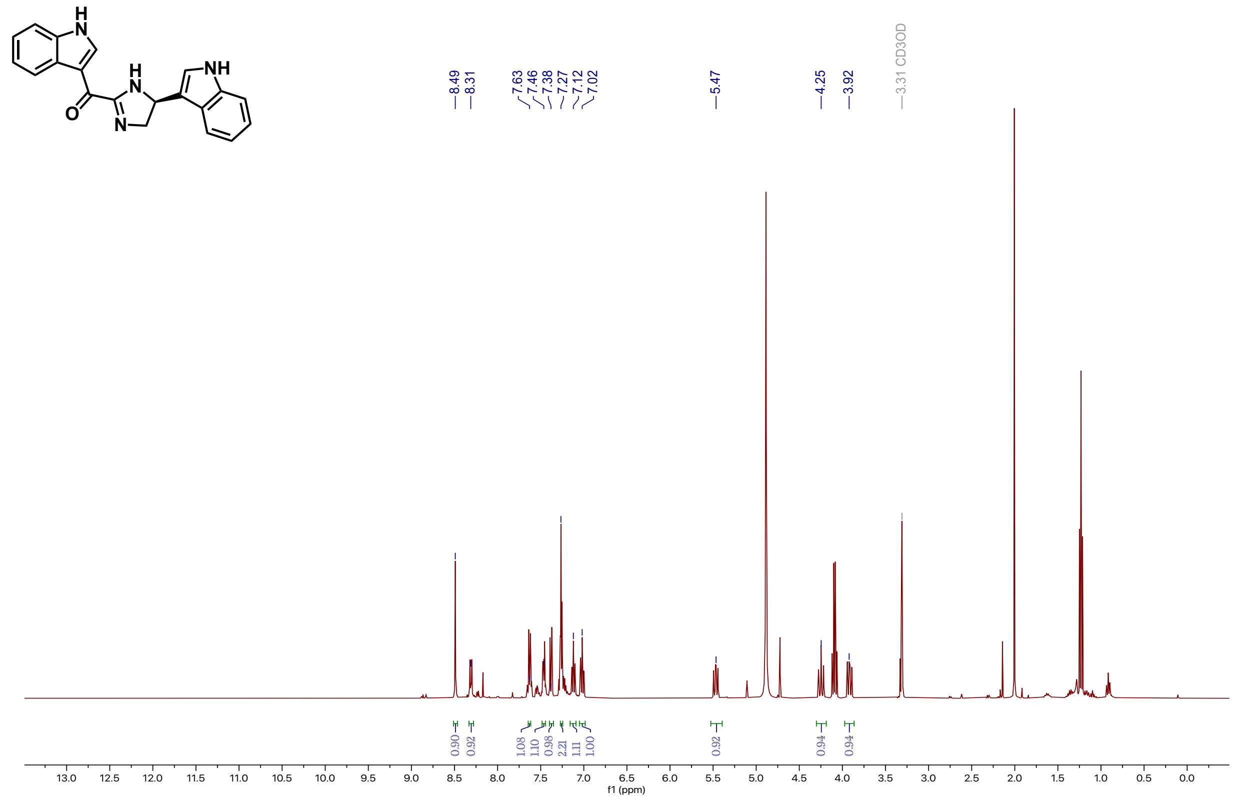
H
N
O
H
N
N
NH
8.49
8.31
7.63
7.46
7.38
7.27
7.12
7.02
5.47
4.25
3.92
3.31 CD3OD
0.90
0.92
1.08
1.10
0.98
2.21
1.11
1.00
0.92
0.94
0.94
13.0 12.5 12.0 11.5 11.0 10.5 10.0 9.5 9.0 8.5 8.0 7.5 7.0 6.5 6.0 5.5 5.0 4.5 4.0 3.5 3.0 2.5 2.0 1.5 1.0 0.5 0.0
f1 (ppm)

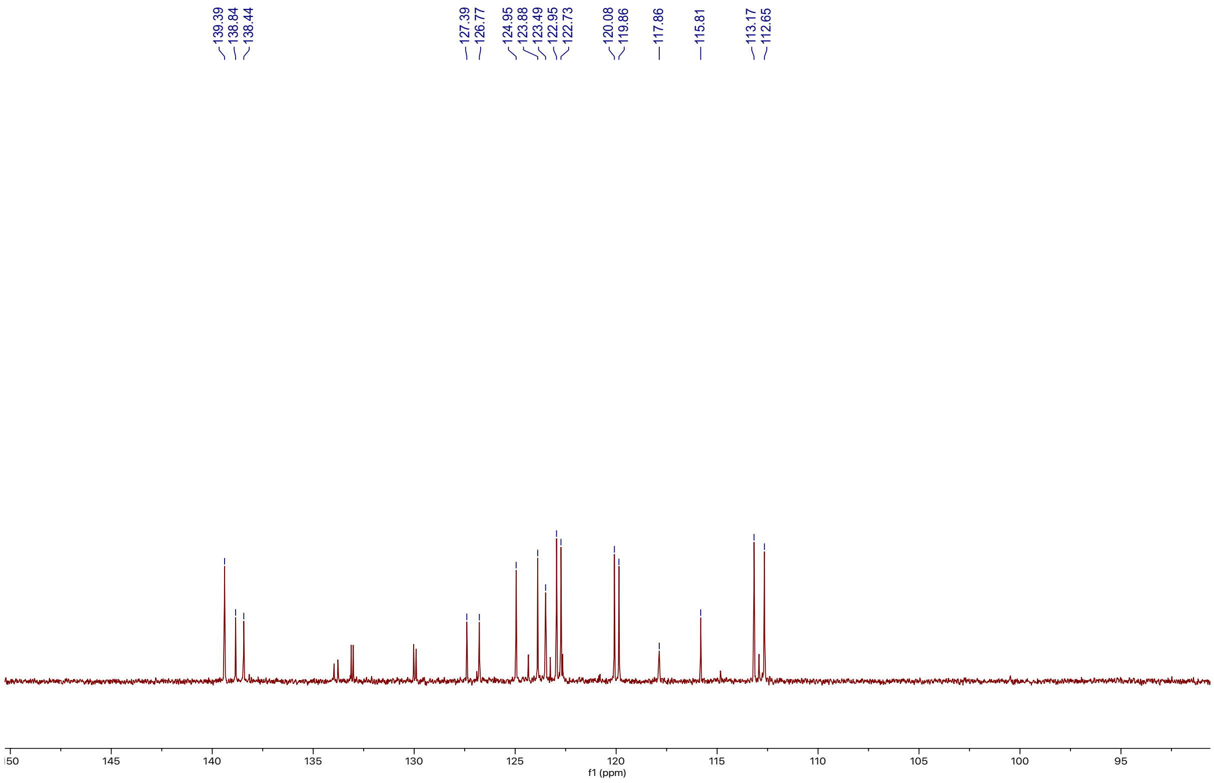
139.39
138.84
138.44
127.39
126.77
124.95
123.88
123.49
122.95
122.73
120.08
119.86
117.86
115.81
113.17
112.65
150 145 140 135 130 125 120 115 110 105 100 95
f1 (ppm)

References

1 Guinchard, X.; Vallée, Y.; Denis, J-N. Total Synthesis of Marine Sponge Bis(indole) Alkaloids of the Topsentin Class. *J. Org. Chem.* **2007**, *72*(10), 3972-3975.

2 Murai, K.; Morishita, M.; Nakatani, R.; Kubo, O.; Fujioka, H.; Kita, Y. Concise Total Synthesis of (-)-Spongotine A. *J. Org. Chem.* **2007**, *72*(23), 8947-8949.

3 Ji, X.; Wang, Z.; Dong, J.; Liu, Y.; Lu, A.; Wang, Q. Discovery of Topsentin Alkaloids and Their Derivatives as Novel Antiviral and Anti-phytopathogenic Fungus Agents. *J. Argic. Food. Chem.* **2016**, *64*(48), 9143-9151.